# Generation of Granitic Magmas in the Lower Crust: A Natural Example from Mt Daniel, Fiordland, New-Zealand

Thesis submitted by

***Shrema Bhattacharya**, B.Sc, M.Sc*

in Aug 2010

For the degree of Doctor of Philosophy

In the School of Earth and Environmental Sciences

James Cook University

# STATEMENT OF ACCESS

I, the undersigned, author of this work, understand that James Cook University will make this thesis available for use within the University Library and, via the Australian Digital Theses network, for use elsewhere.

I understand that, as an unpublished work, a thesis has significant protection under the Copyright Act and I wish this work to be embargoed until August 2010.

After which date I do not wish to place any further restriction on access to this work.

_____ _____

Signature Date

# STATEMENT OF SOURCES DECLARATION

I declare that this thesis is my own work and has not been submitted in any form for another degree or diploma at any university or other institution of tertiary education. Information derived from the published or unpublished work of others has been acknowledged in the text and a list of references is given.

_____ _____

Signature Date

## ELECTRONIC COPY

I, the undersigned, the author of this work, declare that the electronic copy of this thesis provided to the James Cook University Library is an accurate copy of the print thesis submitted, within the limits of the technology available.

_____ _____

Signature Date

# STATEMENT ON THE CONTRIBUTION OF OTHERS

Financial contributions towards this PhD project have included:

- Project funding from the ARC
- James Cook University Graduate Research School scholarship in 2008 and 2009.

General contributions towards this PhD project have included:

- **Prof. Bill Collins**: - supervision throughout the entire project including help in designing the PhD project, field work, sample collection, discussions and revision of all chapters. Particularly the field work and sample collection were completely done by him in the year of 2000. Any further field work could not be carried out during this PhD due to budget constrain.

- **Dr. Tony Kemp**: - supervision through out the PhD project including helping in extensive lab work, discussion, revision of all chapters.

- **Dr. Mike Rubenach**:-helping in thin section study

- **Dr. Carl Spandler**: - Valuable discussion relevant to this research.

- **Dr. K.L. Blake**:-assistance during microprobe analysis at the Advanced Analytical Centre, James Cook University, Townsville.

- **Dr. Yi Hu**:-assistance during LA-ICP-MS analysis at the Advanced Analytical Centre, James Cook University, Townsville.

# ACKNOWLEDGEMENTS

I express my profound sense of gratitude and sincere thanks to my supervisor Prof. Bill Collins and co-supervisor Dr. Tony Kemp for their constant support, guidance and encouragement to come to JCU and do this PhD. I am extremely grateful to Prof.Bill Collins and Dr. Tony Kemp for their continued help and advice throughout the research and without them this PhD would have been impossible.

I would like to thank Prof. Paul Dirks for providing sufficient time for completion of this research successfully. I acknowledge the valuable contributions of Dr. Mike Rubenach and Dr. Carl Spandler by way of stimulating discussions throughout the duration of the project. I would also like to acknowledge the contributions of my co-supervisor Dr. Tony Kemp, Dr. Kevin Blake, Dr. Yi Hu, and other AAC staff for extending enormous help during my Lab work.

I am indebted to my parents Biswabandhu Bhattacharya and Anjali Bhattacharya and very thankful to my sister Souvari Bhattacharya for their encouragement, constant support and love from afar. Huge thanks should go to my friend Kaustav Bose and Sabyasachi Bhattacharya for helping me to complete this reseach.

My office mate Jaiby Ann Jacob is thanked for her support and help even far from Melbroune. I would like to specially acknowledge Jyotindra Sapkota, Ahmed Abusarib, Afroz Shah, Asghar Ali, Ioan Sansilva and all SAMRI guys for their support. Other PhD students, researchers and staff members in the department are also thanked for their friendship and help over the last three years; in particular Glen, Vivian, Judy, Rowena, Haidi, Berit, Ryan, Babo, Darren, Paul, Melissa and Rachel. I would also like to thank my friends abroad Moumita and Rumki and dear ones in Townsville Raj, Rajesh, Prakash, Sreekanth, Manish, Prof Bithin Datta, Anindita Datta, Jashoda Sapkota, Shahid Choudhury and Munni Choudhury. I would like to thanks Dr. Sajeev Krishnan (IISC, India) for providing extensive moral support and help to finish this work.

# ABSTRACT

The base of the 10-20 km thick, batholithic, Western Fiordland Orthogneiss (WFO) is exposed in northern Fiordland as the Mount Daniel Complex (MDC). It forms a ~100-metre thick, sheeted complex between the WFO and the underlying dominantly dioritic basement of Arthur River Complex (ARC). Although previously called a migmatite aureole at the WFO base, field relations show it formed after the WFO was solidified and injected by numerous rectilinear trondhjemitic dykes. U-Pb zircon analysis confirms emplacement of the WFO at 125 Ma, with MDC formation slightly later, between 120-112 Ma. Successive dyke injection and sheeting during tight to isoclinal folding, and fold asymmetry, indicates that the MDC was emplaced syn-tectonically into an active, sinistral reverse shear zone associated with exhumation of the WFO.

The MDC is composed almost entirely of intrusive metre-scale sheets, ranging in composition from mafic dykes, low-Na and high-Na intermediate (trondhjemitic) dykes, high-K granitic dykes and the dominant intermediate-composition Mt Daniel Sheets (MDS) of the complex 55-65% SiO2. The compositional range of MDC vary from 44wt% to 76 wt% $SiO_2$, and has a typically sodic character ($Na_2O$ 4-8 wt %). With the exception of very sodic trondhjemitic dykes ($Na_2O$ >6 wt%), the MDC is similar to coeval high-level granitic plutons of the Separation Point Batholith (SPB), located northward from the study area. WFO shows a different geochemical trend from the other MDC rocks and a more restricted isotopic composition. This data and field evidence suggests that the WFO was not involved in formation of the MDC.

The wide spectrum of MDC rock types requires multiple sources. Flat, MORB-like REE patterns of the mafic dykes indicate derivation from spinel lherzolite (< 70 Km depth). All other rock types come from crustal sources. The trondhjemitic dykes have variably depleted HREE and minor Eu anomalies compared to the other rock-types and high Sr/Y ratios (>40) indicating their derivation from a deep mafic crustal

source ≥13 Kb where garnet was stable and plagioclase unstable. The high-K granites have low Rb content, suggesting residual biotite in the source rock. It is argued, based on published experimental data, that the high-K magmas were hydrous and formed near the granite solidus at ~10 kbar.

Bimodal (felsic and mafic) magmas dominate the lower section of the MDC, but more homogenized intermediate dioritic magmas dominate the upper section. Mixing of the magmas occurred by stirring during intrusion into the active shear zone. Trondhjemitic dyke injection was continuous throughout MDC formation. The isotopic εNd-initial Sr wholerock data and Hf isotopic data of zircon from different rock types show a crust-mantle mixing array, and the coherent major and trace element variation within the MDC is broadly consistent with mixing, rather than fractionation. Mixing of the (high- and low-Na) intermediate dyke magmas with the mafic and granitic dyke magmas can explain the chemical and isotopic variation within the MDC, including the REE and multielement variation patterns.

An alternative explanation for the chemical diversity of the MDC is that bulk assimilation of ARC basement has contributed a major component. Assimilation is most clearly observed in the lower sections of the MDC, but less so in the upper homogenized sections. However, the presence of inherited zircon of Carboniferous age in most samples indicates it was pervasive. The similarities in the Hf isotopic composition of zircons from trondhjemitic dykes and SPB granites with the ARC (136-129 Ma) and Darran Complex (143-136 Ma) suggest they represent the dominant juvenile mafic crustal source or equivalent. Few inherited Mesozoic zircons exist in the MDC, but this probably reflects the lack of zircon in the inferred primitive (gabbroic?) protolith. Evidence for an older evolved source component comes from Carboniferous-aged zircons, which are also present in the ARC. This is probably the major source of the high-K granitic magmas. Thus, this study proposes crustal-assimilation and mixing of four major source components in the lower crust produced the chemical diversity of the MDC.

The short time span (120-112 Ma) represented by MDC rocks, the simultaneous presence of Early Cretaceous magmatic and metamorphic zircons, even within the same rock, and the presence of both

HREE-depleted and non-depleted rims zircon in granites, suggests a very dynamic transitional magmatic-metamorphic environment associated with the MDC formation. The magmatic to metamorphic condition was associated with a change from open to closed system chemical processes.

The formation of trondhjemitic dykes at ~13 Kbar depth after the burial of WFO at ~120 Ma and formation of granites at comparatively lower depth at ~10 Kb (between 120-112 Ma) is consistent with an exhumation path for the MDC at this stage. Thus, the MDC represents the retrograde part of an anticlockwise P-T-t path. Exhumation could have been associated with crustal extension, for which limited evidence exists regionally, or it can be associated with thrusting. If the latter, the crust must have been undergoing rapid erosion during crustal shortening.

The MDC represents a rare exposed example of magma generation in the lower crust. The critical aspect for preservation was the presence of hydrous granitic magmas that froze as the Mt Daniel shear zone crossed the saturated granite solidus. Normally, more anhydrous magmas, possibly also hotter because of mafic input, would move out of the source region and lose the evidence for the incremental granite generation process by sheet/dyke focussing along active shear zones, assimilation and mixing.

The MDC rock types cover the compositional spectrum of the upper crustal SPB, including its sodic, HiSrY character. However, the MDS spectrum reflects mixing whereas the SPB reflects fractionation from relatively homogeneous parent magma. The evidence from the MDC suggests that HiSrY parental, intermediate-composition magmas are produced by large-scale bulk assimilation of the pre-existing lower crust, itself of sodic character, with more sodic dyke material mixed in. The blended magmas segregate and coalesce in upper crustal chambers, where virtually all evidence of the magma generation process is lost.

**TABLE OF CONTENTS**

**Chapter 3: Analytical Techniques**



**Chapter 4: Whole Rock Geochemistry of Mt Daniel Rock Groups**



**Chapter 5: Zircon Morphology and Microstructures of Mt Daniel Rock Groups from CL Images**

**Chapter 6: U-Th-Pb Geochronology of Zircons from Mt Daniel, Fiordland**



**Chapter 7: Electron Probe Microanalysis of zircon and Garnet from Mt Daniel Rocks, Fiordland**

**Chapter 9: Hf isotope geochemistry of Zircons from Mt Daniel, Fiordland**

**Chapter 10: Discussion**

**LIST OF FIGURES**

Chapter: 10

**LIST OF TABLES**

# Chapter 1: Introduction

## 1.1. Advancements in Granite Petrology

Most continental crust is composed of granitoid rocks, so their origin and petrogenesis is important for understanding crustal growth and continental evolution. Up to the 1950s, arguments still existed over whether granitoids were of magmatic or metamorphic origin, but the experimental work of Tuttle and Bowen (1958) demonstrated unequivocally, using experimental evidence, that granites were produced by partial melting of crustal rocks.

During the 1970s and 1980s, the major advance in granite petrology was the discovery that granites were produced from either sedimentary (S-type) or igneous (I-type) sources (Chappell and White, 1974). Based on mineral and chemical differences, they recognized S- (cordierite-bearing, peraluminous) and I-type (hornblende-bearing, metaluminous) granites. This implied that granites were derived from a single source, either metasedimentary (S-type), or metaigneous (I-type), without any input from external sources. From this interpretation, the restite model was developed (White et al., 1977). In other words, granites were considered to "image" their source rocks (White and Chappell, 1983; Chappell, 1984), which implies that granites were formed by closed system processes from specific source rocks (See Fig 1.1) The model predicts that the contrasting source rocks should have significantly different isotopic compositions.

However, with the introduction of whole rock isotopic analyses, it became possible to distinguish different source components (or reservoirs) for magmatic systems (e.g., DePaolo, 1981) and DePaolo suggested differentiation of basaltic magma with simultaneous crustal assimilation.

With the advent and application of whole-rock Sm-Nd isotopic analyses to granitic rocks in the early 1980s, especially when coupled with the Rb-Sr technique (DePaolo, 1981), it became apparent that many granites were mixtures of sources, usually considered to be crust and mantle. Different petrogenetic mixing models (two and three source components) were proposed to explain the chemical and isotopic diversity of Lachlan Fold belt granites of eastern Australia. The two component mixing model was based on the $\epsilon$Nd-Sr isotopic array (Gray 1984) and implies mixing of basaltic magma with variable proportion of melts derived from deeply buried Ordovician sedimentary rocks (See Fig 1.1.b). In this model, felsic melts produced from metasedimentary rocks mixed with high-Ca basalts to produce I-types, and similar melts mixed with low-Ca basalts to produce S-type granites. This model failed to explain the chemical variations across the plutons (e.g. Bega batholith) which have similar isotopic composition. The isotopic variations cannot explain the chemical variation based on inferred bulk composition of the source rocks. So, the bulk rock chemistry and isotopic variability can be better explained by the presence of another component. Thus a three component model was proposed by Keay et al (1997).

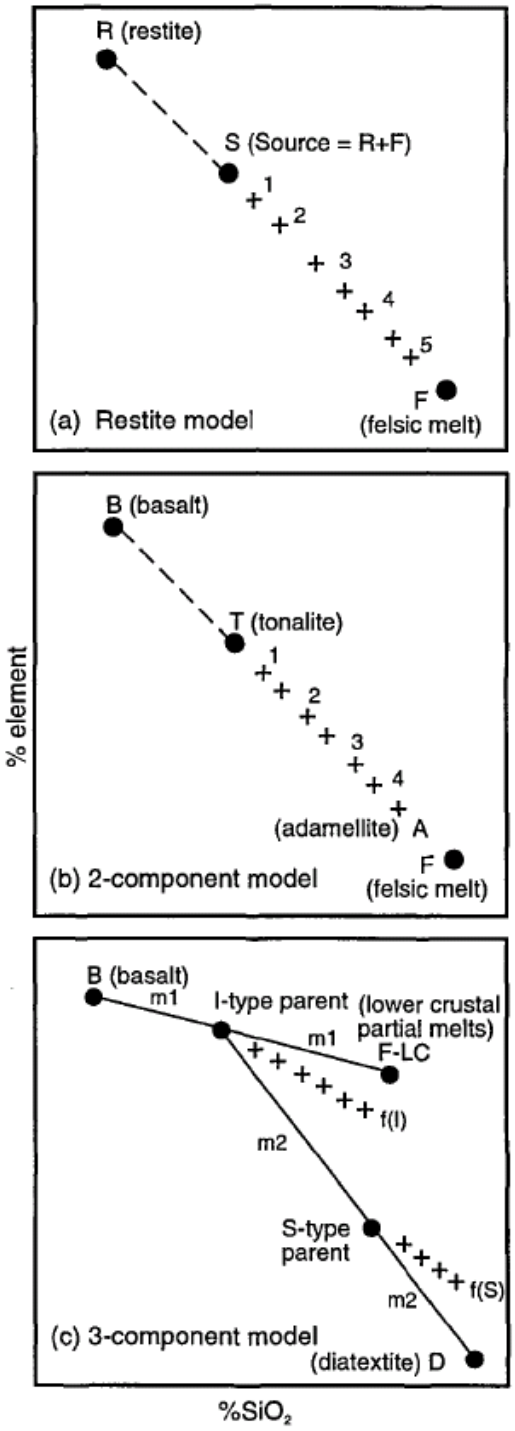


***Figure 1.1.*** *Chemical implications of three different models for the generation of granitic plutons at Lachlan fold belt, Eastern Australia (after Collins, 1998).* ***(a)*** *Restite (single source model);* ***(b)*** *Two component magma mixing model;* ***(c)*** *Three component magma mixing models.*

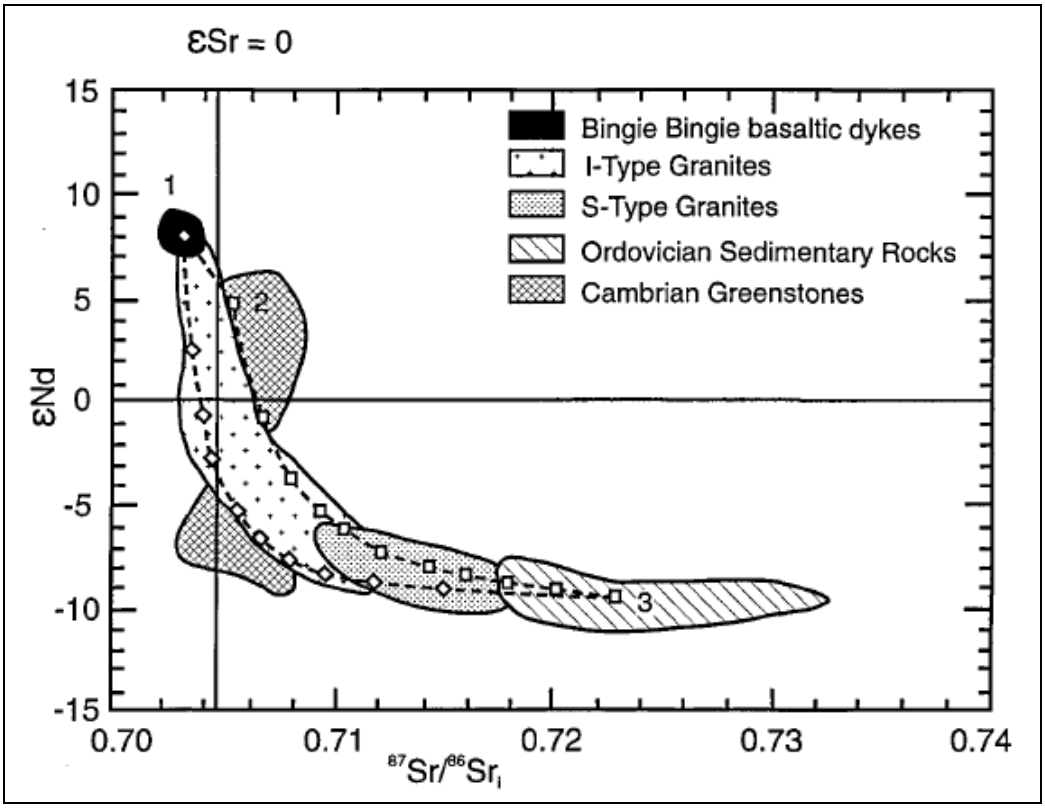


***Figure 1.2.*** *εNd and initial Sr isotopic array for three-component mixing model (after Collins, 1998). 1) Partial melts from the Cambrian greenstone; 2) The granitoids become progressively contaminated; 3) to generate the typical Lachlan Fold Belt granitoid.*

This model suggested that Lachlan I-type granite magmas are a mix between basaltic magma and a metaigneous crustal source believed to be Cambrian greenstones, and formed in the lower crust. These I-type magmas can be variably contaminated by Ordovician metasedimentary rocks to produce S-type granites. This model was supported by modeling of the chemical end-members (Fig 1.1.c.) and isotopic arrays (Fig 1.2.) (Collins, 1998). The different merits and demerits of these three different models in reference to the formation of the Lachlan granites are broadly discussed by Collins (1998).

Much of the petrological work on granites through the 1990s and in the early part of this century has reinforced a position of the presence of at least two source components in response to formation of granitic plutons. More recently, Kemp et al (2007), on the basis of Hf-O isotopic signature of

zircons from Lachlan Fold Belt granites, suggested they were formed by reworking of older crustal material with mafic mantle-derived magmas and not by the remelting of older metaigneous rocks. The two component model was re-emphasized by Gray and Kemp (2009) who proposed the granitic magmas were produced by partial melting of quartzo feldspathic metasedimentary rock mixing with variable amounts of basaltic magma dominantly derived from basalts. The derivation of granitic magmas from local metasedimentary rocks was identified by their similar geochemical signature of Sr, $Na_2O$ and $K_2O$. They suggested that the high-alumina basalt is a basic component in the petrogenesis of orogenic granitic rocks.

The idea of mixing of the magmas in different crustal level before emplacement to the upper crust to form plutons is widely applied in the development of petrogenesis of the Eastern Australian granites as discussed above, and for other batholiths around the world. For example, the Searchlight pluton, Eldorado Mountains, Nevada shows a nearly homogeneous magma composition across the pluton and suggested that the major part of the pluton probably have solidified in a monotonic fashion (Bachl et al, 2001, Miller et al., 1995). However the synplutonic hornblende gabbro and dioritic mafic pods are enclosed within the basal part (quartz-monzonite) and lower part of granite (in the centre of pluton) are isotopically distinct from the main-sequence magma. Distinct injection of these mafic pods into the magma chamber also support that they are not strongly contaminated by the main-sequence magma. Isotopically the main-sequence magma is of intermediate composition between the regional crust and mafic pods which bear enriched mantle like signature. So the Searchlight pluton is modeled to have formed in the lower crust from hybrid magma with ~60% mantle component, and emplaced as a high level pluton (Bachl et al, 2001, Miller et al., 1995). Barnes et al., (2002) suggested that crustal anatexis associated with emplacement of mafic plutons into the middle crust caused melting of the crust and transformation of migmatites to diatexite. The abundance of diatexite dykes in the contact zone is interpreted as the zone of contact migmatization which is caused by the heat of pluton emplacement. The hybridisation of mafic

magma with diatexites and high-K leucosome magmas are observed within the aureole and distinctive porphyritic contact granites are common at pluton contacts. Similarities in mineralogy of the contact granites with the diatexites but their isotopically distinct characters and mass balance calculations suggest that the mixing of high-K leucosomes with dioritic magmas are more consistent with the granite formation. Partial melting, magma accumulation, hybridisation and melt transport to the upper crust are the main mechanism to form granitic plutons at the Bindal batholith, Norway. This 'crustal intraplating' may be a general mechanism to explain formation of many hybrid 'anatectic' granites (cf., Elburg and Nicholls, 1995).

Several experimental approaches were made in order to understand the generation of granitic magma. With few exceptions, experiments were based on a low-K basaltic starting material, giving an end-result with high $Na_2O/K_2O$ which is unlike common granites and rhyolites. However, low-K sources might help to understand the formation of low-K intermediate to silicic rocks like Archean TTG (Winther and Newton, 1991; Rapp et al., 1991) or provide an understanding of the fate of low-K subducted oceanic crust (Sen and Dunn 1994).

A recent experimental study by Sisson at al. (2005) points towards the basic question of how the silicic rocks formed? Their approach was to produce high-K common granitic or rhyolitic magma by the partial melting of medium to high-K, moderately hydrous (1.7-2.3 wt %) arc-derived basalts at 700 MPa, with $fO_2$ controlled in the range of Ni-NiO -1.3 to +4. This source successfully produced melts matching true granite or rhyolite compositions. Ratajeski et al. (2005) also showed from experimental and geochemical evidence that generation of the El Captain Granite of the Sierra Nevada batholith, California, can be produced by partial melting of mafic magma similar to coeval mafic intrusions in the area. Such granitic melts formed in this way may also act as the silicic end member composition of the mixing system that formed the large volume plutons of the Sierra Nevada batholith.

To assess the mixing process in detail, different microanalytical approaches have been developed to characterize mineral zoning patterns using trace element and isotopic compositions of minerals such as plagioclase, zircon, apatite, rutile, monazite, and xenotime. Wark and Miller (1993) suggested that the compositional and textural characteristics of the accessory minerals such as zircon, xenotime and monazite control the trace element geochemistry of granitic partial melts, and record the minute compositional changes in the magma during differentiation.

Davidson et al. (1999) analysed plagioclase phenocrysts having variable $^{87}Sr/^{86}Sr$ isotopic ratios and recorded significant changes associated with mixing and mingling processes in silicic lava domes from Chaos Crags, Lassen volcanic centre, California. This approach, in combination with disequilibrium textural features of phenocrysts, known eruption frequencies in volcanoes, and inferred crystal residence times of plagioclase, are taken to indicate that magma chamber are commonly intermittently replenished (Davidson et al., 2000).

Another microanalytical approach to granite petrogenesis is through the study of zircons. Zircons have geochemical and isotopic information that allows the magmatic evolution of plutonic systems to be tracked because they are abundant in granitic rocks, robust in nature, acquire growth zones during crustal melting events, record thermal episodes and tend to preserve the isotopic record at the time of crystallization. Zircon is an isotopic reservoir of U-Pb, Lu-Hf and O.

U-Pb allows individual zones within zircons to be precisely dated. Hf mainly accumulates in the continental crust during crust formation and thus results in unradiogenic and radiogenic Hf isotopic ratios in crust and depleted mantle respectively (Patchett et al., 1981). Thus Lu-Hf isotopic system is used as an isotopic tracer used to understand the generation of silicic magma and an excellent tool to track the petrogenetic history of the rocks, nature of the source from which they derived (e.g. depleted mantle, mafic crust or older continental crust) and give a detail insight into the crust-mantle process during formation of the rocks.

How mixing occurs in granitic magmas and contribution of isotopically different sources in formation of granites using Hf isotopes is described by Kemp et al., (2007). An important feature of Hf isotope data is the wide range of ϵHf values exhibited by zircons of the same rock (up to 10 ϵ units) (epsilon notation signifies deviation of the isotope ratio from a chondritic reference in parts per ten thousand) (Fig 1.3.).

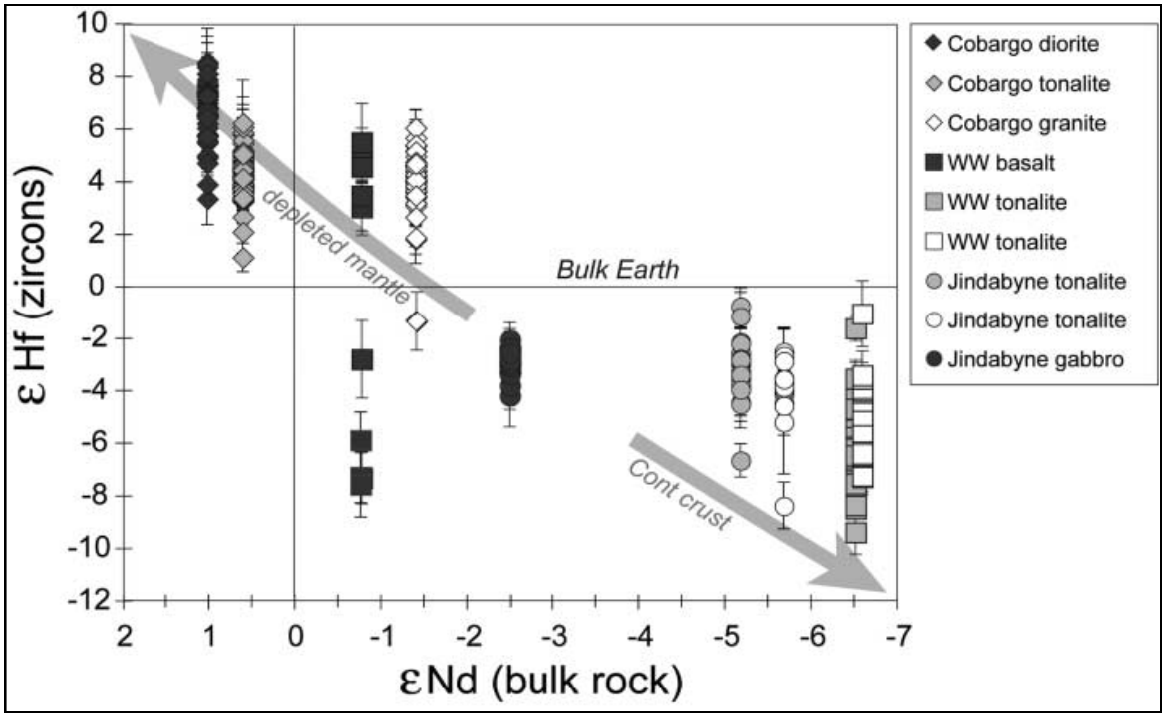


***Figure 1.3.*** *The Hf isotope composition of melt-precipitated zircons from samples of each suite as a function of whole-rock Nd isotope composition at the time of crystallization (WW, Why Worry) showing variable crust-mantle mixing. Error bars represent 2 SEM (after Kemp et al., 2007).*

This wide variation within a single sample can only be possible if an open magmatic system was operating (e.g. mixing). Open system processes are capable of shifting the $^{176}Hf/^{177}Hf$ ratio of the melt from which zircon precipitated. Hf isotope changes within the zircons can be coupled with trace element data to identify the open system process.

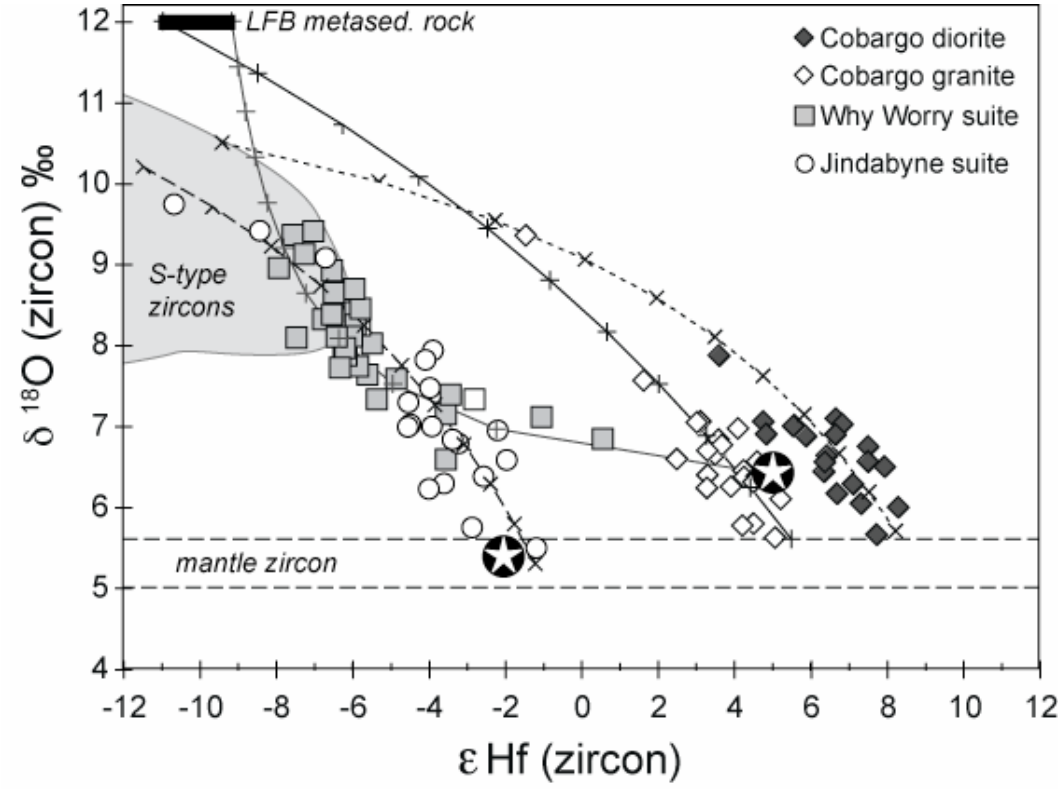


***Figure 1.4.*** *εHf versus $\delta^{18}O$ for zircons of three I-type granite suites of eastern Australia (ε Hf is the departure of the measured $^{176}Hf/^{177}Hf$ from that of chondrites (average Earth) in parts per ten thousand). The star symbols show the composition of igneous mantle-derived mafic rocks associated with the Why Worry and Jyndabyne Suites, which are inferred to be parental magmas to the granites. The $\delta^{18}O$ of zircons in equilibrium with mantle melts is shown by the dashed field; higher $\delta^{18}O$ values in zircon diagnose the recycling of sedimentary material. The ultimate mantle heritage is only retained by the earliest-crystallizing zircons of each suite. All data are presented from Kemp et al., (2007).*

Hf isotopes coupled with O isotopes provides an important tool to understand the mixing process more precisely and can determine the contribution of different source components. Kemp et al., (2007) identified the process of formation of three I-type Lachlan granite suites with the help of Hf-O isotope study of zircons. Their model defines four curves from the isotopic arrays (Fig 1.4.). For each suite ε Hf and $\delta^{18}O$ are correlated with zircons. Each curve has an elevated $\delta^{18}O$ and low $\delta^{18}O$ end-member value corresponding to the isotopic composition of the end-member source

components. The data reveal that these granites formed from low $\delta^{18}O$ magmas with high εHf, similar to igneous rocks directly derived from the mantle. Furthermore, the projection back toward "S-type zircons" for each I-type suite shows that the magma has been progressively contaminated by sedimentary material. Thus the curves indicate the interaction between two end member components during zircon crystallization, respectively parental magma and metasedimentary materials.

In addition, crystallisation thermometers for zircon and rutile have been devised by Watson et al. (2005), which will help to reveal the temperature of crystallisation of zircon cores and rims.

## 1.2. The Mount Daniel Complex as a window into lower crustal melting processes

All the above scenarios reflect upper to middle crustal processes as recorded in high-level plutons and volcanic rocks, recording the final product of the entire petrogenetic process. However the basic questions about how and where granitic magmas form remain unanswered. Are granitic plutons simply an upper crustal phenomena, resulting from assembly of melt increments from the lower crust (e.g., Wiebe and Collins, 1998; Coleman et al., 2004)? Are those melt increments mixed in the lower crust (e.g., Hildreth and Moorbath, 1988), or does that mixing occur in upper crustal reservoirs where mafic and silicic magmas possibly interact (e.g., Davidson et al., 2000)?

In an attempt to answer these questions, rare exposures of lower crust arc rocks from Fiordland, on the South Island of New Zealand, were examined. There, the base of the crust is exposed in a continental margin arc setting, which was metamorphosed to granulite facies conditions (Bradshaw 1985, Mattinson et al., 1986). These rocks include the ~120 Ma Western Fiordland Orthogneiss (WFO), which was considered by Muir et al. (1995, 1998) to be the deep crustal equivalent of the upper crustal ~120 Ma Separation Point Batholith, located several hundred km farther north. Based on metamorphic studies the WFO is known to have been emplaced at ~8-12 kbar (Clarke et al.,

2000; Daczko et al., 2001, 2002a), i.e. in the lower crust. The base of the WFO batholith is exposed at Mt Daniel in northern Fiordland (e.g., Hollis et al., 2004, Daczko et al, 2002), so it is here that the study is focused.

As discussed in detail below in chapter 2, the lower WFO contact on Mount Daniel comprises an intrusive, sheeted complex of mafic, intermediate and felsic dykes, known as the Mount Daniel Complex (MDC). It is underlain by Paleozoic to Early Cretaceous granulite facies rocks of the Arthur River Complex (ARC). This study focuses on the origin of the dykes and sheets of the MDC. Close examination of each melt increment, from mafic to felsic, and processes involved in the formation of MDC are determined using zircon trace element and isotopic studies. This study also helps to determine to what extent homogeneous upper crustal magma chambers reflect their end-member source components.

The geochemical and tectonic contexts of the MDC relative to the plutonic systems in New Zealand and within the circumPacific batholithic systems in general are described below and in Chapter-2 respectively.

## 1.3. Whole-Rock Geochemical Variation of Different Suites from Fiordland

The major granitoid suites present in Fiordland are the Western Fiordland Orthogneiss (WFO) and Arthur River complex (ARC). The Separation Point batholith (SPB) from further north is added to evaluate the assertion by Muir et al (1995) that it is an upper crustal equivalent of the WFO. The SPB and WFO data other than from MDC are provided by Allibone et al., (2009) and ARC data is the repository from Hollis et al., (2003). Whole rock XRF analyses of MDC samples were undertaken at the University of Newcastle, as were most trace element analyses. REE, Th, U and Nb analyses of MDC samples were done by ICPMS at James Cook University. Wholerock Sm-Nd and Rb-Sr isotopic ratios of MDC samples were analysed at the University of Adelaide.

**Major Element Geochemical Variation of Fiordland Rock Groups**

The ARC and MDC follow a single trend of steadily increasing $K_2O$ with increasing $SiO_2$ whereas the WFO has a much steeper trend on $K_2O$ variation diagrams (Fig 1.5.a.). The SPB show nearly constant $K_2O$ (0.4-3.1 wt %) with varying $SiO_2$ (53-71 wt %) (Fig 1.5.a.).

The MDC, ARC and SPB show a nearly coherent trend for $Na_2O$ and $Al_2O_3$ plot, but the MDC shows a comparatively higher $Na_2O$ (2.4-8.6 wt%) and $Al_2O_3$ content (12.6-22.7 wt%) (Fig 1.5.b and c). The SPB shows a nearly constant $Na_2O$ (5.16-6.52 wt%) and increasing $Al_2O_3$ (14.9-21.8 wt%) with varying $SiO_2$ content (53-71 wt %). In ARC rocks, $Na_2O$ increases with increasing silica content and $Al_2O_3$ content (15.2-20.4 wt%) is nearly constant. The WFO follows a trend that is similar to the ARC, with slightly lower $Na_2O$ and $Al_2O_3$ relative to SPB and MDC.

CaO decreases with increasing $SiO_2$ content and all rock groups from Fiordland formed a coherent curvilinear trend in CaO variation (Fig 1.5.d.). MgO, $TiO_2$ and $P_2O_5$ also decrease with increasing $SiO_2$ content (Fig 1.5.e, g, h). The ARC, MDC and SPB show a single coherent trend, but the ARC has very little correlation between MgO-$SiO_2$ (Fig 1.5.e.). $FeO_{total}$ shows a nearly coherent trend in the four suites but SPB and some MDC rocks have low $FeO_{total}$ (Fig 1.5.f.).

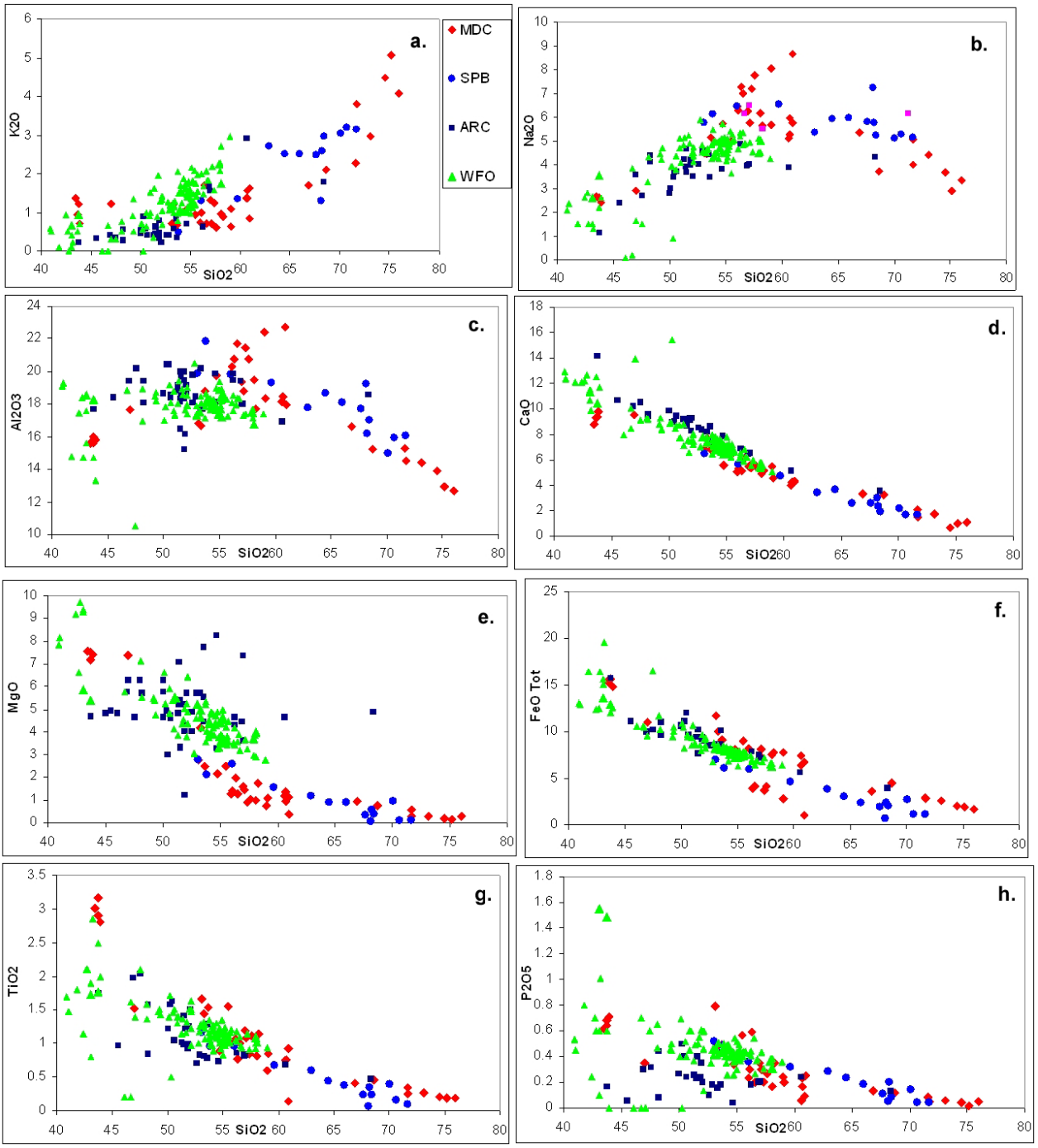


***Figure 1.5.*** *Major Element Harker diagrams of different rock groups of Fiordland.* ***(a)*** *$SiO_2$-$K_2O$;* ***(b)*** *$SiO_2$-$Na_2O$;* ***(c)*** *$SiO_2$-$Al_2O_3$,;* ***(d)*** *$SiO_2$-CaO;* ***(e)*** *$SiO_2$-MgO;* ***(f)*** *$SiO_2$-$Fe_2O_3$,;* ***(g)*** *$SiO_2$- $TiO_2$ and* ***(h)*** *$SiO_2$-$P_2O_5$.*

## Trace Element Geochemical Variation of Fiordland Rock Groups

Ba and Rb increases with increasing silica content for all rock groups (Fig 1.6.a and b). ARC and intermediate groups of the MDC have nearly coherent trends in the Ba and Rb plots but MDC and SPB mostly have some scattered values with higher concentrations of Rb and Ba (Fig 1.6.a and b). Sr decreases with increasing silica content mainly for the SPB and some of the MDC samples. ARC and WFO have a constant Sr content (Fig 1.6.c.).

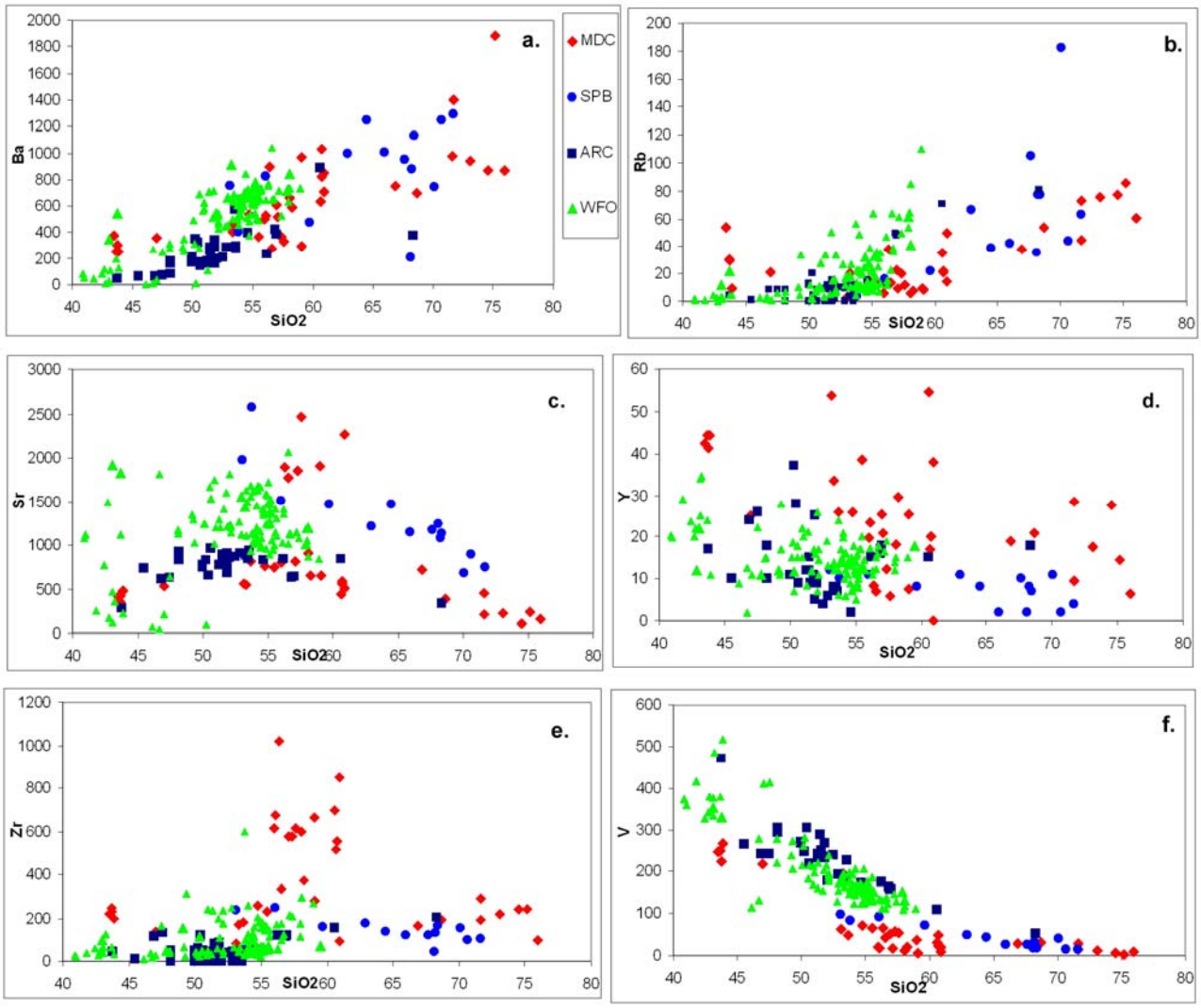


***Figure 1.6.*** *Trace element Harker diagrams of different rock groups of Fiordland.* ***(a)*** *$SiO_2$-Ba;* ***(b)*** *$SiO_2$-Rb;* ***(c)*** *$SiO_2$-Sr;* ***(d)*** *$SiO_2$-Y;* ***(e)*** *$SiO_2$-Zr;* ***(f)*** *$SiO_2$-V.*

The WFO typically has relatively high concentrations of Ba and Rb. Sr is also high in the WFO, and is matched only by the SPB trend.

Y does not show any systematic changes with the silica variation (Fig 1.6.d.), although the SPB is generally lowest, with most values <10ppm. MDC and SPB have some higher Sr and lower Y contents (Fig 1.6.d.). The MDC has some samples with the highest Zr content, the ARC has the lowest Zr contents and other samples of the MDC and SPB have nearly constant Zr content with varying silica (Fig 1.6.e.).

V decreases with increasing silica content (Fig 1.6.f.). Some of the MDC and SPB samples have low V contents (Fig 1.6.f.).

In summary, all the Fiordland rocks are relatively sodic, with high contents of elements that follow feldspar (Na, Al, Ba and Sr). The ARC basement rocks follow a trend similar to the mafic and intermediate rocks of the MDC rocks, between $SiO_2$ 48-53 wt %. The MDC rocks, ARC and SPB in most of cases follow a single trend and SPB rocks fit into the gap between the felsic and intermediate rock groups of MDC. MDC covers the whole range of chemical variation present in other two suites (ARC and SPB) but some rocks of the MDC also show a comparatively higher $Na_2O$, $Al_2O_3$, Sr, Zr and low Y content. These trends show that the rock groups of Fiordland may be genetically related or inter-linked by different magmatic processes, which will be evaluated in the later chapters.

## 1.4. Comparison of Whole Rock Geochemistry with other Circum Pacific Batholiths

A comparison of the geochemical composition of different batholithic bodies around the world, all related to circumPacific subduction zone magmatism, provides a broader tectonic context for the MDC rocks. The data from different batholiths used in this study are Mesozoic batholiths of Sierra Nevada (SN) and Peninsula Ranges (PR) of the North American cordillera, the Mesozoic Coastal batholith of Peru (PC), the Paleozoic Bega-I type and Berridale-I type batholiths of the Lachlan fold belt from Eastern Australian, as well as the ~120 Ma Separation Point batholith (SPB). The North and South American data was provided by Dr. AIS Kemp, and data from the batholiths of the Lachlan fold belt were provided by Prof. WJ Collins.

**Comparison of Major and Trace Element Chemistry of Different Batholiths**

All the data from different granitic batholiths formed a coherent geochemical array in Harker variation diagrams with only some scattered data from SN and PR batholiths (Fig 1.7.). The data range from $SiO_2$ ~50-78 wt%. Despite its small size (~100 m thick sheeted complex), the MDC shows a similar $SiO_2$ ~50-76 wt% variation with other batholiths, but with a greater concentration of samples with intermediate compositions (50-60% $SiO_2$). The mafic groups of the MDC extend the silica range to 43% $SiO_2$, lower than any other sample from the circumPacific batholiths.

$K_2O$ (Fig 1.7.a.) is the only major oxide that increases with $SiO_2$ and most of the data is clustered around 0.2-5.40 wt%. The MDC rocks have the lowest concentration of $K_2O$ compared to other batholiths, although a distinctly low $K_2O$ group exists in the PRB, which is the La Posta Suite (Tulloch and Kimbrough 2003). The $Na_2O$ content of the MDC is distinctly different to all batholiths except the SPB (Fig 1.7.b.). Not only does the MDC have the highest values of all represented circumPacific batholiths, typically 5-9 wt % $Na_2O$ at intermediate silica compositions (50-60% $SiO_2$), but $Na_2O$ content varies inversely with $SiO_2$ from 56-76 wt% silica. Thus, the high silica samples plot in the main field for other batholiths. Only the SPB has comparable $Na_2O$ values

at intermediate compositions, but the $Na_2O$ content remains high (~5 wt%) at high silica contents. The PRB (>70 wt% $SiO_2$) has some high $Na_2O$ content.

$Al_2O_3$ (Fig 1.7.c.) increases (~12-22 wt %) with decreasing silica for all the batholiths. The MDC rocks and SPB have comparatively higher $Al_2O_3$ content than other batholiths and the MDC has the highest $Al_2O_3$ content (up to 28 wt %). The SN and PR batholiths also plot on the higher side of the main $Al_2O_3$ cluster.

The variation diagrams for CaO (Fig 1.7.d.), MgO (Fig 1.7.e.), $Fe_2O_3$ (Fig 1.7.f.), $TiO_2$ (Fig 1.7.g.) and $P_2O_5$ (Fig 1.7.h.) show progressive decreases with increasing $SiO_2$ content. The MDC rocks and the SPB show lower contents of CaO and MgO for similar silica contents compared to the other batholiths. The $P_2O_5$ content of the MDC is very similar to other rock types, but intermediate dykes and rocks have quite scattered values (Fig 1.7.a, e, g and h.).

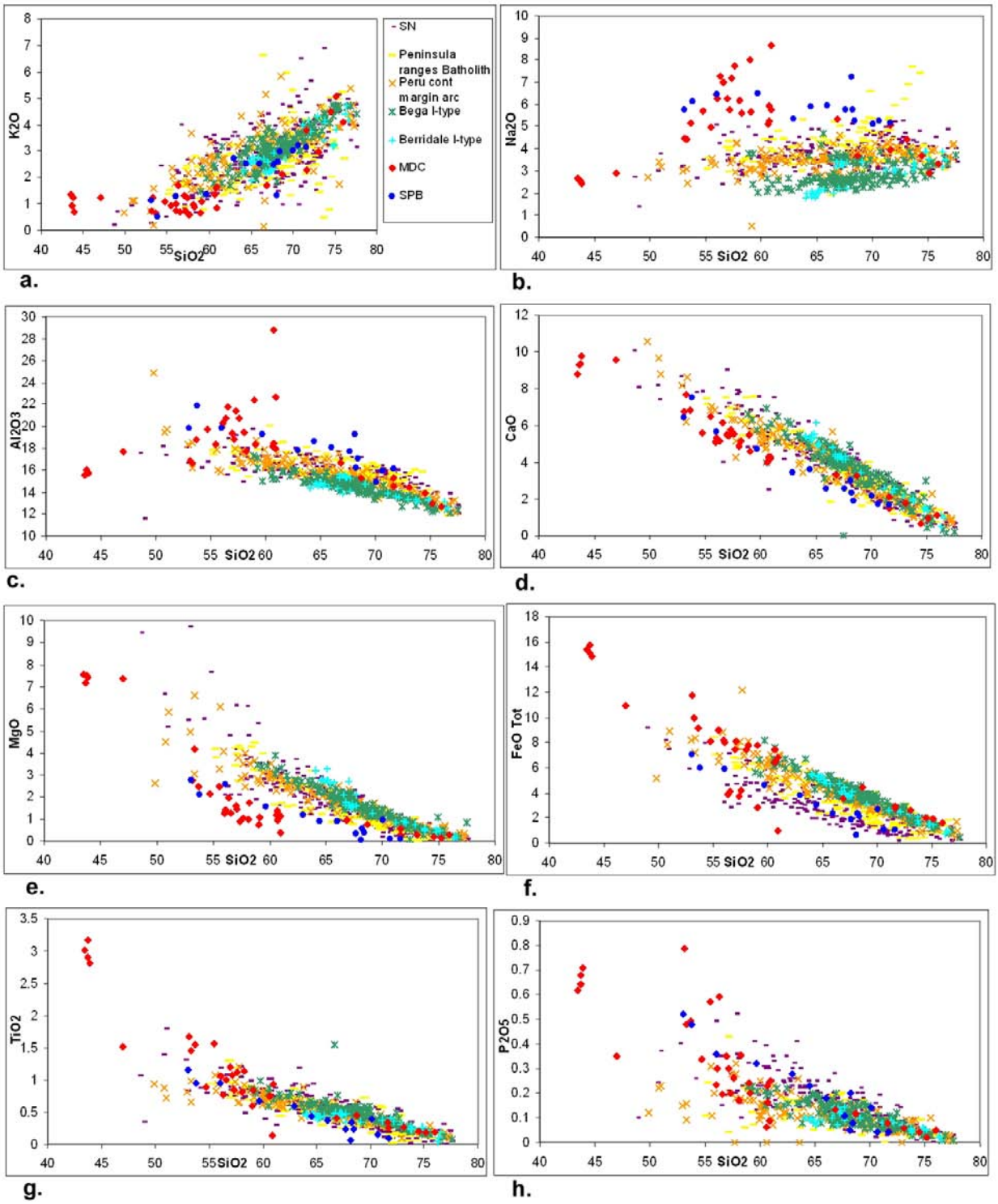


***Figure 1.7.*** *Major element Harker diagrams of different batholiths* ***(a)*** *$SiO_2$-$K_2O$;* ***(b)*** *$SiO_2$-$Na_2O$;* ***(c)*** *$SiO_2$-$Al_2O_3$;,* ***(d)*** *$SiO_2$-CaO;* ***(e)*** *$SiO_2$-MgO;* ***(f)*** *$SiO_2$-$Fe_2O_3$;,* ***(g)*** *$SiO_2$- $TiO_2$ and* ***(h)*** *$SiO_2$-$P_2O_5$.*

Trace element data obtained from the Separation Point, Bega and Berridale I-type batholiths are compared with the MDC rocks. The data are obtained from the same sources mentioned earlier.

Ba generally increases with $SiO_2$ in MDC and SPB (Fig 1.8.a.). Other batholiths have nearly constant Ba content with variable silica content. In general, Rb increases with increasing silica content (Fig 1.8.b.) but MDC rocks and the SPB have lower contents of Rb compare to other batholiths for similar silica contents. SPB and some MDC samples have higher Sr contents compare to Lachlan Fold Belt batholiths (Fig 1.8.c.).

Y does not show any systematic changes with the silica variation and the data are mostly scattered (Fig 1.8.d.). The SPB and some MDC samples have the lowest Y contents (~2-18 ppm). The Zr content is nearly constant for different batholiths except some of the MDC samples have very high Zr content upto 1000ppm (Fig 1.8.e.).

V varies inversely with $SiO_2$ content. V increases sharply (~3-183 ppm) in the Bega and Berridale batholith with decreasing silica and has comparatively much higher contents than the MDC and SPB (~8-97 ppm) (Fig 1.8.f.).

The lower Rb content of MDC rocks compared to other batholiths is clearly observed in the Rb-Ba-Sr triangular plot (Fig 1.9.). The Lachlan fold belt granites show increasing Rb at the expense of Ba in the Rb-Sr-Ba plot (Fig 1.9.) whereas MDC samples show a flat trend along the Sr-Ba line, reflecting very low Rb contents, even when $K_2O$ is >3 wt%.

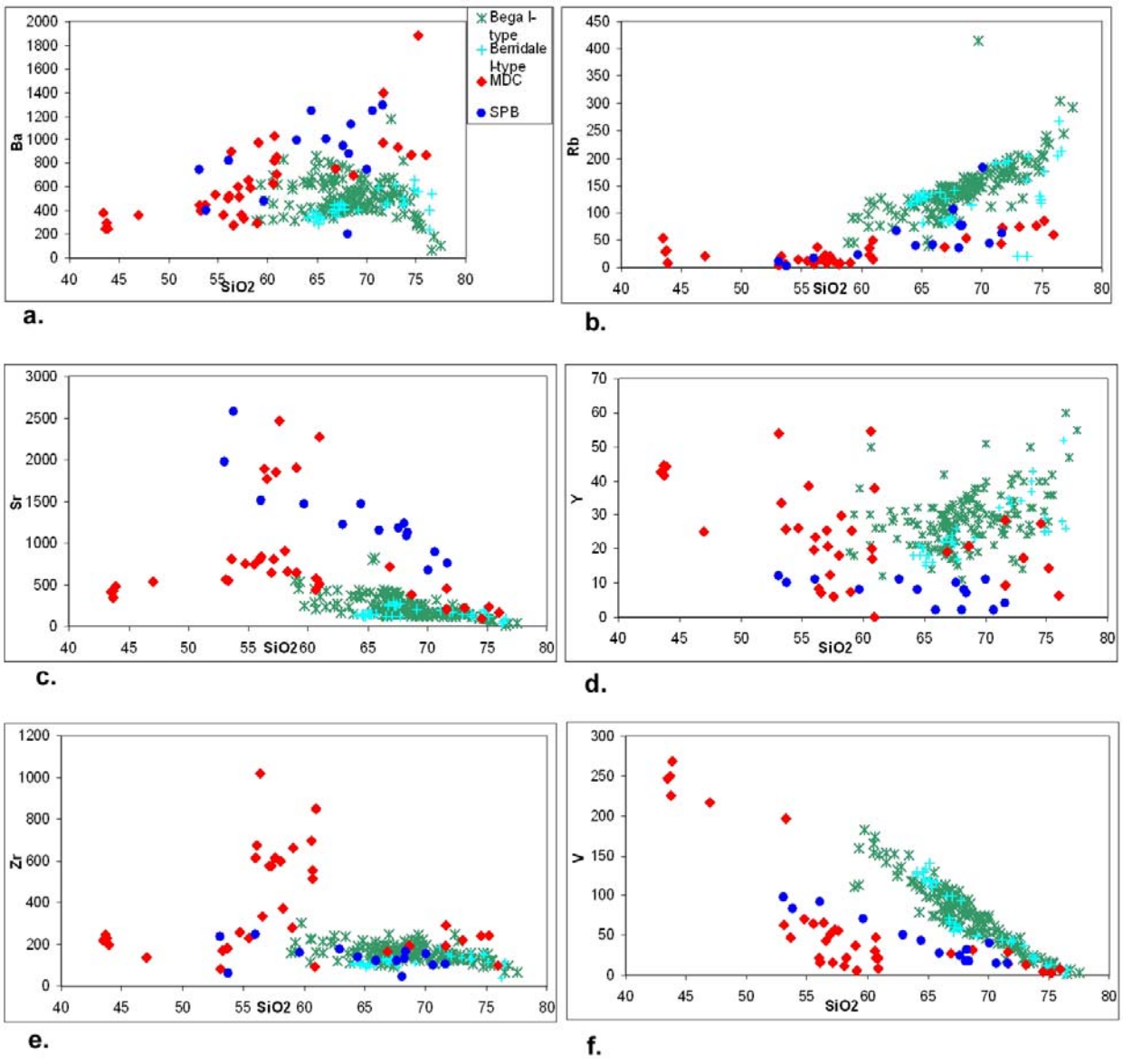


***Figure 1.8.*** *Trace element Harker diagrams of different batholiths.* ***(a)*** *$SiO_2$-Ba;* ***(b)*** *$SiO_2$-Rb;* ***(c)*** *$SiO_2$-Sr;* ***(d)*** *$SiO_2$-Y;* ***(e)*** *$SiO_2$-Zr;* ***(f)*** *$SiO_2$-V.*

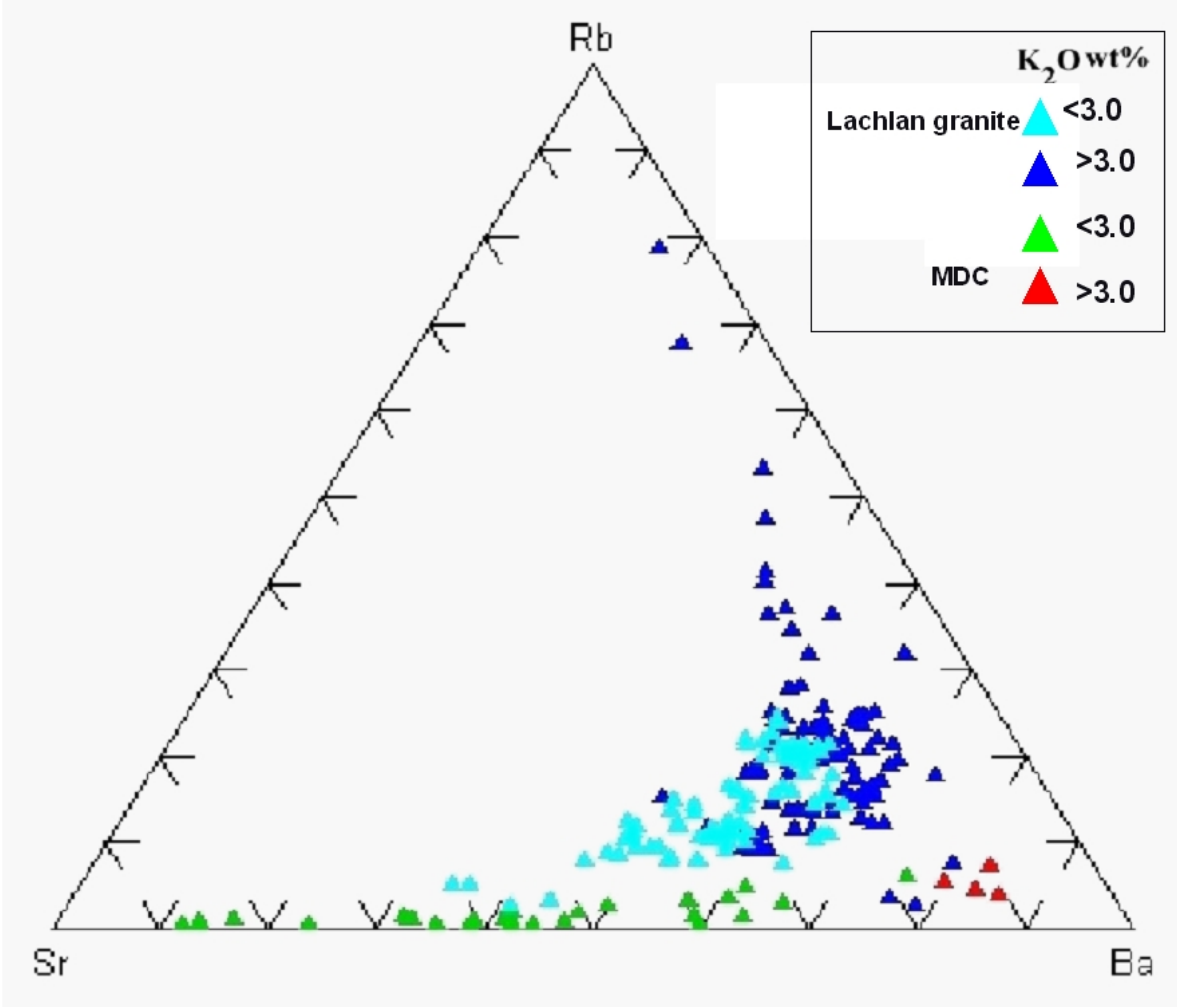


***Figure 1.9.*** *Sr-Rb-Ba triangular plot shows different trend of Lachlan fold belt granites and Mt Daniel Complex rocks.*

## 1.5. Summary and Thesis Context

The granitic rocks from Fiordland are distinctive compared to other granitic CircumPacific batholiths. They are unusually sodic ($Na_2O$ ~ up to 8.6 wt % in MDC), have higher Sr, Ba and variable but high Zr at low silica values. They also have slightly higher $Al_2O_3$, $FeO_{total}$ and $TiO_2$, but distinctly lower MgO and CaO, Rb and V. This suggests that the Fiordland rocks formed from sources that were different, or were produced under different melting conditions, compared to other circumPacific batholiths.

The Fordland granites have been described as HiSY types by Tulloch and Kimbrough (2003).

HiSY granitoids are high in Sr/Y >40 and low in Y content. The high Sr/Y field has been previously termed “adakitic” (Defant and Drummond 1990), though we prefer not to use this term as it has too many petrogenetic connotations, not the least being that adakites form by slab melting. We will use the term “trondhjemitic” to describe these HiSY granitoids, because they are also very sodic.

Therefore, the study of the MDC, from the lower crust of Fiordland, New Zealand, is one where the petrogenesis of HiSY or trondhjemitic magmas can be ascertained by field and geochemical studies. Not only does it become immediately obvious that these sodic granitic rocks were produced by melting of deeply buried arc crust, as discussed by many authors (see Chapter 2), but the opportunity exists to examine in minute detail the petrogenetic processes involved in the generation of a diverse range of rock types in a small “controlled” geological environment. The range of rock types in the MDC also allows the interrelations of such a diverse group to be studied intimately. Moreover, the overall similarity of the MDC with the upper crustal HiSY granites of the SPB means that the observations in the deep crust provide a framework for understanding the partial melting and melt assembly mechanism before transfer of these unusual sodic magmas toward the Earth’s surface, where they accumulate in the upper crust.

These possibilities are addressed in step by step processes, beginning with field observations and a tectonic overview, followed by an analysis of the whole rock geochemistry, then a microanalytical approach to understanding the trace element and isotopic variation in zircons from each rock group. Finally, the results can then be applied to the origin of other batholiths at convergent margins around the world.

# Chapter 2: Regional Geology of Fiordland and Field Relations at Mt Daniel

## 2.1. Regional Geology of Fiordland, New-Zealand

New Zealand represents a wide variety of Cambrian to Early Cretaceous rocks that preserve a record of Gondwana convergent margin activity. The basement rocks of New-Zealand can be described in terms of three major provinces which incorporate a number of tectonostratigraphic terranes (e.g., Mortimer, 2003). This chapter will briefly describe the regional geology to provide a setting for the Mt Daniel Complex.

The South Island of New Zealand is divided into three parts (Fig 2.1.) (Landis and Coombs, 1967; Kimbrough et al., 1993 and 1994; Mortimer et al., 1999).

1. The Eastern Province,
2. The Median Tectonic Zone (MTZ) or Median batholith and
3. The Western Province

The boundaries between the provinces are largely fault controlled but stitching plutons show that amalgamation of the Eastern Province with the MTZ occurred by the late Triassic (William and Harper, 1978) and the MTZ with the Western Province by the Early Cretaceous (Hollis et al, 2003) periods. All three terranes have been disrupted and displaced by 480 km along the Tertiary Alpine Fault (e.g., Klepeis et al, 2003).

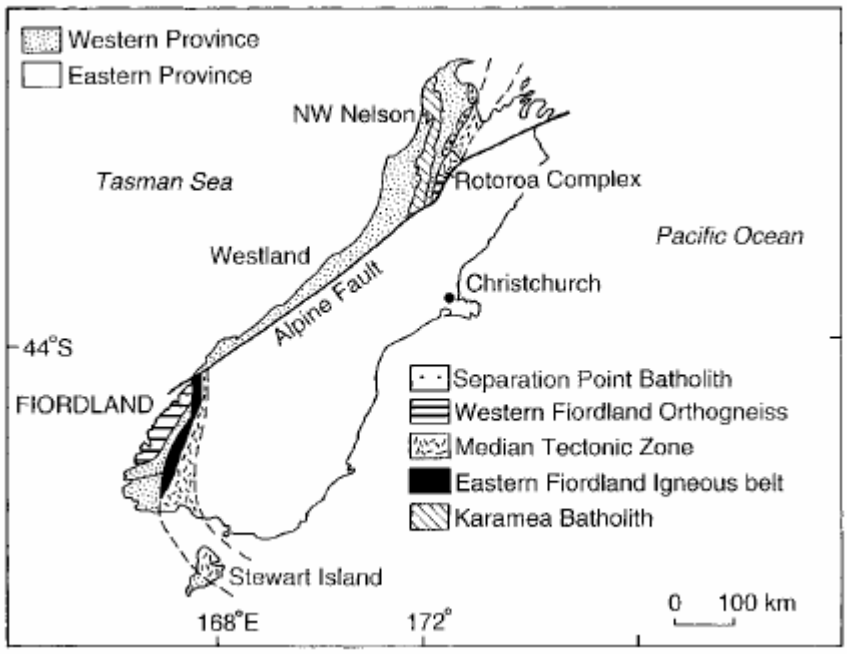


***Figure 2.1.*** Geological map of the South Island, New-Zealand showing Eastern and Western provinces and the Median Tectonic Zone (after Muir et al., 1998). The Eastern Fiordland igneous belt (terms modified from Oliver and Coggan 1979) forms part of the MTZ.

**1.** The Eastern Province comprises dominantly turbiditic, volcanic and volcanoclastic sedimentary rocks of Permian to Early Cretaceous time. These are dominated by the greenschist facies metasedimentary rocks of the Torlesse Supergroup, Caples Group and Haast Schist. Permo-Triassic predominantly volcanoclastic rocks including the Maitai, Murihiku and Brook St Terranes are present in the south and west of the Eastern province (Kimbrough et al., 1992).

**2.** The MTZ is a narrow (10-35 km) corridor comprising plutonic, volcanic and sedimentary rocks associated with subduction-related activity. The zone is thought to be a part of a remnant magmatic arc system developed along the Pacific Gondwana margin (Storey et al., 1992). Two distinct phases of magmatic activity occurred at 345-195 Ma and 168-137 Ma (Bradshaw, 1993; Kimbrough et al., 1993, 1994; Muir et al., 1998).

The major magmatic events are recognized by the emplacement of different plutons. The MTZ includes the Darren complex which is in fault contact on its western side with the Arthur River Complex (ARC) in Northern Fiordland and composed of mainly weakly metamorphosed, shallower-level gabbroic to dioritic rocks of 141-137 Ma age (Blattner 1978; Mattinson et al., 1986; Kimbrough et al 1994; Muir et al., 1998; Wandres et al 1998; Clarke et al, 2000; Nathan et al., 2000).

**3.** The Western Province is divided into two segments: the upper crustal Nelson/Westland and the lower crustal Fiordland regions, once contiguous and displaced by the Alpine fault (Klepeis et al., 2003). The Western Province comprises Lower Palaeozoic metasediments and Palaeozoic and Mesozoic orthogneisses representing the low grade rocks in upper and amphibolite to granulite facies rocks in lower sections respectively of continental Mesozoic Gondwana crust (Hollis et al., 2004).

The Western Province suffered two major magmatic and metamorphic events during the Mid Paleozoic Tuhua Orogeny (380-330 Ma). During 380-360 Ma significant calc-alkaline plutonism resulted in the emplacement of several plutons in this region. Voluminous pluton emplacement occurred in the Karamea Batholith in the Westland region during this time (Muir et al., 1994, 1996; Ireland and Gibson, 1998; Gibson and Ireland, 1999). High-T, low-P metamorphism of the metasedimentary rocks in both Fiordland and Westland region occurred during this orogeny (Gibson et al., 1988; Gibson, 1992; Ireland and Gibson 1998) followed by high-P metamorphism in Fiordland at 330Ma (Ireland and Gibson 1998).

Other major plutons were emplaced during the Cretaceous, including the ARC (Arthur River Complex, age discussed below), WFO (Western Fiordland Orthogneiss) (126-116 Ma, Mattinson et al., 1986; Muir et al., 1998; Tulloch and Kimbrough 2003; Hollis et al., 2004) and SPB (Separation Point Batholith, 126-105 Ma, Muir et al, 1995, 1998, Tulloch and Kimbrough 2003).

The ARC is discussed in detail in this section and a comparative study between the WFO and the SPB is discussed in section 2.2.

## 2.2. Geological and Geochronological Setting of Fiordland

Fiordland, the study area, is situated in the Western Province. Fiordland mainly comprise mid to lower crustal rocks (>25 km depth) (Bradshaw 1989, Clarke et al., 2000) and can be subdivided into 3 distinct geological regions (Oliver and Loggan, 1979; Bradshaw, 1985) (Fig 2.2.).These regions/belts are separated by major faults and have different tectono-metamorphic histories.

1. The Western Fiordland Belt
2. The Eastern Fiordland Belt
3. The South West Fiordland Block

**1. The Western Fiordland Belt** is a deep crustal level metamorphic core complex (Gibson et al.1988; Gibson 1990; Gibson and Ireland 1995) in which Early Cretaceous granulite facies rocks are structurally overlain by Paleozoic amphibolite facies metasedimentary and meta-plutonic rocks.

### Arthur River Complex (ARC)

The rock types and structure of the ARC are heterogeneous (Clark et al., 2000). The ARC consists of garnet-hornblende bearing mafic gabbroic gneiss named the Milford Gneiss, banded dioritic gneiss termed the Harrison Gneiss and lesser migmatite and ultramafic rocks. The Pembroke Granulite is a part of the Milford Gneiss and is composed of two-pyroxene-hornblende-bearing gabbroic and dioritic gneisses.

The emplacement age of ARC is debatable. Hollis et al., (2003) suggested that the diorite to gabbroic protoliths of the ARC were emplaced between 136-129 Ma, whereas Tulloch et al. (2000, 2010) suggested a Paleozoic age of emplacement, followed by granulite facies metamorphism in the Cretaceous. The ARC in Northern Fiordland thought to represent the final stages magmatism of MTZ shortly after the amalgamation of the MTZ and the Western Province and prior to the

emplacement of WFO during 126-119 Ma (Bradshaw, 1985, 1989b; Mattinson et al., 1986; McCulloch et al., 1987; Hollis et al., 2003). Tulloch et al., (2000, 2010) found prismatic zircons with oscillatory zoning of Paleozoic (357 Ma) age and ovoid with sector or patchy zoned zircons of Cretaceous age (133 Ma). Both of the ages are overgrown by younger Cretaceous (120 Ma) metamorphic zircons. Tulloch et al., (2010) interpreted the morphology to mean that the initial emplacement and crystallization of ARC pluton happened at ~357 Ma followed by the granulite facies metamorphism at around 134 Ma. The ARC suffered at least four deformational/metamorphic events (Clarke et al., 2000; Daczko et al., 2001a).

This study considers both the aforesaid theories regarding age of the ARC as working hypothesis because any independent work on ARC samples is not carried out. However, the two different hypotheses will be tried to evaluate further by means of geochemical and isotopic study of MDC samples and field relations.

The Cretaceous granulites are known as Western Fiordland Orthogneiss (WFO). Allibone et al., 2009 described the plutonic rocks of western Fiordland between Breaksea and Sutherland Sounds. The WFO is the dominant phase along with some smaller bodies of Paleozoic and Cretaceous granitoid, but their age relations are not well constrained (Allibone et al., 2009). The Paleozoic granitoids includes Pandora Orthogneiss (500 Ma), All Round Pluton (340 Ma), Deas Cove Granite (372 Ma), possibly the Straight River Granite and widespread sills within Paleozoic metasedimentary rocks related to the Pandora Orthogneiss.

According to Allibone et al. (2009) the WFO consists of at least 7 major dioritic and monzodioritic plutonic bodies in western Fiordland, one in central Fiordland and one in Stewart Island emplaced during 125-116 Ma. The WFO is mainly gabbroic to dioritic in composition and metamorphosed to amphibolite and granulite facies and was emplaced between 122-119 Ma shortly after the emplacement of the ARC at 136-129 Ma (Bradshaw, 1985, 1989; Mattinson et al., 1986; McCulloch et al., 1987; Hollis et al., 2003).

The WFO in Western Fiordland is considered a lower crustal equivalent of the SPB (present in both Nelson and Fiordland) based on their HiSY chemistry and similar emplacement age (Tulloch and Rabone 1993; Muir et al., 1995; Tulloch and Kimbrough 2003). Recent studies by Allibone et al. (2009) suggested that they were likely derived from different sources. The HiSY character of the two rocks suggested their derivation from the same depth where residual plagioclase is stable, but it is not necessary to have a common source. The Separation Point Suite rocks generally contain greater Sr, Na, Al and have lower Sr/Rb ratios compared to WFO rocks with similar $SiO_2$ composition. The Separation Point Suite represents a more fractionated product compare to WFO and was regarded as a different suite by Allibone et al. (2009). The generation of these HiSY magmas (Tulloch et al., 2003, Bolhar et al., 2008) is discussed in detail in section 2.4.

The study area at Mt Daniel (Northern Fiordland) is part of the Western Fiordland Belt where the WFO is in intrusive contact with ARC. The Mt Daniel Complex is overlain and underlain by WFO and ARC respectively. 123 Ma trondjhemitic dykes are found to crosscut the WFO at Mt Daniel (Hollis et al., 2004). Bradshaw (1990) described the well developed igneous features and an intrusive contact with the ARC at this locality and the field relations are thoroughly discussed in the section 2.4. of this chapter.

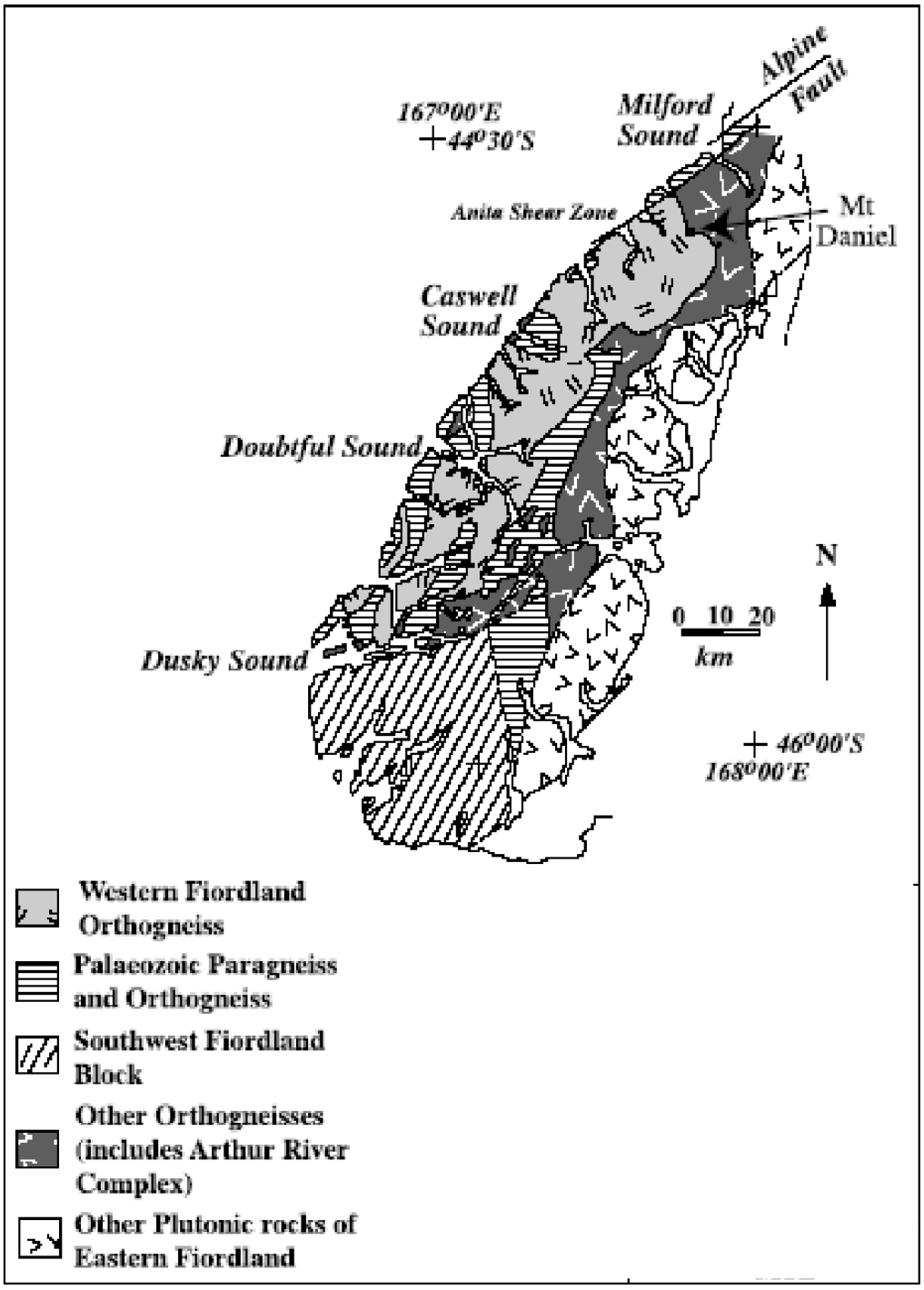


***Figure 2.2.*** *Geological map of Fiordland showing major lithological units (after Bradshaw, 1990). Mt Daniel is located at the northern contact of ARC and WFO.*

**2. The Eastern Fiordland belt** is dominated by Mesozoic Plutonic rocks with subordinate metamorphosed volcanic and sedimentary rocks, and ranges from Mid Jurassic to Early Cretaceous age (168-137 Ma, Muir et al., 1998). The plutonic rocks are termed the Darran Suite which is cut across by 124 Ma old Separation Point Batholith (Muir et al., 1998). The contact between the Eastern and Western Fiordland Belts is separated by the Wall Mountain Fault system of Gibson (1992).

**3. The SW Fiordland Block** consists of mainly low grade metasedimentary rocks and granitoids. This is regarded as an extension of western province terranes of NW Nelson-Westland, which are Lower Paleozoic in age. (Cooper, 1989). Its occurrence is not relevant to the present study and is not discussed further.

## 2.3. Metamorphic History of Fiordland

Bradshaw (1985) and Mattinson et al. (1986) reported that the granulite facies metamorphism in Fiordland is restricted to the two-pyroxene dioritic rocks of the WFO. The WFO concordantly underlies and intrudes mid Palaeozoic ortho- and paragneisses which were metamorphosed to amphibolite facies. The WFO includes both granulites and their retrogressed equivalents.

A low-P/high-T metamorphic event was recognized as the oldest metamorphic event (360 Ma) in Fiordland (Ireland and Gibson 1998). Peak metamorphic event was recorded by sillimanite-kfeldspar assemblages in pelitic rocks and occurred due to the emplacement of different Devonian granitic intrusions, such as Karamea Batholith (Ireland and Gibson 1998). The second Paleozoic event (330 Ma) was recorded by kyanite bearing assemblages indicating a medium P-T condition in Fiordland region and the third major metamorphism was recorded in the Early Cretaceous (125-110 Ma) (Ireland and Gibson 1998).

During Early Cretaceous metamorphism two pyroxene hornblende gneissic assemblages of ARC (preserved in Pembroke Granulite) and WFO reflect a low P<8 Kbar and T>750$^0$ C early metamorphic history (Clarke et al., 2000, Daczko et al., 2001b). This earliest metamorphic event possibly occurred soon after the emplacement of igneous protoliths. During later deformation and metamorphism the two-pyroxene hornblende was replaced by garnet granulite at T > 750$^0$C and P~ 14 kb.

The most common granulite facies assemblage in the WFO is orthopyroxene + clinopyroxene + plagioclase (<An40) ± pargasitic hornblende; granulite sub-assemblages of garnet + clinopyroxene ± quartz are also present locally in a mesoscopic reaction zone overprinting feldspathic rocks (Blattner 1976; Oliver 1977, Bradshaw 1985). Eclogite rocks are also reported locally, as a product of similar garnet-forming reactions from hornblende-rich ultramafic rocks (Oliver 1976; Bradshaw 1985).

However, the peak metamorphic mineral assemblages of the samples collected from the field area at Mt Daniel lack both pyroxenes and include quartz, feldspar, biotite, hornblende, clinozoisite ± garnet, reflecting a range of rock types ranging from mafic to silicic compositions.

The process of melt production associated with granulite facies metramorphism of the ARC is important for understanding the igneous and metamorphic history of the area. Daczko et al., (2001) suggested that the metamorphism of diorites in the ARC was mostly controlled by hornblende breakdown under water undersaturated conditions leaving garnet in residual leucosomes. A small amount of partial melt was extracted from the lower crust via fracture networks and ductile shear zones (Daczko et al. 2001). Adjacent to the leucosomes, in the fracture networks of the source region, hornblende bearing gabbroic gneiss recrystallized to garnet granulite at T > 750 $^0$C at P= 14 kb, indicating the equilibrium conditions during melt formation (Clarke et al., 2000). The Mt Daniel Complex is an excellent locality to observe melt migration from the ARC and entrapment at the base of the WFO.

Successive hydration and dehydration reactions are observed in the pods of mafic granofels of the Arthur River Complex at Mt Daniel at higher temperatures in the deep to mid crust (Daczko et al., 2002a). According to Daczko et al. 2002a, the granulite facies mafic hornfels were probably produced by the removal of felsic material through the partial melting of ARC diorites and the earliest metamorphic assemblages are preserved in hornfels. These are mainly coarse grained garnet-clinopyroxene hornfels in the core of the pods and pseudomorphous symplectite intergrowths of hornblende and clinozoisite within the rim (Daczko et al., 2002a). The generation of mafic granofels in the ARC may be the result of WFO emplacement (Daczko et al., 2002a). Daczko et al., (2002a) described in detail the hydration-dehydration reaction associated with WFO emplacement and burial under different depth and temperature conditions.

Hydration of the hornfels at 800-850 $^0$C < T < 700-750 $^0$C produced hornblende-clinozoisite mafic gneiss. The hornblende-clinozoisite assemblages were replaced by garnet clinopyroxene during dehydration reactions, forming narrow garnet reaction zones. The dehydration reaction and the formation of garnet reaction zone happened after the burial of WFO to deep crustal level at P~12 kb and T= 700-750 $^0$C. Limited dehydration near garnet reaction zones resulted in the symplectitic intergrowth of clinopyroxene-kyanite and clinozoisite-quartz-kyanite-plagioclase, following cooling of contact aureole (Daczko et al., 2002a).

The sequential reactions are as follows: (from Daczko et al., 2002).

Hydration reaction:

garnet + clinopyroxene + quartz + $H_2O$ = hornblende + clinozoisite ------ (1)

Dehydration reactions:

hornblende + clinozoisite = clinopyroxene + kyanite + $H_2O$-------- (2)

hornblende + clinozoisite = clinopyroxene + kyanite + quartz+ plagioclase + $H_2O$----- (3)

Cooling by 200$^0$C of the ARC under high P conditions is suggested by symplectitic intergrowths of kyanite, quartz, plagioclase occurring as partial pseudomorphs of the earlier high T minerals of the ARC (Daczko et al., 2002b). These kyanite symplectites are also partially pseudomorphed by paragonites (Daczko et al., 2002b). Daczko et al., (2002b) suggested an anticlockwise P-T path associated with emplacement and burial of the WFO at peak T conditions (Fig 2.3.) followed by decompression between 105-90 Ma and juxtaposition with comparatively cooler upper crustal rocks of the Darran Complex.

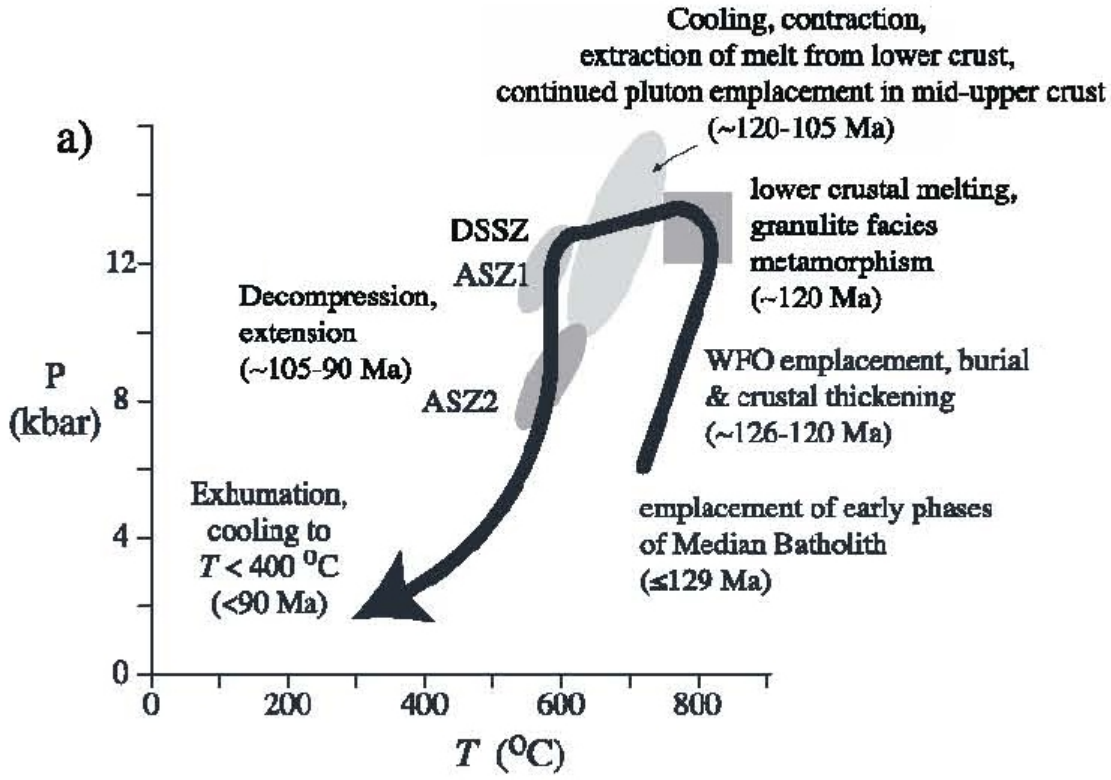


***Figure 2.3.*** *P-T-t path for the lower crust exposed between Caswell and Milford sounds (after Klepeis et al., 2004). Abbreviations are: ASZ-Anita Shear Zone, DSSZ- Doubtful Sound Shear Zone.*

## 2.4. Tectonic Evolution of Fiordland New-Zealand

In Fiordland, the deep root (50 km deep) of a thickened Mesozoic arc is exposed along the Palaeo-Pacific margin of Gondwana (Muir et al., 1998, Klepeis et al., 2003) and is now situated in Western New-Zealand (Klepeis et al., 2003). Neogene uplift associated with dextral movement along the Alpine Fault has produced the present extensive relief in the Southern Alps of New Zealand. Extensive dissection of this uplift terrain by glacial activity has produced the spectacular exposures of Fiordland, such as those at Mt Daniel.

The Mesozoic arc was a site of semi-continuous convergent margin magmatism from 165-105 Ma, and comprises a paired plutonic belt (Tulloch and Kimbrough, 2003). The older outboard belt has low Sr/Y and younger inboard belt has high Sr/Y. The major intrusive features show that the ARC is intruded by >10 km thick WFO of 126-116 Ma age (Mattinson et al., 1986; Tulloch and Kimbrough, 2003; Hollis et al., 2004).

Several studies ( Bradshaw, 1989; Brown, 1996; Clarke et al., 2000, Daczko et al., 2001, 2002a) suggested that the WFO and ARC preserve a change in metamorphic condition from a low P, high-T event ($P<8$Kbar, $T>750^0$C) to a high-P metamorphic event followed by the peak metamorphism ($P\leq16$ kbar, $T>750^0$C) as discussed in section 2.3. Structural studies suggested the high-P metamorphism of these Mesozoic arc rocks is related to the burial by ~25 Km of continental crust due to contraction following pluton intrusion (Clarke et al., 2000; Daczko et al., 2001, 2002a).

Klepeis et al., (2003) examined the evolution of this 50 km thick column of deformed continental crust and proposed three major phases of the tectonic evolution of Fiordland. The three tectonic phases are:

1. Addition of mafic and intermediate magma into the lower crust during the emplacement of WFO between 126-116 Ma, associated with partial melting of the lower crustal host gneisses (ARC).
2. Contractional deformation leading to magmatic arc thickening between 116-105Ma, associated with emplacement of sodic high Sr/Y granitoids in the middle to upper crust.
3. Late orogenic extension, cooling and exhumation 105-90 Ma, prior to opening of the Tasman Sea of *ca*. 84 Ma (Gaina et al., 1998).

According to Klepeis et al., (2003), during the initial stages of magmatism (126-116 Ma); suprasolidus shear zones formed at the upper and lower boundaries of the batholith (WFO). The presence of tightly folded tonalite sheets cut by less deformed sheets is found in the shear zone at Mt Daniel suggest that the deformation occurred under magmatic conditions. This is quite consistent with the detailed field relations of the study area, discussed in detail below. This section is contributed by W.J. Collins as the field work was completely done by him and samples were collected in the year of 2000. Due to budget constrain any further field work in this area could not be carried out during this PhD work.

## 2.5. Field relations of the Mt Daniel Complex, Northern Fiordland

The base of the 10-20 km thick WFO batholith is exposed at Mount Daniel, in northern Fiordland. Directly underlying the base is the Mount Daniel Complex (MDC), forming a ~100-metre thick, sheeted complex between the WFO and underlying batholithic basement of Arthur River Complex (ARC) (Fig.2.4.a). It has been called migmatite (Bradshaw, 1985), but the dominant component of the complex is meta-igneous, and most units have intrusive relations with one another, and they are intrusive into the underlying ARC.

These units consist of banded, schlieric to wispy, medium-grained granitic, intermediate and mafic sheets and low-angle dykes, many isoclinally folded. It is better described as a sheeted complex. The highly attenuated nature of mixed and mingled, isoclinally folded sheets indicate that the complex has been intensely deformed, consistent with the suggestion of Klepies et al (2003), that the MDC is a magmatic shear zone.

Fig 2.4.b. shows the regional relations. The MDC forms the distinctive ~100 meters thick band of white to light grey hues along the ridge crest (centre right) before dipping southeastward under the overlying darker unit of the WFO. The upper contact with the WFO is sharp, but the lower boundary with the ARC is more complex. The ARC and MDC appear to be intimately infolded and inter-sheeted at tens to hundreds of metres scale. Moreover, distinctive, m-scale white granitic dykes cut up the mountainside toward the MDC. In one instance, a 2-metre thick granite cuts at a high-angle through the ARC, but is then deflected sinistrally into a highly attenuated isoclinal fold with wavelength of >50 metres. It reflects the intense strain gradient across the ARC/MDC boundary. Nonetheless, the internal foliation within the dyke on either side of the boundary is virtually non-existent, indicating that the dyke did not record strain associated with the folding at side the shear zone. It suggests that the dyke was still in the magmatic state as it deformed. Syn-tectonic emplacement of dykes is a universal feature of the MDC, as described below.

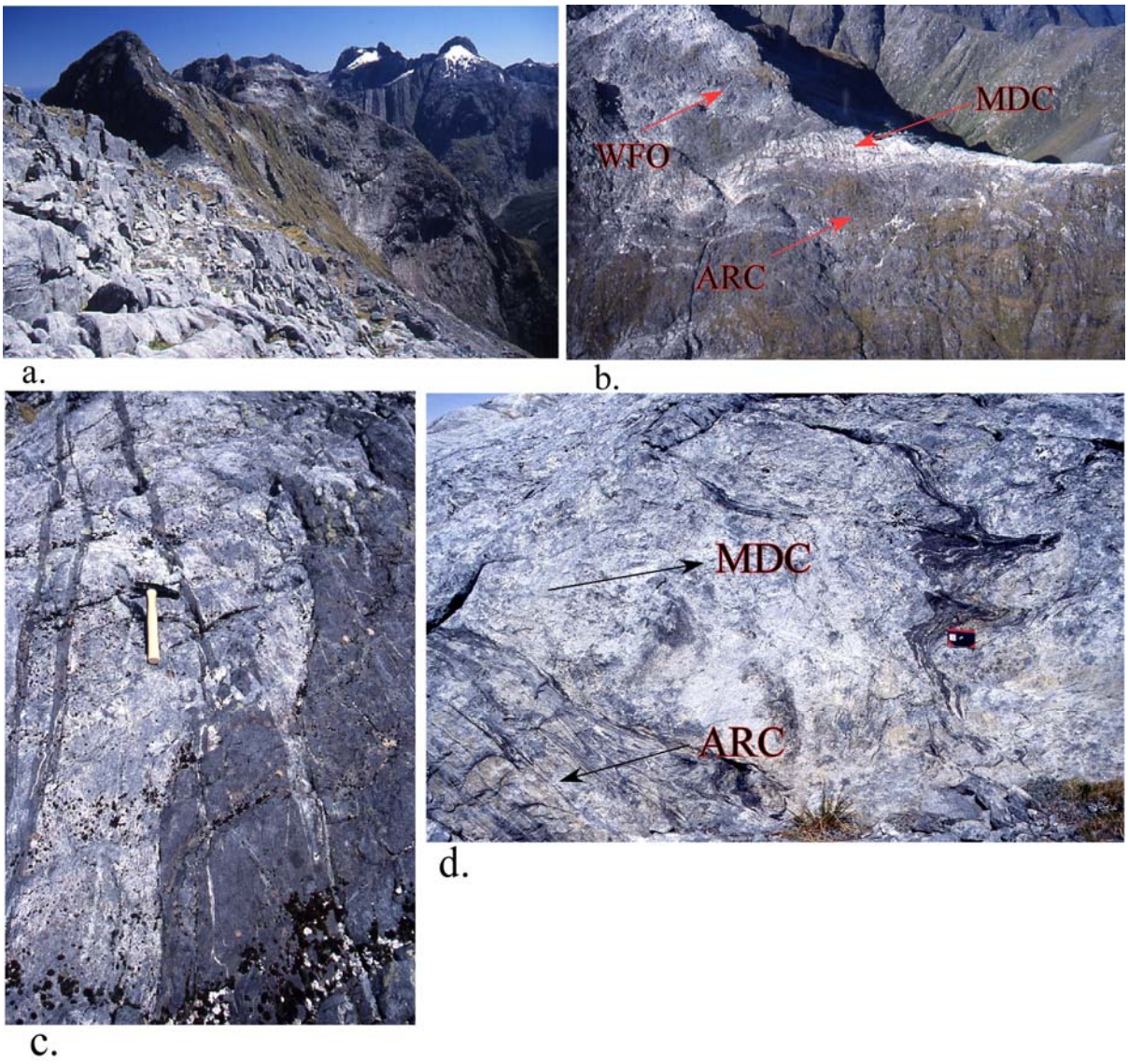


***Figure 2.4.*** *Field Photographs from Mt Daniel, Fiordland.* ***(a)*** *A broad view of the Mt Daniel Complex which is overlain by the WFO and underlain by the ARC;* ***(b)*** *Regional relations show ~100 mt thick sheeted Mt Daniel Complex,* View is to south; relief is ~600 metres. Mt Daniel is at top left; ***(c)*** *Lit per lit granitic intrusion within Arthur River Complex,* View is to SW*;* ***(d)*** *Presence of in-folding and ghost layering of ARC within MDC represents the assimilation of ARC within MDC,* View is to SW.

At the base of the MDC (Fig 2.4.c.) m-scale sheets of granite intrude the ARC. Intrusion is lit-par-lit style, with the sheets appearing to pries along the dominant foliation before widening to form the dominant phase of the MDC, leaving thin septa of ARC country-rock between. The stepping of the dykes to the left suggests emplacement during sinistral transtension.

Advanced stage of dyke widening during granite magma emplacement has forced separation of the septa up to 2 metres, leaving the basement intact (bottom of Fig 2.4.d) which still preserves the isoclinal fold geometry. The folds in the septa are tight, whereas those in the basement are isoclinal, which suggests either the dykes were emplaced during folding (flattening), or post-folding migration and inflation of magma along the axial plane has "unfolded" the earlier folds as the granitic sheets were emplaced. Ghost structure in the granite mimics the open folds on either side of the septa, suggesting initial emplacement of magma along the foliation, for Fig 2.4.c. Nonetheless, the granitic contact cuts across the septa at low angles, and is itself folded, indicating that emplacement began before folding but continued during the flattening. The dyke thins rapidly at bottom centre, and its geometry implies inflation upward and to the left, consistent with emplacement during sinistral transtension.

Fig 2.5.a. shows a detail of Fig 2.4.d. (bottom left). In this example, isoclinal folds in the ARC are defined by leucocratic veins which may have been part of the early intrusive phase of the MDC. The veins are folded and locally highly attenuated within the axial planar foliation (centre), which is concordant with a 30 cm-wide granitic sheet. The sheet is separated from another granitic sheet of similar width (bottom of fig 2.5.a.) by thin, isoclinally folded ARC septa.

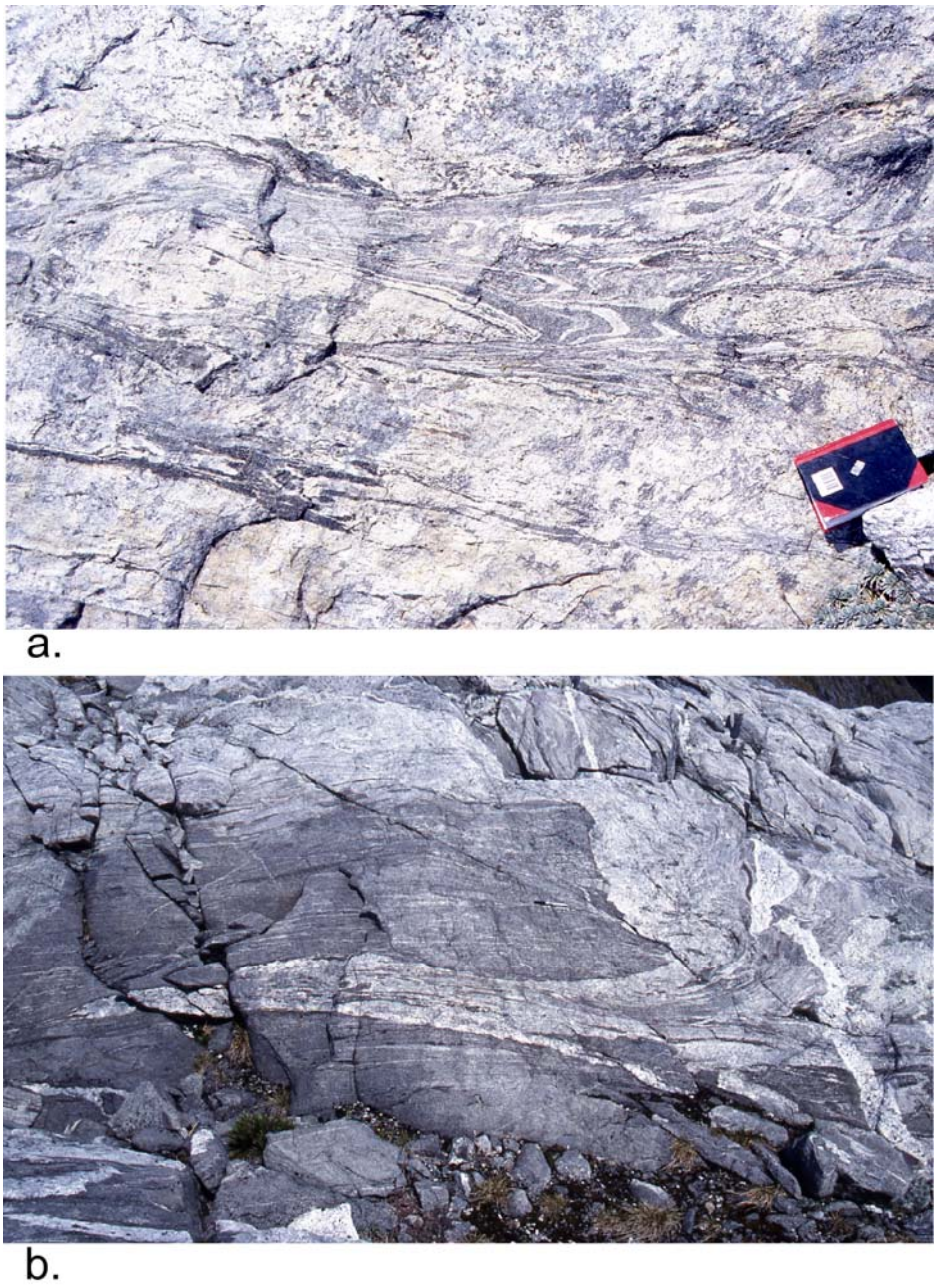


***Figure 2.5.*** *Field Photographs from Mt Daniel, Fiordland.* ***(a)*** *Details of ARC structures from bottom left part of Fig 2.4.d;* ***(b)*** *Granitic dykes cutting strong gneissic foliation of ARC but isoclinally folded within the sequence.*

At centre left in Fig 2.5.a., a thin lens of granite has intruded parallel to the axial plane, and has a deformed rind of country-rock, suggesting it was emplaced early in the folding history. At centre of fig 2.5.a. truncation of sheets in an axial-planar high strain zone probably suggests sinistral offset.

A granitic dyke cuts the strong gneissic foliation of the ARC but is isoclinally folded within the sequence in Fig 2.5.b. This feature commonly occurs within the MDC, but the subsequent isoclinal folding often makes it difficult to recognize such dykes (eg. Fig 2.6.a.). Note that the nose of the folded dyke in Fig 2.5.b. is represented by veins that extend beyond the dyke, concordant with the gneissic foliation in the ARC, indicating that the foliation is partly defined by very fine (mm-scale) sheets. This suggests that magma was present during the early stages of deformation. Also note the heterogeneous nature of the dyke, and the ghost structure within, which is detailed below.

Fig 2.6.b. shows a detail of the contact relations and heterogeneity of the dyke in Fig 2.5.b. The dyke contains diffuse rafts of the ARC that grade into the granitic phase but maintain a “ghost foliation” that mimics the folded dyke outline, including the isoclinally folded hinge (bottom centre). The ARC remnants are progressively dispersed and recrystallised throughout the granite, which is “cleanest” near the dyke margin (top left).

An irregular, trondhjemitic dyke cuts the fold, but is itself weakly folded and sinistrally offset (centre of Fig 2.5.b.). The crenulated margins of the dyke define folds that are axial planar to the isoclinal fold, indicating that it intruded late in the same fold history. The sinistral offset occurred in the magmatic state, as minor granitic apophyses extend across the offset, and are themselves folded. The offset is consistent with other kinematic markers indicating sinistral movement.

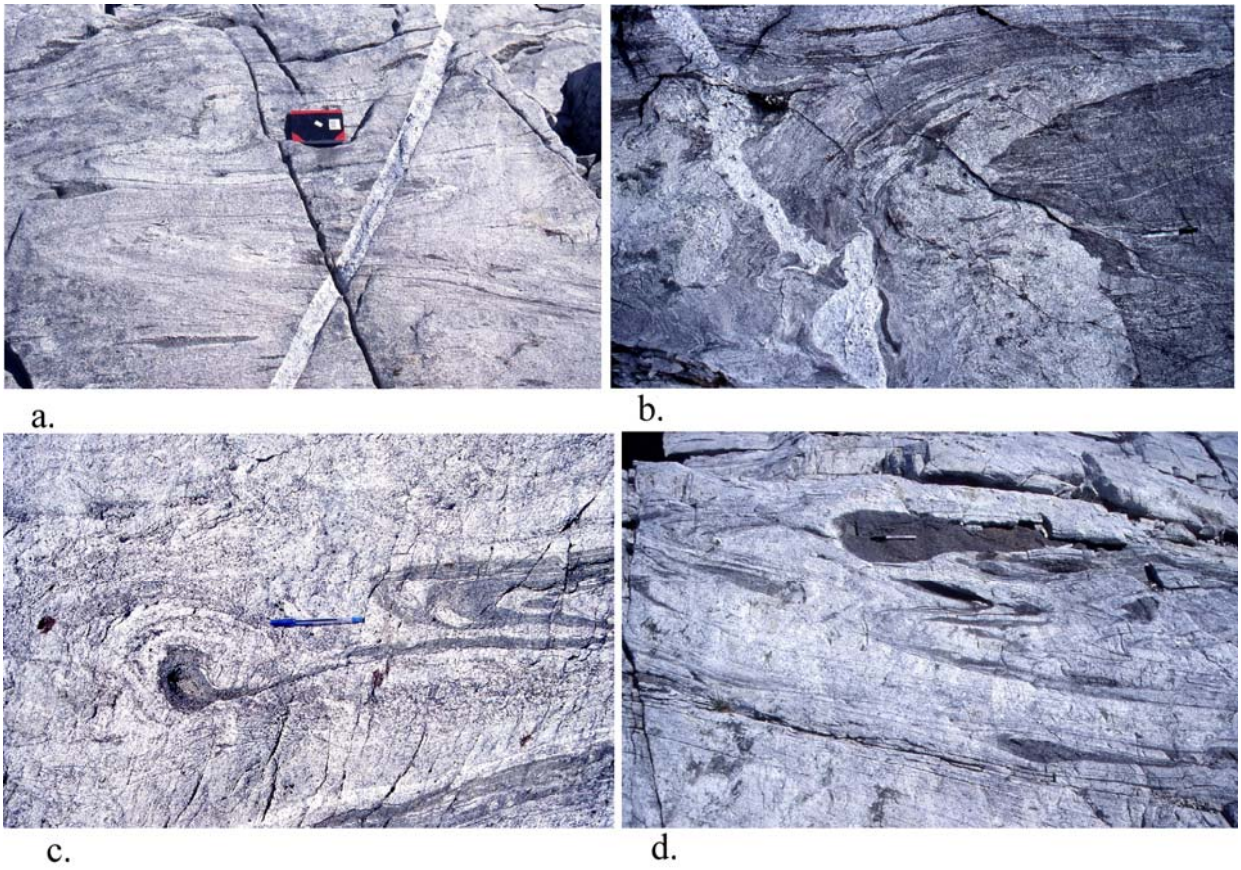


***Figure 2.6.*** *Field Photographs from Mt Daniel, Fiordland.* ***(a)*** *Rectilinear trondhjemite dyke cross cutting MDC;* ***(b)*** *Trondhjemite dyke shows detail contact relation with MDC and associated ARC;* ***(c)*** *Mechanical stirring and mingling of ARC within MDC;* ***(d)*** *Remnant of mafic dykes mixed and mingled within MDC.*

Fig 2.6.c. resembles an imbricate fold-thrust stack. Thin (cm-scale) granitic veins have intruded along the foliation before isoclinal folding, but the geometry of the asymmetric mafic "ball and tail structure" resembles a basal thrust with overlying folds outlined by felsic veins and concordant mafic schlieren defining left (W) verging folds . Very diffuse, W-verging folds are evident at the top of figure. In the nose of the main fold (at and above pen), the granitic dyke widens to be thicker in the hinge zone, suggesting syn-folding emplacement, as discussed above.

Advanced disaggregation of ARC septa during emplacement and deformation is also illustrated by Fig 2.6.c. The western (right) margin of the dyke is well-defined in the hinge, but the eastern margin (pen tip) is diffuse, again suggesting assimilation of ARC into the MDC. Moreover, the diffuse, recrystallised schlieren grades almost imperceptibly into the coarser fabric of the granitic material of the MDC, suggesting assimilation was associated with mineral growth and solidification of magma.

Fig. 2.6.d. is a typical outcrop of the lower half of the MDC, characterized by isoclinal folds of granitic sheets outlined by schlieren of hornblende-rich diorite. The m-scale enclave is hornblende-rich gabbro, and forms one of a "train" of enclaves suggesting it is a disaggregated mafic dyke. It can be distinguished from the ARC by the lack of gneissic fabric. Like other enclaves in the figure, it is stretched into lenses and wisps prior to folding. The variation of enclaves is typical of upper level plutonic rocks that have undergone deformation in the magmatic state, which have undergone varying degrees of solidification before deformation. The marked variation of shape reflects the degree of solidification of the magma: those most solidified are the most rigid and have the greatest viscosity contrast with the host granitic magma, hence are most equant. By contrast, mafic magmas that were least solidified, with viscosity similar to the host granitic magma, have been stretched into diffuse wisps with aspect ratios >100:1. Such wisps become so finely dispersed within the host granite, the schlieren become defined by individual hornblende grains, and then it becomes an integral part of the homogeneous rock.

One example is the enclave that forms a cm-scale fold nose of a granitic dyke (middle of left edge in Fig 2.6.d.); the lower limb of which forms semi-continuous mm-scale schlieren trace that can be followed across figure 2.6.d, defining the lower margin of the white, spotted granitic dyke. Note that the schlieren in the wisps and lenses are magmatic in origin, but appears to be metamorphic in origin (a production of protolith assimilation) near the MDC base.

The granitic dyke can be traced through the MDC. It forms a thickened fold nose near the gabbroic enclave, and the lower limb of the fold, the sheet conformably follows the mm-scale streaks around a second (lower) fold, but then cross-cuts those streaks to become the white, homogeneous granite sheet described above. Equally, on its upper side (below the m-scale enclave described above), the dyke cuts an earlier dyke (defined by dark shadow in centre of Fig. 2.6.d. The trace of the dyke shows the cryptic nature of magma ascent through the MDC. Only locally does it breach an overlying sheet, or cut earlier folds, before itself becoming isoclinally folded. Other, thicker sheets form in the axial plane of the folds, cutting at low angles across the folded surface (top of Fig 2.6.d.) and thus can move up the inclined axial surface, although they too commonly become folded during later progressive deformation (see Fig 2.6.a.).

Fig 2.6.a. is from the upper part of the MDC. The granitic sheets contrast with sheets of the lower part (Fig. 2.6.d.), being of intermediate composition, generally more homogeneous, and containing mafic enclaves. Millimetre- to cm-scale enclaves indicate intimate mingling with intermediate-composition (dioritic) magma (top of Fig. 2.6.d.), which are aligned within the axial planar foliation of the isoclinal folds. Sheets in the lower half of the figure are very diffuse, and the mafic streaks and schlieren are less continuous. Intrusion of the well-defined folded silicic (white) sheet in the centre of the figure, post-dated formation of the tight folds in lower half of figure, as it cuts those folds, but is itself tightly folded (hinge near book). Again, this demonstrates syn-emplacement deformation. A post deformational trondhjemitic dyke cuts all structures.

In this outcrop (Fig 2.6.d.), it is impossible to determine if the hornblende-rich schlieren that defines the sheet margins is derived from assimilated country-rock, or from stretched gabbroic enclaves. Certainly it contrasts with the lensoid enclaves in the lower part of Fig 2.6.d, but where the schlieren thickens to cm-scale lenses (upper part of Fig.2.6.d), the evidence is equivocal: in places, mm-scale lit-par-lit injection resembles that of the country-rock contact (near late dyke), but elsewhere (e.g. top right), the schlieren is coarse-grained and appears metaigneous. A dual origin for the schlieren appears the most likely option, which implies that a significant part of the MDC could contain mafic ARC material.

**Western Fiordland Orthogneiss**

A network of semi-concordant SE-dipping trondhjemitic dykes, which cut the dominant foliation at low angles (Fig. 2.7.a.) are abundant in the WFO (Fig. 2.7.b.). The rectilinear arrangement of the dykes suggests that the WFO was solidified before emplacement of the dykes. A similar arrangement exists locally in the ARC (Clarke et al., 2000), below the MDC. By contrast, trondhjemitic dykes are far less abundant in the MDC, and most are folded to some degree, but usually less than the majority of the sheets. Some trondhjemitic magmas intruded as sheets that are isoclinally folded, but they are difficult to distinguish from high-silica granitic dykes in outcrop, as both rock-types are white, fine-grained and recrystallised. The variably folded nature of the trondhjemitic dykes in the MDC, and their paucity compared to those in the WFO above and the ARC below, suggest that the MDC must have been forming during trondhjemite dyke emplacement.

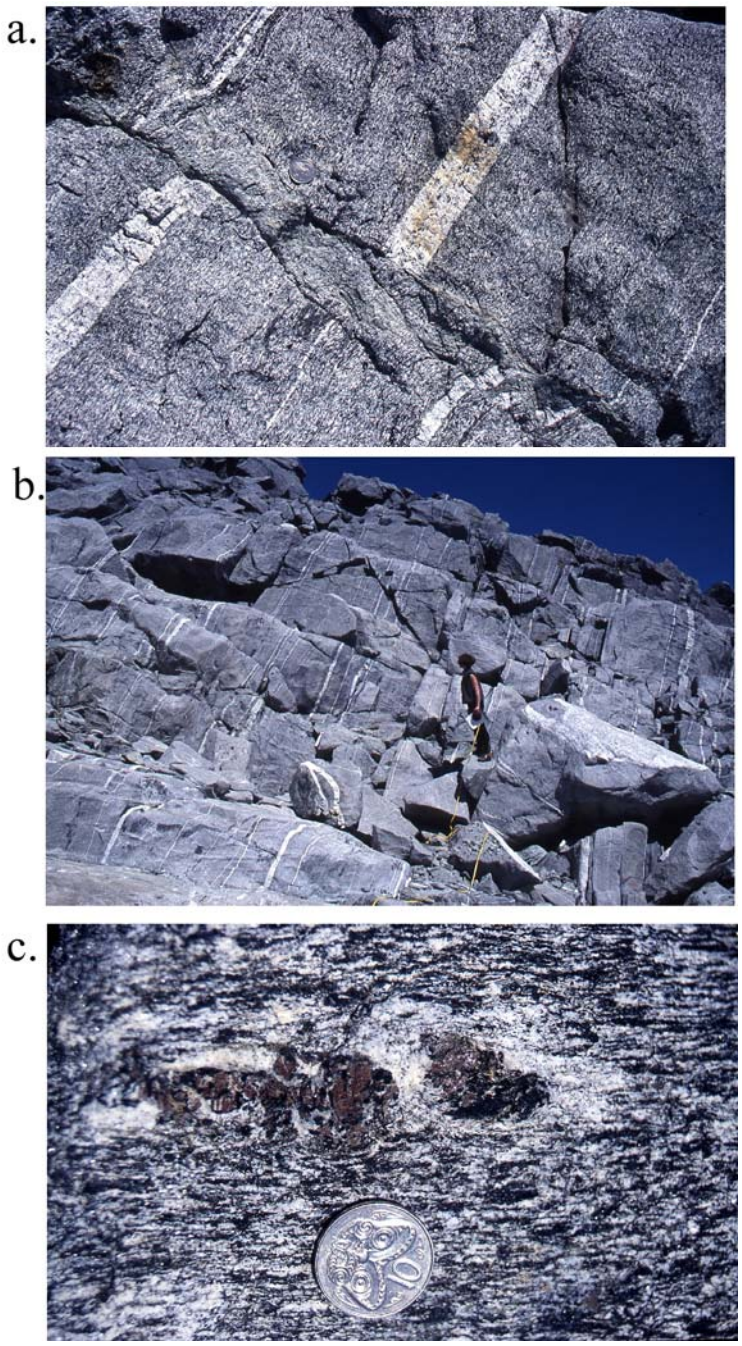


***Figure 2.7.*** *Field Photographs of Western Fiordland Orthogneiss from Mt Daniel, Fiordland.* ***(a)*** *Trondhjemite dykes cross cutting the dominant foliations of WFO at low angles;* ***(b)*** *Abundant rectilinear dykes cross cutting WFO.* ***(c)*** *Presence of leucosomes around peritectic garnet within hornblende rich WFO.*

Figure 2.7.c. is an example of the incipient stages of leucosome development along foliation within the hornblende-rich WFO (Figure 2.7.c.). The cm-scale leucosomes are dominated by sodic plagioclase and quartz, with garnet as a peritectic phase in the core. They formed by the incongruent melting (Clarke 2000, Daczko et al., 2001)

Prg-Hb+OPX+Plag $\longrightarrow$ Grt+Cpx+Qtz+$H_2O$ (Daczko et al., 2001)

The foliation in the WFO is semi-concordant to the axial planar foliation of isoclinal folds in the MDC, again suggesting formation of the leucosomes was occurring during emplacement of the MDC, as described above.

The sodic nature of the dykes, combined with the presence of peritectic garnet, indicate the leucosomes formed at higher pressure (>10kbar) than emplacement of the WFO (~8 kbar) (Clarke et al., 2000). This suggests that the folding during emplacement of the MDC was associated with burial of the entire complex.

The detailed field evidences suggested deformation under magmatic condition similar to that of Klepeis et al., (2003). Syn-tectonic emplacement and subsequent deformation of the dykes and sheets is common at Mt Daniel. The presence of granitic sheets along the foliation and their folded nature suggests emplacement began before deformation and magma was present at the early stage of deformation. Magma flow may have facilitated imbrication of crustal slices during the thickening of the crust (Klepeis et al., 2003). The rectilinear dykes in WFO represent their emplacement after the solidification of WFO. The dykes are continuous across pre, syn and post MDC formation.

## 2.6. HiSY Magma Generation, formation of Dyke Systems in relation to Tectonics in the Mt Daniel Complex, Northern Fiordland

Emplacement of plutonic bodies continued until ~105 Ma, represented by the last stages of the Separation Point Suite (126-105 Ma) in the upper crust of the Fiordland and Nelson regions. The SPS is typically composed of HiSY magmas and WFO was also thought to bear the same HiSY imprints (Muir et al., 1995, 1998, Tulloch and Kimbrough, 2003). Indeed, HiSY magmas are a major plutonic component of the batholiths in Fiordland (Allibone et al., 2009).

The source of these high HiSY granitoid magmas is considered to be mafic crust from the root of the thickened magmatic arc (Muir et al., 1995, 1998). In this model, melting of newly underplated material at the base of the thickened arc occurred at depths >40 km, producing the Na-rich granitoids, leaving a residue of garnet + clinopyroxene + amphibole (Muir et al., 1998). It is this same process observed in the ARC at >10kbar by Clarke et al. (2000).

The Mt Daniel complex possesses numerous HiSY dykes similar to the SPB. They crosscut the WFO and are variably folded within the MDC, indicating emplacement after the solidification of WFO and synchronous with the formation of MDC (see Field description). Tulloch et al. (2003) suggested these HiSY melts were derived from the base of the thickened magmatic arc. Their study suggested that the older (170-128 Ma) LoSY belt represents 30-40 Ma of convergent margin magmatism associated with growth of the underplate, the lower parts of which were in the garnet stability field. This became the source of the HiSY magmas during underthrusting of the arc base and arc migration to a deeper, more continental ward position during shallowing subduction. The melting of underthrusted material (mafic arc base) under high-P produced HiSY partial melts in the inboard belt (126-105) (Tulloch and Kimbrough, 2003). According to this model, the WFO is the first expression of HiSY magmatism, due to the partial melting of the underplate at relatively shallower depths. Contractional deformation and thickening of the crust after the WFO emplacement lead to burial and granulite facies metamorphism of that region, and enhanced generation of HiSY melts at the greater depths (Tulloch and Kimbrough, 2003).

Mantle and Collins (2008) used Ce/Y ratios of basalts from the mafic dykes in the MDC to estimate crustal thickness. The highest Ce/Y suggested a minimum thickness of ~50 km during emplacement of the MDC.

Tectonic switching from contraction and crustal thickening to crustal thinning (extension) and decompression at 105 Ma in Fiordland corresponds to the end of subduction and a reorganization of plate boundaries outboard of Gondwana (Klepeis et al., 2003).

Flowers et al. (2005) revealed the temporal relationship of the burial and exhumation of the magmatic arc from thermochronological data. Their titanite data suggested that the final stages of arc magmatism, thickening and granulite facies metamorphism occurred between 111-113 Ma, followed by prolonged unroofing of the central Fiordland granulites over a 40-45 Ma period.

Therefore, the Mt Daniel Complex records the time of magmatism associated with burial following emplacement of the WFO. The following chapters describe the geochemical and isotopic evolution of the MDC during its emplacement and ongoing deformation and metamorphism during burial to ~50 km depth.

As shown in Chapter 1, the whole rock geochemistry of the MDC covers the entire range of granitoid compositions for the Mesozoic Median Batholith of New Zealand, yet this compositional range occurs within a ~100 wide zone near the base of the crust. A detailed study of the interplay between the whole rock geochemistry, isotopic evolution at bulk rock and mineral scale (with zircons) should yield a comprehensive insight into the origin and evolution of this Cordilleran batholith, from a view close to the source region. Given the general similarity of the MDC to other Cordilleran batholiths, especially those that exhibit a sodic character, the insights from the MDC may have general applicability for the petrogenesis of circum- Pacific batholiths.

# Chapter 3: Analytical Techniques

## 3.1. Introduction

This chapter describes the techniques employed during this study for the analysis of whole rock and minerals from the Fiordland samples, these being zircon, garnet and rutile. The Whole rock major and trace element compositions were determined through X-ray Fluorescence Spectrometry (XRF) using Spectro X'Lab 2000 Energy Dispersive XRF at the New Castle University. Whole rock REE analyses were carried out using LA-ICPMS at the Advanced Analytical Centre, James Cook University, Townsville. Whole rock Nd isotopic analyses were carried out at the Adelaide University using Finigan MAT 262 Thermal Ionisation Mass Spectrometer. All the samples were crushed and powdered before sending to laboratories.

All the mineral analyses were carried out at the Advanced Analytical Centre, James Cook University, Townsville. Zircons were analysed as polished, section crystals in epoxy grains mounts, whereas rutile and garnet were analysed in situ in thin section.

Zircons were separated from 1 to 5 kg pulverized rock by conventional heavy liquid and magnetic separation techniques. Approximately 100-150 grains from each of the sample were mounted in epoxy resin and ground and polished to expose their interior. Zircons of assorted morphologies were selected and all were carefully characterised by cathodoluminescence (CL) and back-scattered electron imaging.

Cathodoluminescence images were taken of zircons using a JSM 5410LV Scanning Electron Microscope (SEM). The accelerating voltage was 20 kV and using monochromatic grayscale CL.

Zircons with cores and rims and with different types of zoning were selected for further analyses by electron microprobe (EMPA) and laser ablation inductively coupled plasma mass spectrometry (LA-ICPMS) for trace element analysis. EMPA zircon analyses were carried out because Hf concentrations are used as an internal standard for trace element analysis using LA-ICPMS. In LA-

ICPMS the whole range of trace elements including REE can be measured, so it is important to carry out both of the analytical techniques for trace element studies of zircon.

Major and trace element analysis of garnet were also carried out through EMPA and LA-ICPMS and trace element analysis of rutile using LA-ICPMS. Polished thin sections with 80μm thickness are used. CaO content has been used as an internal standard for garnet for further trace element analysis by LA-ICPMS. Thus we have carried out both the major element analysis of garnet using EMPA and trace element analysis using LA-ICPMS.

U-Pb isotope age dating of zircon has also been carried out by LA-ICPMS. Analysis was mainly directed towards identifying inherited cores and younger rims to understand the magmatic and metamorphic history of the zircon in individual samples. The major growth phases of the zircon have been precisely dated by U-Pb isotopes and separate Lu-Hf analysis have also been obtained for each growth zone of known age to understand the chemical differentiation of the crust and mantle at that particular time. These data will help to understand the source of the zircon and the evolution of the rocks containing the zircons and will be used to determine the magmatic processes.

## 3.2. Whole Rock Major, Trace, REE and Isotope Analyses

### A. Whole Rock Major and Trace Element (XRF) Analysis

XRF analysis was carried out using a Spectro X'Lab 2000 Energy Dispersive XRF. The instrument is equipped with a Pd anode tube and uses a polarised beam and multiple targets.

A Fusilux Fusion Bead Casting Machine BFF-1 is used to prepare fused beads for major oxide analysis. In this method, powder samples are prepared for analysis by incorporating the test sample, via fusion at 1050ºC, into a borate glass disc. Generally one gram of sample is diluted with six grams of a lithium borate flux. Different composition fluxes are used depending on the expected SiO2 content of the sample. Major oxide analysis is routinely carried out on the "as received" powder. High carbon content samples, including soils and some clays, may need to be dried at

105ºC before fusion. A loss analysis is carried out on all samples that require major oxide determination. The powder is heated at 1050ºC for ten minutes, replicating fusion conditions, and the weight loss calculated. This figure is added to the major oxide values obtained by XRF analysis to give the "total" for the sample.

Two preparation methods are employed at the University of Newcastle for trace element analysis by XRF. Rock powders are pressed into a solid pellet using a small amount of PVA binder in ten grams of rock powder. In this case the amount of binder used is negligible. Soils and high clay or carbon content powders are diluted using approximately one gram of wax binder to five grams of sample. This mixture is then pressed to give a solid pellet for XRF analysis.

Calibration is carried out using certified reference materials. Individual programs are used for each of the three fluxes used in fused bead analysis, and for each of the pressed pellet methods. Matrix corrections are made for inter element effects.

Duplicate analyses and standard checks are used for quality monitoring. A monitor specimen is used to compensate for instrumental variations over time.

**B. Whole Rock REE Analysis**

The samples were digested using a microwave oven (Milestone 1200 Mega), about 0.1 g samples were weighed and then taken into the digestion vessel, 2.5 ml SupraPure (Merk Germany) double distilled HNO3, 1 ml SuperPure HClO4 and 0.5 ml AR Grade HF were added into the vessel. The mixture was in the fumehood for about 1 h to let the reaction complete. The vessels were loaded into the microwave oven and the samples were heated to $220^0$ C and kept at this temperature for 10 minutes. After cooling down, the digested samples were quantitatively transferred into a PTFE beaker and heated on a hotplate to near

dryness and then the samples were dissolved in 10% HNO3 and quantitatively transferred to a 50 ml volumetric flask and diluted to the mark using Milli-Q water.

Sample analysis was carried out by a Varian 820-MS Inductively Coupled Plasma Mass Spectrometer (AAC, JCU, Australia). A series of multi-element standard solutions were used to calibrate the instrument and were also used as the internal standard to correct for instrumental drift and matrix effects. A Certified Reference Material AGV 2 Andesite was used as the quality control sample. It has undergone the same digestion procedure as the samples, and was measured along with all samples, all results showed good agreement with the certified value.

**C. Whole Rock Nd-Sr Isotope Analysis**

Twenty samples were selected for isotopic analyses. All analysis was done on a Finnigan MAT 262 Thermal Ionisation Mass Spectrometer (TIMS) in static mode. Samples were leached in 3 M HCl for 30 minutes at~$100^0$ C. The supernatant was pipetted off. The residue was then analysed for its isotopic composition. The long term Nd reference material measurements used were the La Jolla standard, which gave $^{143}Nd/^{144}Nd$ = 0.511834±9 (n=96) and JNdi-1 gave 0.512092±8 (n=169). Sm μg/g was corrected for a 150 pg Sm blank. SRM987 was used as the Sr reference material with $^{87/86}$ Sr=0.710239 ± 14 (sd) (n=10) (Elburg et al., 2003).

## 3.3. Electron Microprobe Analysis

EMP analyses were carried out using a JEOL JXA 8200 EPMA (electron probe microanalyser) with energy dispersive spectrometer. The probe current was 50nA and the accelerating voltage was 15kV with 20sec counting times on the elemental peaks. The analysis time was 2 min for zircon and 3.3 min for garnet. The spot size was 1-5 microns. Element matrix corrections were made using ZAF 8200 JEOL version Scientific software for zircon and garnet (Armstrong, 1982). Kα and Lα peaks were used for zircon and Kα for garnet. Calibrations are made daily using mineral and synthetic standards and were cross checked against international and in-house standards run prior to each session.

| Date | Session | Sample | %RSD | Average±1SD |
|---|---|---|---|---|
| 12/5/08 | Session 1 | $HfO_2$ | 0.363% | 100.96±0.366 |
| | | T-$ZrO_2$ | 0.313% | 99.96±0.313 |
| | | 91500 | 0.424% | 99.61±0.422 |
| | Session 2 | MTZ | 0.26% | 99.2±0.26 |
| | | TEM-2 | 0.478% | 99.24±0.474 |
| | | 91500 | 0.099% | 99.99±0.099 |
| | Session 3 | MTZ | 0.277% | 100.68±0.28 |
| 29/5/08 | | MTZ | 0.17% | 101.61±.018 |
| 15/9/08 | | MTZ | 0.42% | 100.14±0.42 |

***Table 3.1.a.*** *The results for standard materials for EMPA analytical sessions*

| date 12/5/08 | Sample No | $SiO_2$ | $HfO_2$ | $Y_2O_3$ | $ZrO_2$ | Sum of Cation recalculated to O=12 |
|---|---|---|---|---|---|---|
| session 1 | $HfO_2$ | 0 | 5.714 | 0 | 0.286 | 6.000 |
| | $HfO_2$ | 0 | 5.721 | 0.000 | 0.279 | 6.000 |
| | $HfO_2$ | 0 | 5.714 | 0.000 | 0.286 | 6.000 |
| | | | | | | |
| | T-$ZrO_2$ | 0 | 0.066 | 0.000 | 5.934 | 6.000 |
| | T-$ZrO_2$ | 0 | 0.066 | 0.000 | 5.934 | 6.000 |
| | T-$ZrO_2$ | 0 | 0.063 | 0.000 | 5.937 | 6.000 |
| | | | | | | |
| | 91500 | 2.976 | 0.019 | 0.001 | 3.004 | 6.000 |
| | 91500 | 2.976 | 0.019 | 0.001 | 3.005 | 6.000 |
| | 91500 | 2.975 | 0.019 | 0.000 | 3.007 | 6.000 |
| | 91500 | 2.966 | 0.020 | 0.000 | 3.014 | 6.000 |
| | 91500 | 2.971 | 0.020 | 0.000 | 3.009 | 6.000 |
| | 91500 | 2.972 | 0.018 | 0.001 | 3.009 | 6.000 |
| | | | | | | |
| session 2 | SZ1-MTZ-1 | 3.036 | 0.030 | 0.000 | 2.934 | 6.000 |
| | SZ1-MTZ-2 | 3.028 | 0.030 | 0.000 | 2.942 | 6.000 |
| | SZ1-MTZ-3 | 3.038 | 0.030 | 0.000 | 2.932 | 6.000 |
| | SZ1-MTZ-4 | 3.032 | 0.028 | 0.000 | 2.940 | 6.000 |
| | SZ1-MTZ-5 | 3.040 | 0.030 | 0.000 | 2.930 | 6.000 |
| | SZ1-MTZ-6 | 3.037 | 0.030 | 0.000 | 2.933 | 6.000 |
| | SZ1-MTZ-7 | 3.028 | 0.030 | 0.000 | 2.941 | 6.000 |
| | SZ1-MTZ-8 | 3.042 | 0.030 | 0.000 | 2.928 | 6.000 |
| | SZ1-MTZ-9 | 3.035 | 0.029 | 0.000 | 2.935 | 6.000 |
| | SZ1-MTZ-10 | 3.040 | 0.031 | 0.000 | 2.929 | 6.000 |
| | SZ1-MTZ-11 | 3.039 | 0.029 | 0.000 | 2.933 | 6.000 |
| | SZ1-MTZ-12 | 3.043 | 0.029 | 0.000 | 2.927 | 6.000 |
| | SZ1-MTZ-13 | 3.033 | 0.029 | 0.001 | 2.936 | 6.000 |
| | SZ1-MTZ-14 | 3.038 | 0.031 | 0.000 | 2.931 | 6.000 |
| | SZ1-MTZ-15 | 3.043 | 0.030 | 0.000 | 2.927 | 6.000 |
| | | | | | | |
| | SZ1-TEM-1 | 3.021 | 0.039 | 0.004 | 2.938 | 6.001 |
| | SZ1-TEM-2 | 3.030 | 0.038 | 0.003 | 2.930 | 6.001 |
| | SZ1-TEM-3 | 3.028 | 0.035 | 0.001 | 2.936 | 6.000 |
| | SZ1-TEM-4 | 3.030 | 0.034 | 0.003 | 2.934 | 6.001 |
| | SZ1-TEM-5 | 3.024 | 0.038 | 0.001 | 2.937 | 6.000 |
| | SZ1-TEM-6 | 3.024 | 0.038 | 0.001 | 2.937 | 6.000 |
| | SZ1-TEM-7 | 3.027 | 0.041 | 0.002 | 2.931 | 6.000 |
| | SZ1-TEM-8 | 3.033 | 0.040 | 0.003 | 2.925 | 6.001 |
| | SZ1-TEM-9 | 3.031 | 0.041 | 0.006 | 2.924 | 6.001 |
| | SZ1-TEM-10 | 3.064 | 0.041 | 0.004 | 2.892 | 6.001 |
| | | | | | | |
| | 91500 | 3.009 | 0.019 | 0.000 | 2.972 | 6.000 |
| | 91500 | 2.999 | 0.020 | 0.001 | 2.981 | 6.000 |
| | 91500 | 3.004 | 0.018 | 0.000 | 2.977 | 6.000 |
| session3 | SZ4-MTZ-1 | 1.981 | 0.069 | 0.001 | 3.950 | 6.000 |

| | | | | | | |
|---|---|---|---|---|---|---|
| | SZ4-MTZ-2 | 1.975 | 0.070 | 0.000 | 3.955 | 6.000 |
| | SZ4-MTZ-3 | 1.982 | 0.069 | 0.000 | 3.949 | 6.000 |
| | SZ4-MTZ-4 | 1.965 | 0.069 | 0.000 | 3.966 | 6.000 |
| | SZ4-MTZ-5 | 1.965 | 0.069 | 0.001 | 3.965 | 6.000 |
| | SZ4-MTZ-6 | 1.961 | 0.066 | 0.000 | 3.973 | 6.000 |
| | SZ4-MTZ-7 | 1.964 | 0.069 | 0.000 | 3.967 | 6.000 |
| | SZ4-MTZ-8 | 1.972 | 0.070 | 0.000 | 3.958 | 6.000 |
| | SZ4-MTZ-9 | 1.968 | 0.069 | 0.000 | 3.962 | 6.000 |
| | SZ4-MTZ-10 | 1.973 | 0.070 | 0.000 | 3.956 | 6.000 |
| | SZ4-MTZ-11 | 1.980 | 0.068 | 0.001 | 3.952 | 6.000 |
| | SZ4-MTZ-12 | 1.975 | 0.067 | 0.000 | 3.958 | 6.000 |
| | SZ4-MTZ-13 | 1.979 | 0.073 | 0.001 | 3.946 | 6.000 |
| | SZ4-MTZ-14 | 1.977 | 0.068 | 0.000 | 3.955 | 6.000 |
| | SZ4-MTZ-15 | 1.988 | 0.068 | 0.000 | 3.944 | 6.000 |
| | | | | | | |
| 29/5/08 | SZ3-MTZ-1 | 1.923 | 0.057 | 0.000 | 4.020 | 6.000 |
| | SZ3-MTZ-2 | 1.926 | 0.058 | 0.000 | 4.015 | 6.000 |
| | SZ3-MTZ-3 | 1.924 | 0.068 | 0.000 | 4.008 | 6.000 |
| | SZ3-MTZ-4 | 1.925 | 0.065 | 0.002 | 4.009 | 6.000 |
| | SZ3-MTZ-5 | 1.920 | 0.064 | 0.000 | 4.016 | 6.000 |
| | SZ3-MTZ-6 | 1.918 | 0.067 | 0.001 | 4.015 | 6.000 |
| | SZ3-MTZ-7 | 1.920 | 0.062 | 0.000 | 4.019 | 6.000 |
| | SZ3-MTZ-8 | 1.917 | 0.061 | 0.000 | 4.022 | 6.000 |
| | SZ3-MTZ-9 | 1.916 | 0.061 | 0.000 | 4.023 | 6.000 |
| | SZ3-MTZ-10 | 1.916 | 0.055 | 0.001 | 4.029 | 6.000 |
| | | | | | | |
| 15/9/08 | SZ1-MTZ-1 | 2.964 | 0.032 | 0.000 | 3.004 | 6.000 |
| | SZ1-MTZ-2 | 2.979 | 0.032 | 0.000 | 2.989 | 6.000 |
| | SZ1-MTZ-3 | 2.964 | 0.030 | 0.000 | 3.006 | 6.000 |
| | SZ1-MTZ-4 | 2.978 | 0.030 | 0.000 | 2.992 | 6.000 |
| | SZ1-MTZ-5 | 2.969 | 0.029 | 0.000 | 3.001 | 6.000 |
| | SZ1-MTZ-6 | 2.972 | 0.032 | 0.000 | 2.997 | 6.000 |
| | SZ1-MTZ-7 | 2.970 | 0.029 | 0.001 | 3.000 | 6.000 |
| | SZ1-MTZ-8 | 2.953 | 0.030 | 0.000 | 3.017 | 6.000 |
| | SZ1-MTZ-9 | 2.971 | 0.030 | 0.000 | 2.999 | 6.000 |
| | SZ1-MTZ-10 | 2.985 | 0.030 | 0.000 | 2.985 | 6.000 |

***Table 3.1.b.*** *Number of cations calculated to demonstrate that the results from Electron Microprobe analyses are stochiometric*

| Element | Standard | Crystal | Xray | Pk T (s) | Bckg T (s) |
|---|---|---|---|---|---|
| Si | zircon | TAP | Kα | 20 | 10 |
| Hf | HfO2 | LIFH | Lα | 60 | 30 |
| Y | Y2O3 | PET | Lα | 60 | 30 |
| Zr | zircon | PET | Lα | 20 | 10 |

***Table 3.1.c.*** *The standards used to calibrate the different elements measured in zircons using Electron Microprobe.*

| Element | Standard | Crystal | Xray | Pk T (s) | Bckg T (s) |
|---|---|---|---|---|---|
| Si | Kyanite | TAP | Kα | 20 | 10 |
| Fe | Hematite | LIF | Kα | 20 | 10 |
| Ti | TiO2 | LIFH | Kα | 20 | 10 |
| Mg | Olivine | TAP | Kα | 20 | 10 |
| Ca | Wollastonite | PET | Kα | 20 | 10 |
| Al | Kyanite | TAP | Kα | 20 | 10 |
| Mn | Spessartine | LIF | Kα | 20 | 10 |

***Table 3.1.d.*** *The standards used to calibrate the different elements measured in garnets using Electron Microprobe.*

## 3.4. LA-ICPMS Trace Element Analysis

LA-ICPMS studies of trace elements in zircon, garnet and rutile were carried out on a Coherent Geolas 193 nm ArF laser ablation unit coupled to a Varian 820-MS quadrupole ICPMS. The layout of laser system and observation unit is described in Fig.3.1.a. (Coherent, user manual, GeoLas Pro; 2006) and how the ICPMS and laser system are connected with the gas flow path are described in Fig 3.1.b.

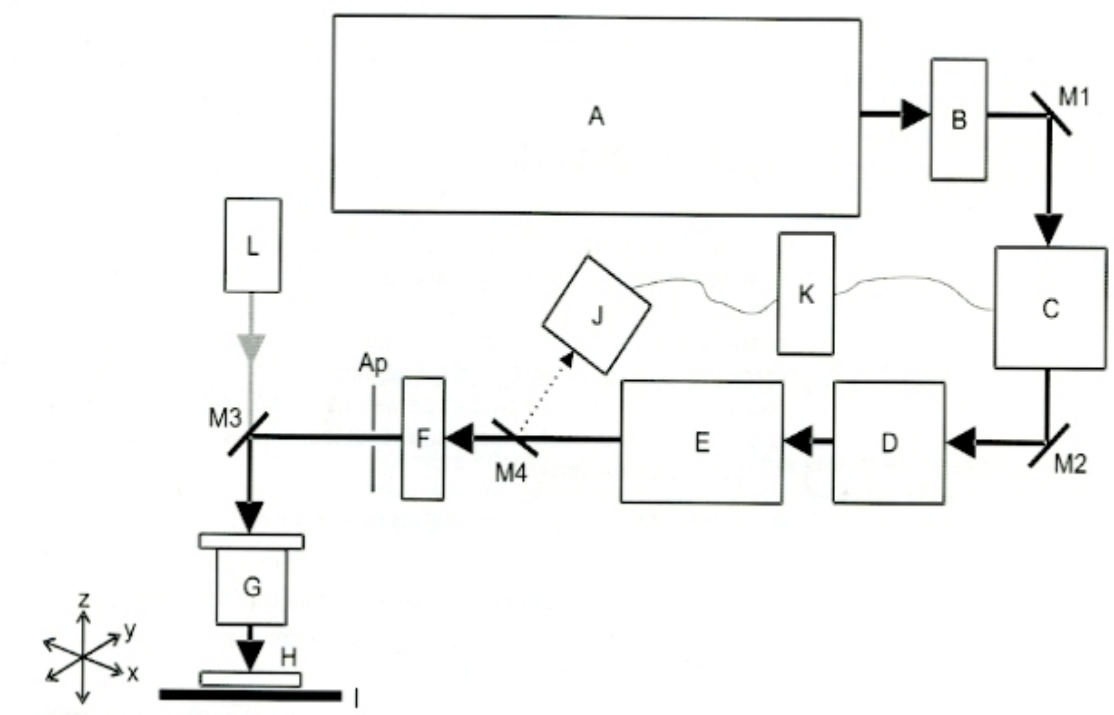


| | | | |
|---|---|---|---|
| A | Laser device | I | XYZ - stage |
| B | Beam shutter | J | Energy monitor |
| C | Attenuator | K | SM1E attenuator control box |
| D | Prism set | L | CCD - camera |
| E | Homogenizer | | |
| F | Field lens | Ap | Aperture |
| G | Schwarzschild objective | Mx | Bending mirror |
| H | Sample | M4 | Beam splitter |

***Figure 3.1.a****. Layout of the GeoLas Pro optical system.*

The laser device (A) is used to generate the laser beam for ablation. The beam shutter (B) is automatically controlled by the software and to open the shutter the high voltage of the laser is needed. The laser beam reflects through deflection mirrors with high reflective coating (M1, M2) into the optical set up to attenuator (C). The attenuator adjusts the high voltage to 150 mJ by a rotating mirror. If the mirror is horizontal no beam can come to the homogenizer (E). Laser beams with different wavelengths come to the homogenizer through prism set (D). The prisms create a laser beam around zero intensity central zone so that it can be accepted by Schwarzschild mirror objective (G). The schwarzschild objective can only accept light around zero intensity. The laser beams with different wave length converted into a single wavelength through the homogenizer (E). The field lens (F) is used to line up the light beams which are diverted behind the aperture. This is

necessary in order to get most of the light from the homogenizer to the Schwarzschild objective. One deflection mirror (M3) with high reflective coating is used to direct the laser beam into the sample chamber (H). The schwarzschild objective (G) is a mirror telescope without any refractive elements. It is totally achromatic and allows for high resolution observations in the visible light spectrum as well as diffraction limited imaging of the aperture at the laser light wavelength. The sample can be observed directly through a microscope or on a LCD display. The image for the LCD display is delivered by a CCD camera (L) mounted on top of the microscope.

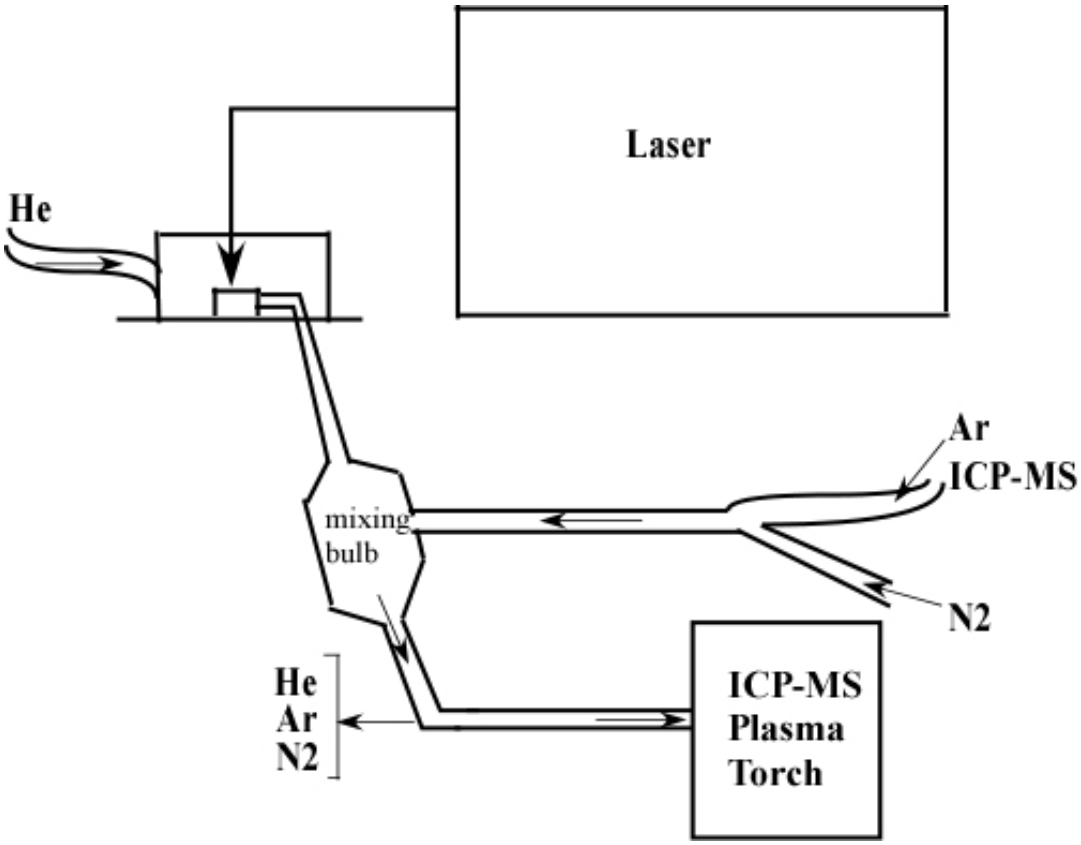


***Figure 3.1.b**. Schematic diagram of how the laser and ICP are connected and the gas flow paths of He, Ar and $N_2$.*

A mixing bulb, 7.5cm in length and 1.8 cm in diameter, was used to smooth the laser signal. The carrier gas used is ultra-high purity Helium with a flow rate of about 235 ml/minute. The instrument was optimized to obtain the highest sensitivity while keeping the Th/U ratio of NIST610 close to 1 to minimize inter-element fractionation, and also maintaining low levels of oxide production (ThO/Th<0.5%). For each session, the LA-ICPMS was tuned to the optimum sensitivity at 6J/cm2 fluence, 5 Hz and with a 44μm aperture. The count rate for $^{238}U$ signal intensity on NIST 610 is 4 million cps. The laser repetition rate was 10 Hz with laser energy fluence of 6.6 $J/cm_2$ measured by External Laser Energy Meter Coherent Field Max II. The laser output energy setting was 150 mJ. Individual trace elements were measured and with a specific dwell time as given below (Table 3.2.).

| Trace element | Dwell time (ms) |
|---|---|
| $^{178}Hf$, $^{181}Ta$ | 10 |
| $^{31}P$, $^{43}Ca$, $^{88}Sr$, $^{89}Y$, $^{157}Gd$, $^{159}Tb$, $^{163}Dy$, $^{165}Ho$, $^{166}Er$, $^{169}Tm$, $^{173}Yb$, $^{175}Lu$, $^{208}Pb$ | 20 |
| $^{93}Nb$, $^{140}Ce$, $^{146}Nd$, $^{147}Sm$, $^{153}Eu$ | 30 |
| $^{49}Ti$, $^{139}La$, $^{141}Pr$, | 40 |

***Table 3.2.*** *Individually measured trace elements with their dwell times (ms) in Coherent Geolas 193 nm ArF laser ablation unit coupled to a Varian 820-MS quadrupole ICPMS.*

Ar is used within the ICPMS and the flow rate was 1 ml/minute. The NIST610 standard was used to calibrate elemental concentrations; with NIST612 as a consistency check and Hf (zircon), CaO (garnet) and $TiO_2$ (rutile) concentrations determined by EMP were used as the internal standards to correct for matrix effects. To check the data quality NIST612 glass and zircon 91500 standards

were run prior to each session and were cross checked after every 10 to 12 analysis using a bracketing system. Aperture (spot size) was selected according to the size of the targeted zircon, garnet and rutile grains, and 31µm and 23 µm were most commonly used. The data were processed using the Glitter data reduction software for the LA-ICPMS (E.Van Achterberg et al., 1999).

## 3.5. (U-Th)-Pb Isotope Dating

U-Pb age data of zircons were obtained using a Coherent Geolas 193 nm ArF laser ablation unit coupled to a Varian 820-MS quadrupole ICPMS operated at high sensitivity mode. Energy output was 150 mJ. Individual isotopes were measured with a specific dwell time as given below (Table 3.3.a.).

| **Isotope** | **Dwell time(ms)** |
|---|---|
| $Si^{29}$ | 10 |
| $Pb^{204}$, $Pb^{206}$, $Pb^{208}$ $Th^{232}$, $U^{238}$ | 20 |
| $U^{235}$ | 30 |
| $Pb^{207}$ | 40 |

***Table 3.3.a.*** *Individually measured isotopes with their dwell time (ms) in Coherent Geolas 193 nm ArF laser ablation unit coupled to a Varian 820-MS quadrupole ICPMS.*

The total time for each analysis was 65 sec. First 25-30sec was used to warm up the laser without starting the ablation, i.e. with the shutter closed (Fig 3.2.a.). In this initial 25-30 sec the signals were very low or almost zero as no material was ablated. The flat part of the signal is called background. The laser shutter was opened and ablation started after 25-30sec of laser warm up. The elements were measured by ICPMS as mean raw cps (counts per second). The backgrounds were also measured in mean raw cps and were subtracted from the measured value of each element.

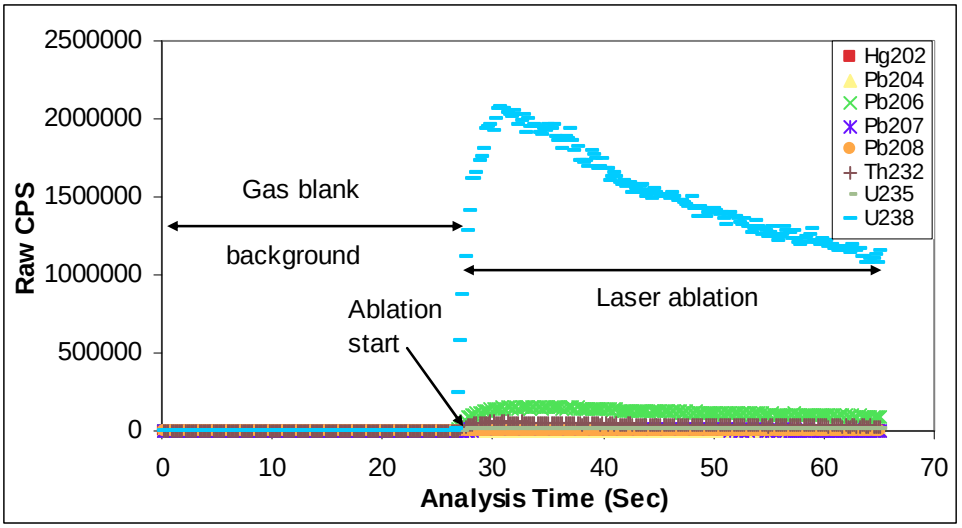


***Figure 3.2.a.*** *A diagram is showing the signal traces for a typical 65sec analysis for U-Pb age dating using LA-ICPMS. Arrows show where the background was measured and when the laser shutter was opened.*

The high purity helium flow rate was about 230-235 ml/min (optimized daily), spot size was 23 µm and the repetition rate was 10 Hz. GJ1 was used as primary standard and Temora2 was used as a secondary standard during most of the analyses (except in one session where we used Temora2 as primary standard). The age of GJ1 is around 609 Ma (Jackson et al., 1996) and Temora2 is of 417 Ma (Black et al., 2004). NIST-610 was used as a standard for correcting the concentration of U, Th and Pb.

| Date | Session | %RSD Primary standard | Secondary standard | Age ± 1SD |
|---|---|---|---|---|
| 8/12/08 | Single | GJ1<br>2.13%<br>(n = 11) | Temora2 (n=5) | 417.7±5.3<br>(RSD 1.28%) |
| 11/11/08 | 1st | Temora2<br>0.043%<br>(n=4) | | |
| | 2nd | GJ1<br>0.3772%<br>(n=4) | Temora2<br>(n=2) | 425±7.495<br>(RSD 1.78%) |
| 30/10/08 | 1st | GJ1<br>2.743%<br>(n=8) | | |
| | 2nd | GJ1<br>2.036%<br>(n=7) | | |
| 23/10/08 | Single | GJ1<br>4.743%<br>(n=10) | Temora 2<br>(n=4) | 421.15±5.18<br>(RSD 1.24%) |

***Table 3.3.b.*** *Reproducibility of standards and secondary standards of (U-Th)-Pb isotope dating for each session using LA-ICPMS, n= number of analysis, 1SD= 1 standard deviation, RSD=reproducibility.*

$^{238}U$ signal was attenuated in automatic mode. The detector of the ICPMS is saturated at about 5 million cps, and $^{238}U$ in some zircon can generate a similar or higher signal, therefore attenuation was set at Auto. When the $^{238}U$ signal is lower than 3 million cps, no attenuation will occur. When signal is higher than that 3 million cps, attenuation will happen but the software will calculate back to the real signal intensity. In this way high $^{238}U$ zircon can also be measured.

The attenuation factors are:

None-Medium- 66.795

Medium-High- 117.702

Data processing includes spike filtering of individual isotopes to obtain a smooth signal. Only the smooth part of the signals was used. Most of the zircons have older cores and younger rims in Fordland samples and sometimes the laser drilled through the boundary of core and rim, resulting in a mixed signal. In the case of mixed signals the signal mostly show different values varying from lower (rim) to higher (core) Pb/U ratio rather than with a constant Pb/U ratio (Fig 3.2.b.).

An undulated graph appears rather than a smooth graph. In that case only the smooth part of the signal was selected. In case of Fig 3.2.b. the first part of the signal from the rim is selected. Fig 3.2.c. shows almost a smooth signal without any mixing effect after laser ablation was started at 25 sec. In this case generally the whole signal will be selected. The age data were processed using Glitter data reduction software for the LA-ICPMS (E.Van Achterberg et al., 1999). The age calculations (weighted mean and intercept) were done using software Isoplot 3.00 *(Ludwig K, 2003).*

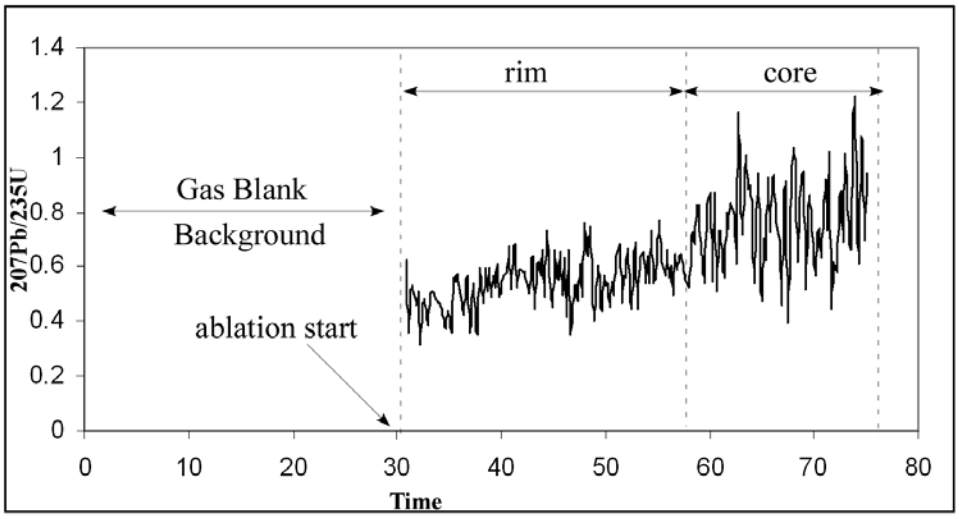


***Figure 3.2.b.*** *The graph is showing $^{207}Pb/^{235}U$ time resolved mixed signal of zircon for U-Pb age dating using LA-ICPMS.*

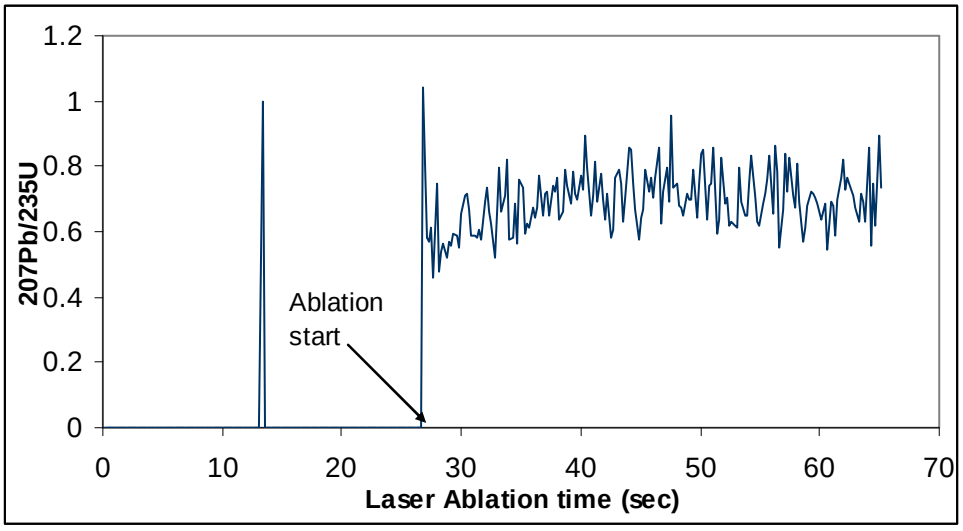


***Figure 3.2.c.*** *The graph is showing $^{207}Pb/^{235}U$ time resolved smooth signal of zircon for U-Pb age dating using LA-ICPMS.*

## 3.6. Lu-Hf Isotope Analysis

Lu- Hf isotope data were obtained using a Thermo-scientific Neptune multi-collector ICPMS coupled to a Coherent Geolas 193 nm ArF laser ablation unit. Laser energy output was maintained at around 6-7 J/cm$^2$. The high purity helium flow rate was set at about 200 ml/min (optimized daily); spot sizes were either 42 µm with 5Hz repetition rate or 58 µm with 4Hz repetition rate. Helium was used as a carrier gas exiting the sample cell and combined with Ar and $N_2$ from the Neptune and mixed in a Y- shaped tube (Fig 3.3.) before transporting into the ICPMS chamber.

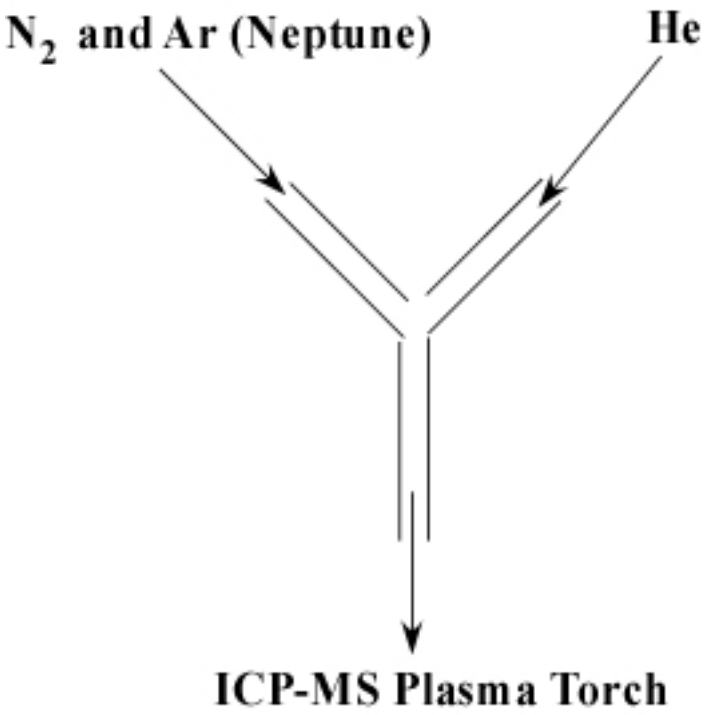


***Figure 3.3.*** *Gas flow paths and configuration of Y-tube in Neptune.*

Mud Tank, FC1 and Temora 2 zircons were used as standards. To check the data quality the standards were run and cross checked after every 12 to 15 analyses. The major issue for the accurate measurement of Hf isotopes in zircon concerns the isobaric interference of $^{176}$Lu and $^{176}$Yb on $^{176}$Hf. The isobaric interference correction of $^{176}$Lu and $^{176}$Yb on $^{176}$Hf has been discussed by number of authors (e.g., Thirwall and Walder, 1995; Griffin et al., 2002; Woodhead et al., 2004; Iizuka and Hirata, 2005; Hawksworth and Kemp, 2006; Wu et al., 2006; Gerdes and Zeh, 2006). The interference correction method in this study mainly followed that of Woodhead et al., (2004). Yb mass bias is obtained by directly measuring $^{173}$Yb/$^{171}$Yb during the run and calculating $^{176}$Yb/$^{177}$Hf using the natural $^{176}$Yb/$^{171}$Yb ratio. The values reported from different authors vary due to variations in using either technique or instrument. To get a close match of $^{176}$Hf/$^{177}$Hf over the range of Yb/Hf ratios with the published Yb pair solution work was carried out (Kemp et al., 2009) to assess which of the published values worked the best for the interference correction. In the Kemp et al., (2009) study, this turned out to be the best match with Segal et al., (2003) values. The match was not perfect because solutions behave differently from ablated aerosols, but the Segal et al., (2003) values also gave the best results on the standard zircons. In this study the analyses carried out at JCU also used the Segal et al., (2003) values. The Lu interference correction has been done by measuring $^{175}$Lu and using $^{176}$Lu/$^{175}$Lu=0.02655 (Vervoort et al., 2004). It is assumed that the mass bias behaviour of Lu is analogous to that of Yb. Time integration of each analysis is 0.524 sec and the number of blocks used was either 120 cycles (in 4Hz repetition rate) or 240 cycles (in 5 Hz repetition rate) depending on the spot size and repetition rate. The total measurement time for each analysis is approximately 1 min.

Different isotopes of Hf, Yb, Lu are set to be measured in Faraday's cup. The faraday cup configuration was used in this study is given in Table 3.4. Six different isotope ratios are measured: $^{176}Hf/^{177}Hf$, $^{178}Hf/^{177}Hf$, $^{179}Hf/^{177}Hf$, $^{180}Hf/^{177}Hf$, $^{173}Yb/^{171}Yb$ and $^{175}Lu/^{177}Hf$.

| Cup No | Species |
|---|---|
| L4 | $^{171}Yb$ |
| L3 | $^{173}Yb$ |
| L2 | $^{175}Lu$ |
| L1 | $^{176}Hf$, $^{176}Lu$, $^{176}Yb$ |
| C (centre) | $^{177}Hf$ |
| H1 | $^{178}Hf$ |
| H2 | $^{179}Hf$ |
| H3 | $^{180}Hf$ |

***Table 3.4.*** *Faraday cup configuration was used in this study in Neptune multi-collector ICPMS.*

# Chapter 4: Whole Rock Geochemistry of Mt Daniel Rock Groups

## 4.1. Introduction

This chapter represents the major and trace element chemistry of the different rock types of the study area in Fiordland. The whole rock geochemistry helps to understand the composition, process of formation and behaviour of different rock groups. In particular, the whole rock geochemistry helps to determine the relationship, if any, between the different rock groups of the area, and the role of magmatic processes (e.g. fractionation, magma mixing/mingling and differentiation) during crystallization of magma. The geochemical results also provide the basis for a detailed study of the individual rock groups as individual or correlated systems to understand the detail petrogenetic processes at the base of the crust.

The major and some trace elements, whole rock REE patterns, multi element spider diagram patterns and whole rock isotope geochemistry of different rock groups of the study area are discussed in detail in this chapter. The different analytical techniques for obtaining whole rock data are described in chapter-3. The geochemical and isotopic data are provided in Appendix 2.

## 4.2. Major & Trace Element Chemistry of Mt Daniel Rock Groups

The rocks studied from Mt Daniel, Fiordland have a wide range of silica variation, from 43 to 76 wt% of $SiO_2$. Of the main rock types: (1) WFO contains 43-58 wt% $SiO_2$; (2) Mafic dykes contain 43-47 wt% $SiO_2$; (3) low-Na intermediate dykes and 4) high-Na (trondhjemitic) intermediate dykes contain $SiO_2$ 56-60 wt%, 5) granitic dykes and the granitic phase in the MDC contain $SiO_2$ >66 wt% and Mount Daniel Sheets (MDS) vary from 53 to 60 wt% of $SiO_2$.

**Western Fiordland Orthogneiss:** The major element composition of WFO rocks show a significant increase in $Na_2O$ (~2.6-5.0 wt %) and $K_2O$ (0.6-2.2 wt %) and decrease in CaO (5.4-11.4 wt %), MgO (3.7-5.8 wt %), $Fe_2O_3$ (6.3-13.6 wt %), $TiO_2$ (1-1.7 wt %), $P_2O_5$ (0.35-1.55) and moderately constant but high $Al_2O_3$ (16.7-18.5 wt %) content with increasing $SiO_2$ (Fig 4.1.). The significant trace element variation is observed for Sr which shows increase in Sr content (1000-2000ppm) with decreasing $SiO_2$ (Fig 4.2.b.). V (131-352) and Zn (75-122) follow a similar trend (Fig 4.3.c, f). Other trace elements like Rb, Ba, Cr, Ni and Zr decrease with decreasing $SiO_2$ (Fig 4.3.a, b, e and 4.2.). Y and Sr/Y do not vary significantly with $SiO_2$ variation (Fig 4.2.c, d).

**Mafic dykes:** The major element compositions of mafic dykes show low $Na_2O$ (2.5-3 wt %) and $K_2O$ (0.7-1.35 wt %) and high MgO (7.16-7.5 wt %), CaO (8.8-9.8 wt %), $Fe_2O_3$ (10.9-15.7) and $TiO_2$ (1.5-3.17 wt %), $P_2O_5$ (0.35-0.7) and a medium $Al_2O_3$ (15.59-17.66 wt %) content (Fig 4.1.). The trace element compositions of mafic dykes show high Y, V, Cr, Ni and Zn content and low Rb, Ba, Zr, Sr, Sr/Y content (Fig 4.2. and 4.3.).

**Low-Na Intermediate Dykes:** The major element compositions show moderate concentration of $Na_2O$ (4.5-5.7 wt %), $K_2O$ (1.09-1.2 wt %), MgO (2.1-4.1 wt %), CaO (5.5-7.7 wt %), $Fe_2O_3$ (8.06-9.98) and $TiO_2$ (0.89-1.45 wt %), $P_2O_5$ (0.2-0.4) and moderate to high $Al_2O_3$ (16.7-19.7 wt %) content (Fig 4.1.). The distinctive trace element composition is very high concentration of Zn (116-181 ppm) (Fig 4.3.f.), high content of Y (Fig 4.2.c.) and moderate to high content of V (Fig 4.3.c.). Cr is high in MD-8 and low in MD-22A (Fig 4.3.d.). Rb, Ba, Ni (Fig 4.3.a, b, e), Zr (Fig 4.2.a.) and Sr content is moderate (Fig 4.2.b.).

**High-Na Intermediate Dykes (trondhjemitic variety):** The major element compositions of trondhjemite dykes show very high $Na_2O$ (7-8.6 wt %) and $Al_2O_3$ (20.7-22.7 wt %), moderate $K_2O$ (0.6-1.7 wt %), MgO (0.3-1.9 wt %), CaO (4.2-6.1 wt %) and low $Fe_2O_3$ (0.9-3.9 wt %), $TiO_2$ (0.7-0.14 wt %) and $P_2O_5$ (0.089-0.59) content (Fig 4.1.). The trace element compositions show a wide range of Zr content (90-1000ppm), extremely high content of Sr (1771-2469ppm) and very low content of Y (<0.5-12.4). They are therefore high Sr/Y granitic rocks. The trondhjemite dykes also show moderate concentrations of Rb and Ba and low concentrations of V, Cr, Ni and Zn (Fig 4.3.).

**Granites:** Granites have high $K_2O$ (1.6-5.0 wt %) content and low $Na_2O$ (2.9-5.3 wt %), MgO (0.2-0.9 wt %), CaO (0.6-3wt %), $Fe_2O_3$ (1.6-4.4 wt %), $TiO_2$ (0.19-0.4 wt %) and $P_2O_5$ (0.04-0.13) with moderate $Al_2O_3$ (12.6-16.6 wt %) (Fig 4.1.). The trace element compositions show the highest content of Rb (37-86 ppm), and moderate to high Ba (699-1883 ppm). Rb and Ba increase with increasing $SiO_2$ (Fig 4.3.a, b). Sr and Zn decrease with increasing $SiO_2$ (Fig 4.2.b and 4.3.f). Granites have moderate Zr, Y , low Sr/Y (Fig 4.2.a, c, d)and very low V, Cr, Ni content (Fig 4.3.c, d, e).

**Mt Daniel Sheets**: Samples from Mount Daniel sheets (MDS) are of intermediate composition. They are denoted as either intermediate rocks or MDC. These rocks show high $Na_2O$ (4.4-6.4 wt %), low $K_2O$ (0.6-1.6 wt %) and moderate $Al_2O_3$ (16.7-20.7 wt %). CaO (4.2-7.7 wt %), MgO (0.9-4.1 wt %), $Fe_2O_3$ (6.4-11.7 wt %) and $TiO_2$ (0.75-1.6 wt %) and $P_2O_5$ (0.06-0.7) all decrease with increasing $SiO_2$ (Fig 4.1.). The trace element compositions show moderate Sr, Y, Rb, Ba (Fig 4.2.b, c and Fig 4.3.a, b) low to moderate Zr (Fig 4.2.a.), moderate to high Zn (Fig 4.3.f.), moderate to low Sr/Y, V (Fig 4.2.d and 4.3.c) and low Cr, Ni content (Fig 4.3.d and e).

**Overall Major Element Geochemical Patterns of Different Rock Groups of Mt Daniel**

All rock groups, with the exception of the WFO and the trondhjemites, form a coherent geochemical array on Harker diagrams. $K_2O$ (Fig 4.1.a.) is the only major oxide that increases with $SiO_2$. $Na_2O$ (Fig 4.1.b.) and $Al_2O_3$ (Fig 4.1.c.) show bell shaped trends with $SiO_2$ with considerable scatter of data. The variation diagram of CaO (Fig 4.1.d.), MgO (Fig 4.1.e.), $Fe_2O_3$ (Fig 4.1.f.), $TiO_2$ (Fig 4.1.g.) and $P_2O_5$ (Fig 4.1.h.) show progressive depletion with increasing $SiO_2$ content. $K_2O$, MgO, $TiO_2$ and $P_2O_5$ show curvilinear trends (Fig 4.1. a, e, g and h.). CaO and $Fe_2O_3$ show a sub-linear trend (Fig 4.1.d. and f.). The two end member compositions of each of these trends are mafic dykes and granite dykes.

The high-Na intermediate (trondjhemitic) dykes have distinctively higher $Na_2O$ and $Al_2O_3$, and low $TiO_2$ and $Fe_2O_3$, compared with all other rock-types. Along with the other two analysed intermediate dykes, which are low-Na (MD-8 and MD-22A), they show a distinctive curvilinear trend that is highly oblique to the MDS array. $Na_2O$ and $Al_2O_3$ increases markedly from MD-8 (low-Na intermediate dyke) to MD-17B (intermediate high-Na trondhjemite dyke). The granites (granitic dykes and granitic phases in MDC) are clustered at the higher silica end with low to medium $Na_2O$ content.

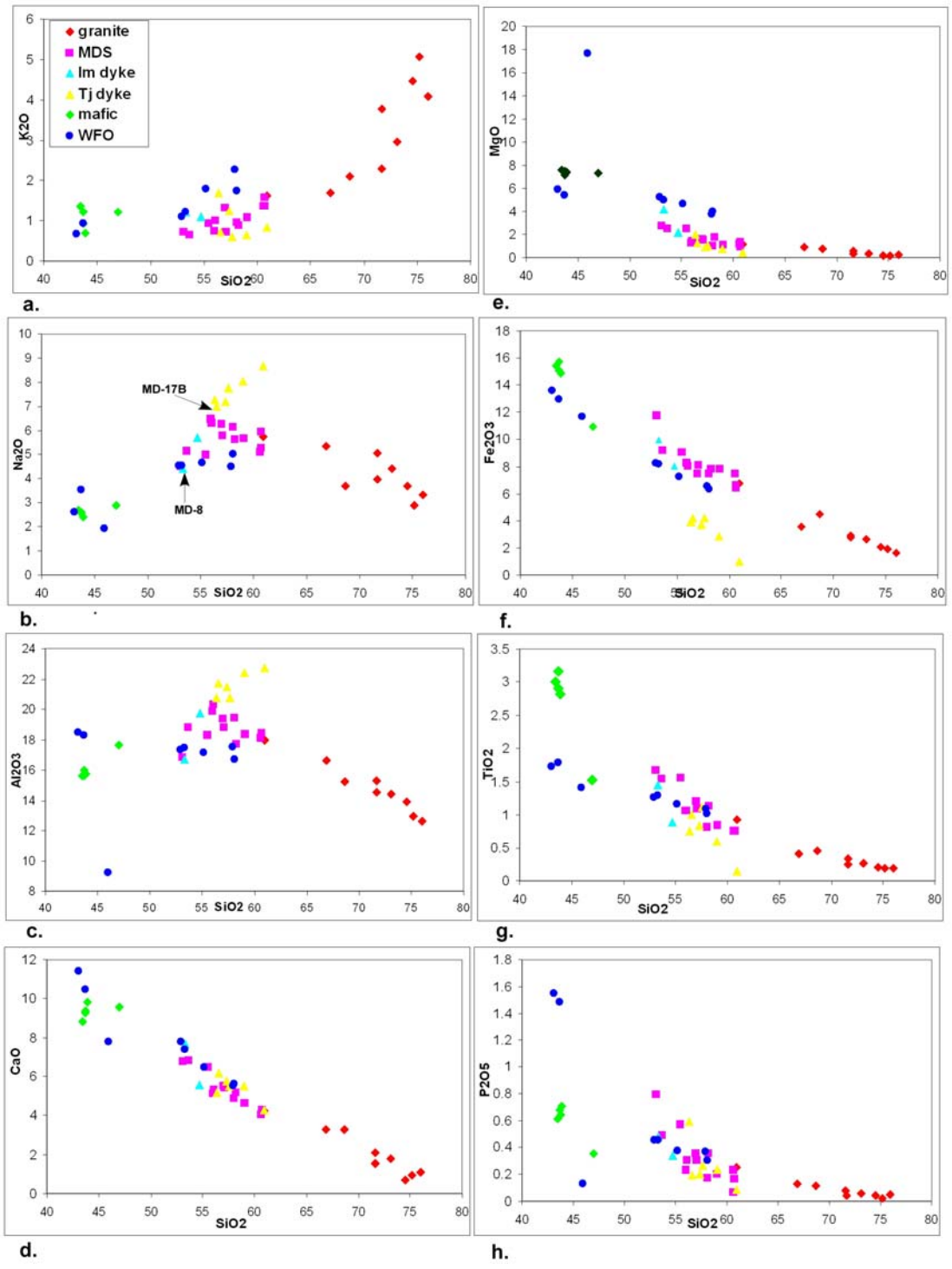


***Figure 4.1.*** *Major element Harker diagrams of Mt Daniel rocks* ***(a)*** *$SiO_2$-$K_2O$ plot shows increasing abundance with increase in silica* ***(b)*** *$SiO_2$-$Na_2O$ and* ***(c)*** *$SiO_2$-$Al_2O_3$ plots show bell shaped trends, except for the high Na-dykes, which plot above that trend;* ***(d)*** *$SiO_2$-CaO;* ***(e)*** *$SiO_2$-MgO;* ***(f)*** *$SiO_2$-$Fe_2O_3$,;* ***(g)*** *$SiO_2$- $TiO_2$ and* ***(h)*** *$SiO_2$-$P_2O_5$ plots show deceasing abundance with increasing silica content.*

**Overall Trace Element Geochemical Patterns of Different Rock Groups of Mt Daniel**

The WFO, mafic dykes, granites and some of the MDC samples have a similar range of Zr content (between 40-370ppm). The WFO shows a linear trend of increasing Zr content with increasing $SiO_2$ (Fig 4.2.a.). The intermediate dykes (low and high-Na) follow a single trend on Zr-$SiO_2$ plots. The Zr decreases in the high Na dykes and increases in the granites with increasing silica content.

The mafic dykes, some of the intermediate rocks (MDC), and granites show a wide range of Sr content (150-900 ppm), among them the granites have the lowest concentration of Sr. The intermediate dykes (low and high-Na) follow a single trend from low to high Sr (Fig 4.2.b.). The Sr content increases with decreasing $SiO_2$ for WFO rocks. The Sr show an opposite trend to Zr where Sr increases in the high-Na dykes and decreases in the granites with increasing silica.

In the Y-$SiO_2$ variation diagram (Fig 4.2.c.), the data are scattered within a range of (0-60 ppm). The high-Na intermediate dykes (trondhjemite dykes) have the lowest concentration and the mafic dykes have the highest concentration of Y. The WFO rocks also contain low to medium Y, which decreases with increasing silica. MDS samples are widely scattered from medium to high Y content. The Y contents of the granites are also scattered between low to medium values. Y-$SiO_2$ plot is similar to Zr- $SiO_2$ plot but more scattered suggesting that Y is controlled by zircon crystallisation. The only group this doesn't hold for is the high-Na intermediate dykes, which presumably have low Y because of having garnet in the source residue.

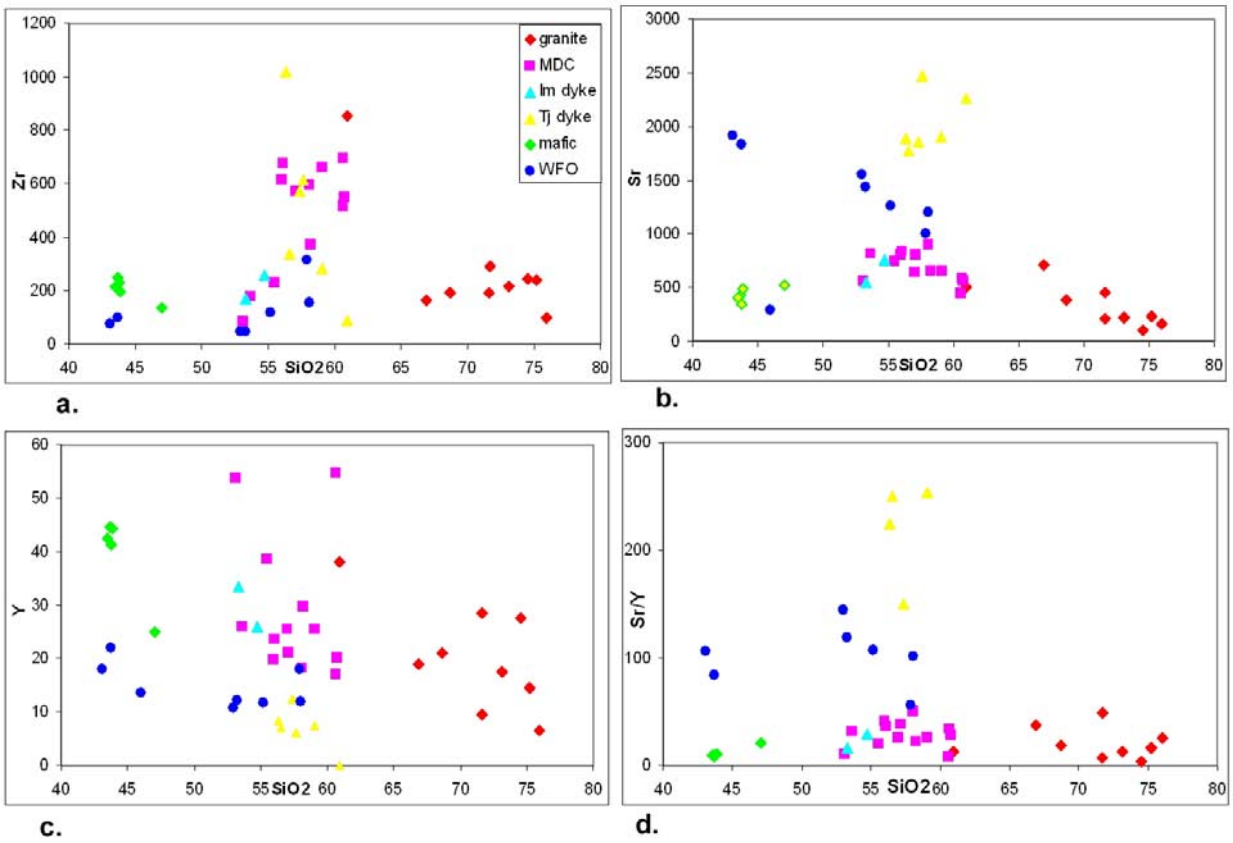


***Figure 4.2.*** *Trace element Harker diagrams of Mt Daniel rocks.* ***(a)*** *$SiO_2$-Zr;* ***(b)*** *$SiO_2$-Sr;* ***(c)*** *$SiO_2$-Y;* ***(d)*** *$SiO_2$- Sr/Y.*

In Sr/Y-$SiO_2$ plots (Fig 4.2.d.), most of the rocks have ratios <60, with only some scattered value towards high Sr/Y. All the High-Na (trondhjemitic) intermediate dykes have very high Sr/Y (Fig 4.2.d.) except one sample MD-17B, which has high Sr content but very low Y content (<0.5ppm) and thus low Sr/Y ratio.

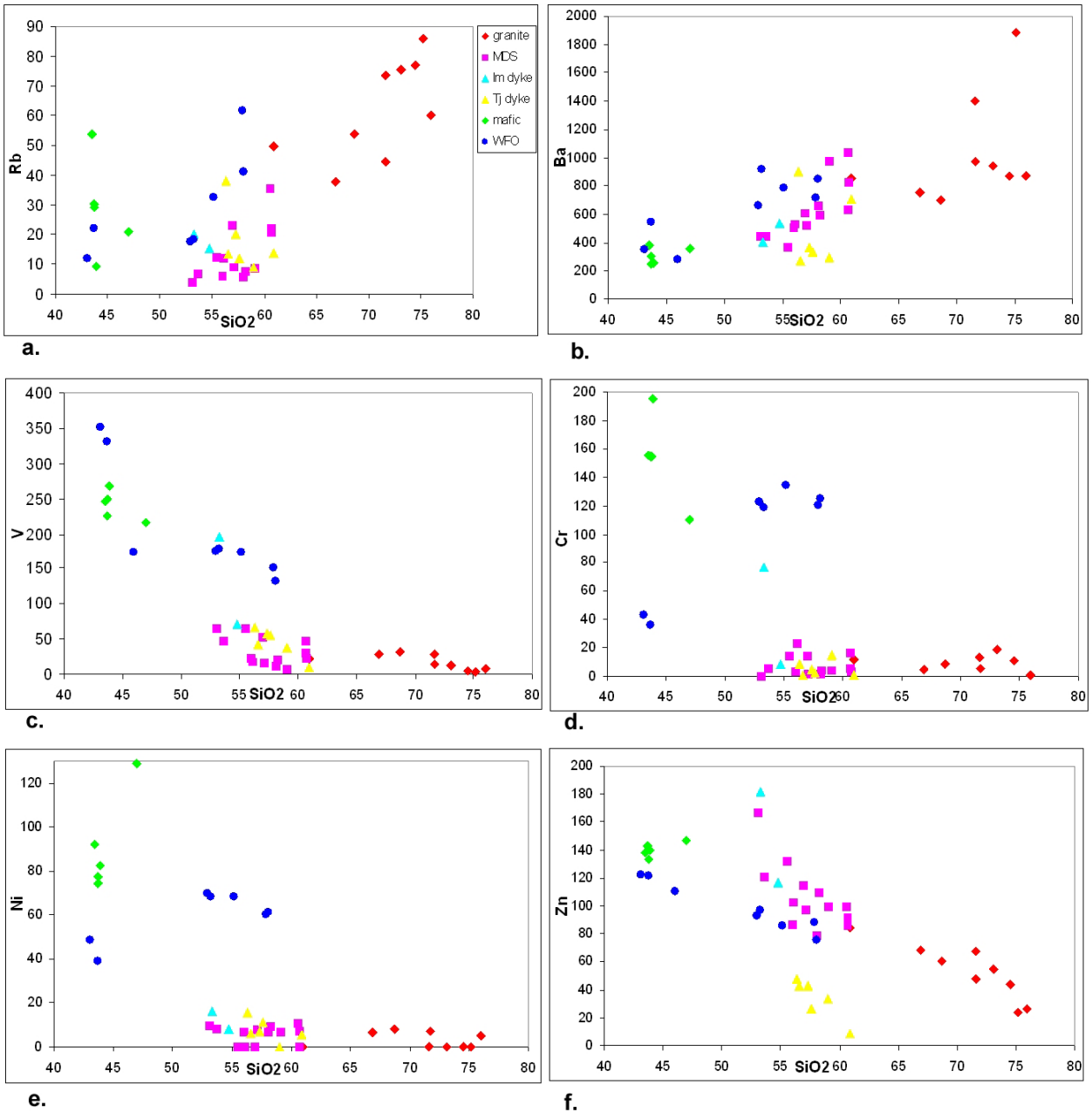


***Figure 4.3.*** *Trace element Harker diagrams of Mt Daniel rocks.* ***(a)*** *$SiO_2$-Rb and* ***(b)*** *$SiO_2$-Ba increases with increasing $SiO_2$;* ***(c)*** *$SiO_2$-V;* ***(d)*** *$SiO_2$-Cr and* ***(e)*** *$SiO_2$-Ni decreases with increasing silica;* ***(f)*** *$SiO_2$-Zn is showing a nearly linear trend where Zn is increasing with decreasing $SiO_2$ and trondhjemites are offset from the trend.*

Other trace elements like Rb (Fig 4.3.a.) and Ba (Fig 4.3.b.) increase with increasing $SiO_2$, similar to $K_2O$, although Ba is significantly lower in the high-Na dykes. V, Cr and Ni (Fig 4.3.c. to e.) decrease with increasing $SiO_2$ and vary in a similar fashion to MgO. Like MgO, all decrease significantly above ~55% SiO2, which contrasts strongly with the WFO, demonstrating they are not linked to that magmatic system. Zn (Fig 4.3.f.) follows a similar trend to $Fe_2O_3$.

## 4.3. REE Patterns of Mt Daniel Rock Groups

REE analysis was undertaken on seventeen representative samples, most of which were further analysed for zircon study. The REE data of representative samples is presented in Appendix 2.2. The REE patterns of individual rock groups show different characteristics.

**Western Fiordland Orthogneiss:** The WFO pattern (Fig 4.4.a) shows a moderate negative slope, with LREE enrichment (~60x chrondrite) but near chondritic HREE (3-4x) values. $(La/Yb)_n$ is13-14. A small negative Eu anomaly is present for both the intermediate and mafic samples.

**Mafic and low–Na intermediate Dykes:** The mafic dykes have a flatter pattern compared to the WFO (Fig 4.4.b), with slightly lower LREE concentrations, but higher HREE concentrations. HREE concentration is around 10 times of chondritic values. There is no Eu anomaly.

The two low-Na, intermediate dykes MD-8 and MD-22A have very similar REE patterns (Fig 4.4.c), which are both similar to the mafic dykes, except that the HREE abundances are slightly lower (<10x chondrite).

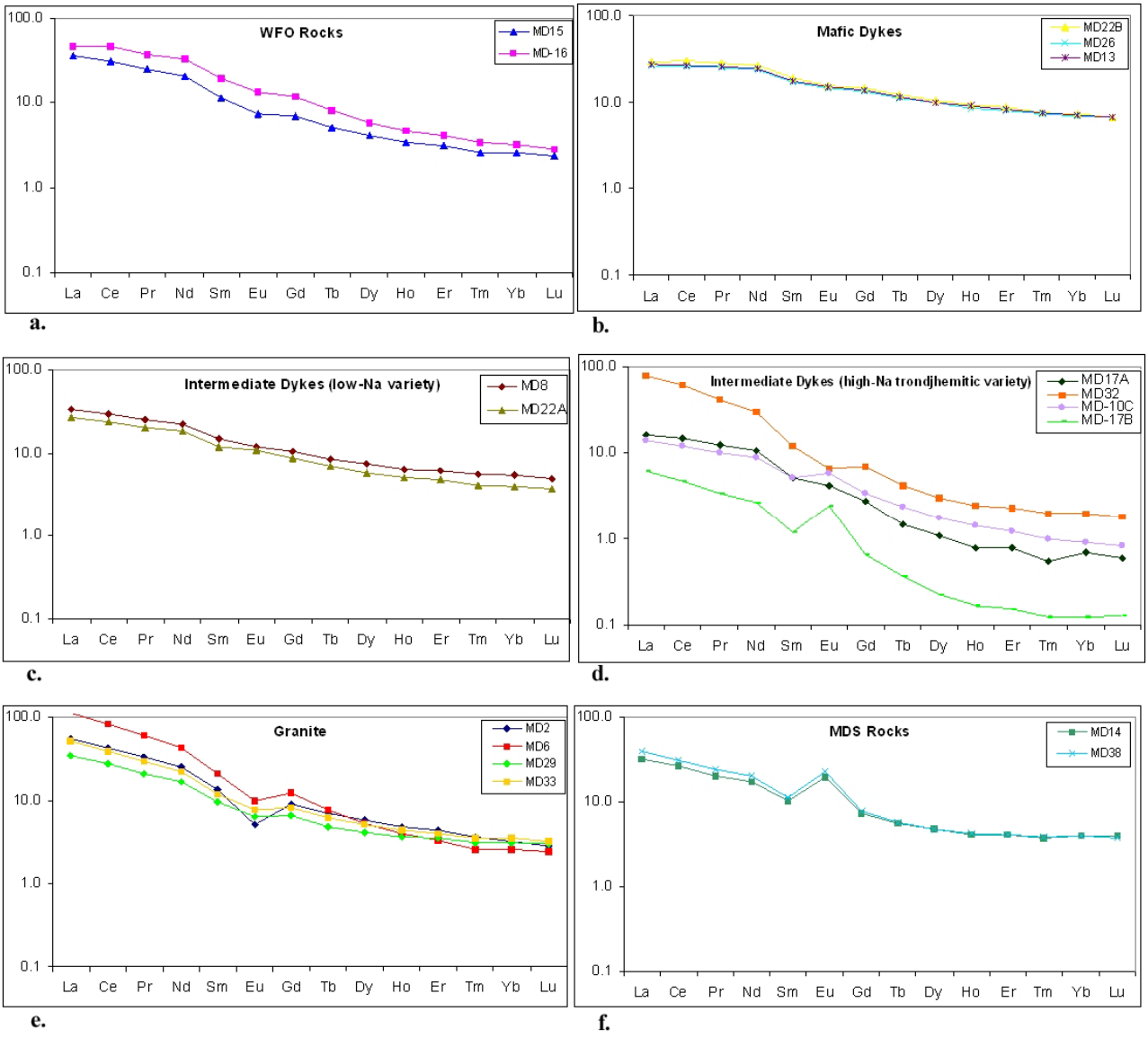


***Figure 4.4.*** *Whole rock Rare Earth Element patterns of mafic, intermediate and granitic rock groups of Mt Daniel, Fiordland normalized to primitive mantle (Sun and McDonough 1989).* ***(a)*** *WFO rocks,* ***(b)*** *Mafic Dykes,* ***(c)*** *Low-Na intermediate Dykes,* ***(d)*** *High-Na intermediate dykes (trondhjemitic variety),* ***(e)*** *Granitic dykes (MD-2 and MD-6) and granitic sheets (MD-29 and MD-33) in MDC.* ***(f)*** *Mt Daniel Sheets.*

**High-Na Intermediate dykes (trondhjemitic variety):** The trondhjemite dykes show (Fig 4.4.d) markedly different REE patterns for different rock types. They show strongly fractionated REE patterns with $(La/Yb)_n$ > 20, with highest ratio of $(La/Yb)_n$ = 50 for MD-17B. MD-17A and MD-10C have LREE abundances similar to the low-Na intermediate dykes, but much lower HREE abundances. The pattern is steep for the MREE but flattens for the HREE. MD-10C has a slight positive Eu anomaly.

MD-32 has a similar pattern to MD-17A and -10C, but with higher concentrations of all REE. It also has a slight negative Eu anomaly. The most distinctly different sample is MD-17B, which has a strong Eu anomaly and strong depletion of MREE and HREE. MD-17B is an end-member composition of the intermediate dyke array, having the highest silica content (60.93 wt %) and lowest MgO, FeO and $TiO_2$ contents. It appears to have mineral accumulations that are opposite that of MD-17A and -10C.

**Granites**: Granites (Fig 4.4.e) have steep negatively sloping LREE, moderate negatively sloping MREE and nearly flat HREE. Granitic dykes and granites in MDC show similar REE patterns. MD-6 is highly fractionated $(La/Yb)_n$ = 46 whereas MD-2, MD-29 and MD-33 are moderately fractionated $(La/Yb)_n$ = 11-17. MD-6 is enriched in LREE compared to the other granites and has the lowest concentration of HREE. The Eu anomaly is strongly negative in MD-6 but weak in MD-2, MD-29 and MD-33. MD-6 has higher LREE and MREE abundance and lowest HREE abundance compared to other granitic varieties. All the rocks have nearly flat HREE patterns and HREE concentration close to 5-6x times of chondritic value. The rocks show strong to medium negative Eu anomalies. The granites show strongest similarity to MD-32, a high-Na intermediate dyke.

**Mt Daniel Sheets:** The two representative MDS (Fig 4.4.e) have a concave up REE pattern with a strong positive Eu anomaly. They are most similar to MD-17A, but with much higher MREE and HREE. LREE abundances are more typical of the low-Na intermediate dykes.

## 4.4. Multi Element "Spider" Diagrams of Mt Daniel Rock Groups

Multi element spider diagrams, normalised to N-MORB, show different patterns for different rock groups.

**Western Fiordland Orthogneiss:** The WFO (Fig 4.5.a) has marked negative Nb and Ta anomalies and Ti and P troughs are present. Positive K, Ba, Pb and Sr spikes also exist. A continuous depletion of HREE from Sm to Lu is observed except Gd. The HREE have values close to N-MORB, though the pattern is sloped, not flat.

**Mafic Dykes:** The mafic dykes have (Fig 4.5.b) a less spiked pattern, though K, Pb and P spikes are observed. An extremely deep Ta-Nb trough might reflect analytical error, as U is also very low. The moderate slope of the pattern suggests the mafic dykes are somewhat alkaline, but they are not OIB like. Rather, they more closely resemble basalts formed in arcs with thick crust (Mantle and Collins, 2008).

**Low-Na Intermediate Dykes:** Low-Na intermediate dykes (Fig 4.5.c) have well developed negative Nb-Ta and Ti anomalies and spikes of Ba, K, Pb and to a lesser extent, Sr. They have lower HFSE abundances than the mafic dykes, and a slightly steeper slope. The overall pattern most closely resembles the WFO rocks, although they have a more subdued K spike, and slightly lower HREE.

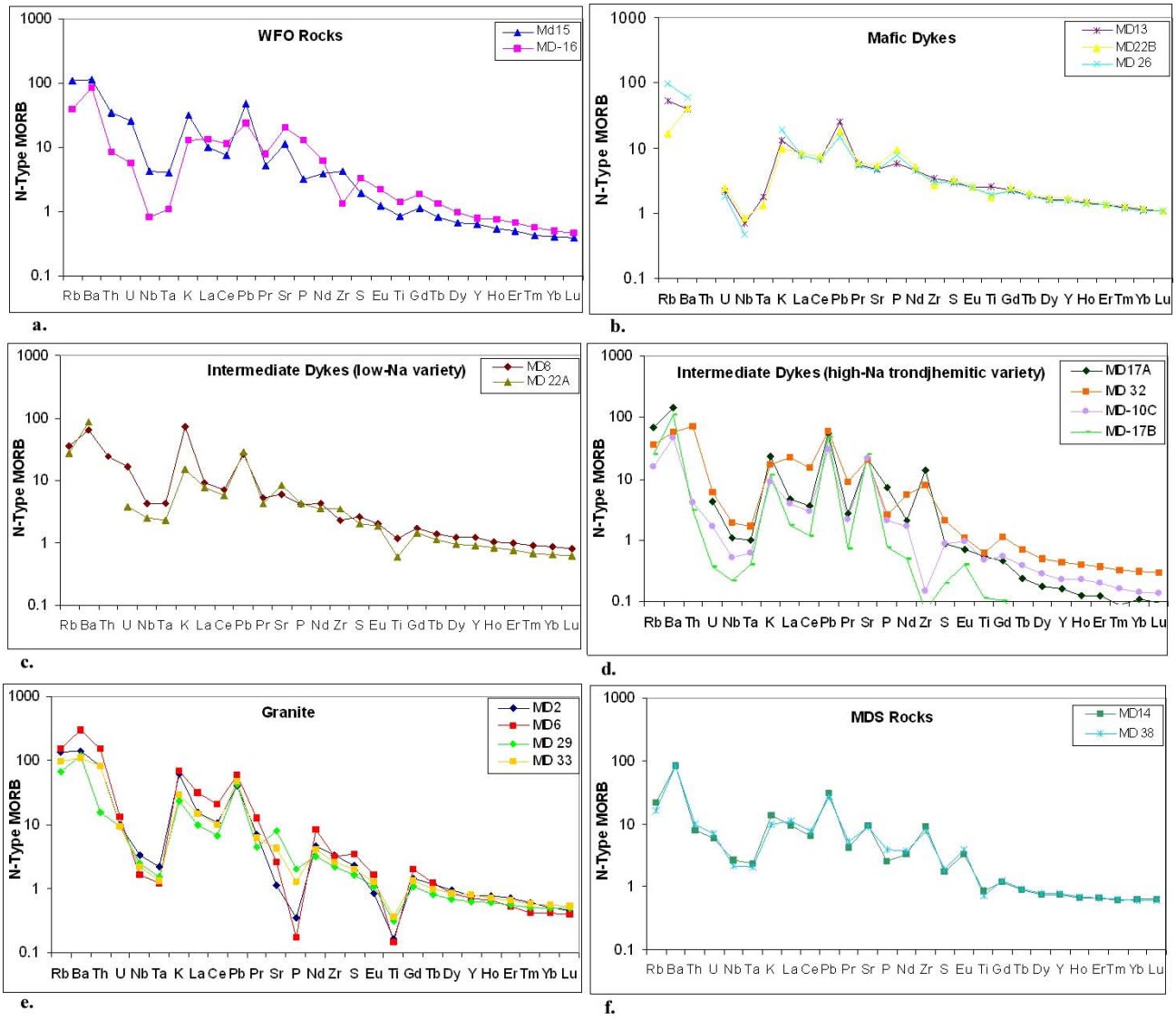


***Figure 4.5.*** *Multi element diagrams of the Mt Daniel rocks normalized to N-type MORB (Sun and McDonough 1989).* ***(a)****WFO rocks;* ***(b)*** *Mafic Dykes;* ***(c)*** *Low-Na intermediate dykes;* ***(d)*** *High-Na intermediate dykes;* ***(e)*** *Granitic dykes (MD-2 and MD-6) and granitic sheets in MDC (MD-29 and MD-33;* ***(f)*** *Mt Daniel Sheets.*

**High-Na Intermediate Dykes (trondhjemitic variety):** Trondhjemite dykes are the most heterogeneous group, but they all have a characteristic pattern. They have (Fig 4.5.d) deep negative U, Nb-Ta, and U anomalies, and marked positive K, Pb, Sr and Zr anomalies (with one exception). However, all but MD-17B have marked HREE depletions.

**Granites:** Granites include both granitic dykes and granitic rocks from the MDC. They show (Fig 4.5.e) strong negative Nb-Ta, U, P and Ti anomalies and positive K, Ba and Pb. MD-6 shows slightly positive Nd and Gd anomalies. All the granites have low Rb content, relative to Ba and K. Hence, they have high K/Rb and Ba/Rb rations. The LILE pattern is somewhat similar to that for the high-Na dykes.

**Mt Daniel Sheets:** The samples from MDS (MD-14 & MD-38) exhibit (Fig 4.5.f) negative Th, U, Nb-Ta, U, and Ti anomaly and positive Ba, K, Pb, Sr, Zr, and Eu anomalies. The HREE pattern and abundances resemble the granites, whereas the LILE pattern is similar to the low-Na intermediate dykes, yet the HFSE pattern is strongly spiked, similar to the high-Na dykes. The MDC rocks therefore appear to have a combination of geochemical characteristics.

## 4.5. Whole Rock Isotope Analysis of Mt Daniel Rock Groups

Nd-Sr whole rock isotopic compositions were determined for 20 samples across the entire silica range. Sm-Nd isotope data of the samples are provided in appendix 2.3.

All of the samples have $^{147}Sm/^{144}Nd$ ratios close to 0.1 and $^{143}Nd/^{144}Nd$ ratios show an average of 0.5125 (see appendix) which is similar to CHUR (DePaolo & Wasserburg 1976). Initial Nd, Sr isotope ratios and εNd values are calculated on the basis of the average emplacement age of the WFO at 125 Ma (see chapter-6).

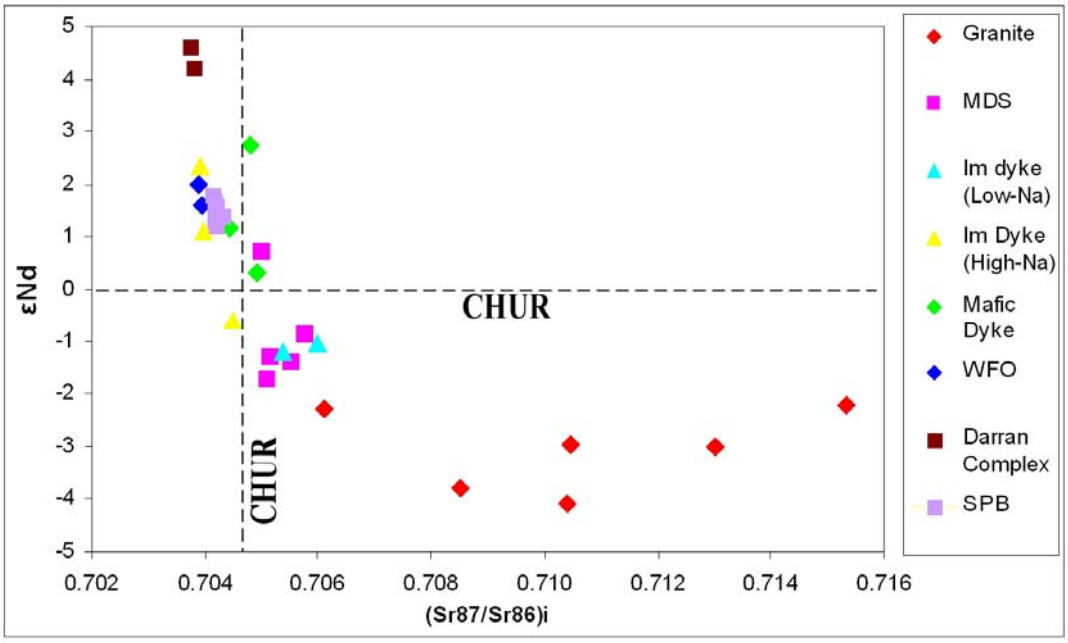


***Figure 4.6.*** εNd vs. $^{87}Sr/^{86}Sr_i$ plot of different rock types from Mt Daniel, Separation Point Batholith (from Muir et al., 1995) and Darran Complex (from McCulloch et al., 1987), Fiordland. The different types of rocks have been shown with different colours.

**Comparison of Isotopic values from Different Rock Types of Mt Daniel**

The εNd vs. $^{87}Sr/^{86}Sr_i$ plot (Fig 4.6.) shows the isotopic variation and trend of MDC rocks. WFO rocks range between εNd 1.59 to 2.01 and low $^{87}Sr/^{86}Sr$ initial ratios 0.7039-0.7040. The εNd and initial Sr values are quite restricted, given the large range of SiO2 composition. The mafic dykes have a range of εNd values vary from 0.32 to 2.74 with very similar $^{87}Sr/^{86}Sr$ initial ratios 0.7044-0.7049. MD-13 has highest εNd +2.74 and MD-26 has the lowest εNd +0.32 values with similar $^{87}Sr/^{86}Sr$ initial ratio of 0.7048 and 0.7049 respectively. The high-Na intermediate dykes (trondhjemitic variety) show ranges of εNd values vary from -0.59 to +2.34 with $^{87}Sr/^{86}Sr$ initial ratios 0.7039-0.7045. The two low-Na intermediate dykes have very similar εNd values -1.04 to -1.20 and initial $^{87}Sr/^{86}Sr$ ratios of 0.7054-0.7060. The granites have a wide range of εNd values -2.22 to -4.09 and initial $^{87}Sr/^{86}Sr$ ratios 0.7061 to 0.7153. MD-2 has the highest initial $^{87}Sr/^{86}Sr$ ratio and lowest εNd value. The MDS rocks have εNd values ranges from -1.73 to 0.72 and initial $^{87}Sr/^{86}Sr$ ratios 0.7050-0.7058.

Whole rock isotopic data from Separation Point Batholith (Muir et al., 1995) are plotted on εNd vs. $^{87}Sr/^{86}Sr_i$ in (Fig 4.6.) and show a very similar signature to the high-Na dykes of the MDC and WFO. Two samples of Darran Complex rocks (McCulloch et al., 1987) are plotted on εNd vs. $^{87}Sr/^{86}Sr_i$ in (Fig 4.6.) have a more mantle like signature (εNd 4.2 to 4.6 and low initial $^{87}Sr/^{86}Sr$ 0.70374 to 0.70380).

## 4.6. Interpretation

Major and trace elements variation diagram trends, REE patterns, patterns of multielement diagrams and eNd-Sr isotopic evidence, suggest that these trends or patterns are controlled by partial melting, magma mixing or fractional crystallization processes, or a combination of all the processes. The chemical variation of the various rock systems at Mount Daniel are briefly explained below, although more detailed explanation will occur in chapter-9 and 10 where the detailed isotopic and geochronological information can also be considered to evaluate different petrogenetic processes.

## A. Evidence for Partial Melting

Some of the rock groups have the mafic dykes, the high-Na intermediate dykes and the granites; record some effect of partial melting supported by their geochemistry, as discussed below.

**Mafic Dykes:** The much flatter REE patterns of mafic dykes, compared to the WFO, suggest they formed in different environments. With REE concentration ~10 times chondrite for the mafic dykes, this suggests an absence of garnet from the magma source region. Equally, absences of Eu anomalies indicate the absence of plagioclase in the source rock. These indicate that the mafic magmas may have derived from a source where garnet and plagioclase both were absent. Presumably, these basaltic melts were produced in the spinel lherzolite stability field.

The isotopic signature shows that the mafic dykes (MD-13 and MD-22B) have positive εNd values (+1 & +3) and low initial $^{87}Sr/^{86}Sr$ ratio (0.7044 & 0.7048), indicating derivation of these magmas from a mantle like source which is isotopically depleted relative to the bulk earth, but less extreme than depleted mantle (DMM). The mafic dyke sample MD-26 has a much lower value of εNd +0.32 which indicates either the effect of crustal assimilation or a higher slab flux component. This will be evaluated in chapters 8 and 9.

**Low-Na Intermediate Dykes:** The two analysed intermediate dykes have very similar REE patterns to the mafic dykes, but with slightly higher LREE/HREE ratios: $(La/Yb)_n$=6-7 versus 3-4 for the mafic dykes. They do not have Eu anomalies. The similarity of patterns suggests they may have been derived from similar sources to the mafic dykes, even though their silica content is ~10% higher. The flat patterns indicate a lack of garnet and plagioclase in the source. However, the isotopic values for the low-Na intermediate dykes are more crustal-like than the mafic dykes (εNd +1 to -2), indicating that other source components may have been involved in their genesis, as discussed in later sections.

**High-Na Intermediate Dykes:** Trondhjemitic dykes show distinctly different, steep, curved, REE patterns with depleted HREE concentrations, compared with the other rock types. Also, the variation of REE patterns within this group of dykes is remarkable. A feature of the variation is that as the REE become more depleted, a positive Eu anomaly develops.

The positive Eu anomalies might suggest plagioclase accumulation in the more sodic dykes, but these dykes have lower Eu content than the mafic or low-Na intermediate dykes. Rather, it appears that the Eu anomaly occurs because the MREE and HREE are being depleted more rapidly than Eu. Given these are narrow, fine grained dykes, this is likely to be a source region effect rather than a result of cumulate processes, where the more $SiO_2$- and $Na_2O$-rich dykes have more efficient removal of HREE-bearing phases during partial melting.

This is likely to be residual garnet and it might reflect either lower degrees of partial melting and/or greater depth of melting for the more silica-rich dykes. The latter possibility raises the intriguing possibility that the source region was undergoing pressure changes during partial melting to form the dykes.

The dyke with the highest abundance of REE (MD-32) has a negative Eu anomaly, and an overall REE pattern more closely resembling the granites. This might suggest the chemical variation in the intermediate dykes might also be a result of interaction of several source components. This is confirmed by the isotopic variation. MD-17A, the most sodic dyke, has a mantle-like signature ($\varepsilon Nd$ +2.34; $Sr_i$ = 0.7039) whereas MD-32 has $\varepsilon Nd$ (-0.59) and an initial Sr ratio of (0.7045). MD-17B has an intermediate value of $\varepsilon Nd$ (1.11) and initial Sr ratio (0.7040). This isotopic variation suggests that the high-Na dykes may have been derived from various sources, as discussed below.

**Granites:** The high K/Rb in the granites (Fig 4.4.f.) is considered to be significant and may suggest that biotite exists in the source rock residue during melting. This is because biotite has much higher mineral/liquid partition coefficients for Rb. The probable presence of biotite in the granitic source rock residue suggests melting in the presence of a fluid, rather than the typical fluid-absent melting to produce granitic melts under granulite facies conditions (e.g. Clemens and Wall, 1981). Hydrous melting of biotite also suggests relatively low degrees of partial melting, which would suggest that the strong negative Ti and P anomalies are due to retention of solid phases in the source region, such as titanate and apatite.

This is evaluated more fully in Chapter 10. The granites have variably negative $\varepsilon Nd$ values (-2 to -4) and have variably high Sr initial ratios of 0.7061-0.7153, suggesting that the magmas were either derived from a variably radiogenic crustal component, or that several source components were involved in their genesis. This is discussed below.

## B. Evidence for Mixing

The most compelling evidence for mixing at Mt Daniel comes from field (chapter-2) and isotopic data (Fig 4.6), which suggests that a series of mafic, intermediate and felsic dykes have mixed to form the measured chemical and isotopic array. The most obvious isotopic array is from the mafic to granitic dykes, with most other samples fitting somewhere between. In particular, the low-Na intermediate dykes cluster in an intermediate position on the isotope array. The REE and multielement patterns of these dykes (MD-8 and MD-22A) also show the combined effects of mixing between the mafic and granitic end-members. The HFSE pattern resembles the mafic rocks, but the LILE pattern resembles the granitic rocks (Fig 4.5.). Therefore, we concluded that at least two source components exist; the mafic dykes and the high-K granitic dykes.

By contrast, the isotopic values for the high-Na intermediate dykes vary by 3 epilson Nd units, indicating that their chemical variation is partly a result of mixing of different source components. However, their chemical trend for almost all elements is highly oblique to the dominant chemical arrays, suggesting that another component must be involved in the mixing. The low-Na intermediate dykes lie at the low silica end of the high-Na (trondhjemitic) chemical array (Fig 4.2). However, they also lie at the more isotopic evolved end of the isotopic array (Fig 4.6.), extending that array by one epsilon Nd unit. The chemical and isotopic variation is consistent with a third "trondhjemitic" dyke component being involved in generation of the petrological array observed at Mt Daniel.

**Mt Daniel Sheets:** The MDS samples are the sheeted complex at Mt Daniel that cluster as a triangular array of points (Fig 4.1. and 4.7.), which fall on the high silica side of the intermediate (low-Na to high-Na) dyke array, projecting toward the granite dyke compositions on Harker diagrams (Fig 4.1.). MDS rocks have a positive Eu anomaly, similar to that seen for MD-17B (one of the high-Na dykes), but the elevated LREE contents and LREE pattern is more similar to the

low-Na dykes, as is the HREE content. The similarities of these REE patterns suggest that the MDS have a similar hybrid origin to the intermediate dykes. They also closely overlap with the low-Na dykes on the isotope array (Fig 4.6.), consistent with this cogenetic relationship.

Nonetheless, the MDS have quite similar REE and multielement patterns with the granitic dykes, which again suggest a mixing of more than two components to give rise to these rocks. This similarity of REE and multielement patterns confirms the Harker variation diagrams, which indicate that the MDS sheets chemically trend toward granitic compositions. Some of the MDS rocks are also rich in Zr, which may due to the fine scale injection of Zr rich trondjhemitic dykes into these rocks. This is supported by field evidence (chapter-2).

## C. Evidence for Fractional Crystallisation

In general the variation of $K_2O$, MgO, CaO, $Fe_2O_3$, $TiO_2$ and $P_2O_5$ all apparently give an impression of fractional crystallization, as they show curvilinear or sub-linear trends from mafic dykes to granitic dykes; the two end member compositions. The high-Na trondjhemitic dykes and WFO are usually not coherent with the trends.

The early removal of Fe, Mg, Mn and Ca during fractionation of magma is commonly related to the crystallization of pyroxenes ± hornblende and plagioclase. The V, Cr, Ni and Zn contents decrease with increasing $SiO_2$ (Fig 4.2.c and 4.3.c to f) and can be attributed to the minor substitutions into magnetite and ferromagnesian minerals. V, Ni, Cr in hornblende substitute for $Mg^{++}$ and $Fe^{++}$. $Zn^{++}$ and $Y^{+++}$ substitute for $Fe^{++}$ and $Fe^{+++}$ in magnetite, hornblende etc and thus follow a similar trend to $Fe_2O_3$.

Rb and Ba increase with $SiO_2$ in a similar fashion to $K_2O$ (Fig 4.3.a and b.). The increase of Rb and Ba can be related by their similar geochemical behaviour. Rb and Ba have similar ionic sizes to K, and commonly substitute for $K^+$ ions during fractionation of potassium bearing minerals such as biotite and alkali feldspar (Gill, 1991). However, isotopic data preclude fractionation crystallisation

as the major cause of geochemical variation between the major rock-types (Fig 4.6). Nonetheless, some intra-group compositional variations may have resulted from fractional crystallisation, as discussed above. This is especially the case for the WFO at Mt Daniel.

**Western Fiordland Orthogneiss:** The case for fractional crystallisation within the WFO is that the two rocks analysed for Sr and Nd isotopes have very similar isotopic compositions, despite a difference of 14wt% $SiO_2$. Moreover, the smooth chemical variation observed in Harker diagrams, REE patterns, and multielement patterns suggest that fractional crystallisation processes were operating at the base of the WFO at Mt Daniel. For most variation diagrams for the WFO, elements follow a linear trend from high to low silica (described in section 3.2.). Also, the REE pattern for the two WFO samples is extremely similar. The higher silica sample has slightly higher content of all REE, suggesting they could be linked by fractional crystallisation, with the fractionating phases having similar partition coefficients for the REE; all slightly incompatible ($\sim K_D \leq 1$). This suggests olivine or pyroxene fractionation, but not garnet or hornblende, which would cause significant HREE depletion. The WFO rocks show that HREE abundance and Eu anomalies decrease with increasing $SiO_2$ content.

It is possible that MD-15 ($SiO_2$ = 57 wt %) is close to the composition of the parent magma for the WFO, and the more mafic samples are cumulates, such as MD-16 ($SiO_2$ = 43 wt %). MD16 has distinctive Sr, Ba, and P spikes, which could indicate plagioclase and apatite accumulation, although a positive Eu anomaly is not present. Lower Zr in MD16 indicates that zircon was not a crystallising phase at this stage.

**In summary,** field evidence shows that the whole spectrum of rock groups at Mt Daniel are a series of dyke systems of different compositions, ranging from mafic-intermediate to felsic, which may have formed by different degrees of partial melting of different sources at varying crustal depths. However, the Sr-Nd isotopic array suggests that mixing is the dominant cause of chemical diversity, although fractional crystallisation of magmas may have caused small intra-group variations.

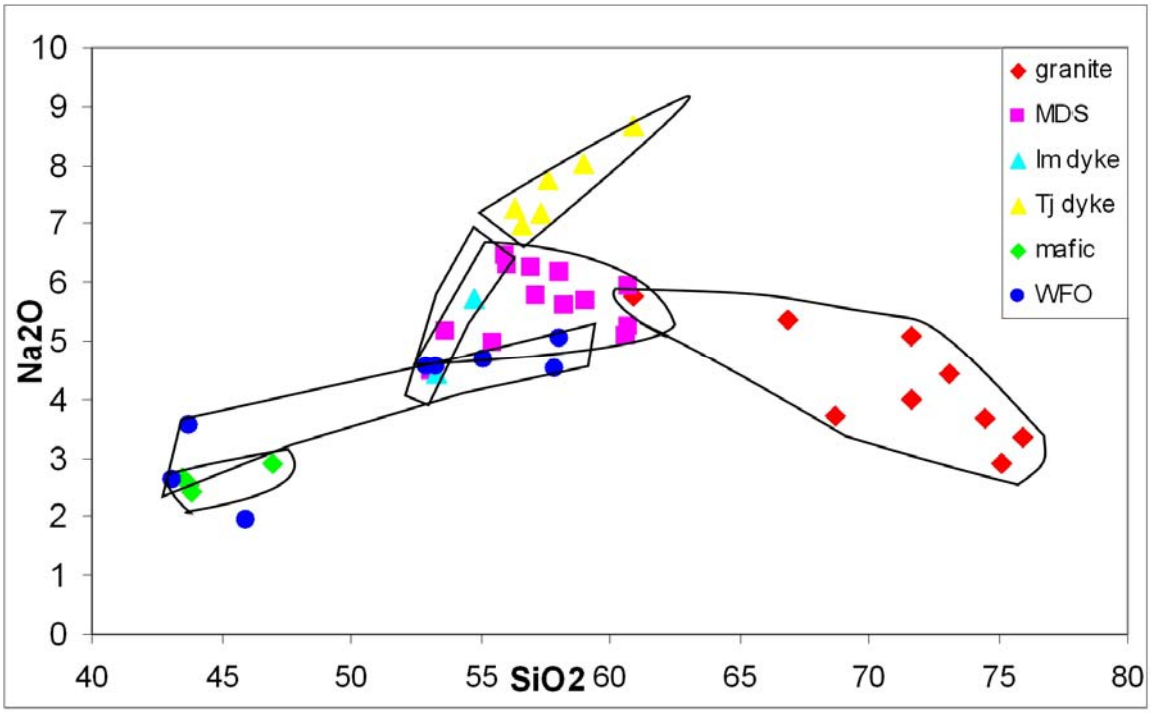


***Figure 4.7.*** *$SiO_2$-$Na_2O$ digagram shows probable mixing fields amon different components Mt Daniel Complex, Fiordland.*

The striking similarities of isotopic composition between SPB and the high-Na intermediate dykes of MDC suggest that the high-Na magmas in both suites are derived from similar sources. The $SiO_2$-$Na_2O$ plot demonstrates this mixing process (Fig 4.7.) very well, where the main mixed magmatic components identified are mafic dykes, high-Na intermediate dykes and granitic dykes.

The granites potentially mix with low silica mafic magmas and high-Na magmas to produce the MDC triangular array. This suggests the MDC may have formed by at least three components of mixing.

Nonetheless, a contribution from assimilated components from the ARC cannot be ruled out, as the ARC clusters as a chemical group near the low-Na mafic end of the MDC triangular array (see chapter-1, section 1.2.). Also, given the chemical, geochronological and age similarity of the ARC with the Darren Complex (Blattner 1991, Hollis et al., 2003), for which limited Sm-Nd and Rb-Sr isotopic data exist (McCulloch et al., 1987), a role for crustal assimilation in the MDC seems likely. Only the WFO seems to be an entirely different system that does not take any part in the mixing. The various possibilities will be further evaluated discussed in the following chapters.

# Chapter 5: Zircon Morphology and Microstructures of Mt Daniel Rock Groups from CL Images

## 5.1. Introduction

Zircon is an extremely robust mineral and has the ability to survive magmatic, metamorphic and weathering and erosional processes that destroy many other common minerals. Zircon has extremely variable external morphology and internal textures. The external morphology refers to the shape and size of zircon. Zircon acquires different shape and size depending on different geological processes, e.g. acicular zircon is commonly found in rapidly crystallized porphyritic, sub volcanic intrusions, high level granites and gabbros (Moser 1997, Corfu and Stott 1998), metamorphically grown or modified zircons are generally characterized by subrounded (van Breemen et al., 1986) and highly resorbed shapes (Pin and Lancelot 1982), euhedral shapes are also possible in metamorphic zircon (Corfu et al., 2003). Zircon growth phases mainly reflect episodes of magmatic crystallization and/or metamorphic recrystallisation processes and thus preserve significant stages in the evolution of the rock. The purpose of this chapter is to describe the external morphology and internal textures of zircons from different rock groups of the study area, Fiordland. Cathodoluminescence (CL) and back-scattered electron (BSE) images are used to document the morphology of zircon. CL images reveal the detailed internal microstructure of zircon and thus can help to understand the origin of zircon, whether it has formed during a magmatic or metamorphic event or within a transitional period between these two (e.g. Corfu et al., 2003). CL images may also preserve evidence for changes in the magmatic environment during zircon growth (e.g. Corfu et al., 2003).

## 5.2. Western Fiordland Orthogneiss: (Sample No: MD 15)

Zircons from the WFO are elongate to subrounded in shape with an average size range of 50-120μm.

The zircons show CL bright and dark grain populations. The dark CL grains are elongate and have planar and sector zoning patterns as typically shown by melt-precipitated zircons of igneous rocks (Fig 5.1.a.). In contrast, the CL-bright grains are typically elongate but have faint or almost no visible zoning with irregular grain boundaries (Fig 5.1.b.). The core and rim structure is absent in zircons of MD15 except in one grain (Fig 5.1.c.). Note this grain appears to show patchy recrystallisation around an inclusion. This is the same as described by Pidgeon (1992). Another type of CL bright subrounded or oval shaped zircon is also present. These grains have fir tree zoning and sector zoning (Fig 5.1.d., 5.1.e.) and also have dark patches and dark planar bands. Sometimes the grain boundaries are highly irregular.

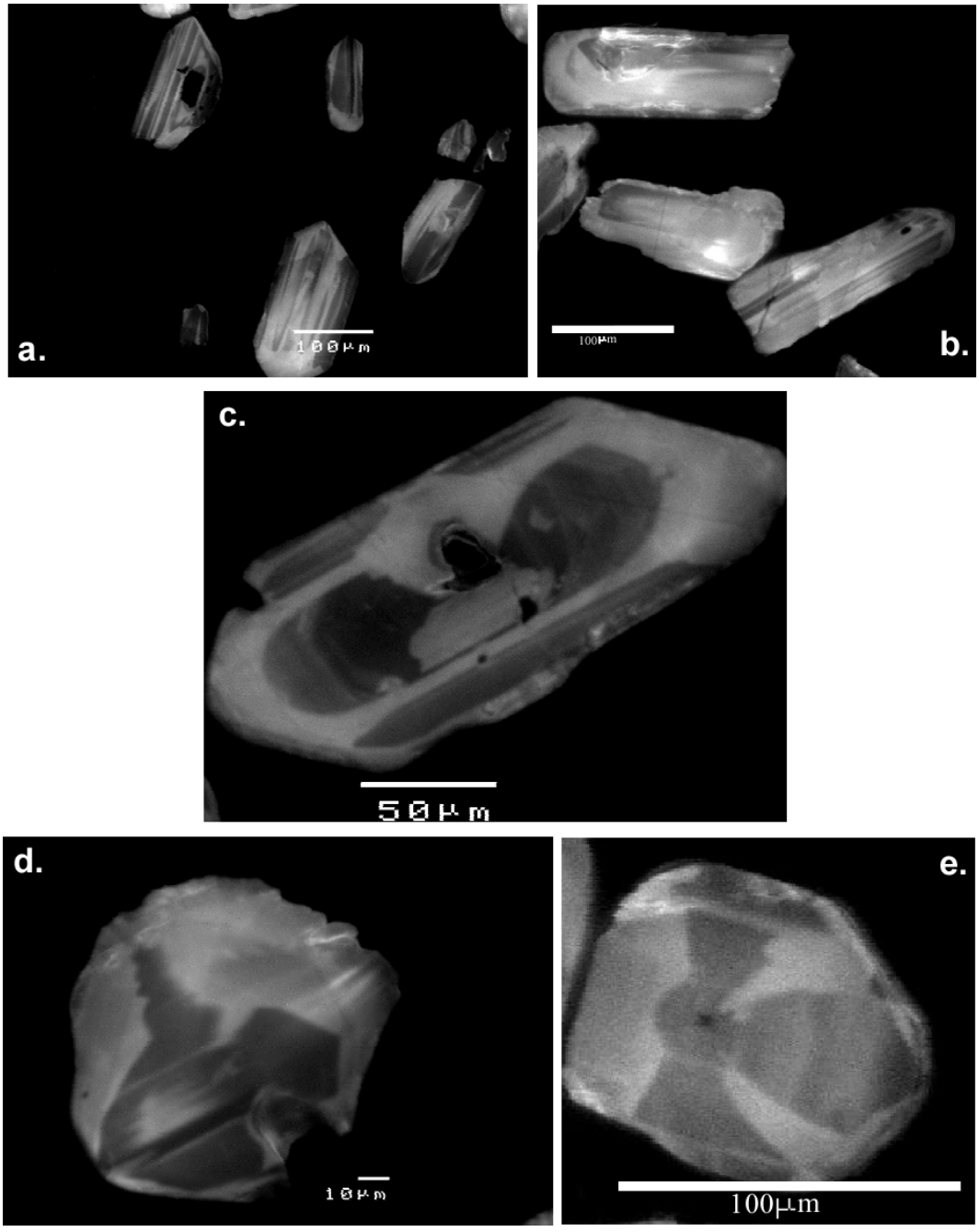


***Figure 5.1.*** *Cathodoluminescence images of zircons from the WFO from Mt Daniel, Fiordland analysed in this study.* ***(a)*** *Planar banding and sector zoning in WFO;* ***(b)*** *CL-bright zircon grains with faintly visible zoning in WFO sample;* ***(c)*** *Core and rim structure of zircon in WFO;* ***(d)*** *Fir tree zoning in WFO;* ***(e)*** *Sector zoning in WFO.*

In summary, the WFO has three different zircon populations; CL-dark elongated grains, CL bright elongated grains and subrounded to oval shaped CL bright grains.

Zoning in the CL dark zircons resembles magmatic zoning. Such zoning in zircon reflects compositional variation of Zr, Si and trace elements such as Hf, P, Y, REE, U and Th (Koppel and Sommerauer 1974, Benisek and Finger 1993, Hanchar and Rudnick 1995, Fowler et al., 2002 and many other studies). It has been suggested that variation of magmatic zoning (here planar zoning) (5.1.a.) formed due to incorporation of trace elements affected by "external forcing" (a process occurring within the magma system and not at the crystal/melt interface, Hoskin, 2000). The impact of external forcing is to increase the frequency of the oscillatory zoning as the magmatic differentiation proceeds (Hoskin, 2000). A transition of zoning patterns from broad to finely spaced oscillatory zones has been documented from the Boggy Plain pluton in southeastern Australia that is compositionally zoned from diorite through granodiorite to aplite (Hoskin 2000). The WFO is dioritic and its constituent zircons show the same broad oscillatory and sector zoning as exhibited by zircons of the Boggy Plain diorite.

Another population of zircons is bright coloured in CL images and elongate in shape with faint or no zoning and with irregular grain boundaries, are shown in (Fig 5.1.b). These grains can be either magmatic or metamorphic. In magmatic zircon when the compositional differences in the magma with respect to trace element concentration are very small, either faintly visible zoning can be formed (Corfu et al., 2003) or sometimes no visible zoning found (Zeck and Williams, 2002). Irregular grain boundaries are a possible sign of resorption and may be indicative of changes in the magmatic environment or of metamorphic growth or recrystallisation.

The subrounded to ovoid shaped zircons resemble metamorphic zircons. The presence of fir tree zoning in these zircons is also commonly observed in granulite facies rocks (Corfu et al., 2003) suggesting a metamorphic origin of the zircons.

## 5.3. Mafic Dykes: (Sample No: MD-22B, MD-26 and MD-13)

The zircons in the studied mafic dykes of Fiordland are mostly 40 to 120 μm in size, rounded to subrounded, ovoid and sometimes with highly resorbed shapes. Some elongated grains are also present.

Most of the CL images of zircons from these mafic dykes are very simple looking (Fig 5.2.a.). The zircons are mainly of two different grain populations. One type of grains has bright CL images and other dark CL images (Fig 5.2.b.). The bright grains are generally rounded to subrounded in shape, mostly featureless, but sometimes show dark patches. A type of zoning described as 'fir tree' zoning (Fig 5.2.c.) is commonly present. Some elongated dark grains have dark and light banding (Fig 5.2.d.). Wide oscillatory growth bands are also present in some dark grains.

The CL dark grains are very common in sample MD-26.The CL-dark grains are elongated and some of them show core and rim structures (Fig 5.2.e.). The core consists of faintly visible oscillatory zoning with some patches followed by a homogeneous dark zone, whereas the rim is featureless. Some cores are dark, featureless and homogeneous (Fig 5.2.f.). Some grains show faintly visible oscillatory zoning (Fig 5.2.g.). These features are not observed in zircons of the other mafic samples.

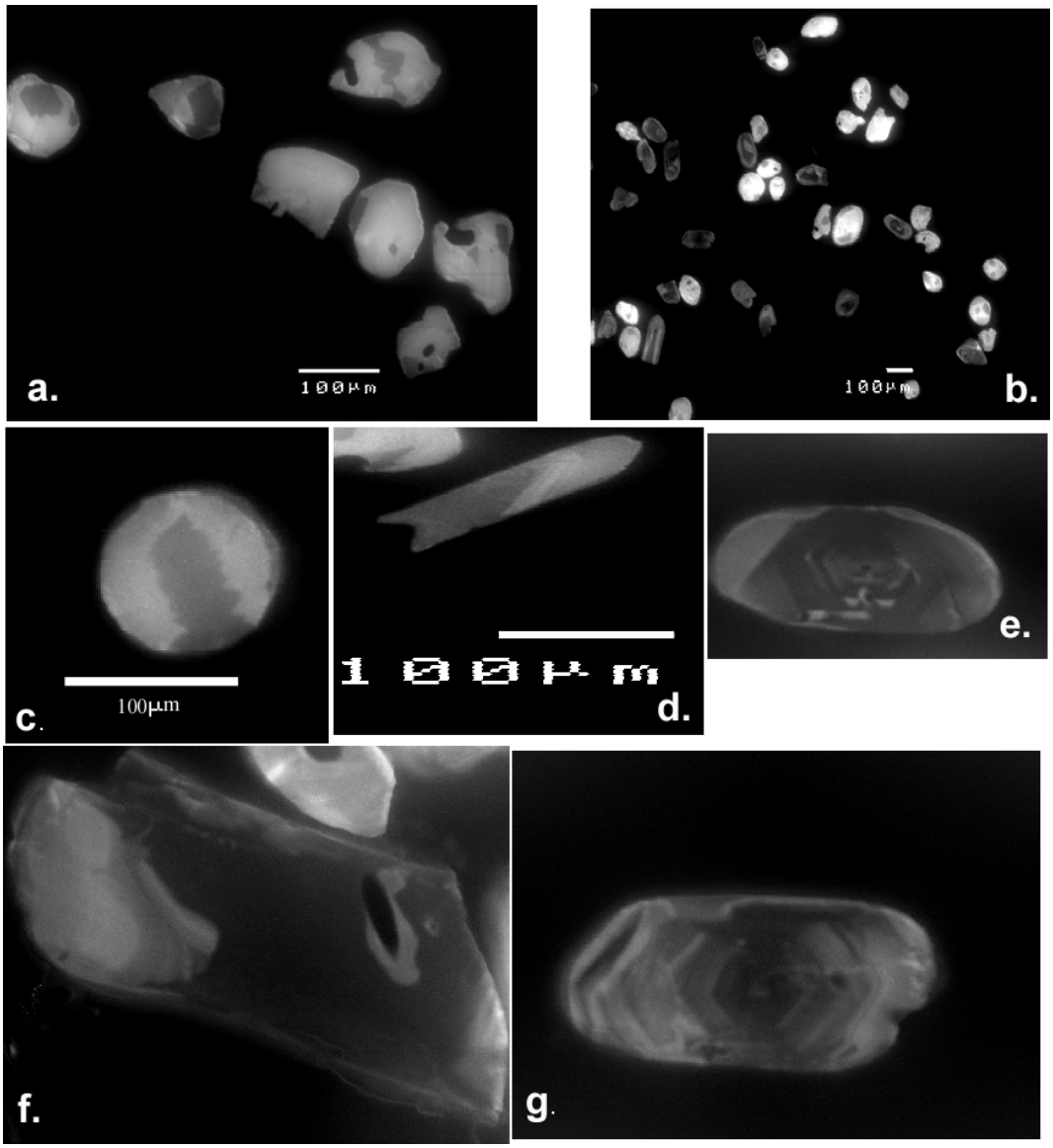


***Figure 5.2.*** *Cathodoluminescence images of zircons from the mafic dykes of Mt Daniel, Fiordland analysed in this study.* ***(a)*** *typical appearance of CL bright zircons commonly present in three mafic dykes (MD-22B, MD-13, MD-26);* ***(b)*** *CL-dark and bright grains in MD-26 are also present in other two mafic dykes;* ***(c)*** *Fir tree zoning is common in three mafic dykes;* ***(d)*** *Planar banding in zircons from mafic dyke are present in (MD-22B);* ***(e)*** *Core and rim structure of zircon in mafic dyke MD-26 where the oscillatory zoned core is overgrown by a homogeneous domain and featureless rim;* ***(f)*** *Dark homogeneous core and rim structure of zircons in mafic dyke MD-26;* ***(g)*** *Faintly visible oscillatory zoning of zircons from mafic dyke samples.*

Most of the zircons with bright CL in mafic dykes could be either of magmatic or metamorphic origin. The CL bright zircons are similar to metamorphic zircon in shape as they are subrounded to rounded and appear to be highly resorbed but these types of zircons are also commonly present as an igneous origin in mafic rocks (Rubatto 2000). Fir tree zoning is also commonly observed in zircons from the Fiordland mafic dykes. The fir tree zoning can be present both in metamorphic granulite facies rocks (Corfu et al, 2003) and also in igneous rocks. Fir tree zoning is thought to reflect strong fluctuations in growth rates (Vavra et al., 1996). CL dark grains of MD-26 samples mostly have dark homogeneous cores with some patches and light coloured rims. The homogeneous dark cores may have formed by recrystallisation. Rims are featureless and may represent either metamorphic or magmatic overgrowths. This will be evaluated by trace element and isotopic data (see chapters 8 and 9). The planar banding in the elongate dark grains in sample MD-22B (see Fig 5.2.d.) resembles magmatic zoning, and these grains also show characteristic igneous shapes that are unlike the rounded morphology of other zircons from the Fiordland mafic dykes. These grains may be of igneous origin. The dominance of subrounded to rounded shaped zircon morphologies and zoning patterns could be of either magmatic or metamorphic origin. The origin of the zircons from mafic dykes will be evaluated in the next chapters.

## 5.4. Low-Na Intermediate Dykes: (Sample No: MD-8 and MD-22A)

The zircons are mainly elongate to elliptical in shape and a few subrounded shaped grains are also present. Grains are mainly 50-100μm in size; a few smaller grains (<50 μm) are also present.

The intermediate dykes show two types of grain populations; CL-dark grains and CL-bright grains. CL bright grains mainly have no inherited cores where as the CL dark zircons have inherited cores (5.3.a.).

Most of the CL-dark zircons have two distinctly different CL domains. The innermost domain is dark and has a range of different types of microstructures (e.g. mottled, smooth, or oscillatory zoning). These are designated as cores. The outermost domain is comparatively thinner (5-60 μm) light coloured, brighter than the cores and often featureless in CL. These are referred to as rims. Thus the CL characteristics of most of the zircons from intermediate dykes have a well defined core and rim structure along with some zircons without cores (Fig 5.3.b.).

Sometime the cores are featureless and appear homogeneous. Homogeneous cores are very common in MD-22A (5.3.c). Patchy zoning is also a common structure in the zircon cores. It resembles a mottled or chaotic pattern (Fig5.3.d.).

Patchy or homogeneous cores are generally overgrown by oscillatory zoning towards the rim (Fig 5.3.b, c and d.). The rims are mostly featureless and narrow. The oscillatory zoning pattern either consists of very narrow growth bands or wide growth bands. The core-rim boundaries are often gradational (5.3.d.).

Some zircons with elongated or subrounded shapes either lack zoning or have dark and light alternate stripes of planar banding in MD-22A (5.3.e.) or broad oscillatory zoning in MD-8 (5.3.f.) and no evidence of cores. The process of formation of these grains is not clear. The lack of zoning can be attributed to many factors such as growth environment or kinetics or destruction of original zoning. These zircons have different brightnesses from grain to grain.

The formation of patchy zoning structure has been attributed to different factors by different authors. Paquette et al. (1995) reported patchy zoning, similar to undulatory extinction in strained quartz, formed due to strain experienced by zircon during final magmatic emplacement or during a late magmatic stage or subsequent metamorphism. Vavra and Hansen (1991) reported somewhat similar patchy zoning in elongated crystals with faint zoning and irregular longitudinal streaks, which they attributed to local recrystallisation along longitudinal microfractures. This kind of patchy zoning is observed in zircons of granite samples. Patchy zoning is considered a disequilibrium texture and has been reported in zircons from metamorphic rocks (Tomaschek et al., 2003; Spandler et al. 2004), pegmatites and granites (Xie et al., 2005) and has been formed experimentally (Geisler et al., 2003; Tomaschek et al., 2004). In all the studies, the texture has been attributed to fluid interaction with zircon. But two lines of evidence argue against this view. Firstly hydrothermal processes occur at the end stage of magmatic evolution but the textures are mainly found in the cores, which represent an early magmatic stage. Secondly, Hoskin and Schaltegger, (2003) suggested that porous zircon followed by oscillatory idiomorphic zoning overgrowths is of typically magmatic origin. Geisler et al., (2007) described a diffusion-limited dissolution-recrystallisation process along a reaction front as a cause for disequilibrium during zircon growth.

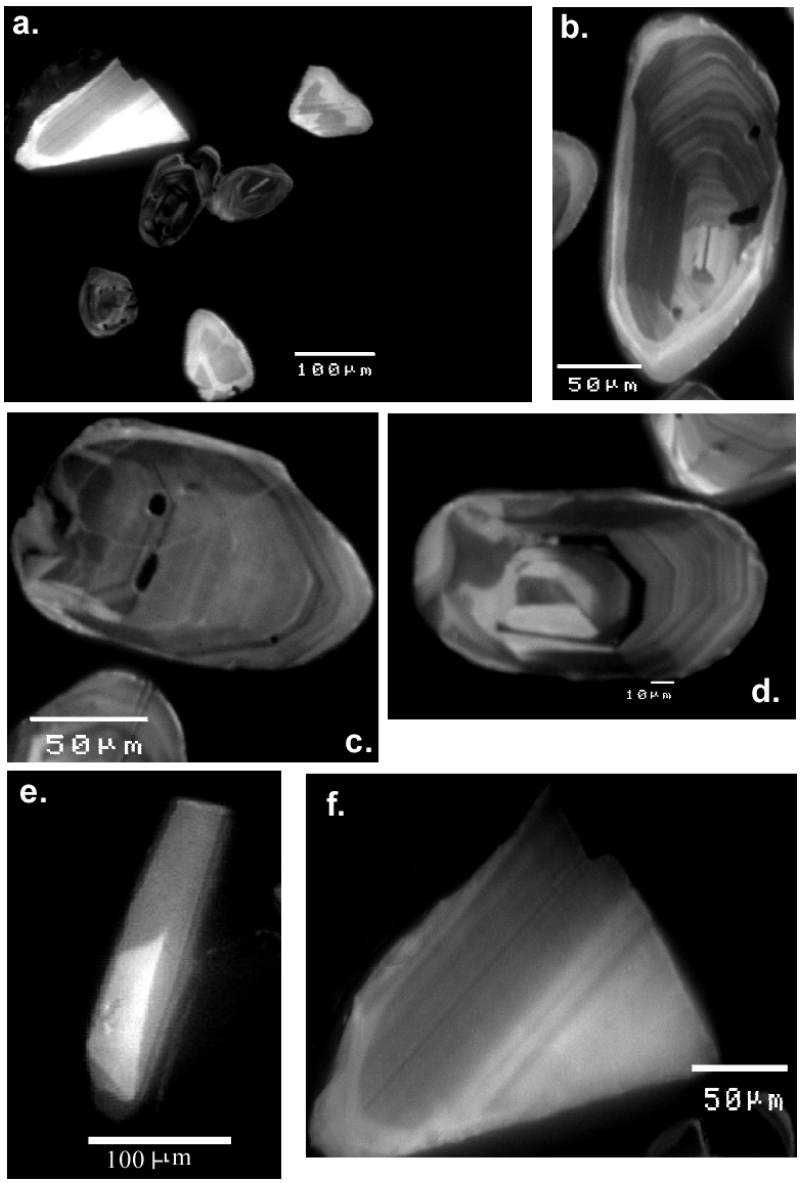


***Figure 5.3.*** *Cathodoluminescence images of zircons from the low-Na intermediate dykes of Mt Daniel, Fiordland analysed in this study.* ***(a)*** *CL-dark and CL-bright zircons in intermediate dykes;* ***(b)*** *Well defined core and thin rim structure of zircons where core is overgrown by oscillatory zoning towards rim;* ***(c)*** *homogeneous zircon core with inclusion trails followed by fine growth zoning towards rim;* ***(d)*** *Patchy zoning in zircon core with gradational core-rim boundary where core is overgrown by oscillatory zoning rim wards;* ***(e)*** *Elongated zircons with dark and bright stripe without any inherited core in intermediate dyke MD-22A;* ***(f)*** *Broad oscillatory zoning without any inherited core in intermediate dyke MD-8.*

Gagnevin et al., (2008) reported that these disequilibrium features closely resemble the patchy zoning texture of zircons from the Monte Capanne pluton (Italy) and suggested that the texture formed by diffusion-limited dissolution-recrystallisation processes at magmatic temperatures which involves progressive replacement of high U-Th-Y zircon by low U-Th-Y zircon. This replacement occurs via magma mixing of peraluminous and metaluminous melts during differentiation where high U-Th-Y zircon are thought to have crystallized from crustal peraluminous melts and in equilibrium with monazite and other accessory phases(apatite, allanite). Most of the patchy zoning in the Fiordland zircons is similar to those described by Gagnevin et al., (2008) and few have longitudinal streaks as discussed before. However the process of formation of patchy zoning in Fiordland zircons is unclear, and will be tested and addressed in the later chapters through detailed trace element and isotopic study.

The different types of narrow and wide banding of oscillatory zoning can be explained by the Hoskin's model as discussed in section 5.2. in this chapter. The origin of growth zoning reflects factors such as interplay between the stage of crystal growth, the nature of the crystal-liquid interface, the degree of supersaturation of the melt, the rates of diffusion and the oxidation state (Mattinson et al., 1996).

## 5.5. High-Na Intermediate Dykes: (Sample No: MD-17A, MD-32)

The zircons are of different shape and size in two different samples of high-Na intermediate dykes (trondhjemitic variety). In one of the samples (MD-17A) the zircons are elongated, acicular in habit, and the grain size is 30-100 μm. Another sample (MD-32) has elliptical, elongated and subrounded large grains, 50-130μm in size.

The sample (MD-17A) with mostly elongated grains shows different types of magmatic zoning. Planar zoning (Fig 5.4.a.) and broad oscillatory zoning (Fig 5.4.b.) are commonly. Sector zoning (Fig 5.4.c.) and patchy zoning are also present in some grains with resorption at the margins (Fig 5.4.d.). Marginal resorption and patchy zoning are also present together in some grains.

Zircons from the other high-Na intermediate dyke sample MD-32 are distinctly different. In some grains two distinctly different domains are present. Some of these grains have core-rim structures (Fig 5.4.e.). The textures of the cores vary from grain to grain. Some of the cores have patchy zoning followed by oscillatory zoning that is sometimes convoluted. Rims are mostly wide and featureless but in some cases contain faint broad oscillatory zoning. A few of the cores are homogeneous and euhedral to subhedral in shape. Resorption along the core boundary is also observed. One subrounded grain shows a homogeneous dark core and a thin light coloured rim (Fig 5.4.f.). Another grain population in MD32 shows a patchy appearance with both dark and bright CL. Some of those grains are nearly homogeneous (Fig 5.4.g.) and some grains contain a faint broad growth zoning (Fig 5.4.h.).

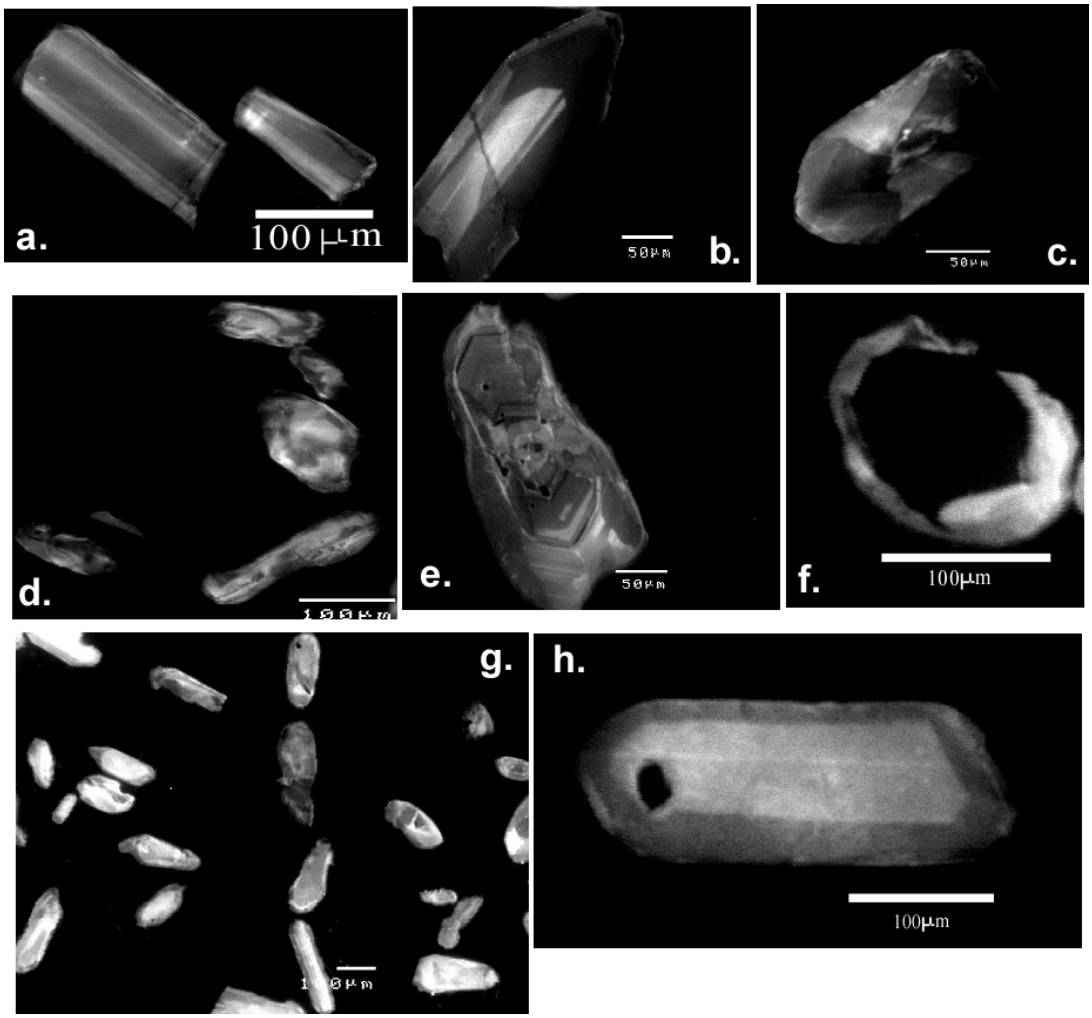


***Figure 5.4.*** *Cathodoluminescence images of zircons from the high-Na intermediate dykes (trondhjemitic variety) of Mt Daniel, Fiordland analysed in this study.* ***(a)*** *Planar zoning of zircon in MD-17A;* ***(b)*** *Broad oscillatory zoning of zircon of MD-17A;* ***(c)*** *Sector zoning of zircon in MD-17A;* ***(d)*** *Patchy zoning of zircon with irregular and resorbed grain boundary in MD-17A;* ***(e)*** *Core and rim structure in MD-32;* ***(f)*** *Very dark homogeneous core with thin rim of zircon in sample MD-32;* ***(g)*** *Patchy zoning of CL- bright and dark grains of zircons in MD-32;* ***(h)*** *Broad and faint growth zoning of zircon of MD32.*

Broad oscillatory zoning patterns in MD-17A suggest that the zircon formed in a magmatic environment where the zones are show a bimodal succession of trace element rich and trace element poor bands.

Formation of sector zoning in magmatic environment is attributed to different factors by different authors as discussed earlier. Sector zoning can be formed in both magmatic and metamorphic zircons, particularly in granulite facies rocks as reported by different authors. But incase of the sample MD-17A it is likely of magmatic origin as the shapes of the zircons are acicular, elongated mainly with planar or oscillatory zoning which strongly resemble to magmatic zircons.

The CL images of the trondhjemite-hosted zircons vary widely in inter and intra-grain populations. In MD-17A most of the zircons show microstructures that strongly indicate an igneous origin but some patchy zoned grains are present with highly resorbed grain boundaries.

The dark homogeneous domain in CL image of sample MD-32 suggests it is either free of zoning because the luminescence may be the result of a high concentration of trace elements and/or metamictization (Corfu et al., 2003). The CL bright homogeneous domains have very low trace element contents (Corfu et al., 2003). These types of zircons with subrounded shapes and with completely homogeneous domains are common in granulite facies rocks (Corfu et al., 2003).

Zircons in the other sample MD-32 are distinctly different in having core and rim structures as well some patchy zoning. Rims are mostly featureless or have some faint oscillatory zoning and cores are patchy or homogenous. These zircons may reflect metamorphic modification or growth.

## 5.6. Granitic Dykes: (Sample No: MD-2, MD-6) and Granitic sheets in MDC (Sample No: MD29 and MD-33)

The zircons in granitic samples from Fiordland are mainly 40-100μm in size, elliptical to subrounded in shape and a few elongated grains are also present. Rounded shapes are also present.

Most of the zircons in granite samples have two distinctly different CL domains. The innermost domain is dark, having different types of textures (e.g. mottled, smooth, or oscillatory zoning). These are designated as cores. The outermost domain is 10-50 μm; light coloured, and mostly featureless in CL. These are referred to as rims. In the zircons of granitic dyke MD-2, cores are abundant whereas rims are absent or very thin. In granitic dyke MD-6 and granitic rocks MD-29 and MD-33 rims have variable thickness from thin (10 μm) to thick (>50 μm) (Fig 5.5.a.).

The boundary between cores and rims is not always well defined and is sometimes gradational. In granitic dyke MD-6 the rims of the zircons are sometimes very thick where as the cores are very small. Cores have different types of internal micro-structure or commonly have a combination of more than one structure. One of the common structures is patchy zoning, which is mainly present within the core and the core-rim boundary is often gradational (Fig 5.5.b.). As mentioned earlier a different type of patchy zoning in elongated grains with irregular longitudinal streaks and faint zoning were reported by Vavra and Hansen (1991). A similar type of zoning is found in zircons of both of the granitic dyke samples (Fig 5.5.c.). Cores with oscillatory zoning and stripes of dark and light planar bands are commonly disrupted and truncated with an irregular homogeneous domain (Fig 5.5.d. and 5.5.e.). It appears to be some embayment or resorption of the cores followed by growth of the homogeneous domain. Few very CL-bright relatively homogeneous grains are present in MD-29 (Fig 5.5.f.).

Homogeneous cores with euhedral to subhedral shapes and featureless rims are also present in different granitic samples but very common in granitic rocks (MD-29 and MD-33) of MDC and often followed rim-wards by fine oscillatory zoning (Fig 5.5.g.). In one of the granitic dykes, MD-

2, partial resorption of the rims of the zircon grains are frequently present (Fig 5.5.c.). Rims are thin, bright in CL images and structureless.

In the granite samples (granitic dykes and granitic rocks of MDC) the zircons mostly show core and rim structures. Rims are mainly overgrowth structures and could be either magmatic or metamorphic in origin. Comparatively small cores and large thick rims of zircons in MD-6 suggest the consumption of the cores either by magmatic assimilation or by metamorphic dissolution processes. The type of patchy zoning in granite is similar to the patchy zoning of intermediate rocks and thought to be formed in the same way as intermediate rocks which were discussed earlier. The patchy zoning in elongated grains with faint zoning and longitudinal streaks is formed by local recrystallisation along longitudinal microfractures (Vavra and Hansen 1991). Formations of the homogeneous domains are attributed to recrystallisation. The structure of granitic dyke MD-6 and granitic rocks MD-29 and MD-33 of MDC are very similar so thought to be formed in the same way. MD-2 may indicate a different environment of formation of the zircons.

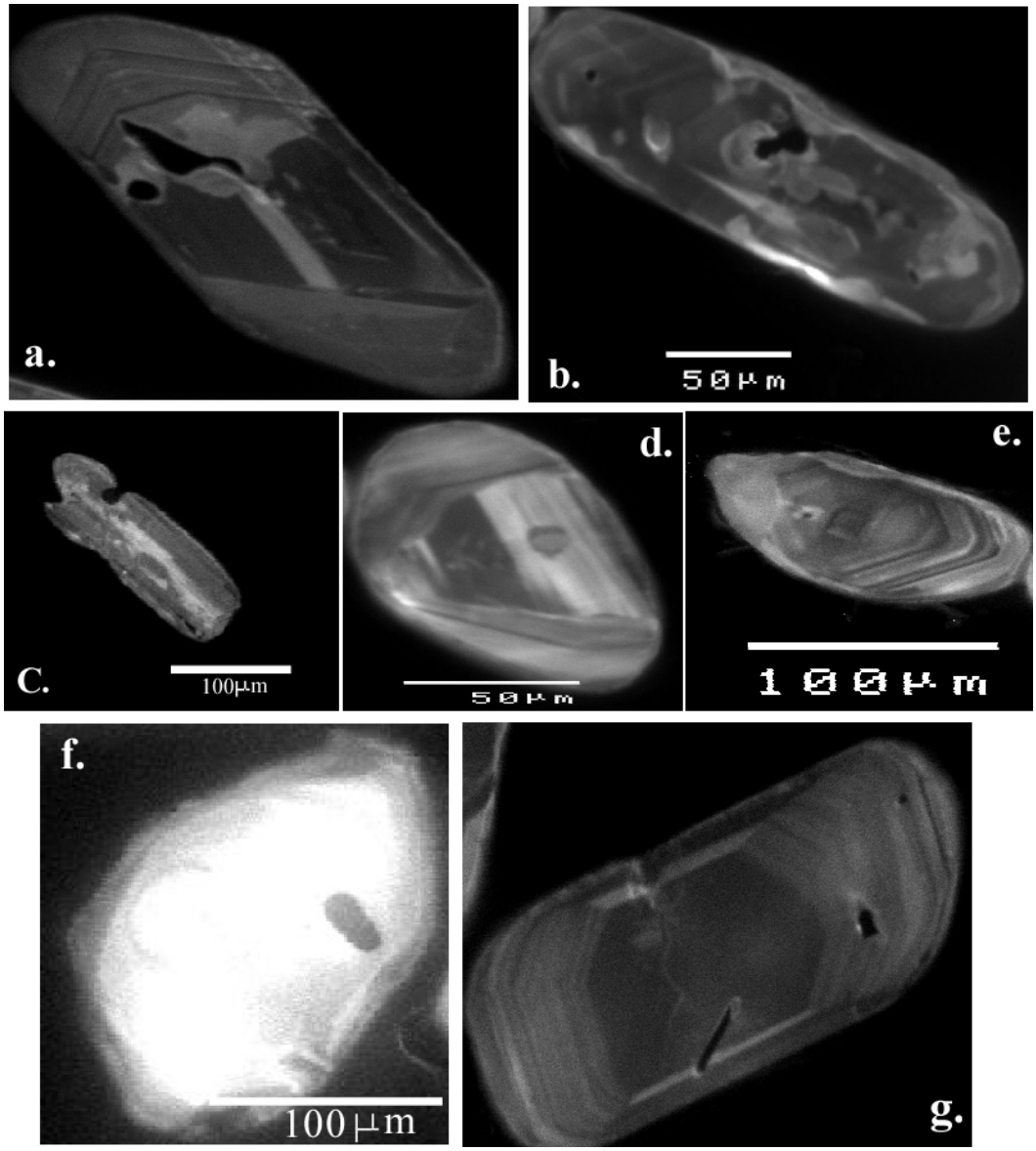


***Figure 5.5.*** *Cathodoluminescence images of zircons from the granites of Mt Daniel, Fiordland analysed in this study.* ***(a)*** *Well defined core and rim structure of zircons in intermediate rocks also showing evidence of local recrystallisation around inclusions;* ***(b)*** *Patchy zoned core of zircon with core and rim gradational boundary in granite samples;* ***(c)*** *Type of patchy zoning with irregular longitudinal streaks in zircons of granitic dykes;* ***(d & e)*** *Planar and oscillatory zoned cores of zircons truncated against an irregular homogeneous domain in granite samples;* ***(f)*** *Very bright oval shaped zircon without zoning from MD-29;* ***(g)*** *Homogeneous zircon cores followed by fine growth zoning.*

## 5.7. Mt Daniel Sheets (Sample No: MD-14 and MD-38)

The zircons are mainly elongate to elliptical in shape and subrounded shaped grains are also present. Grains are mainly 50-100μm in size; a few smaller grains (<50 μm) are also present.

The zircons in MDS samples have two distinctly different CL domains-cores and rim. The core is dark, with various microstructures (e.g. mottled, smooth, or having oscillatory zoning). The rim is comparatively thinner (5-50 μm) light coloured, brighter than the core and often featureless in CL. These are referred to as rims. Thus the CL characteristics of most of the zircons from MDS samples have a well defined core and rim structure (Fig5.6.a.). In the zircons of MD-38 cores are abundant whereas rims are absent or very thin (Fig 5.6.b.).

Patchy zoning is very common structure in the cores. It resembles a mottled or chaotic pattern, sometimes with inclusion trails (Fig 5.6.a and 5.6.b.). Sometimes the cores are featureless and appear homogeneous. Homogeneous cores are very common in MD-14 and sometime consist of inclusion trails (Fig 5.6.c.). The patchy or homogeneous cores are generally overgrown by well developed wide growth zoning towards featureless rims (Fig 5.6.c.). Some zircons have very dark homogeneous cores and bright thick rims without any prominent zoning (Fig 5.6.d.).

Sometimes a reverse sequence is also observed where oscillatory zoning followed by a dark homogeneous domain is truncated by a bright outermost rim (Fig 5.6.e.). Signs of resorption are also present in some cores.

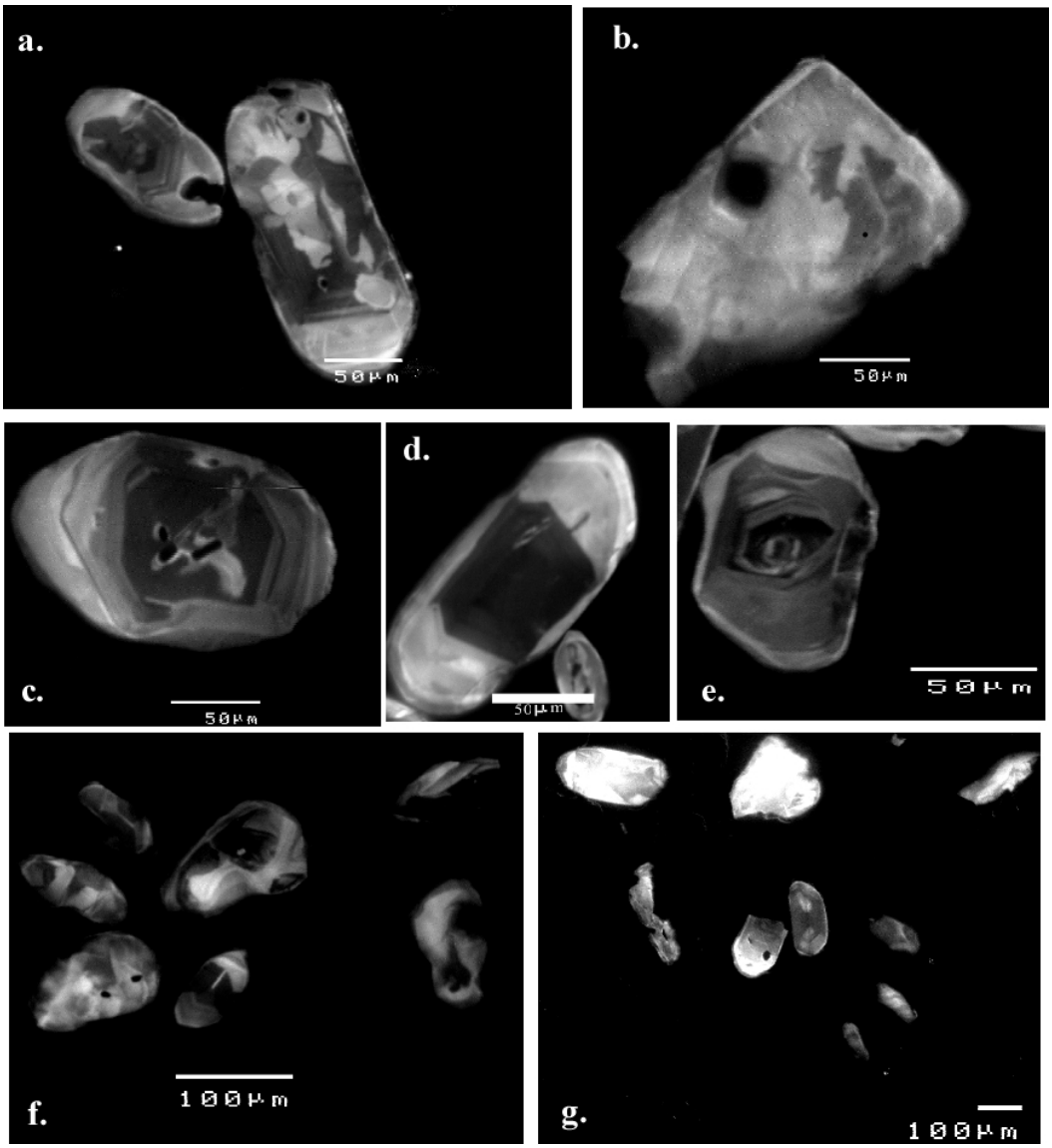


***Figure 5.6.*** *Cathodoluminescence images of zircons from the samples of Mt Daniel Sheet (MD-14and MD-38) of Mt Daniel, Fiordland analysed in this study.* ***(a)*** *Core-rim structure of zircon with patchy zoned zircon core and thick bright rim;* ***(b)*** *Core with patchy zoning in MD-38;* ***(c)*** *Well developed growth bands and homogeneous zircon cores with inclusion trails in intermediate samples also showing evidence of local recrystallisation around inclusions in MD-14;* ***(d)*** *Very dark homogeneous core with bright thick rim of zircon;* ***(e)*** *Oscillatory zoned core followed by homogeneous domain;* ***(f)*** *Oval shaped zircons with irregular patches in MD-14;* ***(g)*** *Irregular, diffuse like auroral-light zoning of zircons in MD-38.*

MD-14 has some ovoid shaped zircons with irregular patches (Fig 5.6.f). These zircons have sometimes smooth subrounded surfaces, multifaceted exteriors and highly resorbed shapes. MD-38 has a number of zircons with irregular diffuse zoning but with comparatively smooth internal textures (Fig 5.6.g.). This type of zoning is very similar to the "auroral light" texture in the zircons from high-pressure rocks (Corfu et al, 2003).

The zircons in MDS samples mostly show core and rim structures but MD-38 has abundant cores and often rims are absent. Rims are mainly overgrowth structures and may be magmatic or metamorphic in origin. The type of patchy zoning in MDC rocks is similar to the patchy zoning of other rock types and thought to be formed in the same way as rock types discussed earlier (section 5.4.). The structures of the homogeneous domains are similar to other rock types which are thought to be formed by recrystallisation.

The different types of narrow and wide banding of oscillatory zoning can be explained by the Hoskin's model as discussed in section 5.2. in this chapter. The origin of growth zoning is attributed to various factors which are already discussed in section 5.4. in this chapter.

The oval shaped zircons with multifaceted exteriors in MD-14 are common in metamorphically grown or modified zircon crystals. In granulite facies rocks zircons sometimes show multifaceted exteriors (Corfu et al, 2003).

Auroral light textures are mainly reported zircons formed at high pressure (Corfu et al, 2003).

## 5.8. Summary

All of the Fiordland samples mainly have two types of zircon microstructures, single zircons of different shapes without core-rim structures and zircons with core-rim structures.

Some obvious igneous looking zircons are present in nearly all of the rock samples excluding granitic rocks and MDS. These zircons are abundant in one high-Na intermediate dyke (MD-17A) and in the WFO but in other rock groups like mafic and in low-Na intermediate dykes these are only occasionally present. These zircons are elongate to subrounded in shape, showing planar zoning, sector zoning and sometimes oscillatory zoning. Another type of zircons found in the mafic dykes and low-Na intermediate dykes. These are subrounded to rounded in shape, highly resorbed, sometimes multifaceted and mainly CL bright grains. They mainly show fir tree zoning and sector zoning. The origin of these zircons could be either magmatic or metamorphic and will be evaluated in the next chapter.

Core and rim structures are common in all rock types except one high-Na intermediate dyke (MD-17A), two mafic dykes (MD-22B and MD-13) and in the WFO (MD-15), where only one grain shows this structure. Where present, cores are mainly patchy, homogeneous or sometimes oscillatory zoned. Oscillatory zoned cores are interrupted by homogeneous overgrowths. Rims are featureless and brighter than cores in CL. Most of the core and rim structures bear some imprints of metamorphism to an extent such as round to ovoid shaped grains, irregular grain boundary, patchy, recrystallised and resorbed structures etc.

It is noticeable that the igneous looking and metamorphic-looking zircons are found in the same rocks. This observation attracts attention, since we will be interested to explore the chemical and isotopic differences between these grains of inferred different origin.

# Chapter-6: U-Th-Pb Geochronology of Zircons from Mt Daniel, Fiordland

## 6.1. Introduction

Information about the timing of rock formation is very important for understanding the geological history. The absolute age can only be determined for a geological time frame by isotopic dating. Different geochronometers are based on isotopic decay schemes (e.g. U/Pb, Sm/Nd, Rb/Sr and K/Ar) and applied to whole rocks and different minerals. Each isotopic scheme and mineral has different advantages and limitations and is used depending on the specific applications.

Zircon is a useful mineral for analyzing the U-Pb decay system as it contains significant amounts of U and Th. Zircon is therefore ideal for U-Pb geochronology as it is abundant in felsic rocks, and is a robust mineral. The closure temperature of zircon is very high (950-1000$^0$ C for Pb in zircon, Black et al., 1986; Claoue-Long et al. 1991; Williams 1992, Lee et al., 1997) and so zircon can retain isotopic information even through high grade metamorphism. So for establishing the timing of magmatic processes in rocks that have experienced subsequent high grade metamorphism (e.g. granulite facies) like in Fiordland, zircon is the most useful geochronological tool. This chapter will deal with the ages of zircons obtained from different samples from Mount Daniel, Fiordland. The systematic variation of ages in conjunction with CL-images (see chapter-5) will be outlined to understand the timing of zircon growth and thus to build up a coherent history of rock forming processes of that area. The analytical techniques for U-Pb dating are described in Chapter-3.

It is important to mention that dating the Fiordland zircons by laser ablation has some limitations, as the zircons are typically small (i.e. usually less than 50 microns in diameter) and commonly have inherited cores and thin rims. Spot analyses commonly intersected core-rim boundaries and give rise to mixed ages formed by the physical mixing of ablated aerosols derived from two different age

populations. These 'mixed' ages were recognized during data processing and are mentioned in the text. The way of processing these mixed signals is discussed in chapter 3.

## 6.2. Western Fiordland Orthogneiss: (Sample No: MD 15)

The zircons from the WFO are interpreted as magmatic based on their elongated to subrounded shapes and planar banding and oscillatory zoning without any evidence of core-rim structures (Fig. 6.1a, b and see section 5.2. in chapter-5). Ten spot analyses have been done on different grains. Nine out of ten analyses give a $^{206}Pb/^{238}U$ age of 125 ± 2 Ma (2σ, MSWD=1.9; Fig 6.2.) with one outlier rejected. One zircon has an older core (see Fig 6.1.b.) of 339 ± 6.

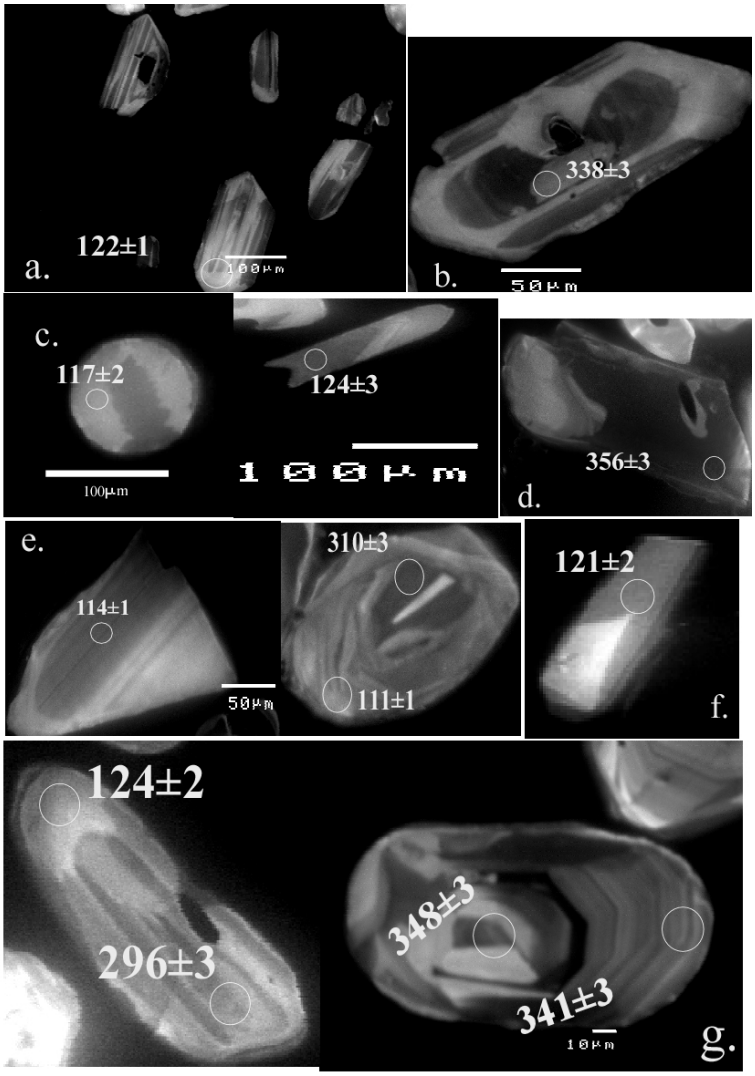


***Figure 6.1.*** *Cathodoluminescence images of representative zircons from different rock types dated by U-Pb isotopes. The ages are in Ma.* ***(a) & (b)*** *CL-images of Zircons dated from WFO (MD15);* ***(c)*** *&* ***(d)*** *CL-images of Zircons dated from mafic rocks (MD-13, MD-22B & MD-26);* ***(e)*** *CL-images of Zircons dated from low-Na intermediate Dyke MD-8;* ***(f) & (g)*** *CL-images of Zircons dated from low-Na intermediate Dyke MD-22A.*

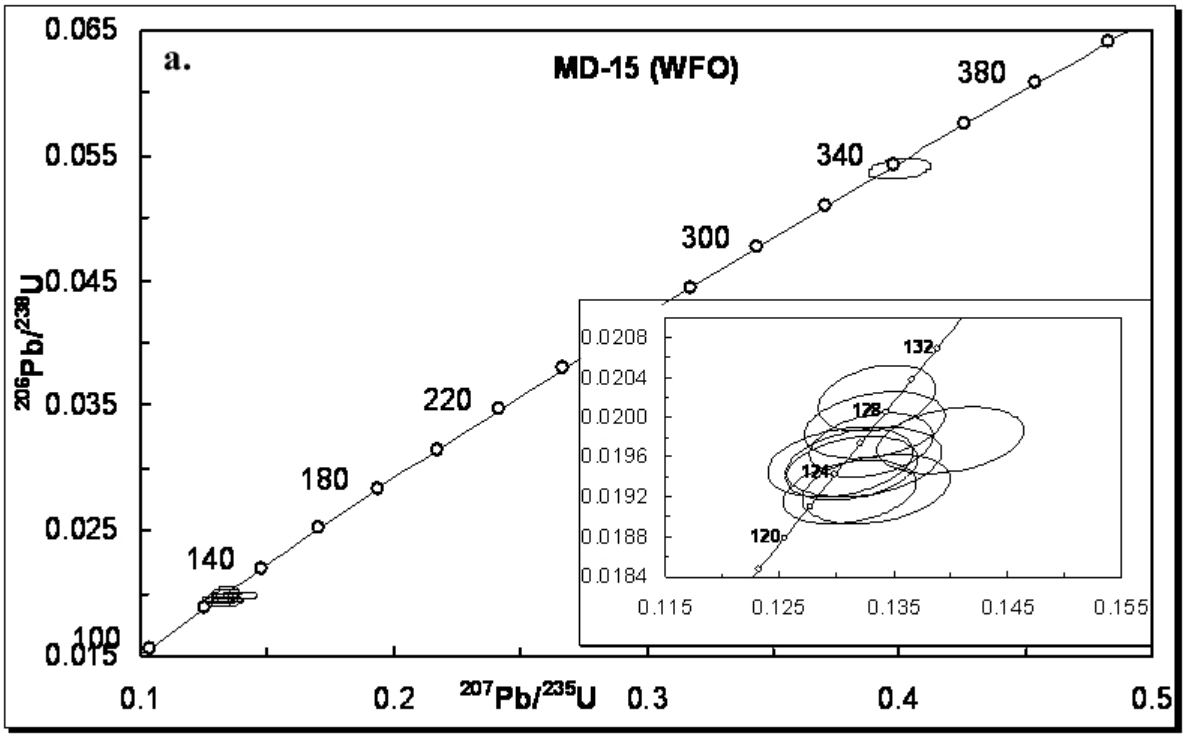


***Figure 6.2.*** *Concordia diagram summarizing U-Pb isotope data from zircons of the WFO (MD-15) of Mt Daniel, Fiordland**.** This and all subsequent Concordia diagrams were constructed using Isoplot 3.00 (Ludwig K, 2003)**.***

## 6.3. Mafic Dykes: (Sample No: MD-13, MD-22B and MD-26)

**MD-13:** The zircons from MD-13 are mostly CL-bright without any evidence for older cores. Sector zoning and fir tree zoning occurs in some grains (see chapter-5).

Ten spot analyses have been done on different grains. Nine out of ten grains give a $^{206}Pb/^{238}U$ age of 123 ± 6 Ma (2σ, MSWD=3.3; Fig 6.3.a.).

**MD-22B:** MD-22B has similar CL-bright zircons without any evidence for inherited cores, and also has some CL-dark grains with acicular shapes (Fig 6.1.c.). Sixteen spot analyses have been done on different grains and three analyses are rejected due to short signals. The data are quite coherent. Twelve out of thirteen grains give a $^{206}Pb/^{238}U$ age of 121±2 Ma (2σ, MSWD=1.14; Fig 6.3.b.).

**MD-26:** The zircons from MD-26 have two different populations of CL-bright and CL dark zircons, where CL-dark grains have evidence of cores (Fig 6.1.d., See chapter-5). Thirteen spot analyses have been performed; five on cores and eight on rims from CL dark grains with and without cores, and from CL-bright grains without any core. The zircons without cores (CL-bright grains and few CL-dark grains, n = 8) give an average $^{206}Pb/^{238}U$ age of 124±6 Ma (2σ, MSWD=2.5; Fig 6.3.c.). The cores have a $^{206}Pb/^{238}U$ age range of 376-306 Ma (Fig 6.3.c.).

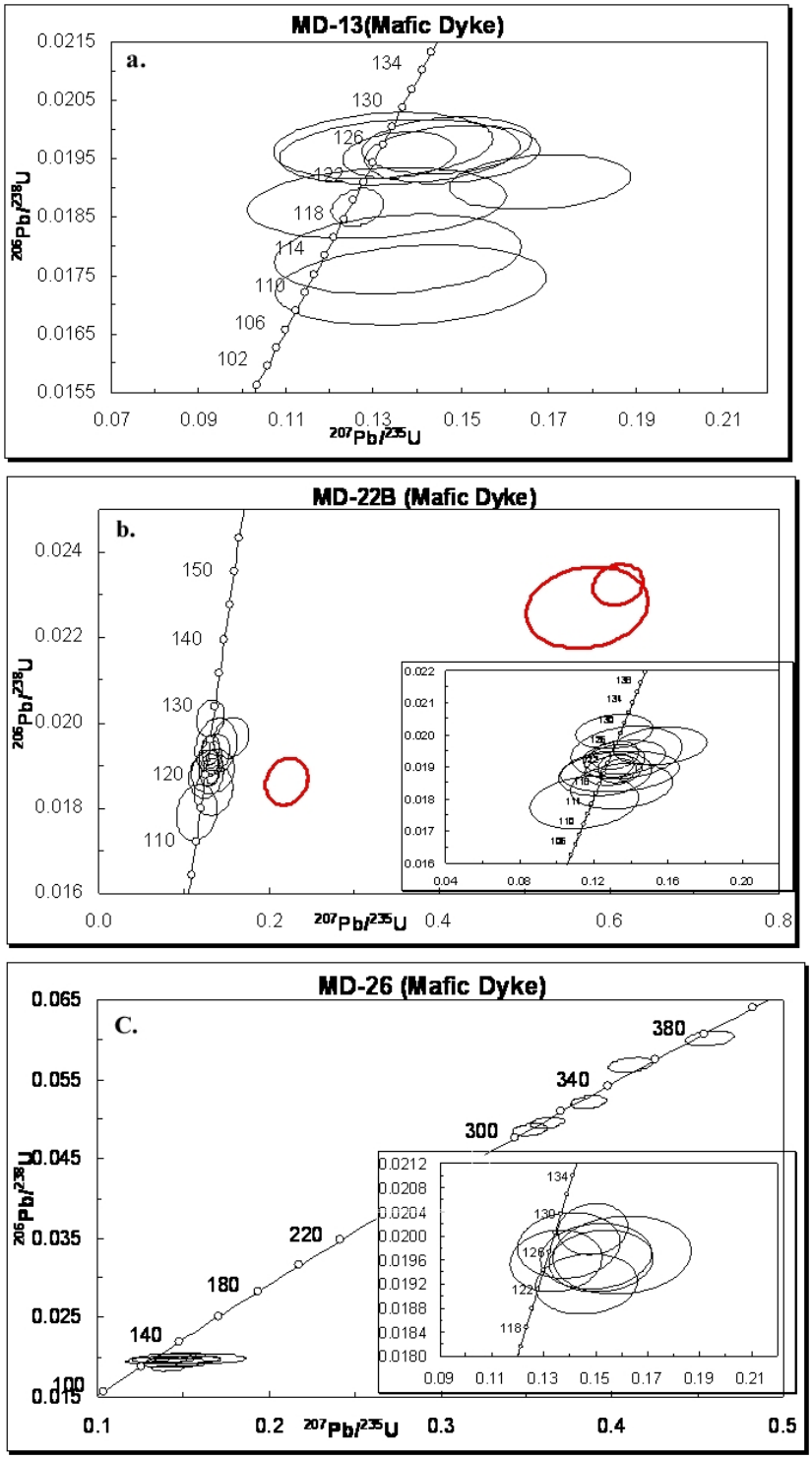


***Figure 6.3.*** *Concordia diagrams summarizing U-Pb data from zircons from different mafic dykes of Mt Daniel, Fiordland;* ***(a)*** *mafic dyke MD-13;* ***(b)*** *mafic dyke MD-22B;* ***(c)*** *mafic dyke MD-26. Rejected analyses are presented in red and accepted analyses are presented in black.*

## 6.4. Low-Na Intermediate Dykes: (Sample No: MD-8 & MD-22A)

**MD-8:** The zircons from low-Na intermediate dyke MD-8 show two different types of grain populations that are similar to those of MD-26. MD-8 has some CL-bright grains and CL-dark grains with inherited cores (Fig 6.1.e). Six spot analyses have been done on cores and rims of different grains. The rims of CL-dark grains and CL bright grains without older cores show a range of $^{206}Pb/^{238}U$ ages of 114-106 Ma and yield a weighted mean of 112±12 Ma (2σ, MSWD=7.1, n=4; Fig 6.4.a.). The two older cores give $^{206}Pb/^{238}U$ ages of 330±3 and 310±3 Ma.

**MD-22A:** CL images of low-Na intermediate dyke MD-22A show a few zircons without inherited cores (Fig 6.1.f.) but most of the zircons in this rock have core and rim structures (Fig 6.1.g.). Twenty-eight analyses have been performed on cores and rims. Only three zircons have Cretaceous $^{206}Pb/^{238}U$ ages and yield a weighted mean of 125±18 Ma (2σ, MSWD=3.2; Fig 6.4.b.). Two of the younger ages are from single grains without inherited cores and one is from a rim around an older core. The single grains are very small and the rim is very thin, thus the signals are short and discordant so they yield a large error. Most of the zircons (20 analyses, from cores) give a $^{206}Pb/^{238}U$ age range of 362-313 Ma. Five analyses have $^{206}Pb/^{238}U$ ages that fall between 296-148 Ma (Fig 6.4.b.).

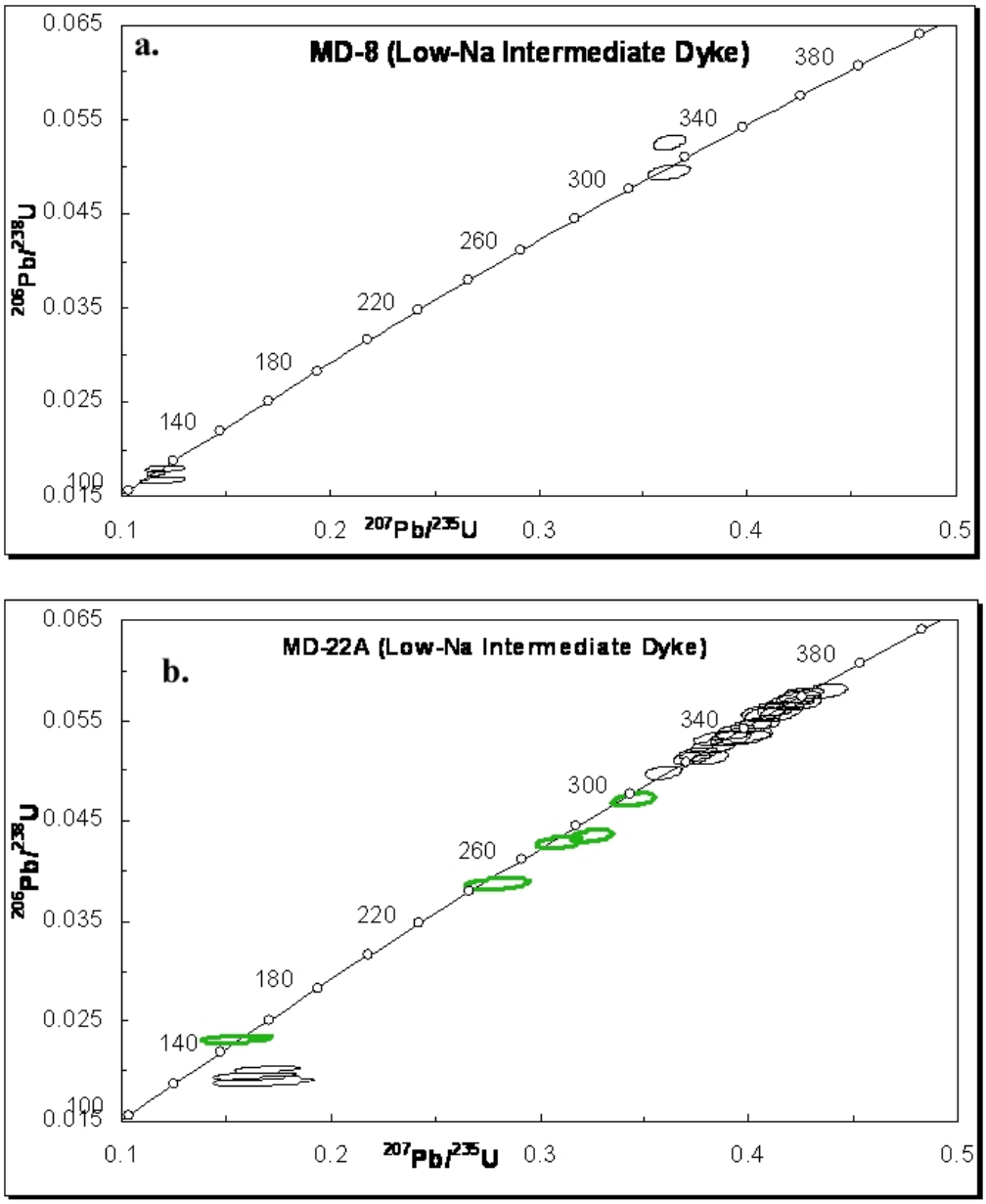


***Figure 6.4.*** *Concordia diagrams summarizing U-Pb isotope data from zircons of low-Na intermediate dykes of Fiordland, Mt Daniel;* ***(a)*** *MD-8;* ***(b)*** *MD-22A. Symbols in green are mixed ages.*

## 6.5. High-Na Intermediate Dykes (Trondhjemitic Variety): (Sample No: MD-17A & MD-32)

**MD-17A:** Zircons of high-Na intermediate dyke MD-17A are interpreted as magmatic based on their elongated shapes and planar banding and oscillatory zoning (Fig 6.5.a.). Twenty-five spot analyses have been done on different zircons and one outlier was rejected. Twenty-five spot analyses yield an average $^{206}Pb/^{238}U$ age of 119±2 Ma (2σ, MSWD=2.4; Fig 6.6.a.).

**MD-32:** High-Na intermediate dyke MD-32 has zircons with core and rim structures. Cores generally show patchy zoning or are unzoned and the thick rims are featureless (Fig 6.5.b. & 6.5.c.). Some zircons show patchy or homogeneous zoning without any cores (Fig 6.5.d.).

Twenty-four spot analyses were done on different zircons. Two analyses are rejected due to short signals (not shown on the plot). Sixteen out of sixteen grains give $^{206}Pb/^{238}U$ ages between 129-110 Ma and yield an weighted mean of 120±6 Ma (2σ, MSWD=8.4; Fig 6.6.b.). The MSWD is high because of scattered Early Cretaceous age range. Five analyses from cores yield a $^{206}Pb/^{238}U$ age range of 344 to 323 Ma (Fig 6.6.b). One of the cores exhibits a $^{206}Pb/^{238}U$ age of 199±4 Ma and shows a mixed time-resolved signal.

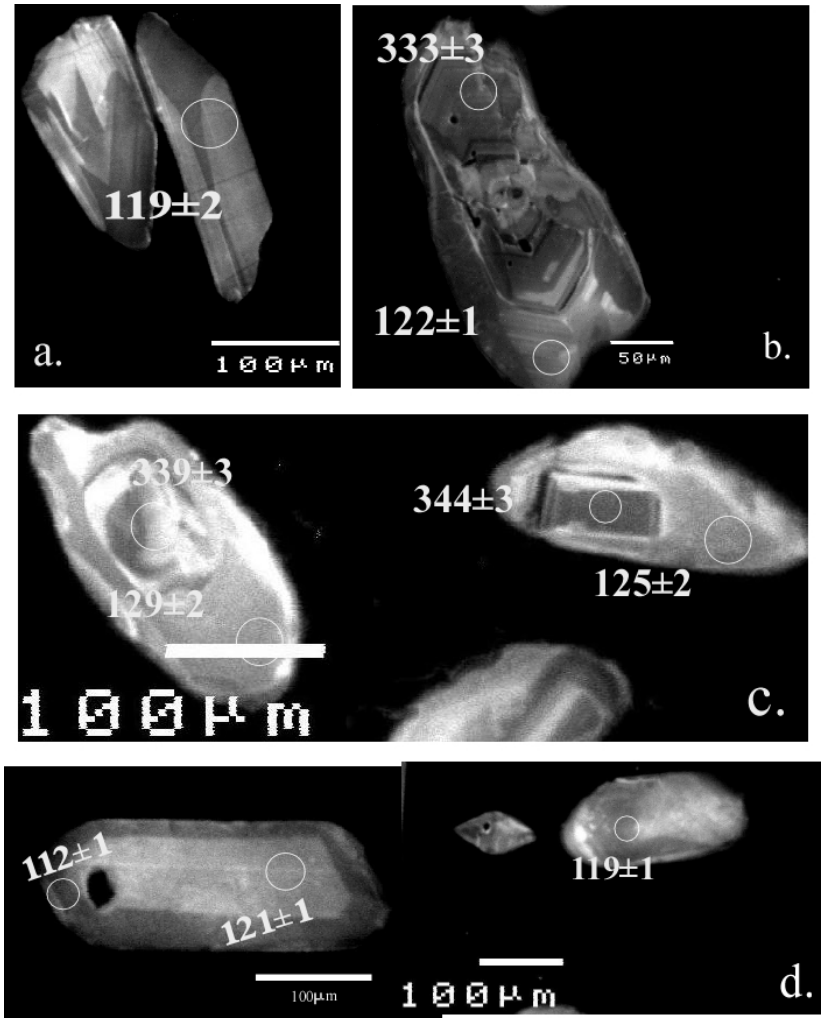


***Figure 6.5.*** *Cathodoluminescence images of representative zircons from intermediate (High-Na, trondhjemitic variety) dykes dated by U-Pb isotopes. The ages are in Myr.* ***(a)*** *Zircons from MD-17A.* ***(b)&(C)*** *Zircons from MD-32****; (d)*** *CL images of Homogeneous and patchy zircons from MD-32****.***

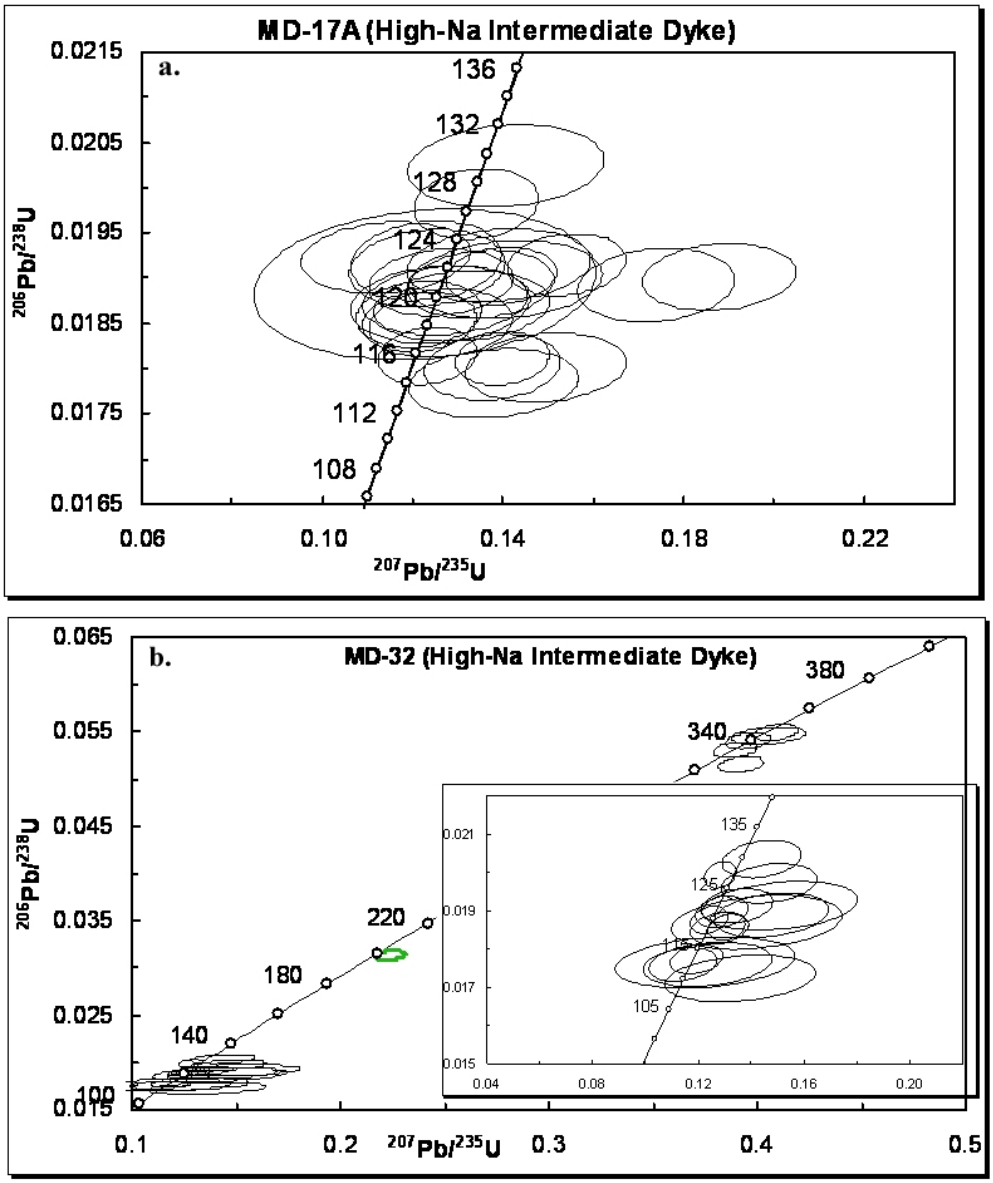


***Figure 6.6.*** *Concordia diagrams summarizing U-Pb isotope data from zircons of intermediate dykes (High-Na Trondhjemitic variety) of Mt Daniel, Fiordland;* ***(a)*** *MD-17A;* ***(b)*** *MD-32.*

## 6.6. Granite Dykes: (MD-2 & MD-6)

**MD-2:** All the zircons in MD-2 have core-rim structures, where the cores generally show patchy zoning or magmatic zoning (see chapter-5) and the rims are very thin (Fig 6.7.a.).

Eighteen spot analyses have been carried out and one analysis is rejected due to reverse discordance. Only two of the zircon rims show Cretaceous $^{206}Pb/^{238}U$ ages of 140±6 Ma and 140±4 Ma (Fig 6.8.a.). Another eight analyses show a range of mixed ages of 305-140 Ma. The remaining seven spot analyses from cores yield a $^{206}Pb/^{238}U$ age range of 347 to 305 Ma (Fig 6.8.a.).

**MD-6:** The zircons in MD-6 have cores and thick rims (Fig 6.7.b.). Twenty-eight spot analyses were done on zircons from cores and rims and six analyses are rejected either due to very short signals or strong discordance (shown in red in Fig 6.8.b.). Eleven rim analyses yield a weighted mean of 112±8 Ma with a large scatter beyond analytical error (2σ, MSWD=27; Fig 6.8.b.), nine core analyses yield a $^{206}Pb/^{238}U$ age range of 334-247 Ma and two analyses yield mixed $^{206}Pb/^{238}U$ ages of 206 and 344 Ma (Fig 6.8.b.).

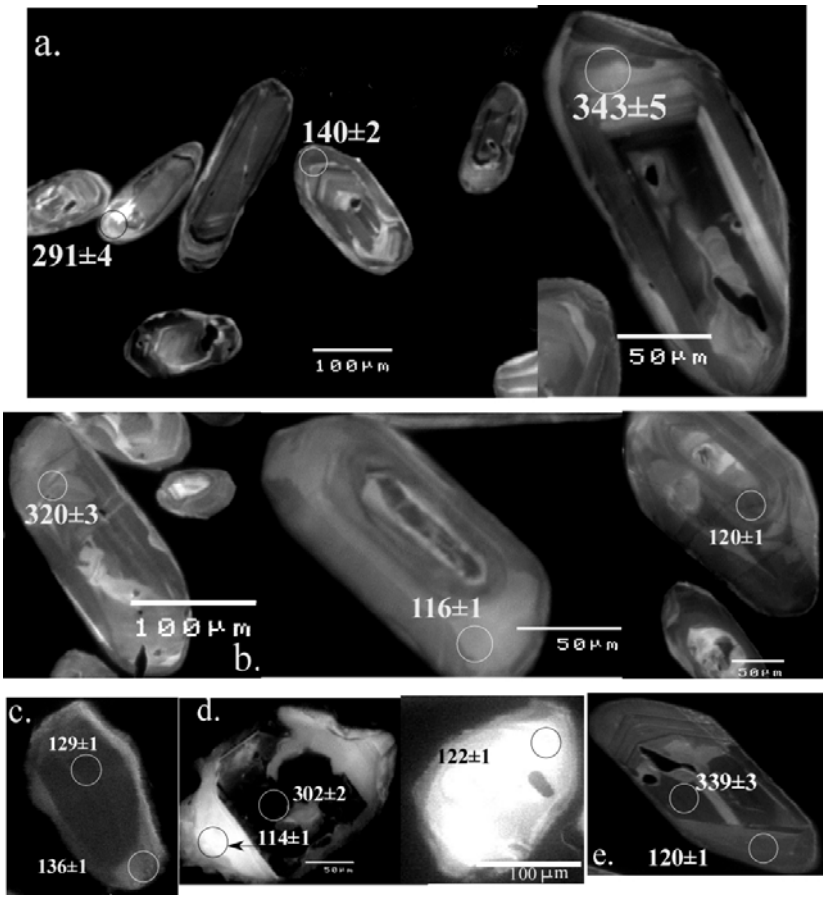


***Figure 6.7.*** *Cathodoluminescence images of representative zircons from granitic dykes and granitic phase in MDC dated by U-Pb isotopes. The ages are in Myr.* ***(a)*** *Granitic dyke MD-2;* ***(b)*** *Granitic dyke MD-6;* ***(c)*** *Unzoned CL-image of zircon dated from granitic sheet in MDC (MD-29);* ***(d)*** *Zircons dated from granitic sheet in MDC (MD-29);* ***(e)*** *Zircon core-rim structure dated from granitic sheet in MDC (MD-33).*

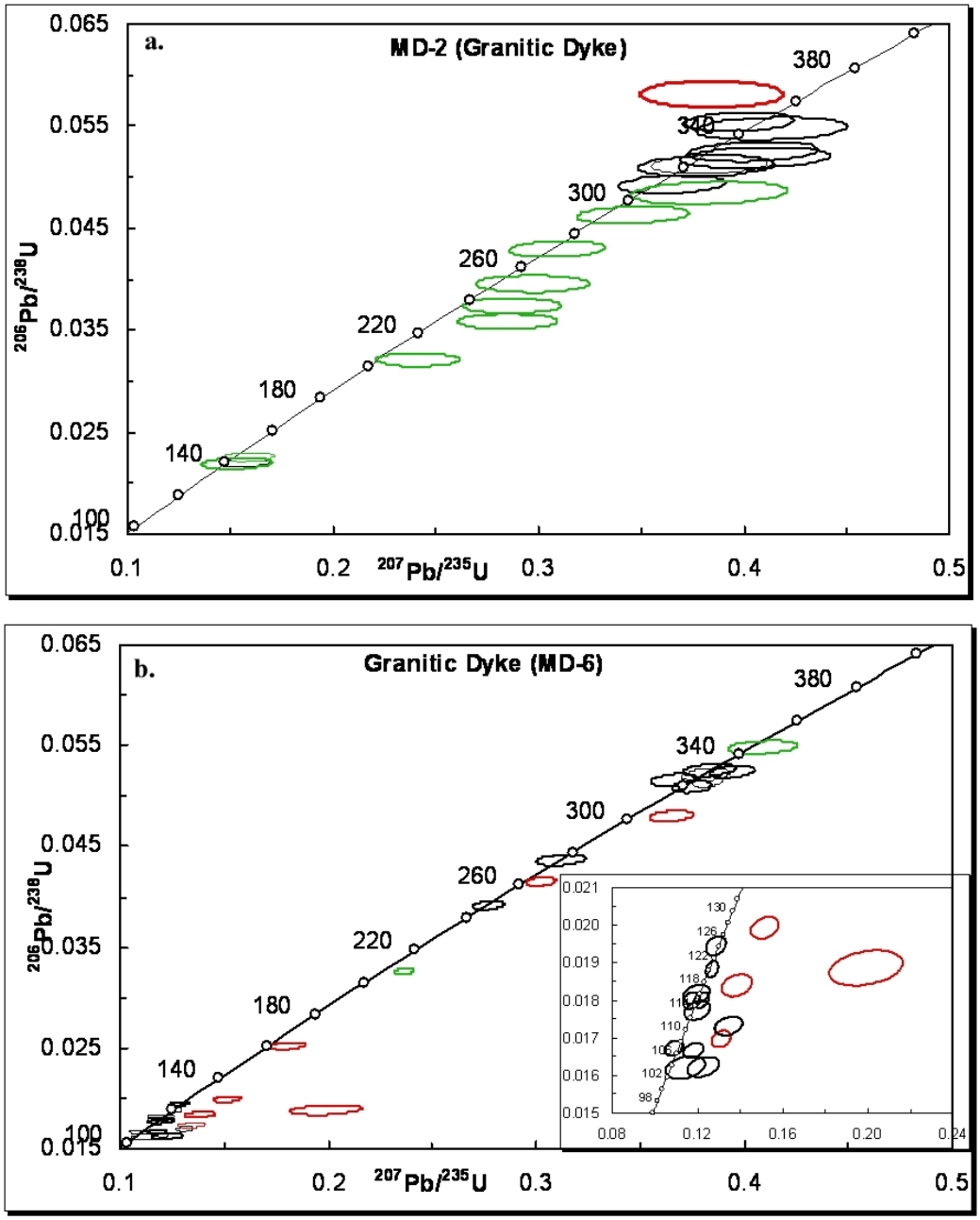


***Figure 6.8.*** *Concordia diagrams summarizing U-Pb isotope data from zircons of granitic dykes and sheets of Fiordland, Mt Daniel;* ***(a)*** *MD-2;* ***(b)*** *MD-6.*

## Granitic Sheets in Mt Daniel Complex: (Sample No: MD-29 & MD-33)

**MD-29:** Most of the zircons in MD-29 have core-rim structures and the rims are usually very thin. Some zircons are dark and unzoned without any evidence for inherited cores (Fig 6.7.c). CL-bright zircons without any inherited cores are also present (Fig 6.7.d.).

Twenty-two spot analyses were done on different grains from cores and rims and three analyses are rejected due to short signals or strong discordance. Only two rim analyses show Early Cretaceous ages of 123±4 and 114±2 Ma. The rims are very thin and those are not viable targets for LA analysis, so good analyses of rims are rarely obtained. Some of the zircon analyses have similar Early Cretaceous ages from 140 to 129 Ma but these ages are older than the emplacement of the WFO and thus cannot represent the igneous crystallization age of MD-29. One of these zircons yields a small difference in core to rim age where the rim gives 129 ± 2 Ma and core 136 ± 2 Ma. The $^{206}Pb/^{238}U$ ages of cores range from 365 to 268 Ma (Fig 6.9.a.).

**MD-33:** The zircons from MD-33 show core and rim structures (Fig 6.7.e.) and rims are usually thin and not viable targets for LA analysis. Twenty-one spot analyses were done and one analysis is rejected due to a short signal. Three analyses give an Early Cretaceous age range of 133-120 Ma, of which the youngest two are 120±2 and 121±2 Ma (yield a weighted mean $^{206}Pb/^{238}U$ age of 121±4 Ma, 2σ, MSWD=0.18; Fig 6.9.b.). The cores have $^{206}Pb/^{238}U$ ages between 373-260 Ma (Fig 6.9.b.).

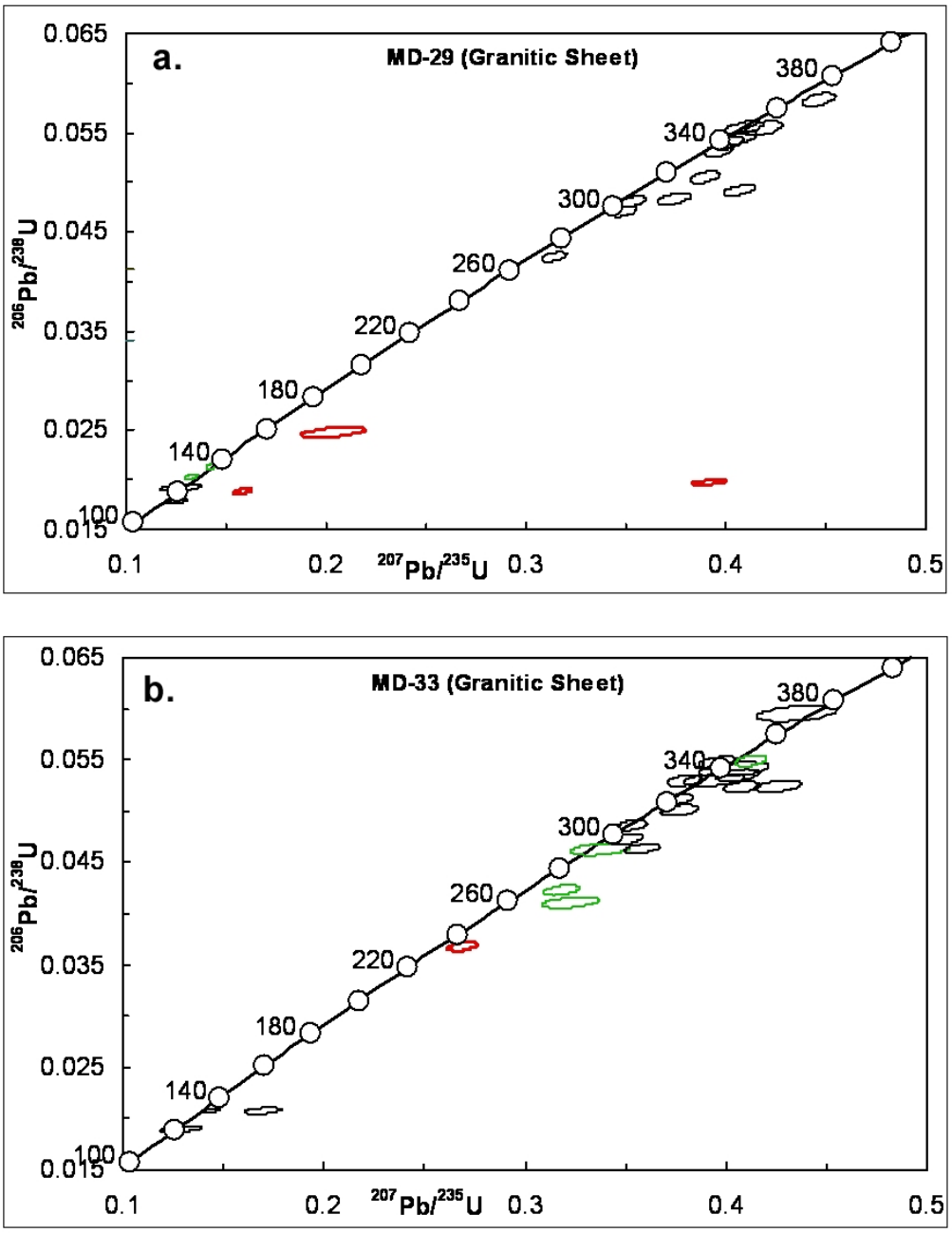


***Figure 6.9.*** *Concordia diagrams summarizing U-Pb isotope data from zircons of different granitic sheets of Fiordland, Mt Daniel;* ***(a)*** *MD-29;* ***(b)*** *MD-33. The rejected analyses are presented in red colour.*

## 6.7. Mt Daniel Sheets: (Sample No: MD-14 & MD-38)

**MD-14:** The zircons from Mt Daniel sheet (MDS) samples show variations in ages from core to rim. The zircons from MD-14 mostly have distinct core-rim structures (Fig 6.10.a.) Some grains show dark and bright striped zonation (Fig 6.10.b.).

A total of thirty-one spot analyses were done on different types of zircons from cores and rims and six of the analyses are rejected. Seven zircon rims give a $^{206}Pb/^{238}U$ age range of 129 to110 Ma and yield a weighted mean of 119±12 (2σ, MSWD=16; Fig 6.11.a.). Eighteen of the spot analyses of zircon cores have a $^{206}Pb/^{238}U$ age range of 332-158 Ma (Fig 6.11.a.) and some of them are mixed ages.

**MD-38:** The zircons in MD-38 mostly show dark patchy zoning. Zircons both with and without core and rim structures occur (Fig 6.10.c.). The core–rim boundaries commonly appear to be gradational.

32 spot analyses have been carried out and two analyses are rejected. Only one zircon with patchy zoning gives a younger age of 125±2 Ma (Fig 6.11.b.). The reminder of the zircon analyses, including the zircons without core-rim structure, yield a $^{206}Pb/^{238}U$ age range of 344-246 Ma (Fig 6.7.b.) including some mixed ages.

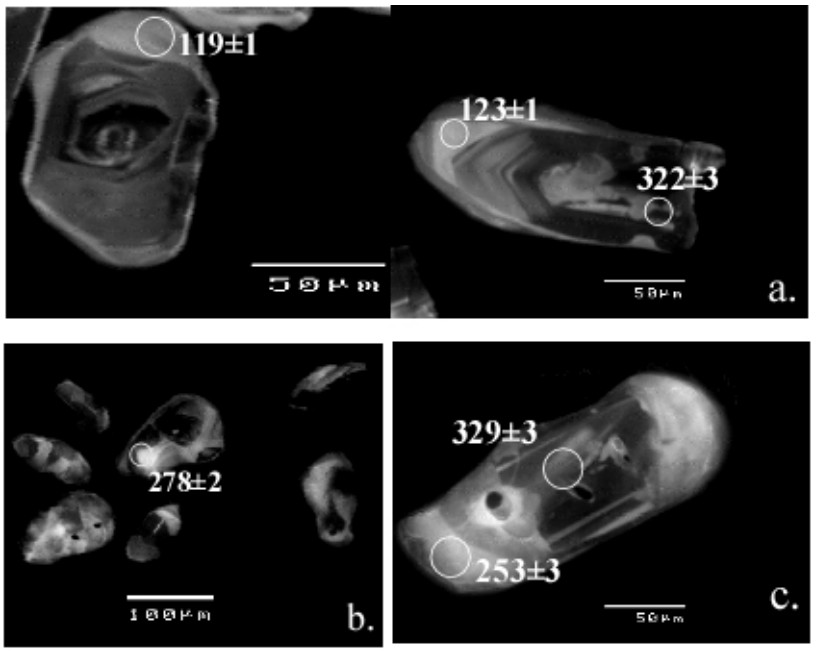


***Figure 6.10.*** *Cathodoluminescence images of representative zircons from intermediate rocks in MDS dated by U-Pb system. The ages are in Ma.* ***(a)*** *CL-images of zircons with core-rim structures dated from MDC rock (MD-14);* ***(b)*** *CL-images of zircons with dark & bright stripes dated from MDC rock (MD-14);* ***(c)*** *Typical CL-image of zircons dated from MDC rock (MD-38).*

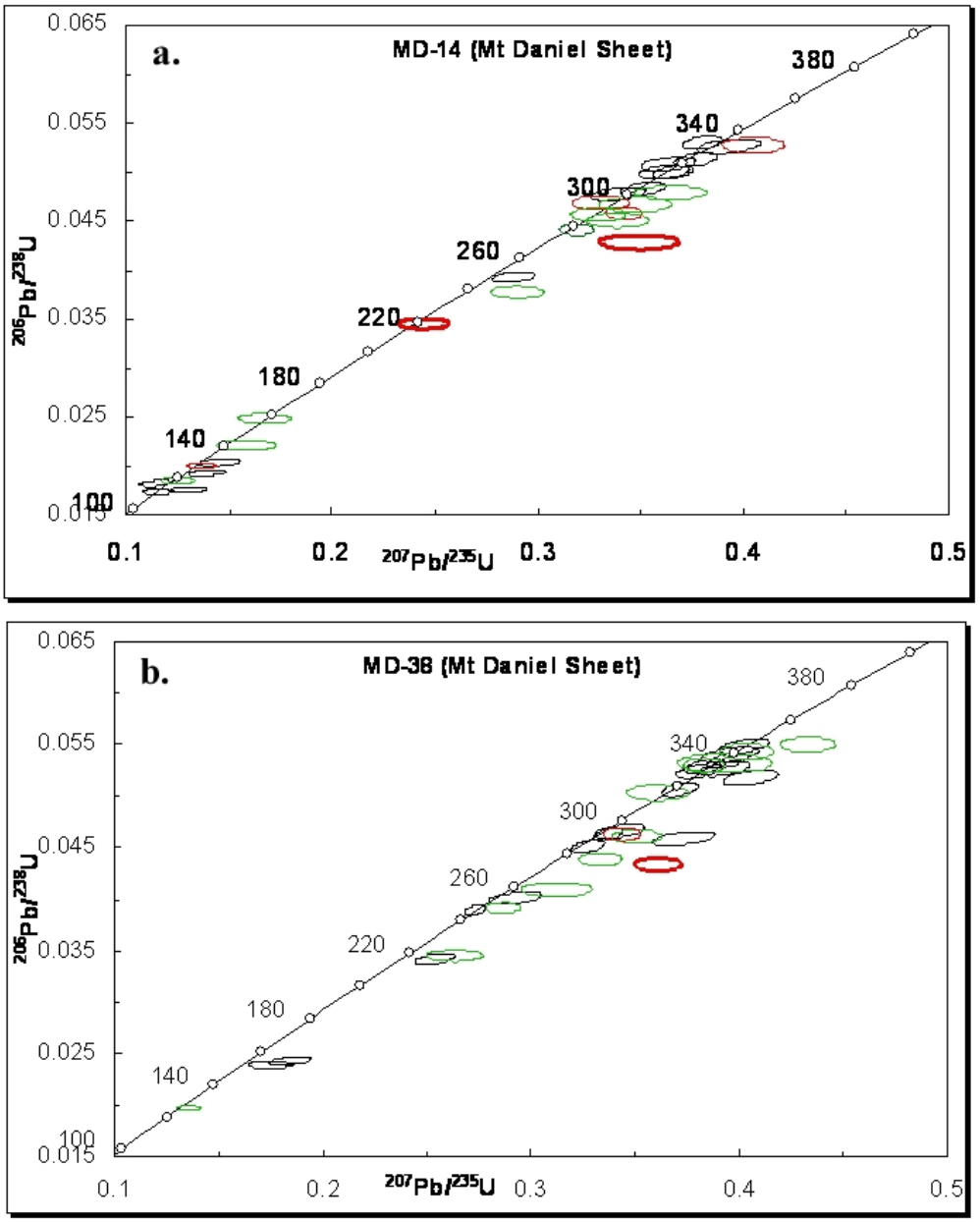


***Figure 6.11.*** *Concordia diagrams summarizing U-Pb isotope data from zircons of Mt Daniel sheets, Fiordland;* ***(a)*** *Concordia diagram from zircons from MDS sample MD-14;* ***(b)*** *Concordia diagram from zircons from MDS sample MD-38.*

## 6.8. Discussion and Interpretation of Age Data of Mt Daniel Rock Groups

The age variation shown by zircons of the different samples is summarized in Table 6.1.

The WFO (MD-15) has magmatic zircons of 125 Ma. A single zircon has an inherited core of Palaeozoic age of 338 Ma. Published ages from the WFO (Mattinson et al., 1986; McCulloch et al., 1987; Gibson et al., 1988, Hollis et al., (2004) are 126-116 Ma, consistent with this study. These ages are considered as the emplacement age of the igneous protolith WFO. Two phases of WFO emplacement have been reported by (Hollis et al., 2004), which are 126 Ma and 114 Ma. They consider that the 126 Ma zircons from WFO were unaffected by metamorphism related to the later phase of WFO emplacement at 114 Ma. This study shows a single growth event of zircons at 125±2 except for the presence of a single inherited core. Similar to Hollis et al., (2004), no evidence was found of new metamorphic zircons or overgrowths at 114 Ma in WFO.

The zircons from different rock types of the Mt Daniel Complex produced a variable age range. The zircons without inheritance and overgrowths from different rock types of the MDC have a coherent Early Cretaceous age ranging from 125-107 Ma. The inherited cores also show a coherent Paleozoic age range from 376-300Ma.

The zircons from mafic dykes MD-13 & MD-22B and high-Na dyke MD-17A do not contain any inheritance. The zircons from these samples yield Early Cretaceous ages of 123-119 Ma. MD-17A has magmatic the population age of 119±2 Ma zircon and can be considered as the magmatic crystallisation age. The zircons from mafic dyke MD-26, low (MD-8 and MD-22A) and high-Na (MD-32) intermediate dykes, granitic dykes and sheets and MDS samples show two main age populations corresponding to core and rim structures. The zircon rims formed during the Early Cretaceous (125-106 Ma) and the cores have Palaeozoic ages (376-300 Ma). Some zircons in mafic dyke MD-26 and low and high-Na intermediate dykes (MD-8 and MD-32 respectively) have single zircons without inherited cores (see chapter-5) and yield similar Early Cretaceous ages (125-106 Ma) which are within error with the age of the rims.

Apart from these ages the zircons from intermediate dyke MD-22A (low-Na) and MD-32 (high Na), granites and the MDS samples have core and rim structures and yield a much more complicated spread of Pb/U ages, commonly ranging between 300-140 Ma and also include older ages. This age range may not directly represent the original age of the zircons for the following reasons:

**1)** Mixed sampling by the laser of Cretaceous rims and Paleozoic cores, particularly where the zircons have thin rims. This is apparent from the time resolved signals. Most of the granitic samples have very thin rims and give a large number of mixed ages. Particularly the zircons from MD-2 have lack of rims. Only few very thin rims were able to analyse but produced a comparatively older mixed ages of 140 Ma. These mixed ages are produced by drilling through core-rim boundary. All the analyses that yield ages within 305-140 Ma in MD-2 show mixed signals. This is older than the emplacement age of the WFO and can not be the crystallisation age of the MD-2 magma as all the granitic dykes cross-cut the WFO.

**2)** Partial Pb-loss from older Palaeozoic cores can in part also cause this variation. Pb-loss is suggested by the recrystallised structure (patchy zoning in CL) along with the 'mixed' signal from the particular analysis. The mixed signals appear in the case of partial Pb-loss of the zircons. During transgressive recrystallisation of older protolith zircon non-essential structural constituent cations with different ionic radii from Zr (Hf) and Si are expelled from the zircon structure. As $Th^{+4}$ has a larger ionic radii than $U^{+4}$, $Th^{+4}$ is preferentially purged from the zircon structure, leading to a decrease in Th/U ratio. The U-Th-Pb ages also decrease correspondingly due to this effect and mixed isotopic ages occur between the recrystallised area and recrystallisation front (Hoskin and Black 2000, Möllar et al, 2002, Tomaschek et al, 2003). The isotopic age of the zircon will be completely reset in case of complete recrystallisation.

In MDC samples, some mixed signals are observed where the spot is on a gradational boundary between core and rim. Some zircons that yield ages within the range of 305-140 Ma have no evidence for mixed signals and lack patchy zoning. These zircons are sometimes unzoned. In these cases it is difficult to distinguish between lead loss and the ages being the original crystallization age of the zircon.

**Examples of possible Pb-loss in different samples of MDC**

A slight change of ages from centre of the grain (core, e.g. 349±6 Ma in grain#2) towards rim (e.g. 334±6 Ma in grain#2) are observed in some zircons of low-Na intermediate dyke MD-22A. In a few cases the cores show younger ages (e.g. 324±6 Ma in grain# 61 of sample 22A) than the rims (e.g.338 ±6 Ma)**.** In both of the cases the slight changes in age are probably due to partial Pb-loss from the original inherited core. Similar cases are commonly encountered in the zircons of granite samples MD-6 and MD-33. The domains of partial Pb-loss are patchy or recrystallized or homogeneous structure with gradational boundaries. The patchy zoning is very common in zircons from MD-38 with recrystallised structures (see chapter-5).

In granite sample MD-29 the wide dispersion of the weighted mean value of the rims **(**MSWD=9.7**)** may be partly due to the small number of analyses (only 3). The two ages (129 Ma and 136 Ma) mentioned earlier (in sec 6.6.) from a single zircon in MD-29 show dark homogeneous cores and thin homogeneous rims in CL. As signals are not mixed it is hard to identify whether the ages are the original age of the zircon or a completely isotopically reset age.

## 6.9. Conclusion

The WFO provides a key age constraint on the formation of the MDC because the MDC is younger than WFO, based on field relations (chapter-2).

Early Cretaceous zircons in mafic dykes, intermediate dykes (low-Na and high-Na) and granites (except MD-2, discussed before) and MDS samples are younger than the inferred WFO emplacement age, but in most cases the average zircon ages are within error. This is consistent with the field evidence (see chapter-2).

The high-Na intermediate dykes show a variation in zircon ages and morphology where both are younger than WFO and also consistent with the study of Hollis et al., (2004). MD-17A shows typical magmatic zircons without any inheritance (see chapter-5) of 119 Ma. In contrast, MD-32 shows both Early Cretaceous zircons without inheritence and overgrowths (120 Ma) on abundant inherited cores of Palaeozoic age.

The abundant inherited Palaeozoic cores in most of the rock-groups suggest an extensive crustal input into the Cretaceous magmas. However, the origin of Cretaceous zircons may have various possibilities as discussed in Chapter-5. The zircons could be magmatic, metamorphic or they could form in a transitional environment where igneous crystallisation and metamorphism overlap. A dynamic environment where magmatism and deformation and metamorphism all happened in a very short time span is consistent with the field evidence (see chapter-2).

| Rock Type | Sample No | Type of newly formed zircons | Age range of newly formed zircons : Early Cretaceous (Ma) | Weighted mean | Presence of mixed ages (Ma) | Age range of inherited cores (Ma) |
|---|---|---|---|---|---|---|
| **WFO** | MD-15 | Magmatic | 128-122 | 125±2 (n=9/10) | Absent | Only 1 grain; 338 |
| **Mafic Dykes** | MD-13 | Cl-bright & Cl-dark zircons without inheritance | 126-110 | 123±6 (n=9/10) | Absent | Absent |
| | MD-22B | Cl-bright and Cl-dark grains without inheritance | 128-114 | 122±2 (n=12/13) | Absent | Absent |
| | MD-26 | Cl-bright grains without inheritance | 128-119 | 124±6 (n=8/8) | Absent | Cores of Cl-dark grains; 376-306 |
| **Intermediate Dykes (low-Na variety)** | MD-8 | Cl-bright grains without core and rims of Cl-dark grains | 114-106 | 112±12 (n=4/4) | Absent | Cores of Cl-dark grains; 330-310 |
| | MD-22A | Rims | 128-121 | 125±18 (n=3/3) | Present | 362-313 |
| **Intermediate Dykes (high-Na trondjhemitic variety)** | MD-17A | Magmatic | 119-115 | 119±2 (n=24/25) | Absent | Absent |
| | MD-32 | Rims | 129-110 | 120±6 (n=16/16) | Present only one | 344-323 |
| **Granite Dykes** | MD-2 | Rims(only 2 grains found) | 140-139 | 140±6 (n=2/2) | Present | 347-305 |
| | MD-6 | Rims | 120-107 | 112±8 (n=11/13) | Present | 329-302 |
| **Granitic phase in MDC** | MD-29 | Rims (Two rims only) | 123-114 | - | Present | 341-300 |
| | MD-33 | Rims (two rims only) | 121-120 | - | Present | Two cores only; 372-339 |
| **MDS** | MD-14 | Rims | 129-110 | 119±12 (n=8/8) | Present | 332-300 |
| | MD-38 | A single Rim | 125 | - | Present | 344-316 |

***Table 6.1****. Summary of zircon U-Pb age data from different samples of Mt Daniel.*

# Chapter 7: Electron Probe Microanalysis of zircon and Garnet from Mt Daniel Rocks, Fiordland

## 7.1. Introduction

Zircon is a significant reservoir of Hf, Y and heavy REE with other elements including Ti, P, U, and Th. Zircon acquires major changes in its chemical composition during different stages of magmatic crystallisation or during metamorphism. The major changes in the trace element composition within individual zircon crystals may track magma crystallization processes (e.g. fractionation, assimilation) or the metamorphic growth history experienced by the zircon (e.g. metasomatism, recrystallisation). These chemical changes help in understanding the geological history and genesis of the magmatic and metamorphic rocks in which the zircon crystallized.

This chapter mainly discusses the results of EPMA (Electron Probe Micro-Analyzer) analyses of zircons and garnets and their significance.

EPMA analysis is mainly conducted because of two reasons: (1) the Hf value of zircon and garnet can be used as an internal standard for further detail trace element and REE analysis in LA-ICP-MS (Varian); (2) major and some trace elements (Zr, $SiO_2$, Hf, Y,) values from EPMA can help to understand the trace elements behaviour in inter and intra zircon populations and if there is any relation with garnet formation. The analytical method has been discussed in detail in (Chapter-3). The detailed EPMA data are presented in Appendix 4.

| Rock Types | Element concentration (average range for individual rock types in ppm) | | | Sample No | Element concentration (range for individual rock samples in ppm) | | |
|---|---|---|---|---|---|---|---|
| | Zr | Hf | Y | | Zr | Hf | Y |
| **WFO** | 476500-487300 | 8750-12300 | 100-1100 | **MD-15** | Same as average value | Same as average value | Same as average value |
| **Mafic Dykes** | 481850-505600 | 5450-10700 | 100-4700 | **MD-13** | 501000-505600 | 6000-8700 | 100-930 |
| | | | | **MD-22B** | 486300-497400 | 5450-10600 | 100-1500 |
| | | | | **MD-26** | 481850-496150 | 6200-10700 | 100-4700 |
| **Intermediate Dykes (low-Na variety)** | 491000-505000 | 6500-13000 | 100-5000 | **MD-8** | Similar to average value | Similar to average value | Similar to average value |
| | | | | **MD-22A** | Similar to average value | Similar to average value | Similar to average value |
| **Intermediate Dyke (high-Na variety)** | 475000-493200 | 7000-19000 | 100-2200 | **MD-17A** | 475700-487800 | 7500-10000 | 100-2200 |
| | | | | **MD-32** | 476200-493200 | 7000-19000 | 100-2200 |
| **Granitic Dykes** | 475000-508600 | 6300-22900 | 100-6350 | **MD-2** | 477400-499500 | 7400-17600 | 100-6350 |
| | | | | **MD-6** | 475000-496700 | 6300-18700 | 100-6300 |
| **Granitic rocks in MDC** | | | | **MD-29** | 489100-508600 | 7150-22900 | 100-5100 |
| | | | | **MD-33** | 477750-493600 | 9140-20100 | 100-5300 |
| **MDC Rocks** | 476800-493200 | 7650-12700 | 100-6800 | **MD-14** | 477700-493200 | 7650-12200 | 100-6800 |
| | | | | **MD-38** | 476800-488700 | 7800-12700 | 100-4200 |

***Table 7.1.*** *Selected EPMA data of zircons from different samples of Mt Daniel.*

## SECTION A: Electron Probe data of Zircons from Mt Daniel Rock Groups

### 7.2. Western Fiordland Orthogneiss: (Sample No: MD 15)

The age of the zircons from the WFO sample MD-15 is 125±2 Ma with only one inherited core at 338 Ma.

The Zr and Hf content of zircons from WFO do not vary widely (Fig 7.1.a) and the values are represented in Table 7.1.a. The Y content varies up to 1100ppm (Fig 7.1.b). There is no specific change in pattern of Hf/Y ratio for individual zircon grains.

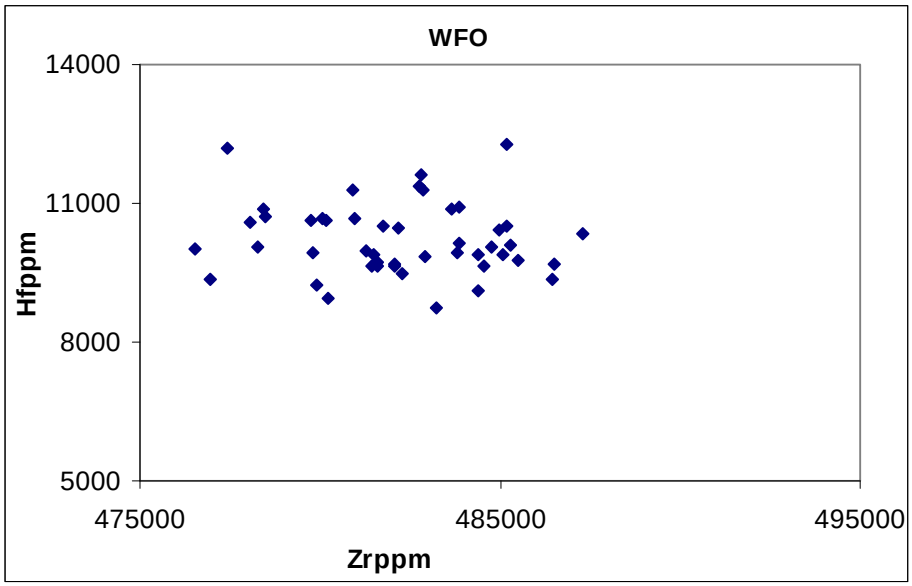


***Figure 7.1. (a)*** Hf-Zr plot of zircons from Western Fiordland Orthogneiss of Mt Daniel, Fiordland.

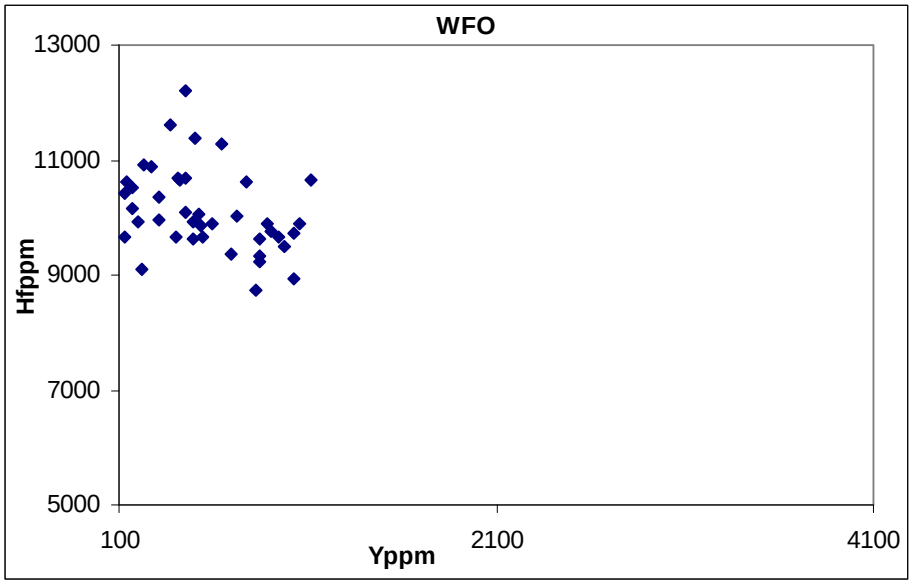


***Figure 7.1. (b)*** Hf-Y plot of zircons from Western Fiordland Orthogneiss of Mt Daniel, Fiordland.

## 7.3. Mafic Dykes: (Sample No: MD13, MD22B, MD 26)

CL-images of zircons from mafic dykes show two different grain populations of CL-bright and CL-dark grains in all three samples. MD-13 and MD-22B show similar Early Cretaceous age 123±6 Ma and 122±2 Ma for both grain populations without no inherited cores. In MD-26 CL-bright grains have an Early Cretaceous age (124±6 Ma) similar to two other mafic samples and the CL-dark grains contain inherited cores with variable ages (376-306 Ma).

The average Zr, Hf and Y concentration of zircons in mafic dykes and in individual samples are presented in Table 7.1.a. The Zr concentration of zircons is almost the same in MD-22B and MD-26, but concentrations are higher in MD-13 and present as a separate cluster (Fig 7.2.a.). The Zr content is high in the zircons' of MD-13 and clustered separately whereas MD-22B and MD-26 zircons have similar values. It may indicate that the Zr content may be higher in the MD-13 magma than MD-22B and MD-26.

Zircons from all the mafic dykes show a similar range of Hf concentration. However, MD-22B has wide range of variation and MD-26 is slightly on the higher side of Hf values as the Paleozoic inherited cores in MD-26 have higher Hf concentration.

Y values of zircons in MD-26 are much higher than other two mafic samples (Table 7.1.a.). The high Y content is mainly from the dark-CL zircons of MD-26 of Palaeozoic age.

Hf and Y value varies in individual zircon from core to rim. The Hf/Y ratio of zircons in all of the mafic rocks increases significantly from core to rim. The general trend of core-rim variation is shown in (Fig 7.2.b.) and core-rim variations of some zircons from representative sample MD-22B are shown in (Fig 7.2.c.). Generally the Y decreases and Hf increases from core to rim but Hf concentration does not change as strongly as Y. This core to rim variation of Hf/Y is commonly present in the zircons with older inherited cores of around 330 Ma and younger rims of around 120-125 Ma rather than the zircons without core and rim structures. Although the Hf/Y ratios of zircons cluster between 100-2000 for varying Hf in mafic rocks (MD-22B and MD-13) and in MD 26 Hf and Y both vary widely. The presence of inherited cores in MD-26 represents a more contaminated-mixed variety rock type than other two mafic dykes.

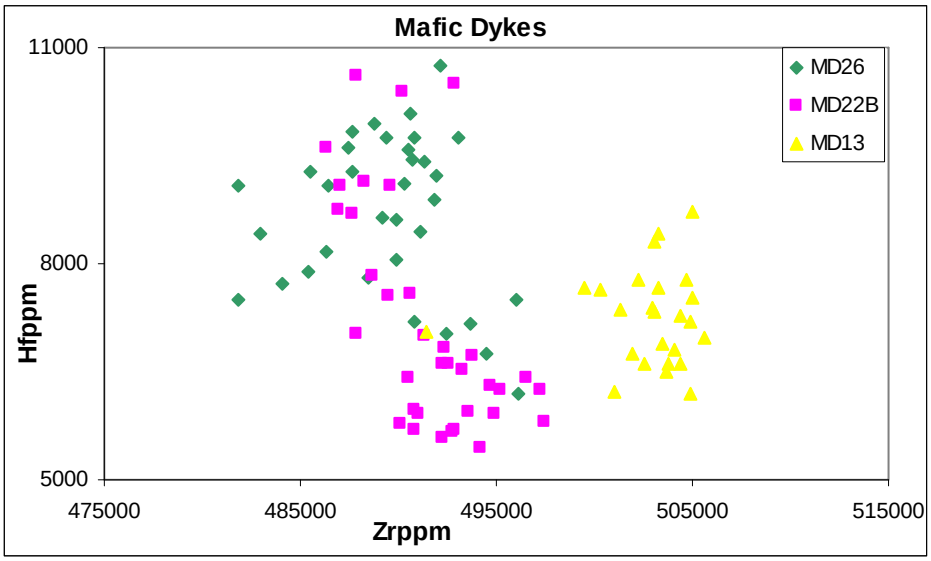


***Figure 7.2. (a)*** *Hf-Zr plot of zircons from 3 different mafic dykes* from Mt Daniel, Fiordland.

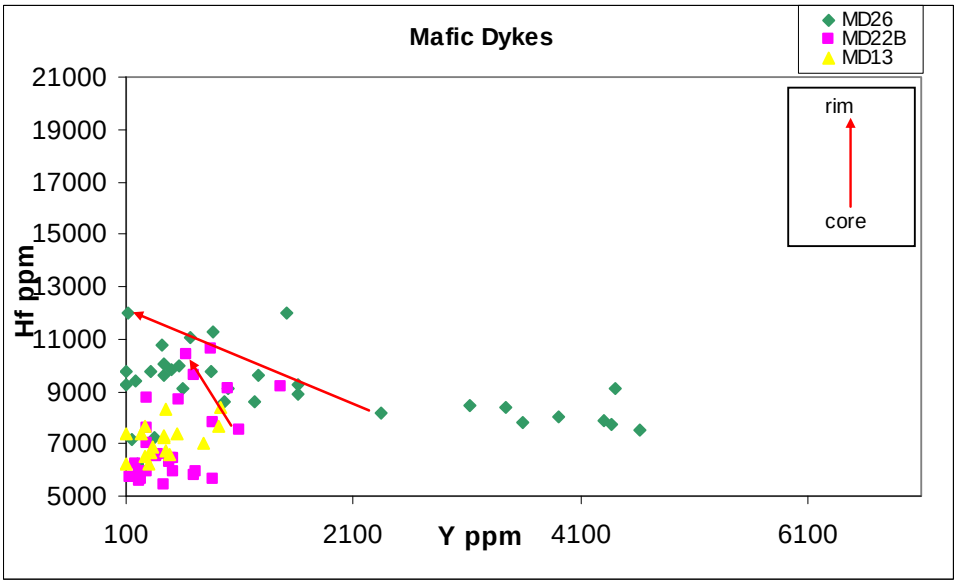


***Figure 7.2. (b)*** *Hf-Y plot of zircons from three different mafic dykes* from Mt Daniel, Fiordland. *Increases of Hf/Y ratio in a single grain of zircon (sample no- MD-22B) has been shown with arrow from core to rim and the arrow is also showing the average direction of increasing Hf/Y ratio from core to rim of most of the zircons.*

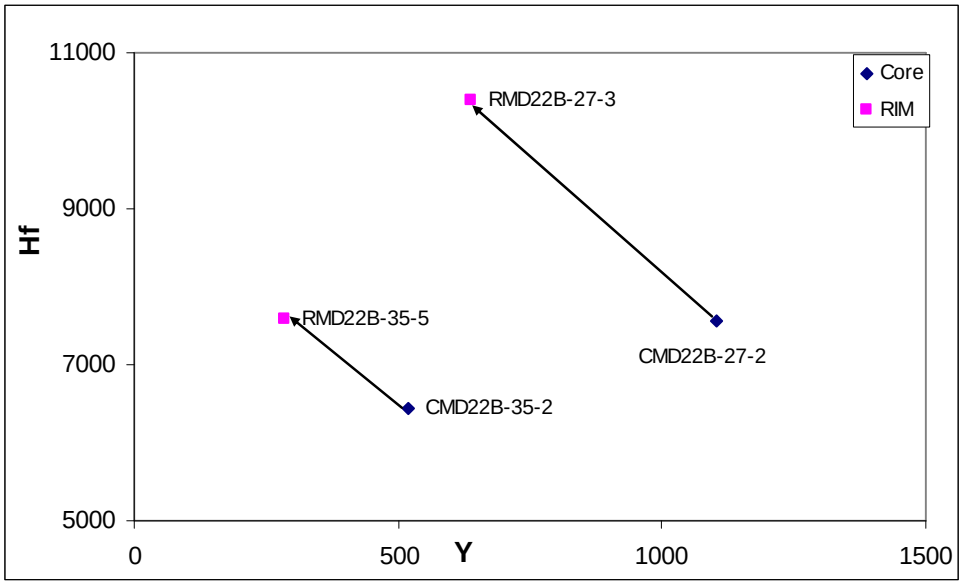


***Figure 7.2. (c)*** *Increases of Hf/Y ratio in two different grains of zircon (from representative sample no- MD-22B)* of mafic dykes from Mt Daniel, Fiordland *has been shown with arrow from core to rim. The other samples follow the same trend.*

## 7.4. Low-Na Intermediate Dykes: (Sample No: MD-8 and MD-22A)

MD-8 has both CL-bright zircons without inheritance and CL-dark zircons with core-rim structures. MD-22A has zircons with inherited cores and rims.

The CL-bright zircons without inheritence and rims of both of the samples are Early Cretaceous in age (125-111 Ma). The inherited cores in MD-8 and MD-22A show a wide range of Palaeozoic ages (362-320 Ma).

Zircons from both of the intermediate dykes (low-Na variety) show a very similar range of Zr, Hf and Y contents (Table 7.1.a). Zr content in these dykes is more restricted where as Hf and Y content varies widely (Fig 7.3.a. and 7.3.b.).

In Fig 7.3.b the Hf contents of zircons remain nearly within the same range for both of the samples while Y contents vary widely upto 5000ppm. Most of the zircons of intermediate dykes show a consistent increase of Hf/Y ratio from core to rim and the general trend is shown in Fig 7.3.b and a

variable trend is also observed. The Hf/Y ratio of zircons in MD8 shows little variation from core to rim (Fig 7.3.c.). It may be because of that the Y content of zircons decreases from dark core to light rim more strongly than Hf. The Y variation is more pronounced in the zircons which are dark in CL with inherited cores than the Cl bright zircons of Early Cretaceous age without having any inherited cores. So the high Y values are mainly from the very dark inherited cores from mafic sample (MD-26).

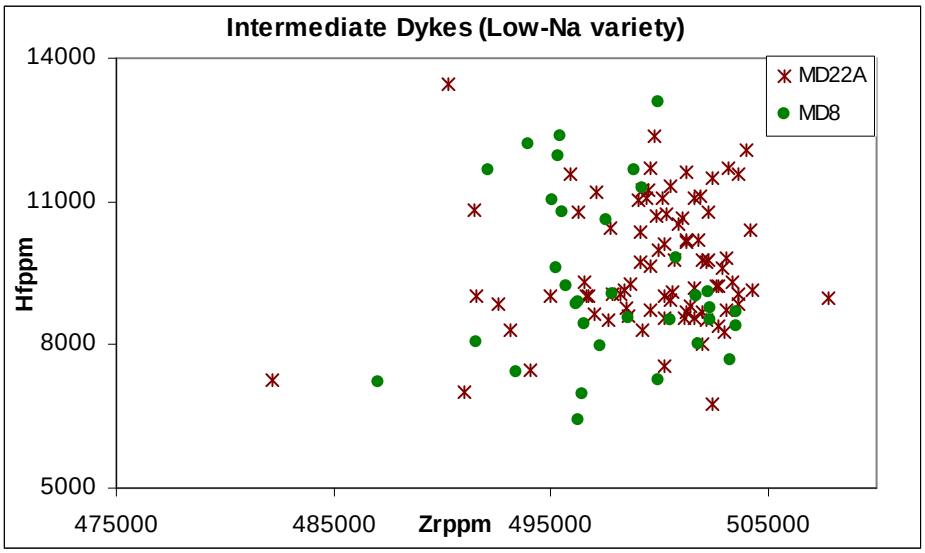


***Figure 7.3. (a)*** *H-Zr plot of zircons from low-Na intermediate dykes of* Mt Daniel, Fiordland.

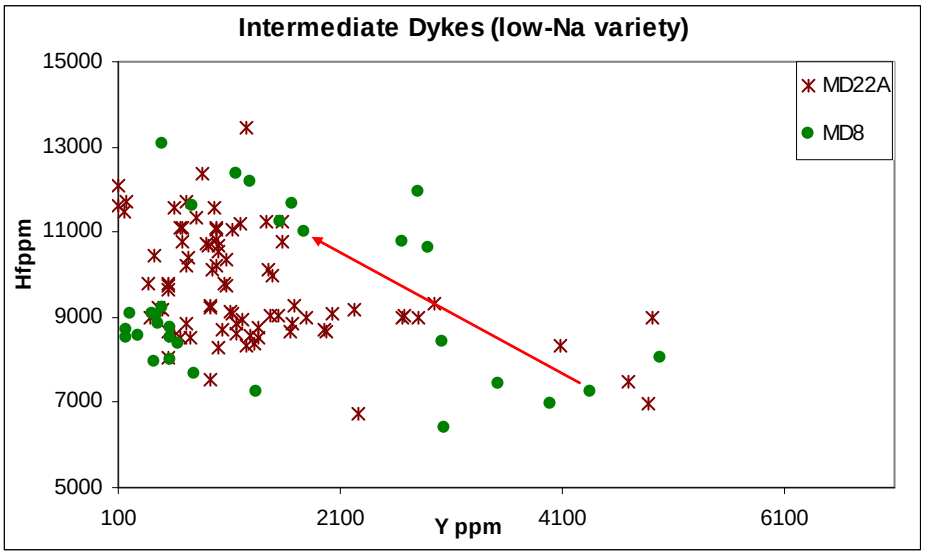


***Figure 7.3. (b)*** *Hf-Y plot of zircons of low-Na intermediate dykes* from Mt Daniel, Fiordland. *Increases of Hf/Y ratio in a single grain of zircon (sample no-MD-8) has been shown with arrow from core to rim and the arrow is showing the average direction of increasing Hf/Y ratio from core to rim of most of the zircons though MD-8 shows a variable directions .*

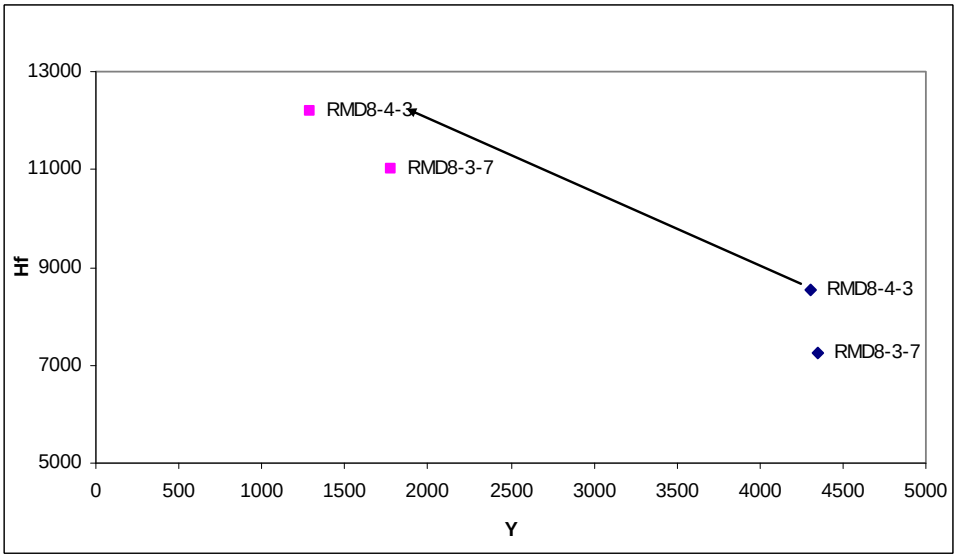


***Figure 7.3. (c)*** *Increasing Hf/Y ratio of zircons from core to rim has been shown with arrow of some representative grains from low-Na intermediate dyke (MD-8).The other sample follows the same trend.*

## 7.5. High-Na Intermediate Dykes: (Sample No: MD17A and MD32)

The zircons from MD-17A exhibits Early Cretaceous age of 119±2 Ma. The inherited cores of zircons from MD-32 show Palaeozoic age of (344-323) Ma and rims show Early Cretaceous age of 120±6 Ma.

The two high-Na intermediate dykes have zircon with different concentrations of Zr, Hf and Y (Table 7.1.a.). The Hf content of zircons of MD-17A does not vary much as MD-32 and Zr content is similar in both of the samples (Fig 7.4.a.). Zircon in MD-32 has two different clusters of Hf concentration; one is similar to MD-17A (7400-9300ppm) and another group has high Hf concentration (1000-18730 ppm, Fig 7.4.a.). The Y concentration of zircons in both of the samples is similar (Fig 7.4.b.).

In MD17A some of the zircons with planar zoning and broad oscillatory-zoning (see chapter 5) show systemic increases in Hf/Y from centre to rim and the general trend is shown in (Fig 7.4.b.) but the zircons with patchy zoning and sector zoning have no such pattern. The core-rim variation of zircons is shown in details in (Fig 7.4.c.). In MD-32 the Hf/Y ratio of zircon is decreases from core to rim. These reverse sequences happen as both the Hf and Y concentrations are decreasing towards the rim.

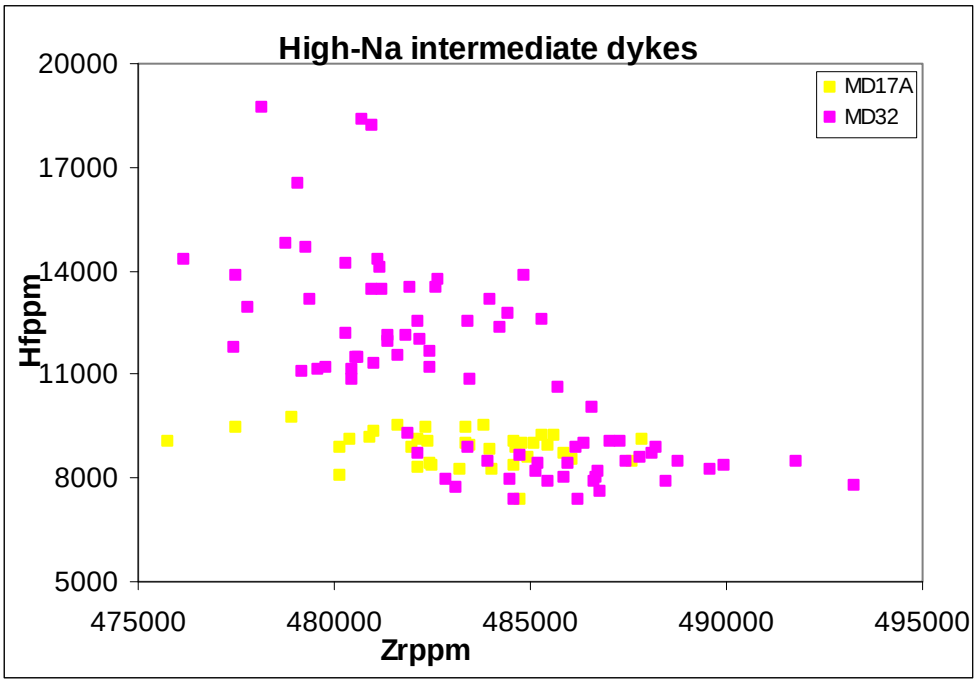


***Figure 7.4. (a)*** *Hf-Zr plot of zircons from two high-Na intermediate dykes* from Mt Daniel, Fiordland.

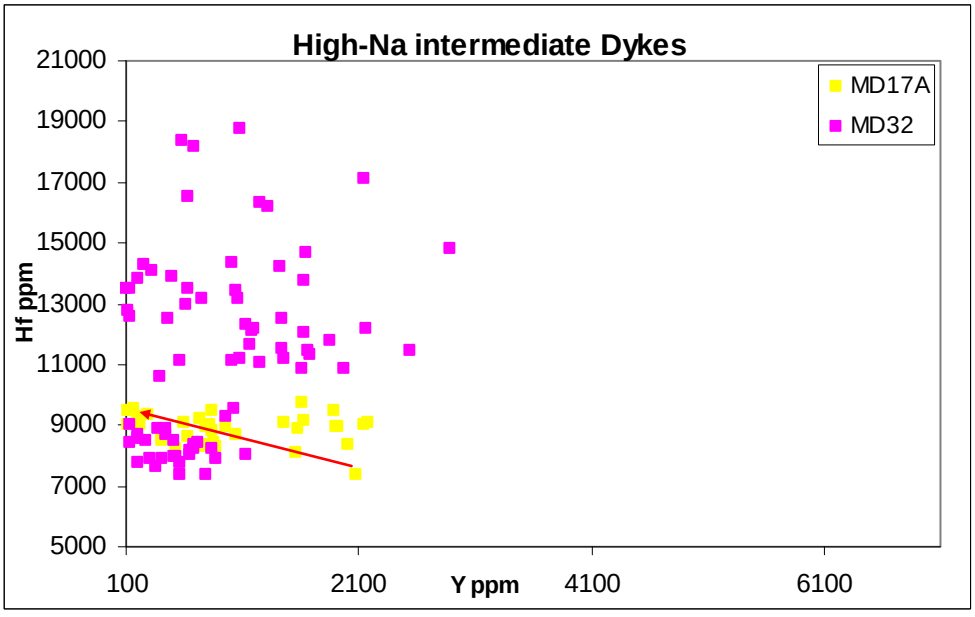


***Figure 7.4. (b)*** *Hf-Y plot of zircons of two samples of high-Na intermediate dykes* from Mt Daniel, Fiordland. *Increases of Hf/Y ratio in oscillatory zoned and planar banded igneous zircon (sample no- MD-17A) is shown with an arrow from core to rim and the arrow is also showing the average direction of increasing Hf/Y ratio from core to rim of most of the zircons.*

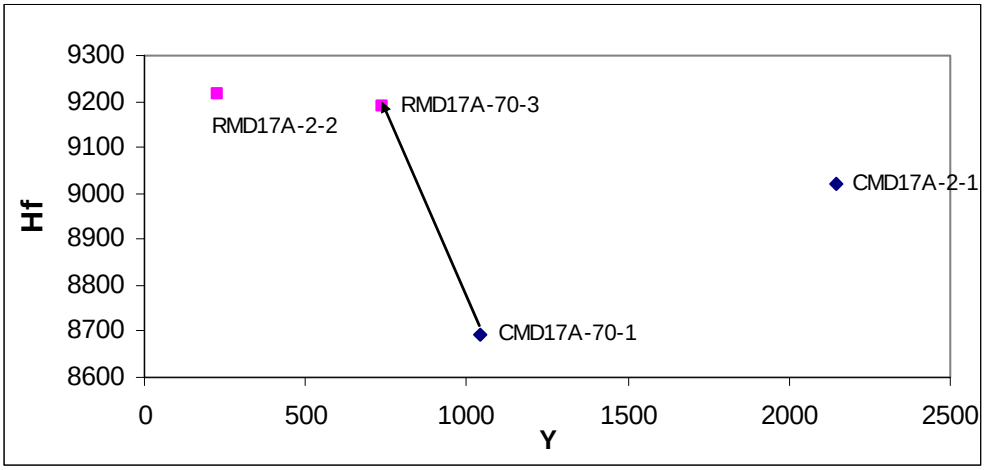


***Figure 7.4. (c)*** *The core-rim variations have been shown with the arrow of some representative zircons of sample MD-17A. The other zircons in MD-17A follow the similar trend.*

## 7.6. Granite Dykes: (Sample No: MD-2 and MD-6)

The zircons from granite dyke MD-6 have core-rim structures where the cores are inherited of Palaeozoic age (329-302 Ma) and rims are 112±8 Ma in age. Zircons from MD-2 do not contain any Early Cretaceous rims and the youngest age obtained from rims is 140±6 Ma and may be consider as a mixed age because of very thin rims (see chapter-6).

The granitic dykes MD-2 and MD-6 have similar ranges in Zr and Hf but the Hf values of zircons above 12000ppm are more common in MD-6 (Fig 7.5.a.). These higher Hf analyses in MD-6 are mainly rims and the inherited cores in MD-2 typically have lower Hf. MD-2 has higher Y contents of zircons than MD-6 (Fig 7.5.b.). These zircons mostly have a dark inherited core and very thin light rim. The Hf/Y ratio increases systematically from core to rim in individual zircons (Fig 7.5.b.).

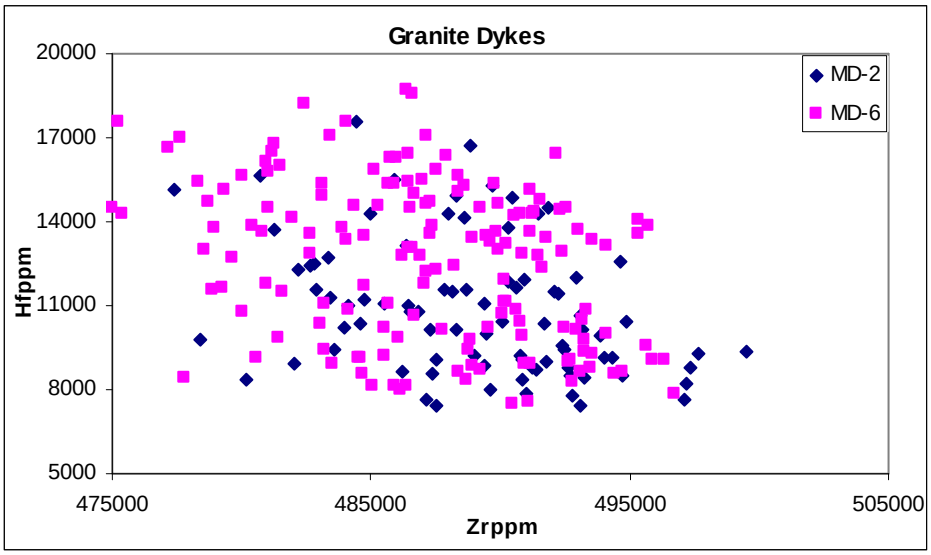


***Figure 7.5. (a)*** *Hf-Zr plots of zircons of two samples of granitic dykes* from Mt Daniel, Fiordland.

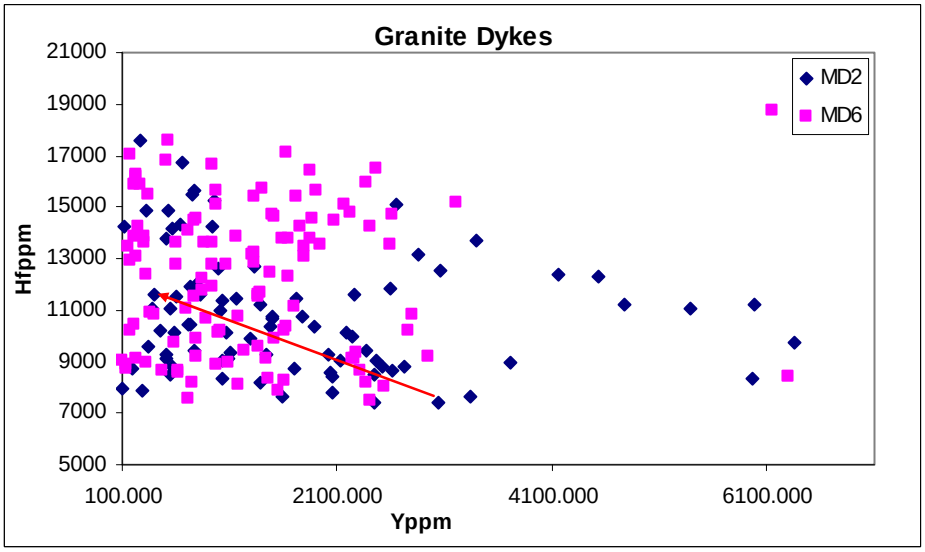


***Figure 7.5. (b)*** *Hf-Y plot of zircons of two granitic dykes* from Mt Daniel, Fiordland. *Increases of Hf/Y ratio in a single grain of zircon (sample no- MD-2) has been shown with arrow from core to rim and the arrow is also showing the average direction of increasing Hf/Y ratio from core to rim of most of the zircons.*

## Granitic Sheets: (Sample No: MD-29 and MD-33)

The MDC granitic sheets show zircon core-rim structures where the cores are inherited of Palaeozoic age and rims are Early Cretaceous in age (123-114 Ma).

MD-29 shows higher Zr content than MD-33 and similar range of Hf content with some scatter in values of higher concentrations of Hf from MD-33 zircons (Fig 7.6.a.). In both of the rocks zircons show similar ranges of Y values and mostly cluster within 100~2100ppm with some scattered data up to ~5000ppm (Fig 7.6.b.). The high Y zircons are mainly dark inherited cores. The Hf/Y ratio increases systematically from core to rim in individual zircons (Fig 7.6.b.).

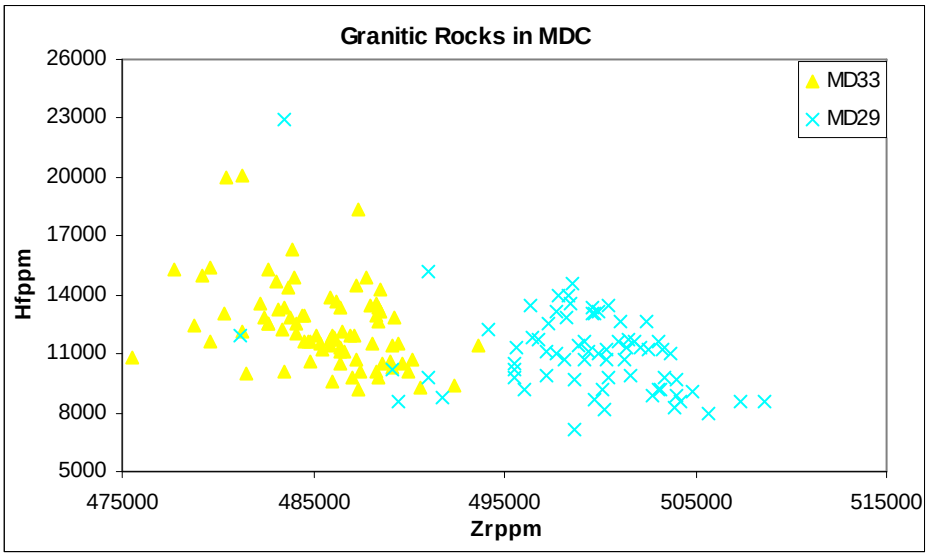


***Figure 7.6. (a)*** *Hf-Zr plots of zircons of two samples of granite* from Mt Daniel, Fiordland.

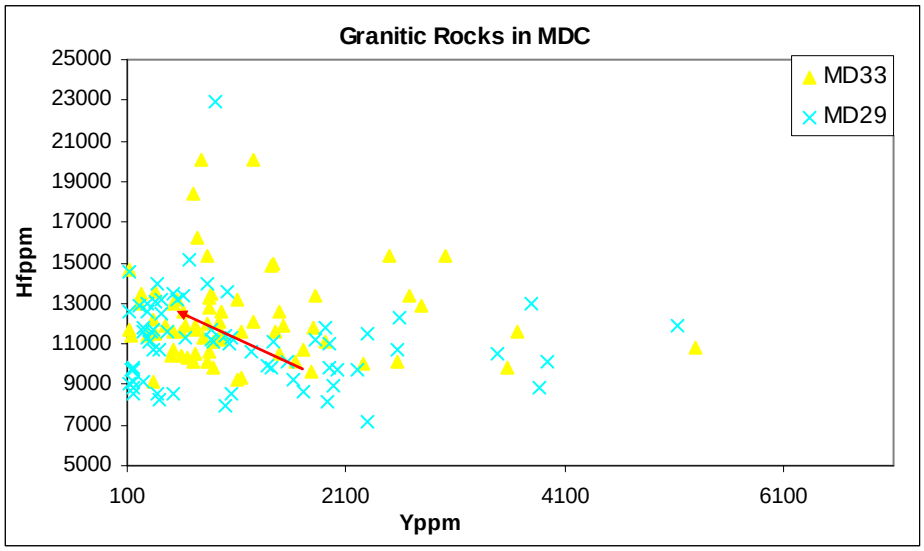


***Figure 7.6. (b)*** *Hf-Y plot of zircons from two granitic sheets* from Mt Daniel, Fiordland. *Increases of Hf/Y ratio in a single grain of zircon (sample no- MD-33) has been shown with arrow from core to rim and the arrow also shows the average direction of increasing Hf/Y ratio from core to rim of most of the zircons.*

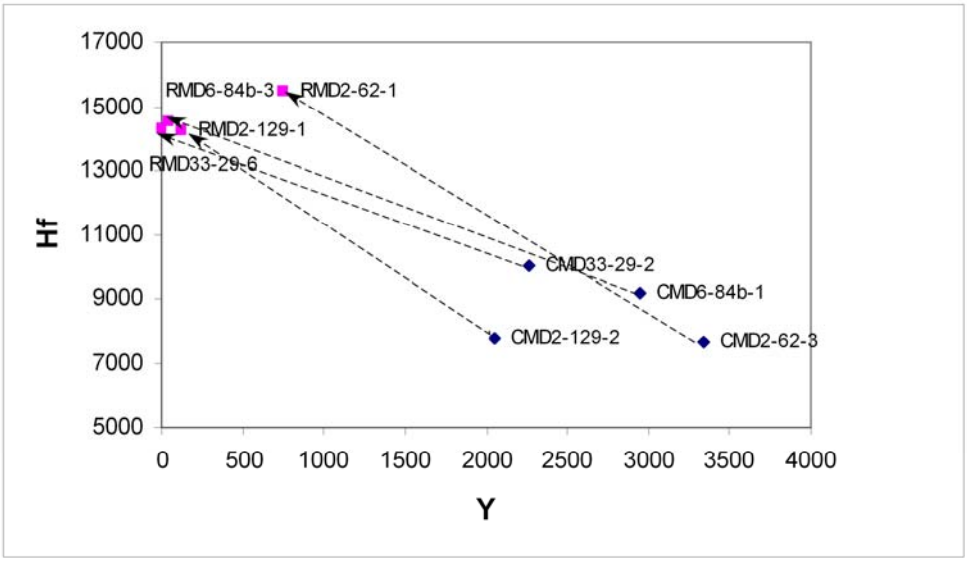


***Figure 7.7.*** *Increasing Hf/Y ratio of zircons from core to rim has been shown from different granite samples of Mt Daniel, Fiordland.*

## 7.7. Mt Daniel Sheets: (Sample No: MD-14 and MD-38)

The zircons from sample MD-14 and MD-38 from MDC rocks show core-rim structures where the cores are inherited, giving Palaeozoic ages ranging from 344-300 Ma. In MD-14 rims are 119±12 Ma and in MD-38 only a single rim gives an Early Cretaceous age of 125 Ma (see chapter-6).

The zircons from both of the samples of MDC sheets show variable Zr, Hf and Y content (Table 7.1.a). The zircons have lower Zr and higher Hf content in MD-38 compare to MD-14 (7.8.a.). Zircons of MD-38 have a restricted range in Y and clusters at values <2000 ppm but MD-14 shows a varied Y content up to 7000 ppm (Fig 7.8.b.).

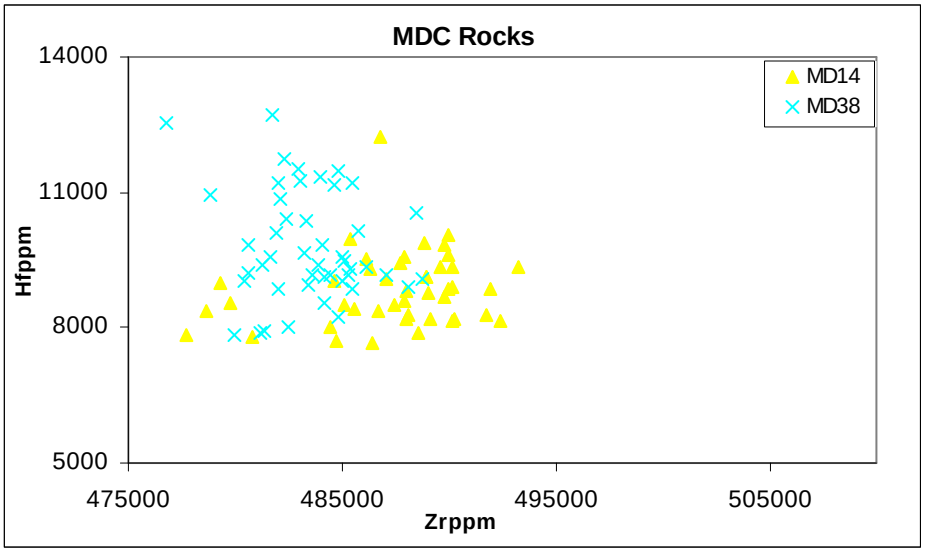


***Figure 7.8. (a)*** *Hf-Zr plots of zircons of two MDS samples* from Mt Daniel, Fiordland.

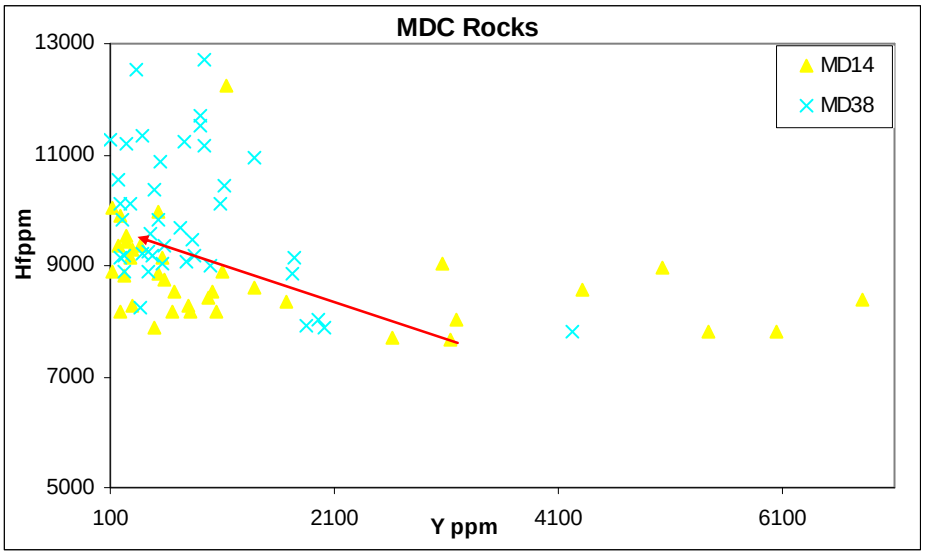


***Figure 7.8. (b)*** *Hf-Y plot of zircon from two MDS samples* of Mt Daniel, Fiordland. *Increases of Hf/Y ratio in a single grain of zircon (sample no- MD-14) is shown with an arrow from core to rim and the arrow also shows the average direction of increasing Hf/Y ratio from core to rim of most of the zircons.*

Most of the zircons of MDC sheets show a consistent increase of Hf/Y ratio from core to rim and the general trend is shown in (Fig 7.8.b.). The Y variation is more pronounced in the zircons with dark inherited cores and younger rims of Early Cretaceous age.

## 7.8. Discussion of Zircon Electron Probe Data from Mt Daniel Rock Groups

A large inter-grain and intra-grain compositional variation is observed in the zircons of the samples from Fiordland. Most of the samples show a steady increase of Hf/Y ratio of zircon from core to rim except the WFO zircons.

The Hf concentration of zircon increases with whole rock $SiO_2$ content (Fig 7.9.a.); granite with highest $SiO_2$ (~66-75 wt %) and Hf content followed by intermediate rocks and thereafter mafic rocks with lowest $SiO_2$ (~42-43wt %) and Hf content (Fig 7.9.b.).

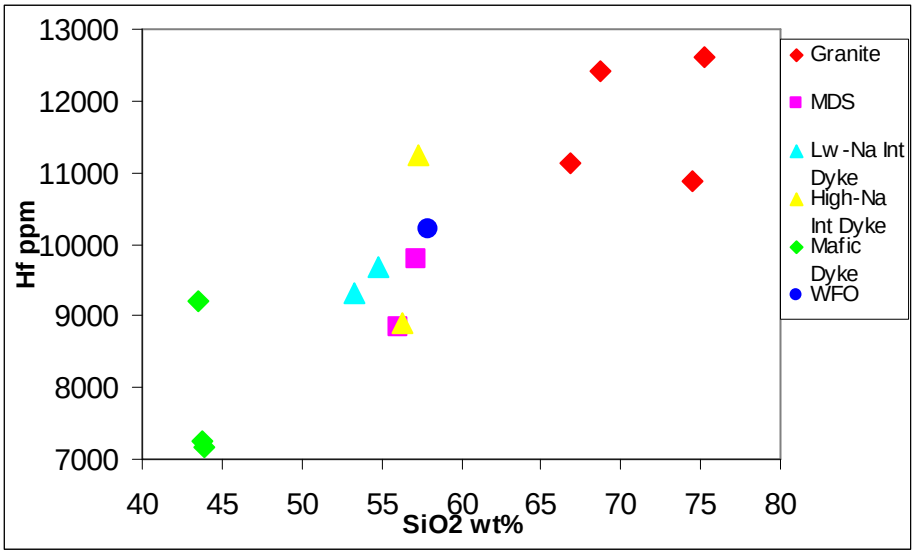


***Figure 7.9. (a)*** *Hf concentration in zircons vs. $SiO_2$ plot from all the rock types of Mt Daniel, Fiordland.*

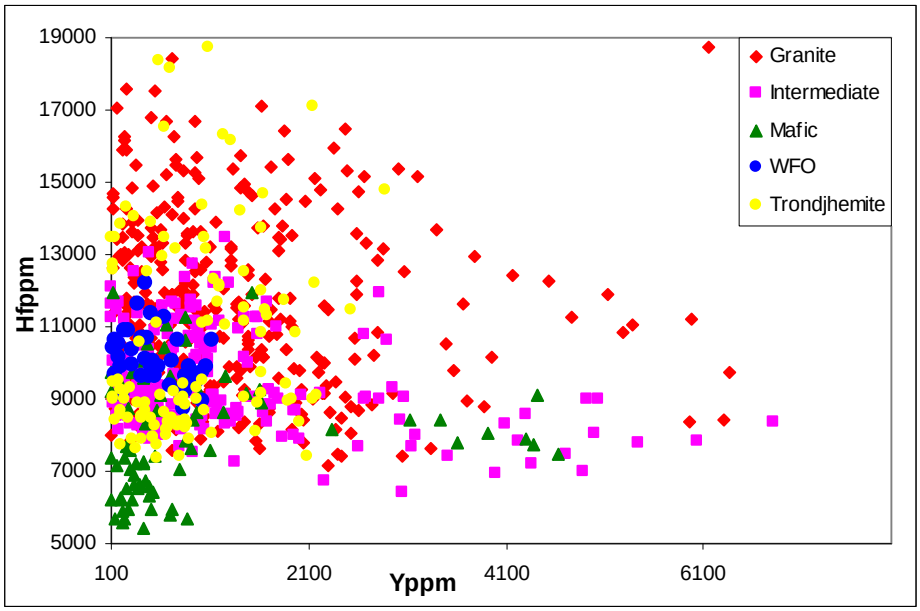


***Figure 7.9. (b)*** *Hf-Y plots of zircons from all the rock types of Mt Daniel, Fiordland.*

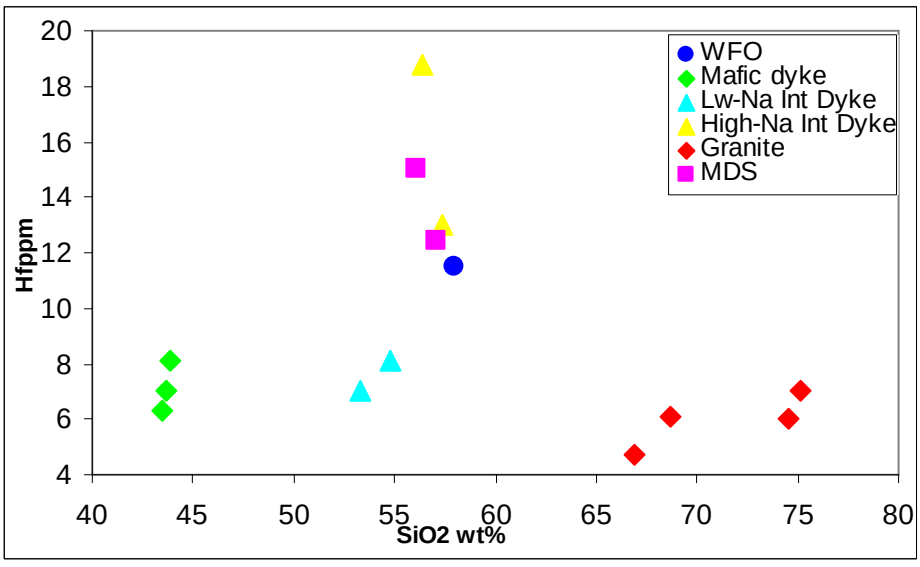


***Figure 7.9. (c)*** Whole-rock *Hf-$SiO_2$ plot of zircons from all the rock types of Mt Daniel, Fiordland.*

Hf concentration varies widely in granites, intermediate and high-Na rock types. It appears that Hf falls with increasing $SiO_2$ at $SiO_2$ above~ 60wt%, so Hf doesn't rise in the melt and that causes Hf in zircon to rise and correspondingly rising Hf/Zr ratio as zircon crystallizes (Fig 7.9.c.) (Claiborne et al., 2006).

These rocks contain higher amount of Paleozoic inherited cores suggesting the profuse crustal contamination of these magmas. Increase of Hf content with differentiation of the magma has also been reported from other intrusive rocks (e.g. the Boggy plain zoned pluton, Australia; Hoskin et al., 2000). The presence of Paleozoic inherited cores in zircons shift the Hf content towards higher values suggesting evolved origin of the cores compare to Early Cretaceous zircons. This effect is observed in mafic dyke MD-26 and High-Na intermediate dyke MD-32. So increasing Hf concentration in zircons is consistent with magma contamination and differentiation. Some of the zircons in most of the rock types, except WFO and high-Na intermediate dykes have high Y content and mostly they are dark inherited cores (Fig 7.9.).

Zircons with high Y content are mostly within the range 3000-6500ppm. These zircons have common characteristics. Their CL images are characterized by very dark cores of 330 Ma and light rims of 120-125 Ma. The cores have higher Y content than the rims. In a single crystal of zircon, the Y content varies between 527-6811ppm. Hoskin and Schaltegger (2003) have linked high-Y zircon to crustal affinity. Zr content doesn't vary much in inter- and intra-grain populations of zircon. The granites and the dykes and sheets of intermediate composition have the greatest range (475000-510000ppm) of Zr content.

## Comparison of Zircon and Whole Rock Data

The comparison of the whole rock Hf/Y vs. $SiO_2$ (Fig 7.10.a.) data with average zircon Hf/Y vs. $SiO_2$ (Fig 7.10.b.) data and whole rock Zr/Y vs. $SiO_2$ (Fig 7.10.c.) data with average zircon Zr/Y vs. $SiO_2$ (Fig 7.10.d.) data show very similar patterns.

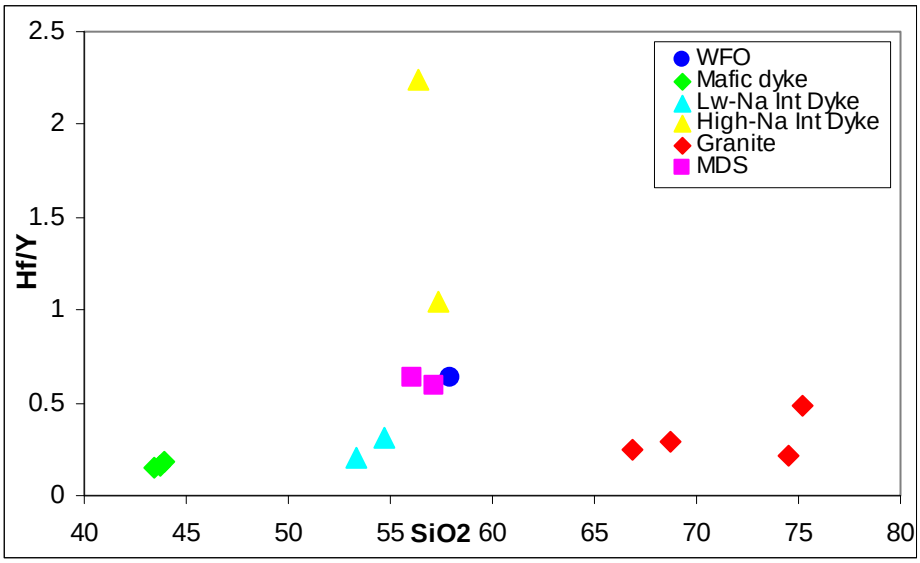


***Figure 7.10. (a)*** *Whole rock Hf/Y-$SiO_2$ plot of different representative samples from Mt Daniel Fiordland.*

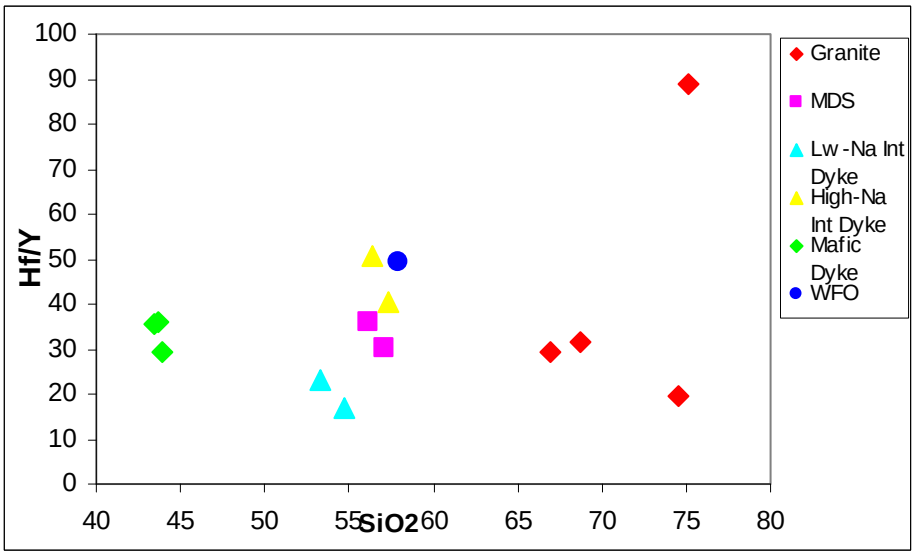


***Figure 7.10. (b)*** *Average Hf/Y-$SiO_2$ plot of zircons from different representative samples of Mt Daniel, Fiordland.*

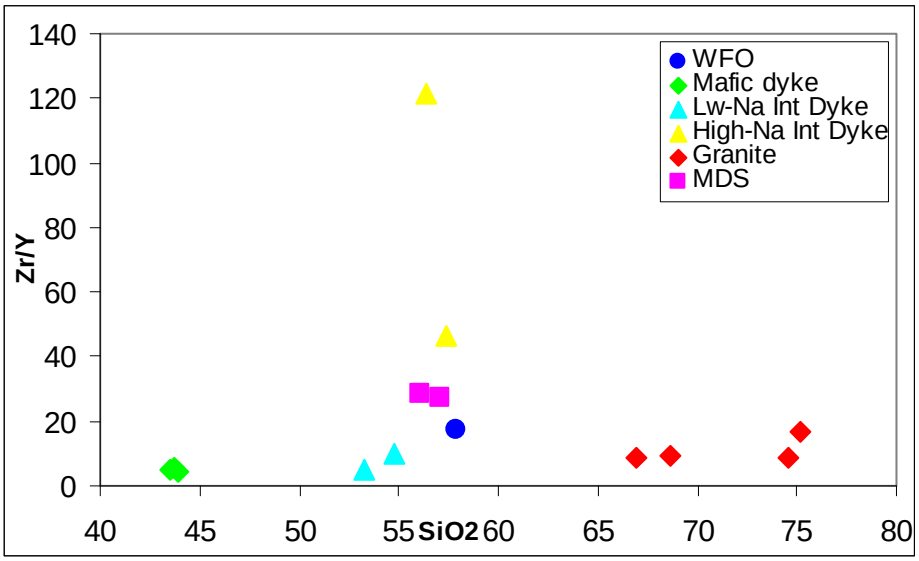


***Figure 7.10. (c)*** *Whole rock Zr/Y-$SiO_2$ plot of different representative samples from Mt Daniel Fiordland.*

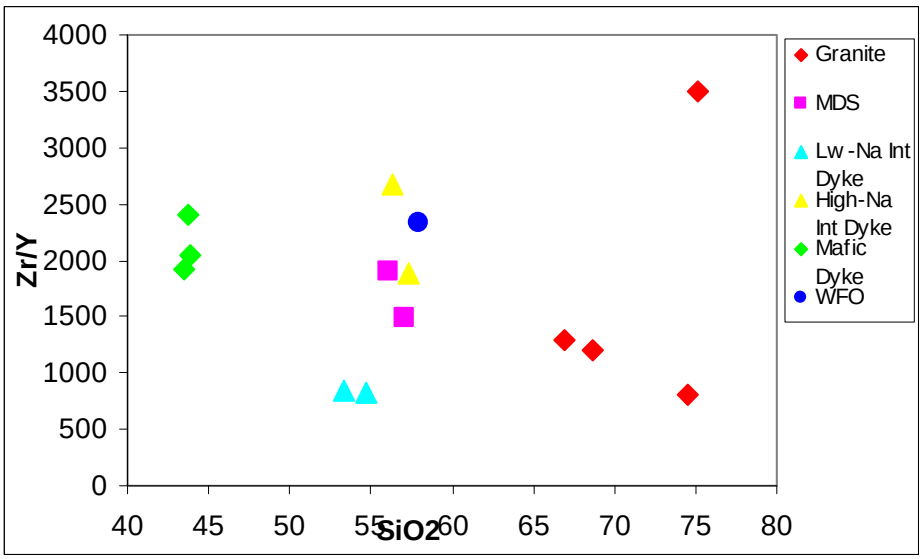


***Figure 7.10. (d)*** *Average Zr/Y-$SiO_2$ plot of zircons from different representative samples of Mt Daniel Fiordland.*

Zr-Hf ratios of zircons do not show much variation in different rock samples, with most of the zircons from each sample clustering together (Fig 7.11.). But there is a general trend to higher Hf/Zr in granites to mafics. The Hf/Zr vs. $SiO_2$ plot (Fig 7.12.a.) of whole rocks shows an opposite trend when compared to average Hf/Zr vs. $SiO_2$ of zircon (Fig 7.12.b.). In the average zircon plot shows increasing Hf/Zr with $SiO_2$ content from mafic to granitic rocks almost in a linear fashion while the whole rock Hf/Zr vs. $SiO_2$ shows more scattered data with higher values of Hf/Zr for mafic dykes and some of the intermediate rocks and WFO. Linnen and Keppler (2002) have experimentally shown the fractionation of Zr and Hf in a melts from which the zircons are crystallizing is related to the Zr/Hf activity coefficient ratio in the melt. Thus, fractional crystallisation of zircon will decrease the Zr/Hf ratio in metaluminous and peraluminous granitic melts and increase the abundance of $HfO_2$ in zircon. So these plots are also consistent with a zircon crystallization effect.

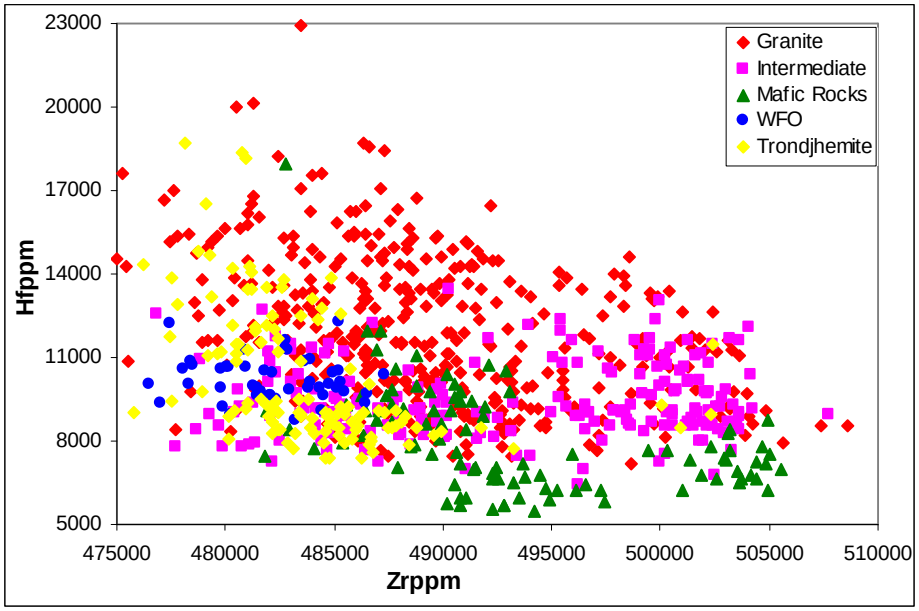


***Figure 7.11.*** *Hf-Zr plot of zircons from all the rock types of Mt Daniel Fiordland. Individual rock types have been represented by different colours and symbol.*

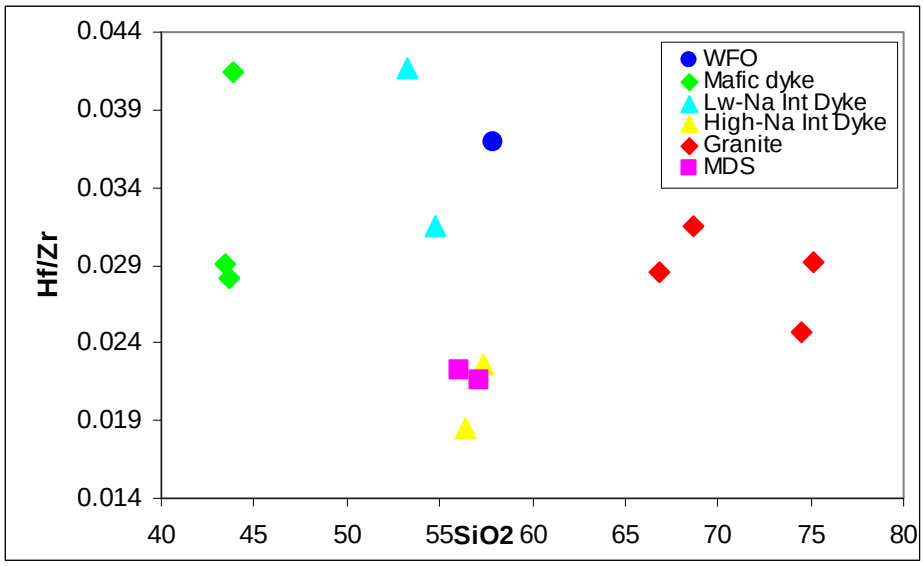


***Figure 7.12. (a)*** *Whole rock Hf/Zr-$SiO_2$ plot of different representative samples from Mt Daniel Fiordland*

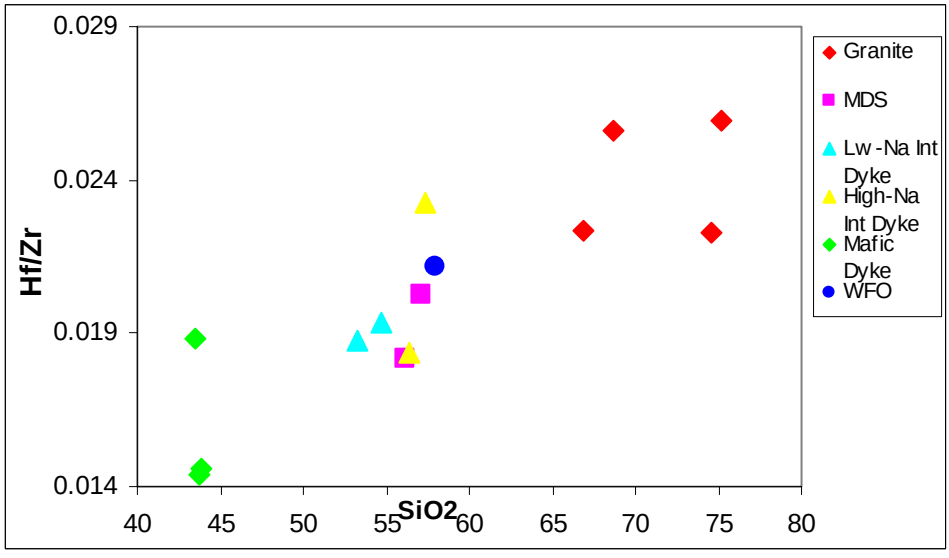


***Figure 7.12. (b)*** *Average Hf/Zr-$SiO_2$ plot of zircons from different representative samples of Mt Daniel, Fiordland.*

The whole rock data and zircon data are compatible with each other with few minor differences.

In summary the EPMA data of zircons show that the different clusters of rock groups and variations of the zircon data in inter and intra rock groups indicate the diverse origin of the different rock groups and even differences within the same rock group. The zircons with Paleozoic inherited cores are more evolved in nature. For example, mafic dyke MD-26 and high-Na intermediate dyke MD-32 both have Paleozoic inherited cores (see chapter-6) and show a more evolved origin which is reflected in the zircon chemistry as well as supported by the whole rock isotope chemistry (see chapter-3). MDS are different than intermediate dykes though both are of intermediate composition. The granites also show variable composition in whole rock and zircon chemistry. The WFO has a more restricted range of data which supports that this may be formed in a closed system process. The variations in trace element composition in inter and intra rock groups suggest a combination of processes operating.

## SECTION B: Electron Probe Data of Garnets from Mt Daniel Rock Groups

Garnets are present in most of the Fiordland samples except WFO and the High-Na intermediate dykes the garnet in low-Na intermediate dyke MD-22A and MDS sample MD-38 were not analysed because the grains are very small and uneven and not suitable for analysis. The garnet is considered to be an important phase help to determine whether it garnet grew during metamorphism and whether it has grown during prograde, peak or retrograde metamorphism. Here the major elements of garnets from different rock types will be discussed to understand the type and formation of the garnet. The average EPMA data of garnet is provided in Table 7.2.

| Rock Types | Sample No | Composition of Garnet core or near-core | Composition of Garnet rim or near-rim |
|---|---|---|---|
| **Mafic Dykes** | MD-13 | $Al_{49}Prp_{19}Grs_{29}Sps_{0.7}$. | |
| | MD-22B | $Al_{29}Prp_{16}Grs_{14}\,Sps_{0.1}$ | $Al_{34}Prp_{8}\,Grs_{14}\,Sps_{1}$ |
| | MD-26 | $Al_{53\text{-}55}Prp_{21}Grs_{24}Sps_{0.9}$ | $Al_{49}Prp_{19}Grs_{29}Sps_{0.7}$ |
| **Intermediate Dyke (low-Na variety)** | MD-8 | $Al_{52\text{-}57}Prp_{8\text{-}11}Grs_{22\text{-}28}\,Sps_{6\text{-}12}$ | |
| **Granitic Dykes** | MD-2 | $Al_{37\text{-}41}\,Prp_{4\text{-}6}\,Grs_{9\text{-}16}\,Sps_{1.07\text{-}1.97}$ | |
| | MD-6 | $Al_{38\text{-}40}Prp_{3\text{-}7}Grs_{12\text{-}17}Sps_{0.5\text{-}1.7}$ | |
| **Granitic Rocks in MDC** | MD-29 | $Al_{35}\,Prp_{8}\,Grs_{15\text{-}16}\,Sps_{0.8\text{-}1.30}$ | $Al_{32\text{-}33}Prp_{7}Grs_{19}Sps_{0.8}$ |
| | MD-33 | $Al_{34}\,Prp_{8}\,Grs_{19}\,Sps_{0.4}$ | $Al_{37}\,Prp_{3}\,Grs_{14}\,Sps_{4}$ |
| **MDS sample** | MD-14 | $Al_{56\text{-}60}Prp_{8\text{-}13}Grs_{26\text{-}30}Sps_{0.8\text{-}1.8}$ | |

***Table 7.2.*** *Composition of garnets of different rock groups of Mt Daniel, Fiordland obtained from EPMA. The garnets with nearly same composition from core to rim are put in between core and rim. The values are averaged based on all of the analyses from each sample.*

## 7.9. Mafic Dykes: (Sample No: MD-13, MD-22B, and MD-26)

In MD-13 the composition of the garnet rims and cores are similar (Fig 7.13.a) and the composition is presented in Table 7.2.

Garnets in MD22B show similar core and rim compositions to MD-13 (Table-7.2.). The cores are slightly depleted in Fe and Mn and enriched in Mg whereas Ca is fairly constant (Fig 7.13.b).

In MD-26 a slight enrichment of Fe and depletion of Ca and Mg present from rim to core where Mn is fairly constant (Fig 7.13.c) but no systematic zoning is found. The composition is varying from rim to near core (Table 7.2.a.).

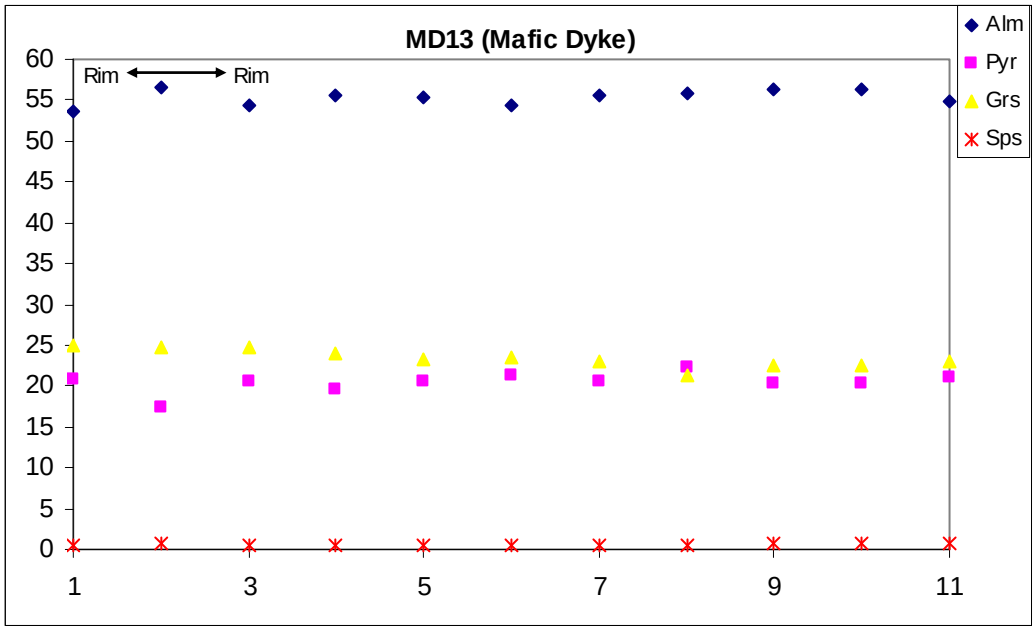


***Figure 7.13. (a)*** *Major element zoning profile across garnet (rim to rim) of MD-13-1. The garnet doesn't show any core-rim variation.*

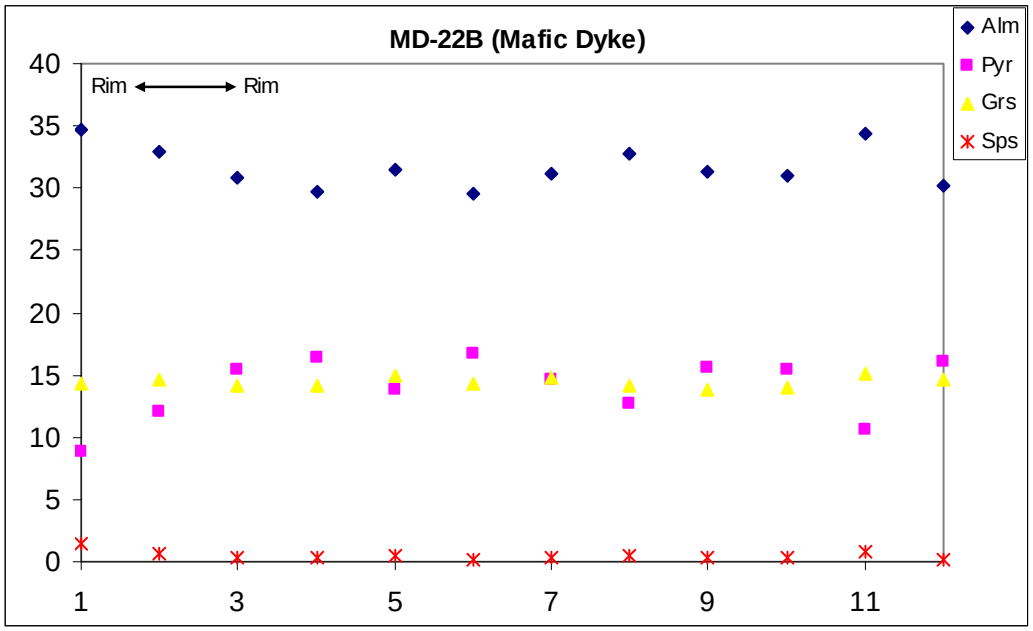


***Figure 7.13. (b)*** *Major element zoning profiles across garnet (rim to rim) of MD-22B-1. The garnet shows slightly Fe and Mn depleted and Mg enriched core.*

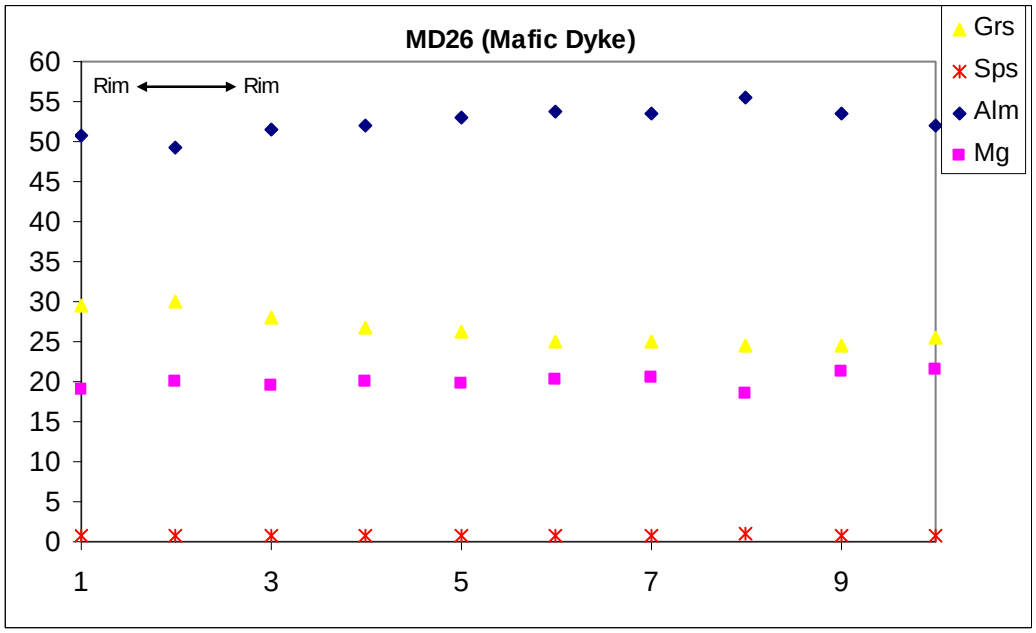


***Figure 7.13. (c)*** *Major element zoning profiles across garnet (rim to rim) of MD-26-1. The garnet doesn't show any systematic variation from core to rim.*

## 7.10. Low-Na Intermediate Dykes: (Sample No: MD-8)

The garnets of MD-8 also don't show any systematic variation from core to rim (Fig7.14.). The compositions of the garnets do not vary much from core to rim but have high Sps content (Table 7.2.).

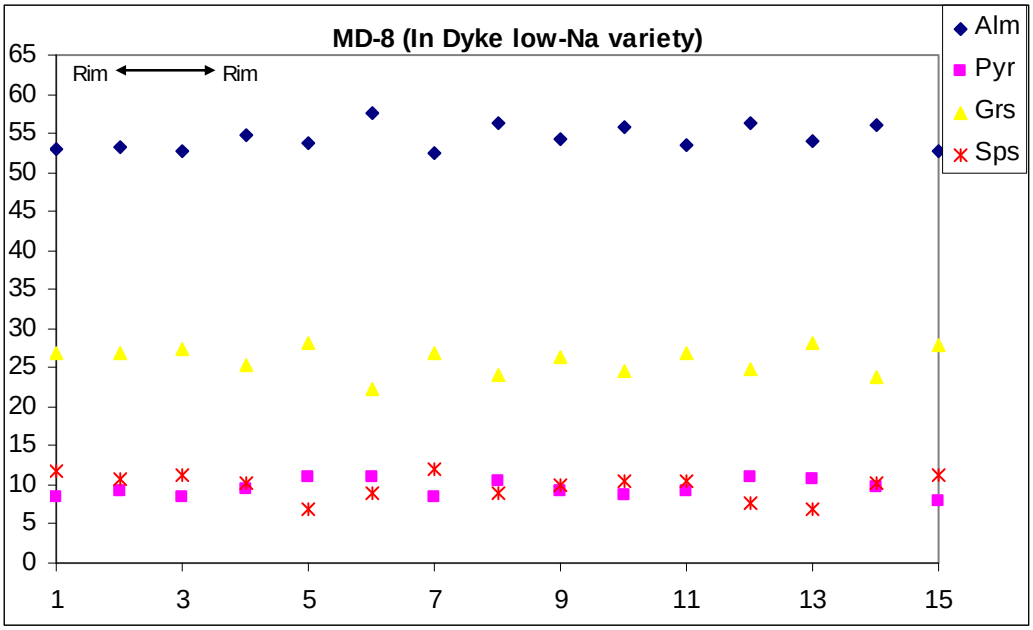


***Figure 7.14. (a)*** *Major element zoning profiles across garnet (rim to rim) of MD-8-3. The garnet doesn't show any systematic variation from core to rim.*

## 7.11. Granitic Dykes and Sheets: (Sample No: MD-2, MD-6, MD-29 and MD-33)

The garnets in MD-2 do not show much variation from rim to core (Table 7.2.) but one of the garnets shows slight depletion of Fe and enrichment of Ca in the core (Fig 7.15.a.).

The garnets in MD-6 do not show much variation from rim to core but a slight depletion of Fe and slight enrichment of Ca observed in the core (Fig 7.15.b.). But the compositions of the garnets are nearly homogeneous (Table 7.2.a). One of the garnets in MD-6 shows a higher range of composition of $Al_{64\text{-}65}\,Prp_{10\text{-}11}\,Grs_{21\text{-}24}\,Sps_{0.79\text{-}1.5}$.

The garnets in MD-29 show a slight core to rim variation (Table 7.2.). The garnet cores are slightly depleted in Fe and Mn and enriched in Ca (near point 5) (Fig 7.16.a.).

The garnets in MD-33 show no systematic change from core to rim (Fig 7.16.b.) and nearly same composition range (Table 7.2.).

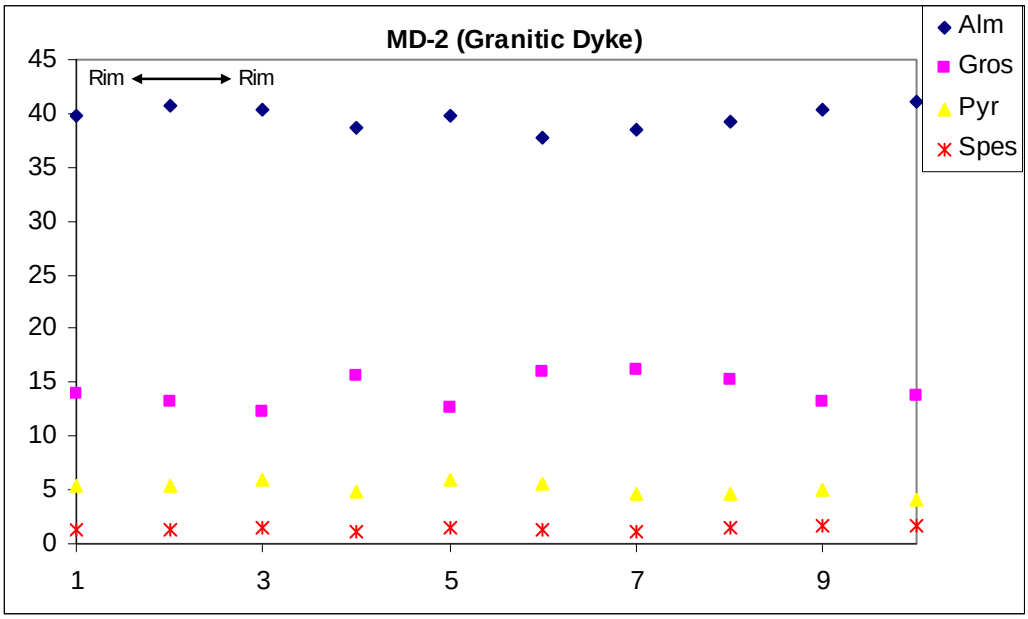


***Figure 7.15. (a)*** *Major element zoning profiles across garnet (rim to rim) of MD-2-2.*

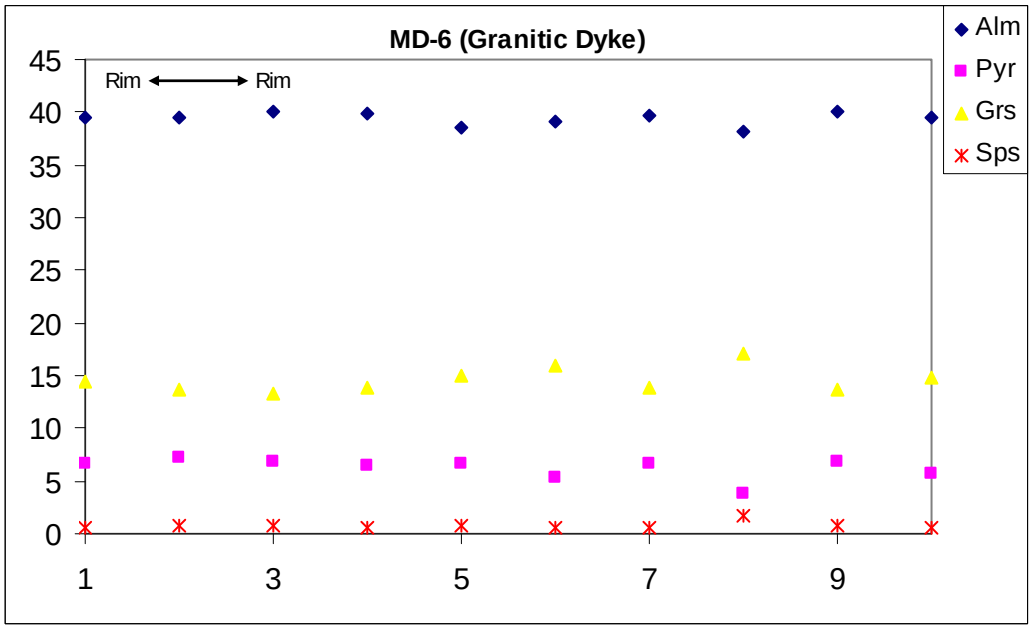


***Figure 7.15. (b)*** *Major element zoning profiles across garnet (rim to rim) of MD-6-3. The garnets don't show any systematic variation from core to rim.*

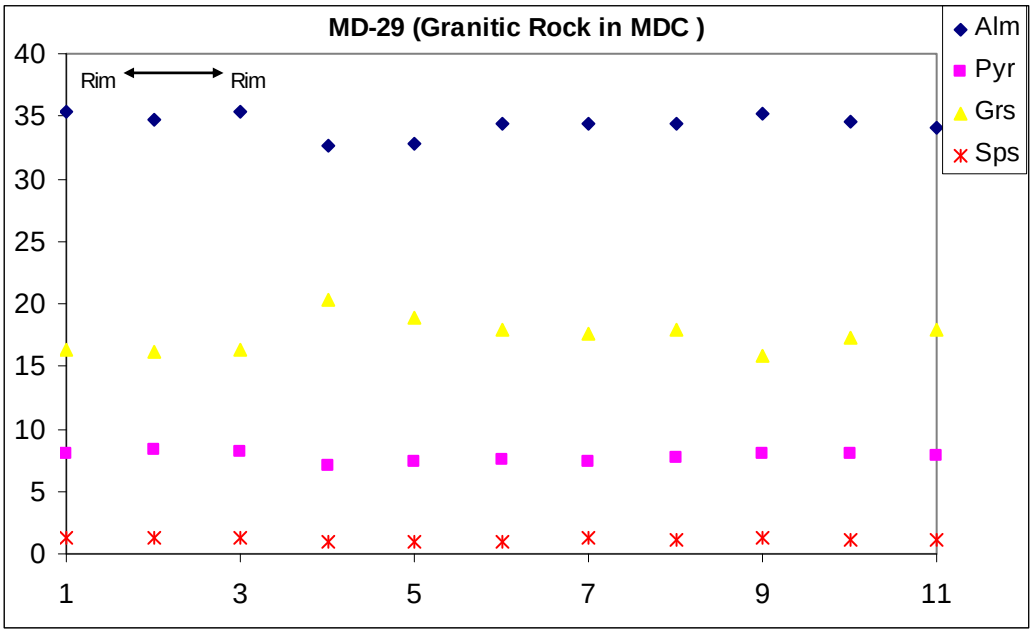


***Figure 7.16. (a)*** *Major element zoning profiles across garnet (rim to rim) of MD-29-3.*

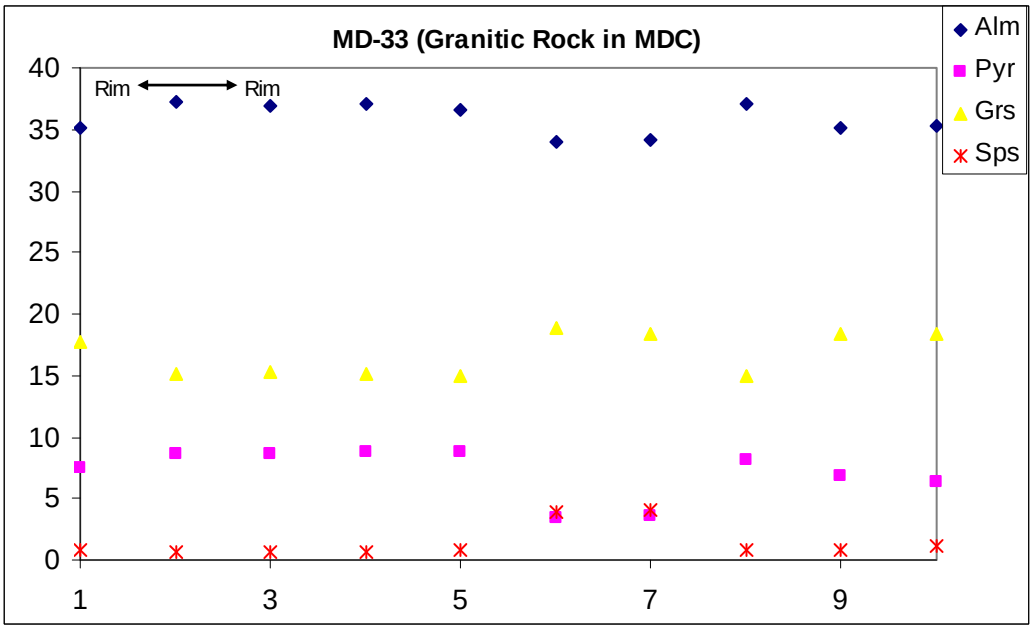


***Figure 7.16. (b)*** *Major element zoning profiles across garnet (rim to rim) of MD-33-3. The garnets don't show any systematic variation from core to rim.*

## 7.12. Mt Daniel Sheet: (Sample No: MD-14)

In MDC rocks only MD-14 contains garnets. The garnets in MD-14 don't show any systematic variation from core to rim (Fig 7.17.).

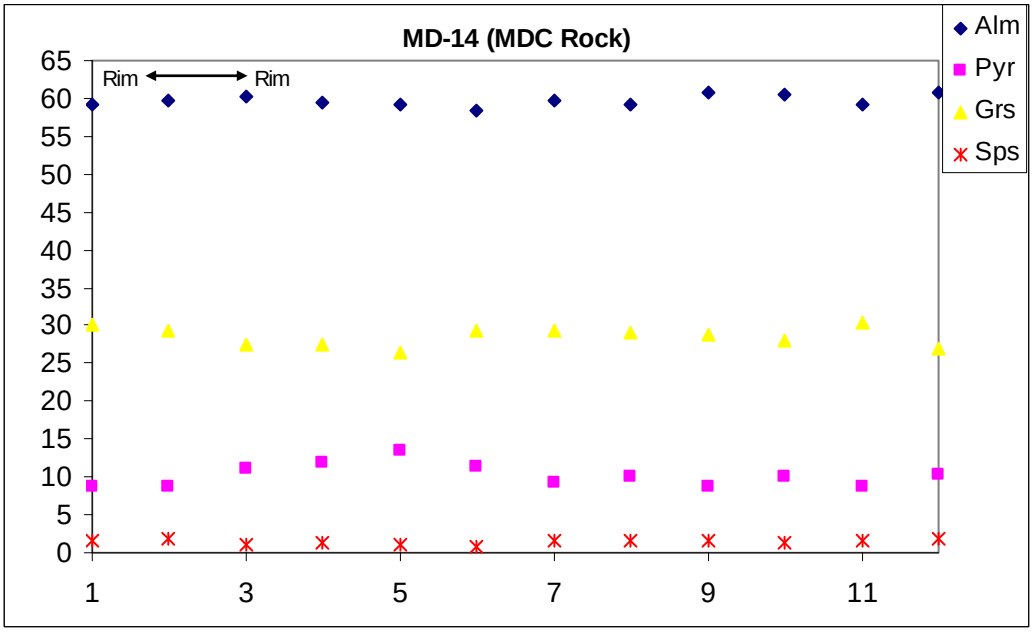


***Figure 7.17.*** *Major element zoning profiles across garnet (rim to rim) of MD-14-3 and 3a. The garnets don't show any systematic variation from core to rim.*

In summary the garnets show nearly uniform patterns without any systematic variation from core to rim in most of the rocks of Mt Daniel Complex (see Table 7.2.). A slight increase of Ca and decrease of Fe in some garnet cores from some of the rocks are observed but no conclusion can be derived from the available data regarding garnet forming environment and the relationship with zircons in Mt Daniel rocks

# Chapter 8: Trace Element Chemistry of Zircon, Garnet and Zircon-Rutile Thermometry of Mt Daniel Rock Groups

## 8.1. Introduction

Trace elements are very important and useful in the study of magmatic processes. The trace element behaviour is more sensitive than major elements to igneous processes. For example during differentiation of the magma different minerals (e.g. zircon) selectively incorporate or exclude trace elements more sensitively than major elements. Thus the origin of the melt systems and their evolutionary processes can be better understood by trace element studies. As already mentioned in previous chapters, zircon is a significant reservoir of a large number of trace elements (20-25) and Hf, Y (sometime considered as minor elements in zircon), REE, P, U, Th are present in abundance. These elements can be substituted into zircon either by simple or coupled substitution (e.g.Fronndel 1953, Hoskin et al., 2000, Hinton and Upton 1991).

The REE (rare earth elements), from lanthanum (La) to lutetium (Lu), are members of Group IIIA of the periodic table that have similar chemical and physical properties. They all have 3+ oxidation states though (Ce can be +4 and Eu +2) and their ionic radius decreases steadily with increasing atomic number, called the lanthanide contraction. The chondrite-normalized REE patterns of zircon show some distinctive characteristics. They generally show a steeply rising slope from the LREE to the HREE with a positive Ce anomaly (Ce/Ce*) and they commonly (but not always) have a negative Eu anomaly (Eu/Eu*). Ce/Ce* values varies upward from 1 and Eu/Eu* usually varies between 1 and 0. The cause of these anomalies is attributed to $fO_2$ and bulk rock composition of $Ce^{4+}$ & $Eu^{2+}$. In a highly oxidising environment the $Ce^{4+}/Ce^{3+}$ ratio is increased resulting in a positive Ce anomaly, because $Ce^{4+}$ is more compatible in zircon than $Ce^{3+}$ (Hinton and Upton, 1991). Similarly oxidizing conditions promote elevated $Eu^{3+}/Eu^{2+}$ ratios that favour partitioning of Eu into zircon and thus small to negligible Eu anomalies.

Another controlling factor of the Eu anomaly is plagioclase crystallization, which can deplete Eu from the magma prior or during zircon formation. This is especially true under reducing conditions where Eu is preferentially partitioned into plagioclase (Drake and Weill 1975, Weill and Drake 1973). So, negative Eu anomalies in zircon can thus reflect either a reducing environment with low $O_2$ or zircon crystallised in the presence of plagioclase. Other minerals with high Kd for Sm and Gd can also control Eu anomalies. The simultaneous crystallisation of zircon and garnet minerals are very significant to understand different rock forming environment as HREE partitioned into both zircon and garnet and can cause HREE depletion in a closed system process (Rubatto, 2002). The Mt Daniel Complex (MDC) rocks are meta-igneous and have suffered granulite facies metamorphism (see chapter-2) and garnet is present as an important phase in most of the rocks. So it is important to understand the magmatic vs. metamorphic processes and under which conditions the different rocks are formed. To understand the physico-chemical condition of the rock forming process this study analysed both of the minerals, zircon and garnet from different samples. Rutile was analysed to allow the zircon-rutile thermometry of the rocks. The detail study of trace elements in zircon, garnet and rutile of individual rock groups will provide an idea about their petrogenesis and metamorphic histories. Trace element analyses of zircon, garnet and rutile were carried out on a Coherent Geolas 193 nm ArF laser ablation unit coupled to a Varian 820-MS quadrupole ICP-MS. The details of the technique are provided in chapter-3. The trace element compositions of zircon, garnet and rutile from the different samples are listed in Appendix 5.

## Section A: Zircon Trace Element Analyses of Mt Daniel Rocks

### 8.2. WFO: (Sample No: MD-15)

The zircons from the WFO are of Early Cretaceous age (125±2 Ma) are interpreted as magmatic based on their elongated to subrounded shape and planar banding and oscillatory zoning and have moderate Th and U contents and Th/U ratios ≥ 0.5 (see Table 8.1.). The REE patterns are uniform, with steep HREE pattern (Fig 8.1.a.). The zircons of WFO have a strong positive Ce anomaly and negative Eu anomaly (see Table 8.1.).

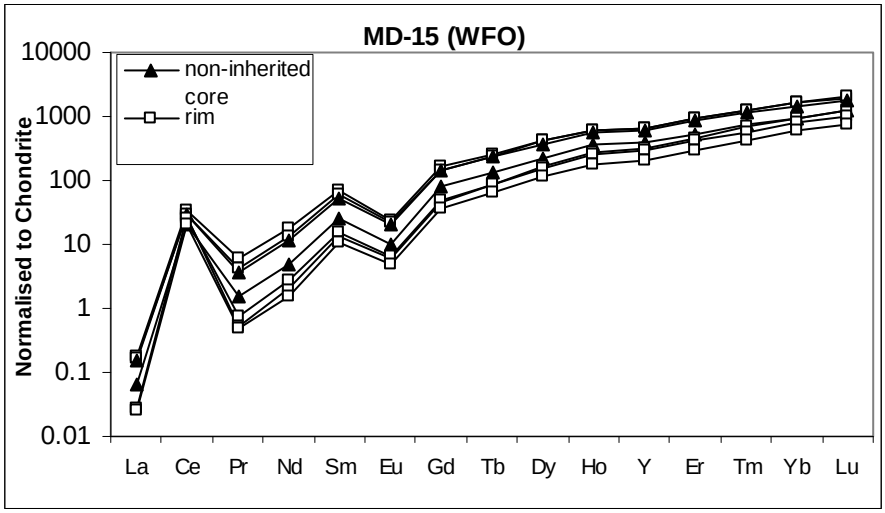


***Figure 8.1.*** *The REE patterns of zircons from WFO of Mt Daniel, Fiordland. The non-inherited cores from single zircons are shown with filled triangles and rims with open square symbol.* ***(a)*** *The REE patterns of zircons from MD-15 show similar patterns from centre to rim. Ce anomaly were calculated using* Ce/Ce* = Ce/√(La x Pr) and Eu anomaly were calculated using Eu/Eu* = Eu/√(Sm x Gd).

| Rock Type | Sample No | Zircon Type with age | Age (Ma) | Th ppm | U ppm | Th/U | Ce/Ce* | Eu/Eu* |
|---|---|---|---|---|---|---|---|---|
| **WFO** | **MD-15** | Magmatic | 125±2 | 122-331 | 155-292 | 0.75-1.18 | 33-218 | 0.22-0.24 |
| **Mafic Dykes** | **MD-13** | CL-bright and CL-dark grains without inheritence | 123±6 | 7-25 | 15-36 | 0.49-1.27 | Not detectable | 0.31-0.6 |
| | **MD-22B** | CL-bright and CL-dark grains without inheritence | 122±2 | 8-90 | 19-74 | 0.39-1.53 | 12-63 | 0.4-0.8 |
| | **MD-26** | Cl-bright grains without inheritance & rims of CL-dark grains | 124±6<br>unknown | 7-70 | 23-187 | 0.31-0.38 | Not detectable | 0.6-0.8 |
| | | CL-dark grains with core | 376-306 | 146-430 | 215-380 | 0.6-11 | 10-95 | 0.2-0.3 |
| **Intermediate Dykes (low-Na variety)** | **MD-8** | Cl-bright grains without core and rims of Cl-dark grains | 112±12 | 56-325 | 67-282 | 0.74-1.17 | 12-70 | 0.2-0.3 |
| | **MD-22A** | Rims & Cores | 125±18 & 362-313 | 20-468 | 35-544 | 0.3-0.8 | 18-38 | 0.1-0.2 |
| **Intermediate Dykes (high-Na trondjhemitic variety)** | **MD-17A** | Magmatic | 119±2 | 30-170 | 41-119 | 0.75-1.43 | 58-239 | 0.76-0.81 |
| | **MD-32** | Rims & | 120±6 | 36-104 | 62-587 | 0.06-0.72 | 81-243 | 0.5-0.7 |
| | | Cores | 344-323 | 209-712 | 732-953 | 0.28-0.77 | 18-211 | 0.1-0.2 |

| | | | | | | | | |
|---|---|---|---|---|---|---|---|---|
| **Granite Dykes** | **MD-2** | Rims & cores | 140±6 & 347-305 | 32-270 | 275-1095 | 0.02-1.3 | Mostly not detectable | 0.1-0.6 |
| | **MD-6** | Rims | 112±8 | 7-67 | 240-1277 | 0.01-0.05 | Mostly not detectable , only have two values 312 & 357 | 0.25-0.7 |
| | | Cores | 329-302 | 160-389 | 363-1549 | 0.25-0.44 | 39-357 | 0.20-0.03 |
| **Granitic phase in MDC** | **MD-29** | Rims | 123-114 | 3-358 | 93-4357 | 0.003-0.34 | Mostly not detectable, only two values 210 & 394 | 0.04-0.6 |
| | | Cores | 341-300 | 119-398 | 361-644 | 0.33-0.75 | 75-91 | 0.15-0.26 |
| | **MD-33** | Rims | 121-120 | 22-93 | 250-670 | 0.03-0.2 | 204-267 | 0.1-0.6 |
| | | Cores | 372-339 | 96-537 | 182-818 | 0.4-0.9 | 52-298 | 0.09-0.3 |
| **MDC rocks** | **MD-14** | Rims | 119±12 | 39-60 | 147-203 | 0.2-04 | Mostly not detectable , only one value 30 | 0.3-0.4 |
| | | cores | 332-300 | 78-688 | 153-650 | 0.4-1.05 | 41-52 | 0.1-0.41 |
| | **MD-38** | Rims | 125 | 57-79 | 126-432 | 0.1-0.4 | Mostly not detectable, only two values 102& 117 | 0.2-0.44 |
| | | Cores | 344-316 | 148-418 | 276-566 | 0.3-0.8 | 16-102 | 0.1-0.3 |

***Table 8.1.*** *Trace element composition of zircons from different samples of Fiordland. All the age errors are quoted in 2 sigma.*

## 8.3. Mafic Dykes: (Sample No: MD-13, MD-22B and MD-26)

**MD-13:** The zircons from MD-13 have CL-bright and CL-dark grains of Early Cretaceous age (123±6 Ma) without inheritance. The zircons of MD-13 have the lowest Th and U contents and the Th/U ratio is > 0.3 (see Table 8.1.). The zircons show uniform REE patterns with positive Ce anomalies and small negative Eu anomalies (Fig 8.2.a.).

**MD-22B:** The mafic dyke MD-22B mainly has Early Cretaceous (122±2 Ma) CL-bright and CL-dark zircons without any inheritance. Zircons from MD-22B have low to moderate Th and U contents and a few CL-dark grains are high in Th and U (see Table 8.1.). The REE patterns of zircons are uniform with positive Ce anomalies and small negative Eu anomalies (Fig 8.2.b.).

**MD-26:** The mafic dyke MD-26 has CL-bright zircons (124±6 Ma) and CL-dark zircons with inheritance (376-306 Ma). The zircons from MD-26 have variable Th and U contents (see Table 8.1.). The CL-bright zircons and rims of CL-dark zircons from MD-26 (not dated see chapter-6) have similar, comparatively low Th/U ratios (0.3) compared to inherited cores (>0.6) (see Table 8.1.). The REE patterns of Early Cretaceous zircons show steep LREE to HREE enrichment with positive Ce anomalies and small negative Eu anomalies (Fig 8.2.c.). The inherited cores of CL-dark zircons in sample MD-26 have strongly negative Eu anomalies and higher REE abundance (Fig 8.2.c.) than CL-bright zircons. Both Paleozoic cores and rims show similar MREE and HREE enrichment (Fig 8.2.c.). It is important to note that the Early Cretaceous zircons in mafic dykes lack significant Eu anomalies.

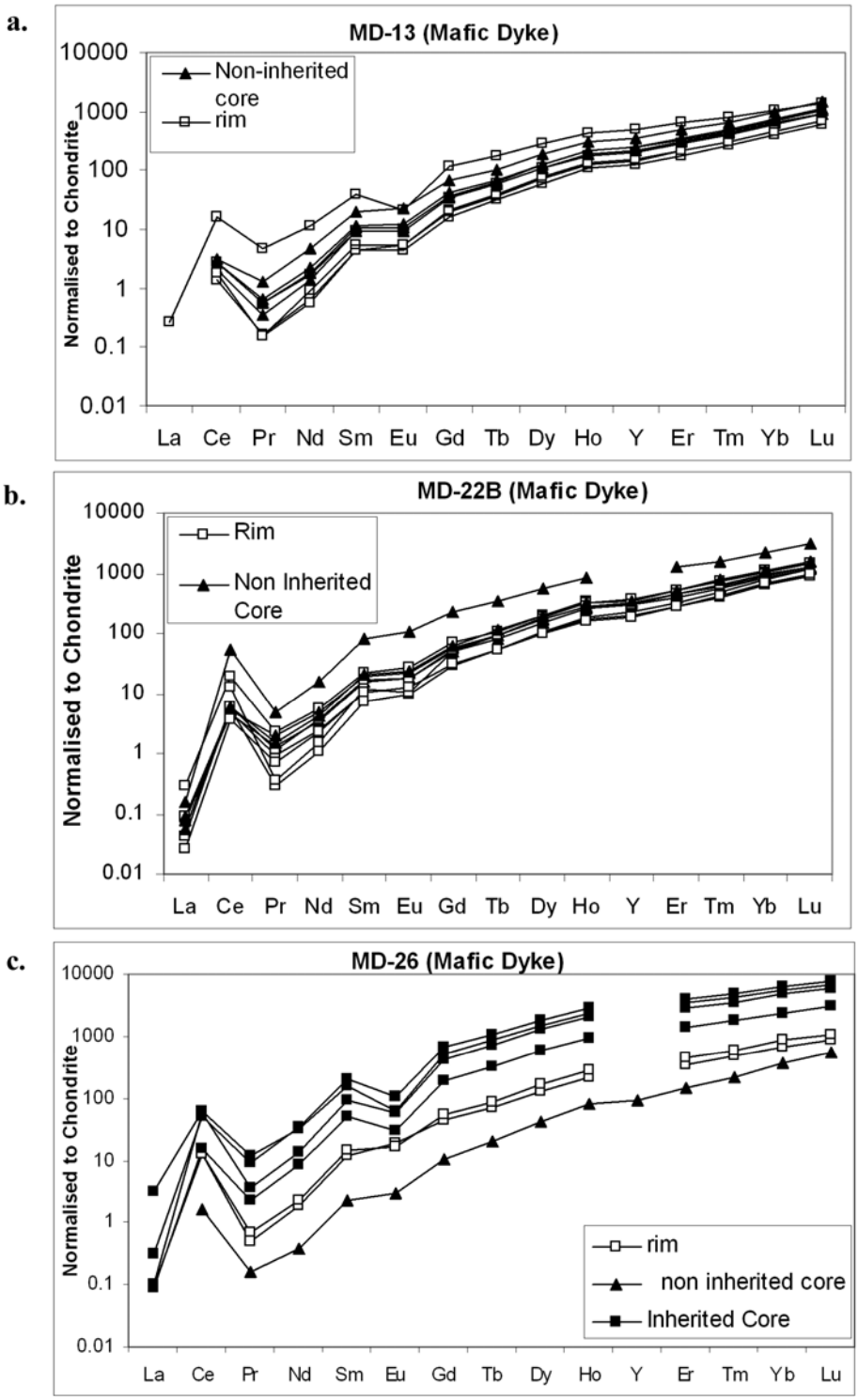


***Figure 8.2.*** *REE patterns of zircons from mafic dykes of Mt Daniel, Fiordland. The inherited cores are shown with close square symbol and rims with open square symbol.* ***(a)*** *MD-13;* ***(b)*** *MD-22B and* ***(c)*** *MD-26.*

## 8.4. Low-Na Intermediate Dykes: (Sample No: MD-8 & MD-22A)

**MD-8:** The zircons from MD-8 have both CL-bright single zircons of Early Cretaceous age and CL-dark zircons with inherited Paleozoic cores. The CL-dark grains were not analysed due to small grain size and presence of thin rims and only the CL-bright grains from MD-8 were analysed. These zircons have moderate Th and U contents and Th/U ratio $\geq 0.7$ (see Table 8.1.). The zircons show uniform REE patterns with strong positive Ce anomaly and negative Eu anomaly (Fig 8.3.a.).

**MD-22A:** MD-22A contains zircons with Paleozoic inherited cores and Early Cretaceous thick featureless rims. The zircons of both ages have moderate to high Th and U and the rims mainly show lower Th/U ratios (0.2-0.4) compare to inherited cores with Th/U ratios of 0.45- 1.05. The REE patterns of zircons from MD-22A show nearly uniform patterns of cores and rims with strong positive Ce anomalies and negative Eu anomalies but cores usually have higher REE enrichment compare to rims of the same grains (Fig 8.3.b.).

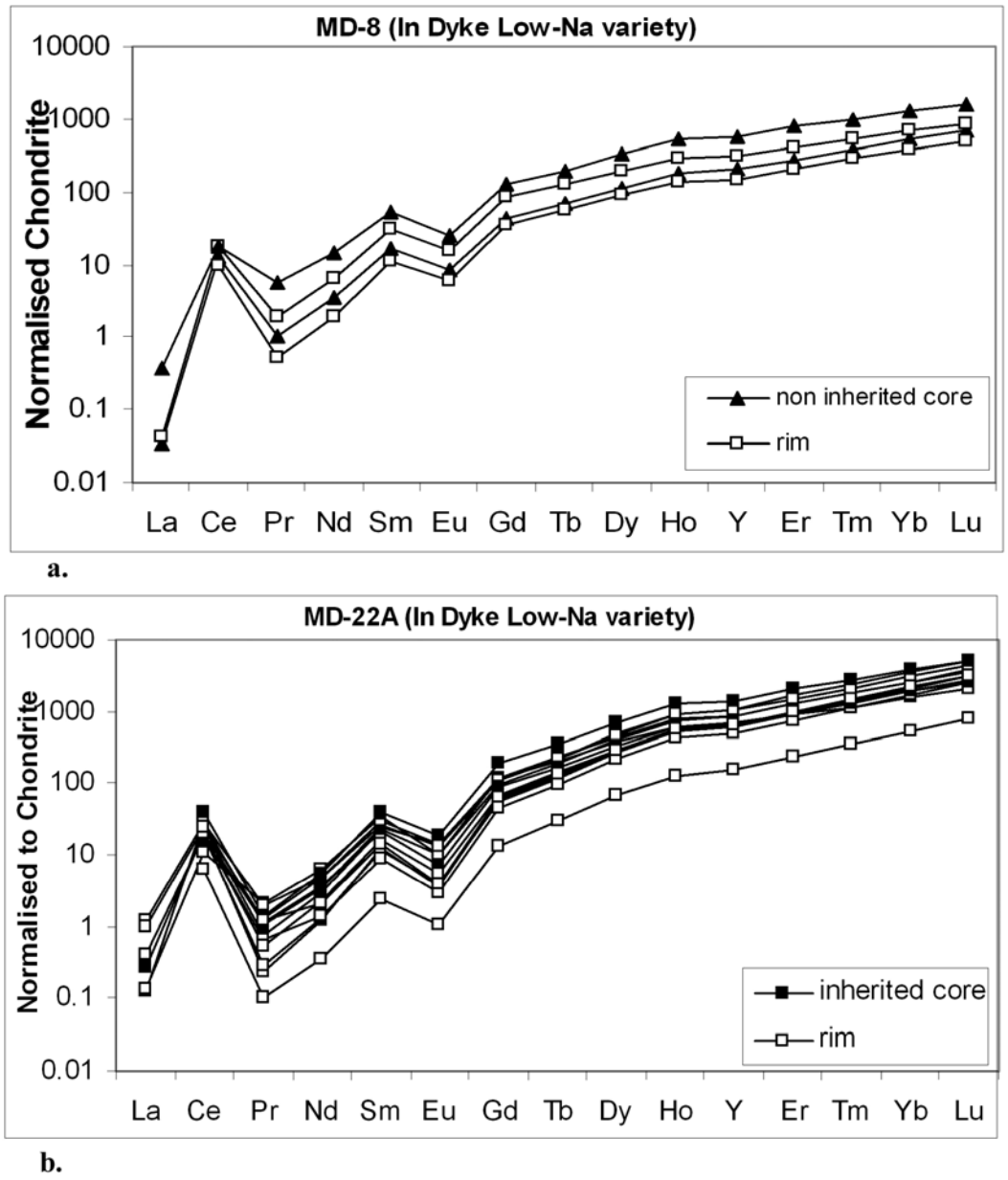


***Figure 8.3.*** *REE patterns of zircons from intermediate dykes of Mt Daniel, Fiordland;* ***(a)*** *MD-8 and* ***(b)*** *MD-22A.*

## 8.5. High-Na Intermediate Dyke (trondhjemitic variety): (Sample No: MD-17A & MD-32)

**MD-17A:** Zircons from MD-17A has are interpreted as magmatic based on their elongated shapes and planar banding and oscillatory zoning of Early Cretaceous age (117±2 Ma) without inheritance. The zircons of MD-17A have moderate Th and U content and high Th/U ratios ≥ 0.7 (See Table 8.1.). The REE patterns of the zircons from MD-17A are very uniform with positive Ce anomalies and negligible Eu anomalies (8.4.a.).

**MD-32:** The zircons in MD-32 have Paleozoic cores and Early Cretaceous rims (120±6 Ma) that are either featureless or zoned (see chapter-5), and also have some Early Cretaceous zircons without inheritance and with or without zoning (see chapter-5).

The zircons of MD-32 with Palaeozoic cores and Early Cretaceous rims have medium to high Th and U content and variable Th/U ratios (0.06-0.77) (See Table 8.1.). The Early Cretaceous zircons usually have both high (1.17) and low (0.06) Th/U ratios. The zircons from MD-32 mostly show uniform REE patterns from core to rim with positive Ce anomalies. But cores usually have higher HREE contents than rims and stronger negative Eu anomalies. The Early Cretaceous zircons have high Th/U ratio (1.17), high REE enrichment, positive Ce anomalies and small negative Eu anomaly (Fig 8.4.b.).

.

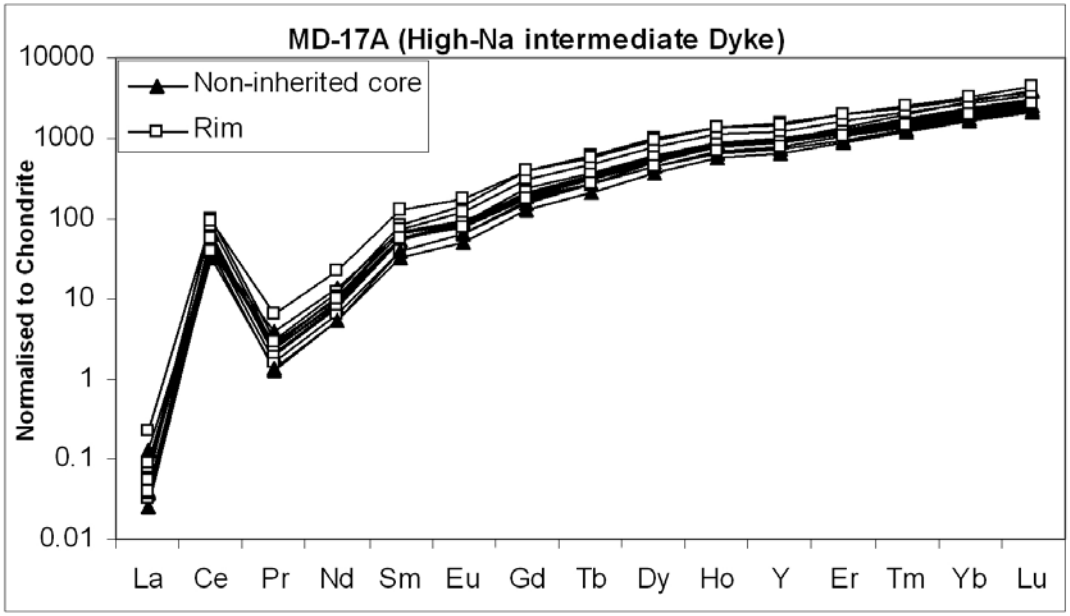


**a.**

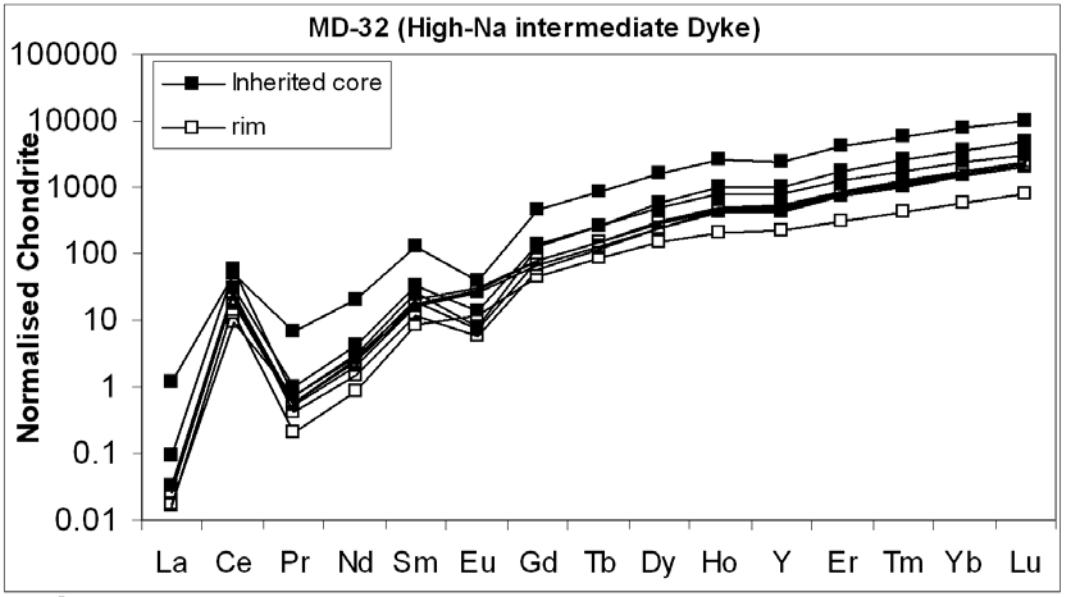


**b.**

***Figure 8.4.*** *The REE patterns of zircons from trondhjemites of Mt Daniel, Fiordland;* ***(a)*** *MD-17A and* ***(b)*** *MD-32.*

## 8.6. Granite Dykes: (Sample No: MD-2 and MD-6)

**MD-2:** The zircons from MD-2 show core-rim structures, where Paleozoic cores exhibit variable zoning patterns (patchy, oscillatory, homogeneous and planar) and have thin and bright featureless rims. Zircons from sample MD-2 do not contain any Cretaceous rims and the youngest age obtained from the rim is around 140 ± 6 Ma and is considered as a mixed age (see chapter-6).

The zircons have high Th and U content (see Table 8.1.) with Th/U ratio (0.02-1.31) and age data suggest they may all have Paleozoic cores. The REE patterns of the zircons from MD-2 (Fig 8.5.a.) show steeply rising slopes from LREE to HREE with positive Ce and negative Eu anomalies (0.1-0.6) for both cores and rims. One of the rims has higher HREE abundance compare to cores but the age is not well constrained in this rock.

**MD-6:** The zircons from MD-6 have Paleozoic cores and Early Cretaceous rims of 112±8 Ma.

MD-6 zircons have very high to medium U and medium to low Th content (see Table 8.1.) and generally a low Th/U ratio (0.05-0.4). The Th/U ratio is fairly low in the rims (0.01-0.05) compared to cores (0.2-0.4).

The REE patterns of zircons from sample MD-6 are widely variable from core to rim (Fig 8.5.b.). Cores have steeply rising slope from LREE to HREE with positive Ce and negative Eu anomalies. The rims are variably depleted both in MREE and HREE and also have extremely depleted HREE patterns. The rims have positive Ce anomaly but small negative Eu anomalies (0.3-0.7). The extremely HREE depleted rims have very small negative Eu anomalies.

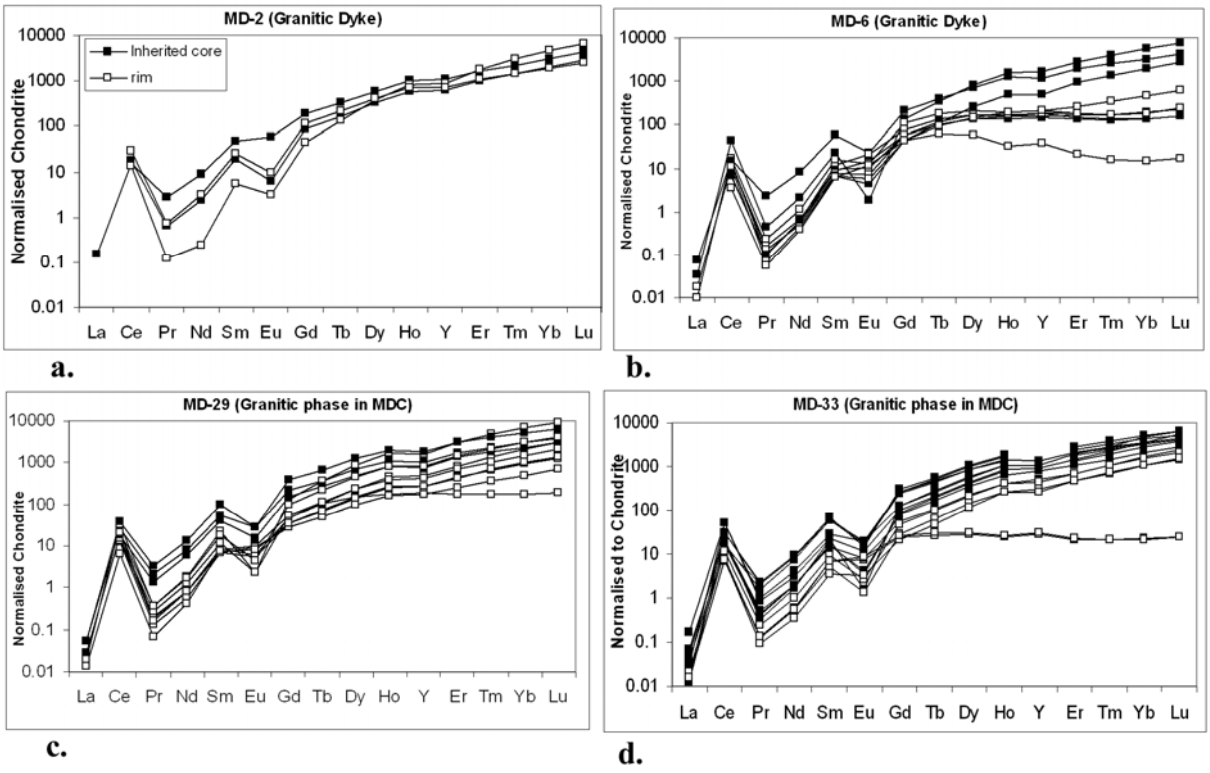


***Figure 8.5.*** *The REE patterns of zircons from different granite samples of Mt Daniel, Fiordland.* ***(a)*** *Granitic dyke MD-2 and* ***(b)*** *MD-6;* ***(c)*** *granitic sheets MD-29 and* ***(d)*** *MD-33.*

## Granitic Sheets in MDC: (Sample No: MD-29 & MD-33)

**MD-29:** MD-29 has zircons with Paleozoic inherited cores and thin featureless Early Cretaceous rims (see chapter-5 and 6). The rims have low Th/U ratio (0.003-0.3) compare to inherited cores (0.6-0.75). The REE patterns of the cores are uniform with positive Ce and negative Eu anomalies (Fig 8.5.c.). The REE patterns of the zircon rims show both HREE depleted and non-depleted nature (Fig 8.5.c.). A single HREE-depleted rim has small negative Eu anomaly whereas the non HREE-depleted rims have both small and large negative Eu anomalies (Fig 8.5.c.).

**MD-33:** MD-33 zircons have Paleozoic inherited cores and thin featureless Early Cretaceous rims (see chapter-5 and 6). As with MD29, the rims have lower Th/U ratios (0.03-0.26) compared to cores (0.48-0.97). The REE patterns of the cores are uniform with positive Ce and negative Eu anomalies and the rims are both HREE depleted and non-depleted in nature (Fig 8.5.d.). The depleted rims have small negative Eu anomalies and the non depleted rims have comparatively large Eu anomalies (Fig 8.5.d.).

## 8.7. Mt Daniel Sheets: (Sample No: MD-14 and MD-38)

**MD-14:** The zircons from sample MD-14 have Paleozoic inherited cores and Early Cretaceous featureless rims of 119±12. Some zircons in MD-14 are ovoid in shape with irregular patches that are commonly attributed to metamorphic growth or modification (see-chapter-5). The ovoid shaped zircons in MD-14 exhibit mixed ages of 278 Ma (see chapter-6). In MD-14 zircons have moderate to high Th and U content and Th/U ratio is 0.23-1.05 (see Table 8.1.) The rims have lower Th/U ratio (0.2-0.4) compare to cores (Th/U=0.45- 1.05).

The REE patterns of zircons from MD-14 show similar patterns of cores and rims with positive Ce and negative Eu anomalies (Fig 8.6.a.). Some cores are enriched in REE compared to the rims. These grains are very dark homogeneous inherited cores and bright thick rims (see chapter-5) or oscillatory zoned cores with the signs of resorption. The metamorphic looking grains (ovoid shaped with irregular patches) in MD 14 have the lowest abundance of REE and the other characteristics (smaller negative Eu anomaly, lower Th/U ratios than cores) are very similar to the rims.

**MD-38:** The zircons from MD-38 show core-rim structures where Paleozoic cores are patchy or homogeneous and sometimes with oscillatory zoning and rims are featureless and sometimes gradational (see chapter-5 and 6). Only a single rim was found with an Early Cretaceous age of 125 Ma (see chapter-6) as the rims are very thin and not viable targets for laser ablation.

The zircons from MD-38 have moderate Th and U content and Th/U ratio is 0.33-0.86 ppm (see Table 8.1.). The rims have lower Th/U compare to cores. The zircons have nearly the same REE patterns of cores and rims with positive Ce and negative Eu anomalies. The core-rim variations are not well constrained in MD-38 (Fig 8.6.b.) due to the absence of well developed rims and/or the presence of usually very thin or gradational rims which could not be analysed (see chapter-5 & 6).

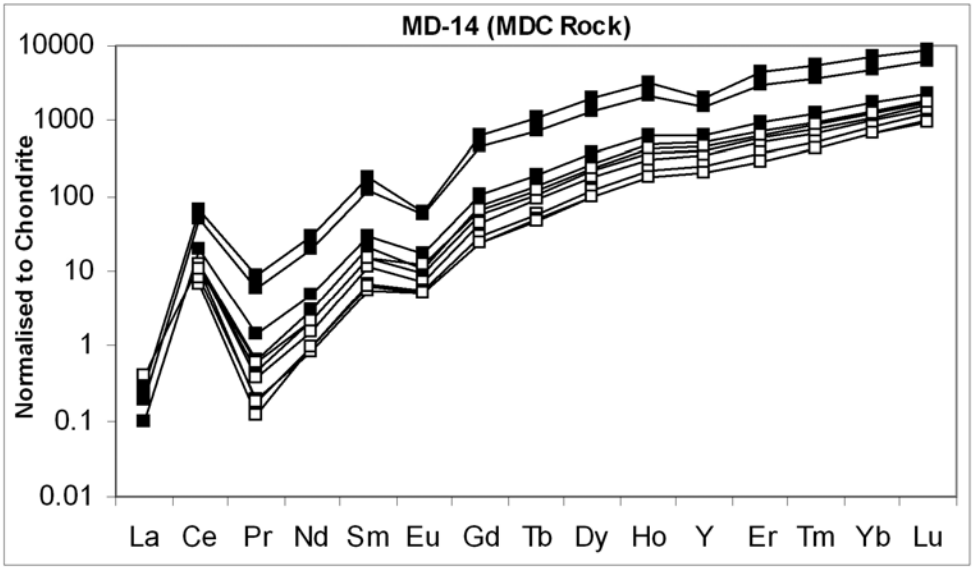


a.

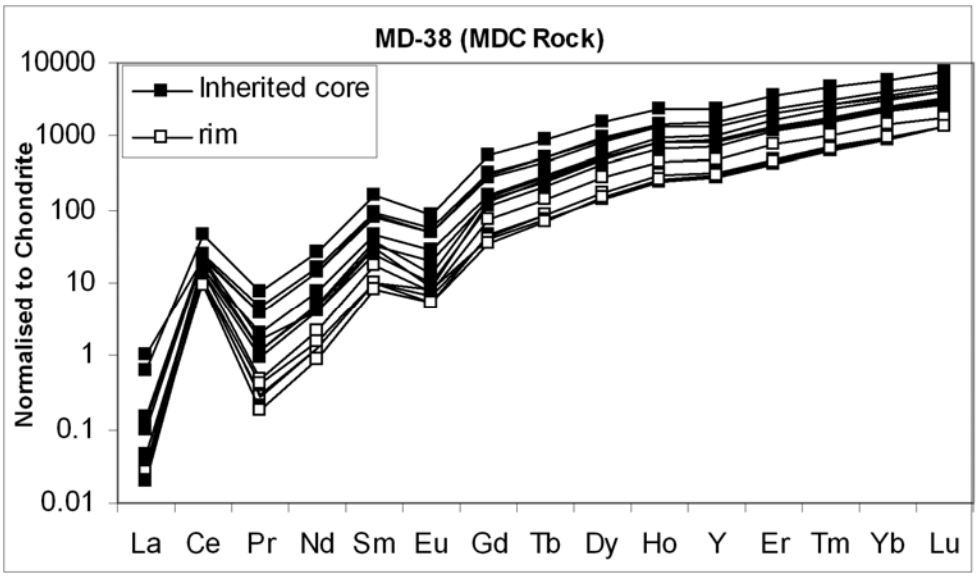


b.

***Figure 8.6.*** *The REE patterns of zircons of samples from Mount Daniel sheets from Mt Daniel Fiordland;* ***(a)*** *MD-14 and* ***(b)*** *MD-38.*

## Section B: Garnet Trace Element Analyses of Mt Daniel Rocks

Garnets are only present in mafic, low-Na intermediate and granitic rocks and absent in WFO and high-Na intermediate rocks. Garnet is an important mineral phase because the coexistence of garnet and zircon may affect the trace element budget of both minerals depending on their time of formation and growth environment (Rubatto, 2002). In this section the REE patterns of garnets will therefore be discussed. The garnet-bearing rock types are mafic dykes, granites, low-Na intermediate dykes and MDS sample MD-14. REE analyses of garnets are not obtained from low-Na intermediate dyke MD-22A because of very rough grain surfaces.

### 8.8. Mafic Dykes: (Sample No: MD-13, MD-22B and MD-26)

**MD-13:** The garnets in MD13 (Fig 8.7.a.) show similar LREE patterns for core and rim and steeply increasing from La-Sm (La is below detection limit in most of the analyses). The garnets have no Eu anomalies. The HREE have progressively decreasing abundance from core to rim.

**MD-22B:** Garnets in MD-22B are analysed from core, intermediate and rim part. The LREE (La-Sm) show steeply increasing slope and small negative Eu anomalies, MREE (Gd-Dy) are nearly constant showing flat profiles but from Ho to Lu HREE show slightly decreasing slope (Fig 8.7.b.). The REE patterns are uniform from core to rim with increasing LREE to MREE and slightly decreasing abundance of HREE. The MREE and HREE have progressively decreasing abundance from rim to core which is the opposite trend to that seen in other samples (Fig 8.7.b.).

**MD-26:** In MD-26 the garnets show quite similar REE patterns (Fig 8.7.c.) to MD-13, where the HREE have progressively decreasing abundance from core to rim.

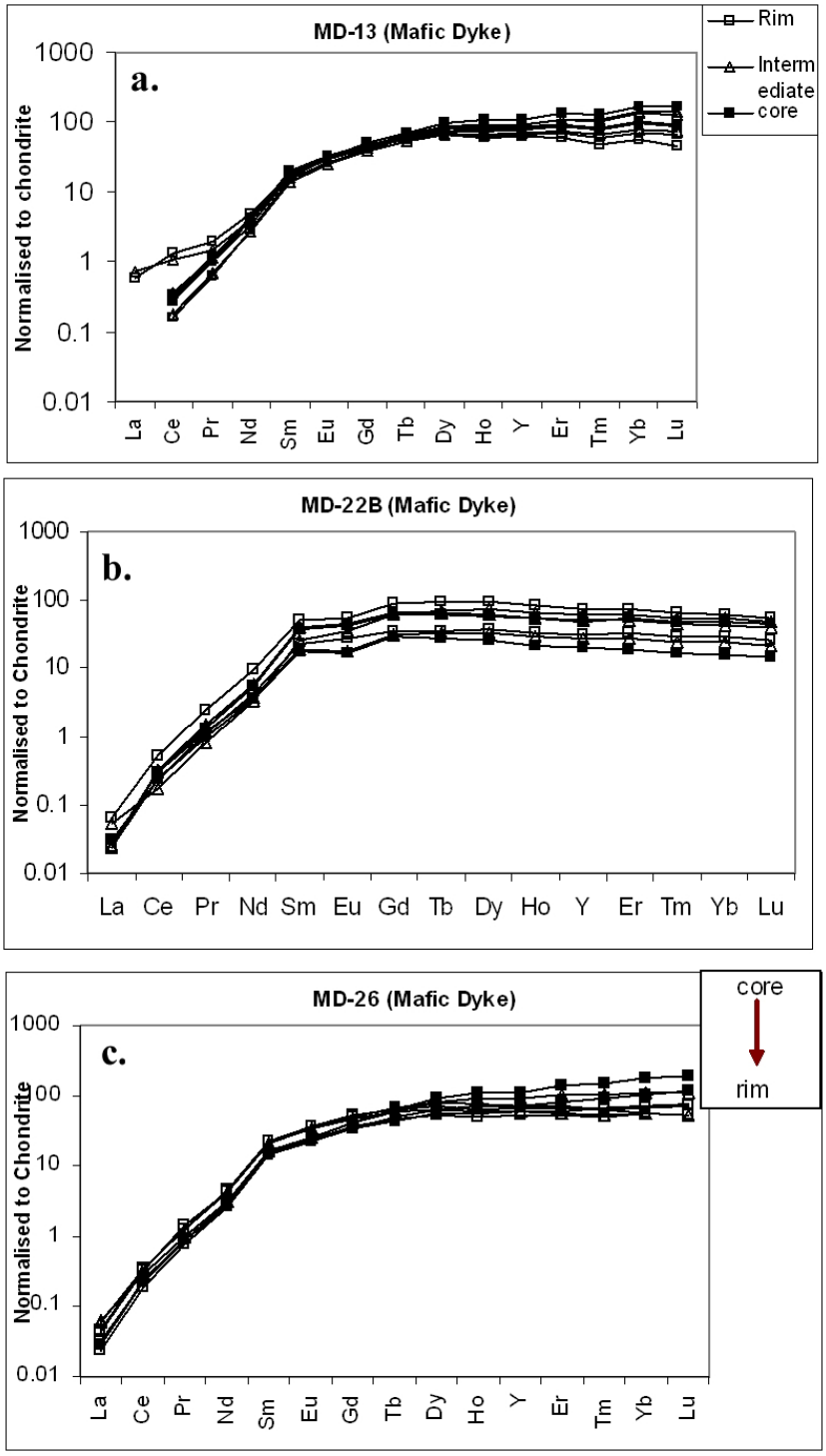


***Figure 8.7.*** *REE patterns of garnets from mafic rocks of Mt Daniel, Fiordland. The cores have been shown with closed square symbols and rims with open square symbols and points from intermediate zones have been shown with open triangles.* ***(a)*** *MD-13;* ***(b)*** *MD-22B;* ***(c)*** *MD-26. The key legends are similar to Fig 8.7.(a) in subsequent graphs showing REE patterns of garnets from different samples.*

## 8.9. Low-Na Intermediate Dyke: (Sample No: MD-8)

In intermediate dykes garnets from MD-8 have been analysed. Garnets from MD-8 show quite similar REE patterns (Fig 8.8.a.) to garnets from mafic rocks (MD-26 and MD-13). REE patterns show little variation from core to rim. The LREE have steeply increasing slope (La is below detection limit), MREE have moderately increasing slope to nearly flat patterns of HREE. The garnets have no Eu anomalies.

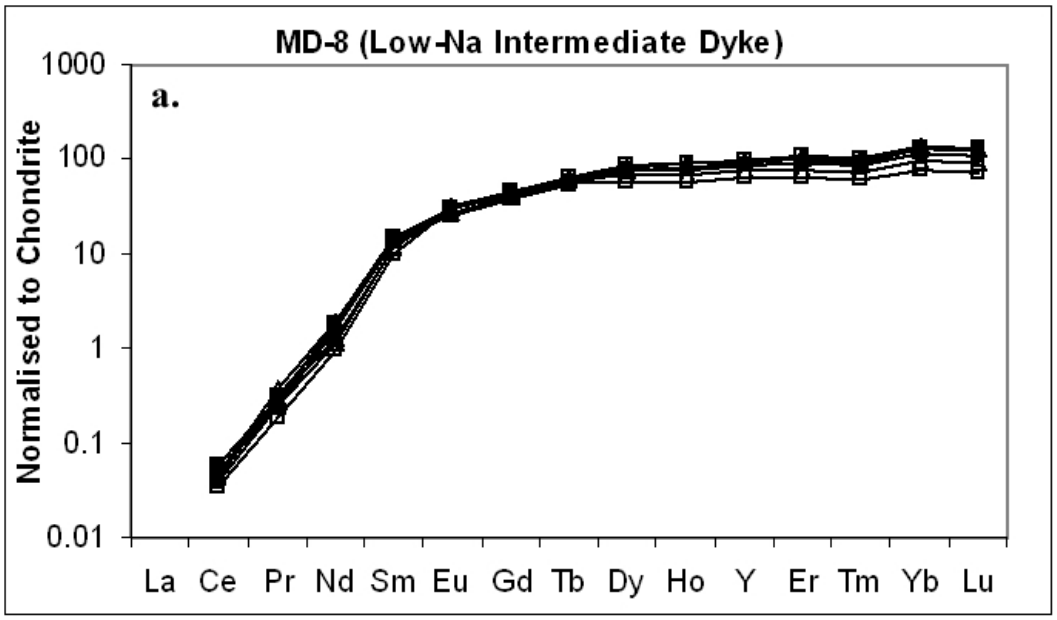


***Figure 8.8.*** *REE patterns of garnets from low-Na intermediate dykes of Fiordland.* ***(a)*** *MD-8.*

## 8.10. Granite: (Sample No: MD-2, MD-6, MD-29 and MD-33)

**MD-2:** MD-2 shows nearly uniform REE patterns of garnets from core to rim. LREE have steeply rising slopes from (La-Sm) with small Eu anomalies (Fig 8.9.a.). Only one core has a large Eu anomaly. MREE have slightly increasing slopes from (Gd-Dy). From Dy to Y the REE patterns are nearly flat and the HREE (Er-Lu) have decreasing slopes. The decreasing slope of the HREE in MD-2 is different than that observed in previous rock types. In general, cores have higher REE abundance than rims. The cores to rims values are not widely variable and vary within the range of 100 to near 1000 of chondritic value.

**MD-6:** Garnet REE patterns in MD-6 display a steeply increasing LREE (La-Sm) and a striking progressive depletion of MREE and HREE from core to rim (Fig 8.9.b.). Cores also have comparatively large negative Eu anomalies compare to rims. All the garnet rims are extremely depleted in HREE.

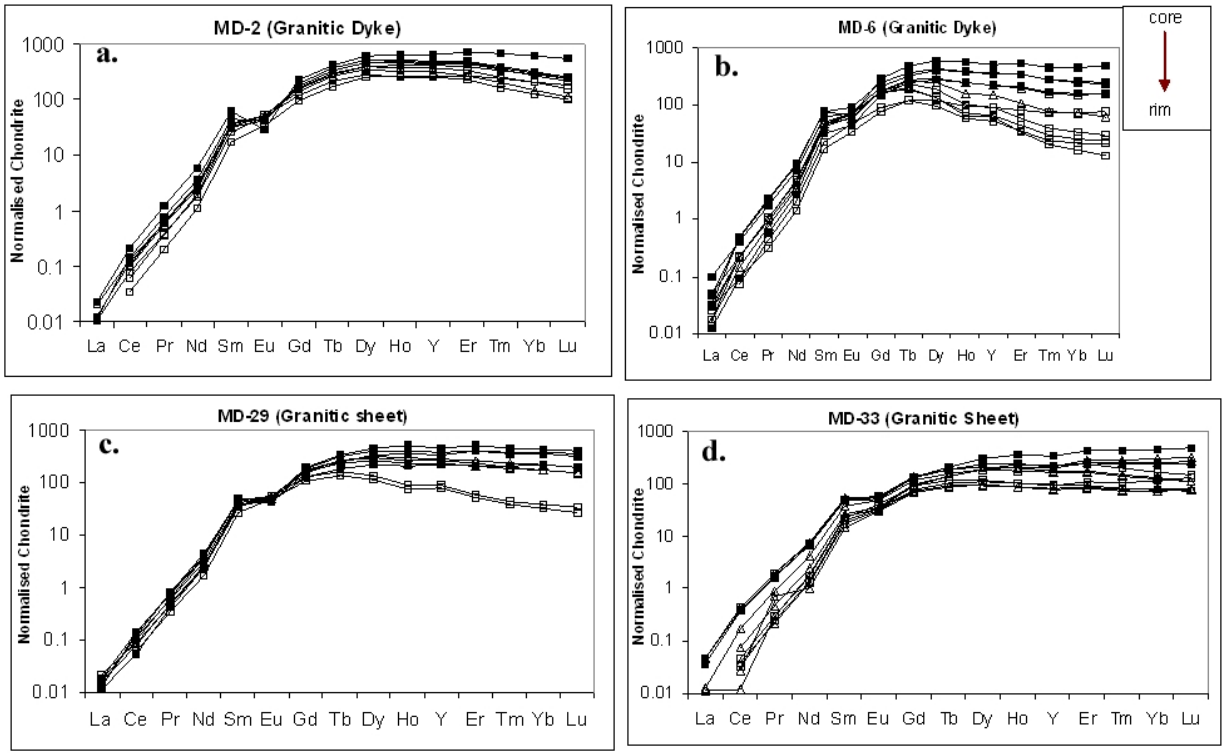


***Figure 8.9.*** *REE patterns of garnets from granites of Mt Daniel, Fiordland;* ***(a)*** *Granitic dyke MD-2 and* ***(b)*** *MD-6,* ***(c)*** *Granitic sheet MD-29 and* ***(d)*** *MD-33.*

**MD-29:** MD-29 shows a wide variation in REE patterns of garnets from core to rim (Fig 8.9.c.). The LREE patterns are uniform from core to rim and steeply increasing from La to Sm, with small Eu anomalies and mostly flat HREE patterns. However, the garnets in MD-29 show both MREE and HREE depleted and non-depleted rims. The non-HREE depleted garnets generally show a slight decrease in MREE and HREE abundances towards rim and garnet with HREE-depleted rims show a wide variation in REE abundances from core to rim. The HREE depleted rims have smaller negative Eu anomalies than cores.

**MD-33:** The REE patterns of garnet in MD-33 are nearly same as the HREE undepleted garnets in MD-29.

## 8.11. Mt Daniel Sheet: (Sample No: MD-14)

MD-14 has quite different REE patterns of garnets (Fig 8.10.a.) from other samples. The LREE patterns are steeply increasing and have a positive Eu anomaly. MREE and HREE patterns are nearly flat, with slightly lower abundances.

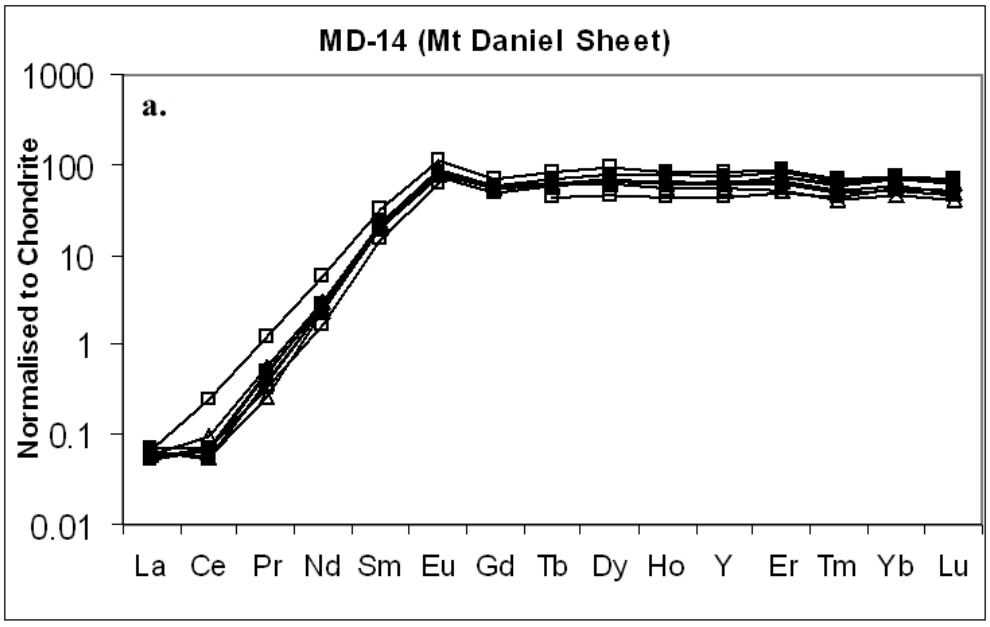


***Figure 8.10.*** *REE patterns of garnets Mt Daniel sheet (MDS) MD-14 from Mt Daniel, Fiordland.*

In summary garnets in mafic rocks show similar REE patterns with small Eu anomalies from core to rim and decreasing abundance of HREE from core to rim. The low-Na intermediate dyke MD-8 shows nearly flat HREE from core to rim with no Eu anomalies. The granites show different REE patterns for individual samples. MD-2 shows nearly uniform core to rim compositions where HREE have slightly decreasing slope and Eu anomalies are generally small. MD-6 shows wide variation and progressive depletion of MREE and HREE from core to rim. Cores have larger Eu anomalies than rims. MD-29 and MD-33 both show progressive depletion of MREE and HREE from core to rim, with small Eu anomalies. MDS sample MD-14 shows positive Eu anomaly with nearly flat MREE and HREE. An important observation is that the zircons and garnets from the same rock

exhibit similar REE patterns and the relation between zircon and garnet will be discussed in details in the section 8.18.

## SECTION C: Geothermometry for Zircon and Rutile of Mt Daniel Rocks

Crystallisation thermometers for zircon and rutile have been devised by Watson and Harrison (2005). The thermometers are based on the temperature dependent uptake of Ti in zircon and Zr in rutile under rutile and zircon saturated conditions respectively, where activity of $TiO_2$, $SiO_2$ and $ZrO_2$ are assumed to be 1. $T_{crystallisation}$ were calculated according to

$T\ (^0C)_{zircon} = [(5080\pm30)/(6.01\pm0.03)-(\log (Ti))]-273$ and

$T\ (^0C)_{rutile} = [(4470\pm120)/(7.36\pm0.10)-(\log (Zr))]-273$ (Equation. 7 and 9 Watson et al., 2006) using Ti and Zr concentrations obtained from LA-ICPMS. The rutile thermometry has been attempted for only mafic rocks because the rutile is abundantly present in mafic dykes but is lacking in other rock types.

The zircon thermometry can reveal the thermal condition of crystallisation of the zircon cores and rims. Th/U and Zr/Hf have been used as indicators in several studies to delineate compositional changes of the zircon-forming environment (e.g. Bolhar et al., 2008a, Fu et al., 2008). U is more compatible than Th in zircon crystal structures. As differentiation proceeds the Th/U ratios tend to decrease with falling temperatures as zircon crystallises from the magma. Zr/Hf also varies in similar fashion. Thus high Hf and low Zr/Hf ratios in zircons indicate the zircons formed from a fractionated melt (Claiborne et al., 2006).

The decrease in Th/U ratio is also attributed to the presence of Th rich accessory minerals like monazite or allanite as a fractionating phase. A low Th/U ratio is also an indicator of metamorphically grown zircon where Th has been expelled from zircon structure as it has larger ionic radii than U and also because U is more mobile in fluids than Th. But Th/U ratio is not an

independent tool and needs to be combined with other data carefully to evaluate the zircon forming environment.

Zircon thermometry alone may also not be an independent monitor to evaluate the magmatic and metamorphic thermal history. Zircon thermometry can be influenced by pressure, the activity of $SiO_{2,}$ errors in calibration, subsolidus resetting of Ti contents, non-Henry's Law of substitution of Ti in zircon, disequilibrium crystallisation from melts and growth of zircon in late hydrous melt (Fu et al., 2008).

In this section, zircon and rutile thermometry will be used along with the trace element compositions of zircon and garnet and CL-images of zircons to evaluate the magmatic and/or metamorphic thermal history of the Fiordland samples. The temperatures obtained from Ti in zircon and Zr in Rutile (where present) of different Fiordland samples are given in Table 8.2.

| Rock Type | Sample No | Range of Ti in Zircon $T^0C$ | Average $T^0C$ Ti in Zircon of Early Cretaceous rim | Average $T^0C$ Ti in Zircon of Cores | Range of Zr in Rutile $T^0C$ | Average Zr in Rutile $T^0C$ |
|---|---|---|---|---|---|---|
| **WFO** | **MD-15** | 773-841 | 815±22 | - | - | - |
| **Mafic Dykes** | **MD-13** | 734-784 | 749±17 | - | 586-674 | 609±12 |
| | **MD-22B** | CL-bright-(829-922) CL-Dark-(674-825) | 822±72 | - | 586-674 | 642±30 |
| | **MD-26** | 667-870 | 700±47$^o$C | 789±70$^o$C | 561-634 | 601±26 |
| **Intermediate Dykes (low-Na variety)** | **MD-8** | 731-892 | 814±68 | - | - | - |
| | **MD-22A** | 634-791 | 658±23$^o$C | 721±49$^o$C | - | - |
| **Intermediate Dykes (high-Na trondhjemitic variety)** | **MD-17A** | 732-846 | 784±35 | - | - | - |
| | **MD-32** | 659-798 | 724±80$^o$C | 738±52$^o$C | - | - |
| **Granite Dykes** | **MD-2** | 660-753 | unknown | 682±47 $^o$C | - | - |
| | **MD-6** | 651-683 | 663±10$^o$C | 673±11$^o$C | - | - |
| **Granitic phase in MDC** | **MD-29** | 648-728 | 684±29$^o$C | 685±38$^o$C | - | - |
| | **MD-33** | 643-719 | 664±24$^o$C | 679±29$^o$C | - | - |
| **MDS rocks** | **MD-14** | 641-877 | 658±23$^o$C | 721±49$^o$C | - | - |
| | **MD-38** | 651-831 | unknown | 707±50$^o$C | - | - |

***Table 8.2.*** *Ti in zircon and Zr in rutile temperatures from different samples of Mt Daniel, Fiordland. All the errors are quoted in 1 sigma.*

## 8.12. WFO: (Sample No: MD-15)

The WFO sample MD-15 shows a small Ti in zircon temperature range of 773-841$^{o}$C with an average of 815±22$^{o}$C. The WFO zircons show a slight decrease in Th/U and Zr/Hf from centre to rim (Fig 8.11.a & b) with a more restricted temperature range, although there are insufficient data to determine whether systematic core-rim trends exist.

## 8.13. Mafic Dykes: (Sample No: MD-13, MD-22B and MD-26)

**MD-13** shows quite restricted range Ti-in-zircon temperature 749±17$^{o}$C (Table 8.2.). The Zr in rutile thermometer yields lower temperatures 609±12 $^{o}$C of Early Cretaceous zircons.

**MD-22B** shows the highest range of Ti-in-zircon temperatures of 674-906$^{o}$C (Table 8.2.) for Early Cretaceous zircons. The different types of grain exhibit a wide variation of Ti-in-zircon temperature. The CL-bright grains exhibit a higher Ti-in-zircon temperature around 825-922$^{o}$C and CL-dark grains show a comparatively lower Ti-in-zircon temperature range 674-752$^{o}$C. The average Ti-in-zircon temperature of MD-22B is 822±72$^{o}$C. The Zr in rutile temperatures are quite low and restricted (586-674$^{o}$C, average 642±30$^{o}$C).

**MD-26** shows a range of Ti-in-zircon temperatures of 667-870$^{o}$C. The rims of CL-dark grains generally show a lower Ti-in-zircon temperature (667-699$^{o}$C) and the single CL bright grains show a comparatively higher Ti-in-zircon temperature (755-795$^{o}$C). The Paleozoic zircon cores have higher temperature with an average of 789±70$^{o}$C and the Early Cretaceous zircons have comparatively lower temperature with an average of 700±47$^{o}$C (Table 8.2.). The Zr in rutile temperature has a lower range than MD-22B (561-634 $^{o}$C, average 601±26 $^{o}$C).

The CL-dark zircons in mafic dykes usually have lower Ti in zircon temperatures compare to CL-bright grains.

Zircons of the mafic rocks show a high Th/U and high Ti-in-zircon temperature.

As discussed earlier, the Paleozoic cores generally have higher Th/U ratios compare of to Early Cretaceous zircons (MD-26) and Early Cretaceous zircons show similar values from centre to rim and no systematic patterns are observed in Th/U or Zr/Hf with the temperature variation (Fig 8.11.a, b.).

## 8.14. Low-Na Intermediate Dykes: (Sample No: MD-8 & MD-22A)

**MD-8** shows Ti in zircon temperature range of 731-892$^{o}$C with an average of 814±68 $^{o}$C (Table 8.2.) of Early Cretaceous zircons. The Ti in zircon temperature gives a range of values of CL-bright grains of same age of 112±12 Ma. The Ti in zircon thermometer records a 50$^{o}$C difference within a single CL bright grain. Paleozoic cores are not analysed in this sample due to smaller grain size.

**MD-22A** shows a lower Ti in zircon temperature range of 634-791$^{o}$C. Inherited cores show comparatively slightly higher Ti in zircon temperature with an average of 721±49$^{o}$C than the Early Cretaceous zircons/overgrowths with an average of 658±23$^{o}$C (Table 8.2.).

The T$^{o}$C-Th/U plot (Fig 8.11.c.) shows a general core to rim decrease of Th/U with decreasing temperature. In contrast, no distinct core-rim patterns are observed in the T$^{o}$C-Zr/Hf plot (Fig 8.11.d.).

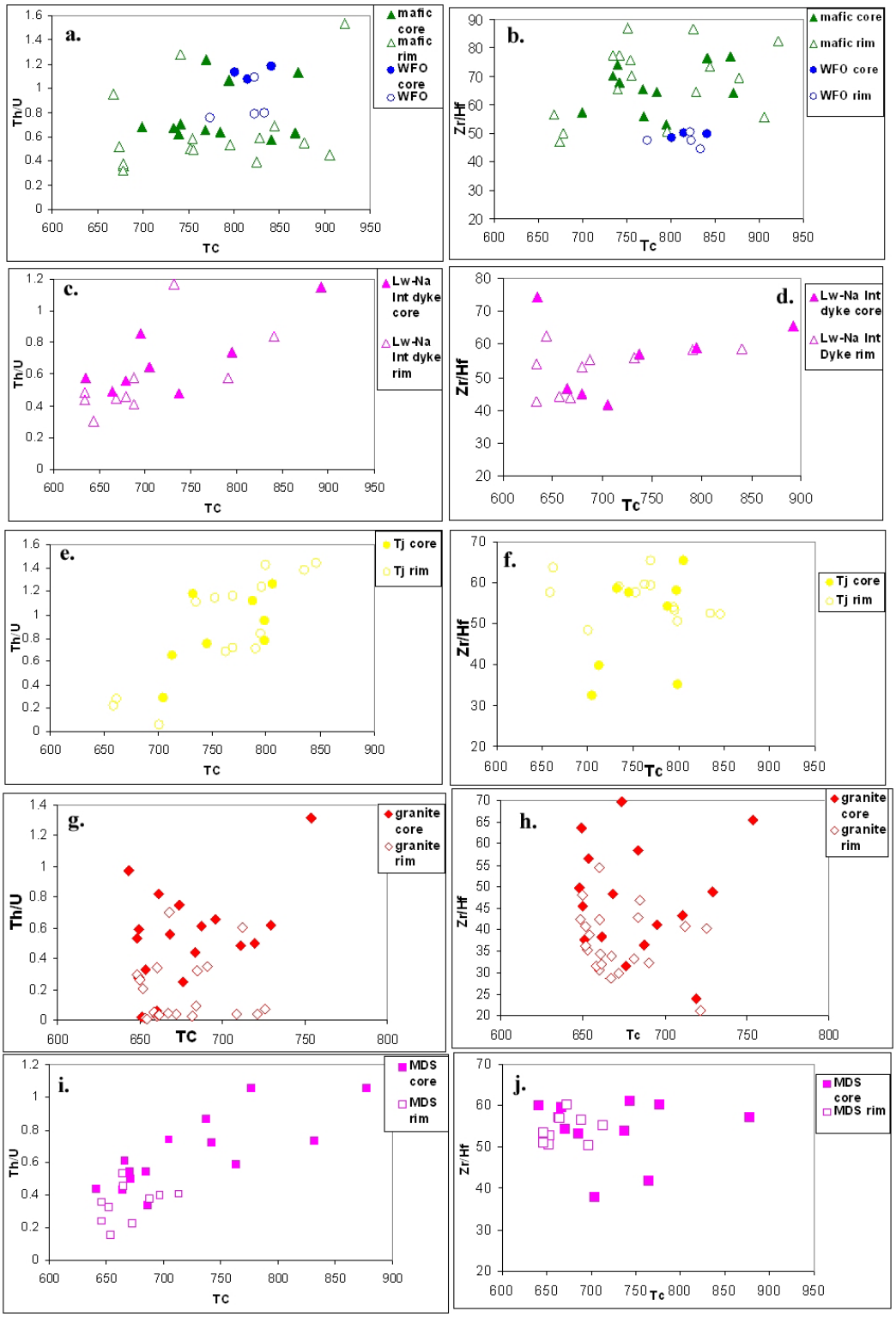


***Figure 8.11.*** ***(a)*** *Th/U -T°C and* ***(b)*** *Zr/Hf-T°C plots of zircon inherited and non-inherited cores and rims from mafic samples (MD-13, MD-22B and MD-26) and WFO of Fiordland;* ***(c)*** *Th/U -T°C and* ***(d)*** *Zr/Hf-T°C plots from low-Na intermediate dykes;* ***(e)*** *Th/U -T°C and* ***(f)*** *Zr/Hf-T°C plots from*

*high-Na intermediate dykes;* ***(g)*** *Th/U -T$^{o}$C and* ***(h)*** *Zr/Hf-T$^{o}$C plots from granite samples of Fiordland;* ***(i)*** *Th/U -T$^{o}$C and* ***(j)*** *Zr/Hf-T$^{o}$C plots from MDS samples from Mt Daniel, Fiordland.*

## 8.15. High-Na Intermediate Dykes (Trondhjemitic Variety): (Sample No: MD-17 and MD-32)

**MD-17A** zircons yield an average Ti in zircon temperature of 784±35$^{o}$C (Table 8.2.). The zircons of Early Cretaceous age are interpreted as magmatic based on their elongated shapes and planar banding and oscillatory zoning without inherited cores. Zircons show both a decrease in temperature from the centre of the grain towards rim and also a reverse trend is observed in some zircons. Th/U (Fig 8.11.e.) and Zr/Hf (Fig 8.11.f.) show a very similar range from centre to rim of the zircons.

**MD-32** shows Ti in zircon temperature range of 659-798$^{o}$C. The inherited cores have slightly higher temperate with an average of 738±52$^{o}$C than the Early Cretaceous zircons with an average of 724±80$^{o}$C (Table 8.2.). A single Early Cretaceous zircons show a higher Ti in zircon temperature of 884 $^{o}$C. The zircons show a slight decrease in Th/U ratio (Fig 8.11.e.) and Zr/Hf (Fig 8.11.f.) from core to rim and a reverse trend is also observed. However the variations are small.

.

## 8.16. Granitic Dykes: (Sample No: MD-2 & MD-6)

**MD-2** has Ti in zircon temperature range of 660-753$^{o}$C with an average Ti in zircon temperature of 682±47$^{o}$C (Table 8.2.). As the age of the Early Cretaceous rims are not well constrained due to the presence of very thin rims (see chapter-6), the temperature variation between core and rim can not be calculated.

**MD-6** shows a Ti in zircon temperature range of 651-683$^{o}$C. The Paleozoic cores show a slightly higher Ti in zircon temperature with an average of 673±11$^{o}$C than the Early Cretaceous zircon rims with an average of 663±10$^{o}$C (Table 8.2.).

## Granitic Sheets in MDC: (Sample No: MD-29 & MD-33)

**MD-29 and MD-33** show a very similar Ti in zircon temperature ranges of 648-728$^{o}$C and 643-719$^{o}$C respectively. The Paleozoic cores and Early Cretaceous rims have very similar Ti in zircon temperature for MD-29 with an average of 685±38$^{o}$C and 684±29$^{o}$C respectively (Table 8.2.). MD-33 has slightly higher Ti in zircon temperature of cores with an average of 679±29$^{o}$C than Early Cretaceous rims of 664±24$^{o}$C (Table 8.2.). Some of the grains show temperature reversals from core to rim.

The Th/U and Zr/Hf vs. temperature (Fig 8.11.g.) & (Fig 8.11.h.) plots do not show any systematic trends in different samples. MD-2 doesn't have core, rim data from single grains but still rims have the low Th/U and Zr/Hf compare to core but the age of the rims are not well constrained in this sample (see chapter-6). MD-6, MD-29 and MD-33 generally show a core to rim decrease of Th/U and Zr/Hf.

## 8.17. Mt Daniel Sheets: (Sample No: MD-14 and MD-38)

**MD-14** shows a Ti in zircon temperature range of 641-877$^{o}$C. A consistent decrease in temperature is observed from zircon core to rim. The very dark inherited core of zircons yields a higher temperature with an average of 721±49$^{o}$C where rims generally show a lower temperature with an average of 658±23$^{o}$C. The zircons with patchy zoning or recrystallized zircon cores (see Chapter-5) show similar lower temperatures to rims.

**MD-38** shows a Ti in zircon temperature range of 651-831$^{o}$C and the average temperature of the Paleozoic cores is 707±50$^{o}$C and the rims observed in CL-images are unknown but presumed Cretaceous ages show a comparatively lower temperature than zircon cores.

The MDS zircons have variable Th/U but a restricted range of Zr/Hf ratio. There is a general core to rim decrease of Th/U with decreasing T$^{o}$C from core to rim (Fig 8.11.i.). The minimum drop of temperature is 20$^{o}$C from core to rim. The Zr/Hf doesn't vary much with varying temperature (Fig 8.11.j.).

## 8.18. Interpretation and Discussion

Zircons of the MDC dykes and sheets are widely variable in inter- and intra-group compositions. So even within the same group these grains may record a different petrogenetic history. The MDC samples show Early Cretaceous zircons/overgrowths and Paleozoic inherited cores. The origin of these two different zircon populations are evaluated here based on their morphology, microstructure and trace element characteristics. Th/U ratio, REE pattern, Ce and Eu anomaly and zircon thermometry are used as key characteristics to distinguish magmatic and metamorphic zircons. Zircon and garnet REE patterns are also compared to understand whether they recorded any change in physicochemical condition occurred due to the transition of the zircon forming environment. In this section the nature of zircons, their growth environment and condition of formation in each rock

group will be discussed in order to evaluate the petrogenetic history of different rock types in the Mt Daniel Complex.

**WFO**

The Early Cretaceous zircons without inherited cores from WFO are interpreted as magmatic based on their elongated to subrounded shapes, planar banding, oscillatory and sector zoning.

The trace element compositions of zircons have high Th/U ratios, positive Ce and strongly negative Eu anomalies with steep HREE patterns and high Ti in zircon temperatures which are also consistent with the igneous origin. The positive Ce anomaly indicates an oxidizing environment and negative Eu anomaly suggests the involvement of plagioclase causing depletion of the Eu/*Eu ratio. There is no difference observed in trace element chemistry and REE patterns for different looking grains observed in CL-images (see Chapter-5). The zircon crystallizing temperature is quite high as appropriate for magmatic conditions but with a restricted range of values and without any significant change in trace element composition (Th/U and Zr/Hf) from centre to rim (Fig 8.11.a and b.). This may indicate that the zircons crystallised in a closed system without any significant temperature variation within a short time span. All lines of evidence reinforce the magmatic origin of the WFO zircons.

**Mafic Dykes**

The zircons from mafic dykes (MD-13, MD-22B and MD-26) are mainly of Early Cretaceous age without inherited cores except MD-26. The zircons are subrounded to rounded in shape with mainly sector and fir tree zoning and could imply either magmatic or metamorphic origin. These zircons mainly have high Th/U, strong positive Ce and small negative Eu anomalies with higher concentration of HREE and high Ti in zircon temperatures. All the

evidence needs to evaluate in detail for understanding the origin of the zircons from mafic dykes and are discussed below.

The small Eu anomalies in the zircons can be attributed to two factors; either the absence of plagioclase - where the zircons do not compete with feldspar for Eu or a highly oxidizing environment - whereby trivalent Eu was dominant. Plagioclase is abundant in these rocks, but the timing of plagioclase formation relative to zircon is unknown. It has also been recognized that small to negligible negative Eu anomalies are common in metamorphic zircons (Rubatto, 2002).

The Th/U of these zircons is ≥0.1, which does not diagnose a magmatic or high-T metamorphic origin. Zircons formed from a partial melt or metamorphic fluid tends to have high Th/U ratio (Th/U > 0.15 and up to 3.2; Carson et al. 2002; Kelly and Harley 2005; Pidgeon, 1992; Schaltegger et al., 1999; Vavra et al., 1999; Harley et al., 2001; Hokada and Harley 2004; Schaltegger et al., 1999; Hoskin and Black, 2000; Rubatto et al., 2001; Rubatto, 2002).

The REE patterns of zircons and garnets do not show any depletion of HREE towards rims. The non depleted patterns both in zircon and garnet suggesting that they may have crystallised from a large volume reservoir, such as magma, where the supply of HREE can be considered as essentially infinite. So the zircons and garnets formed in an open system process.

Ti-in-zircon thermometry reveals that temperatures are high in the zircons of mafic dykes where as the Zr in rutile temperature is low. Also there is no significant change observed in trace element composition of zircon (Th/U and Zr/Hf) with the temperature variation from centre to rim (Fig 8.11.a and b.) suggesting that the zircons may not have a simple fractional crystallisation history from a mafic magma, unless they formed during the final stages of magma crystallisation which is commonly observed in case of mafic magmas.

The trace element compositions, REE patterns of zircon and garnet, and thermometry do not show any significant variation between Early Cretaceous CL-bright and CL-dark zircons. The difference in their CL-images and minor variation in chemistry suggest they may have formed synchronously.

In summary the Early Cretaceous grains and rims from mafic dykes with fir tree and sector zoning have higher concentrations of HREE, high-Th/U ratio and high Ti in zircon temperature. All the evidence goes in favour of a magmatic origin of the zircons from mafic dykes and it can be suggested that the zircons may have formed during late stage magmatic crystallisation in an open system process. This interpretation will be considered in the light of the zircon Hf isotope data presented in Chapter 9.

**The Paleozoic inherited cores** of MD-26 mainly have oscillatory, patchy and homogeneous zoning (see chapter-5) with uniform REE patterns, strong positive Ce anomalies, strongly negative Eu anomalies with high Th/U ratios indicating that they may have derived from igneous protolith. This conclusion is applicable to all Paleozoic inherited cores from other samples.

### Low-Na Intermediate Dykes

**MD-8:** The CL-bright Early Cretaceous zircons of MD-8 are very similar to the zircons from mafic dykes. The zircons have high Th/U ratios, uniform HREE enriched patterns with positive Ce anomalies and negative Eu anomalies and high Ti in zircon temperatures. The zircon and garnet rims do not have any HREE depletion suggesting that they have formed in an open system process. The planar banding and different growth zones observed indicate the zircons may have formed in a magmatic environment.

**MD-22A:** The Cretaceous rims of the zircons from MD-22A have Th/U ratios $\geq 0.3$ which is not like typical metamorphic zircons. The REE patterns are uniform and without any core to rim depletion and have a lower Ti in zircon temperature compare to core which proportionally varies with Th/U (Fig 8.11.c.). The lack of oscillatory zoning in the rims suggests that the thin zircon overgrowths may have formed during metamorphism probably by subsolidus recrystallisation

and/or from partial melting during peak metamorphic conditions. The exact formation process of zircons will be addressed in the next chapter.

**High-Na Intermediate Dykes**

**MD-17A:** The origin of the Early Cretaceous MD-17A zircons is quite straightforward. The zircons are interpreted as magmatic based on their elongated shapes and planar banding and oscillatory zoning. They have high Th/U; uniform HREE enriched pattern with positive Ce and small or almost no Eu anomalies and also show a high Ti in zircon crystallisation temperature consistent with a magmatic origin of these zircons. The cause of the positive Ce anomaly and small negative Eu anomaly is already discussed in the mafic dyke section. The increase of Th/U and Zr/Hf ratios from centre to rim of the zircons with increasing temperature suggest systematic crystallisation of zircons from the magma in an open system process. Some temperature reversals of zircons from centre to rim suggest that the system may have been replenished by more hot magma.

**MD-32:** The Early Cretaceous zircon overgrowths of MD-32 have variable morphologies /microstructures and broad range of trace element compositions. Mainly the oscillatory zoned overgrowths and single zircons with subhedral crystal structure with planar banding or unzoned, having similar characteristics with high Th/U ratios, enriched uniform HREE patterns, low Eu anomalies and high Ti in zircon temperature consistent with the magmatic origin of these zircons/overgrowths. Some zircons record temperature reversals from core to rims suggesting consecutive replenishment of the system by hot magma/melts during the zircon growth.

The thick, featureless Early Cretaceous overgrowths on the other hand show low Th/U ratio (0.06-0.2), lower HREE enrichment of the rims but not depleted and low Ti in zircon temperature suggesting a metamorphic origin of these overgrowths. Thus the presence of igneous and metamorphic zircons in MD-32 suggests a transitional environment continuous across magmatic to metamorphic conditions.

## Granites

**MD-2:** As discussed in chapter-6, the core-rim boundaries are often gradational and extremely thin in the zircons of MD-2. So the trace element analyses have been done on core-rim gradational boundaries rather than on pure rims. This study is thus unable to provide the exact trace element compositions of the zircon rims.

**Other Granites (Sample No: MD-6, MD-29 and MD-33)**

The other granite samples mostly have featureless, thick (MD-6) or thin (MD-29 and MD-33) overgrowths. They show both HREE non-depleted and HREE depleted zircon rims of Early Cretaceous age. The depleted rims have low Th/U ratios and low Eu anomalies and low Ti in zircon temperature suggesting that the rims may have a metamorphic origin. The non depleted rims have comparatively high Th/U ratio and Ti in zircon temperature but Eu anomalies are variable from small to large. The garnet rims also show variable depletion from core to rim suggest that the zircon and garnet rims are formed synchronously under equilibrium conditions.

The HREE depleted and non depleted Early Cretaceous growth of zircon and garnet can be possible in two ways. These zircons may have been formed during the burial and solidification of magma, where crystal growth and/or recrystallisation are continuous across the igneous to metamorphic transition. Lithostatic pressure increases due to burial of the Mt Daniel area causes late stage garnet crystallisation in the magma, which rapidly depletes the residual liquid in HREE. This signature is then reflected in the crystallizing zircons whereas any earlier formed zircon grains will be non-depleted in HREE. The HREE depleted rims suggest that they have been formed in a typical metamorphic environment, in a finite reservoir which implies a closed system process

The irregular homogeneous domains are present in zircons which cut across the growth zoned of cores (see chapter-5). These domains might have formed by recrystallisation which may be promoted by the presence of magmatically derived aqueous fluids in depth (Pidgeon 1992,

Nemchin and Pedgeon 1997, Schaltegger et al., 1999). These interpretations will be evaluated more precisely with the help of Hf isotopic data in the next chapter.

**Mt Daniel Sheets**

The featureless Early Cretaceous zircon overgrowths from both of the MDS samples have uniform REE patterns but rims have generally lower abundance of HREE compare to cores. The rims have moderately low Th/U ratios, small Eu anomalies and low Ti in zircon temperature compared to cores. The restricted range of Zr/Hf without any systematic variation from core to rim with temperature indicates that these grains may not have formed from a purely igneous process (e.g. fractional crystallisation). The zircon morphology along with trace element study suggests that the zircons have formed in a metamorphic environment.

The HREE non depletion in zircon and garnet rims suggest that they have crystallised in an infinite reservoir, possibly in the presence of melts. These rims may have crystallised from partial melts formed during peak metamorphism in granulite facies conditions, suggesting the presence of an open system process thus not causing any depletion of HREE in the zircon and garnet rims.

**In summary**- Early Cretaceous zircons without inheritance in mafic dykes and low-Na intermediate dykes may have formed in igneous environment and possibly formed during late stage magmatic crystallisation in an open system process.

Magmatic zircons are present in the WFO and high-Na intermediate dyke MD-17A. The WFO zircons may have formed in a close system process where as the zircons from MD-17A suggest an open system. In contrast the zircons of dyke MD-32, formed in a transitional environment having both magmatic and metamorphic overgrowths. The temperature reversals towards rim in high-Na dykes could suggest replenishment by the hot magma in an open system process.

Zircons of the granites MD-6, MD-29 and MD-33 also formed in a transitional environment-continuous across late magmatic stage to metamorphism. Simultaneous crystallisation of garnets and zircons led to the HREE depletion of both the minerals.

All the other zircon overgrowths from different rock types – low-Na intermediate dyke (MD-22A) and MDS samples (MD-14 and MD-38) may have crystallised from partial melts that formed during peak metamorphic conditions and do not have HREE depleted zircon.

The Paleozoic inherited cores probably derived from an igneous protolith. In general the cores have formed at higher temperature than rims.

Zircons from the MDC indicate that these rocks formed in contrasting environments and bear different effects of metamorphism. The simultaneous presence of typical igneous and metamorphic zircons even within the same rock suggests dynamic processes where the both of these high temperature processes are nearly simultaneous or overlapping.

# Chapter-9: Hf isotope Geochemistry of Zircons from Mt Daniel, Fiordland

## 9.1. Introduction

Lu-Hf isotope is an important tool for understanding crust-mantle differentiation processes (Patchett et al 1981, Vervoort and Blichert-Toft, 1999; Vervoort and Patchett, 1996; Blichert-Toft and Albarede, 1997; Vervoort et al., 1999; Chauvel and Blichert-Toft, 2001). Zircon is a very good reservoir of different isotopes (U-Th-Pb and Lu-Hf) and trace elements. U-Pb-Th are used as geochronometers (see chapter-6) and Lu-Hf can be used as crustal evolutionary tracers in zircon. The chemical behaviour of Hf and Zr are similar. Hf is the member of group IVB lithophile elements in the periodic table. Hf is more incompatible than Lu during melting of spinel-garnet peridotite, thus Hf becomes concentrated in the continental crust relative to Lu, resulting in unradiogenic and radiogenic $^{176}Hf/^{177}Hf$ ratios in the crust and depleted mantle reservoir respectively (Patchett et al., 1981). Due to low Lu/Hf ratios (typically < 0.002), zircon preserves $^{176}Hf/^{177}Hf$ ratios very close to the initial $^{176}Hf/^{177}Hf$ ratios inherited from the magma during the formation. The intra-crystalline diffusion rate of Hf in zircon is very low (Cherniak et al., 1999), allowing the preservation of isotopic variations induced by interaction between various magmas (Griffin et al., 2002) or the presence of components from different ages during zircon crystallisation. So Hf isotopes in zircon are an important tool for understanding the evolution of silicic magmas and thus the generation and evolution of continental crust. This chapter discusses the Hf isotope data from zircons of different rock types of Mt Daniel, Fiordland, and tries to evaluate the nature of source rock/s of different magmas and the compositional evolution of different magma types. The analytical techniques for obtaining Lu-Hf isotopic data are described in Chapter-3. The Hf isotope data are provided in appendix 6. This chapter will mainly deal with the Hf isotope compositions of different rock types and their significance.

## 9.2. Early Cretaceous Zircon εHf and Whole Rock εNd in Relation to the Formation of Mt Daniel Rocks

The Early Cretaceous zircons are representative of the formation of Mt Daniel Complex (MDC) after the formation of Western Fiordland Orthogneiss (WFO) at 125 Ma. The Early Cretaceous zircon εHf and whole rock εNd data are broadly correlated in individual rock types (Fig 9.1.) of MDC and fall along the "terrestrial array" defined by Vervoort et al., (1999).

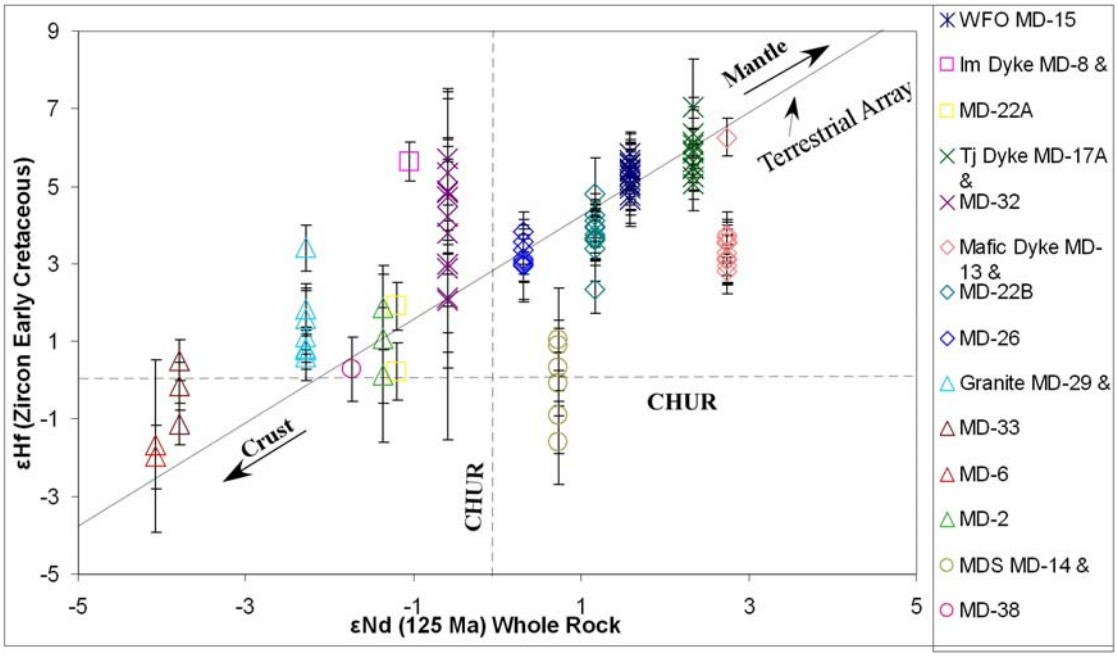


***Figure 9.1.*** *Hf isotopic composition of zircons from Mt Daniel correlated with whole rock Nd isotope at the time of their crystallisation. Error bars represent 2 standard error.*

Samples from Mt Daniel Sheets, MD-14 slightly plots off from this terrestrial array (Fig 9.1.). All the other rock types are within the terrestrial array forming a best fit mixing line between crust and mantle but mafic dyke MD-13 and low-Na intermediate dyke MD-8 are not consistent with this trend (Fig 9.1.).

The slight shift from the mixing line may reflect the effect of metamorphism in these rocks. The presence of other Hf rich mineral phases during metamorphism may contribute Hf to the system which affects the original Hf isotopic composition of the zircons. The end member representatives of this line are high-Na intermediate dyke (trondjhemitic variety) MD-17A and granitic dyke MD-6. This is also consistent with the whole rock isotopic study, where these samples plot at opposing ends of the Sr-Nd isotope array (see chapter-3). MD-17A shows most radiogenic and the granitic dyke MD-6 shows least radiogenic. So this array could reflect mixing between the mafic and felsic crustal components. All other rocks from different groups (Fig 9.1.) are within this general mixing trend.

The Separation Point Batholith shows a more radiogenic signature than the Mt Daniel rock types ($\varepsilon Hf = 3.2\pm0.2$ to $11.2\pm0.6$ of similar Early Cretaceous age (Fig 9.2.a.).

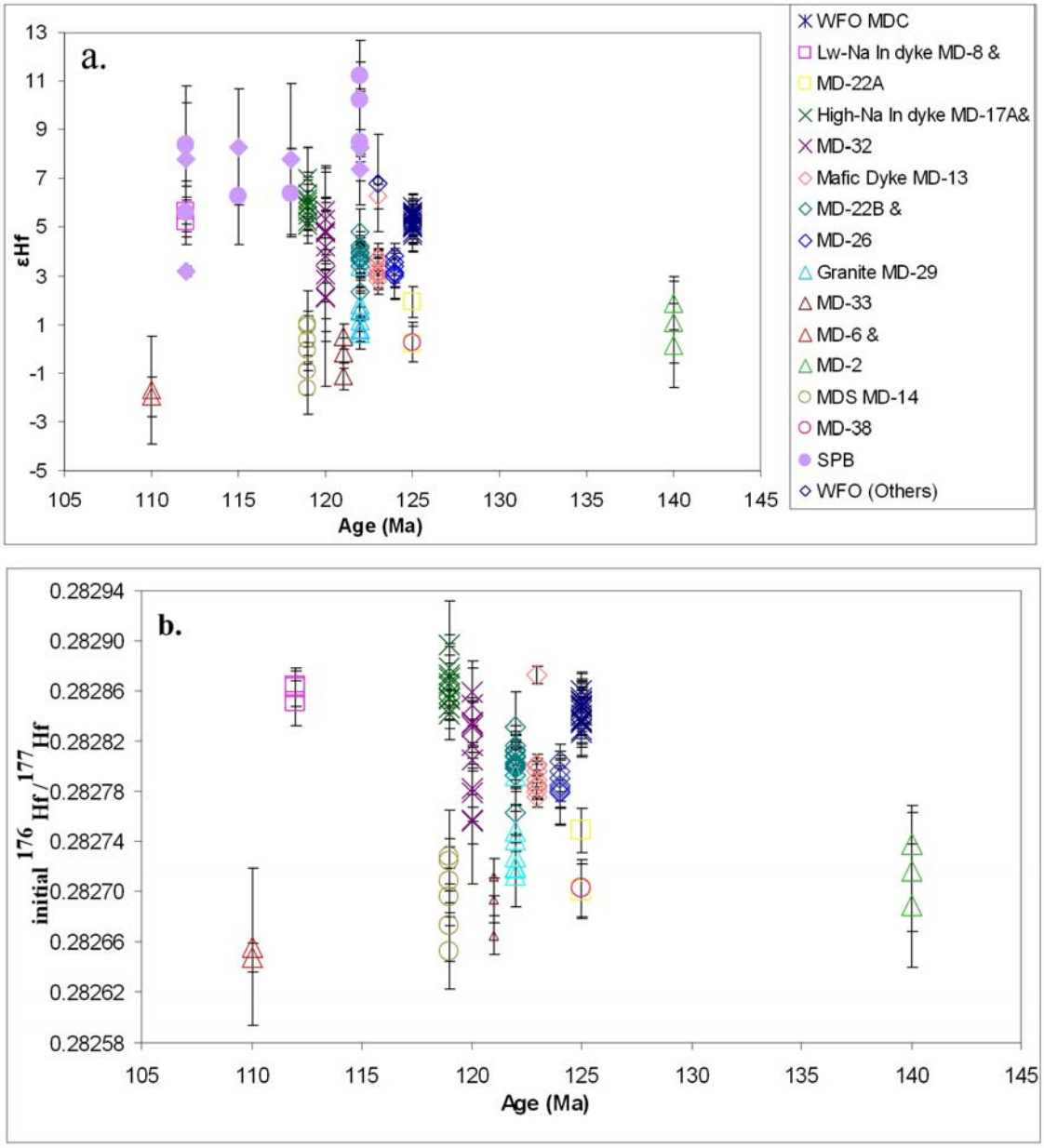


***Figure 9.2.*** *Hf isotopic composition variation of Early Cretaceous zircons with age.* ***(a)*** εHf *vs. age from Mt Daniel and Separation point batholith (from Bolhar et al., 2008).* ***(b)*** *Initial Hf isotopic composition of zircons vs. age of Mt Daniel Complex rocks.*

## 9.3. Comparison of Hf Isotope Composition of Early Cretaceous Zircons from Different Rock Groups of Mt Daniel

The Hf isotope analyses of Early Cretaceous zircons are mostly obtained near to the spots of U-Th-Pb analyses.

**Western Fiordland Orthogneiss (WFO): (Sample No: MD-15)**

The Hf isotope composition of WFO zircons shows a very restricted range of initial $^{176}Hf/^{177}Hf$ (Table 9.1.) with an average of 0.282845±0.000017 (2 SD, n=26) and εHf values ranges from 4.7±0.6 to 5.8±0.5 (2SE).

**Mafic Dykes: (Sample No: MD-13, MD-22B and MD-26)**

The Hf isotope composition of zircons from mafic dyke MD-13 show limited dispersion of initial $^{176}Hf/^{177}Hf$ composition (Table 9.1.) with an average 0.282797±0.000053 (2 SD, n=11) similar to other mafic dykes. The εHf values range from 2.8±0.4 to 3.7±0.5 (2SE) and a single zircon shows a higher εHf (t=123 Ma) value 6.3±0.4. This zircon does not contain any inheritance found in U-Pb age dating and is CL dark.

The Hf isotope compositions of zircons from MD-22B show variable initial $^{176}Hf/^{177}Hf$ values (Table 9.1.) compare to the other mafic dykes with a comparative higher average initial $^{176}Hf/^{177}Hf$ value of 0.282803±0.000030 (2 SD, n=15) but within error with other mafic dykes and corresponding εHf (t=122 Ma) values are in range of 2.3±0.6 to 4.8±0.9 (2SE).

The zircons from mafic dyke MD-26 also show a similar restricted range of initial $^{176}Hf/^{177}Hf$ compositions with other mafic dykes and having an average of 0.282788±0.000018 (2 SD, n=7) and εHf (t=124 Ma) values ranges from 3.0±0.9 to 3.8±0.5 (2SE).

**Low-Na Intermediate Dykes: (Sample No: MD-8 and MD-22A)**

The zircons from low-Na intermediate dyke MD-8 have a higher average initial $^{176}Hf/^{177}Hf$ composition of 0.282858±0.000014 (2SD, n=3) than initial $^{176}Hf/^{177}Hf$ composition of 0.282725±0.000068 (2SD, n=2) from MD-22A (Table 9.1.). The εHf (t=112 Ma) composition of zircons show a different, more radiogenic range in MD-8, from 5.2±0.6 to 5.7±0.5 (2SE) than the unradiogenic εHf (t=125 Ma) values of MD-22A 1.9±0.6 and 0.2±0.7 (2SE).

**High-Na Intermediate Dykes: (Sample No: MD-17A and MD-32)**

The zircons from high-Na intermediate dyke MD-17A have limited variability in initial $^{176}Hf/^{177}Hf$ values (Table 9.1.) with an average 0.282865±0.000031 (2SD, n=12) and variation in εHf (t=116 Ma) ranges 5.0±0.7 to 7.0±1.2 (2SE).

The Early Cretaceous overgrowths and single zircons from high-Na intermediate dyke MD-32 (see chapter-5 and 6) show a large variation in initial $^{176}Hf/^{177}Hf$ composition (Table 9.1.) with respect to MD-17A having an similar average of 0.282809±0.000072 (2SD, n=11) (Fig 9.2.) and also highly variable εHf (t=120 Ma) values from more radiogenic to less radiogenic variety ranges from 2.1±0.7 to 5.7±0.9 (2SE).

**Granitic Dyke: (Sample No: MD-2)**

The zircon overgrowths from granitic dyke MD-2 as discussed in (chapter-5 & 6) have very thin rims with (most likely) mixed U-Pb ages (chapter-6) having average initial $^{176}Hf/^{177}Hf$ compositions 0.282715±0.000049 (2 SD, n=3) and εHf (t=140 Ma) values 0.1±1.7 to 1.9±1.0 (2SE). As the 140 Ma age is more likely to be a mixed age, εHf values of overgrowths are also calculated at 125 Ma to observe any significant change in εHf composition. 125 Ma is the emplacement age of WFO (Hollis et al., 2003) and all the Mt Daniel Complex dykes and sheets are thought be formed during or after the WFO emplacement which is evidence by field relations, U-Pb age studies and by

different other studies (see chapter-1, 2 and 6). The εHf values do not show any significant difference in both cases so the 140 Ma is used in this study to calculate the εHf values, which may also give a mixed isotopic value. But in this study the Hf isotopic composition of MD-2 will not be discussed further, as this is probably not the true composition of the Early Cretaceous zircons.

**Other Granites: (Sample No: MD-6, MD-29 and MD-33)**

In the granitic group MD-6 is granitic dyke and MD-29 and MD-33 are granitic sheets in MDC show a nearly similar Hf isotopic compositions.

The zircon overgrowth from granitic dyke MD-6 have average initial $^{176}Hf/^{177}Hf$ composition 0.282652±0.000011 (2 SD, n=2) and εHf (t=110 Ma) values -1.7±2.2 and -2.0±0.4 (2SE) which is less radiogenic than other granitic samples.

The zircon overgrowths from sample MD-29 have variable initial $^{176}Hf/^{177}Hf$ composition (Fig 9.2.b.) with an average of 0.282738±0.000051 (2 SD, n=8) and εHf (t=122 Ma) values that range from 0.6±0.5 to 3.4±0.5 (2SE).

The zircon overgrowths from sample MD-33 have average initial $^{176}Hf/^{177}Hf$ compositions 0.282690±0.000046 (2 SD, n=3) and less variable than MD-29 (Fig 9.2.b.) The εHf (t=121 Ma) values of rims from -1.1±0.5 to 0.5±0.5 (2SE).

**Mt Daniel Sheets: (Sample No: MD-14 and MD-38)**

The zircon overgrowths from sample MD-14 have a wide range of initial $^{176}Hf/^{177}Hf$ compositions (Table 9.1.) with an average of 0.282697±0.000059 (2 SD, n=6) and εHf (t=119 Ma) values that range from -1.6±1.0 to 1.1±0.6 (2SE).

MD-38 has a single Cretaceous zircon with initial $^{176}Hf/^{177}Hf$ composition 0.282702±0.000023 and εHf (t=125 Ma) value 0.3±0.8 which is in within error with MD-14.

## 9.4. Discussion of Hf Isotopic Composition of Early Cretaceous Zircons from Different rock groups of Mt Daniel

**WFO: (Sample No: MD-15)**

The εHf range in zircons from WFO show a radiogenic signature but less radiogenic than depleted mantle like values (~+16 εHf, Vervoort and Blichert-Toft, 1999). The magma either derived from a less radiogenic mantle source or from the remelting of a juvenile mafic crustal source. The restricted intra-grain variability of the Hf isotopic composition of WFO zircons (Fig 9.2.a. and b) suggests that the zircons from WFO sample MD-15 may have crystallised from a closed system magmatic process.

**Mafic Dykes: (Sample No: MD-13, MD-22B and MD-26)**

The similar Hf isotopic composition of zircons from the three mafic dyke samples suggests that they the host magmas may have been derived from similar sources.

The Hf isotopic values show similar radiogenic signature of these dykes (εHf +3.3 to +3.6) but far less radiogenic than the depleted mantle (~+16 εHf, Vervoort and Blichert-Toft, 1999) suggesting they may have derived either from a less-depleted mantle source or melting of a mafic crustal source.

The intra-grain variability of Hf isotopes in zircons is different in the three mafic dykes but within error of each other (Fig 9.2.a. and b.). MD-13 and MD-26 have a restricted range of composition. But in MD-13, a single grain has higher εHf (+6.3). MD-22B shows more variable Hf isotopic compositions of zircons (Fig 9.2.a. and b). The variation in zircon Hf isotopic compositions in MD-13 and MD-22B suggest the interaction between different sources. The variation in Hf isotopic compositions of zircons in MD-22B may be due to mixing between crustal and mantle source and/or crustal assimilation during the ascent of a more mafic magma, thus shifting the isotopic composition towards less radiogenic values.

The whole rock geochemistry (see chapter-3) suggests a spinel-lherzolite mantle origin of these dykes. The zircon with higher εHf in MD-13 may suggest either a further addition of a more radiogenic component or εHf ~+6.3 is the parent composition of the magma made progressively more unradiogenic by crustal assimilation; however, the shift is not along the mixing trend and plots slightly off the terrestrial array (Fig 9.1.). Figure 9.1. shows a more evolved Hf isotope composition of MD-26. The restricted intra-grain variability of Hf isotopic compositions of the zircons may indicate the zircon growth from a closed system process in this dyke and melt derived from comparatively evolved origin than other dykes.

**Low-Na Intermediate Dykes: (Sample No: MD-8 and MD-22A)**

The two low-Na intermediate dykes show extremely different Hf isotopic composition (Fig 9.2.a. and b) where the zircons from MD-8 show more radiogenic signature and MD-22A shows less-radiogenic signature. The zircons from MD-8 probably crystallised from a melt derived from either less radiogenic (i.e. enriched) mantle source or from remelting of the mafic crustal source or some crustal assimilation during the ascent of more mafic magma.

The MD-22A zircons are crystallised either from the remelting of isotopically heterogeneous crustal source or the mixing between crustal and mantle derived magmas. The mixing between mantle and crustal sources cannot be properly evaluated due to small number of analyses (presence of very few Early Cretaceous rims/zircons).

**High-Na Intermediate Dykes: (Sample No: MD-17A and MD-32)**

The zircons from high-Na intermediate dykes show variable Hf isotopic compositions.

The Hf isotopic compositions of MD-17A show the most radiogenic signature of any Mount Daniel rock types (Fig 9.2.a. and b) but less radiogenic than depleted mantle. MD-32 shows the highest intra-grain variability from more radiogenic to less radiogenic compositions (Fig 9.2.a. and b).

The variations in Hf isotopic composition of zircons suggest the interplay of isotopically-distinct sources. The magma may be derived either by mixing of melts derived from heterogeneous crust, the mixing of crustal and mantle magmas, and/or crustal assimilation by mantle-derived magmas.

**Granites: (Sample No: MD6, MD-29 and MD-33)**

The Hf isotopic composition of zircon rims indicates that they have crystallised from unradiogenic sources, such as crustal rocks (Fig 9.2.a. and b). Some intra-grain variability is present in MD-29 and MD-33 but can not be determined in MD-6 due to few numbers of analyses. MD-29 shows an isotopic variability from more radiogenic to less radiogenic composition. This variation can cause either by mixing of crustal and mantle derived magmas (Griffin et al., 2002; Belousovaet al., 2006; Kemp et al., 2007) or by melting of a heterogeneous crustal source (V. Murgulov et al., 2007).

**Mt Daniel Sheets: (Sample No: MD-14 and MD-38)**

The MDS samples MD-14 and MD-38 have similar zircon Hf isotope compositions (Fig 9.2.a. and b), although MD-38 has only a single Early Cretaceous zircon. The zircons from MD-14 show a wide range of unradiogenic Hf isotopic compositions, suggesting the interaction/mixing of isotopically different sources.

## 9.5. Hf Isotope Characteristics of Zircon Cores

**Mafic Dyke: (Sample no: MD-26)**

Only zircons from sample MD-26 contain Paleozoic inherited cores and show a range of initial $^{176}Hf/^{177}Hf$ compositions (Table 9.1.) with an average of 0.282681±0.000063 (2 SD, n=4). The εHf (t=376-306 Ma) values of cores show a range from 3.4±0.5 to 5.2±0.6 (2SE) (Fig 9.3).

**Low-Na Intermediate Dykes: (Sample No: MD-8 and MD-22A)**

MD-8 has some zircons with inherited cores where as MD-22A has abundant inherited cores. The zircon cores have average initial $^{176}Hf/^{177}Hf$ composition 0.282715±0.000032 (2SD, n=3) and the range presented in Table 9.1.The cores show a range of εHf (t=330-300 Ma) values from 3.9±0.4 to 5.6±0.6 (2SE) (Fig 9.3).

The initial $^{176}Hf/^{177}Hf$ compositions of zircons from MD-22A show a more restricted range of values (Table 9.1.) than MD-8 with a lower average of 0.282676±0.000031 (2SD, n=7). The εHf (t=362-313 Ma) values of cores show a wider range from 2.7±0.8 to 4.9±0.6 (2SE) (Fig 9.3).

**High-Na Intermediate Dyke: (Sample No: MD-32)**

Only zircons from sample MD-32 contain Paleozoic inherited cores. The Hf isotope composition shows limited dispersion of initial $^{176}Hf/^{177}Hf$ values (Table 9.1.) with an average of 0.282665±0.000035 (2 SD, n=5) and εHf (t=344-323 Ma) values ranges from 2.8±0.7 to 4.4±0.7 (2SE) (Fig 9.3).

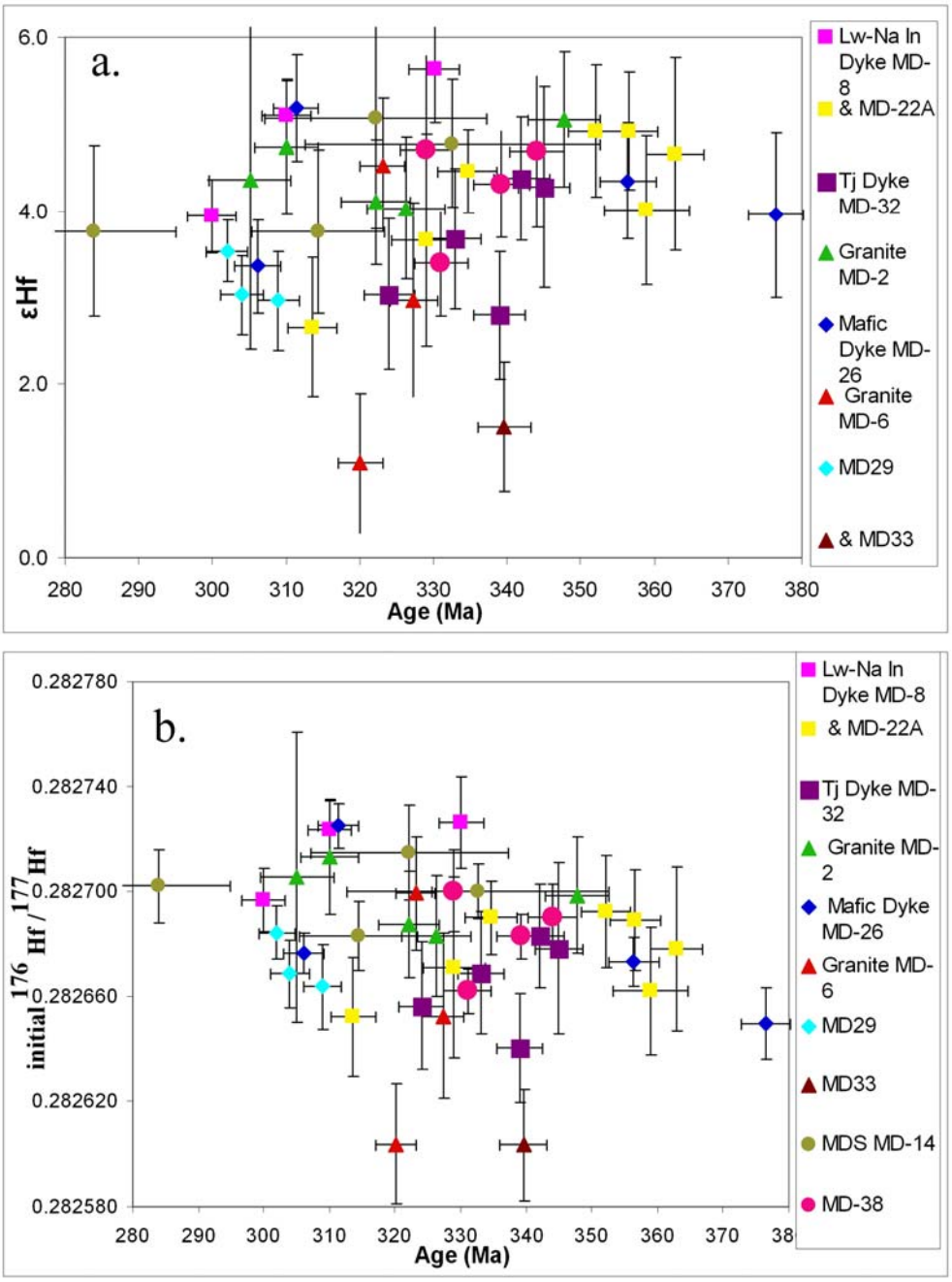


***Figure 9.3.*** *Hf isotopic composition variation of Paleozoic inherited cores with age.* ***(a)*** εHf *vs. age from Mt Daniel Complex rocks.* ***(b)*** *Initial Hf isotopic composition of inherited cores vs. age of Mt Daniel Complex rocks.*

**Granites: (Sample No: MD-2, MD-6, MD-29 and MD-33)**

Zircons from all granitic samples contain abundant Paleozoic inherited cores.

**MD-2:** The initial $^{176}Hf/^{177}Hf$ of inherited cores show a restricted compositional range of values (Table 9.1.) with average 0.282698±0.000025 (2SD, n=5) and restricted range of εHf (t=347-305 Ma) values from 4.0±0.8 to 5.1±0.7 (2SE) (Fig 9.3).

**MD-6:** Initial $^{176}Hf/^{177}Hf$ composition shows limited dispersion of values (Table 9.1.) with an average of 0.282652±0.000095 (2SD, n=3) and a wider ranges of εHf (t=329-320 Ma) values from 1.1±0.8 to 4.5±0.7 (2SE) (Fig 9.3).

**MD-29:** The initial $^{176}Hf/^{177}Hf$ composition shows a restricted range of initial $^{176}Hf/^{177}Hf$ values (Table 9.1.) with an average of 0.282672±0.000021 (2SD, n=3) and εHf (t=309-302 Ma) values ranges from 3.0±0.4 to 3.5±0.3 (2SE) (Fig 9.3).

**MD-33:** The initial $^{176}Hf/^{177}Hf$ compositions of the two cores are very similar 0.282601±0.000019 and 0.282603±0.00002 and εHf values of are -0.4±0.6 to 1.5±0.7 (2SE) (Fig 9.3).

**Mt Daniel Sheets: (MD-14 and MD-38)**

**MD-14:** The initial $^{176}Hf/^{177}Hf$ compositions show similar ranges of inherited cores (Table 9.1.) with an average of 0.282700±0.000026 (2SD, n=4) and the εHf (t=373-284 Ma) values of cores are from 3.8±0.9 to 5.1±1.2 (2SE) (Fig 9.3).

**MD-38:** Five Paleozoic inherited cores and one Cl-bright zircon without core and rim structure (see chapter-5) with the age of 152 Ma show a similar initial $^{176}Hf/^{177}Hf$ composition (Table 9.1.) with an average of 0.282682±0.000029 (2SD, n=6). The εHf (t=344-329 Ma) values of cores ranges from 3.4±0.6 to 4.7±1.0 (2SE) and 152 Ma zircon -0.02±0.5 (2SE) (Fig 9.3).

## 9.6. Difference in Isotopic Composition of Cores within intra and inter Rock Groups and the Probable Source of the Older Cores

The Paleozoic inherited cores have a very similar Hf isotopic compositional range within and between rock groups (Fig 9.4.a and b). All the inherited cores from different rock groups also have limited dispersion of initial $^{176}Hf/^{177}Hf$ composition from 0.282601±0.000019 to 0.282715±0.000032 (Fig 9.4.b.).

The similar isotopic signature of inherited cores (Fig 9.4.a and b) suggests their derivation from a similar source. The ARC present at the base of the MDC (see chapter-2) has a similar Paleozoic age range (Tulloch et al., 2003, 2010), so it could be a potential source of the inherited zircons. The field evidence also supports the assimilation of ARC within MDC (see chapter-2). The hypothesis on ARC by Hollis et al., (2003) can not be examined due to lack of any existing Hf isotopic data of zircons from those samples and thus the emplacement age of ARC during Cretaceous time can not be ruled out. In that case the ARC and MDC may have derived from similar source.

This study tested the source of inherited zircons whether they have come from Arthur River Complex (ARC) or derived from any other source. The Hf isotopic data of ARC zircons are provided by Tulloch et al., (2010) from Milford orthogenesis sample, which is gabbronorite to diorite in composition. These rocks contain more radiogenic varieties of zircons than MDC cores, but some 130 Ma cores from the Tulloch et al. (2010) study are very similar in composition to the inherited cores from Mt Daniel rocks (Fig 9.4.a and b). The William Granite is an Early Carboniferous plutonic body present in the out board Median Batholith of Fiordland (Scott et al., 2009).

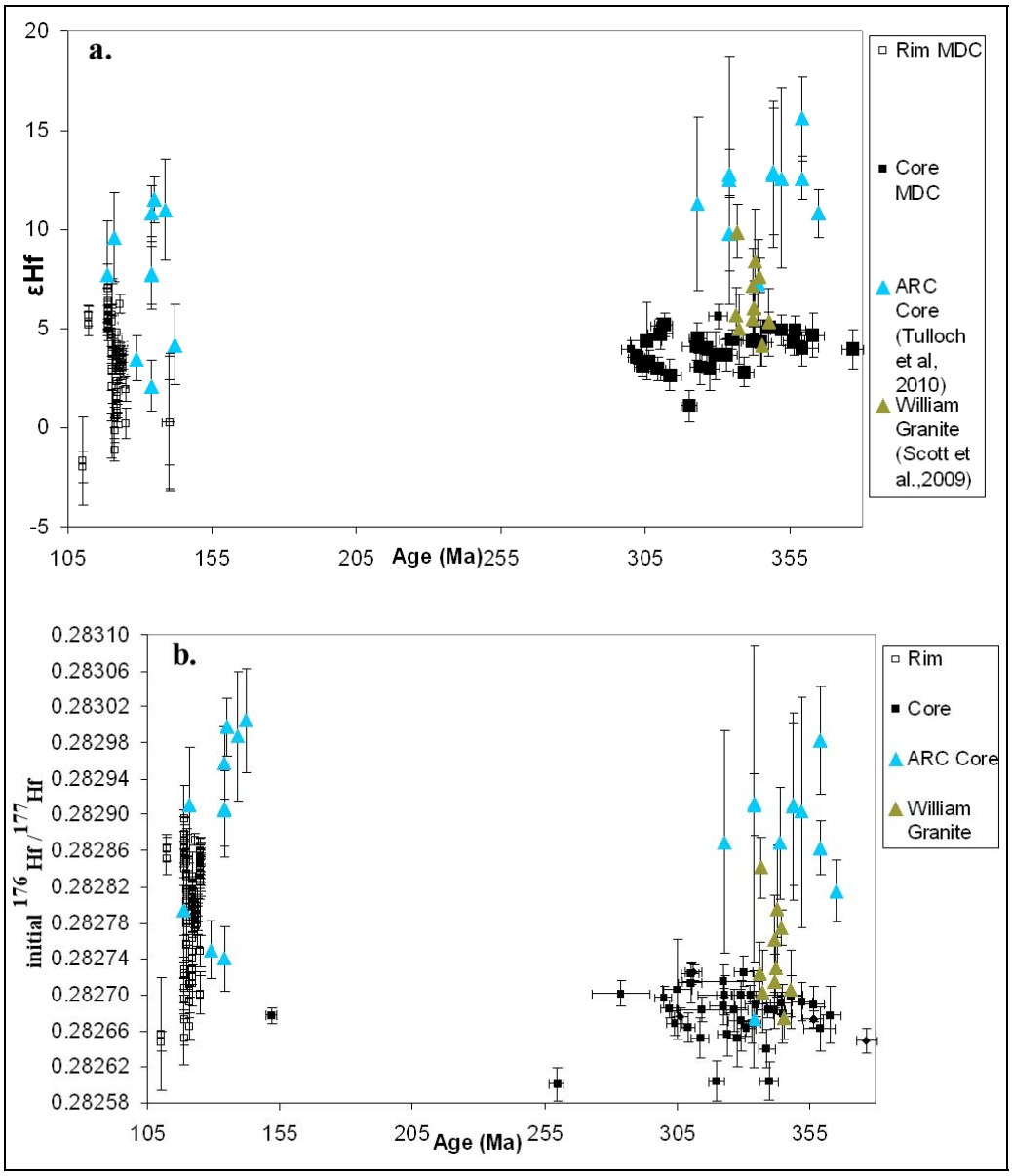


***Figure 9.4.*** *Hf isotope composition of zircons showing the isotopic distribution between two different age populations found in Mt Daniel, Fiordland. The zircon Hf isotopic composition of ARC rocks presented by Tulloch et al., (2010) and the William Granite from Scott et al., (2009) are compared with the Mt Daniel rocks. The open symbols represent the Early Cretaceous zircons and closed represent the inherited cores.*

So it can be suggested that a comparatively less radiogenic source than the ARC, more similar to some of the 130 Ma ARC cores, may also have been present at 330 Ma, as a potential source of the Paleozoic zircon cores at Mt Daniel. The similarities between the Hf isotopic composition of inherited cores of MDC and the less radiogenic variety of William Granite (346 Ma) suggest (Fig 9.4.a.) that the William Granite also can be a potential source of the inherited cores of MDC. The nature of the comparatively less radiogenic domains of ARC (330 Ma) which may have been present at the base of Mt Daniel Complex can not be constrained due to paucity of data.

## 9.7. Core–Rim Relationships of Different Samples from MDC Rock Groups

### Different Hf Isotopic Composition of the Core and Rim

The CL-bright zircons without inheritance from mafic dyke MD-26 and low-Na intermediate dyke MD-8 and the younger rims and single zircons without inheritance from high-Na intermediate dyke MD-32 have distinctly different initial $^{176}Hf/^{177}Hf$ compositions from their inherited cores (Fig 9.5. a to c). The cores have lower initial $^{176}Hf/^{177}Hf$ than the Early Cretaceous zircons and the reasons for these differences are discussed below.

### Reason of Variation

The differences in initial $^{176}Hf/^{177}Hf$ composition in core and rim of MD-26, MD-8 and MD-32 could suggest the derivation of the magma from isotopically distinct sources. The Early Cretaceous zircons without inheritance from these samples have more radiogenic Hf than the older cores, implying their derivation from relatively more juvenile sources. One interpretation could be that the Early Cretaceous zircons are derived from a more radiogenic mantle source.

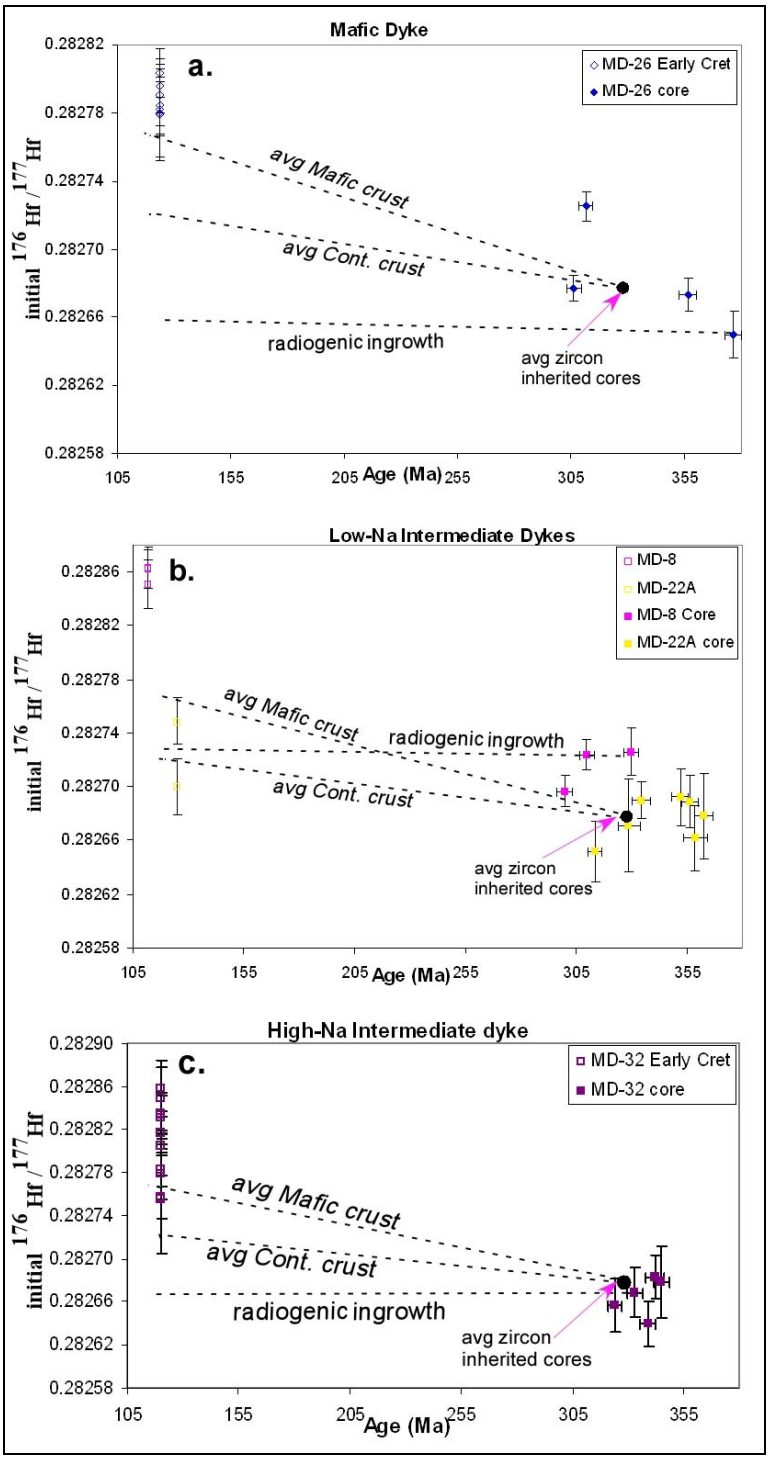


***Figure 9.5.*** *Hf isotopic variation of Early Cretaceous zircons and Paleozoic cores from different rock types of Mt Daniel, Fiordland and their evolution compared with average crustal growth curves.* ***(a)*** *Mafic dyke (MD-26),* ***(b)*** *Low-Na intermediate dykes (MD-8 & MD-22A),* ***(c)*** *High-Na intermediate dyke (MD-32).*

The trace element variations compared to the isotopic variations in zircons from different rock groups may help to understand the origin of the isotopic variations. Yb/Hf composition of the Early Cretaceous zircons from different rock groups mainly shows two types of variations (Fig 9.6.).

The Early Cretaceous zircons without inheritence from WFO, mafic dyke MD-13 and MD-26 and low-Na intermediate dyke MD-8 show a restricted range of Yb/Hf composition. MD-22B show a slightly variable Yb/Hf but this variation is insignificant. All these zircons are without inheritance. This may suggest that these magmas did not experience pronounced mixing of isotopically different magmas or crustal assimilation which is supported by the Hf data from Cretaceous zircon rims (Fig 9.2.a and b).

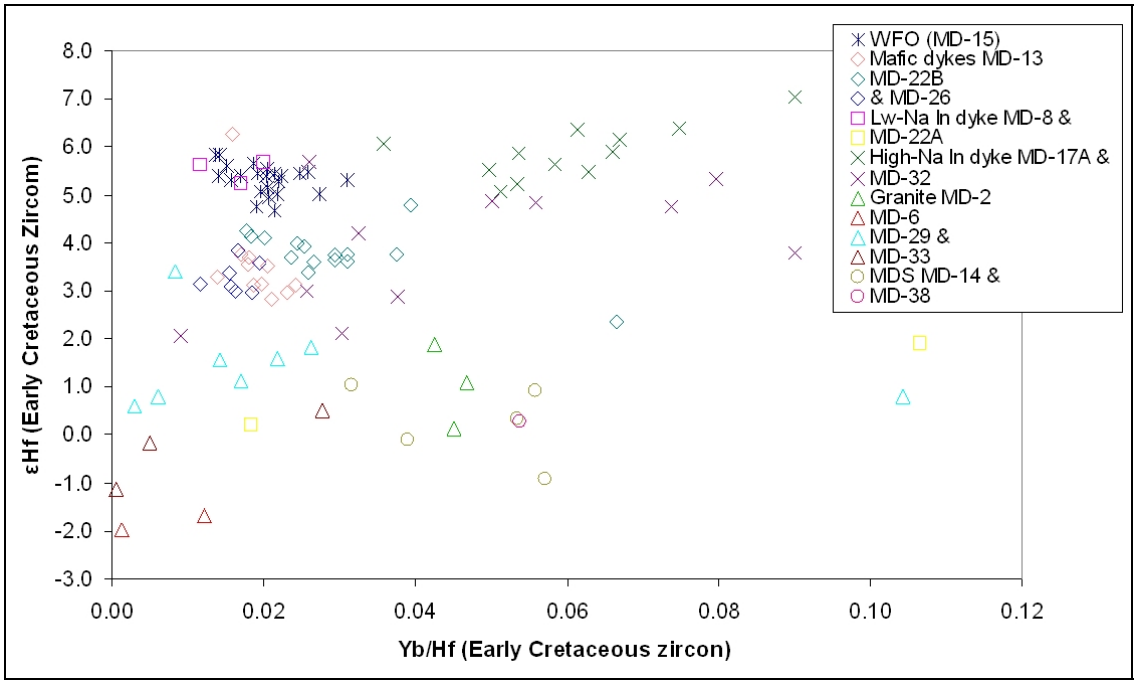


***Figure 9.6.*** *Yb/Hf vs. εHf composition of Early Cretaceous zircons from different rocks of Mt Daniel, Fiordland.*

Only magmatic zircons from MD-17A show a positive correlation between Yb/Hf and εHf indicating a systematic crystallisation of the zircons and also mixing of isotopically different magmas or crustal assimilation which cause the isotopic variability among the different grains.

The Yb/Hf data are quite scattered and do not follow any trend in the rest of samples, i.e. low-Na intermediate dyke MD-22A, high-Na intermediate dyke MD-32, granitic and MDS rocks. These rocks contain mainly zircon overgrowths and some zircons without inheritence. The scattered variation of Yb/Hf data may suggest that the zircons do not record any systematic crystallisation process and rather record an effect mixing of variable components and/or metamorphism.

**Similar Hf Isotopic Composition of the Core and Rim**

The single younger zircon rim and older inherited cores in MD-22A show a similar isotopic composition and the single zircon has slightly higher initial $^{176}Hf/^{177}Hf$ value but within the error range of the core composition (Fig 9.5.b.). Inspite of insufficient data it can be suggested that the rim and inherited cores may incorporate Hf from a similar source.

Granites and MDS samples show very similar initial $^{176}Hf/^{177}Hf$ compositions of older cores and younger rims (Fig 9.7. a and b) suggesting that they may have derived from common sources.

**Reason of Similarities**

The rims of intermediate dyke MD-22A, granites and MDS samples show similar isotopic compositions with the cores (Fig 9.5.b. and 9.7.). Based on this evidence, the rims could either be formed by the dissolution of cores during crustal melting in an open or closed system process, or by solid state recrystallisation of cores in a closed system. The cores and rims from the same zircons were calculated at the crystallisation age of the rims from these samples and only granitic dyke MD-6 show an identical isotopic composition of the core and rim (Fig 9.7.a.) indicating that the rims are formed in a closed system process either by solid state recrystallisation of the cores or by dissolution of the cores during crustal melting.

The morphologies of these zircons suggest variable dissolution of the cores and sometimes faint zoning of the rims indicating that at least some of the rims crystallized from a crustal melt.

However the formation of the rims by solid state recrystallisation also can not be ruled out as only a few analyses were done. The zircon rims from other samples do not have identical isotopic composition with cores but have a similar range of Hf isotopic composition to the cores. The cores are have limited dissolution structures. According to Flowerdew et al., (2006) the Hf isotopic heterogeneity in the melt can be induced from the isotopic heterogeneity of the cores during their partial dissolution. If the Hf budget of the melt is mainly controlled by the dissolved cores and if mixing and homogenization does not occur, then Hf isotopic heterogeneity will be present in the rims, which are forming from this melt in a closed system process. Other Hf rich minerals also can contribute Hf to the melt but their discrete Hf isotopic character can not be distinguished as they may have mixed with the whole range of initial $^{176}Hf/^{177}Hf$ composition of melts. The limited inferred dissolution structures in zircon cores and the wide range of initial $^{176}Hf/^{177}Hf$ composition of the rims suggest the formation of the rims in an open system process (Flowerdew et al., 2006). Zircons from the granite samples MD-29 and MD-33 have both HREE depleted and non-depleted rims (see chapter-8). The cores have limited dissolution structures and the average $^{176}Hf/^{177}Hf$ compositions of the rims are slightly more radiogenic than the cores (Fig 9.7.a.) suggesting either the mixing of melts from isotopically different domains from the same crustal source or contribution of Hf rich minerals into the melt in a closed system process.

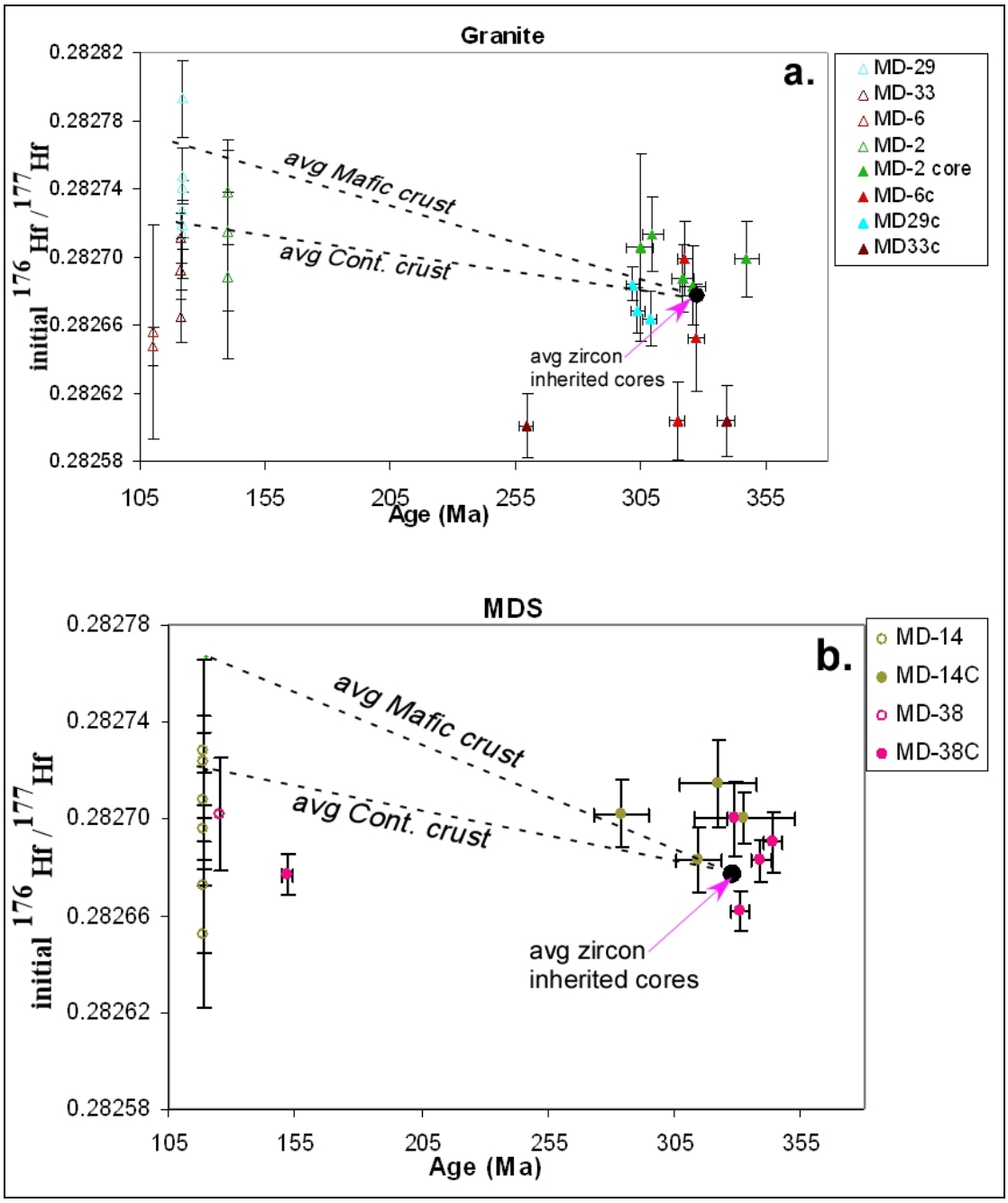


***Figure 9.7.*** *The Hf isotopic variation between Early Cretaceous rims of zircons and their Paleozoic cores from the different samples of Mt Daniel, Fiordland.* ***(a)*** *Granites* ***(b)*** *Mt Daniel Sheets (MDS).*

It can be suggested that the HREE non-depleted rims formed in an open system and HREE depleted rims formed during or after garnet growth in a closed system environment. This can be possible where zircon crystallization is continuous across the igneous to metamorphic realm (see chapter-8) or from the peak to retrograde metamorphism when contributions of the melts to the system become progressively reduced. In that case variation in Hf isotopic composition of the rims still can be induced by dissolving Hf rich minerals into the melt (Flowerdew et al., 2006) and thus the depleted rims can be comparatively more radiogenic than the cores.

Some HREE non-depleted zircon rims (e.g. MD-14) have similar initial $^{176}Hf/^{177}Hf$ isotopic range to cores with limited dissolution structures, but the rims have a wide range of compositional variation (Fig 9.7.b.). This may suggest an open system process involving the mixing of the melts derived from isotopically different domains from a crustal source.

## 9.8. Discussion

Irrespective of the local processes (zircon dissolution, recrystallisation etc) operating in the formation of the Mount Daniel zircons, the Hf isotopic variation of different rock groups suggest that melting of isotopically different crustal sources and a mildly enriched mantle source, mixing of these sources and/or crustal assimilation are predominant in the formation of the different rock types in the Mt Daniel area.

The magmatic zircons without inheritence (mafic dykes, MD-17A, MD-8) and some overgrowths (MD-8, MD-32) have higher $^{176}Hf/^{177}Hf$ than the metamorphic overgrowths (granite and MDS) of the same age. These more radiogenic values may have derived from a mafic crustal source(s). The Hf isotopic compositions of mafic dykes suggest the presence of mildly enriched mantle source(s). This study tested the probable crustal sources present at the base of the arc system in Fiordland (Fig 9.8.). The Hf isotopic composition of the Darran Suite and William Granite (Scott et al., 2009),

Separation Point Batholith (Bolhar et al., 2008), ARC (Tulloch et al., 2010) and MDC are used to derive the source components.

The Darran Suite has variable (εHf~5.8-13.7) Hf isotopic compositions of zircons (Fig 9.8.). The less radiogenic data from the Darran Suite and the 130 Ma ARC are similar to the most radiogenic MDC zircons (like those of MD-17A) (Fig 9.8.). The Hf isotopic compositions of both 130 Ma and 330 Ma ARC and Darran Suite zircons overlap with zircon Hf isotope data from the Separation Point Batholith (SPB) (Fig 9.8.), consistent with these rocks being the source of the SPB magma.

The partial melting of older continental crust like ARC and William Granite of Paleozoic ages is the source of granitic magmas of the MDC. The Hf isotopic values of Early Cretaceous zircons in MDC (except metamorphic overgrowths) are more radiogenic than the average mafic crust (Fig 9.5. and 9.7.).

So the input from more radiogenic source than average mafic crust to form these isotopic variations is required. This can be a more juvenile mafic crust present at the base of the arc system and consistent with the presence of ARC and Darran Suite during (~346-130 Ma) (Fig 9.8.).

They may be the main sources of more radiogenic magmas. The average initial Hf isotopic composition of all the inherited zircon cores in the MDC approximates the Hf isotope composition of crustal source at 330 Ma. From this initial composition, the isotope evolution of continental crust and mafic crust is plotted on Fig 9.5, 9.7 and 9.8.

The Hf isotopic evolution of the 330 Ma crust is calculated using average $^{176}Lu/^{177}Hf = 0.011$ *and* $0.023$ respectively. Most zircons from the Mt Daniel Complex have higher εHf values than either of the crustal reservoirs, thus indicating the contribution of a more juvenile source component.

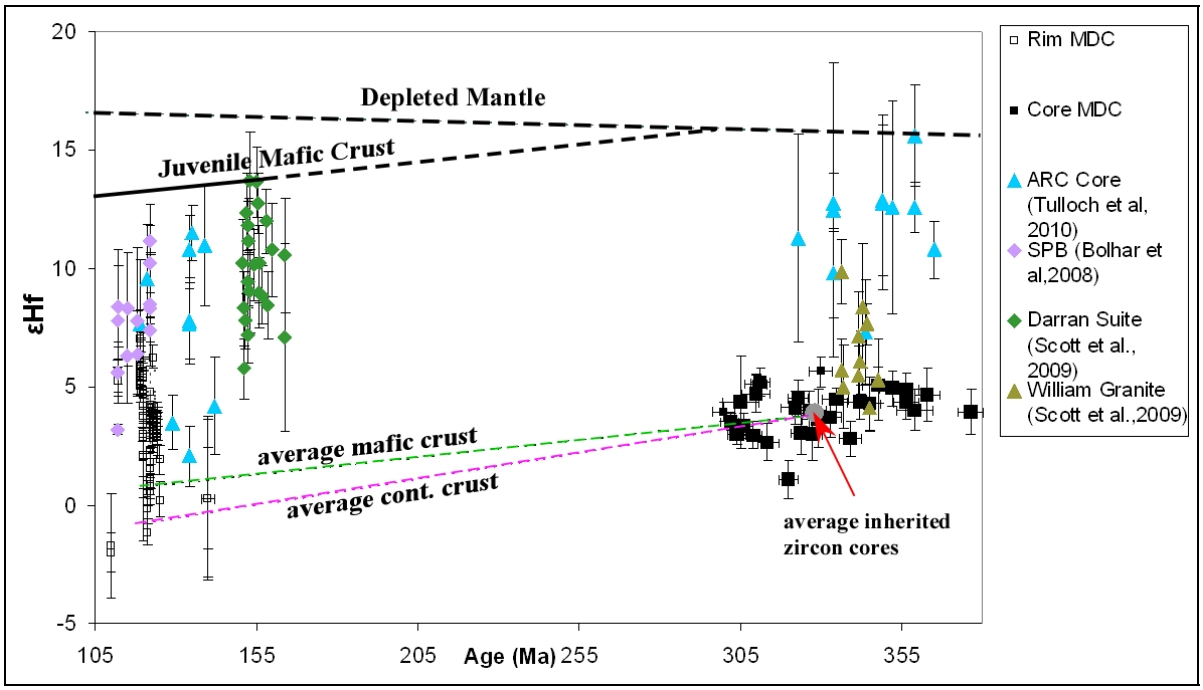


***Figure 9.8.*** *Hf isotopic compositions of MDC rocks, Separation Point Batholith (Bolhar et al., 2008), Arthur River Complex (Tulloch et al., 2010), Darren Suite and William Granite (Scott et al., 2009). The depleted mantle curve is calculated from data in Griffin et al., (2000). The average continental crust and mafic crust are calculated on the basis of* $^{176}Lu/^{177}Hf$ *= 0.011 and 0.023 respectively.*

So from the Hf isotopic data presence of three probable sources can be possible (Fig 9.8.), these being (1) a mildly enriched mantle source, as the whole rock chemistry of the mafic dykes also indicates towards a mantle source, (2) a juvenile mafic crustal source as represented by the Darran Suite and which is present at the base of the magmatic arc and (3) older continental crustal source(s) of Paleozoic age (ARC and William Granite).The later two sources are evident from various Hf isotopic data.

The mixing of melt increments from these isotopically variable sources is evident from the wide variations in Hf isotopic compositions of zircon overgrowths from different rock types (MD-32, MD-29, MD-33, and MD-14). So mixing along with crustal assimilation could be the key processes

in producing the isotope spectrum in rocks of the Mt Daniel Complex and will be address in the discussion chapter.

The isotopic evidence suggests a dynamic process include partial melting, magma mixing, crustal assimilation, metamorphism and episodic magma replenishment operating at the base of the crust at Mt Daniel. The different extent of mixing and mingling of different magmas like mafic and felsic magmas and reworking of older crustal material at depth are the underlying process of formation of the granitic plutons in Fiordland. This raises the possibility that such processes are important for the generation of the granitic batholiths around the circum Pacific belt (see discussion). The reworking of the comparatively juvenile crustal material of Paleozoic to Mesozoic age is an important process in the formation of high-Na granitic batholiths in Fiordland region (e.g. SPB).

| Rock Type | Sample No | Type of newly formed zircons | Cretaceous age at which εHf calculated | Range of initial $^{176}Hf/^{177}Hf$ of Early Cretaceous zircons/rims (2SE) | Average of Initial $^{176}Hf/^{177}Hf$ of Early Cretaceous zircons (2SD) | Range of εHf values of Early Cretaceous zircons (2SE) | Average εHf value of Early Cretaceous zircons (2SD) | Age range of inherited cores (Ma) | Range of initial $^{176}Hf/^{177}Hf$ of Palaeozoic cores (2SE) | Average of Initial $^{176}Hf/^{177}Hf$ of Palaeozoic cores (2SD) | Range of εHf values of Palaeozoic cores (2SE) |
|---|---|---|---|---|---|---|---|---|---|---|---|
| **WFO** | MD-15 | Magmatic | 125 | 0.282826±19 to 0.282860±15 | 0.282845±17 | 4.7±0.6 to 5.8±0.5 (n=) | 5.3±0.6 | Only 1 grain; 338 | - | - | - |
| **Mafic Dykes** | MD-13 | Cl-bright & Cl-dark zircons without inheritance | 123 | 0.282776±12 to 0.282802±15 & a single zircon has 0.282873±13 | 0.282797±53 | 2.8±0.4 to 3.7±0.5& a single zircon have 6.3±0.4 (n=) | 3.6±1.9 | Absent | - | - | - |
| | MD-22B | Cl-bright and Cl-dark grains without inheritance | 122 | 0.282763±12 to 0.282832±27 | 0.282803±30 | 2.3±0.6 to 4.8±0.9 (n=) | 3.6±0.9 | Absent | - | - | - |
| | MD-26 | Cl-bright grains without inheritance | 124 | 0.282779±27 to 0.282803±14 | 0.282788±18 | 3.0±0.9 to 3.8±0.5 (n=7) | 3.3±0.6 | Cores of Cl-dark grains; 376-306 | 0.282650±27 to 0.282725±17 | 0.282681±63 | 3.4±0.5 to 5.2±0.6 (n=4) |
| **Low-Na Intermediate Dykes** | MD-8 | Cl-bright grains without core and rims of Cl-dark grains | 112 | 0.282851±18 to 0.282863±15 | 0.282858±14 | 5.2±0.6 to 5.7±0.5 (n=3) | 5.5±0.5 | Cores of Cl-dark grains; 330-300 | 0.282697±12 to 0.282726±18 | 0.282715±32 | 3.9±0.4 to 5.6±0.6 (n=3) |
| | MD-22A | Rims | 125 | 0.282700±21 to 0.282749±17 | 0.282725±68 | 1.9±0.6 to 0.2±0.7 (n=2) | 1.1±2.4 | 362-313 | 0.282652±23 to 0.282692±18 | 0.282676±31 | 2.7±0.8 to 4.9±0.6 (n=7) |

| | | | | | | | | | | | |
|---|---|---|---|---|---|---|---|---|---|---|---|
| **High-Na Intermediate Dykes** | MD-17A | Magmatic | 116 | 0.282841±20 to 0.282897±35 | 0.282865±31 | 5.0±0.7 to 7.0±1.2 | 5.8±1.1 | Absent | - | - | - |
| | MD-32 | Rims | 120 | 0.282756±51 to 0.282858±26 | 0.282809±72 | 2.1±0.7 to 5.7±0.9 | 4.1±2.6 | 344-323 | 0.282640±21 to 0.282683±20 | 0.282665±35 | 2.8±0.7 to 4.4±0.7 |
| **Granite Dykes** | MD-2 | Rims | 140 | 0.282689±49 to 0.282738±31 | 0.282715±49 | 0.1±1.7 to 1.9±1.0 | 1.0±1.8 | 347-305 | 0.282683±23 to 0.282713±22 | 0.282698±25 | 4.0±0.8 to 5.1±0.7 |
| | MD-6 | Rims | 110 | 0.282648±11 to 0.282656±63 | 0.282652±11 | -1.7±2.2 to -2.0±0.4 | -1.8±0.4 | 329-320 | 0.282604±23 to 0.282699±22 | 0.282652±95 | 1.1±0.8 to 4.5±0.7 |
| **Granitic phase in MDC** | MD-29 | Rims | 122 | 0.282713±16 to 0.282793±17 | 0.282738±51 | 0.6±0.5 to 3.4±0.5 | 1.5±1.8 | 309-302 | 0.282664±16 to 0.282684±10 | 0.282672±21 | 3.0±0.4 to 3.5±0.3 |
| | MD-33 | Rims | 121 | 0.282665±16 to 0.282711±15 | 0.282690±46 | -1.1±0.5 and 0.5±0.5 | -0.6±1.4 | Single core with age of 339 and the other age is 259 Ma | 0.282603±21 and 0.282601±19 | - | 1.5±0.7 and -0.4±0.6 |
| **MDS** | MD-14 | Rims | 119 | 0.282652±30 to 0.282728±38 | 0.282697±59 | -1.6±1.0 and 1.1±0.6 | -0.05±2.1 | 332-284 | 0.282683±27 to 0.282715±36 | 0.282700±26 | 3.8±0.9 to 5.1±1.2 |
| | MD-38 | A single Rim | 125 | 0.282702±23 | - | - | 0.3±0.8 | 344-329 and single grain of 152 Ma | 0.282662±17 to 0.282700±31 | 0.282682±29 | 3.4±0.6 to 4.7±1.0 and for 152 Ma 0.02±0.5 |

***Table 9.1.*** *Hf Isotopic composition of zircons from different rock samples of Mt Daniel, Fiordland.*

# Chapter-10: Discussion

## 10.1. Introduction

This chapter discusses the key findings of this research regarding the evolution and interrelation of the different major source components of the Mt Daniel Complex (MDC) in Fiordland. In Chapter 1, it was established from previous work on P-T conditions that the MDC formed at the base of the crust, at 10-13 kbar. In subsequent chapters various analytical approaches like whole rock chemistry and zircon microanalysis were used in order to understand the probable different sources, their processes of formation and interrelationship. Here, the study will combine all the previous results to understand the generation of different source components, the underlying mechanisms of combining different sources in the lower crust to produce equivalent upper crustal plutons and their contributions in crustal growth processes in an arc system. The Mt Daniel Complex can be compared to the Separation Point Batholith, which is a higher crustal pluton formed during the same Early Cretaceous period, 124-112 Ma (Muir et al., 1995, 1998; Tulloch and Kimbrough 2003, Bolhar et al., 2008).

## 10.2. Key Findings of the Previous Chapters

### Chapter-1

The relation with the other plutonic system in New-Zealand and the Circum-Pacific batholithic systems in general indicate that the Mt Daniel Complex (MDC) belongs to the HiSY (high Sr, low Y after Tulloch and Kimbrough 2003) suite of magmatism at continental margins.

The different plutonic systems from the South Island of New-Zealand are the Separation Point Batholith (SPB), Arthur River Complex (ARC) and the Western Fiordland Orthogneiss (WFO). The SPB fits in a similar geochemical trend (major and trace) to the MDC, whereas the ARC concentrates at the mafic, low-Na end of the MDC spectrum. The WFO shows a different compositional trend on variation diagrams. The MDC also shows a very wide variation of composition compared to other plutons, with silica contents 43-76 wt%. Some trondhjemitic dykes and sheets in the MDC have exceptionally high contents of $Na_2O$, $Al_2O_3$, Zr and Sr.

### Chapter-2

The MDC is composed of numerous dykes and sheets of variable compositions. The field relations suggest syntectonic emplacement and ongoing deformation of dykes and sheets of the MDC. However, the emplacement of the dykes and sheets post-dates emplacement of the WFO and many of the rectilinear trondhjemitic dykes within it, so it can not be a contact aureole to the WFO, as suggested by others. The upper part of the MDC is more homogenous and of intermediate composition, whereas the lower part has a more bimodal character, giving the rocks a migmatitic appearance. However, most of this distinctly streaky to wispy appearance is due to synchronous emplacement of silicic and mafic magmas, followed by shearing under magmatic conditions, so that the mixing is mechanically enhanced by the ongoing deformation. Therefore, the Mt Daniel Complex records the time of magmatism associated with burial *after* solidification of the WFO.

## Chapter-3

This chapter mainly described the detailed analytical techniques used in this study. The techniques used in this study can be divided into two groups: whole-rock analyses and microanalytical study of different minerals. Whole-rock analyses include major and trace element analyses using XRF, whole-rock REE analyses using LA-ICPMS and Nd-Sr isotopic analyses using TIMS method.

Different microanalytical studies of zircons, garnets and rutile were carried out. Major element analyses of zircon and garnet using EPMA, REE and trace element analyses of zircon, garnet and rutile and U-Th-Pb age analyses of zircon using LA-ICPMS were done. Hf isotope analyses of zircons were carried out using Neptune multi collector LA-ICPMS.

## Chapter-4

Whole rock geochemical studies show the presence of six different rock groups at Mt Daniel, including the WFO. However, the WFO plots as a distinctive suite on Harker diagrams and is not part of the MDC.

The rock groups present in MDC are mafic dykes, high-Na intermediate dykes, low-Na intermediate dykes, granitic dykes and sheets and Mt Daniel sheets (MDS) of intermediate compositions. The whole rock major and trace element variation diagrams, evident in Harker diagrams, chondrite normalized REE patterns and N-MORB normalized multielement patterns, suggest that mixing processes could have produced the geochemical diversity, consistent with the field data. Sr-Nd isotopic data confirm that mixing is the major process in the formation of the MDC rather than fractionation.

High-Na intermediate magmas, mafic and granitic magmas are recognized as the three major magmatic source components of the MDC. Another source is the ARC, which appears to be locally assimilated near the base of the MDC. The fact that ARC compositions cluster at one of the mafic apex of the MDC strongly supports the suggestion that it was a source component in the MDC.

Strongly varying REE patterns in the trondhjemitic dykes also suggest varying amounts of residual garnet in the source region, possibly indicating that these dykes formed at varying depth, as observed from metamorphic studies of the complex (Daczko et al., 2001a, b). Mixing of the trondhjemitic magmas with mafic magmas can explain the formation of low-Na intermediate dykes. Mixing of those dykes with granitic dykes, combined with ARC assimilation, can explain the wide chemical and isotopic variations present within MDC.

## Chapter-5

Cathodoluminescence imaging of zircon mainly showed two different types of zircon morphologies: zircons without any evidence of inherited cores, and zircons with inherited cores and rims. The zircons without inheritence are of two types:

a) Zircons with elongated subhedral shapes and with planar banding, oscillatory zoning, and sector zoning inferred to be of igneous origin. They are mainly present in the WFO and in high-Na intermediate dykes (mainly in MD-17A). Sector zoning was mainly present in mafic dykes, and low-Na intermediate dykes.

b) Subrounded zircons with fir tree zoning.

Granites and MD sheets do not contain any zircons without inheritence.

Zircons with core-rim structures show cores having various structures such as magmatic zoning, patchy zoning, recrystallisation and dissolution structures. Rims have variable thickness (usually granites and MDS samples have very thin rims), are featureless and CL-bright and occasionally have magmatic zoning. Granites, MDS and one mafic dyke (MD-26), low-Na intermediate dykes and high-Na intermediate dyke (MD-32) have the majority of these types of zircons.

## Chapter 6

U-Pb age dating of zircons from different rock groups of MDC shows that the zircons without inherited cores and all zircon rims are of Early Cretaceous age from 124-112 Ma, and the inherited cores are of Palaeozoic age from 376-300 Ma. This study shows the emplacement age of the WFO is 125±2 Ma, which is in line with other studies (e.g., Hollis et al., 2004).

The age data, along with the field evidence, suggest that the MDC formed after the WFO. Nonetheless, the emplacement of the WFO, its burial, and MDC formation, all happened within a very short time span.

## Chapter-7

**Zircons:** Inter and intra group variation of trace elements in zircon suggests diverse origins of the rock types, even within same rock group. Most of the samples show a steady increase of Hf/Y ratio of zircon from core to rim except the WFO zircons, which show a restricted range and may have formed by closed system processes. The Hf concentration of zircon increases with whole rock $SiO_2$ content, which could reflect differentiation of magma, crustal contamination and/or mixing with an Hf-rich silicic end-member.

## Chapter-8

The trace element studies suggested that the Early Cretaceous zircons without inherited cores are consistent with a magmatic origin on the basis of the presence of planar banding and oscillatory zoning, high Th/U ratio, strongly positive Ce and negative Eu anomalies, higher concentration of HREE and high Ti in zircon temperature. The Paleozoic inherited cores show similar HREE enriched patterns with positive Ce and negative Eu anomalies and are probably derived from an igneous protolith, whereas featureless Early Cretaceous rims are mostly of metamorphic origin with some igneous overgrowths. The thin featureless rims are both depleted and non-depleted in nature

and both are in equilibrium with garnet. The depleted rims are mainly present in granitic rocks and probably crystallised from closed system process whereas non-depleted rims may have crystallised during open system processes (like mixing). Some temperature reversal observed in high-Na intermediate dyke (MD-17A) from centre to rim of the igneous zircons suggests intermittent input of hot mafic melts within the system. This is consistent with a mixing origin for some of these dykes, as suggested from wholerock geochemical and isotopic data (Chapter 3).

**Chapter-9**

The Hf isotopic study suggest that the mafic dykes were derived from a relatively non- depleted mantle source, that high-Na magmas were derived from mafic crustal sources, and that granitic magmas were derived from an older (Carboniferous) continental crustal source. A range of Hf isotopic compositions for these old zircons suggest derivation from a granitic source, like the adjacent Carboniferous William Granite, and from a less radiogenic domain of the ARC (cf., Tulloch et al., 2010). A mafic juvenile underplate possibly similar to the ARC and Darran Complex appears to have been the main source of high-Na magmas in the MDC and SPB.

## 10.3. How the Different Source Components were formed

**Mafic Dykes:** Whole rock geochemical data for the mafic dykes shows a low $SiO_2$ content 43-47 wt% with flat REE patterns but with LREE concentration near 10-times chondritic values (see chapter-3). The whole rock and Hf isotopic (Fig 10.1.a. and b.) data from zircons show a positive ε, mantle like signature with εNd +3 to +1 and εHf values 3.3.-3.6, consistent with derivation of these magmas from a relatively non-depleted mantle source. One of the mafic dykes (MD-26) has a much lower value of εNd (0.32) suggesting the possible involvement of a crustal component, which will be addressed in the next section. The REE patterns show no Eu anomalies and the high REE concentrations (Fig 10.2.a.) suggest that these magmas are derived from a source where both plagioclase and garnet were absent. The mafic magmas were probably produced in the spinel-lherzolite stability field of the upper mantle.

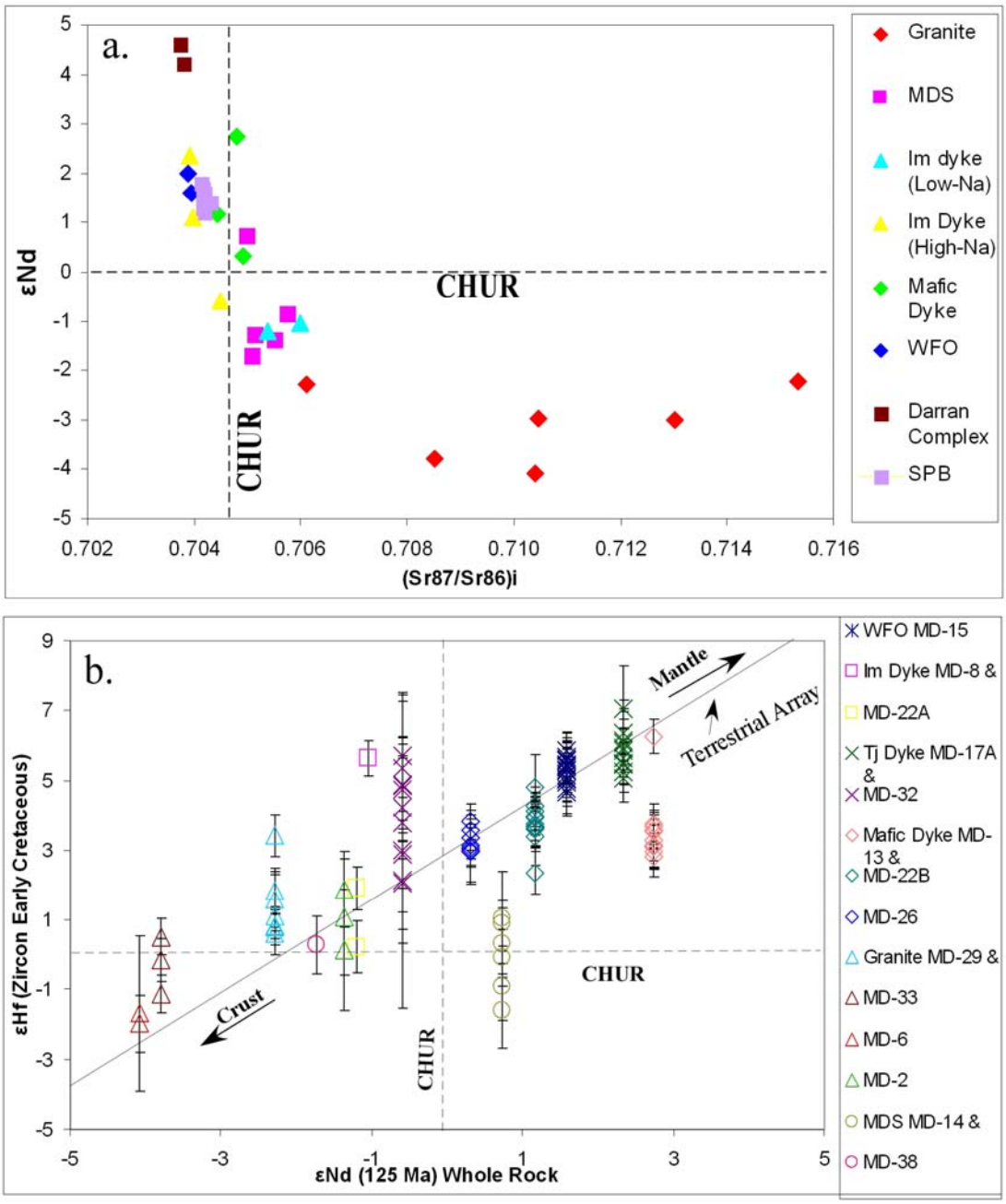


***Figure 10.1***. *Isotopic compositions of zircons from Mt Daniel, Fiordland.* ***(a)*** *Whole rock* εNd vs. $^{87}Sr/^{86}Sr_i$ plot of different rock types of Fiordland. The different types of rocks have been shown with different colours; ***(b)*** *Hf isotopic composition of zircons from Mt Daniel, Fiordland and Darran Complex from McCulloch et al., (1987) correlated with whole rock Nd isotope at the time of their crystallisation. Error bars represent 2 standard error.*

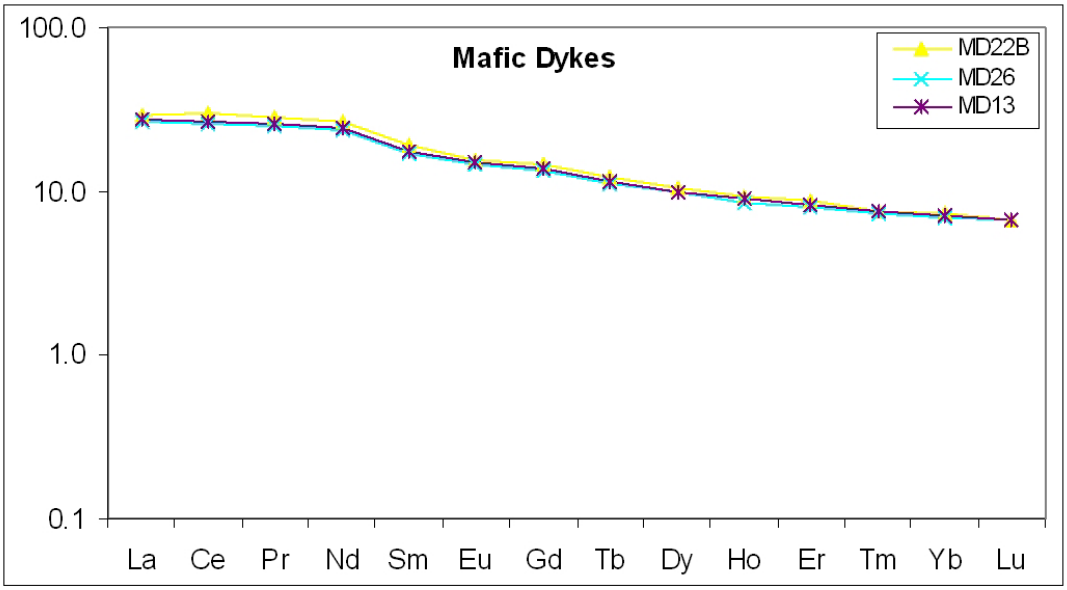


**a.**

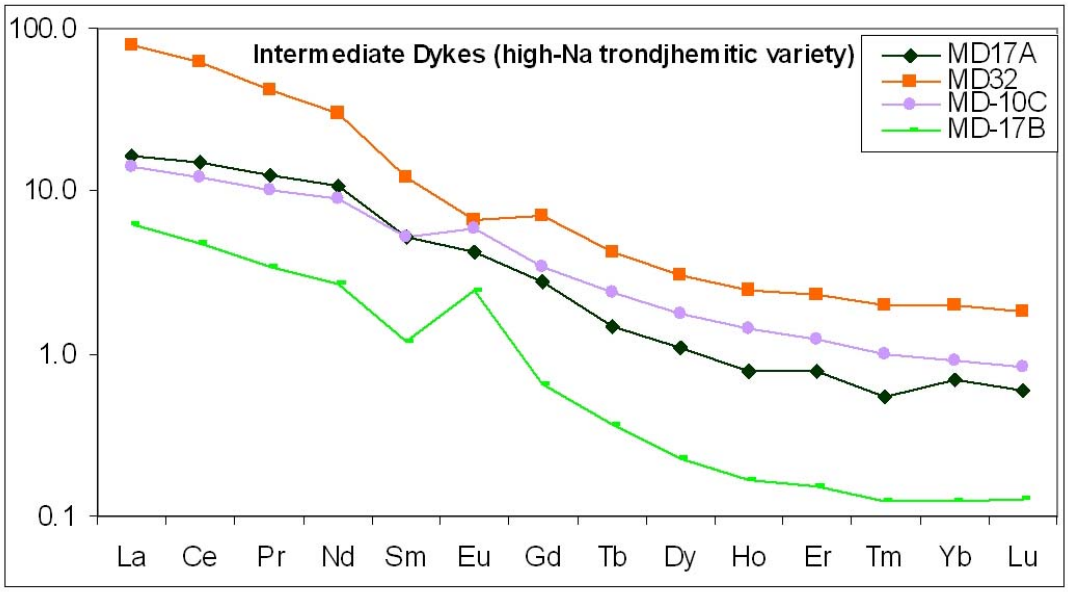


**b.**

***Figure 10.2***. ***(a)*** *REE patterns of mafic dykes from Mt Daniel Complex, Fiordland;* ***(b)*** *REE patterns of high-Na intermediate dykes from Mt Daniel Complex, Fiordland.*

**High-Na Intermediate Dykes:** The high-Na (trondhjemitic) dykes have silica content 56-60 wt% with high-$Na_2O$ (7-8.6 wt %), high $Al_2O_3$ (20.7-22.7 wt %), high-Sr (1771-2469ppm), very low Y (<0.5-12.4), high Zr (90-1000ppm) and extremely depleted HREE and no Eu anomalies (Fig 10.2.b.). The lack of Eu anomalies and extreme depletion of HREE suggests the plagioclase was absent and garnet and/or amphibole were present in the source rock residue. The presence of trondhjemite leucosome around peritectic garnet in the WFO and ARC (Fig 10.3.a.) suggest that they have formed by incongruent melting reaction(Clarke 2000, Daczko et al., 2001)-

Prg-Hb+OPX+Plag $\longrightarrow$ Grt+Cpx+Qtz+$H_2O$ (Daczko et al., 2001)

These leucosomes have mineralogy similar to the trondhjemite dykes, suggesting the sodic dykes have formed by similar processes. The leucosomes may reflect the initiation of trondhjemite dyke formation and strongly indicates the presence of garnet in the source rock residue. On the Sr/Y-Y plot (Fig 10.3.b.), the high-Na intermediate dykes and most WFO samples fall within the adakite field of ($Sr/Y \geq 40$) as defined by Defant and Drummond (1990).

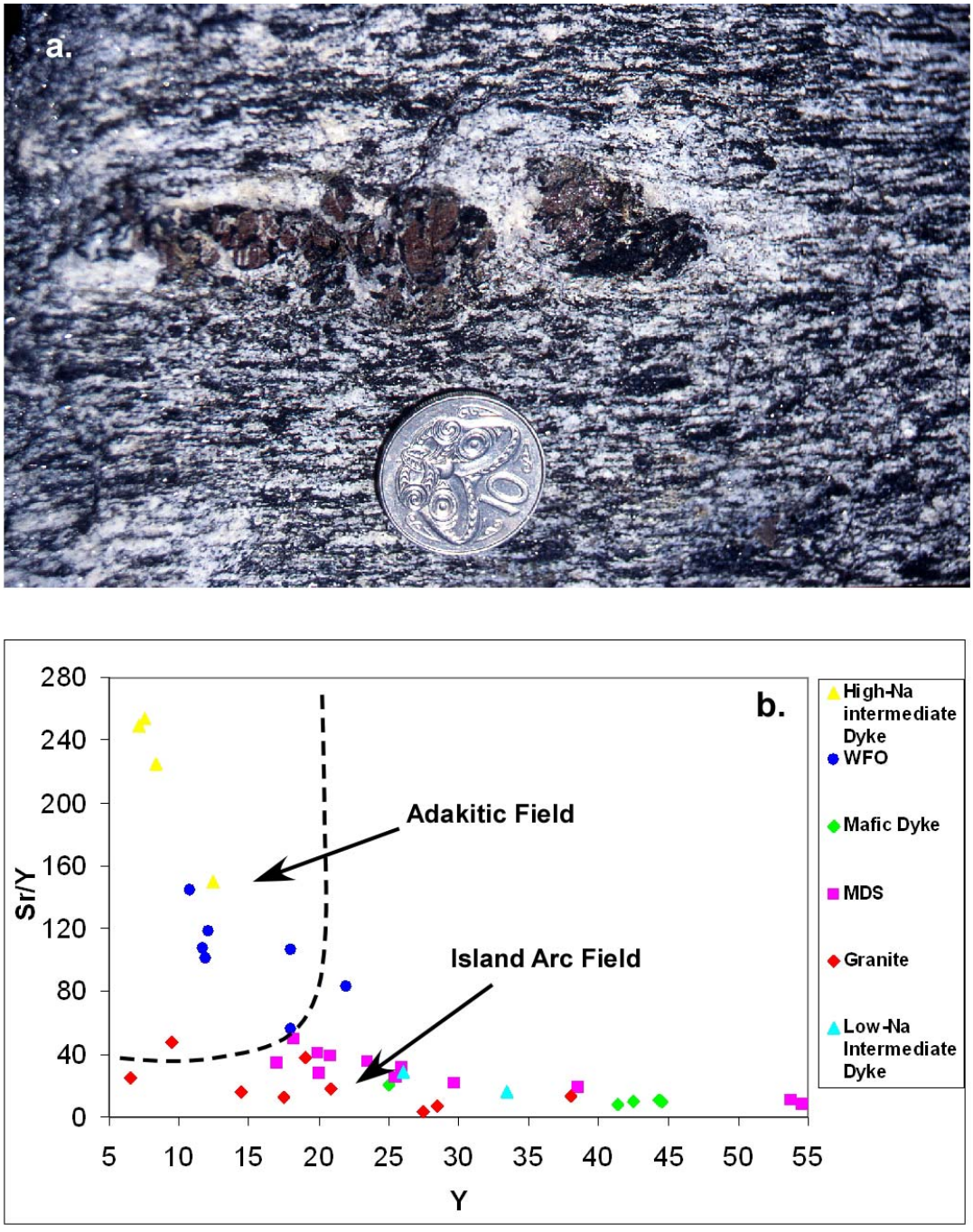


***Figure 10.3. (a)*** *Field photograph shows leucosome formation around peritectic garnet;* ***(b)*** *Sr-Y vs. Y plot shows that MDC rocks plot on the adakitic field and Island Arc field.*

The high-Na dykes have the higher Sr/Y content than WFO and all other MDC rock groups are below Sr/Y≤40, falling within the island arc field. So the whole rock geochemistry, along with field evidence, strongly suggests that the high-Na magmas have residual garnet in the source region and were derived from a higher crustal depth than 10 Kb. This depth was within the garnet stability field and beyond the plagioclase stability field. At crustal depths ≥10 Kb plagioclase is unstable and is dissolved into the melt, so the magma acquires a highly sodic nature with high Sr content. Several other studies (Muir et al, 1995, 1998, Tulloch and Kimbrough 2003, Bolhar et al., 2008) suggested that these high-Na magmas were derived from thickened mafic crust at the base of the arc system in Fiordland, which is consistent with this thesis.

The whole rock isotopic values and Hf isotopic values of zircons from the MDC (Fig 10.1.a and b.) show a mantle-like signature where εNd +2.34 and average εHf +5.8 to +4.1 to more evolved values of εNd +0.59 and individual εHf values of zircons varies up to +2.1. A comparative Hf isotopic study of zircons from major plutons of Fiordland shows that the isotopic signature of high-Na magmas of MDC and SPB are very similar to isotopic composition of the ARC and Darren complex (Fig 10.4.).

This study suggests the presence of a juvenile mafic crustal source at the base of the crust, similar to the most radiogenic isotopic compositions of Carboniferous cores found in the ARC by Tulloch et al (2010) or the Jurassic Darran Suite (Scott et al., 2009). So the partial melting of the juvenile mafic crust at depth ≥10 Kb is probably the main source of the high-Na (trondhjemitic) magmas in Fiordland.

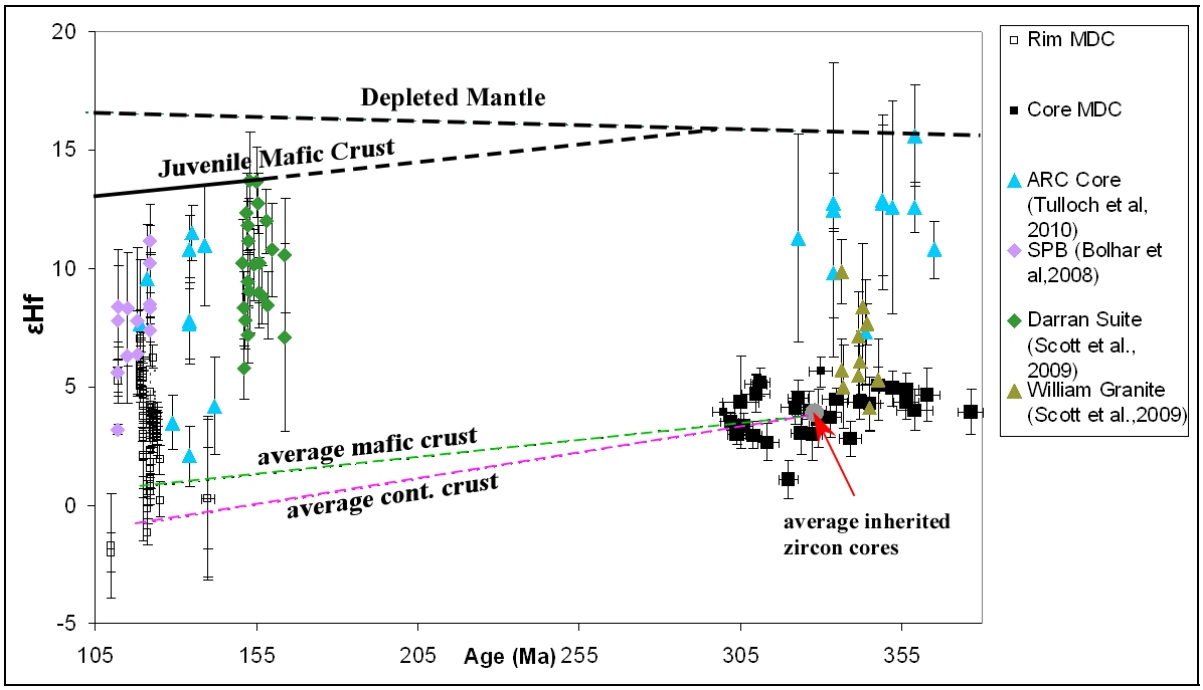


***Figure 10.4.*** *Hf isotopic compositions of MDC rocks, Separation Point Batholith (Bolhar et al., 2008), Arthur River Complex (Tulloch et al., 2010), Darren Suite and William Granite (Scott et al., 2009). The Depleted mantle value calculated from Griffin et al., 2000. The average continental crust and mafic crust calculated on the basis of* $^{176}Lu/^{177}Hf = 0.11$ *and0.023 respectively.*

**Granites:** The striking similarities of Hf isotopic composition between Early Cretaceous rims and inherited zircon cores within the granites, suggest that the rims have formed by dissolving the cores (see chapter-9). The Paleozoic inherited cores have a similar isotopic composition to the William Granite of Fiordland (Scott et al., 2009), which has a similar Carboniferous age (346Ma). This relation suggests that similar Carboniferous granite was the protolith of the granitic magma (Fig 10.4.).

The granites have high silica content 66-76 wt% with high $K_2O$ (1.6-5.0 wt %), but very low Rb (37-86 ppm) content. The strikingly low Rb content, compared to other granitic batholiths (Fig 10.5.), shows that the granitic rocks of the MDC are an unusual variety.

The Lachlan granites show an increase Rb with the increase in $K_2O$ content. The samples with $K_2O>3.0$ wt % have higher Rb content where as samples with $K_2O<3.0$ wt % have low Rb content. The curved trend for Lachlan granites can be explained by feldspar fractionation where the samples with low-Rb content and higher-Sr values were produced by early plagioclase fractionation and as the differentiation proceeded, orthoclase became a liquidus phase thereby depleting the magma of Ba. As a result, the more incompatible Rb increased in the residual melt.
In contrast to the Lachlan granites, the MDC granites do not follow this fractionation trend with all MDC samples falling on the Sr-Ba baseline. The high-Na magmas concentrate at the Sr end and the high-K granitic magmas at the Ba end.

As Rb is intriguingly low in MDC granite, it is suggested that biotite was present in the source rock residue, so that Rb partitioned into biotite and derivative granitic melts had low Rb content. If correct, the presence of biotite in the source region suggests fluid-present melting of the source rock or at least meting under high water activity.

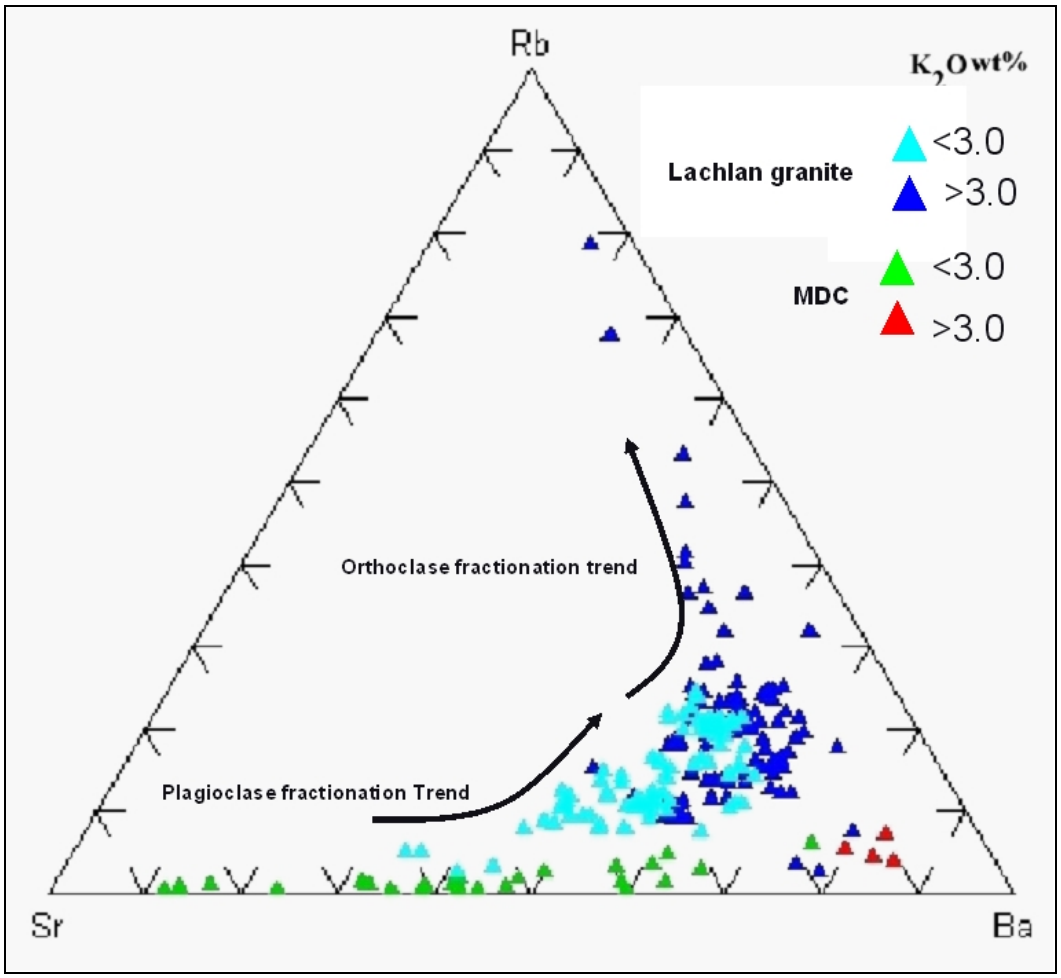


***Figure 10.5.*** *Rb-Sr-Ba plot shows difference between the Rb concentrations of MDC rocks and Lachlan granite. The curve line indicate plagioclase-orthoclase fractionation trend.*

As discussed earlier, the MDC is a lower crustal section that formed between 10-13 Kbar (Klepeis et al., 2004). An important question is whether high K granitic magmas can be produced at these pressures. Usually, high K magmas are associated with melting, or at least crystal-melt equilibrium, a upper crustal levels (<5 Kbar) (Johannes and Holtz,, 1996, page 173-176). This thesis has examined whether wet melting of granite at such higher pressure condition can produce high K granites with residual biotite in the source region.

The experimental work by Conrad et al, (1988) shows that high-K granitic magmas can be produced at 10Kb pressure by melting of dacite at varying $xH_2O$ content. On a Q-Ab-Or diagram (Fig 10.6.), the MDC data overlap with the experimental dataset from Conrad et al., (1988) and occupy the same quadrilateral field. The experimental data show that melts are generally more sodic when water-rich ($xH_2O$ >0.5), and K-rich melts form when $xH_2O$~0.25 at temperatures at ≥800 $^0$C, which is above the biotite breakdown reaction. This presents a dilemma, because this thesis suggests that biotite was a residual product of the melting reaction.

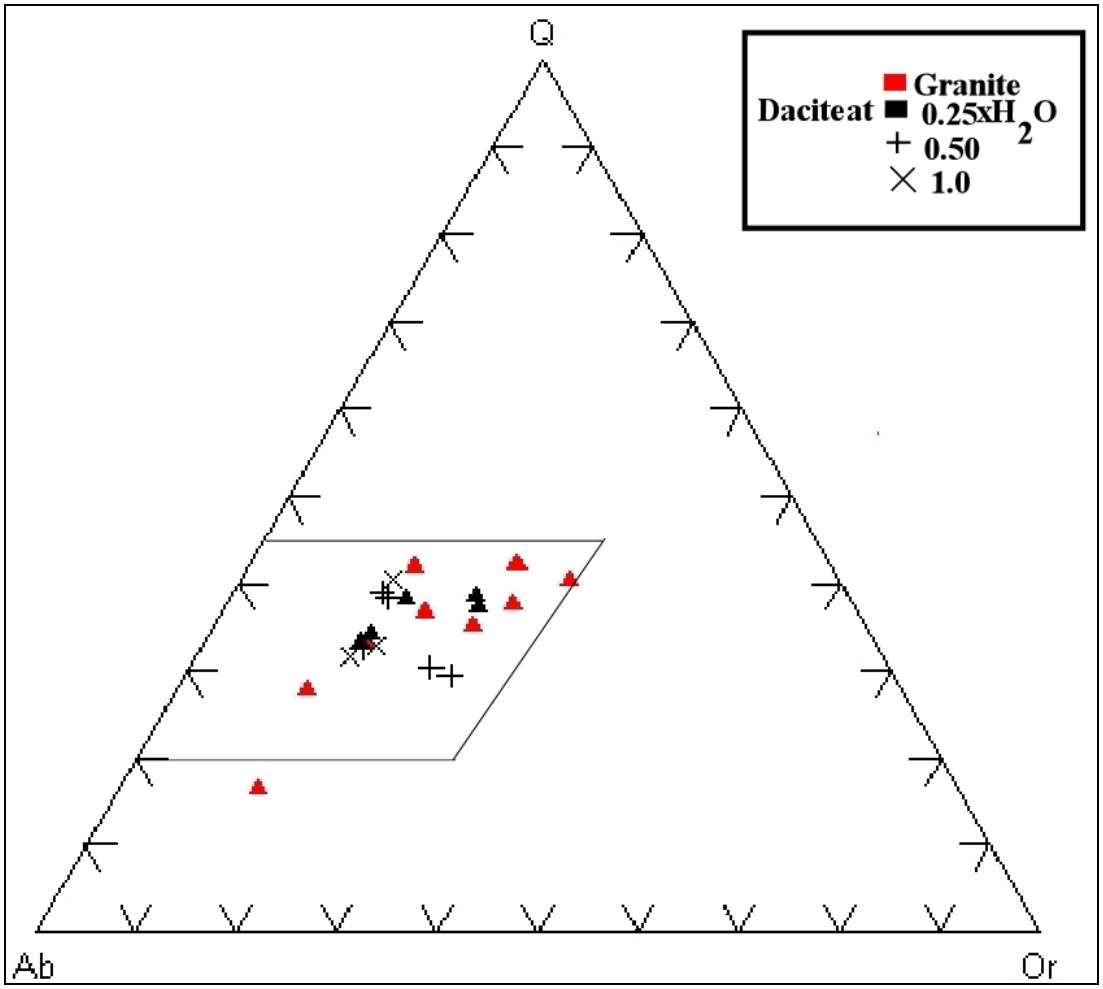


***Figure 10.6.*** *Q-Ab-Or diagram showing experimental dacite field at 10 Kb with different $xH_2O$ from Conrad et al., 1988 and the granites from Mt Daniel Complex plots on the similar quadrilateral field.*

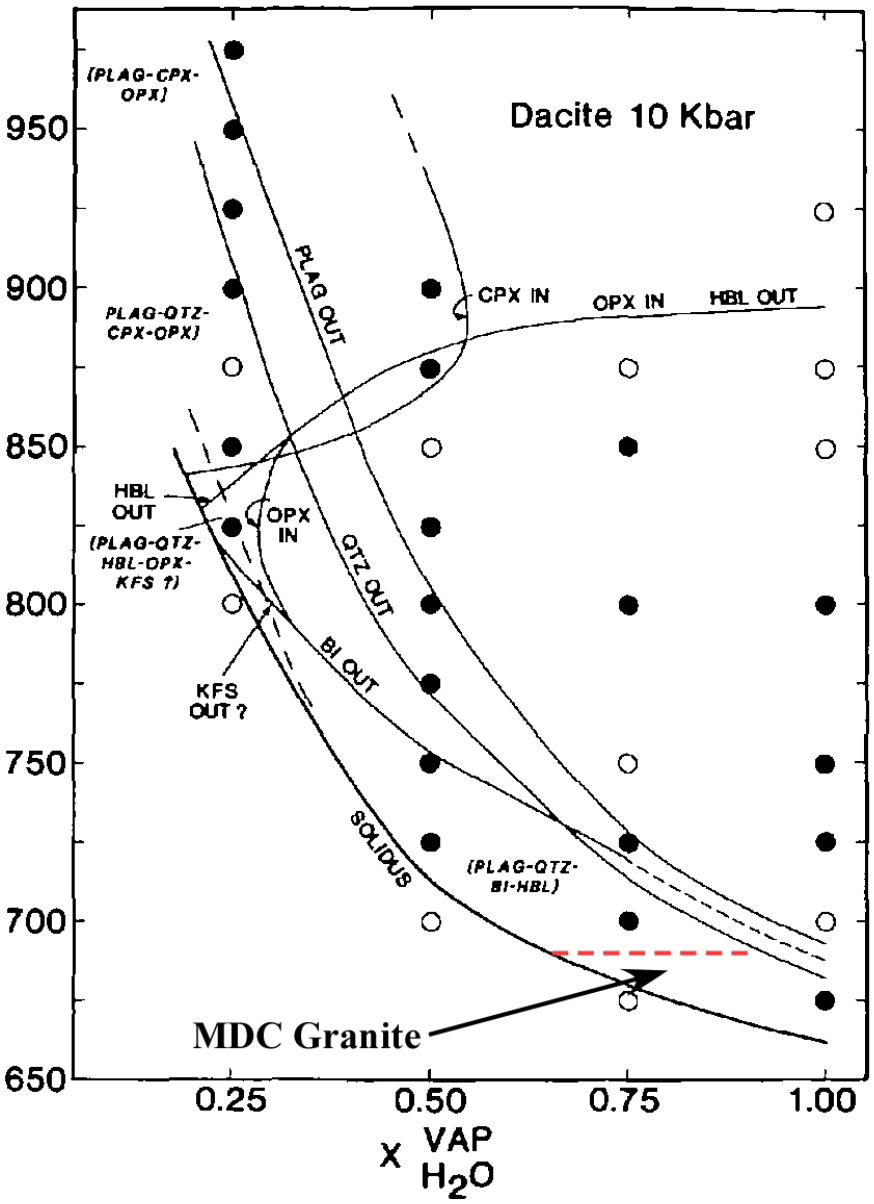


***Figure 10.7.*** *Phase diagram show biotite stability fields of Dacite at 10 Kb pressure with variable $xH_2O$ from Conrad et al., 1988. The granites from MDC occupy the field on the phase diagram is shown by arrow below the dashed red line.*

An independent estimate of the melting temperature for granitic rocks of the MDC was derived from Ti in zircon thermometry, which varied between 650-683$^0$C. This is lower than the inferred temperatures of melting of dacite at $xH_2O$~0.25 (Conrad et al., 1988), but is within the P-T range (at 10Kbar) where biotite is stable (Fig 10.7). Under these P-T conditions $xH_2O$ is >0.5.

A suggestion to resolve this problem is provided. This study previously suggested that the source of the granitic magmas was a protolith similar to the William Granite of eastern Fiordland (Scott et al., 2009), based on Hf isotope data. This is one of several Carboniferous plutonic remnants that exist in the Darran Complex (Allibone et al, 2009). The classification of the granite can only be speculated on. It is likely to have a higher $K_2O$ content compared to the experimental dacite of Conrad et al (1988), which has a $K_2O$ content of 1.7wt% at 65wt % $SiO_2$. The $K_2O$ content of ARC rocks at 65wt% $SiO_2$ is within 2.5-3.5 wt% (Hollis et al, 2003, fig. 8d). If this is representative of the Carboniferous protoliths in the ARC, the much higher $K_2O$ content suggests that higher amounts of $K_2O$ would have been released into the MDC granitic melts at lower degrees of partial melting, following Le Chatelier's principle. Therefore, we suggest that under the P-T conditions of MDC melting, (T = 650-683$^0$C and P = ~10 Kbar), a higher amount of $K_2O$ was released into the magma, even though biotite was a stable residual phase.

**Low-Na Intermediate Dykes and Mt Daniel Sheets:** The intermediate silica content (53 to 60 wt %) with moderate concentrations of other major element ($Na_2O$, $K_2O$, $Al_2O_3$, CaO etc) and related trace elements, similarities of REE patterns of the low-Na intermediate dykes with the mafic dykes and MDS with granites (see chapter-3) and whole rock isotope and Hf isotopic data of zircons (Fig 10.1.) suggest a mixed origin of these rock groups. The details of formation of these rock groups will be discussed in the next section.

## 10.4. How the Different Source Components Combined to form the Mt Daniel Complex

The dominant component of the MDC is meta-igneous, with the exception of the assimilated ARC, and each rock has intrusive relationships as they emanate as dykes from the ARC basement (see field evidence in chapter-2). These magmatic units consist of banded schlieric to wispy medium grained granitic, intermediate, mafic sheets and low angle dykes, many of which are tightly to isoclinally folded. The dykes were folded under magmatic conditions.

Assimilation of ARC with the dykes is well developed in the lower part of the MDC and occurred during emplacement and solidification of the magmas. The remnants of mafic dykes within MDC were stretched into lenses and wisps prior to folding, suggesting mechanical stirring and mixing of different magmas. Ghost layering of the ARC is also folded, indicating that assimilation occurred before folding. The lower part of the MDC is bimodal, where discrete magma batches can be identified, whereas the upper part of the MDC is more homogenised, suggesting more thorough mixing of the magmas. This does not mean to say that ARC assimilation did not occur in the upper part; just that it is more homogenised, so the field evidence is lost.

The rectilinear arrangement of the high-Na intermediate dykes (i.e. trondhjemite dykes) within the WFO suggests it was solidified before dyke emplacement. However, they are much less abundant in the MDC, which suggests MDC emplacement began after the rectilinear dykes formed. Nonetheless, the trondhjemitic dykes are folded to varying degrees (Chapter 2), indicating that they were still intruding during MDC formation. The field relations show that the MDC formed after solidification of the WFO and after it was intruded by the rectilinear trondhjemitic dykes and veins.

The geochemical and isotopic evidence show three possibilities of forming MDC: (**1)** Mixing of three major source components and (**2)** Crustal assimilation of ARC like mafic crust along with variable mixing of atleast two major components, high-Na magma and granitic magma, or **(3)** a combination of both.

**Possibility -1:**

The geochemical and isotopic evidence show that the MDC formed by the combination of different components derived from isotopically distinct sources. The potential major source components are – mantle-derived basaltic dykes, high-Na melts derived by partial melting of mafic juvenile crust, high-K granitic magmas derived by wet melting of older continental crust, and assimilation of the ARC (see section 10.2.).

The mixing of these contrasting magmas from different sources is major phenomena in producing most of the variety of Mt Daniel sheets. The wholerock major and trace element (Chapter-3) and isotopic evidence (Fig 10.1.a.) shows that the low-Na intermediate dykes and MDS rocks bear a mixed signature that can be explained by mutual injection and mixing of basalt, high-K granitic dykes and trondhjemitic dykes. The REE patterns of low-Na intermediate dykes are more similar to basaltic dykes, but the MDS shows chemical trends more similar to the granite dykes (Fig 10.8.). On Harker diagrams, all the intermediate dykes and sheets of MDC occupy the field in-between these three major source components.

Furthermore, the whole rock and zircon isotopic study emphasized mixing of these dykes as a dominant process of MDC formation. The curved isotopic array between primitive (basaltic and trondhjemite dykes) and crustal (high-K granitic dykes) end members on the εNd vs. $^{87}Sr/^{86}Sr_i$ plot (Fig 10.1.a.) also suggest a combination of mixing among at least two of these three source components. The granitic sheets are also a mixed variety. The MDS samples closely overlap with the low-Na dykes on the isotope array (Fig.10.1.a), consistent with a cogenetic mixing relationship.

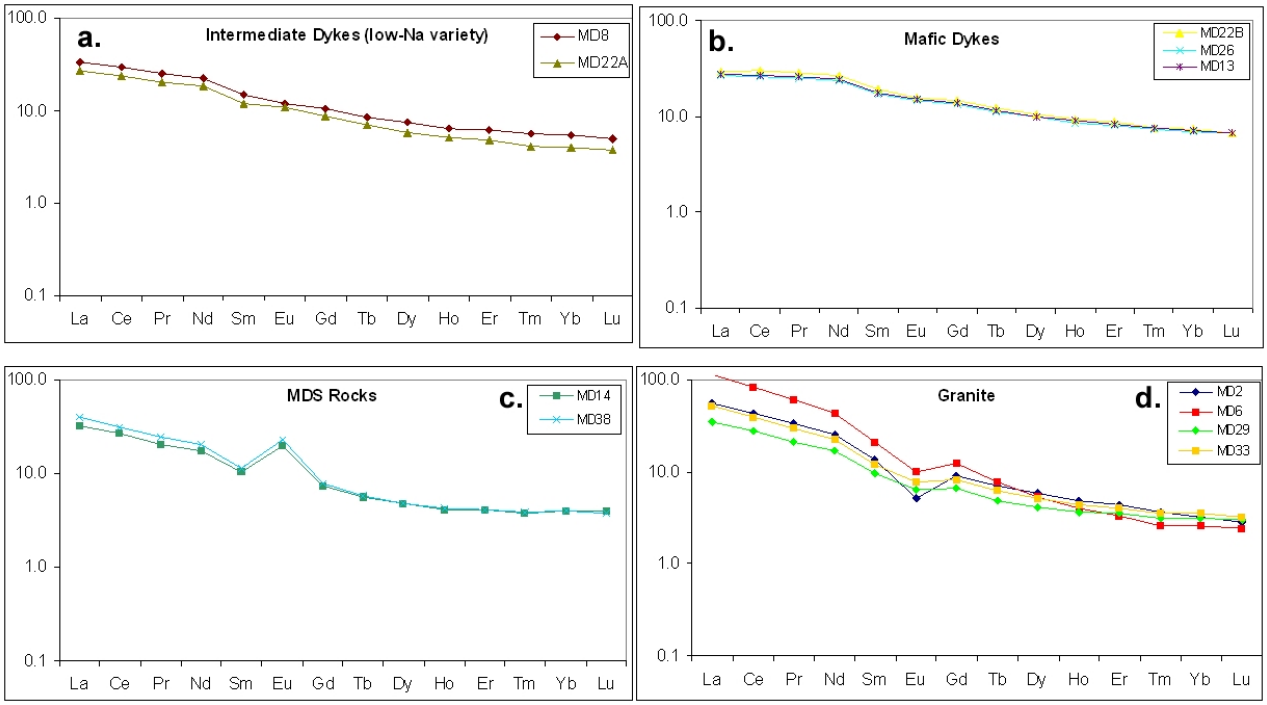


***Figure10.8.*** *Wholerock Rare Earth Element patterns shows the similarities between mafic, low-Na intermediate dykes and MDS and granites from MDC, Fiordland normalized to primitive mantle (Sun and McDonough 1989).* ***(a)*** *Intermediate Dykes (low-Na variety) and* ***(b)*** *Mafic Dykes;* ***(c)*** *MDS and* ***(d)*** *Granitic dykes (MD-2 and MD-6) and granitic sheets (MD-29 and MD-33) in MDC.*

The Hf isotope study of zircons shows a pronounced effect of mixing of each of the melt sources. A similar mixing trend among high-Na magmas, basaltic magmas and granitic magmas is observed in εHf-εNd plot (Fig 10.1.b.). The wide variation of Hf compositions of Early Cretaceous zircons from different samples (Fig 10.9.) suggest the mixing was pronounced even within each melt increment, and therefore that most of the MDC formed by an open system process.

In summary, mixing of mafic to intermediate magmas with the high-K granitic magmas can produce the large chemical variation in the MDC rocks, at least the $SiO_2$~ 60-76 wt % part. Combined with the more mafic melt increments (43-50 wt% $SiO_2$), the compositional variation for this small 100-metre thick complex, formed by mixing of dyke-fed magmas, some of which already hybridised, is more than that observed in large upper-crustal batholiths (see chapter-1).

**Possibility -2:**

Field evidence suggests that assimilation of ARC also occurred in formation of the MDC magmas. Given that the ARC clusters close to the mafic apex of MDC compositions, the geochemical and isotopic trends of the MDC can be explained by crustal assimilation during injection of the various dyke systems. In addition to the field evidence, the presence of a large amount of inherited cores within all the MDC magmatic components (including mafic intermediate and granitic dykes) strongly suggest crustal contamination was involved in the genesis and/or emplacement of the MDC.

Limited wholerock isotopic data exist to further test this possibility. The Darran Complex and ARC are found to be similar in terms of whole rock chemistry, age (Blattner 1991, Hollis et al., 2003) and Hf isotopic composition (Fig 10.4.). The whole rock isotopic data from two leucogabbros of the Darran Complex (Fig 10.1.a.) and the measured Hf isotopic composition of ARC components (Fig 10.4.) indicate that the more primitive members of the MDC could be derived from the ARC basement. Indeed, besides a mantle component, it is difficult to envisage any other source than heterogeneous ARC basement.

Intra-group variation of each of the source components is commonly observed. For example, the mafic dykes show a variation in isotopic signature from less evolved εNd (+3.0) to more evolved εNd (0.32) (MD-26) origin (Fig 10.1.a.), but the Hf isotopic signature is not variable among these dykes (Fig 10.1.b. and 10.9.). The presence of inherited cores of zircons only within mafic dyke MD-26 (see chapter-5 and 9) suggests that the magma may have picked up wall rock xenocrysts during its ascent.

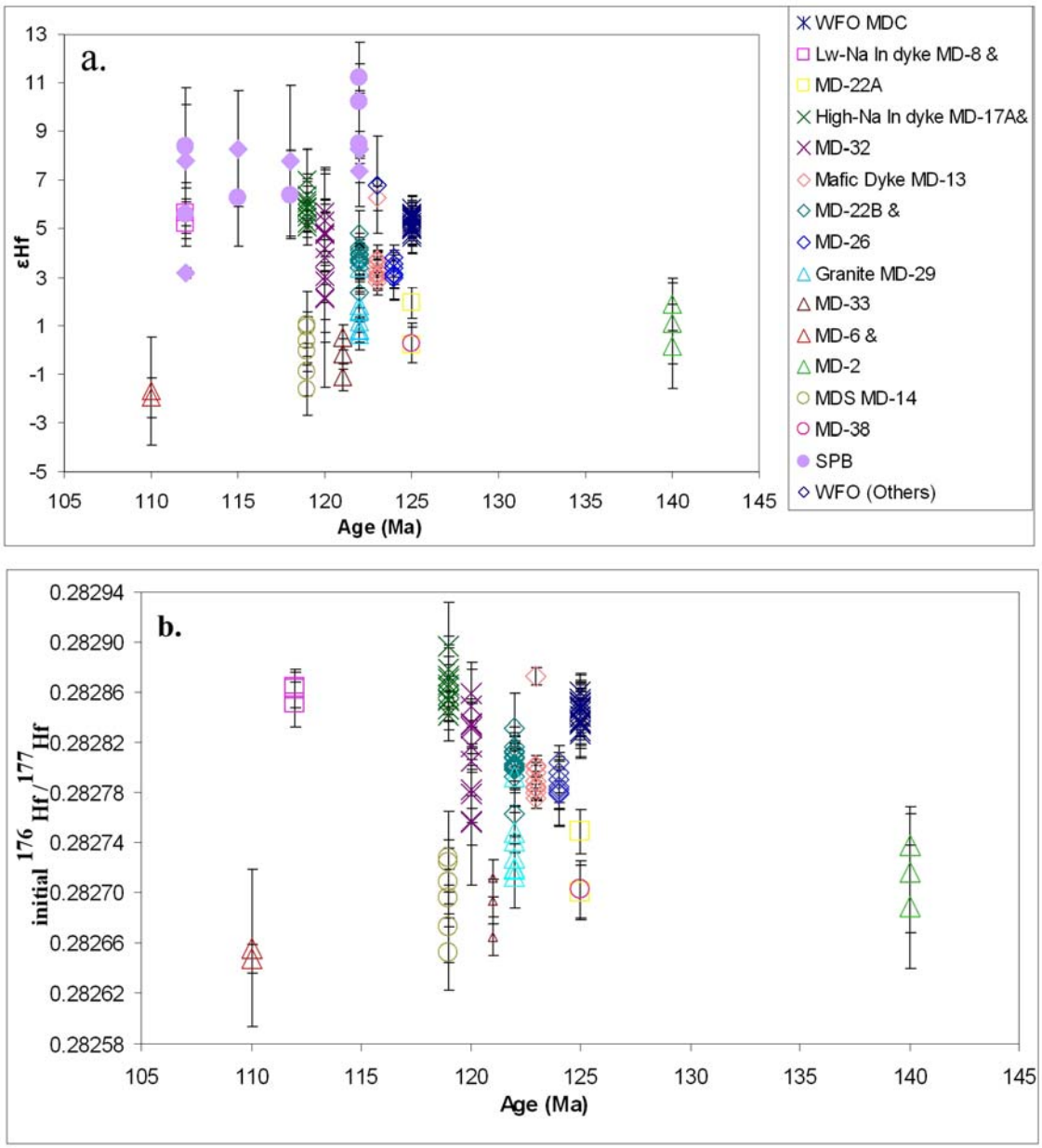


***Figure 10.9.*** *Hf isotopic composition variation of Early Cretaceous zircons with age.* ***(a)*** εHf *vs. age from Mt Daniel, Separation point batholith and WFO (from Bolhar et al., 2008).* ***(b)*** *Initial Hf isotopic composition of zircons vs. age of Mt Daniel Complex rocks. The error bar represents 2 standard error.*

The initial Hf compositions of zircons in mafic dykes have quite a restricted range (Fig 10.9.), suggesting that the xenocrystic zircons were not sufficiently equilibrated after assimilation with the magma to shift its isotopic composition. However, the extent of crustal assimilation may be variable in individual melt increments as Hf isotopic variations are different in individual dykes.

For example, one of the mafic dykes (MD-22B) has comparatively large variations in Hf isotopic composition (+2.3 to +4.8), compared to the other mafic dykes (Fig 10.9.), but it does not contain any inherited cores. This suggests either the zircons were completely dissolved or not picked up by the dyke, or the variation may be caused by mixing with more evolved magma. Thus, crustal assimilation and mixing is evident in the basaltic dykes.

The wide variations of Hf isotopic compositions of zircons from high-Na intermediate dykes indicate derivation from isotopically different sources (Fig. 10.9 and 10.1.b). The more radiogenic (+7.0) to less εHf radiogenic signature (+2.1) indicate interaction with evolved crustal sources. The presence of inherited cores in one of these dykes suggests that the magmas may have undergone crustal contamination with ARC-like mafic crust.

The different magmas may have assimilated different isotopic domains of the ARC protolith in varying proportions. These different isotopic domains of ARC associated with different magma source are discussed in details in Chapter-9. The granitic magmas have assimilated continental crust similar to the William Granite, which represents a Carboniferous protolith within the ARC, whereas high-Na magmas were derived from more primitive mafic crust similar to the Cretaceous ARC and/or Darran Complex.

**Possibility -3:**

If the assimilation model is accepted, significant involvement of basaltic magma to form the MDC is not required. Indeed, mixing of just the three dyke components (if pure melts) cannot explain the presence of large amount of inherited cores in Mt Daniel rocks. However, mafic dykes *are* present and have evolved Hf isotopic compositions, indicating they were involved in the hybridization process, as shown by field relations. The intermittent input of hot mantle-derived mafic melts is also suggested by the zircon trace element study (see chapter-8), which records temperature reversal in Early Cretaceous igneous zircons.

Therefore, the low-Na to high-Na (trondhjemitic) dykes can also form by mixing. Indeed, intrusion of mafic magma is probably a necessity to raise the crustal temperatures sufficiently to melt the crust in the first place (cf., Annen et al, 2006). Therefore, this thesis proposes a model combining both possibilities of mixing and crustal assimilation.

Fig 10.10 shows how the different source components might have been combined. The model is based on the $Na_2O$-$SiO_2$ variation diagram where the basaltic magma at the lower silica-end, granitic magma at high-silica end and high-Na intermediate magma at the top apex are the major magmatic end members. The composition of the ARC is in between the basaltic and high-Na magmas. Variable mixing of high-Na magmas with assimilated ARC can produce the intermediate-composition dioritic magmas of the MDC. More silicic varieties are produced by variable mixing with granitic magmas.

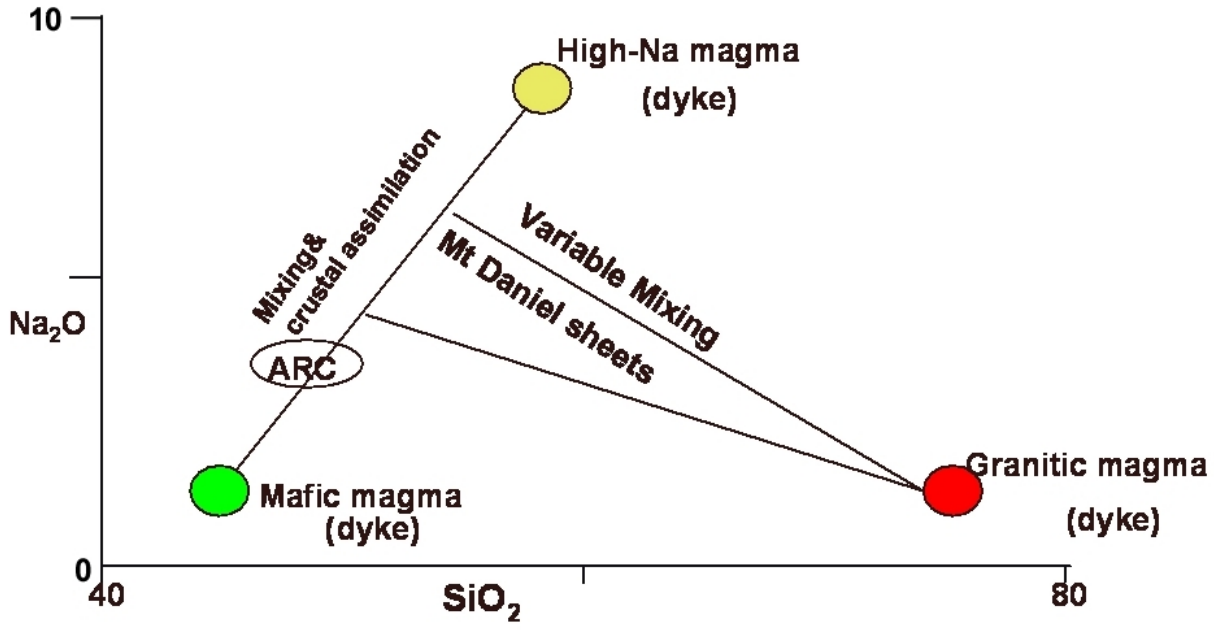


***Figure 10.10.*** *Mixing model shows the mixing among different source components and crustal assimilation combined together to produce Mt Daniel Complex.*

## 10.5. The Dynamics of the Region during MDC Emplacement

The structural and field relations at Mt Daniel suggest that the MDC was a magma-filled shear zone that formed after the WFO had solidified. The emplacement age of the WFO is 125 Ma (this study; Hollis et al., 2004) and the MDC shows ages within a range of 124-112 Ma, although the period of emplacement was probably much shorter. So the solidification and burial of WFO to ~13 Kbar, and formation of MDC, was probably very rapid.

The zircon trace element study gave a detailed account of the complex conditions during formation of the MDC. The CL-image structures, combined with trace element chemistry of zircons, suggest a transition from igneous to metamorphic conditions of growth during the Early Cretaceous. Igneous zircons are commonly present in mafic dykes, high-Na intermediate dykes and low-Na intermediate dykes suggesting they crystallised in a magmatic condition. However some zircons in these dykes have metamorphic overgrowths of the same age, suggesting the crystallisation was continuous across the magmatic to metamorphic transition.

Some of the granites have both HREE-non depleted and HREE depleted zircon and metamorphic garnet rims, suggesting that the non-depleted rims have formed in an open system environment and the depleted rims and garnet grew in a finite reservoir leading to depletion of HREE. The latter situation is considered the metamorphic condition and suggests a transformation from open to closed system chemical processes during the igneous to metamorphic transition. The field evidence and U-Pb age data suggest that the granites analysed from MDC are the youngest phases to intrude into the MDC, and they rapidly crystallised. Similar granitic melts which produced these granites acted as one of the important sources to the MDC. Thus, their emplacement, crystallisation and metamorphism happened in a very short time span suggesting a very dynamic process operated at the base of the crust at Mt Daniel.

Different magmas were generated at different depths, as described in section 10.2. The high-Na intermediate magmas formed at greater crustal depth (≥ 13 Kbar) (eg., (Klepeis et al., 2004), whereas the granites were derived from a comparatively lower crustal depth (≤10Kb). So the highest pressure of 13 Kbar can be correlated to the high-Na intermediate dyke formation.

To observe the correlation of changing depth with the evolution of different source components with time; the high-Na intermediate dykes, granitic dykes, and one hybrid low-Na intermediate dykes, are plotted on Q-Ab-Or diagram (Fig 10.11.). The triangular diagram shows the variation of their normative compositions is defined by a curve that connects the water-saturated melt compositions of sodic (trondhjemitic) rocks with high-K granitic rocks, reflecting the transition from higher pressure to lower pressure. The normative composition of the high-Na intermediate dykes plot on the sodic side of the triangular plot, along the Ab-Or baseline. These are silica undersaturated magmas. However, the granites plot near the water-saturated minima at 10 kbar. Basically the curve shows an ~3 Kbar (10 km) decrease in pressure from high-Na dykes approximately at 13 Kb (see section 10.2.) to granites approximately at 10 Kb (see section 10.2). High-K granites record the lowest pressure of any rock type at Mt Daniel.

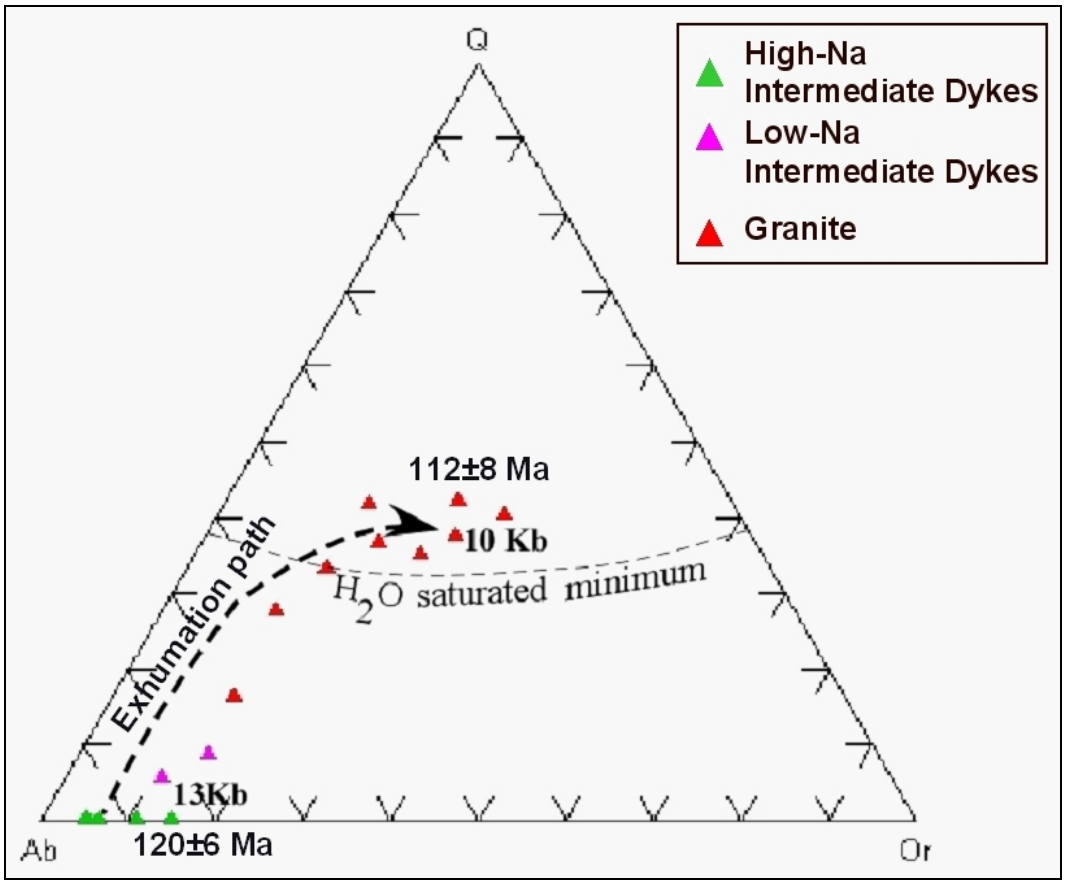


***Figure 10.11.*** *Q-Ab-Or triangular plot shows the formation of Mt Daniel Complex follow the decompression-exhumation path.*

Therefore, the granites formed in a lower P field related to ~10 km of decompression, which suggested that the Mt Daniel Complex formed during a decompression-exhumation event after the burial and solidification of Western Fiordland Orthogneiss. This is consistent with the field relations and geochronological data. So this study suggests that the MDC formed immediately following the peak temperature condition associated with the granulite facies metamorphism and initial formation of the trondhjemitic dykes. The observed P-T-t path was anticlockwise (Fig 10.12) similar to that described by (Klepies et al., 2004), but the key difference with their model is that the MDC did not form as a metamorphic aureole during WFO emplacement or burial.

According to Klepeis et al (2004), the Mt Daniel Shear Zone formed during ongoing compression associated with burial (increasing P), whereas we consider that the MDSZ formed during exhumation (decreasing P). Klepeis et al (2004) described arrays of discordant veins and fractures filled with trondhjemitic leucosome that occur above and below the shear zone. We agree with this observation, but do not see those leucosomes cutting "all ductile fabrics". Rather, some do and some do not, as discussed in Chapter 2. So this thesis suggests that the rectilinear fracture systems were associated with burial and record dehydration at the garnet granulite facies, before the hydration associated with the MDC during shearing along the Mt Daniel Shear Zone.

As pointed out by Klepeis et al. (2004) the development of a relatively cool lower crust ($T^o$ 650–700 C) at Mt Daniel at 120-112 Ma, contrasts with the higher temperatures (T >800$^o$C) at~107 Ma recorded in granulite facies mineral assemblages at Doubtful Sound, some 100 km to the south (Gibson and Ireland, 1995). Furthermore, trondhjemitic magmas continued to be emplaced into the middle and upper crust until ~105 Ma (Tulloch and Kimbrough, 2003) in this region. In addition, Forster and Lister (2003) provided evidence that exhumation associated with extension in southern New Zealand began between 112-109 Ma, forming the regional subhorizontal fabrics in the Otago

Schist to the east of Fiordland. This information suggests that the Mt Daniel Shear Zone could have been kinematically linked with the extensional Doubtful Sound Shear Zone (Klepeis et al., 2004).

Alternatively, the Mt Daniel Shear Zone was one of a series of thrusts associated with the Carswell fold-thrust belt (Klepeis et al, 2004), but if so, thrusting was associated with exhumation rather than burial, at least from ~120 Ma onward. For this to occur, the upper crust must have been removed by erosion at tectonic rates. Perhaps the decompression-related metamorphism focused in the syntaxes of the Himalayan collision zone (eg., Koons et al, 2002) provides an explanation for simultaneous thrusting and exhumation known as tectonic aneurysms (Zeitler et al., 2001). A Tectonic aneurysm describes the rapid uplift and erosion of deep continental crust at piercement points in a collisional orogen. Key examples are the syntaxes of NE and NW India, within the Himalayan orogen. There, continental crust is rising so rapidly that the crust cannot thermally equilibrate, thereby generating high-temperature, low-pressure metamorphism in the aneurysm by isothermal decompression. So a process similar to tectonic aneurysms (Zeitler et al., 2001) might be associated with the development and exhumation of Mt Daniel Complex.

Irrespective of the deformation mechanism associated with formation of the Mt Daniel Shear Zone, magmas would continue to be emplaced into it until the zone crossed the granite solidus at ~10 Kb. At this stage, all MDC magmas would freeze, because they were hydrous, thereby providing a unique example of preservation of magma generation processes in the lower crust. Elsewhere, where melting and mixing probably continued under more typical water-undersaturated (granulite facies) conditions (such as Doubtful Sound), the more anhydrous magmas were also hotter and thus capable of rising to higher crustal levels. At this stage they would have become more homogenized and lost the evidence associated with assembly of melt increments in the lower crust, as preserved

at Mt Daniel. Indeed, magmatic activity at shallow crustal levels, such as the SPB, is compatible with the regional structural data from Fiordland, which suggest that ductile shear zones helped extract melt from the lower crust and transfer it to the upper crust (e.g., Klepeis and Clarke, 2003).

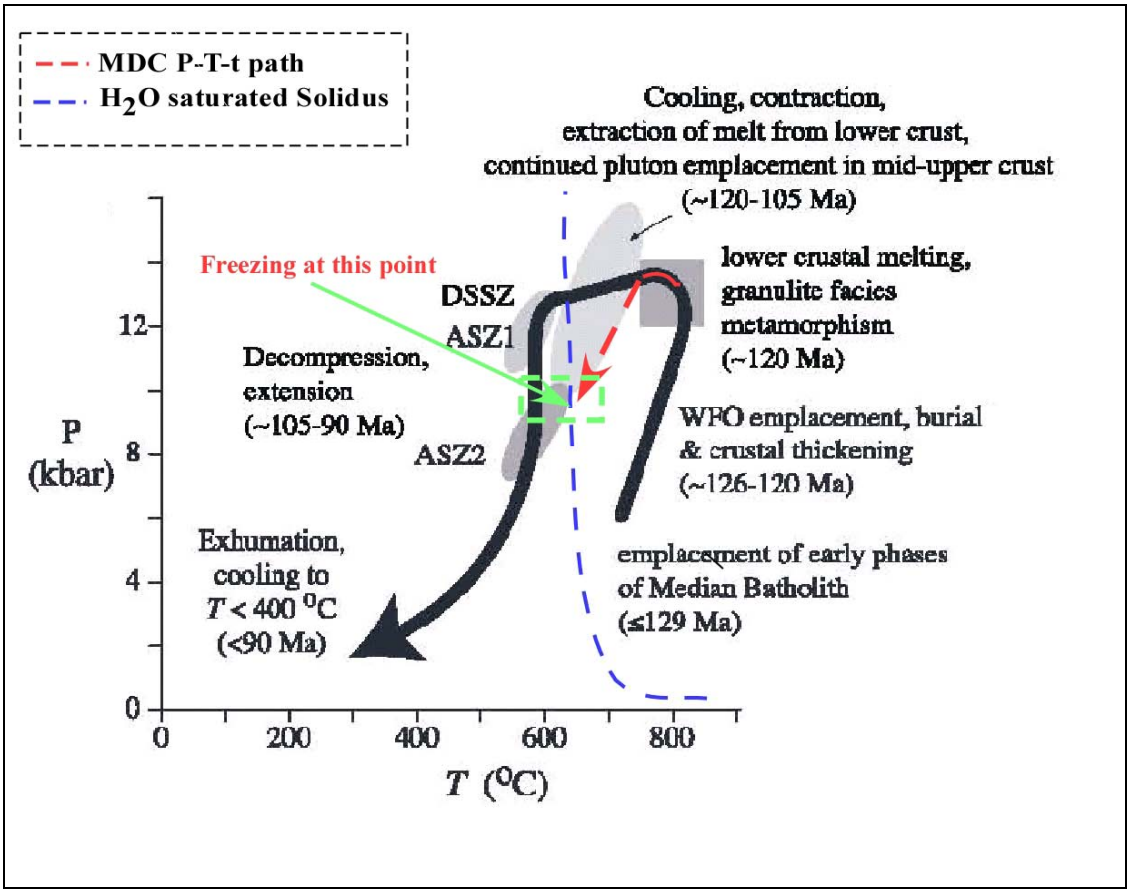


***Figure 10.12.*** *The decompression-exhumation path of Mt Daniel Complex modified on the P-T-t path after Klepies et al., (2004).*

## 10.6. Implications for Generation of HiSrY Granites

Finally, it is relevant to compare the cause of geochemical and isotopic variations of SPB, of similar Early Cretaceous age and composition to the MDC. The Hf isotopic compositions of zircons from the SPB (Fig 10.9.a, Bolhar et al., 2008) show a more mantle-like signature than the MDC, suggesting that the SPB magmas were not contaminated by the isotopically evolved, high-K granitic dykes as at Mt Daniel. Rather, it seems that the SPB may have formed by variable amounts of contamination of mafic juvenile crust (ARC and Darran Complex) with high-Na (sodic) magmas derived during deep burial of the arc.

The critical contribution required to produce HiSY granites seems to be the amount of sodic dykes injected into the magmatic system. The highly sodic components of MDC are not present in SPB, so it is their contribution that raises the sodium content (and $Al_2O_3$, Sr, Ba), as plagioclase progressively breaks down in the source region. These dykes can mix variably with basaltic magma to form an array of intermediate-composition (55-60% $SiO_2$) sodic dioritic magmas that are the equivalent to the mafic SPB granitoids, and thus are possible parental magmas for the SPB.

Alternatively, as detailed at Mt Daniel, trondhjemitic dykes formed in the deeper parts of the basement, but became trapped along an active deep crustal shear zone (>25 km depth). Once established, the shear zone becomes the locus of magma emplacement, and, given the already high ambient temperatures at this depth (~700$^{o}$C), the shear zone itself becomes a site of partial melting. This is evident at Mt Daniel because the ARC granulites below the MDC are garnet-rich and biotite-poor, reflecting a chemically depleted character (e.g., Klepeis et al, 2004). By contrast, the ARC components in the shear zone directly above became dissolved and progressively assimilated into the intruding magmas. Presumably, ingress of water along the shear zone, either from the crystallising trondhjemitic magmas or externally derived (hydrous arc basalts?), increased the water activity along the zone and facilitated fluid-present melting. The potential effect was to rapidly

produce large amounts of melt just above the solidus, from the ARC. Under such fluid-present conditions, residual material could be incorporated *en mass* into the developing magma and begin to move along the shear zone. Movement of magma would virtually be restricted to the shear zone because it represented a zone of mechanical weakening. Injections of externally derived magma (trondhjemitic dykes and later granitic dykes) as the crust moved to higher levels, would then feed into the fluidised shear zone.

However, once the magma-rich shear zone reached ~10 kbar, magma transfer along the zone would stop because the magmas would freeze. This was the case at Mt Daniel. If a similar structural model is applied to the SPB, it requires either that the magmas coalescing in the shear zone were less hydrous, or that additional magmatic heat was being advected into the system from mafic dykes. Few mafic dykes exist in the MDC, which might help explain its preservation, but primitive mantle-derived magma, entering a shear zone at ~1000-1100$^{o}$C, would have the potential to keep the magmatic temperature elevated for longer. This provides the opportunity for the magmas to rise to higher crustal levels, like the SPB, particularly if active pathways were being developed under the existing stress regime (e.g., Klepeis et al., 2004).

The more isotopically primitive character of the SPB, relative to the MDC, is consistent with a greater mantle input. The greater mantle input also provides the opportunity for greater degrees of crustal melting and/or assimilation of basement rocks along the actively forming shear zone. If the amount of melt becomes large, it is probable that it would siphon off from the shear zone as dykes and transfer to higher crustal levels, incrementally feeding into upper crustal magma chambers. These dykes are likely to be relatively homogenised as they would represent magmas with the highest melt fraction (lowest residual material). The dykes could then be further homogenised within the active chamber, in which case much of the evidence for source complexity would be almost, if not completely, lost.

Subsequent chemical diversity in the relatively homogenised, upper crustal magma chamber would occur by a range of processes involving some sort of crystal fractionation from parent magma. Upper crustal contamination is probably limited to local wall-rock assimilation, but should not strongly affect the magma chemistry. Thus, the isotopic signature of the magma chamber should not change significantly with increasing silica.

Although crystal fractionation is the likely cause of chemical variation in the SPB, it was not the case for the MDC. For the MDC, increasing silica was associated with mixing of a more isotopically evolved end-member. However, this represents only a small proportion of the total magma produced in the MDC, and homogenisation with the more abundant intermediate (and primitive) magmas would effectively remove this isotopic spike. Thus, the mixing of the evolved, high-K, crustal end-member at Mt Daniel reflected only a transient (and terminal) condition in the generation of the sodic magmas of Fiordland.

Much more commonly, sodic magmas were produced by plagioclase breakdown under high-P conditions during growth and burial of the arc, but the effect was enhanced by the systemic melting and assimilation of pre-existing (generally sodic) protoliths, probably adjacent to active shear zones like at Mt Daniel. Thus, once the arc was sufficiently thick to generate sodic magmas, the HiSrY condition was enhanced through successive partial melting and assimilation events until arc magmatism terminated.

# Bibliography

***Allibone, A. H., Jongens, R., Turnbull, I. M., Milan, L. A., Daczko, N. R., De Paoli, M. C., Tulloch, A. J.,*** 2009, Plutonic rocks of western Fiordland, New Zealand: field relations, geochemistry, correlation and nomenclature, New Zealand Journal of Geology and Geophysics, 52, 4; p. 379-415.

***Annen, C., Blundy, J.D., Sparks, R.S.J.,*** 2006, The sources of granitic melt in Deep Hot Zones, Transactions of the Royal Society of Edinburgh-Earth Sciences, 97, 4; p. 297-309.

***Armstrong, J.T.,*** 1982, New ZAF and α factor correlation procedures for the quantitative analysis of individual microparticles, In: K.F.J. Heinrich, Ed., Microbeam Analysis, San Francisco Press; p. 175-180.

***Bachl, C.A., Miller, C.F., Miller, J.S., Faulds, J.E.,*** 2001, Construction of a pluton: Evidence from an exposed cross section of the Searchlight pluton, Eldorado Mountains, Nevada, *GSA Bulletin*, 113 (9); p. 1213–1228.

***Barnes, C.G., Yoshinobu, A.S., Nordgulen T.P.O., Haraldur, R.K., and Sundvoll*, B.,** 2002, Mafic magma intraplating; anatexis and hybridization in arc crust, Bindal Batholith Norway, Journal of Petrology, 43(12); p. 2171-2190.

***Benisek, A. & Finger, F.,*** 1993, Factors controlling the development of prism faces in granite zircons: A microprobe study, Contrib Mineral Petrol, 114; p. 441-451.

***Belousova, E.A., Griffin, W.L., O' Reilly, S.Y., 2006,*** Zircon crystal morphology, trace element signatures and Hf isotope compositions as a tool for petrogenetic modeling: examples from eastern Australian granitoids, Journal of Petrology, 47 (2); p. 329-353.

***Black, L.P., Sheraton, J.W., James, P.R.,*** 1986, Late Archean granites of the Napier Complex, Enderby Land, Antarctica: a comparison of Rb-Sr, Sm-Nd and U-Pb isotopic systematics in a complex terrain, Precambrian Research, 32; p. 343-386.

***Black, L.P., Kamo, S.L., Allen, C.M., Davis, D.W., Aleinikoff, J.N., Valley, J.W., Mundil, R., Campbell, I.H., Korsch, R.J., Williams, I.S., Foudoulis, C.,*** 2004, Improved 206Pb/238U microprobe geochronology by the monitoring of a trace-element-related matrix effect: SHRIMP, ID–TIMS, ELA–ICP–MS and oxygen isotope documentation for a series of zircon standards, Chemical Geology, 205; p. 115–140.

***Blattner, P***., 1976, Replacement of hornblende by garnet in granulite facies assemblages near Milford Sound, New Zealand, Contrib Mineral Petrol, 55; p.181-019.

***Blattner, P.,*** 1978, Geology of the crystalline basement between Milford Sound and the Hollyford Valley, New Zealand, New Zealand Journal of Geology and Geophysics, 21; p. 33–47.

***Blattner, P.,*** 1991, North Fiordland transcurrent convergence, New Zealand Journal of Geology and Geophysics, 34; p. 533–542.

***Blichert-Toft, J. & Albarede, F.,*** 1997, The Lu–Hf isotope geochemistry of chondrites and the evolution of the mantle–crust system, Earth Planet Sc Lett, 148; 42, p. 243–258.

***Bolhar, R., Weaver, S.D., Whitehouse, M.J., Palin, J.M., Woodhead, J.D., Cole***, ***J.W.,*** *2008*, Sources and evolution of arc magmas inferred from coupled O and Hf isotope systematics of plutonic zircons from the Cretaceous Separation Point Suite (New Zealand), Earth Planet Sc Lett, 268; p. 312–324.

***Bolhar, R., Weaver, S.D., Palin, J.M.,*** 2008a, Systematics of zircon crystallisation in the Cretaceous Separation Point Suite, New Zealand, using U/Pb isotopes, REE and Ti geothermometry , Contrib Mineral Petrol, 156, 2; p. 133-160.

***Bradshaw, J.Y.,*** 1985, Geology of the Northern Franklin Mountains, Northern Fiordland, New Zealand, with Emphasis on the Origin and Evolution of Fiordland Granulites, Unpublished Ph.D. Thesis, University of Otago, Dunedin, New Zealand.

***Bradshaw, J.Y.,*** *1989,* Origin and metamorphic history of an early Cretaceous polybaric granulite terrain Fiordland, sourhwest New Zealand, Contrib Mineral Petrol, 103; p. 346-360.

***Bradshaw, J.Y.,*** 1990, Geology of crystalline rocks of northern Fiordland: details of the granulite facies Western Fiordland Orthogneiss and associated rock units, New Zealand Journal of Geology and Geophysics, 33; p. 465–484.

***Bradshaw, J.Y.,*** 1993, A review of the Median Tectonic Zone terrane boundaries and terrane amalgamation near the Median Tectonic Line, New Zealand Journal of Geology and Geophysics, 36; p. 117–125.

***Brown, E. H.,*** 1996, High-pressure metamorphism caused by magma loading in Fiordland, New Zealand, Journal of Metamorphic Geology, 14; p. 441–452.

***Carson, C.J., Ague, J.J., Coath, C.D.,*** 2002, U–Pb geochronology from Tonagh Island, East Antarctica: implications for the timing of ultra-high temperature tamorphism in the Napier Complex, Precambrian Research, 116; p. 237-263.

***Chappell, B.W. & White, A.J.R.,*** 1974, Two contrasting granite types, *Pacific Geology,* 8; p. 173-174.

***Chappell, B.W.,*** 1984, Source rocks of S- and I-type granites in the Lachlan Fold Belt, southeastern Australia, Philosophical Transactions of the Royal Society of London, A310; p. 693-707.

***Chauvel, C. & Blichert-Toft, J.***, 2001, A hafnium isotope and trace element perspective on melting of the depleted mantle, Earth Planet Sc Lett, 190; p. 137– 151.

***Cherniak, D.J., Hanchar, J.M., Watson, E.B.,*** 1999, Diffusion of tetravalent cations in zircon, Contrib Mineral Petrol, 127; p. 383–390.

***Claibone, L.L., Miller, C.F., Walker, B.A., Wooden, J.L., Mazdab, F.K., Bea, F.,*** 2006, Tracking magmatic processes through Zr/Hf ratios in rocks and Hf and Ti zoning in zircons: an example from the Spirit mountain batholith, Nevada, Mineral Mag, 70; p. 517-543.

***Claoue-Long, J.C., Sobolev, N.N., Shatsky, V.S., Sobolev, A.V.,*** 1991, Zircon response to diamond-pressure metamorphism in the Kokchetav Massif, USSR, Geology, 95; p. 87-105.

***Clarke, G.L., Klepeis, K.A., Daczko, N.R.,*** 2000, Cretaceous high-P granulites at Milford Sound, New Zealand: metamorphic history and emplacement in a convergent margin setting, Journal of Metamorphic Geology, 18; p. 359–374.

***Clemens, J. D. & Wall, V. J.,*** 1981, Origin and crystallization of some peraluminous (S-type) granitic magmas, Can. Miner. 19; p. 111-31.

***Coherent, user manual, GeoLas Pro*;** 2006.

***Coleman, D.S., Gray, W., Glazner, A.F.,*** 2004, Rethinking the emplacement and evolution of zoned plutons: Geochronologic evidence for incremental assembly of the Tuolumne Intrusive Suite, California, Geology, 32, (5); p. 433-436.

***Collins, W.J***., 1998, Evaluation of petrogenetic models for Lachlan Fold Belt granitoids: Implications for crustal architecture and tectonic models', Australian Journal of Earth Sciences, 45, 4; p. 483-500.

***Conrad, W.K., Nicholls, I.A., Wall, V.J.,*** *1988, Water-saturated melting of metaluminous and peraluminous crustal compositions at 10kb: Evidence for the origin of silicic magmas in the Taupo Volcanic Zone, New-Zealand, and other Occurrences, Journal of Petrology, 29, 4; p. 765-803.*

***Cooper, R.A.,*** 1989, *Early Paleozoic terranes of New Zealand, Journal of the Royal Society of New Zealand, 19; p. 73-112.*

***Corfu, F., Stott, G.M.,*** 1998, The Shebandowan greenstone belt, western Superior Province: U-Pb ages, tectonic implications and correlations, Geol Soc Am Bull, 110; p. 1467-1484.

***Corfu, F., Hanchar, J.M., Hoskin, P.W.O., Kinny, P.,*** 2003, Atlas of zircon textures, Reviews in Mineralogy and Geochemistry, Mineralogical Society of America, 53; p. 469-495.

***Daczko, N.R., Klepeis, K.A., Clarke, G.L.,*** 2001a, Evidence of Early Cretaceous collisional-style orogenesis in northern Fiordland, New Zealand and its effects on the evolution of the lower crust, Journal of Structural Geology, 23; p.693–713.

***Daczko, N.R., Clarke, G.L., Klepeis, K.A.,*** 2001b, Transformation of two-pyroxene hornblende granulite to garnet granulite involving simultaneous melting and fracturing of the lower crust, Fiordland, New Zealand, Journal of Metamorphic Geology, 19; p. 547–560.

***Daczko, N.R., Stevenson, J.A., Clarke, G.L. & Klepeis, K.A.,*** 2002a, Successive hydration and dehydration of a high-P mafic hornfels involving clinopyroxene-kyanite symplectites, Mt Daniel, Fiordland, New Zealand, Journal of Metamorphic Geology, 20; p. 669-682.

***Daczko, N.R., Clarke, G.L., Klepeis, K.A.,*** 2002b, Kyanite-paragonite-bearing assemblages, northern Fiordland, New Zealand: rapid cooling of the lower crustal root to a Cretaceous magmatic arc, Journal of Metamorphic Geology, 20; p.887-902,

***Davidson J.P., Tepley F.J., Clynne, M.A.,***1999, Magmatic Interactions as Recorded in Plagioclase Phenocrysts of Chaos Crags, Lassen Volcanic Center, California, Journal of Petrology, 5, 40; p.787-806.

***Davidson, J.P., Tepley, F.J., Tilling, R.I., Arth, J.G.,*** 2000, Magma mixing, Recharge and eruption histories recorded in plagioclase phenocrysts from El Chichon Volcano, Maxico, Journal of Petrology, 9, 41; p.1397-1411.

***Defant, M.J. & Drummond, M.S.,*** 1990, Derivation of some modern arc magmas by melting of young subducted lithosphere, Nature, 347; p. 662-665.

***Depaolo, D.J., Wasserburg, G.J.,*** 1976, Nd isotopic variations and petrogenetic models, Geophysical Research Letters, 3, 5; p. 249-252.

***DePaolo, D.J***., 1981, A neodymium and strontium isotopic study of Mesozoic calc-alkaline granitic batholiths of the Sierra Nevada and Peninsular Ranges, California, Journal of Geophysical Research, 86; p.10470–10488.

***Drake, M.J. & Weill, D.F.,*** 1975, Partition of Sr, Ba, Ca, Y, $Eu^{2+}$, $Eu^{3+}$ and other REE between plagioclase feldspar and magmatic liquid-Experimental study, Geochim Cosmochim Acta, 5, 39; p. 689-712.

***Elburg, M.A. & Nicholls, I.A.,*** 1995, Origin of microgranitoid enclaves in the S-type Wilson's Promontory Batholith, Victoria; evidence for magma mingling, *Australian Journal of Earth Sciences*, 42(4); p.423-435.

***Elburg, M.A., Bons, P.D., Foden, J.,*** 2003, A newly defined Late Ordovician magmatic-thermal event in the Mt Painter Province, Northern Flinders Ranges, South Australia, Australian Journal of Earth Sciences, 50, 4; p. 611-631.

***Flowerdew, M.J., Miller, I.L., Vaughan, A.P.M., Horstwood, M.S.A., Fanning, C.M***., 2006, The source of granitic gneisses and migmatites in the Antarctic Peninsula: a combined U-Pb SHRIMP and laser ablation Hf isotope study of complex zircons, Contrib Mineral Petrol, 151; p. 751-768.

***Flowers, R.M., Bowring, S.A., Tulloch, A.J., Klepeis , K.A.,*** 2005, Tempo of burial and exhumation within the deep roots of a magmatic arc, Fiordland, New Zealand, Geology, Jan 2005; 33; p. 17 - 20.

***Forster, M.A., Lister, G.S.,*** 2003, Cretaceous metamorphic core complexes in the Otago Schist, New Zealand, Australian Journal of Earth Sciences, 50; p. 181-198.

***Fowler, A., Prokoph, A., Stern, R., Dupuis, C.,*** 2002, Organization of oscillatory zoning in Zircon: Analysis, scaling, geochemistry and model of a zircon from Kipawa, Quebec, Canada, Geochim Cosmochim Acta, 66; p. 311-328.

***Frondel, C.,*** 1953, Hydroxyl substitution in thorite and zircon, Am Mineral, 38; p. 1007-1018.

***Fu, B., Page, F.Z., Cavosie, A.J., Fournelle, J., Kita, N.T., Lackey, J.S., Wilde, S.A., Valley, J.W.,*** 2008, Ti-in-zircon thermometry: applications and limitations, Contrib Mineral Petrol, 2, 156; p. 197-215.

***Gagnevin, D., Daly, J.S., Kronz,*** 2010, A zircon texture and chemical composition as a guide to magmatic processes and mixing in a granitic environment and coeval volcanic system, Contrib. Mineral Petrol, 4, 159; p. 579-596.

***Gaina, C., Müller, D.R., Royer, J.Y., Stock, J., Hardebeck, J., & Symonds, P.,*** 1998, The tectonic history of the Tasman Sea: A puzzle with thirteen pieces, Journal of Geophysical Research, 103; p. 12,413–12,433.

***Geisler, T., Pidgeo, R.T., Kurtz, R., van Bronswijk, W., Schleicher, H.,*** 2003, Experimental hydrothermal alteration of partially metamict zircon, American Mineralogist, 86; p.1496-1518.

***Geisler, T., Schaltegger, U., Tomaschek, F.,*** 2007, Re-equilibration of zircon in aqueous fluids and melts, Elements, 3(1); p. 43-50.

***Gerdes, A., Zeh, A.,*** 2006, Combined U–Pb and Hf isotope LA-ICP-MS analyses of detrital zircons: comparison with SHRIMP and new constraints for the provenance and age of an Amorican metasediment in Central Germany, Earth Planet Sc Lett, 249; p. 47–61.

***Gibson, G.M., McDougall, I., Ireland, T.R.,*** 1988, Age constraints on metamorphism and the development of a metamorphic core complex in Fiordland, southern New Zealand. Geology, 16; p. 405–408.

***Gibson, G.M.,*** 1990, Uplift and exhumation of middle and lower crustal rocks in an extensional tectonic setting, Fiordland, New Zealand. In: Salisbury, M.H. & Fountain D.M. (eds) Exposed Cross-Sections of the Continental Crust, Kulwer Academic Publishers, Netherlands; p.71-101.

***Gibson, G.M.,*** 1992, Medium-high pressure metamorphic rocks of theTuhua Orogen, western New Zealand, as lower crustal analogues of the Lachlan Fold Belt, southeastern Australia, Tectonophysics, 214; p. 145-157.

***Gibson, G. M. & Ireland, T. R.,*** 1995, Granulite formation during continental extension in Fiordland, New Zealand. Nature, 375; P. 479–482.

***Gray, C.M.,*** 1984, An isotopic mixing model for the origin of granitic rocks in southeastern Australia, Earth Planet Sc Lett, 70; p. 47-60.

***Gray, C.M., Kemp, A.I.S.,*** 2009, The two component model for the genesis of granitic rocks in southeastern Australia-Nature of the metasedimentary-derived and basaltic end members, Lithos, 111; p. 113-124.

***Griffin, W.L., Pearson, N.J., Belousova, E.A., Jackson, S.E.,O'Reilly, S.Y., van Achterberg, E., Shee, S.R.,*** 2000, The Hf-isotope composition of cratonic mantle: LAM-MC-ICPMS analysis of zircon megacrysts in kimberlites, Geochim Cosmochim Acta, 64; p. 133–147.

***Griffin, W.L., Wang, X., Jackson, S.E., Pearson, N.J., O'Reilly, S.Y., Xu, X., Zhou, X.,*** 2002, Zircon chemistry and magma mixing, SE China: in-situ analysis of Hf isotopes, Tonglu and Pingtan igneous complexes, Lithos, 61; p. 237– 269

***Hanchar, J.M., Rudnick, R.L.,*** 1995, Revealing hidden structures: the application of cathodoluminescence and backscattered electron imaging to dating zircons from lower crustal xenoliths, Lithos, 36; p. 289-2003.

***Harley, S.L., Kinny, P.D., Snape, I., Black, L.P.,*** 2001, Zircon chemistry and the definition of events in Archaean granulite terrains. In: Cassidy KF, Dunphy JM, van Kranendonk MJ (eds) Extended Abstracts of 4th International Archaean Symposium, AGSO-Geoscience Australia Record, Canberra, 37; p. 511-513.

***Hawkesworth, C.J., Kemp, A.I.S.,*** 2006, Using hafnium and oxygen isotope in zircon to unravel the record of crustal evolution, Chemical Geology, 226; p. 144-162.

***Helz, R.T.,*** 1976, Phase relations of basalts in their melting ranges at PH2O = 5 kb. Part II. Melt compositions, Journal of Petrology, 17; p. 139–193.

***Hildreth, W., Moorbath, S.,*** 1988, Crustal contributions to arc magmatism in the Andes and central Chil, Contrib Mineral Petrol, 98; p. 455–489.

***Hinton, R.W., Upton, B.G.J.,*** 1953, The chemistry of zircon: variations within and between large crystals from syenite and alkali basalt xenoliths. Geochim Cosmochim Acta, 55; p. 3287-3302.

***Hirsch, D.M., Prior, D.J., Carlson, W.D.,*** 2003, An overgrowth model to explain multiple, dispersed high-Mn regions in the cores of garnet porphyroblasts, American Mineralogist, 88; p. 131–141.

***Hokada, T., Harle, S.L.***,2004, Zircon growth in UHT leucosome: constraints from zircon garnet rare earth element (REE) relations in Napier Complex, East Antarctica, Journal of Mineralogical and Petrological Sciences, 99; p. 180-190.

***Hollis, J.A., Clarke, G.L., Klepeis, K.A., Daczko, N.R., Ireland, T.R.,*** 2003, Geochronology and geochemistry of high-pressure granulites of the Arthur River Complex, Fiordland, New Zealand: Cretaceous Magmatism and Metamorphism on the Palaeo-Pacific Margin, Journal of Metamorphic Geology, 21; p. 299–313.

***Hollis, J.A., Clarke, G.L., Klepeis, K.A., Daczko, N.R., Ireland, T.R.,*** 2004, U–Pb zircon geochronology of Cretaceous granulites from Fiordland, New Zealand: rapid burial and uplift along the Mesozoic Pacific Gondwana margin. Journal of Metamorphic Geology, 22; p. 607–627.

**Hoskin, P.W.O.,** 2000, Patterns of chaos: Fractal statistics and the oscillatory chemistry of zircon, Geochim Cosmochim Acta 64; p.1905-1923.

***Hoskin, P.W.O. & Black, L.P.,*** 2000, Metamorphic zircon formation by solid-state recrystallisation of protolith igneous zircon, Journal of Metamorphic Geology, 18; p. 423-429.

***Hoskin, P.W.O., Kinny, P.D., Wyborn, D., Chappell, B.W.,*** 2000, Identifying accessory mineral saturation during differentiation in granitoid magmas: an integrated approach, Journal of Petrology, 41; p.1365-1396.

***Hoskin, P.W.O. & Schaltegger, U.,*** 2003, The composition of zircon and igneous and metamorphic petrogenesis, Rev Mineral Geochem, 53; p. 27-62.

***Ireland, T. R., Gibson, G. M.,*** 1998, SHRIMP monazite and zircon geochronology of high-grade metamorphism in New Zealand. Journal of Metamorphic Geology, 16; p. 149–167.

***Iizuka, T. & Hirata, T.,*** 2005**,** Improvements of precision and accuracy in situ Hf isotope microanalysis of zircon using the laser ablation MC-ICPMS technique, Chemical Geology, 220; p. 121–137.

***Jackson, S.E., Longerich, H.P., Horn, I., Dunning, G.R.,*** 1996, The application of laser ablation microprobe (LAM)–ICP–MS to in situ U–Pb zircon geochronology, J. Conf. Abstr, 1; 283.

***Johannes, W. & Holtz, F.***, 1996, Petrogenesis and Experimental Petrology of Granitic Rocks, Minerals and rocks; p. 173-176.

***Keay, M., Collins,W.J., Mcculloch, M.T***., 1997, A three-component mixing model for granitoid genesis: Lachlan Fold Belt, eastern Australia, *Geology*, 25; p. 307-310.

***Kelly, N.M. & Harley, S.L.,*** 2005, An integrated microtextural and chemical approach to zircon geochronology: refining the Archaean history of the Napier Complex, east Antarctica, Contrib. Mineral. Petrol, 149; p. 57-84.

***Kemp, A.I.S., Hawkesworth, C.J., Foster, G.L., Paterson, B.A., Woodhead, J.D., Hergt, J.M., Gray, C.M., Whitehouse, M.J.,*** 2007, Magmatic and crustal differentiation history of granitic rocks from hafnium and oxygen isotopes in zircon. Science, 315; p. 980–983.

***Kemp, A.I.S., Foster, G.L., Scherstén, A., Whitehouse, M.J., Darling, J., Storey, C.,*** 2009, Concurrent Pb–Hf isotope analysis of zircon by laser ablation multi-collector ICP-MS, with implications for the crustal evolution of Greenland and the Himalayas, Chemical Geology, 261; p. 244–260.

***Kimbrough, D. L., Mattinson, J. M., Coombs, D. S., Landis, C. A., Johnston, M. R.,*** 1992, Uranium-lead ages from the Dun Mountain ophiolite belt and Brook Street Terrane, South Island, New Zealand, Geological Society of America Bulletin, 104; p. 429–443.

***Kimbrough, D.L., Tulloch, A., Geary, E., Coombs, D.S., Landis, C.A.,*** 1993, Isotope ages from the Nelson region of South Island, New Zealand: structure and definition of the Median Tectonic Zone, Tectonophysics, 225; p. 433–448.

***Kimbrough, D.L., Tulloch, A.J., Coombs, D.S., Landis, C.A., Johnston, M.R., Mattinson, J.M.,*** 1994, Uranium-lead zircon ages from the Median Tectonic Zone, New Zealand, New Zealand Journal of Geology and Geophysics, 37; p. 393-419.

***Klepeis, K.A., Clarke, G.L. & Daczko, N.R.,*** 2000, Cretaceous high-P granulites at Milford Sound, New Zealand: their metamorphic history and emplacement in a convergent margin setting, Journal of Metamorphic Geology, 18; p. 359-374.

***Klepeis, K.A. & Clarke, G.L.,*** 2003, Evolution of an exposed lower crustal attachment zone in Fiordland, New Zealand, In: Vertical coupling and decoupling in the lithosphere, Grocott, J., McCaffrey, K., Taylor, G., Tikoff, B. (eds), Geological Society Special Publications.

***Klepeis, K.A., Clarke, G.L., Gehrel, G., Vervoort, J.,*** 2004, Processes controlling vertical coupling and decoupling between the upper and lower crust of orogens: results from Fiordland, New Zealand Journal of Structural Geology, 26; p. 765–791.

***Koons, P.O., Zeitler, P.K., Chamberlain, C.P., Craw, D., Meltzer, A.S.,*** 2002, Mechanical links between erosion and metamorphism in Nanfa Parbat, Pakistan Himalaya, American Journal of Science, 302, 9; p. 749-773.

***Koppel, V., Sommerauer, J.,*** 1974, Trace element and the behaviour of the U-Pb system in inherited and newly formed zircons, Contrib Mineral Petrol, 43; p.71-82.

***Landis, C.A. & Coombs, D.S.,*** 1967, Metamorphi*c* belts and orogenesis in southern New Zealand, Tectonophysics, 4; p. 501–518.

***Lee, J.K.W., Williams, I.S., Ellis, D.J., 1997,*** Pb, U and Th diffusion in natural zircon, Nature (London), 390(6656); p. 159-162.

***Linnen, R.L., Keppler, H.,*** 2002, Melt composition control of Zr/Hf fractionation in magmatic processes, Geochim Cosmochim Acta, 66; p. 3293-3301.

***Lizuka, T. & Hirata, T.,*** 2005, Improvements of precision and accuracy in situ Hf isotope microanalysis of zircon using the laser ablation MC-ICPMS technique, Chemical Geology, 220; p. 121–137.

***Ludwig, K., 2003,*** User's Manual for Isoplot 3.00, A Geochronological Toolkit for Microsoft Excel: Berkeley Geochronology Center, No. 4a, Berkeley, California.

***Mantle, G.W., Collins, W.J.,*** Quantifying crustal thickness variations in evolving orogens: Correlation between arc basalt composition and Moho depth, 2008, Geology, 36, 1; p. 87-90.

***Mattinson, J.L., Kimbrough, D.L., Bradshaw, J.Y***, 1986, Western Fiordland Orthogneiss: Early Cretaceous arc magmatism and granulite facies metamorphism, New Zealand, Contrib Mineral Petrol, 92; p. 383–392.

***Mattinson, J.M., Graubard, C.M., Parkinson, D.L., McLelland, W.C.,*** 1996, U-Pb reverse discordance in zircon: the role of fine scale oscillatory zoning and submicroscopic transport of Pb, Am Geophys Union, Geophys Mongr, 95; p. 355-370.

***McCulloch, M.T., Bradshaw, J.Y., Taylor, S.R.,*** 1987, Sm–Nd and Rb–Sr isotopic and geochemical systematics in Phanerozoic granulites from Fiordland, southwest New Zealand, Contrib Mineral Petrol, 97; p. 183–195.

***Miller, C.F., Bachl, C.A., Miller, J.S., Wooden, J.L., Faulds, J.E., Shaw, M.L.,*** 1995, Mid-crustal plutons of the Eldorado Mountains: evidence for large-scale magmatic modification and reorganization of the crust in the Colorado River extensional corridor: A435; Boulder, Colorado, Geological Society of America Abstracts with Programs, 27 (6); p. A435

***Möllar, A., O'Brien, P.J., Kennedy, A., Kröner, A.,*** 2002, Polyphase zircon in ultrahigh-temperature granulites (Rogaland, SW Norway): constraints for Pb diffusion in zircon, Journal of Metamorphic Geology, 20; p. 727-740.

***Mortimer, N., Tulloch, A.J., Spark, R.,*** 1999, Median batholith and Median Suite of New Zealand: new perspectives on the Phanerozoic igneous record of southern Gondwanaland, African Journal of Earth Sciences, 29; p. 257–268.

***Mortimer, N.,*** *2003,* New Zealand's geological foundations, Gondwana Research, 7(1); p. 261-272.

***Moser, D.E.,*** 1997, Dating the shock wave and thermal imprint of the giant Vredefort impact, South Africa, Geology, 25; p. 7-10.

***Muir, R.J., Ireland, T.R., Weaver, S.D., Bradshaw, J.D., Waight, T.E., Jongens, R. & Eby, G. N.,*** 1997, SHRIMP U–Pb geochronology of Cretaceous magmatism in Northwest Nelson, Westland, South Island, New Zealand, New Zealand Journal of Geology and Geophysics, 40; p. 453–463.

***Muir, R. J., Weaver, S. D., Bradshaw, J. D., Eby, G. N. & Evans, J. A.,*** 1995, The Cretaceous Separation Point batholith, New Zealand: granitoid magmas formed by melting of mafic lithosphere, Journal of the Geological Society of London, 152; p. 689–701.

***Muir, R.J., Ireland, T.R., Weaver, S.D., Bradshaw, J.D., Evans, J.A., Eby, G.N., Shelly, D.,*** 1998, Geochronology and geochemistry of a Mesozoic magmatic arc system, Fiordland, New Zealand, Journal of the Geological Society of London, 155; p. 1037–1053.

***Murgulov, V., Beyer, E., Griffin W.L., O'Reilly, S.Y., Walters, S.G., Stephens, D.,*** *2007, Crustal evolution in the Georgetown Inlier, North Queensland, Australia: a detrital zircon grain study, Chemical Geology, 245; p. 198-218.*

***Nabelek, P.I., Russ-Nabelek, C., Denison, J.R.,*** 1992, The generation and crystallisation conditions of the Proterozoic Harney Peak leucogranite, Black Hills, South Dakota, USA: petrologic and geochemical constraints, Contrib Mineral Petrol, 110; p.173-191.

***Nathan, S., Thurlow, C., Warnes, P., Zucchetto, R.,*** 2000, Geochronology Database for New Zealand Rocks, 2nd edn.1961) 99. Institute of Geological and Nuclear Sciences report 2000／11; p. 51.

***Nemchin, A.A., Pidgeon, R.T.,*** 1997, Evolution of the Darling Range Batholith, Yilgarn Craton, Western Australia: A SHRIMP zircon study, Journal of Petrology, 38; p. 625-649.

***Oliver, G. J. H.,*** 1976, The high grade metamorphic rocks of Doubtful Sound, Fiordland, New Zealand; a study of the lower crust University of Otago, Dunedin, New Zealand, Doctoral thesis.

***Oliver, G.J.H.,*** 1977, Feldspathic hornblende and garnetgranulites and associated anorthosite pegmatites from Doubtful Sound, Fiordland, New Zealand, Contrib Mineral Petrol, 65; p. 111–121.

***Oliver, G.J.H. & Coggon, J.H.,*** 1979, Crustal structure of Fiordland, New Zealand, Tectonophysics, 54; p. 253–292.

***O'Reilly, S.Y., Van Achterberg, E., Shee, S.R.,*** 2000, The Hf isotope composition of cratonic mantle: LAM-MC-ICPMS analysis of zircon megacrysts in kimberlites, Geochim Cosmochim Acta, 64; p. 133–147.

***Paquette, J.L., Monchoux, P., Coutirier, M.,*** 1995, Geochemical and isotopic study of a norite-eclogite transition in the Europian Variscan belt: Implications for U-Pb zircon systematics in metabasic rocks, Geochim Cosmochim Acta, 59; p. 1611-1622.

***Patchett, P.J., Kouvo, O., Hedge, C.E., Tatsumoto, M.***, 1981, Evolution of Continental crust and mantle heterogeneity: Evidence from Hf isotopes, Contrib Mineral Petrology, 778; p. 279-297.

***Pidgeon, R.T.,*** 1992, Recrystallisation of oscillatory zoned zircon: some geochronological and petrological implications. Contrib Mineral Petrol, 110; p. 463-472.

***Pin, C. & Lancelot, J.,*** 1982, U-Pb dating of an Early Paleozoic bimodal magmatism in the French Massif Central and its further metamorphic evolution. Contrib Mineral Petrol, 79; p. 1-12.

***Rapp, R.P., Watson, E.B., Miller, C.F.,*** 1991, Partial melting of amphibolite/eclogite and the origin of Archean trondhjemites and tonalites, Precambrian Research, 51; p. 1–25.

***Ratajeski, K., Sisson, T.W., Glazner, A.F.,*** 2005, Experimental and geochemical evidence for derivation of the El Capitan Granite, California, by partial melting of hydrous gabbroic lower crust, Contrib Mineral Petrol ,149; p. 713–734.

***Rubatto, D. & Gebauer, D.,*** 2000, Use of cathodoluminescence for U-Pb zircon dating by ion microprobe; some examples from theWestern Alps, In: Cathodoluminescence in Geosciences (eds Pagel, M., Barbin, V., Blanc, P. & Ohnenstetter, D.) Springer, Berlin; p. 373–400.

***Rubatto, D., Williams, I.S., Buick, I.S.,*** 2001, Zircon and monazite to prograde metamorphism in the Reynolds Range, central Australia, Contrib Mineral Petrol, 140; p. 458-468.

***Rubatto, D.,*** 2002, Zircon trace element geochemistry: partitioning with garnet and the link between U-Pb ages and metamorphism, Chemical Geology, 184; 1-2; p. 123-138.

***Schaltegger, U., Fanning, C.M., Günther, D., Maurin, J.C., Schulmann, K., Gebauer, D.***, 1999, Growth, annealing and recrystallization of zircon and preservation of monazite in high-grade metamorphism: conventional and in-situ U-Pb isotope, cathodoluminescence and microchemical evidence, Contrib Mineral Petrol, 134; p.186-201.

***Scott, J.M., Cooper, A.F., Palin, J.M., Tulloch, A.J., Kula, J., Jongens, R., Spell, T.L., Pearson N.J.***, 2009, Tracking the influence of a continental margin on growth of a

magmatic arc, Fiordland, New Zealand, using thermobarometry, thermochronology and zircon U-Pb and Hf isotopes, Tectonics, 28; TC6007.

***Segal, I., Halicz, L., Platzner, I.T.,*** 2003, Accurate isotope ratio measurements of ytterbium by multi-collector inductively coupled plasma mass spectrometry applying erbium and hafnium in an improved double external normalisation procedure, J. Anal. At. Spectrom, 18, p. 1217– 1223.

***Sen, C., Dunn T.,*** 1994, Dehydration melting of a basaltic composition amphibolite at 1.5 and 2.0 Gpa: implications for the origin of adakites, Contrib Mineral Petrol, 117; p. 394–409.

***Simon, E.J., Norman, J.P., William, L.G.,*** 2004, The application of laser ablation inductively coupled plasma-mass spectrometry to in-situ U-Pb zircon geochronology, Chemical Geology, 211; p. 47-69.

***Sisson, T.W., Ratajeski, K.R., Glazner, A.F.,*** 2005, Voluminous granitic magmas from common basaltic sources, Contrib Mineral Petrol, 148; p. 635–661.

***Spandler, C., Hermann, J., Rubatto, D***., 2004, Exsolution of thortveitite, yttrialite, and xenotime during low-temperature recrystallization of zircon from New Caledonia, and their significance for trace element incorporation in zircon**,** American Mineralogist; 89; p. 1795 - 1806.

***Storey, B.C., Alabaster, T., Hole, M.J., Pankhurst, R.J., Wever, H.E.,*** 1992, Role of subduction-plate boundary forces during the initial stages of Gondwana break-up: evidence from the proto-Pacific margin of Antarctica, In: Storey, B.C., Alabaster, T. & Pankhurst, R.J. (eds) Magmatism and the Causes of Continental Break-up, Geological Society Special Publications, 68; p. 149–163.

***Sun, S. & McDonough, W.F.,*** 1989, Chemical and isotopic systematics of oceanic basalts: Implications for mantle composition processes, In: Saunders,A.D.&Norry,M.J.(eds) Magmatism in the Ocean Basins, Geological Society, London, Special Publications, 42; p. 313–345.

***Tomaschek., F., Kennedy, A.K., Villa, I.M., Lagos, M., Ballahaus, C.***, 2003, Zircons from Syros, Cyclades, Greece-Recrystallisation and mobilization of zircon during high-P metamorphism, Journal of Petrology, 44(11); p.1977-2002.

***Tomaschek, F.,*** 2004, Zircon reequilibration by dissolution-reprecepitation: reaction textures from flux-grown solid solutions, Beihefte zum, European Journal of Mineralogy, 12; p.214.

***Tulloch, A.J. & Kimbrough, D.L.,*** 1989, The Paparoa metamorphic core complex, New Zealand: Cretaceous extension associated with fragmentation of the Pacific margin of Gondwana. Tectonics, 8; p. 1217–1234.

***Tulloch, A. J. & Rabone, S. D. C.,*** 1993, Mo-bearing granodiorite porphyry plutons of the Early Cretaceous Separation Point Suite, West Nelson, New Zealand, New Zealand Journal of Geology and Geophysics, 36; p. 401–408, A. A. Balkema, Rotterdam: New York.

***Tulloch, A.J., Ireland, T.R., Walker, N.W., Kimbrough, D.L***., 2000, U-Pb zircon ages from the Milford Orthogneisses, Milford Sound, northern Fiordland: Palaeozoic igneous emplacement and Early Cretaceous metamorphism, Report, 6, Institute of Geological and Nuclear Sciences Science, City.

***Tulloch, A.J. & Kimbrough, D.L.,*** 2003, Paired plutonic belts in convergent margins and the development of high Sr/Y magmatism: the Peninsular Ranges Batholith of California and the Median Batholith of New-Zealand, Geological Society of America Special Paper, 374; p. 275-295.

***Tulloch, A.J., Ireland, T.R.., Kimbrough, D.L., Griffin, W.L., Ramezani, J.***, 2010, Autochthonous inheritance of zircon through Cretaceous partial melting of Carboniferous plutons: the Arthur River Complex, Fiordland, New Zealand, Contrib Mineral Petrol, DOI: 10.1007/s00410-010-0539-6.

***Tuttle, O.F. & Bowen,* N.L.,** 1958, Origin of granite in the light of experimental studies in the system $NaAlSi_3O_8$-$KAiSi_3O_8$-$SiO_2$-$H_2O$, Geol. Soc. Am Mem, 74; 153.

***Thirlwall, M.F. & Walder, A.J.,*** 1995, In situ Hf isotope ratio analysis of zircon by inductively coupled plasma multiple collector mass spectrometry, Chemical Geology, 122; p. 241–247.

***van Achterberg, E., Ryan, C.G., Griffin, W. L.,*** 1999, Glitter: online intensity reduction for ablation inductively coupled plasma spectrometry, 9th Goldschmidt Conference, Boston, MA, 1999; p.305.

***van Breemen, O., Davidson, A., Loveridge, W.D., Sullivan, R.W.,***1986, U-Pb zircon geochronology of Grenville tectonics, granulite and igneous precursors, Parry Sound, Ontario, In The Grenville Province, Moore JM, Davidson A, Baer AJ (eds) Geol Assoc Can Spec Paper, 3; p.191-207.

***Vavra, G., Hansen, BT.,*** 1991, cathodoluminescence studies and U-Pb dating of zircons in pre-Mesozoic gneisses of the Tauern Window: Implication for Pennine basement evolution. Geol Rundsch, 80; p. 703-715.

***Vavra, G., Gibauer, D., Schmid, R., Compston, W.,*** 1996, Multiple zircon growth and recrystallisation during polyphase Late Carboniferous to Triassic metamorphism in granulites of the Ivrea zone (South Alps): an ion micro-probe (SHRIMP) study, Contrib Mineral Petrol, 12; p. 337-358.

***Vavra, G., Schmid, R., Gebauer, D.,*** 1999, Internal morphology, habit and U-Th-Pb microanalysis of amphibolite-to-granulite facies zircons: geochronology of the Ivrea Zone (Southern Alps), Contrib Mineral Petrol, 134; p. 380-404.

***Vervoort, J.D., Patchett, P.J.,*** 1996, Behaviour of hafnium and neodymium isotopes in the crust: constraints from Precambrian crustally-derived granites, Geochim Cosmochim Acta, 60; p. 3717–3733.

***Vervoort, J.D. & Blichert-Toft, J.,*** 1999, Evolution of the depleted mantle: Hf isotope evidence from juvenile rocks through time, Geochim Cosmochim Acta, 63; p. 533–566.

***Vervoort, J.D., Patchett, P.J., Blichert-Toft, J., Albarede, F.,*** 1999, Relationships between Lu–Hf and Sm–Nd isotopic systems in the global sedimentary system, Earth Planet Sc Lett, 168; p. 79– 99.

***Vervoort, J.D., Patchett, P.J., Söderlund, U., Baker, M.,*** 2004, The isotopic composition of Yb and the precise and accurate determination of Lu concentrations and Lu/Hf ratios by isotope dilution using MC-ICPMS, Geochemistry Geophysics Geosystems, DOI 2004GC000721RR.

***Wandres, A.M., Weaver, S.D., Shelley, D., Bradshaw, J.D.,*** 1998, Change from calc-alkaline to adakitic magmatism recorded in the early Cretaceous Darran Complex, Fiordland, New Zealand, New Zealand Journal of Geology and Geophysics, 41; p. 1–14.

***Wark, D.A. & Miller, C.F.,*** 1993, Accessory mineral behavior during differentiation of a granite suite: monazite, xenotime and zircon in the Sweetwater Wash pluton, southeastern California, U.S.A. Chemical Geology, 110; p. 49-67.

***Watson, E.B. & Harrison, T.M.,*** 2005, Zircon thermometer reveals minimum melting conditions on earliest Earth, Science, 308; p. 841–844.

***Watson, E.B., Wark, D.A., Thomas, J.B.,*** 2006, Crystallization thermometers for zircon and rutile Contrib. Mineral Petrol, 151; p. 413–433.

***Weill, D.F. & Drake, M.J.,*** 1973, Europium anomaly in plagioclase feldspar-Experimental results and semiquantitative model, Science, 4090, 180; p. 1059-1060.

***White, A.J.R. & Chappell, B.W.,*** 1977, Ultrametamorphism and granitoid genesis, Tectonophysics, 43; p. 7-22.

***White, A.J.R., Chappell, B.W.,*** 1983, Granitoid types and their distribution in the Lachlan Fold Belt, southeastern Australia, Geol Soc Am Mem, 59; p. 21–34.

***Wiebe, R.A. & Collins, W.J.,*** 1998, Emplacement and crystallization of the Tuross Head Tonalite (Australia); evidence from tilted basal stratigraphic sections (in, Anonymous) Abstracts with Programs - Geological Society of America, 30(5); p. 70.

***Williams, J.G. & Harper, C.T.,*** 1978, Age and status of the Mackay Intrusives in the Eglinton-Upper Hollyford area, New Zealand Journal of Geology and Geophysics, 21; p. 733–742.

***Williams, I.S.,*** 1992, Some observation on the use of zircon U-Pb geochronology on the study of granitic rocks, Transactions of the Royal Society of Edinburgh, Earth Sciences, 83; p. 447-458.

***Winther, K.T. & Newton, R.C.,*** *1*991, Experimental melting of hydrous low-K tholeiite: evidence on the origin of Archean cratons, Bull Geol Soc Denmark, 39; p.213–228.

***Woodhead, J.D., Hergt, J.M., Shelley, M., Eggins, S., Kemp, R.,*** 2004, Zircon Hf-isotope analysis with an excimer laser, depth profiling, ablation of complex geometries, and concomitant age estimation, Chemical Geology, 209; p. 121–135.

***Wu, F.Y., Yang, Y.H., Xie, L.W., Yang, J.H., Xu, P.,*** 2006, Hf isotopic compositions of the standard zircons and baddeleyites used in U–Pb geochronology, Chemical Geology, 234; p. 105–126.

***Xie, L., Wang, R., Chen, X., Qiu, J., Wang, D.,*** 2005, Th rich zircon from peralkaline A-type granite: Mineralogical features and petrological implications. Chinese Science Bulletin, 50; 809-817.

***Zeck, H.P., Williams. I.S.,*** 2002, Inherited and magmatic Zircon from Neogene Hoyazo Cordierite dacite, SE Spain anatectic source rock provenance and magmatic evaluation, Journal of Petrology, 43; p.1089-1104.

***Zeitler, P.K., Meltzer, A.S., Koons, P.O., Craw, D., Hallet, B., Chamberlain, C.P., Kidd, W.S.F., Park, S.K., Seeber, L., Bishop, M., Shroder, J.,*** 2001, Erosion, Himalayan Geodynamics and Geomorphology of Metamorphism, Geological Society of America, 11(1); p. 4-9.

***Zharikov, V.A., Khodorevskaya, L.I.,*** 1996, Amphibolite melting: Compositions of partial liquids at 5–25 kbar, Trans (Doklady) Russ Acad Sci Earth Sci Sect, 344; p.66–271.

# Appendices

## *Appendix 1 – List of Samples from Mt Daniel*

| JCU Ref No | Sample ID | Rock Types |
|---|---|---|
| 74854 | MD11 | Western Fiordland Orthogneiss |
| 74855 | MD15 | Western Fiordland Orthogneiss |
| 74856 | MD16 | Western Fiordland Orthogneiss |
| 74857 | MD18 | Western Fiordland Orthogneiss |
| 74858 | MD19 | Western Fiordland Orthogneiss |
| 74859 | MD20 | Western Fiordland Orthogneiss |
| 74860 | MD21 | Western Fiordland Orthogneiss |
| 74861 | MD23 | Western Fiordland Orthogneiss |
| 74862 | MD10B | Mafic Dyke |
| 74863 | MD13 | Mafic Dyke |
| 74864 | MD22B | Mafic Dyke |
| 74865 | MD26 | Mafic Dyke |
| 74866 | MD36 | Mafic Dyke |
| 74867 | MD8 | Low-Na Intermediate dyke |
| 74868 | MD22A | Low-Na Intermediate dyke |
| 74869 | MD10C | Hi-Na Intermediate Dyke (Trondhjemite variety) |
| 74870 | MD17A | Hi-Na Intermediate Dyke (Trondhjemite variety) |
| 74871 | MD17B | Hi-Na Intermediate Dyke (Trondhjemite variety) |
| 74872 | MD25 | Hi-Na Intermediate Dyke (Trondhjemite variety) |
| 74873 | MD32 | Hi-Na Intermediate Dyke (Trondhjemite variety) |
| 74874 | MD34 | Hi-Na Intermediate Dyke (Trondhjemite variety) |
| 74875 | MD2 | Granite |
| 74876 | MD3 | Granite |
| 74877 | MD4 | Granite |
| 74878 | MD5 | Granite |
| 74879 | MD6 | Granite |
| 74880 | MD28 | Granite |
| 74881 | MD29 | Granite |
| 74882 | MD30 | Granite |
| 74883 | MD33 | Granite |
| 74884 | MD7 | Mt Daniel Sheet (MDS) |
| 74885 | MD9 | Mt Daniel Sheet (MDS) |
| 74886 | MD10A | Mt Daniel Sheet (MDS) |
| 74887 | MD14 | Mt Daniel Sheet (MDS) |
| 74888 | MD24 | Mt Daniel Sheet (MDS) |
| 74889 | MD27 | Mt Daniel Sheet (MDS) |
| 74890 | MD31 | Mt Daniel Sheet (MDS) |
| 74891 | MD35 | Mt Daniel Sheet (MDS) |
| 74892 | MD35B | Mt Daniel Sheet (MDS) |
| 74893 | MD37 | Mt Daniel Sheet (MDS) |
| 74894 | MD38 | Mt Daniel Sheet (MDS) |
| 74895 | MD39 | Mt Daniel Sheet (MDS) |
| 74896 | MD40 | Mt Daniel Sheet (MDS) |

# *Appendix 2: Whole Rock Geochemistry of Mt Daniel Rocks*

## *Appendix 2.1. Major and Trace Element of Mt Daniel Rocks*

| | MD11 | MD15 | MD16 | MD18 | MD19 | MD20 | MD21 | MD23 | MD10B | MD13 | MD22B | MD26 | MD36 |
|---|---|---|---|---|---|---|---|---|---|---|---|---|---|
| SiO2 | 43.1 | 57.92 | 43.72 | 55.18 | 52.97 | 45.98 | 53.27 | 58.07 | 47 | 43.7 | 43.89 | 43.48 | 43.73 |
| TiO2 | 1.73 | 1.09 | 1.78 | 1.16 | 1.27 | 1.41 | 1.3 | 1.02 | 1.52 | 3.17 | 2.81 | 3.01 | 2.9 |
| Al2O3 | 18.5 | 17.54 | 18.3 | 17.17 | 17.31 | 9.18 | 17.48 | 16.73 | 17.66 | 16 | 15.77 | 15.59 | 15.63 |
| Fe2O3 | 13.6 | 6.53 | 12.96 | 7.28 | 8.26 | 11.65 | 8.17 | 6.33 | 10.98 | 15.7 | 14.87 | 15.43 | 15.08 |
| MnO | 0.11 | 0.09 | 0.1 | 0.1 | 0.11 | 0.15 | 0.11 | 0.08 | 0.17 | 0.24 | 0.21 | 0.22 | 0.21 |
| MgO | 5.88 | 3.72 | 5.42 | 4.65 | 5.21 | 17.68 | 4.98 | 4.01 | 7.37 | 7.16 | 7.4 | 7.56 | 7.51 |
| CaO | 11.4 | 5.51 | 10.47 | 6.47 | 7.8 | 7.8 | 7.4 | 5.62 | 9.56 | 9.29 | 9.81 | 8.82 | 9.35 |
| Na2O | 2.62 | 4.5 | 3.54 | 4.67 | 4.56 | 1.92 | 4.54 | 5.03 | 2.9 | 2.6 | 2.43 | 2.67 | 2.56 |
| K2O | 0.67 | 2.26 | 0.93 | 1.8 | 1.1 | 1.02 | 1.21 | 1.75 | 1.22 | 0.93 | 0.7 | 1.36 | 1.23 |
| P2O5 | 1.55 | 0.37 | 1.48 | 0.37 | 0.46 | 0.13 | 0.45 | 0.31 | 0.35 | 0.68 | 0.71 | 0.62 | 0.64 |
| SO3 | 0.06 | <0.002 | 0.19 | 0.02 | 0.04 | 0.12 | 0.02 | 0.01 | 0.01 | 0.05 | 0.05 | 0.03 | 0.06 |
| LOF | 0.97 | 0.8 | 1.11 | 0.66 | 0.42 | 2.52 | 0.57 | 0.56 | 1.61 | 0.59 | 0.96 | 0.8 | 0.7 |
| Total | 100.35 | 100.36 | 100.08 | 99.52 | 99.51 | 99.55 | 99.51 | 99.53 | 100.58 | 100.27 | 99.61 | 99.58 | 99.59 |
| P | - | - | - | 2400 | 2932 | 462 | 2911 | 1920 | - | - | 4886 | 3884 | 3825 |
| S | - | - | - | <4.8 | <4.8 | <6.5 | <5.4 | <5.2 | - | - | 9.6 | <5.9 | <5.6 |
| Cl | 240 | 84 | 329 | 240.8 | 131.6 | 250.1 | 170.9 | 152.6 | 148 | 454.5 | 217.3 | 580.2 | 519.1 |
| Sc | - | - | - | 16.9 | 27.8 | > 38.0 | > 29.7 | 14.4 | - | - | > 68 | > 59 | > 67 |
| Ti | - | - | - | 6556 | 6271 | 7171 | 6529 | 5547 | - | - | 13280 | 14330 | 13590 |
| V | 352 | 151 | 331.5 | 174.8 | 176.3 | 173.7 | 179 | 131.7 | 217 | 250 | 267.9 | 246.9 | 225.2 |
| Cr | 42.5 | 120.5 | 35.5 | 134.5 | 123.3 | 851.3 | 118.7 | 125.3 | 110.5 | 154.5 | 195.4 | 155.5 | 154.8 |
| Mn | - | - | - | 743.7 | 827.1 | 1111 | 813.2 | 626.7 | | | 1715 | 1709 | 1684 |
| Co | 59.5 | 35.5 | 43 | 50.3 | 47.8 | 93.3 | 42.9 | 49.1 | 50.5 | 54 | 42.3 | 49.7 | 28.6 |
| Ni | 48.5 | 60 | 39 | 68.1 | 70 | 537.8 | 68.1 | 61.4 | 129 | 74.5 | 82.7 | 92 | 77.4 |
| Cu | 74 | 41 | 84 | 82.1 | 82.1 | 27.8 | 77.3 | 11.6 | 4 | 40.5 | 56.1 | 20.3 | 12.3 |
| Zn | 122 | 88 | 121.5 | 85.8 | 92.5 | 110.5 | 96.7 | 75.4 | 147 | 142.5 | 139.6 | 137.8 | 133.4 |
| Ga | 25.5 | 22 | 24.5 | 21.8 | 21.9 | 15 | 22 | 20.9 | 19 | 22 | 22.5 | 23.4 | 22 |
| Ge | - | - | - | 0.5 | 0.5 | 0.5 | <0.6 | 0.7 | - | - | 0.7 | 0.6 | <0.6 |
| As | - | - | - | <0.4 | <0.4 | <0.3 | <0.4 | <0.4 | - | - | <0.4 | 2.1 | 1.8 |
| Se | - | - | - | 0.4 | 0.7 | <0.2 | 0.4 | 0.4 | - | - | 0.5 | <0.3 | <0.3 |
| Br | - | - | - | 0.7 | 0.4 | 0.2 | 0.9 | 0.9 | - | - | 0.5 | <0.2 | <0.2 |
| Rb | 12 | 61.5 | 22 | 32.4 | 17.6 | 21.4 | 18.4 | 40.9 | 21 | 29 | 9.2 | 53.6 | 30.4 |
| Sr | 1915 | 1009.5 | 1829.5 | 1258 | 1556 | 289.9 | 1437 | 1206 | 528 | 426.5 | 485.1 | 411.2 | 346.9 |
| Y | 18 | 18 | 22 | 11.7 | 10.8 | 13.5 | 12.1 | 11.9 | 25 | 44.5 | 44.3 | 42.5 | 41.4 |
| Zr | 73 | 312 | 100.5 | 116.2 | 48.7 | 65.5 | 46.1 | 152.8 | 136.5 | 248.5 | 195.8 | 217 | 231.6 |
| Nb | 9 | 11 | 10 | 5.8 | 4.6 | 4.7 | 4.3 | 7 | 14.5 | 24.5 | 12.4 | 10 | 10 |
| Mo | - | - | - | <1 | <1 | 0.5 | <1 | <1 | - | - | 1.3 | 1.1 | 2.1 |
| Ag | - | - | - | <0.6 | <0.6 | <0.6 | <0.6 | <0.6 | - | - | <0.6 | <0.6 | <0.6 |
| Cd | - | - | - | <0.5 | 0.3 | <0.5 | 0.3 | 0.3 | - | - | 0.4 | 0.4 | 0.5 |
| In | - | - | - | <0.7 | <0.7 | <0.7 | <0.7 | <0.7 | - | - | <0.7 | <0.7 | <0.7 |
| Sn | - | - | - | 1.8 | 1.6 | 1.7 | 1.5 | 2.2 | - | - | 2 | 2.2 | 2.6 |
| Sb | - | - | - | <1.5 | <1.5 | <1.5 | <1.5 | <1.5 | - | - | <1.5 | <1.5 | <1.5 |
| Te | - | - | - | <1.5 | <1.5 | <1.5 | <1.5 | <1.5 | - | - | <1.5 | <1.5 | <1.5 |
| I | - | - | - | <1.5 | <1.5 | <1.5 | <1.5 | <1.5 | - | - | <1.5 | <1.5 | <1.5 |
| Cs | - | - | - | 1.8 | <1.5 | <1.5 | <1.5 | 0.9 | - | - | <1.5 | 2.2 | <1.5 |
| Ba | 352.5 | 717.5 | 545 | 783.9 | 663.8 | 279.6 | 914.8 | 846.7 | 361 | 248 | 253.4 | 380.3 | 300.7 |
| La | 38 | 30.5 | 30 | 20.9 | 17.6 | 6.8 | 18.4 | 17.2 | 21 | 19.5 | 17.5 | 15.4 | 15.7 |
| Ce | 33.5 | 40 | 32 | 45.2 | 40.6 | 26.4 | 43.6 | 43.8 | 23.5 | 33.5 | 55.1 | 45.6 | 50.9 |
| Pr | - | - | - | <5 | <5 | <5 | <5 | <5 | - | - | <5 | <5 | <5 |
| Nd | - | - | - | 24.3 | 31 | 15.3 | 23.7 | 18.4 | - | - | 34.7 | 23 | 38.2 |
| Hf | 10 | 11.5 | 11.5 | 5.3 | 4.8 | 3 | 5.2 | 5.2 | 6 | 7 | 8.1 | 6.3 | 6.6 |
| Ta | - | - | - | <5.2 | <5.3 | <5 | <5.2 | <3.1 | - | - | <5.5 | <4.4 | <4.1 |
| W | - | - | - | 143.6 | 103.1 | 26.4 | 125.7 | 165.3 | - | - | 74.7 | 54.7 | 66.5 |
| Hg | - | - | - | <0.2 | <0.2 | <0.2 | <0.2 | <0.2 | - | - | <0.3 | <0.2 | <0.2 |
| Tl | - | - | - | 2.2 | 2.1 | 1 | 2.3 | 2.3 | - | - | 2.2 | 1.2 | 1 |
| Pb | 9 | 14.5 | 7 | 13.4 | 11.3 | 2.9 | 11.6 | 13.4 | 8 | 7.5 | 5.5 | 4.4 | 8 |
| Bi | - | - | - | 1.1 | 1.4 | <0.3 | 0.8 | 1 | - | - | 1.2 | <0.4 | <0.4 |
| Th | 10 | 11.5 | 10 | <1.5 | <1.5 | <1.5 | <1.5 | <1.5 | 8.5 | 6.5 | <1.5 | 1.1 | <1.5 |
| U | - | - | - | <1.5 | <1.5 | 1 | <1.5 | <1.5 | - | - | <1.5 | 1.1 | 1.3 |

| | MD8 | MD22A | MD10C | MD17A | MD17B | MD25 | MD32 | MD34 | MD2 | MD3 | MD4 | MD5 |
|---|---|---|---|---|---|---|---|---|---|---|---|---|
| **SiO2** | 53.3 | 54.74 | 59.02 | 56.35 | 60.93 | 57.61 | 57.34 | 56.56 | 74.53 | 73.1 | 71.65 | 60.94 |
| **TiO2** | 1.45 | 0.89 | 0.59 | 0.76 | 0.14 | 1.12 | 0.85 | 1 | 0.21 | 0.26 | 0.34 | 0.93 |
| **Al2O3** | 16.7 | 19.76 | 22.43 | 20.74 | 22.73 | 20.76 | 21.43 | 21.72 | 13.88 | 14.4 | 15.27 | 17.97 |
| **Fe2O3** | 9.98 | 8.07 | 2.86 | 3.93 | 0.98 | 4.19 | 3.73 | 4.17 | 2.06 | 2.6 | 2.76 | 6.78 |
| **MnO** | 0.17 | 0.16 | 0.03 | 0.04 | 0.01 | 0.03 | 0.05 | 0.05 | 0.05 | 0.07 | 0.05 | 0.19 |
| **MgO** | 4.17 | 2.17 | 0.74 | 1.98 | 0.38 | 1.04 | 0.9 | 1.25 | 0.2 | 0.3 | 0.57 | 1.14 |
| **CaO** | 7.71 | 5.56 | 5.48 | 5.17 | 4.28 | 5.51 | 5.75 | 6.13 | 0.69 | 1.78 | 2.1 | 4.22 |
| **Na2O** | 4.43 | 5.71 | 8.04 | 7.26 | 8.66 | 7.76 | 7.19 | 6.99 | 3.68 | 4.42 | 5.08 | 5.75 |
| **K2O** | 1.22 | 1.09 | 0.64 | 1.7 | 0.84 | 0.6 | 1.24 | 0.71 | 4.47 | 2.97 | 2.29 | 1.63 |
| **P2O5** | 0.48 | 0.34 | 0.24 | 0.59 | 0.09 | 0.26 | 0.2 | 0.2 | 0.04 | 0.06 | 0.08 | 0.25 |
| **SO3** | 0.08 | 0.02 | 0.06 | 0.04 | 0.01 | 0.05 | 0.06 | 0.08 | <0.002 | 0.02 | 0.04 | 0.01 |
| **LOF** | 0.48 | 1.13 | 0.59 | 0.77 | 0.45 | 0.48 | 0.71 | 0.7 | 0.47 | 0.29 | 0.46 | 0.59 |
| **Total** | 100.24 | 99.64 | 100.74 | 99.33 | 99.51 | 99.4 | 99.45 | 99.54 | 100.43 | 99.97 | 100.6 | 100.47 |
| **P** | - | 2195 | - | 3698 | 861 | 1839 | 1299 | 1330 | - | - | - | - |
| **S** | - | <5.1 | - | 57.3 | <4.6 | <4.9 | 10.6 | <4.6 | - | - | - | - |
| **Cl** | 262 | 63.3 | - | 144.5 | 9.1 | 111.9 | 52.1 | 81.5 | - | - | 42.5 | 106 |
| **Sc** | - | 24.1 | - | 13.7 | <12 | 18.6 | 24.6 | 27.9 | - | - | - | - |
| **Ti** | - | 4390 | - | 4156 | 821 | 5227 | 4698 | 4675 | - | - | - | - |
| **V** | 196.5 | 70.9 | 37.5 | 66 | 9.1 | 55.5 | 57.9 | 42.4 | 4.5 | 12.5 | 28 | 21.5 |
| **Cr** | 76.5 | 8.6 | 14.5 | 8.2 | 1.1 | 2.1 | 4.5 | 0.7 | 11 | 19 | 13.5 | 12 |
| **Mn** | - | 1129 | - | 286.9 | 71.2 | 229.2 | 350.8 | 300.8 | | - | - | - |
| **Co** | 41.5 | 19.7 | 50.5 | 40.1 | 38.4 | 39.7 | 37.6 | 39.3 | 42 | 81.5 | 33.5 | 37.5 |
| **Ni** | 16 | 8.1 | <3 | 15.8 | 5.8 | 11.2 | 7.2 | 5.9 | <3 | <3 | <3 | <3 |
| **Cu** | 18.5 | 25 | - | > 302.7 | 4.2 | 110 | 41.6 | 20.2 | | 10 | 46 | 5 |
| **Zn** | 181.5 | 116.6 | 33.5 | 47.8 | 9 | 25.8 | 42.8 | 42.5 | 44 | 55 | 47.5 | 84.5 |
| **Ga** | 22 | 24.9 | 19 | 20.4 | 18 | 19.8 | 19 | 18.3 | 17.5 | 18.5 | 17 | 23 |
| **Ge** | - | 0.9 | - | 1.3 | 1.1 | 1 | 1 | 0.4 | - | - | - | - |
| **As** | - | <0.4 | - | 1 | <0.4 | 0.5 | 1.1 | 0.6 | - | - | - | - |
| **Se** | - | 0.4 | - | 1.2 | 1.3 | 1.8 | 1.4 | 0.8 | - | - | - | - |
| **Br** | - | 0.5 | - | 0.8 | 0.9 | 1.3 | 1.3 | 0.8 | - | - | - | - |
| **Rb** | 20 | 15.4 | 9 | 38.2 | 14 | 12.1 | 20 | 13.5 | 77 | 75.5 | 44.5 | 49.5 |
| **Sr** | 553 | 756.5 | 1904 | 1888 | 2269 | 2469 | 1854 | 1771 | 102.5 | 222 | 458.5 | 501.5 |
| **Y** | 33.5 | 26 | 7.5 | 8.4 | <0.5 | 6 | 12.4 | 7.1 | 27.5 | 17.5 | 9.5 | 38 |
| **Zr** | 168 | 256.9 | 281.5 | 1018 | 90.8 | 615 | 573.4 | 335.2 | 243 | 217.5 | 194.5 | 851.5 |
| **Nb** | 16.5 | 7.6 | - | 0.6 | 0.5 | 1.3 | 2.7 | 1.5 | 5.5 | 6 | | 16.5 |
| **Mo** | - | 0.5 | - | 0.8 | <1 | <1 | <1 | <1 | - | - | - | - |
| **Ag** | - | <0.6 | - | <0.6 | <0.6 | <0.6 | <0.6 | <0.6 | - | - | - | - |
| **Cd** | - | 0.4 | - | <0.5 | <0.5 | 0.3 | 0.4 | <0.5 | - | - | - | - |
| **In** | - | <0.7 | - | <0.7 | <0.7 | <0.7 | <0.7 | <0.7 | - | - | - | - |
| **Sn** | - | 1.4 | - | 1.4 | <1 | 1.7 | 1.6 | 1.4 | - | - | - | - |
| **Sb** | - | <1.5 | - | <1.5 | <1.5 | <1.5 | <1.5 | <1.5 | - | - | - | - |
| **Te** | - | <1.5 | - | <1.5 | <1.5 | <1.5 | <1.5 | <1.5 | - | - | - | - |
| **I** | - | <1.5 | - | <1.5 | 1.2 | <1.5 | <1.5 | <1.5 | - | - | - | - |
| **Cs** | - | <1.5 | - | 3.5 | 2.7 | <1.5 | 1.7 | <1.5 | - | - | - | - |
| **Ba** | 406 | 539.3 | 297.5 | 899.9 | 704.4 | 333.3 | 364.9 | 274.2 | 873.5 | 941.5 | 976 | 856 |
| **La** | 15.5 | 19.1 | - | 15.4 | 6.3 | 6.3 | 76.3 | 6.1 | 47 | 39 | 43.5 | 37 |
| **Ce** | 39.5 | 45 | - | 30.9 | 11.1 | 14.2 | 131.9 | 13.5 | 53 | 65 | 61.5 | 54.5 |
| **Pr** | - | <5 | - | 5.9 | <5 | <5 | 15.1 | <5 | - | - | - | - |
| **Nd** | - | 22.7 | - | 25.5 | <5 | <5 | 50.2 | 12.4 | - | - | - | - |
| **Hf** | 7 | 8.1 | 11 | 18.8 | 5.3 | 16.9 | 13 | 8.5 | 6 | 6 | 7 | 17 |
| **Ta** | - | <3.5 | - | <8.4 | 2.6 | <5.7 | <3.8 | <3.1 | - | - | - | - |
| **W** | - | 111.2 | - | 133.6 | 236 | 130.7 | 161.7 | 158.3 | - | - | - | - |
| **Hg** | - | <0.2 | - | <0.2 | > 0.2 | > 0.4 | <0.2 | <0.2 | - | - | - | - |
| **Tl** | - | 1.6 | - | 2.5 | 2.6 | 4.3 | 3.2 | 1.8 | - | - | - | - |
| **Pb** | 8 | 8.8 | 9 | 16.9 | 14.3 | 18.9 | 17.9 | 9.4 | 12 | 33.5 | 12.5 | 15.5 |
| **Bi** | - | 0.7 | - | 1.2 | 1.4 | 3 | 1.8 | 0.9 | - | - | - | - |
| **Th** | 8.5 | <1.5 | 13 | <1.5 | <1.5 | <1.5 | 6.6 | <1.5 | 15.5 | 16.5 | 11 | 15 |
| **U** | - | <1.5 | - | <1.5 | <1.5 | <1.5 | <1.5 | <1.5 | | | | |

| | MD6 | MD28 | MD29 | MD30 | MD33 | MD7 | MD9 | MD10A | MD14 | MD24 | MD27 | MD31 |
|---|---|---|---|---|---|---|---|---|---|---|---|---|
| **SiO2** | 75.18 | 75.99 | 66.89 | 71.66 | 68.68 | 56.98 | 60.7 | 55.5 | 56.1 | 58.08 | 59.09 | 58.25 |
| **TiO2** | 0.19 | 0.19 | 0.41 | 0.25 | 0.45 | 1.2 | 0.75 | 1.56 | 1.06 | 0.81 | 0.85 | 1.14 |
| **Al2O3** | 12.94 | 12.66 | 16.64 | 14.52 | 15.25 | 19.34 | 28.8 | 18.3 | 20.3 | 19.46 | 18.33 | 17.71 |
| **Fe2O3** | 1.91 | 1.64 | 3.56 | 2.94 | 4.46 | 7.48 | 6.41 | 9.01 | 8.06 | 7.49 | 7.81 | 7.82 |
| **MnO** | 0.04 | 0.03 | 0.08 | 0.08 | 0.09 | 0.2 | 0.16 | 0.22 | 0.24 | 0.22 | 0.23 | 0.22 |
| **MgO** | 0.16 | 0.29 | 0.96 | 0.29 | 0.74 | 1.61 | 1.34 | 2.47 | 1.41 | 0.98 | 1.1 | 1.73 |
| **CaO** | 0.96 | 1.09 | 3.3 | 1.52 | 3.26 | 5.48 | 4.26 | 6.46 | 5.29 | 4.87 | 4.59 | 5.16 |
| **Na2O** | 2.91 | 3.34 | 5.34 | 3.98 | 3.7 | 6.26 | 5.94 | 4.96 | 6.29 | 6.16 | 5.67 | 5.62 |
| **K2O** | 5.06 | 4.08 | 1.69 | 3.79 | 2.11 | 1.31 | 1.37 | 0.93 | 1 | 0.96 | 1.08 | 0.89 |
| **P2O5** | 0.02 | 0.05 | 0.13 | 0.05 | 0.12 | 0.35 | 0.23 | 0.57 | 0.3 | 0.17 | 0.2 | 0.35 |
| **SO3** | <0.002 | 0.01 | 0.02 | 0.02 | 0.01 | 0 | 0.03 | 0 | 0 | 0.02 | 0.02 | 0.02 |
| **LOF** | 0.32 | 0.34 | 0.64 | 0.49 | 0.77 | 0.48 | 0.74 | 0.42 | 0.77 | 0.36 | 0.59 | 0.71 |
| **Total** | 99.66 | 99.71 | 99.65 | 99.58 | 99.65 | 100.36 | 100.61 | 100.6 | 100.73 | 99.58 | 99.56 | 99.61 |
| **P** | - | 258.6 | 1043 | 265 | 647 | - | - | - | - | 1338 | 1441 | 2255 |
| **S** | - | <3.5 | <4.5 | <4.2 | <4.2 | - | - | - | - | <5 | <5.1 | <5.5 |
| **Cl** | | 43.4 | 119.2 | 114.1 | 98.9 | 134 | | 60.5 | 24 | 38.1 | 42 | 98 |
| **Sc** | - | <5.8 | <10 | <7.5 | <11 | - | - | - | - | 33.2 | 20.8 | > 37.4 |
| **Ti** | - | 1089 | 2339 | 1497 | 2739 | - | - | - | - | 4104 | 4854 | 6367 |
| **V** | 3 | 7.6 | 27.9 | 14.8 | 30.9 | 51 | 47.5 | 65 | 16.5 | 11.7 | 5.6 | 20.9 |
| **Cr** | - | 0.7 | 4.3 | 5.1 | 8.6 | 14 | 16 | 14 | 22.5 | 1.6 | 3.9 | 4 |
| **Mn** | - | 208.7 | 574.4 | 601 | 657.2 | - | - | - | - | 1561 | 1604 | 1590 |
| **Co** | 75.5 | 35.2 | 30.3 | 67 | 63 | 40 | 28 | 33 | 22.5 | 28.4 | 27.2 | 29.2 |
| **Ni** | <3 | 4.9 | 6.6 | 7.1 | 7.9 | <3 | <3 | <3 | <3 | 6.8 | 6.6 | 8.9 |
| **Cu** | | 11.3 | 7.7 | 11 | 3.2 | 3 | 13.5 | 27.5 | 7 | 25.9 | 44 | 22.6 |
| **Zn** | 23.5 | 25.9 | 68.3 | 67.1 | 60.3 | 114 | 85.5 | 132 | 102 | 78.2 | 99.1 | 109.8 |
| **Ga** | 16 | 14.4 | 19.4 | 21.1 | 20.7 | 22 | 21 | 22.5 | 23 | 22.7 | 23.5 | 22.2 |
| **Ge** | - | 1 | 1.2 | 1.1 | 1.6 | - | - | - | - | 0.5 | 1.5 | 0.8 |
| **As** | - | <0.3 | 0.8 | 0.6 | 0.9 | - | - | - | - | <0.4 | 0.5 | <0.4 |
| **Se** | - | <0.3 | 0.4 | 0.3 | 0.7 | - | - | - | - | 0.3 | 1.1 | 0.4 |
| **Br** | - | 0.2 | 0.5 | 0.4 | 1 | - | - | - | - | 0.2 | 0.8 | 0.2 |
| **Rb** | 86 | 60.1 | 37.6 | 73.4 | 53.6 | 23 | 22 | 12.5 | 12 | 5.5 | 8.6 | 7.5 |
| **Sr** | 236 | 164.4 | 715.3 | 208.7 | 382 | 642.5 | 580.5 | 745.5 | 835 | 901.7 | 649.9 | 657.1 |
| **Y** | 14.5 | 6.5 | 19 | 28.5 | 20.9 | 25.5 | 17 | 38.5 | 23.5 | 18.2 | 25.4 | 29.7 |
| **Zr** | 240 | 97.3 | 164.8 | 289.5 | 193.8 | | 513.5 | 230 | 676 | 594.8 | 662.8 | 370.7 |
| **Nb** | | 3.5 | 5.1 | 8.1 | 5 | 20.5 | 7.5 | 21.5 | 9.5 | 4.4 | 7.1 | 12.1 |
| **Mo** | - | <1 | <1 | 0.8 | 0.7 | - | - | - | - | <1 | 0.7 | 0.5 |
| **Ag** | - | <0.6 | <0.6 | <0.6 | <0.6 | - | - | - | - | <0.6 | <0.6 | <0.6 |
| **Cd** | - | <0.5 | <0.5 | 0.4 | 0.3 | - | - | - | - | <0.5 | 0.4 | <0.5 |
| **In** | - | <0.7 | <0.7 | <0.7 | <0.7 | - | - | - | - | <0.7 | <0.7 | <0.7 |
| **Sn** | - | 0.9 | 1.8 | 2.9 | 1.8 | - | - | - | - | 1.5 | 1.4 | 1 |
| **Sb** | - | <1.5 | <1.5 | <1.5 | <1.5 | - | - | - | - | <1.5 | <1.5 | <1.5 |
| **Te** | - | <1.5 | <1.5 | 1.8 | <1.5 | - | - | - | - | <1.5 | <1.5 | <1.5 |
| **I** | - | 2.5 | 1.1 | 2.4 | <1.5 | - | - | - | - | <1.5 | <1.5 | <1.5 |
| **Cs** | - | 5.5 | 5.5 | 5.6 | 1.9 | - | - | - | - | <1.5 | 1.3 | <1.5 |
| **Ba** | 1883.5 | 872.4 | 754.8 | 1401 | 699.4 | 606 | 1033 | 366.5 | 527.5 | 664.2 | 972.2 | 590.2 |
| **La** | 81.5 | 32.2 | 34 | 41 | 39.9 | 20.5 | 30 | 40.5 | 24.5 | 21 | 23.2 | 28 |
| **Ce** | 118 | 48.9 | 51.9 | 69.9 | 74.4 | 37.5 | 64 | 52 | 44 | 37.9 | 42.8 | 60 |
| **Pr** | - | 18.6 | 8.4 | 13.2 | 7.1 | - | - | - | - | <5 | 9.2 | <5 |
| **Nd** | - | 24.5 | 26.5 | 35.8 | 32.7 | - | - | - | - | 21.4 | 30.6 | 35.9 |
| **Hf** | 7 | 4.1 | 4.7 | 8.7 | 6.1 | 12.5 | 13 | 8.5 | 15 | 12.3 | 14 | 9.2 |
| **Ta** | - | <2.4 | <2.6 | <2.8 | 2.2 | - | - | - | - | <3.5 | <4 | <3.4 |
| **W** | - | 287.8 | 245.1 | > 472.3 | 459.2 | - | - | - | - | 158.5 | 208.2 | 243.6 |
| **Hg** | - | <0.2 | <0.3 | <0.3 | <0.3 | - | - | - | - | <0.2 | <0.3 | <0.3 |
| **Tl** | - | 1.4 | 2 | 1.9 | 3.2 | - | - | - | - | 1.5 | 2.6 | 1.6 |
| **Pb** | 18 | 15.2 | 12.8 | 26.8 | 14.5 | 12 | 10.5 | 10.5 | 9 | 10.5 | 11.1 | 8.9 |
| **Bi** | - | 0.6 | 0.7 | 0.9 | 1.5 | - | - | - | - | 0.9 | 1.3 | 0.5 |
| **Th** | 15.5 | 5.3 | <1.5 | 12 | 11.3 | 8.5 | 6 | 7 | 8.5 | <1.5 | 2.1 | 1.7 |
| **U** | | <1.5 | <1.5 | <1.5 | <1.5 | - | - | - | - | <1.5 | <1.5 | <1.5 |

| | MD35 | MD35B | MD37 | MD38 | MD39 | MD40 |
|---|---|---|---|---|---|---|
| **SiO2** | 56 | 53.11 | 60.73 | 57.12 | 60.62 | 53.66 |
| **TiO2** | 1.06 | 1.67 | 0.75 | 1.09 | 0.76 | 1.54 |
| **Al2O3** | 19.89 | 16.84 | 18.44 | 18.78 | 18.12 | 18.79 |
| **Fe2O3** | 8.23 | 11.74 | 6.58 | 8.13 | 7.47 | 9.15 |
| **MnO** | 0.18 | 0.33 | 0.17 | 0.22 | 0.15 | 0.22 |
| **MgO** | 1.25 | 2.77 | 0.96 | 1.47 | 1.18 | 2.5 |
| **CaO** | 5.08 | 6.76 | 4.26 | 5.41 | 4.01 | 6.81 |
| **Na2O** | 6.47 | 4.49 | 5.25 | 5.77 | 5.09 | 5.15 |
| **K2O** | 0.74 | 0.72 | 1.58 | 0.72 | 1.36 | 0.65 |
| **P2O5** | 0.23 | 0.79 | 0.16 | 0.3 | 0.06 | 0.49 |
| **SO3** | 0.02 | 0.02 | 0.01 | 0.01 | 0.02 | 0.03 |
| **LOF** | 0.43 | 0.41 | 0.7 | 0.58 | 0.74 | 0.64 |
| **Total** | 99.58 | 99.65 | 99.6 | 99.59 | 99.59 | 99.62 |
| **P** | 1786 | 5165 | 1136 | 1940 | 676 | 3252 |
| **S** | <5.3 | <5.8 | <5.2 | <5.2 | <4.7 | <5.3 |
| **Cl** | 93.7 | 199.4 | 65.8 | 56.6 | 119.4 | 138.2 |
| **Sc** | 18.4 | > 52.7 | 19.1 | 32.2 | 14.7 | > 46.2 |
| **Ti** | 5374 | 8351 | 4223 | 5485 | 4378 | 7128 |
| **V** | 21.3 | 63.8 | 21.9 | 15.8 | 30.3 | 47.7 |
| **Cr** | 3.4 | <1.5 | 2.9 | 1.9 | 5.2 | 5.1 |
| **Mn** | 1263 | 2415 | 1171 | 1505 | 1131 | 1474 |
| **Co** | 35.8 | 21.7 | 27 | 23.3 | 40.7 | 17.1 |
| **Ni** | 6.7 | 9.4 | 7.2 | 7.8 | 10.4 | 7.9 |
| **Cu** | 13.8 | 13.1 | 3.6 | 10.1 | 16.5 | 29.9 |
| **Zn** | 86.9 | 166.7 | 91.3 | 96.8 | 98.9 | 121 |
| **Ga** | 25.3 | 23.5 | 22.1 | 23.4 | 28.2 | 23.5 |
| **Ge** | 1 | 0.4 | 0.8 | 0.9 | 1.8 | 0.4 |
| **As** | <0.4 | <0.4 | <0.4 | <0.4 | 1.8 | <0.4 |
| **Se** | 0.6 | <0.3 | 0.4 | <0.3 | 1.1 | <0.3 |
| **Br** | 0.9 | 0.3 | 0.6 | 0.2 | 0.8 | 0.3 |
| **Rb** | 5.9 | 3.6 | 20.6 | 8.9 | 35.6 | 6.8 |
| **Sr** | 804 | 562.1 | 563.9 | 810.8 | 441.1 | 814.2 |
| **Y** | 19.9 | 53.8 | 20 | 20.9 | 54.6 | 25.9 |
| **Zr** | 615.3 | 84.8 | 550.7 | 573.1 | 694.5 | 178.1 |
| **Nb** | 48.7 | 16.3 | 6.8 | 6.4 | 7.1 | 10.8 |
| **Mo** | <1 | <1 | 0.6 | 0.8 | 2.2 | <1 |
| **Ag** | <0.6 | <0.6 | <0.6 | <0.6 | <0.6 | <0.6 |
| **Cd** | 0.4 | 0.5 | <0.5 | <0.5 | 0.6 | <0.5 |
| **In** | <0.7 | <0.7 | <0.7 | <0.7 | <0.7 | <0.7 |
| **Sn** | 1.6 | 2 | 1.1 | 1.5 | 3.6 | 1.2 |
| **Sb** | <1.5 | <1.5 | <1.5 | <1.5 | <1.5 | <1.5 |
| **Te** | <1.5 | <1.5 | <1.5 | <1.5 | <1.5 | <1.5 |
| **I** | <1.5 | <1.5 | <1.5 | <1.5 | <1.5 | <1.5 |
| **Cs** | <1.5 | <1.5 | <1.5 | <1.5 | <1.5 | <1.5 |
| **Ba** | 503.9 | 447 | 822 | 520.2 | 633.9 | 447.2 |
| **La** | 25.2 | 45.6 | 24.7 | 28.4 | 65.3 | 25.7 |
| **Ce** | 50.3 | 106.9 | 49 | 55.6 | 146.2 | 59.5 |
| **Pr** | <5 | 6.5 | <5 | <5 | 14.2 | <5 |
| **Nd** | 24.1 | 70.9 | 24.4 | 30.2 | 74.7 | 34.9 |
| **Hf** | 13.9 | 5.3 | 10.9 | 12.4 | 17.4 | 5.9 |
| **Ta** | <3.1 | <3.5 | <2.6 | <3 | 5 | <3.8 |
| **W** | 175.8 | 173.1 | 196.7 | 163.7 | 232.3 | 112.9 |
| **Hg** | <0.3 | <0.3 | <0.3 | <0.3 | <0.3 | <0.2 |
| **Tl** | 2.6 | 0.9 | 2.2 | 1.4 | 3.3 | 1.3 |
| **Pb** | 10.2 | 8.6 | 12.9 | 8 | 18.9 | 9.8 |
| **Bi** | 1.1 | <0.4 | 0.8 | 0.7 | 1.6 | <0.3 |
| **Th** | 1.1 | <1.5 | 2.7 | <1.5 | 30.4 | <1.5 |
| **U** | <1.5 | <1.5 | <1.5 | <1.5 | <1.5 | <1.5 |

## *Appendix 2.2. Whole Rock REE of selected samples from Mt Daniel Rocks*

| | MD15 | MD-16 | MD22B | MD26 | MD13 | MD8 | MD22A | MD17A | MD32 |
|---|---|---|---|---|---|---|---|---|---|
| La | 25.3 | 32.7 | 20.8 | 19 | 19.2 | 23.4 | 19.3 | 11.7 | 55.4 |
| Ce | 55.9 | 84.2 | 54.5 | 48 | 48.5 | 53.4 | 42.9 | 27.6 | 112 |
| Pr | 6.96 | 10.4 | 7.85 | 6.92 | 7.15 | 7.11 | 5.6 | 3.49 | 11.6 |
| Nd | 28.1 | 45.1 | 36.6 | 32.3 | 33 | 30.8 | 25 | 14.8 | 40.3 |
| Sm | 5.13 | 8.51 | 8.48 | 7.59 | 7.73 | 6.67 | 5.37 | 2.28 | 5.35 |
| Eu | 1.23 | 2.21 | 2.61 | 2.46 | 2.51 | 2.02 | 1.85 | 0.717 | 1.12 |
| Gd | 4.17 | 6.92 | 8.81 | 7.92 | 8.11 | 6.3 | 5.24 | 1.66 | 4.19 |
| Tb | 0.545 | 0.878 | 1.32 | 1.21 | 1.23 | 0.93 | 0.754 | 0.159 | 0.459 |
| Dy | 3.04 | 4.33 | 7.76 | 7.2 | 7.35 | 5.48 | 4.3 | 0.792 | 2.21 |
| Ho | 0.553 | 0.771 | 1.53 | 1.39 | 1.47 | 1.05 | 0.845 | 0.127 | 0.397 |
| Er | 1.48 | 1.99 | 4.15 | 3.87 | 3.96 | 2.95 | 2.29 | 0.376 | 1.1 |
| Tm | 0.194 | 0.255 | 0.566 | 0.539 | 0.559 | 0.41 | 0.305 | 0.0406 | 0.146 |
| Yb | 1.23 | 1.53 | 3.52 | 3.34 | 3.4 | 2.6 | 1.93 | 0.328 | 0.945 |
| Lu | 0.176 | 0.208 | 0.497 | 0.487 | 0.491 | 0.37 | 0.281 | 0.0438 | 0.135 |
| Y | 17.7 | 21.7 | 47.5 | 43.5 | 43.8 | 33.5 | 25.5 | 4.46 | 12 |
| U | 1.19 | 0.265 | 0.116 | 0.087 | 0.101 | 0.78 | 0.177 | 0.205 | 0.282 |
| Th | 4.06 | 1.02 | <= 0.05 | <= 0.05 | <= 0.05 | 2.97 | <= 0.05 | <= 0.05 | 8.64 |
| Nb | 9.71 | 1.91 | 1.96 | 1.09 | 1.57 | 9.93 | 5.89 | 2.53 | 4.4 |
| Ta | 0.533 | 0.144 | 0.174 | <= 0.1 | 0.231 | 0.56 | 0.303 | 0.132 | 0.221 |
| Hf | 0.236 | 0.903 | 0.526 | 0.436 | 0.47 | 0.44 | 0.201 | 0.227 | 0.218 |

| | MD-10C | MD-17B | MD2 | MD6 | MD29 | MD33 | MD14 | MD38 |
|---|---|---|---|---|---|---|---|---|
| La | 9.98 | 4.4 | 38.8 | 79.8 | 24.5 | 36.9 | 23 | 28.2 |
| Ce | 22.2 | 8.65 | 79 | 154 | 51 | 72.7 | 48.4 | 57.6 |
| Pr | 2.82 | 0.946 | 9.19 | 16.7 | 5.91 | 8.17 | 5.69 | 6.75 |
| Nd | 12.2 | 3.66 | 34.1 | 59.6 | 22.8 | 30.4 | 23.5 | 27.4 |
| Sm | 2.33 | 0.522 | 6.1 | 9.16 | 4.21 | 5.28 | 4.54 | 4.99 |
| Eu | 0.984 | 0.415 | 0.862 | 1.64 | 1.08 | 1.29 | 3.28 | 3.9 |
| Gd | 2.02 | 0.383 | 5.36 | 7.33 | 3.88 | 4.9 | 4.33 | 4.63 |
| Tb | 0.254 | 0.0401 | 0.768 | 0.833 | 0.529 | 0.674 | 0.608 | 0.625 |
| Dy | 1.28 | 0.164 | 4.3 | 3.89 | 3.08 | 3.75 | 3.49 | 3.54 |
| Ho | 0.23 | 0.0269 | 0.788 | 0.651 | 0.596 | 0.709 | 0.679 | 0.7 |
| Er | 0.594 | 0.0722 | 2.09 | 1.58 | 1.67 | 1.92 | 1.96 | 1.96 |
| Tm | 0.0729 | 0.00926 | 0.271 | 0.19 | 0.228 | 0.26 | 0.273 | 0.287 |
| Yb | 0.432 | 0.0592 | 1.52 | 1.24 | 1.48 | 1.69 | 1.93 | 1.89 |
| Lu | 0.0616 | 0.00944 | 0.208 | 0.179 | 0.22 | 0.239 | 0.29 | 0.28 |
| Y | 6.28 | 0.864 | 21.9 | 19.5 | 17.5 | 22.7 | 21.2 | 22.3 |
| U | 0.0778 | 0.0171 | 0.459 | 0.611 | 0.437 | 0.438 | 0.276 | 0.33 |
| Th | 0.49 | 0.372 | 9.76 | 18.6 | 1.88 | 9.77 | 0.943 | 1.16 |
| Nb | 1.2 | 0.501 | 7.83 | 3.88 | 5.85 | 5.18 | 6.27 | 5.1 |
| Ta | 0.0825 | 0.0522 | 0.294 | 0.163 | 0.199 | 0.174 | 0.311 | 0.269 |
| Hf | 0.346 | 0.339 | 0.153 | 0.0775 | 0.0647 | 0.0787 | 0.126 | 0.18 |

## *Appendix 2.3. Whole Rock Isotope data of selected samples of Mt Daniel Rocks*

| Sample ID | Rbppm | Srppm | $^{87}Rb/^{86}Sr$ | $^{87}Sr/^{86}Sr$ | $(^{87}Sr/^{86}Sr)_i$ | Sm ppm | Nd ppm | $^{147}Sm/^{144}Nd$ | $^{143}Nd/^{144}Nd$ | $(^{143}Nd/^{144}Nd)_i$ | εNd |
|---|---|---|---|---|---|---|---|---|---|---|---|
| MD2 | 77 | 102.5 | 2.120 | 0.7191041 | 0.715337 | 8.33 | 47.98 | 0.1050 | 0.512449 | 0.5123634 | -2.22 |
| MD3 | 75.5 | 222 | 0.960 | 0.7121572 | 0.710452 | 5.43 | 31.92 | 0.1029 | 0.512409 | 0.5123251 | -2.97 |
| MD6 | 86 | 236 | 1.029 | 0.7122397 | 0.710412 | 9.37 | 61.40 | 0.0923 | 0.512343 | 0.5122677 | -4.09 |
| MD28 | 60.1 | 164.4 | 1.032 | 0.7148469 | 0.713014 | 2.35 | 17.06 | 0.0832 | 0.512392 | 0.5123239 | -2.99 |
| MD29 | 37.6 | 715.3 | 0.148 | 0.7063844 | 0.706121 | 4.82 | 26.53 | 0.1098 | 0.512450 | 0.5123599 | -2.29 |
| MD33 | 53.6 | 382 | 0.396 | 0.7092154 | 0.708512 | 6.37 | 37.44 | 0.1030 | 0.512367 | 0.5122830 | -3.79 |
| MD7 | 23 | 642.5 | 0.101 | 0.7057010 | 0.705521 | 1.7 | 9.1 | 0.1133 | 0.512498 | 0.5124053 | -1.40 |
| MD10A | 12.5 | 745.5 | 0.047 | 0.7052640 | 0.705180 | 1.1 | 8.5 | 0.0786 | 0.512475 | 0.5124107 | -1.30 |
| MD14 | 12 | 835 | 0.041 | 0.7050980 | 0.705026 | 6.1 | 26 | 0.1429 | 0.512631 | 0.5125142 | 0.72 |
| MD38 | 8.9 | 810.8 | 0.031 | 0.7051606 | 0.705106 | 5.16 | 28.61 | 0.1092 | 0.512478 | 0.5123885 | -1.73 |
| MD8 | 20 | 553 | 0.102 | 0.7061710 | 0.705990 | 2.1 | 9.4 | 0.1385 | 0.512537 | 0.5124238 | -1.04 |
| MD22A | 15.4 | 756.5 | 0.057 | 0.7054785 | 0.705376 | 3.39 | 28.80 | 0.0713 | 0.512474 | 0.5124155 | -1.20 |
| MD17A | 38.2 | 1888 | 0.057 | 0.7040292 | 0.703928 | 2.91 | 18.97 | 0.0928 | 0.512673 | 0.5125973 | 2.34 |
| MD17B | 14 | 2269 | 0.017 | 0.7039987 | 0.703968 | 0.67 | 4.80 | 0.0844 | 0.512603 | 0.5125342 | 1.11 |
| MD32 | 20 | 1854 | 0.030 | 0.7045397 | 0.704486 | 6.69 | 53.01 | 0.0763 | 0.512509 | 0.5124470 | -0.59 |
| MD13 | 29 | 426.5 | 0.192 | 0.7051260 | 0.704785 | 4 | 23.2 | 0.1043 | 0.512703 | 0.5126177 | 2.74 |
| MD22B | 9.2 | 485.1 | 0.054 | 0.7045404 | 0.704445 | 8.33 | 35.57 | 0.1417 | 0.512653 | 0.5125372 | 1.17 |
| MD26 | 53.6 | 411.2 | 0.368 | 0.7055608 | 0.704907 | 7.89 | 33.90 | 0.1409 | 0.512609 | 0.5124934 | 0.32 |
| MD15 | 61.5 | 1009.5 | 0.172 | 0.7042643 | 0.703959 | 5.50 | 30.76 | 0.1081 | 0.512647 | 0.5125584 | 1.59 |
| MD16 | 22 | 1829.5 | 0.034 | 0.7039450 | 0.703885 | 2.6 | 14.2 | 0.1125 | 0.512672 | 0.5125800 | 2.01 |

# *Appendix 3- U-Th-Pb Analyses of Mt Daniel Samples*

| Isotope ratios | | | | | | | | | | | Isotopic ages | | | | | | | |
|---|---|---|---|---|---|---|---|---|---|---|---|---|---|---|---|---|---|---|
| Sample No | zoning | Pb207/Pb206 | ± 2SE | Pb207/U235 | ± 2SE | Pb206/U238 | ± 2SE | Pb208/Th232 | ± 2SE | error corr. | Pb207/Pb206 | ± 2SE | Pb206/U238 | ± 2SE | Pb207/U235 | ± 2SE | Pb208/Th232 | ± 2SE |
| MD15-2-1r | pln | 0.049 | 0.003 | 0.132 | 0.009 | 0.020 | 0.0005 | 0.0065 | 0.0004 | 0.34 | 165 | 145 | 125 | 3 | 126 | 8 | 132 | 8 |
| MD15-8-1c | pln | 0.049 | 0.003 | 0.130 | 0.008 | 0.020 | 0.0005 | 0.0063 | 0.0004 | 0.36 | 155 | 139 | 125 | 3 | 124 | 8 | 128 | 8 |
| MD15-20-1r | osc | 0.049 | 0.003 | 0.131 | 0.008 | 0.019 | 0.0004 | 0.0060 | 0.0003 | 0.37 | 140 | 128 | 123 | 3 | 125 | 7 | 121 | 6 |
| MD15-29-1r | pln | 0.050 | 0.003 | 0.133 | 0.009 | 0.019 | 0.0005 | 0.0060 | 0.0004 | 0.37 | 201 | 135 | 123 | 3 | 127 | 8 | 121 | 7 |
| MD15-64-1r | sec | 0.049 | 0.003 | 0.133 | 0.008 | 0.020 | 0.0004 | 0.0064 | 0.0004 | 0.36 | 133 | 133 | 127 | 3 | 127 | 7 | 129 | 7 |
| MD15-69-1r | pln, sec | 0.049 | 0.002 | 0.133 | 0.007 | 0.020 | 0.0004 | 0.0063 | 0.0004 | 0.40 | 149 | 115 | 126 | 3 | 127 | 6 | 127 | 7 |
| MD15-161-1r | pln, sec | 0.051 | 0.003 | 0.140 | 0.008 | 0.020 | 0.0004 | 0.0064 | 0.0004 | 0.37 | 253 | 129 | 126 | 3 | 133 | 8 | 128 | 7 |
| MD15-144c | hm | 0.049 | 0.003 | 0.131 | 0.008 | 0.019 | 0.0004 | 0.0060 | 0.0003 | 0.37 | 151 | 125 | 124 | 3 | 125 | 7 | 121 | 7 |
| MD15-81c | hm | 0.049 | 0.002 | 0.134 | 0.007 | 0.020 | 0.0004 | 0.0065 | 0.0003 | 0.43 | 127 | 109 | 129 | 3 | 127 | 6 | 131 | 7 |
| MD15-145-1c | pchy | 0.053 | 0.002 | 0.400 | 0.016 | 0.054 | 0.0011 | 0.0167 | 0.0010 | 0.49 | 349 | 77 | 339 | 7 | 342 | 12 | 334 | 20 |
| MD13-27-1c | hm | 0.064 | 0.010 | 0.168 | 0.027 | 0.019 | 0.0006 | 0.0071 | 0.0006 | 0.20 | 726 | 321 | 122 | 4 | 158 | 24 | 144 | 12 |
| MD13-30-1c | hm | 0.054 | 0.009 | 0.147 | 0.026 | 0.020 | 0.0006 | 0.0069 | 0.0005 | 0.19 | 390 | 363 | 126 | 4 | 139 | 23 | 138 | 11 |
| MD13-31-1c | hm | 0.049 | 0.012 | 0.132 | 0.033 | 0.020 | 0.0007 | 0.0066 | 0.0008 | 0.15 | 129 | 536 | 126 | 5 | 126 | 30 | 132 | 17 |
| MD13-29-1c | hm | 0.049 | 0.006 | 0.136 | 0.017 | 0.020 | 0.0005 | 0.0062 | 0.0004 | 0.21 | 151 | 277 | 125 | 3 | 129 | 15 | 126 | 7 |
| MD13-12-1c | hm | 0.052 | 0.012 | 0.136 | 0.037 | 0.018 | 0.0009 | 0.0066 | 0.0030 | 0.18 | 292 | 492 | 114 | 6 | 129 | 33 | 134 | 59 |
| MD13-16-1c | hm | 0.054 | 0.014 | 0.139 | 0.041 | 0.017 | 0.0009 | 0.0059 | 0.0026 | 0.18 | 358 | 533 | 111 | 6 | 132 | 37 | 118 | 53 |
| MD13-19-1c | hm | 0.054 | 0.009 | 0.148 | 0.026 | 0.020 | 0.0007 | 0.0061 | 0.0005 | 0.19 | 364 | 372 | 125 | 4 | 140 | 23 | 124 | 11 |
| MD13-34-1c | hm | 0.049 | 0.003 | 0.126 | 0.008 | 0.019 | 0.0004 | 0.0061 | 0.0002 | 0.36 | 126 | 138 | 119 | 3 | 121 | 7 | 122 | 5 |
| MD13-42-1c | hm | 0.049 | 0.013 | 0.136 | 0.036 | 0.020 | 0.0007 | 0.0063 | 0.0007 | 0.14 | 126 | 569 | 125 | 5 | 129 | 33 | 126 | 15 |
| MD13-50-1c | hm | 0.049 | 0.014 | 0.131 | 0.039 | 0.019 | 0.0008 | 0.0074 | 0.0008 | 0.14 | 143 | 629 | 120 | 5 | 125 | 35 | 149 | 17 |
| MD22B-4-1c | hm | 0.047 | 0.014 | 0.115 | 0.039 | 0.018 | 0.0011 | 0.0062 | 0.0033 | 0.18 | 56 | 638 | 114 | 7 | 110 | 35 | 125 | 66 |
| MD22B-6-1c | hm | 0.048 | 0.008 | 0.131 | 0.021 | 0.019 | 0.0007 | 0.0065 | 0.0006 | 0.22 | 119 | 354 | 122 | 4 | 125 | 19 | 131 | 12 |
| MD22B-7-1c | hm | 0.087 | 0.015 | 0.221 | 0.040 | 0.019 | 0.0009 | 0.0082 | 0.0008 | 0.27 | 1356 | 319 | 119 | 6 | 203 | 33 | 164 | 17 |
| MD22B-8-1c | pchy | 0.048 | 0.012 | 0.126 | 0.033 | 0.019 | 0.0009 | 0.0058 | 0.0007 | 0.19 | 82 | 557 | 120 | 6 | 121 | 30 | 118 | 14 |
| MD22B-16-1r | hm | 0.050 | 0.016 | 0.134 | 0.042 | 0.019 | 0.0008 | 0.0056 | 0.0009 | 0.14 | 190 | 652 | 121 | 5 | 128 | 38 | 114 | 17 |
| MD22B-21-1c | ft | 0.053 | 0.014 | 0.135 | 0.036 | 0.018 | 0.0009 | 0.0063 | 0.0010 | 0.19 | 315 | 548 | 118 | 6 | 129 | 33 | 127 | 21 |
| MD22B-24-1r | hm, ft | 0.050 | 0.011 | 0.137 | 0.029 | 0.019 | 0.0007 | 0.0061 | 0.0006 | 0.17 | 188 | 457 | 123 | 4 | 130 | 26 | 123 | 13 |
| MD22B-35-1c | hm,sec | 0.048 | 0.010 | 0.131 | 0.028 | 0.020 | 0.0007 | 0.0061 | 0.0006 | 0.17 | 113 | 454 | 128 | 4 | 125 | 25 | 122 | 12 |
| MD22B-29-1r | pln | 0.193 | 0.013 | 0.610 | 0.048 | 0.023 | 0.0008 | 0.0147 | 0.0009 | 0.42 | 2768 | 110 | 148 | 5 | 484 | 30 | 295 | 19 |
| MD22B-48-1c | hm | 0.052 | 0.005 | 0.133 | 0.013 | 0.019 | 0.0005 | 0.0060 | 0.0004 | 0.28 | 275 | 201 | 121 | 3 | 127 | 11 | 121 | 7 |
| MD22B-42-1r | hm | 0.050 | 0.008 | 0.131 | 0.020 | 0.019 | 0.0006 | 0.0064 | 0.0005 | 0.21 | 216 | 335 | 121 | 4 | 125 | 18 | 129 | 10 |
| MD22B-55-1c | hm | 0.057 | 0.012 | 0.156 | 0.034 | 0.020 | 0.0008 | 0.0076 | 0.0008 | 0.18 | 502 | 434 | 126 | 5 | 147 | 29 | 152 | 16 |
| MD22B-27-1c | pln | 0.050 | 0.005 | 0.132 | 0.013 | 0.019 | 0.0005 | 0.0062 | 0.0004 | 0.27 | 183 | 207 | 122 | 3 | 126 | 11 | 125 | 8 |

Abbreviations used: c=core, r= rim, pln=planar banding, osc=oscillatory zoning, hm=homogeneous zoning, sec=sector zoning, pchy=patchy zoning, ft=fir tree zoning, fl=featureless.

| Isotope ratios | | | | | | | | | | | Isotopic ages | | | | | | | |
|---|---|---|---|---|---|---|---|---|---|---|---|---|---|---|---|---|---|---|
| Sample No | zoning | Pb207/Pb206 | ± 2SE | Pb207/U235 | ± 2SE | Pb206/U238 | ± 2SE | Pb208/Th232 | ± 2SE | error corr. | Pb207/Pb206 | ± 2SE | Pb206/U238 | ± 2SE | Pb207/U235 | ± 2SE | Pb208/Th232 | ± 2SE |
| MD22B-28-1r | hm | 0.048 | 0.006 | 0.131 | 0.017 | 0.019 | 0.0006 | 0.0063 | 0.0005 | 0.23 | 119 | 289 | 124 | 4 | 125 | 16 | 126 | 9 |
| MD22B-11-1r | pln | 0.048 | 0.014 | 0.138 | 0.040 | 0.019 | 0.0011 | 0.0058 | 0.0008 | 0.19 | 123 | 599 | 124 | 7 | 131 | 35 | 116 | 17 |
| MD22B-10-1r | hm | 0.174 | 0.032 | 0.574 | 0.117 | 0.023 | 0.0016 | 0.0266 | 0.0035 | 0.34 | 2597 | 288 | 145 | 10 | 461 | 75 | 531 | 69 |
| MD26-10-1c | hm | 0.057 | 0.010 | 0.150 | 0.028 | 0.020 | 0.0007 | 0.0062 | 0.0006 | 0.19 | 486 | 382 | 126 | 5 | 142 | 25 | 125 | 13 |
| MD26-23-1c | hm | 0.054 | 0.009 | 0.146 | 0.026 | 0.019 | 0.0007 | 0.0069 | 0.0006 | 0.19 | 367 | 369 | 123 | 4 | 139 | 23 | 138 | 13 |
| MD26-27-1r | hm | 0.051 | 0.009 | 0.140 | 0.026 | 0.020 | 0.0007 | 0.0063 | 0.0006 | 0.19 | 257 | 393 | 127 | 5 | 133 | 23 | 126 | 12 |
| MD26-18-1c | hm | 0.054 | 0.002 | 0.386 | 0.014 | 0.052 | 0.0011 | 0.0199 | 0.0009 | 0.59 | 354 | 69 | 328 | 7 | 332 | 10 | 398 | 18 |
| MD26-31-1r | pln | 0.053 | 0.002 | 0.352 | 0.013 | 0.049 | 0.0010 | 0.0201 | 0.0010 | 0.55 | 317 | 73 | 306 | 6 | 307 | 10 | 403 | 20 |
| MD26-37-1c | hm,pchy | 0.054 | 0.002 | 0.457 | 0.019 | 0.060 | 0.0012 | 0.0189 | 0.0009 | 0.51 | 380 | 78 | 377 | 8 | 382 | 13 | 379 | 18 |
| MD26-32-1r | hm | 0.053 | 0.006 | 0.149 | 0.018 | 0.020 | 0.0006 | 0.0066 | 0.0004 | 0.23 | 315 | 253 | 128 | 4 | 141 | 16 | 132 | 9 |
| MD26-50-1r | hm | 0.051 | 0.009 | 0.135 | 0.024 | 0.020 | 0.0007 | 0.0067 | 0.0006 | 0.20 | 226 | 370 | 125 | 4 | 128 | 21 | 136 | 12 |
| MD26-48-1r | hm | 0.059 | 0.012 | 0.160 | 0.035 | 0.020 | 0.0009 | 0.0072 | 0.0009 | 0.20 | 550 | 434 | 126 | 5 | 151 | 31 | 145 | 19 |
| MD26-39-1c | hm | 0.055 | 0.005 | 0.142 | 0.013 | 0.019 | 0.0005 | 0.0060 | 0.0003 | 0.30 | 416 | 194 | 119 | 3 | 135 | 12 | 122 | 7 |
| MD26-54-1c | hm | 0.053 | 0.002 | 0.411 | 0.017 | 0.057 | 0.0013 | 0.0259 | 0.0014 | 0.53 | 342 | 79 | 356 | 8 | 350 | 12 | 518 | 27 |
| MD26-63-1r | hm | 0.057 | 0.010 | 0.152 | 0.026 | 0.020 | 0.0007 | 0.0066 | 0.0007 | 0.20 | 477 | 355 | 125 | 4 | 144 | 23 | 133 | 13 |
| MD26-64-1c | hm | 0.053 | 0.002 | 0.362 | 0.013 | 0.049 | 0.0010 | 0.0162 | 0.0008 | 0.56 | 327 | 71 | 311 | 6 | 314 | 10 | 325 | 15 |
| MD8-6-1c | osc,pln | 0.049 | 0.005 | 0.121 | 0.013 | 0.018 | 0.0005 | 0.0056 | 0.0003 | 0.25 | 155 | 232 | 114 | 3 | 116 | 11 | 112 | 5 |
| MD8-1-1r | hm | 0.052 | 0.006 | 0.119 | 0.014 | 0.017 | 0.0005 | 0.0050 | 0.0003 | 0.24 | 278 | 261 | 107 | 3 | 115 | 13 | 100 | 6 |
| MD8-5-1r | hm,ft | 0.069 | 0.016 | 0.174 | 0.041 | 0.018 | 0.0007 | 0.0071 | 0.0007 | 0.17 | 889 | 448 | 118 | 5 | 162 | 35 | 144 | 14 |
| MD8-3-1c | pchy | 0.053 | 0.001 | 0.363 | 0.010 | 0.053 | 0.0011 | 0.0457 | 0.0018 | 0.74 | 311 | 59 | 330 | 7 | 314 | 8 | 904 | 34 |
| MD8-4-1r | fl | 0.048 | 0.002 | 0.117 | 0.006 | 0.018 | 0.0004 | 0.0062 | 0.0008 | 0.47 | 122 | 108 | 112 | 3 | 112 | 5 | 126 | 16 |
| MD8-4-2c | pchy | 0.053 | 0.002 | 0.362 | 0.014 | 0.049 | 0.0011 | 0.0145 | 0.0006 | 0.58 | 346 | 76 | 311 | 7 | 314 | 10 | 291 | 11 |
| MD22A-2-1 r | fl | 0.053 | 0.002 | 0.391 | 0.016 | 0.053 | 0.0012 | 0.0158 | 0.0006 | 0.54 | 333 | 82 | 335 | 7 | 335 | 12 | 317 | 13 |
| MD22A-2-2 c | pln | 0.054 | 0.002 | 0.415 | 0.016 | 0.056 | 0.0012 | 0.0170 | 0.0007 | 0.57 | 376 | 77 | 350 | 7 | 353 | 11 | 341 | 14 |
| MD22A-3-1c | hm | 0.060 | 0.009 | 0.170 | 0.026 | 0.020 | 0.0006 | 0.0062 | 0.0005 | 0.20 | 602 | 307 | 129 | 4 | 159 | 22 | 126 | 10 |
| MD22A-6-1c | hm | 0.054 | 0.002 | 0.420 | 0.019 | 0.057 | 0.0013 | 0.0169 | 0.0007 | 0.51 | 363 | 89 | 357 | 8 | 356 | 13 | 338 | 14 |
| MD22A-9-1c | hm | 0.054 | 0.002 | 0.413 | 0.015 | 0.056 | 0.0012 | 0.0163 | 0.0006 | 0.60 | 357 | 73 | 352 | 7 | 351 | 11 | 326 | 13 |
| MD22A-12-1r | fl | 0.053 | 0.002 | 0.383 | 0.018 | 0.052 | 0.0012 | 0.0156 | 0.0007 | 0.49 | 349 | 92 | 329 | 7 | 329 | 13 | 313 | 13 |
| MD22A-12-2c | hm | 0.054 | 0.002 | 0.424 | 0.017 | 0.057 | 0.0013 | 0.0175 | 0.0007 | 0.56 | 369 | 79 | 359 | 8 | 359 | 12 | 350 | 14 |
| MD22A-14-1r | fl | 0.049 | 0.008 | 0.155 | 0.027 | 0.023 | 0.0007 | 0.0074 | 0.0007 | 0.17 | 129 | 377 | 148 | 4 | 146 | 24 | 149 | 13 |
| MD22A-14-2c | osc | 0.054 | 0.002 | 0.436 | 0.018 | 0.058 | 0.0013 | 0.0169 | 0.0007 | 0.54 | 378 | 81 | 363 | 8 | 368 | 13 | 339 | 14 |
| MD22A-15-1r | fl | 0.053 | 0.004 | 0.280 | 0.025 | 0.039 | 0.0010 | 0.0115 | 0.0006 | 0.29 | 332 | 182 | 245 | 6 | 250 | 20 | 231 | 13 |
| MD22A-15-2c | osc | 0.053 | 0.002 | 0.373 | 0.015 | 0.051 | 0.0011 | 0.0149 | 0.0006 | 0.56 | 319 | 79 | 322 | 7 | 322 | 11 | 300 | 12 |

| Isotope ratios | | | | | | | | | | | Isotopic ages | | | | | | | |
|---|---|---|---|---|---|---|---|---|---|---|---|---|---|---|---|---|---|---|
| Sample No | zoning | Pb207/Pb206 | ± 2SE | Pb207/U235 | ± 2SE | Pb206/U238 | ± 2SE | Pb208/Th232 | ± 2SE | error corr. | Pb207/Pb206 | ± 2SE | Pb206/U238 | ± 2SE | Pb207/U235 | ± 2SE | Pb208/Th232 | ± 2SE |
| MD22A-18-1r | fl | 0.060 | 0.012 | 0.164 | 0.032 | 0.020 | 0.0007 | 0.0064 | 0.0011 | 0.17 | 594 | 396 | 125 | 4 | 154 | 28 | 129 | 23 |
| MD22A-18-2c | osc,pchy | 0.053 | 0.002 | 0.345 | 0.017 | 0.047 | 0.0011 | 0.0152 | 0.0007 | 0.46 | 333 | 98 | 297 | 7 | 301 | 13 | 306 | 13 |
| MD22A-31-1r | fl | 0.054 | 0.002 | 0.425 | 0.017 | 0.058 | 0.0013 | 0.0169 | 0.0007 | 0.54 | 375 | 82 | 361 | 8 | 360 | 12 | 338 | 14 |
| MD22A-31-2c | osc | 0.054 | 0.002 | 0.425 | 0.016 | 0.057 | 0.0012 | 0.0168 | 0.0007 | 0.57 | 384 | 76 | 356 | 8 | 360 | 12 | 337 | 14 |
| MD22A-32-1c | hm | 0.052 | 0.002 | 0.359 | 0.014 | 0.050 | 0.0011 | 0.0139 | 0.0006 | 0.55 | 299 | 82 | 314 | 7 | 312 | 11 | 280 | 11 |
| MD22A-27-1c | pln | 0.054 | 0.003 | 0.325 | 0.017 | 0.043 | 0.0010 | 0.0136 | 0.0006 | 0.45 | 385 | 104 | 274 | 6 | 286 | 13 | 273 | 12 |
| MD22A-22-1c | hm | 0.053 | 0.004 | 0.392 | 0.030 | 0.053 | 0.0013 | 0.0172 | 0.0008 | 0.32 | 330 | 154 | 335 | 8 | 336 | 22 | 345 | 16 |
| MD22A-61-1r | fl | 0.053 | 0.002 | 0.394 | 0.015 | 0.054 | 0.0012 | 0.0160 | 0.0006 | 0.57 | 349 | 78 | 338 | 7 | 337 | 11 | 321 | 13 |
| MD22A-61-2c | osc | 0.053 | 0.002 | 0.376 | 0.015 | 0.052 | 0.0011 | 0.0152 | 0.0006 | 0.55 | 330 | 81 | 325 | 7 | 324 | 11 | 306 | 12 |
| MD22A-55-11 | pln | 0.053 | 0.002 | 0.407 | 0.018 | 0.056 | 0.0012 | 0.0174 | 0.0007 | 0.51 | 322 | 87 | 350 | 8 | 347 | 13 | 349 | 14 |
| MD22A-73-1r | fl | 0.053 | 0.003 | 0.309 | 0.018 | 0.043 | 0.0010 | 0.0134 | 0.0006 | 0.41 | 338 | 117 | 270 | 6 | 274 | 14 | 268 | 13 |
| MD22A-73-2 c | hm,osc | 0.054 | 0.002 | 0.405 | 0.017 | 0.055 | 0.0012 | 0.0166 | 0.0007 | 0.54 | 359 | 83 | 343 | 7 | 345 | 12 | 333 | 14 |
| MD22A-87-1 c | pln | 0.054 | 0.003 | 0.397 | 0.024 | 0.054 | 0.0012 | 0.0169 | 0.0008 | 0.39 | 353 | 120 | 336 | 8 | 340 | 17 | 338 | 16 |
| MD22A-139-1c | hm | 0.064 | 0.015 | 0.168 | 0.039 | 0.019 | 0.0007 | 0.0071 | 0.0010 | 0.16 | 756 | 455 | 121 | 5 | 157 | 34 | 144 | 20 |
| MD22A-101-1c | pchy | 0.054 | 0.002 | 0.382 | 0.014 | 0.051 | 0.0011 | 0.0151 | 0.0006 | 0.59 | 378 | 74 | 322 | 7 | 328 | 10 | 303 | 12 |
| MD22A-4-1c | pchy,osc | 0.053 | 0.002 | 0.407 | 0.015 | 0.056 | 0.0012 | 0.0166 | 0.0007 | 0.60 | 347 | 73 | 349 | 7 | 347 | 11 | 334 | 13 |
| MD22A-4-2 r | fl | 0.053 | 0.002 | 0.401 | 0.016 | 0.054 | 0.0012 | 0.0155 | 0.0006 | 0.56 | 345 | 78 | 342 | 7 | 342 | 11 | 310 | 12 |
| MD17a-1c | pln | 0.048 | 0.012 | 0.126 | 0.033 | 0.019 | 0.0007 | 0.0057 | 0.0011 | 0.14 | 119 | 596 | 119 | 4 | 121 | 31 | 115 | 21 |
| MD17a-38r | osc | 0.049 | 0.008 | 0.122 | 0.021 | 0.019 | 0.0005 | 0.0061 | 0.0011 | 0.17 | 126 | 386 | 118 | 3 | 116 | 20 | 124 | 22 |
| MD17a-72c | hm | 0.048 | 0.009 | 0.121 | 0.023 | 0.019 | 0.0006 | 0.0063 | 0.0011 | 0.17 | 123 | 425 | 119 | 4 | 116 | 22 | 126 | 22 |
| MD17a-30c | pln | 0.056 | 0.006 | 0.140 | 0.017 | 0.018 | 0.0005 | 0.0063 | 0.0011 | 0.22 | 450 | 249 | 116 | 3 | 133 | 16 | 126 | 22 |
| MD17a-51c | osc | 0.049 | 0.012 | 0.131 | 0.032 | 0.019 | 0.0006 | 0.0063 | 0.0012 | 0.14 | 139 | 555 | 119 | 4 | 125 | 30 | 126 | 24 |
| MD17a-21c | hm | 0.048 | 0.007 | 0.123 | 0.018 | 0.018 | 0.0005 | 0.0062 | 0.0011 | 0.20 | 103 | 321 | 116 | 3 | 118 | 17 | 124 | 22 |
| MD-17A-22-1c | sec,hm | 0.057 | 0.010 | 0.138 | 0.025 | 0.018 | 0.0006 | 0.0054 | 0.0007 | 0.19 | 487 | 363 | 115 | 4 | 131 | 22 | 108 | 15 |
| MD-17A-23-1c | hm | 0.049 | 0.024 | 0.123 | 0.062 | 0.019 | 0.0014 | 0.0054 | 0.0013 | 0.14 | 127 | 999 | 121 | 9 | 118 | 56 | 109 | 25 |
| MD-17A-31-1r | pln | 0.051 | 0.010 | 0.135 | 0.027 | 0.019 | 0.0006 | 0.0064 | 0.0009 | 0.17 | 246 | 415 | 121 | 4 | 129 | 24 | 128 | 18 |
| MD-17A-53-1c | hm | 0.046 | 0.010 | 0.123 | 0.027 | 0.019 | 0.0007 | 0.0051 | 0.0008 | 0.17 | 0 | 458 | 123 | 5 | 118 | 25 | 102 | 17 |
| MD-17A-68-1c | osc | 0.054 | 0.013 | 0.139 | 0.033 | 0.019 | 0.0007 | 0.0061 | 0.0010 | 0.14 | 366 | 492 | 122 | 4 | 132 | 30 | 122 | 19 |
| MD-17A-90-1c | pln | 0.048 | 0.011 | 0.123 | 0.028 | 0.019 | 0.0007 | 0.0064 | 0.0011 | 0.16 | 79 | 491 | 122 | 4 | 118 | 25 | 129 | 22 |
| MD-17A-106-1c | pln | 0.050 | 0.008 | 0.134 | 0.023 | 0.020 | 0.0006 | 0.0056 | 0.0009 | 0.19 | 209 | 354 | 127 | 4 | 128 | 20 | 113 | 18 |
| MD-17A-121-1c | pln | 0.049 | 0.012 | 0.141 | 0.036 | 0.020 | 0.0007 | 0.0069 | 0.0009 | 0.14 | 138 | 535 | 129 | 5 | 134 | 32 | 138 | 18 |
| MD-17A-139-1c | hm | 0.066 | 0.010 | 0.174 | 0.028 | 0.019 | 0.0007 | 0.0061 | 0.0008 | 0.21 | 817 | 310 | 121 | 4 | 163 | 25 | 123 | 15 |
| MD-17A-159-1c | pchy | 0.042 | 0.011 | 0.114 | 0.031 | 0.019 | 0.0006 | 0.0067 | 0.0008 | 0.12 | 0 | 181 | 123 | 4 | 110 | 28 | 134 | 17 |

| Isotope ratios | | | | | | | | | | | Isotopic ages | | | | | | | |
|---|---|---|---|---|---|---|---|---|---|---|---|---|---|---|---|---|---|---|
| Sample No | zoning | Pb207/Pb206 | ± 2SE | Pb207/U235 | ± 2SE | Pb206/U238 | ± 2SE | Pb208/Th232 | ± 2SE | error corr. | Pb207/Pb206 | ± 2SE | Pb206/U238 | ± 2SE | Pb207/U235 | ± 2SE | Pb208/Th232 | ± 2SE |
| MD-17A-154-1c | pln | 0.075 | 0.011 | 0.188 | 0.028 | 0.019 | 0.0006 | 0.0058 | 0.0007 | 0.21 | 1064 | 275 | 121 | 4 | 175 | 24 | 117 | 15 |
| MD-17A-189-1c | sec | 0.050 | 0.010 | 0.126 | 0.026 | 0.019 | 0.0006 | 0.0054 | 0.0007 | 0.16 | 209 | 435 | 118 | 4 | 121 | 23 | 109 | 14 |
| MD-17A-255-1c | hm | 0.053 | 0.007 | 0.140 | 0.020 | 0.019 | 0.0005 | 0.0055 | 0.0007 | 0.19 | 329 | 298 | 121 | 3 | 133 | 18 | 112 | 13 |
| MD-17A-241-1c | pchy | 0.048 | 0.010 | 0.126 | 0.026 | 0.019 | 0.0006 | 0.0056 | 0.0007 | 0.15 | 86 | 450 | 121 | 4 | 121 | 24 | 112 | 14 |
| MD-17A-277-1r | pln | 0.062 | 0.012 | 0.150 | 0.029 | 0.018 | 0.0006 | 0.0058 | 0.0008 | 0.18 | 689 | 381 | 115 | 4 | 142 | 26 | 116 | 15 |
| MD-17A-278-1c | hm | 0.053 | 0.013 | 0.141 | 0.035 | 0.019 | 0.0007 | 0.0061 | 0.0009 | 0.15 | 349 | 509 | 121 | 4 | 134 | 31 | 122 | 18 |
| MD-17A-294-1c | pln | 0.060 | 0.008 | 0.154 | 0.021 | 0.019 | 0.0006 | 0.0058 | 0.0008 | 0.21 | 603 | 275 | 122 | 4 | 146 | 19 | 118 | 15 |
| MD-17A-295-1c | pln | 0.049 | 0.011 | 0.127 | 0.030 | 0.019 | 0.0006 | 0.0061 | 0.0008 | 0.14 | 125 | 501 | 120 | 4 | 122 | 27 | 122 | 17 |
| MD-17A-296-1r | pln | 0.055 | 0.012 | 0.138 | 0.031 | 0.018 | 0.0006 | 0.0060 | 0.0009 | 0.16 | 427 | 456 | 114 | 4 | 131 | 28 | 122 | 17 |
| MD32-1-1r | osc | 0.051 | 0.007 | 0.135 | 0.018 | 0.019 | 0.0006 | 0.0063 | 0.0004 | 0.23 | 251 | 287 | 122 | 4 | 128 | 16 | 127 | 7 |
| MD32-1-2c | pchy,osc | 0.053 | 0.002 | 0.390 | 0.014 | 0.053 | 0.0011 | 0.0170 | 0.0006 | 0.59 | 348 | 73 | 334 | 7 | 334 | 10 | 341 | 12 |
| MD32-2-1r | fl | 0.047 | 0.003 | 0.128 | 0.008 | 0.020 | 0.0005 | 0.0069 | 0.0007 | 0.37 | 28 | 139 | 127 | 3 | 123 | 7 | 139 | 14 |
| MD32-2-2c | pchy,osc | 0.054 | 0.003 | 0.406 | 0.024 | 0.055 | 0.0013 | 0.0176 | 0.0007 | 0.40 | 389 | 113 | 343 | 8 | 346 | 17 | 352 | 14 |
| MD32-3-1r | fl | 0.052 | 0.004 | 0.131 | 0.009 | 0.019 | 0.0005 | 0.0066 | 0.0004 | 0.35 | 281 | 153 | 119 | 3 | 125 | 8 | 133 | 9 |
| MD32-3-2c | hm | 0.052 | 0.002 | 0.224 | 0.009 | 0.031 | 0.0007 | 0.0115 | 0.0004 | 0.52 | 267 | 88 | 199 | 4 | 205 | 8 | 231 | 8 |
| MD32-10-1r | fl | 0.055 | 0.009 | 0.147 | 0.024 | 0.020 | 0.0007 | 0.0062 | 0.0006 | 0.21 | 408 | 338 | 126 | 4 | 139 | 21 | 124 | 11 |
| MD32-10-2c | hm | 0.054 | 0.002 | 0.409 | 0.014 | 0.055 | 0.0012 | 0.0174 | 0.0006 | 0.61 | 357 | 70 | 345 | 7 | 348 | 10 | 348 | 12 |
| MD32-15-1r | fl | 0.048 | 0.001 | 0.127 | 0.004 | nd | nd | 0.0061 | 0.0003 | nd | 107 | 62 | -NaN | nd | 121 | 3 | 123 | 6 |
| MD32-15-2c | hm | 0.049 | 0.002 | 0.184 | 0.008 | 0.027 | 0.0006 | 0.0097 | 0.0006 | 0.50 | 163 | 94 | 175 | 4 | 172 | 7 | 196 | 12 |
| MD32-8c | hm | 0.052 | 0.006 | 0.128 | 0.015 | 0.019 | 0.0005 | 0.0057 | 0.0003 | 0.25 | 274 | 246 | 118 | 3 | 122 | 13 | 115 | 6 |
| MD32-16-1r | fl | 0.052 | 0.007 | 0.144 | 0.020 | 0.020 | 0.0006 | 0.0067 | 0.0005 | 0.23 | 295 | 291 | 130 | 4 | 137 | 18 | 135 | 10 |
| MD32-16-2c | pchy,hm | 0.054 | 0.002 | 0.396 | 0.014 | 0.054 | 0.0012 | 0.0185 | 0.0007 | 0.60 | 354 | 73 | 339 | 7 | 338 | 10 | 370 | 14 |
| MD32-21-1c | hm | 0.055 | 0.002 | 0.392 | 0.014 | 0.052 | 0.0011 | 0.0162 | 0.0006 | 0.58 | 428 | 72 | 324 | 7 | 336 | 10 | 325 | 11 |
| MD32-21-2r | fl | 0.056 | 0.011 | 0.148 | 0.029 | 0.019 | 0.0008 | 0.0068 | 0.0006 | 0.21 | 463 | 393 | 121 | 5 | 140 | 25 | 136 | 13 |
| MD32-83-1c | pln | 0.049 | 0.018 | 0.123 | 0.045 | 0.018 | 0.0009 | 0.0054 | 0.0010 | 0.14 | 159 | 752 | 113 | 6 | 117 | 41 | 109 | 20 |
| MD32-94-1c | hm | 0.049 | 0.004 | 0.124 | 0.009 | 0.019 | 0.0005 | 0.0060 | 0.0005 | 0.32 | 140 | 167 | 120 | 3 | 119 | 8 | 122 | 11 |
| MD32-95-1c | hm | 0.049 | 0.005 | 0.129 | 0.013 | 0.019 | 0.0005 | -0.0005 | 0.0011 | 0.28 | 147 | 222 | 121 | 3 | 123 | 12 | -9 | 23 |
| MD32-95-2r | fl | 0.048 | 0.007 | 0.114 | 0.017 | 0.018 | 0.0006 | 0.0059 | 0.0003 | 0.22 | 92 | 329 | 112 | 4 | 110 | 15 | 120 | 6 |
| MD32-97-1c | hm | 0.056 | 0.015 | 0.136 | 0.038 | 0.017 | 0.0008 | 0.0061 | 0.0007 | 0.17 | 456 | 554 | 110 | 5 | 129 | 34 | 123 | 13 |
| MD32-100-1c | hm | 0.053 | 0.016 | 0.142 | 0.043 | 0.019 | 0.0009 | 0.0077 | 0.0010 | 0.16 | 321 | 608 | 119 | 6 | 135 | 38 | 155 | 20 |
| MD32-109-1c | hm | 0.049 | 0.013 | 0.123 | 0.032 | 0.018 | 0.0008 | 0.0064 | 0.0006 | 0.17 | 144 | 552 | 112 | 5 | 118 | 29 | 129 | 12 |
| MD32-108-1c | hm | 0.057 | 0.014 | 0.151 | 0.039 | 0.019 | 0.0008 | 0.0086 | 0.0008 | 0.17 | 471 | 516 | 122 | 5 | 143 | 34 | 173 | 15 |
| MD32-105-1c | osc | 0.050 | 0.005 | 0.119 | 0.013 | 0.018 | 0.0005 | 0.0057 | 0.0002 | 0.26 | 184 | 240 | 113 | 3 | 114 | 12 | 114 | 5 |

| Isotope ratios | | | | | | | | | | | Isotopic ages | | | | | | | |
|---|---|---|---|---|---|---|---|---|---|---|---|---|---|---|---|---|---|---|
| Sample No | zoning | Pb207/Pb206 | ± 2SE | Pb207/U235 | ± 2SE | Pb206/U238 | ± 2SE | Pb208/Th232 | ± 2SE | error corr. | Pb207/Pb206 | ± 2SE | Pb206/U238 | ± 2SE | Pb207/U235 | ± 2SE | Pb208/Th232 | ± 2SE |
| MD2-1-1r | fl | 0.054 | 0.005 | 0.397 | 0.044 | 0.055 | 0.0016 | 0.0172 | 0.0014 | 0.26 | 387 | 210 | 348 | 10 | 340 | 32 | 345 | 27 |
| MD2-1-2c | hm,pchy | 0.049 | 0.006 | 0.385 | 0.057 | 0.058 | 0.0021 | 0.0164 | 0.0017 | 0.24 | 145 | 293 | 364 | 13 | 330 | 42 | 329 | 34 |
| MD2-21-1c | hm | 0.053 | 0.005 | 0.365 | 0.043 | 0.049 | 0.0014 | 0.0165 | 0.0013 | 0.25 | 340 | 224 | 310 | 9 | 316 | 32 | 331 | 26 |
| MD2-4-1c | pchy | 0.052 | 0.006 | 0.241 | 0.033 | 0.032 | 0.0011 | 0.0156 | 0.0014 | 0.24 | 304 | 263 | 204 | 7 | 219 | 27 | 313 | 29 |
| MD2-23-1r | fl | 0.051 | 0.005 | 0.157 | 0.019 | 0.022 | 0.0007 | 0.0107 | 0.0010 | 0.25 | 228 | 236 | 140 | 4 | 149 | 17 | 216 | 19 |
| MD2-24-1r | fl | 0.057 | 0.007 | 0.287 | 0.039 | 0.037 | 0.0012 | 0.0158 | 0.0014 | 0.24 | 481 | 251 | 237 | 8 | 256 | 30 | 317 | 29 |
| MD2-25-1r | fl | 0.053 | 0.006 | 0.346 | 0.045 | 0.046 | 0.0014 | 0.0171 | 0.0015 | 0.24 | 348 | 245 | 292 | 9 | 302 | 34 | 343 | 30 |
| MD2-39-1r | fl | 0.052 | 0.006 | 0.309 | 0.038 | 0.043 | 0.0013 | 0.0147 | 0.0012 | 0.24 | 277 | 240 | 271 | 8 | 274 | 30 | 294 | 25 |
| MD2-41-1c | pchy | 0.054 | 0.006 | 0.383 | 0.046 | 0.051 | 0.0015 | 0.0161 | 0.0013 | 0.24 | 367 | 229 | 322 | 9 | 329 | 34 | 323 | 26 |
| MD2-62-1c | pln | 0.055 | 0.006 | 0.404 | 0.052 | 0.053 | 0.0016 | 0.0178 | 0.0015 | 0.24 | 397 | 241 | 330 | 10 | 345 | 37 | 356 | 30 |
| MD2-80-1c | hm | 0.055 | 0.007 | 0.405 | 0.059 | 0.052 | 0.0017 | 0.0167 | 0.0015 | 0.22 | 415 | 276 | 326 | 10 | 346 | 43 | 335 | 30 |
| MD2-116-1r | fl | 0.057 | 0.007 | 0.285 | 0.040 | 0.036 | 0.0012 | 0.0148 | 0.0014 | 0.24 | 481 | 262 | 227 | 7 | 254 | 31 | 297 | 27 |
| MD2-118-1c | pln | 0.055 | 0.008 | 0.383 | 0.062 | 0.048 | 0.0018 | 0.0150 | 0.0016 | 0.23 | 415 | 304 | 305 | 11 | 329 | 46 | 300 | 31 |
| MD2-130-1r | fl | 0.055 | 0.007 | 0.381 | 0.054 | 0.051 | 0.0017 | 0.0155 | 0.0015 | 0.24 | 393 | 268 | 322 | 10 | 328 | 40 | 312 | 29 |
| MD2-124-1r | fl | 0.050 | 0.006 | 0.159 | 0.021 | 0.023 | 0.0007 | 0.0102 | 0.0009 | 0.23 | 181 | 262 | 144 | 4 | 150 | 18 | 205 | 18 |
| MD2-138-1r | fl | 0.054 | 0.007 | 0.297 | 0.045 | 0.040 | 0.0014 | 0.0145 | 0.0014 | 0.23 | 354 | 289 | 250 | 8 | 264 | 35 | 291 | 29 |
| MD2-149-1r | fl | 0.054 | 0.007 | 0.413 | 0.060 | 0.055 | 0.0018 | 0.0170 | 0.0016 | 0.23 | 388 | 274 | 344 | 11 | 351 | 43 | 342 | 32 |
| MD2-149a-1r | fl | 0.049 | 0.008 | 0.153 | 0.028 | 0.022 | 0.0009 | 0.0100 | 0.0013 | 0.23 | 166 | 360 | 140 | 6 | 145 | 25 | 201 | 25 |
| MD6-84ac | pchy | 0.054 | 0.002 | 0.382 | 0.019 | 0.052 | 0.0010 | 0.0167 | 0.0006 | 0.39 | 377 | 101 | 327 | 6 | 328 | 16 | 334 | 12 |
| MD6-84ar | fl | 0.056 | 0.003 | 0.131 | 0.007 | 0.017 | 0.0004 | 0.0123 | 0.0010 | 0.38 | 434 | 123 | 108 | 2 | 125 | 7 | 247 | 21 |
| MD6-84bc | pchy | 0.055 | 0.002 | 0.365 | 0.017 | 0.048 | 0.0009 | 0.0159 | 0.0005 | 0.42 | 406 | 95 | 302 | 6 | 316 | 15 | 319 | 11 |
| MD6-80c | osc,sec | 0.055 | 0.002 | 0.394 | 0.017 | 0.052 | 0.0010 | 0.0175 | 0.0006 | 0.44 | 408 | 89 | 329 | 6 | 337 | 15 | 350 | 12 |
| MD6-62c | pln | 0.054 | 0.002 | 0.383 | 0.011 | 0.051 | 0.0009 | 0.0175 | 0.0006 | 0.62 | 353 | 65 | 323 | 6 | 329 | 10 | 351 | 11 |
| MD6-62r | fl | 0.053 | 0.002 | 0.237 | 0.007 | 0.033 | 0.0006 | 0.0154 | 0.0005 | 0.59 | 328 | 69 | 207 | 4 | 216 | 7 | 308 | 10 |
| MD6-124c | faint osc | 0.049 | 0.002 | 0.127 | 0.005 | 0.019 | 0.0004 | 0.0067 | 0.0015 | 0.49 | 128 | 92 | 120 | 2 | 121 | 5 | 136 | 29 |
| MD6-130c | pchy | 0.055 | 0.002 | 0.375 | 0.015 | 0.051 | 0.0010 | 0.0170 | 0.0006 | 0.46 | 403 | 85 | 320 | 6 | 323 | 13 | 340 | 12 |
| MD6-138r | fl | 0.049 | 0.004 | 0.119 | 0.010 | 0.018 | 0.0004 | 0.0072 | 0.0031 | 0.27 | 129 | 199 | 116 | 3 | 115 | 10 | 144 | 63 |
| MD-6-10-1r | fl | 0.047 | 0.003 | 0.117 | 0.006 | 0.018 | 0.0004 | 0.0056 | 0.0007 | 0.36 | 58 | 125 | 115 | 2 | 112 | 6 | 112 | 13 |
| MD-6-11-1r | fl | 0.053 | 0.003 | 0.312 | 0.019 | 0.044 | 0.0009 | 0.0161 | 0.0009 | 0.33 | 338 | 122 | 275 | 6 | 276 | 15 | 323 | 17 |
| MD-6-10-2c | hm | 0.053 | 0.002 | 0.383 | 0.020 | 0.053 | 0.0010 | 0.0158 | 0.0007 | 0.37 | 319 | 103 | 330 | 6 | 330 | 15 | 317 | 14 |
| MD-6-12-1r | fl | 0.049 | 0.002 | 0.122 | 0.006 | 0.018 | 0.0003 | 0.0058 | 0.0006 | 0.39 | 161 | 107 | 115 | 2 | 117 | 5 | 118 | 11 |
| MD-6-17-1r | fl | 0.054 | 0.005 | 0.123 | 0.012 | 0.016 | 0.0004 | 0.0105 | 0.0021 | 0.27 | 366 | 208 | 104 | 3 | 118 | 11 | 210 | 42 |
| MD-6-17-2c | hm | 0.053 | 0.002 | 0.302 | 0.012 | 0.041 | 0.0008 | 0.0128 | 0.0005 | 0.47 | 308 | 80 | 262 | 5 | 268 | 9 | 257 | 11 |
| MD-6-17-3c | hm | 0.052 | 0.002 | 0.366 | 0.017 | 0.052 | 0.0010 | 0.0140 | 0.0007 | 0.42 | 274 | 93 | 324 | 6 | 317 | 13 | 281 | 14 |

| Isotope ratios | | | | | | | | | | | Isotopic ages | | | | | | | |
|---|---|---|---|---|---|---|---|---|---|---|---|---|---|---|---|---|---|---|
| Sample No | zoning | Pb207/Pb206 | ± 2SE | Pb207/U235 | ± 2SE | Pb206/U238 | ± 2SE | Pb208/Th232 | ± 2SE | error corr. | Pb207/Pb206 | ± 2SE | Pb206/U238 | ± 2SE | Pb207/U235 | ± 2SE | Pb208/Th232 | ± 2SE |
| MD-6-43-1r | fl | 0.053 | 0.004 | 0.181 | 0.014 | 0.025 | 0.0006 | 0.0171 | 0.0017 | 0.31 | 342 | 156 | 161 | 4 | 169 | 12 | 343 | 34 |
| MD-6-72-1r | fl | 0.056 | 0.004 | 0.152 | 0.011 | 0.020 | 0.0005 | 0.0120 | 0.0009 | 0.33 | 435 | 145 | 127 | 3 | 143 | 9 | 241 | 19 |
| MD-6-93-1r | fl | 0.052 | 0.002 | 0.277 | 0.012 | 0.039 | 0.0007 | 0.0131 | 0.0006 | 0.42 | 293 | 91 | 248 | 5 | 248 | 10 | 263 | 11 |
| MD-6-95-1r | fl | 0.049 | 0.003 | 0.129 | 0.008 | 0.019 | 0.0004 | 0.0084 | 0.0008 | 0.36 | 128 | 132 | 124 | 3 | 123 | 7 | 168 | 15 |
| MD-6-110-1r | fl | 0.052 | 0.007 | 0.114 | 0.015 | 0.016 | 0.0005 | 0.0141 | 0.0034 | 0.23 | 279 | 280 | 104 | 3 | 110 | 14 | 282 | 68 |
| MD-6-113-1r | fl | 0.050 | 0.004 | 0.120 | 0.010 | 0.018 | 0.0004 | 0.0097 | 0.0011 | 0.29 | 207 | 178 | 113 | 3 | 115 | 9 | 196 | 22 |
| MD-6-117-1r | fl | 0.084 | 0.011 | 0.199 | 0.028 | 0.019 | 0.0008 | 0.0499 | 0.0064 | 0.28 | 1283 | 250 | 120 | 5 | 184 | 24 | 983 | 123 |
| MD-6-120-1c | hm | 0.055 | 0.003 | 0.409 | 0.027 | 0.055 | 0.0011 | 0.0158 | 0.0007 | 0.30 | 421 | 126 | 344 | 7 | 348 | 20 | 318 | 14 |
| MD-6-132-1r | fl | 0.057 | 0.005 | 0.138 | 0.012 | 0.018 | 0.0005 | 0.0116 | 0.0017 | 0.30 | 490 | 176 | 118 | 3 | 132 | 11 | 233 | 33 |
| MD-6-147-1r | fl | 0.056 | 0.004 | 0.135 | 0.011 | 0.017 | 0.0004 | 0.0144 | 0.0021 | 0.29 | 451 | 164 | 111 | 3 | 128 | 10 | 288 | 42 |
| MD-6-175-1c | hm | 0.052 | 0.003 | 0.118 | 0.008 | 0.017 | 0.0003 | 0.0089 | 0.0015 | 0.29 | 284 | 146 | 107 | 2 | 113 | 7 | 180 | 29 |
| MD-6-175-2r | fl | 0.048 | 0.003 | 0.109 | 0.007 | 0.017 | 0.0003 | 0.0070 | 0.0013 | 0.30 | 94 | 148 | 107 | 2 | 105 | 6 | 140 | 27 |
| MD29-1-1r | fl | 0.051 | 0.003 | 0.125 | 0.009 | 0.018 | 0.0004 | 0.0068 | 0.0007 | 0.32 | 228 | 153 | 114 | 3 | 120 | 8 | 138 | 13 |
| MD29-1-2c | pchy | 0.053 | 0.002 | 0.353 | 0.011 | 0.048 | 0.0009 | 0.0127 | 0.0005 | 0.60 | 337 | 65 | 303 | 6 | 307 | 8 | 256 | 10 |
| MD29-6-1r | fl | 0.054 | 0.002 | 0.409 | 0.015 | 0.056 | 0.0011 | 0.0175 | 0.0007 | 0.52 | 356 | 75 | 348 | 7 | 348 | 11 | 351 | 15 |
| MD29-6-2c | hm | 0.059 | 0.002 | 0.407 | 0.013 | 0.049 | 0.0009 | 0.0172 | 0.0006 | 0.59 | 572 | 63 | 309 | 6 | 347 | 9 | 344 | 13 |
| MD29-5-1c | hm | 0.048 | 0.002 | 0.147 | 0.006 | 0.022 | 0.0005 | 0.0077 | 0.0025 | 0.56 | 107 | 84 | 141 | 3 | 139 | 5 | 155 | 50 |
| MD29-32-1r | fl | 0.048 | 0.002 | 0.143 | 0.005 | 0.021 | 0.0004 | 0.0071 | 0.0023 | 0.56 | 118 | 80 | 136 | 3 | 136 | 5 | 143 | 46 |
| MD29-32-2c | hm | 0.048 | 0.002 | 0.132 | 0.005 | 0.020 | 0.0004 | 0.0058 | 0.0019 | 0.52 | 105 | 87 | 129 | 3 | 126 | 5 | 117 | 38 |
| MD29-9-1c | hm | 0.054 | 0.002 | 0.349 | 0.011 | 0.047 | 0.0009 | 0.0155 | 0.0006 | 0.61 | 353 | 64 | 297 | 6 | 304 | 8 | 310 | 11 |
| MD29-12-1c | hm | 0.056 | 0.002 | 0.447 | 0.014 | 0.058 | 0.0011 | 0.0192 | 0.0007 | 0.64 | 439 | 60 | 365 | 7 | 375 | 10 | 385 | 14 |
| MD29-47-1c | hm | 0.256 | 0.009 | 1.456 | 0.068 | 0.041 | 0.0009 | 0.0129 | 0.0006 | 0.47 | 3222 | 56 | 261 | 6 | 912 | 28 | 258 | 13 |
| MD29-33-1r | fl | 0.048 | 0.002 | 0.158 | 0.008 | 0.019 | 0.0004 | -0.0130 | 0.0045 | 0.47 | 98 | 109 | 120 | 3 | 149 | 7 | -264 | 92 |
| MD29-52-1c | fl | 0.054 | 0.002 | 0.408 | 0.012 | 0.055 | 0.0011 | 0.0176 | 0.0006 | 0.64 | 379 | 62 | 342 | 6 | 348 | 9 | 352 | 13 |
| MD29-53-1r | fl | 0.054 | 0.002 | 0.397 | 0.012 | 0.053 | 0.0010 | 0.0177 | 0.0007 | 0.65 | 384 | 62 | 334 | 6 | 339 | 9 | 355 | 13 |
| MD29-66-1r | fl | 0.053 | 0.002 | 0.314 | 0.010 | 0.043 | 0.0008 | 0.0135 | 0.0006 | 0.57 | 345 | 68 | 268 | 5 | 277 | 8 | 270 | 12 |
| MD29-67-1r | fl | 0.055 | 0.002 | 0.419 | 0.015 | 0.055 | 0.0012 | 0.0170 | 0.0008 | 0.58 | 397 | 71 | 348 | 7 | 355 | 11 | 341 | 15 |
| MD29-69-1c | hm | 0.056 | 0.002 | 0.374 | 0.014 | 0.048 | 0.0010 | 0.0161 | 0.0007 | 0.55 | 436 | 71 | 304 | 6 | 323 | 10 | 323 | 13 |
| MD29-70-1c | hm | 0.048 | 0.006 | 0.127 | 0.017 | 0.019 | 0.0005 | 0.0064 | 0.0007 | 0.20 | 104 | 292 | 123 | 3 | 122 | 15 | 128 | 15 |
| MD29-86-1r | fl | 0.060 | 0.007 | 0.203 | 0.027 | 0.025 | 0.0008 | 0.0092 | 0.0007 | 0.24 | 602 | 258 | 158 | 5 | 188 | 22 | 185 | 14 |
| MD29-86-2c | osc | 0.054 | 0.002 | 0.402 | 0.012 | 0.054 | 0.0011 | 0.0171 | 0.0006 | 0.64 | 384 | 62 | 339 | 6 | 343 | 9 | 342 | 13 |
| MD29-90-1r | fl | 0.049 | 0.001 | 0.131 | 0.004 | nd | nd | 0.0064 | 0.0003 | nd | 153 | 66 | nd | nd | 125 | 4 | 129 | 7 |

| Isotope ratios | | | | | | | | | | | Isotopic ages | | | | | | | |
|---|---|---|---|---|---|---|---|---|---|---|---|---|---|---|---|---|---|---|
| Sample No | zoning | Pb207/Pb206 | ± 2SE | Pb207/U235 | ± 2SE | Pb206/U238 | ± 2SE | Pb208/Th232 | ± 2SE | error corr. | Pb207/Pb206 | ± 2SE | Pb206/U238 | ± 2SE | Pb207/U235 | ± 2SE | Pb208/Th232 | ± 2SE |
| MD29-91-1r | fl | 0.143 | 0.005 | 0.392 | 0.014 | 0.020 | 0.0004 | 0.1181 | 0.0052 | 0.57 | 2267 | 55 | 126 | 3 | 336 | 10 | 2257 | 95 |
| MD29-101-1c | hm | 0.056 | 0.002 | 0.390 | 0.012 | 0.051 | 0.0010 | 0.0167 | 0.0006 | 0.63 | 444 | 61 | 318 | 6 | 334 | 9 | 335 | 13 |
| MD33-43c | pchy | 0.059 | 0.005 | 0.170 | 0.015 | 0.021 | 0.0005 | 0.0107 | 0.0021 | 0.26 | 569 | 173 | 132 | 3 | 159 | 14 | 215 | 42 |
| MD33-29c | hm,pchy | 0.055 | 0.003 | 0.404 | 0.028 | 0.054 | 0.0012 | 0.0183 | 0.0034 | 0.31 | 405 | 126 | 340 | 7 | 344 | 24 | 367 | 69 |
| MD33-29r | fl | 0.048 | 0.003 | 0.124 | 0.010 | 0.019 | 0.0004 | 0.0053 | 0.0013 | 0.29 | 95 | 151 | 120 | 3 | 119 | 9 | 107 | 26 |
| MD33-2c | hm | 0.058 | 0.003 | 0.323 | 0.023 | 0.041 | 0.0009 | 0.0153 | 0.0029 | 0.30 | 517 | 128 | 260 | 6 | 284 | 21 | 308 | 59 |
| MD33-2r | fl | 0.050 | 0.004 | 0.132 | 0.011 | 0.019 | 0.0004 | 0.0065 | 0.0015 | 0.27 | 206 | 169 | 121 | 3 | 126 | 11 | 131 | 30 |
| MD33-58c | pchy,osc | 0.053 | 0.003 | 0.435 | 0.033 | 0.060 | 0.0013 | 0.0189 | 0.0037 | 0.29 | 348 | 135 | 373 | 8 | 367 | 27 | 378 | 74 |
| MD33-58r | fl | 0.054 | 0.003 | 0.338 | 0.024 | 0.046 | 0.0010 | 0.0154 | 0.0031 | 0.30 | 351 | 128 | 292 | 6 | 295 | 21 | 308 | 61 |
| MD-33-3-1r | fl | 0.052 | 0.002 | 0.380 | 0.014 | 0.053 | 0.0009 | 0.0160 | 0.0006 | 0.46 | 279 | 75 | 333 | 5 | 327 | 10 | 322 | 13 |
| MD-33-9-1r | fl | 0.050 | 0.002 | 0.144 | 0.007 | 0.021 | 0.0004 | 0.0091 | 0.0010 | 0.38 | 211 | 106 | 133 | 2 | 137 | 6 | 182 | 20 |
| MD-33-22-1r | osc | 0.053 | 0.002 | 0.376 | 0.013 | 0.051 | 0.0008 | 0.0164 | 0.0006 | 0.49 | 350 | 70 | 322 | 5 | 324 | 9 | 329 | 13 |
| MD-33-18-1r | fl | 0.053 | 0.002 | 0.269 | 0.012 | 0.037 | 0.0007 | 0.0134 | 0.0006 | 0.41 | 311 | 94 | 233 | 4 | 242 | 10 | 268 | 11 |
| MD-33-24-1r | fl | 0.055 | 0.002 | 0.406 | 0.018 | 0.054 | 0.0009 | 0.0171 | 0.0007 | 0.41 | 419 | 84 | 336 | 6 | 346 | 13 | 342 | 14 |
| MD-33-28-1r | fl | 0.056 | 0.002 | 0.358 | 0.014 | 0.046 | 0.0008 | 0.0159 | 0.0007 | 0.43 | 453 | 79 | 292 | 5 | 311 | 11 | 318 | 13 |
| MD-33-32-1r | fl | 0.053 | 0.002 | 0.350 | 0.014 | 0.047 | 0.0008 | 0.0155 | 0.0006 | 0.43 | 328 | 81 | 298 | 5 | 305 | 10 | 311 | 12 |
| MD-33-32-2c | hm | 0.053 | 0.003 | 0.394 | 0.025 | 0.053 | 0.0010 | 0.0179 | 0.0008 | 0.30 | 307 | 127 | 333 | 6 | 337 | 18 | 359 | 15 |
| MD-33-48-1r | hm | 0.056 | 0.002 | 0.408 | 0.015 | 0.052 | 0.0009 | 0.0162 | 0.0006 | 0.47 | 469 | 73 | 329 | 5 | 347 | 11 | 324 | 13 |
| MD-33-33-1r | fl | 0.053 | 0.002 | 0.353 | 0.012 | 0.049 | 0.0008 | 0.0149 | 0.0006 | 0.51 | 335 | 70 | 306 | 5 | 307 | 9 | 298 | 11 |
| MD-33-48-2r | fl | 0.054 | 0.002 | 0.377 | 0.015 | 0.050 | 0.0009 | 0.0161 | 0.0006 | 0.43 | 368 | 82 | 315 | 5 | 325 | 11 | 323 | 12 |
| MD-33-40-1r | fl | 0.052 | 0.002 | 0.396 | 0.016 | 0.055 | 0.0009 | 0.0174 | 0.0007 | 0.43 | 264 | 83 | 344 | 6 | 339 | 12 | 349 | 14 |
| MD-33-51-1r | hm | 0.054 | 0.002 | 0.412 | 0.013 | 0.055 | 0.0009 | 0.0176 | 0.0006 | 0.52 | 365 | 66 | 345 | 6 | 350 | 9 | 353 | 13 |
| MD-33-72-1r | fl | 0.054 | 0.002 | 0.318 | 0.015 | 0.042 | 0.0008 | 0.0146 | 0.0006 | 0.39 | 352 | 96 | 267 | 5 | 280 | 11 | 294 | 13 |
| MD-33-84-1c | pchy | 0.059 | 0.002 | 0.426 | 0.019 | 0.052 | 0.0009 | 0.0196 | 0.0008 | 0.40 | 560 | 85 | 330 | 6 | 360 | 13 | 392 | 16 |
| MD14-11-1 r | fl | 0.053 | 0.003 | 0.339 | 0.022 | 0.048 | 0.0011 | 0.0164 | 0.0008 | 0.35 | 314 | 131 | 301 | 7 | 296 | 17 | 328 | 17 |
| MD14-10-1r | fl | 0.053 | 0.006 | 0.145 | 0.017 | 0.020 | 0.0006 | 0.0069 | 0.0006 | 0.24 | 320 | 248 | 130 | 4 | 137 | 15 | 139 | 12 |
| MD14-10-2c | hm | 0.053 | 0.002 | 0.380 | 0.016 | 0.053 | 0.0011 | 0.0178 | 0.0008 | 0.49 | 333 | 85 | 333 | 7 | 327 | 12 | 356 | 16 |
| MD14-6-1r | fl | 0.050 | 0.004 | 0.137 | 0.012 | 0.020 | 0.0005 | 0.0065 | 0.0004 | 0.30 | 179 | 186 | 128 | 3 | 130 | 10 | 130 | 8 |
| MD14-6-2c | hm,osc | 0.053 | 0.002 | 0.366 | 0.016 | 0.050 | 0.0011 | 0.0160 | 0.0007 | 0.50 | 345 | 85 | 314 | 7 | 317 | 12 | 321 | 14 |
| MD14-15-1r | fl | 0.054 | 0.002 | 0.342 | 0.014 | 0.046 | 0.0010 | 0.0157 | 0.0010 | 0.52 | 384 | 83 | 289 | 6 | 299 | 11 | 315 | 20 |
| MD14-18-1r | fl | 0.049 | 0.006 | 0.167 | 0.021 | 0.025 | 0.0008 | 0.0074 | 0.0009 | 0.25 | 164 | 272 | 158 | 5 | 157 | 18 | 149 | 18 |
| MD14-24-1r | fl | 0.054 | 0.004 | 0.365 | 0.029 | 0.048 | 0.0011 | 0.0176 | 0.0011 | 0.30 | 389 | 152 | 302 | 7 | 316 | 21 | 353 | 21 |
| MD14-30-1r | fl | 0.051 | 0.007 | 0.158 | 0.024 | 0.022 | 0.0008 | 0.0079 | 0.0008 | 0.25 | 237 | 316 | 141 | 5 | 149 | 21 | 159 | 17 |

| Isotope ratios | | | | | | | | | | | Isotopic ages | | | | | | | |
|---|---|---|---|---|---|---|---|---|---|---|---|---|---|---|---|---|---|---|
| Sample No | zoning | Pb207/Pb206 | ± 2SE | Pb207/U235 | ± 2SE | Pb206/U238 | ± 2SE | Pb208/Th232 | ± 2SE | error corr. | Pb207/Pb206 | ± 2SE | Pb206/U238 | ± 2SE | Pb207/U235 | ± 2SE | Pb208/Th232 | ± 2SE |
| MD14-29-1c | hm | 0.051 | 0.004 | 0.244 | 0.020 | 0.035 | 0.0009 | 0.0113 | 0.0007 | 0.32 | 257 | 171 | 219 | 6 | 222 | 16 | 227 | 14 |
| MD14-32-1r | hm | 0.053 | 0.002 | 0.351 | 0.018 | 0.048 | 0.0011 | 0.0153 | 0.0007 | 0.44 | 346 | 102 | 304 | 7 | 306 | 14 | 307 | 14 |
| MD14-33-1r | fl | 0.053 | 0.003 | 0.393 | 0.025 | 0.053 | 0.0012 | 0.0162 | 0.0008 | 0.37 | 344 | 124 | 330 | 8 | 337 | 18 | 324 | 16 |
| MD14-35-1c | pchy | 0.051 | 0.003 | 0.330 | 0.023 | 0.047 | 0.0012 | 0.0154 | 0.0009 | 0.36 | 259 | 140 | 295 | 7 | 290 | 18 | 309 | 17 |
| MD14-40-1r | fl | 0.052 | 0.003 | 0.329 | 0.022 | 0.046 | 0.0011 | 0.0159 | 0.0008 | 0.38 | 299 | 133 | 288 | 7 | 289 | 17 | 319 | 17 |
| MD14-50-1r | osc | 0.052 | 0.005 | 0.139 | 0.014 | 0.019 | 0.0005 | 0.0072 | 0.0006 | 0.27 | 293 | 219 | 123 | 3 | 133 | 13 | 145 | 11 |
| MD14-50-2c | osc | 0.053 | 0.002 | 0.377 | 0.017 | 0.051 | 0.0011 | 0.0165 | 0.0008 | 0.48 | 329 | 90 | 322 | 7 | 325 | 13 | | 15 |
| MD14-51-1c | pln | 0.053 | 0.004 | 0.348 | 0.029 | 0.047 | 0.0013 | 0.0152 | 0.0010 | 0.34 | 340 | 162 | 294 | 8 | 303 | 22 | 304 | 19 |
| MD14-43-1r | fl | 0.063 | 0.007 | 0.163 | 0.018 | 0.019 | 0.0006 | 0.0080 | 0.0007 | 0.29 | 704 | 215 | 119 | 4 | 154 | 16 | 160 | 14 |
| MD14-48-1r | osc | 0.054 | 0.003 | 0.405 | 0.025 | 0.053 | 0.0013 | 0.0169 | 0.0008 | 0.39 | 376 | 119 | 331 | 8 | 345 | 18 | 339 | 16 |
| MD14-63-1r | fl | 0.056 | 0.004 | 0.290 | 0.022 | 0.038 | 0.0010 | 0.0155 | 0.0008 | 0.34 | 464 | 147 | 239 | 6 | 259 | 17 | 310 | 17 |
| MD14-64-1r | fl | 0.049 | 0.005 | 0.115 | 0.011 | 0.017 | 0.0005 | 0.0060 | 0.0006 | 0.28 | 124 | 219 | 111 | 3 | 111 | 10 | 121 | 12 |
| MD14-66-1r | fl | 0.046 | 0.005 | 0.114 | 0.013 | 0.018 | 0.0005 | 0.0062 | 0.0006 | 0.26 | 8 | 249 | 116 | 3 | 110 | 12 | 125 | 12 |
| MD14-69-1r | fl | 0.053 | 0.002 | 0.274 | 0.013 | 0.037 | 0.0009 | 0.0137 | 0.0009 | 0.48 | 327 | 97 | 236 | 5 | 246 | 11 | 275 | 18 |
| MD14-68-1r | fl | 0.054 | 0.006 | 0.130 | 0.015 | 0.018 | 0.0006 | 0.0056 | 0.0005 | 0.29 | 377 | 232 | 112 | 4 | 124 | 13 | 112 | 11 |
| MD14-71-1r | fl | 0.059 | 0.005 | 0.349 | 0.032 | 0.043 | 0.0012 | 0.0139 | 0.0009 | 0.32 | 562 | 171 | 270 | 8 | 304 | 24 | 280 | 19 |
| MD14-42-1r | hm | 0.051 | 0.003 | 0.364 | 0.022 | 0.051 | 0.0012 | 0.0162 | 0.0008 | 0.39 | 250 | 120 | 320 | 7 | 315 | 16 | 324 | 15 |
| MD14-79-1r | fl | 0.054 | 0.004 | 0.339 | 0.025 | 0.045 | 0.0011 | 0.0143 | 0.0008 | 0.34 | 357 | 146 | 284 | 7 | 297 | 19 | 287 | 16 |
| MD14-89-1c | pln | 0.049 | 0.005 | 0.125 | 0.013 | 0.018 | 0.0005 | 0.0060 | 0.0005 | 0.27 | 166 | 233 | 118 | 3 | 120 | 12 | 122 | 9 |
| MD14-110-1c | hm | 0.053 | 0.003 | 0.289 | 0.017 | 0.039 | 0.0009 | 0.0141 | 0.0007 | 0.39 | 336 | 121 | 248 | 6 | 257 | 14 | 282 | 14 |
| MD14-128-1r | pchy | 0.054 | 0.002 | 0.319 | 0.014 | 0.044 | 0.0010 | 0.0172 | 0.0008 | 0.49 | 353 | 89 | 278 | 6 | 281 | 11 | 344 | 15 |
| MD14-130-1r | pchy | 0.054 | 0.003 | 0.362 | 0.020 | 0.050 | 0.0011 | 0.0163 | 0.0007 | 0.41 | 366 | 109 | 314 | 7 | 313 | 15 | 327 | 14 |
| MD38-23-1r | fl | 0.055 | 0.005 | 0.184 | 0.017 | 0.024 | 0.0007 | 0.0086 | 0.0006 | 0.30 | 417 | 186 | 155 | 4 | 172 | 14 | 173 | 11 |
| MD38-23-2c | pchy | 0.056 | 0.003 | 0.351 | 0.020 | 0.046 | 0.0011 | 0.0151 | 0.0006 | 0.41 | 463 | 111 | 290 | 7 | 305 | 15 | 304 | 12 |
| MD38-2-1c | hm | 0.054 | 0.002 | 0.403 | 0.019 | 0.055 | 0.0012 | 0.0166 | 0.0006 | 0.47 | 354 | 94 | 344 | 7 | 344 | 14 | 333 | 12 |
| MD38-27-1r | fl | 0.054 | 0.002 | 0.394 | 0.016 | 0.053 | 0.0012 | 0.0165 | 0.0006 | 0.54 | 353 | 81 | 336 | 7 | 338 | 12 | 331 | 12 |
| MD38-27-2c | pln | 0.054 | 0.002 | 0.393 | 0.020 | 0.053 | 0.0012 | 0.0162 | 0.0006 | 0.45 | 350 | 100 | 331 | 7 | 337 | 14 | 324 | 12 |
| MD38-47-1c | pchy | 0.053 | 0.005 | 0.175 | 0.017 | 0.024 | 0.0007 | 0.0083 | 0.0005 | 0.28 | 326 | 210 | 152 | 4 | 164 | 15 | 168 | 11 |

| Isotope ratios | | | | | | | | | | | Isotopic ages | | | | | | | |
|---|---|---|---|---|---|---|---|---|---|---|---|---|---|---|---|---|---|---|
| Sample No | zoning | Pb207/Pb206 | ± 2SE | Pb207/U235 | ± 2SE | Pb206/U238 | ± 2SE | Pb208/Th232 | ± 2SE | error corr. | Pb207/Pb206 | ± 2SE | Pb206/U238 | ± 2SE | Pb207/U235 | ± 2SE | Pb208/Th232 | ± 2SE |
| MD38-101-1c | pchy | 0.053 | 0.003 | 0.361 | 0.025 | 0.050 | 0.0012 | 0.0143 | 0.0009 | 0.36 | 347 | 135 | 317 | 7 | 313 | 18 | 287 | 17 |
| MD38-129-1r | fl | 0.055 | 0.005 | 0.393 | 0.037 | 0.053 | 0.0015 | 0.0186 | 0.0011 | 0.29 | 410 | 183 | 334 | 9 | 337 | 27 | 373 | 21 |
| MD38-132-1c | pln | 0.055 | 0.004 | 0.263 | 0.022 | 0.035 | 0.0009 | 0.0132 | 0.0006 | 0.31 | 417 | 170 | 219 | 6 | 237 | 18 | 266 | 12 |
| MD38-147-1c | pchy | 0.056 | 0.005 | 0.312 | 0.028 | 0.041 | 0.0011 | 0.0116 | 0.0007 | 0.29 | 443 | 178 | 258 | 7 | 276 | 22 | 232 | 14 |
| MD38-172-1r | fl | 0.054 | 0.003 | 0.343 | 0.020 | 0.047 | 0.0011 | 0.0144 | 0.0006 | 0.41 | 389 | 116 | 294 | 7 | 299 | 15 | 289 | 11 |
| MD38-174-1r | fl | 0.053 | 0.002 | 0.287 | 0.014 | 0.039 | 0.0009 | 0.0166 | 0.0005 | 0.48 | 335 | 98 | 247 | 5 | 256 | 11 | 332 | 10 |
| MD38-174-2c | hm | 0.053 | 0.002 | 0.372 | 0.014 | 0.051 | 0.0011 | 0.0167 | 0.0005 | 0.57 | 369 | 112 | 212 | 5 | 276 | 15 | 304 | 29 |
| MD38-170-1c | hm | 0.054 | 0.003 | 0.396 | 0.023 | 0.054 | 0.0012 | 0.0168 | 0.0006 | 0.40 | 369 | 111 | 212 | 5 | 277 | 15 | 304 | 29 |
| MD38-169 r | pchy | 0.055 | 0.007 | 0.347 | 0.048 | 0.046 | 0.0013 | 0.0143 | 0.0012 | 0.20 | 369 | 110 | 213 | 5 | 277 | 15 | 305 | 29 |
| MD38-169-1r | fl | 0.053 | 0.004 | 0.292 | 0.021 | 0.040 | 0.0010 | 0.0122 | 0.0005 | 0.34 | 369 | 109 | 213 | 5 | 278 | 15 | 305 | 29 |
| MD38-169-2c | pchy | 0.053 | 0.002 | 0.381 | 0.018 | 0.052 | 0.0012 | 0.0159 | 0.0005 | 0.47 | 369 | 109 | 214 | 5 | 278 | 15 | 306 | 29 |
| MD38-183-1r | fl | 0.059 | 0.004 | 0.373 | 0.025 | 0.046 | 0.0011 | 0.0149 | 0.0007 | 0.37 | 369 | 108 | 214 | 5 | 278 | 15 | 306 | 29 |
| MD38-183-2c | pchy | 0.057 | 0.003 | 0.406 | 0.022 | 0.052 | 0.0012 | 0.0160 | 0.0006 | 0.43 | 369 | 107 | 215 | 5 | 279 | 15 | 307 | 29 |
| MD38-194-1r | fl | 0.054 | 0.003 | 0.254 | 0.016 | 0.034 | 0.0008 | 0.0123 | 0.0007 | 0.38 | 369 | 106 | 215 | 5 | 279 | 15 | 307 | 29 |
| MD38-194-2r | fl | 0.061 | 0.003 | 0.361 | 0.018 | 0.043 | 0.0010 | 0.0135 | 0.0005 | 0.45 | 369 | 105 | 215 | 5 | 280 | 15 | 308 | 30 |
| MD38-194-3c | hm | 0.055 | 0.003 | 0.404 | 0.021 | 0.054 | 0.0012 | 0.0175 | 0.0006 | 0.44 | 369 | 105 | 216 | 5 | 280 | 15 | 308 | 30 |
| MD38-195-1r | fl | 0.053 | 0.002 | 0.344 | 0.015 | 0.046 | 0.0010 | 0.0188 | 0.0006 | 0.52 | 370 | 104 | 216 | 5 | 280 | 15 | 309 | 30 |
| MD38-201-1r | fl | 0.055 | 0.003 | 0.334 | 0.017 | 0.044 | 0.0010 | 0.0164 | 0.0005 | 0.45 | 370 | 103 | 217 | 5 | 281 | 15 | 309 | 30 |
| MD38-135-1c | pchy | 0.053 | 0.002 | 0.384 | 0.016 | 0.053 | 0.0012 | 0.0162 | 0.0005 | 0.54 | 370 | 102 | 217 | 5 | 281 | 15 | 310 | 30 |
| MD38-134-1c | pchy | 0.053 | 0.002 | 0.328 | 0.013 | 0.045 | 0.0010 | 0.0148 | 0.0004 | 0.55 | 370 | 101 | 218 | 5 | 281 | 15 | 310 | 30 |
| MD38-133-1r | fl | 0.053 | 0.002 | 0.337 | 0.012 | 0.046 | 0.0010 | 0.0163 | 0.0006 | 0.63 | 370 | 101 | 218 | 5 | 282 | 15 | 311 | 30 |
| MD38-133-2c | fl | 0.052 | 0.002 | 0.273 | 0.009 | 0.039 | 0.0008 | 0.0140 | 0.0005 | 0.69 | 370 | 100 | 219 | 5 | 282 | 15 | 311 | 30 |
| MD38-135a-1c | pchy | 0.058 | 0.003 | 0.433 | 0.021 | 0.055 | 0.0012 | 0.0226 | 0.0007 | 0.46 | 370 | 99 | 219 | 5 | 283 | 15 | 312 | 30 |
| MD38-37-1c | pchy | 0.050 | 0.004 | 0.136 | 0.010 | 0.020 | 0.0005 | 0.0071 | 0.0005 | 0.34 | 370 | 98 | 219 | 5 | 283 | 15 | 312 | 30 |
| MD38-40-1r | fl | 0.053 | 0.002 | 0.383 | 0.016 | 0.053 | 0.0012 | 0.0165 | 0.0005 | 0.54 | 370 | 97 | 220 | 5 | 283 | 15 | 313 | 30 |
| MD38-40-2c | hm,osc | 0.052 | 0.002 | 0.376 | 0.013 | 0.052 | 0.0011 | 0.0164 | 0.0005 | 0.61 | 370 | 97 | 220 | 5 | 284 | 15 | 313 | 30 |
| MD38-42-1r | hm | 0.053 | 0.002 | 0.376 | 0.015 | 0.051 | 0.0011 | 0.0187 | 0.0009 | 0.57 | 370 | 96 | 221 | 5 | 284 | 14 | 314 | 30 |

# *Appendix 4- Electron Probe Microanalyses of Mt Daniel Samples*

***Appendix 4.1. Zircon Major Element Analyses of Mt Daniel Samples, recalculated on the basis of oxygen=12,*** *abbreviations are: cent=centre (used for the grains without inherited cores), int=intermediate.*

| | | IN wt % | | | | | Cation | | | | | In ppm | | |
|---|---|---|---|---|---|---|---|---|---|---|---|---|---|---|
| SL NO | | SiO2 | HfO2 | Y2O3 | ZrO2 | Total | Si | Hf | Y | Zr | SUM | Hf | Y | Zr |
| MD15-20-1 | rim | 32.58 | 1.33 | 0.00 | 65.22 | 99.14 | 3.02 | 0.04 | 0.000 | 2.95 | 6 | 11269 | 0 | 482853 |
| MD15-20-2 | cent | 32.79 | 1.14 | 0.07 | 65.12 | 99.12 | 3.03 | 0.03 | 0.003 | 2.94 | 6 | 9649 | 543 | 482083 |
| MD15-20-3 | rim | 32.65 | 1.14 | 0.05 | 65.05 | 98.89 | 3.03 | 0.03 | 0.003 | 2.94 | 6 | 9649 | 402 | 481573 |
| MD15-20-5 | cent | 32.89 | 1.19 | 0.00 | 65.48 | 99.56 | 3.03 | 0.03 | 0.000 | 2.94 | 6 | 10056 | 16 | 484771 |
| MD15-20-6 | rim | 32.91 | 1.15 | 0.13 | 65.06 | 99.25 | 3.04 | 0.03 | 0.006 | 2.93 | 6 | 9742 | 1031 | 481602 |
| MD15-18-1 | rim | 32.79 | 1.45 | 0.00 | 65.54 | 99.78 | 3.02 | 0.04 | 0.000 | 2.94 | 6 | 12269 | 0 | 485207 |
| MD15-18-2 | int | 32.61 | 1.22 | 0.04 | 65.82 | 99.69 | 3.01 | 0.03 | 0.002 | 2.96 | 6 | 10353 | 307 | 487280 |
| MD15-18-3 | cent | 32.67 | 1.28 | 0.01 | 65.33 | 99.29 | 3.02 | 0.03 | 0.000 | 2.95 | 6 | 10879 | 71 | 483668 |
| MD15-18-4 | int | 32.74 | 1.20 | 0.02 | 65.36 | 99.33 | 3.02 | 0.03 | 0.001 | 2.94 | 6 | 10141 | 173 | 483890 |
| MD15-18-5 | rim | 32.71 | 1.07 | 0.03 | 65.43 | 99.24 | 3.02 | 0.03 | 0.001 | 2.95 | 6 | 9098 | 220 | 484386 |
| MD15-29-1 | rim | 32.91 | 1.26 | 0.05 | 64.85 | 99.07 | 3.04 | 0.03 | 0.003 | 2.92 | 6 | 10667 | 425 | 480055 |
| MD15-29-2 | cent | 32.98 | 1.17 | 0.11 | 65.04 | 99.30 | 3.04 | 0.03 | 0.005 | 2.92 | 6 | 9878 | 882 | 481469 |
| MD15-29-3 | rim | 32.83 | 1.23 | 0.01 | 65.13 | 99.21 | 3.03 | 0.03 | 0.001 | 2.93 | 6 | 10463 | 87 | 482157 |
| MD15-14-1 | rim | 32.66 | 1.06 | 0.13 | 64.87 | 98.71 | 3.03 | 0.03 | 0.006 | 2.94 | 6 | 8945 | 1024 | 480210 |
| MD15-14-2 | cent | 32.69 | 1.17 | 0.08 | 65.53 | 99.46 | 3.02 | 0.03 | 0.004 | 2.95 | 6 | 9887 | 591 | 485082 |
| MD15-14-3 | rim | 32.75 | 1.17 | 0.04 | 65.01 | 98.97 | 3.03 | 0.03 | 0.002 | 2.93 | 6 | 9954 | 307 | 481262 |
| MD15-8-1 | rim | 32.88 | 1.24 | 0.01 | 65.54 | 99.67 | 3.03 | 0.03 | 0.000 | 2.94 | 6 | 10514 | 47 | 485207 |
| MD15-8-2 | int | 32.65 | 1.10 | 0.09 | 64.43 | 98.27 | 3.04 | 0.03 | 0.004 | 2.93 | 6 | 9352 | 693 | 476975 |
| MD15-50-1 | rim | 32.93 | 1.28 | 0.03 | 64.63 | 98.87 | 3.05 | 0.03 | 0.002 | 2.92 | 6 | 10870 | 268 | 478441 |
| MD15-50-2 | int | 32.77 | 1.25 | 0.10 | 64.81 | 98.93 | 3.04 | 0.03 | 0.005 | 2.93 | 6 | 10616 | 780 | 479774 |
| MD15-50-3 | rim | 32.83 | 1.19 | 0.07 | 64.61 | 98.69 | 3.04 | 0.03 | 0.003 | 2.92 | 6 | 10073 | 528 | 478278 |
| MD15-47-1 | int | 32.98 | 1.18 | 0.09 | 64.37 | 98.62 | 3.06 | 0.03 | 0.005 | 2.91 | 6 | 10031 | 724 | 476516 |
| MD15-47-2 | int | 32.87 | 1.26 | 0.14 | 64.86 | 99.12 | 3.04 | 0.03 | 0.007 | 2.92 | 6 | 10641 | 1118 | 480159 |
| MD15-47-3 | rim | 32.98 | 1.25 | 0.02 | 64.58 | 98.83 | 3.05 | 0.03 | 0.001 | 2.91 | 6 | 10607 | 142 | 478078 |
| MD15-47-4 | rim | 32.94 | 1.17 | 0.06 | 64.82 | 98.99 | 3.05 | 0.03 | 0.003 | 2.92 | 6 | 9912 | 496 | 479825 |
| MD15-56-1 | cent | 32.81 | 1.26 | 0.05 | 64.63 | 98.75 | 3.04 | 0.03 | 0.003 | 2.92 | 6 | 10700 | 417 | 478471 |
| MD15-56-2 | cent | 32.79 | 1.26 | 0.06 | 64.97 | 99.07 | 3.03 | 0.03 | 0.003 | 2.93 | 6 | 10675 | 457 | 480943 |
| MD15-56-3 | cent | 32.87 | 1.37 | 0.05 | 65.22 | 99.51 | 3.03 | 0.04 | 0.002 | 2.93 | 6 | 11616 | 370 | 482809 |
| MD15-56-4 | int | 32.53 | 1.14 | 0.12 | 65.12 | 98.90 | 3.02 | 0.03 | 0.006 | 2.95 | 6 | 9666 | 945 | 482046 |
| MD15-64-1 | rim | 32.69 | 1.12 | 0.12 | 65.15 | 99.09 | 3.03 | 0.03 | 0.006 | 2.94 | 6 | 9488 | 976 | 482305 |
| MD15-64-2 | cent | 32.79 | 1.14 | 0.06 | 65.03 | 99.03 | 3.03 | 0.03 | 0.003 | 2.93 | 6 | 9641 | 488 | 481447 |
| MD15-64-3 | rim | 32.73 | 1.34 | 0.06 | 65.21 | 99.35 | 3.02 | 0.04 | 0.003 | 2.94 | 6 | 11370 | 504 | 482772 |
| MD15-101-1 | cent | 32.74 | 1.15 | 0.12 | 65.58 | 99.59 | 3.02 | 0.03 | 0.006 | 2.95 | 6 | 9768 | 906 | 485489 |
| MD15-101-2 | rim | 32.63 | 1.17 | 0.03 | 65.35 | 99.18 | 3.02 | 0.03 | 0.001 | 2.95 | 6 | 9912 | 197 | 483816 |
| MD15-110-1 | cent | 32.75 | 1.23 | 0.02 | 65.51 | 99.51 | 3.02 | 0.03 | 0.001 | 2.95 | 6 | 10429 | 126 | 484985 |
| MD15-110-2 | rim | 32.81 | 1.29 | 0.03 | 65.36 | 99.49 | 3.03 | 0.03 | 0.001 | 2.94 | 6 | 10912 | 228 | 483882 |
| MD15-110-3 | int | 32.92 | 1.33 | 0.08 | 64.96 | 99.29 | 3.04 | 0.04 | 0.004 | 2.92 | 6 | 11269 | 646 | 480891 |
| MD15-110-4 | int | 32.79 | 1.19 | 0.06 | 65.56 | 99.59 | 3.02 | 0.03 | 0.003 | 2.95 | 6 | 10090 | 449 | 485311 |
| MD15-145-1 | cent | 32.74 | 1.17 | 0.13 | 65.43 | 99.46 | 3.02 | 0.03 | 0.007 | 2.94 | 6 | 9878 | 1055 | 484371 |
| MD15-145-2 | cent | 32.79 | 1.03 | 0.11 | 65.27 | 99.20 | 3.03 | 0.03 | 0.005 | 2.94 | 6 | 8750 | 827 | 483209 |
| MD15-145-3 | rim | 32.94 | 1.14 | 0.02 | 65.72 | 99.82 | 3.03 | 0.03 | 0.001 | 2.94 | 6 | 9675 | 134 | 486518 |
| MD15-145-4 | cent | 32.79 | 1.14 | 0.11 | 65.45 | 99.49 | 3.02 | 0.03 | 0.005 | 2.94 | 6 | 9641 | 850 | 484534 |
| MD15-145-5 | cent | 32.89 | 1.10 | 0.11 | 65.71 | 99.81 | 3.02 | 0.03 | 0.005 | 2.94 | 6 | 9344 | 843 | 486444 |
| MD15-167-1 | rim | 32.75 | 1.44 | 0.06 | 64.49 | 98.73 | 3.04 | 0.04 | 0.003 | 2.92 | 6 | 12201 | 449 | 477412 |
| MD15-167-2 | cent | 32.59 | 1.09 | 0.11 | 64.83 | 98.61 | 3.03 | 0.03 | 0.005 | 2.94 | 6 | 9225 | 850 | 479914 |
| MD15-167-3 | rim | 32.73 | 1.24 | 0.02 | 65.08 | 99.06 | 3.03 | 0.03 | 0.001 | 2.94 | 6 | 10514 | 173 | 481765 |
| MD15-167-4 | cent | 32.67 | 1.16 | 0.07 | 65.23 | 99.13 | 3.02 | 0.03 | 0.003 | 2.94 | 6 | 9844 | 535 | 482912 |

| | | IN wt % | | | | | Cation | | | | | In ppm | | |
|---|---|---|---|---|---|---|---|---|---|---|---|---|---|---|
| SL NO | | SiO2 | HfO2 | Y2O3 | ZrO2 | Total | Si | Hf | Y | Zr | SUM | Hf | Y | Zr |
| MD13-3-1 | int | 32.80 | 0.83 | 0.10 | 66.39 | 100.12 | 3.01 | 0.02 | 0.005 | 2.97 | 6 | 7046 | 787 | 491456 |
| MD13-3-2 | cent | 32.79 | 0.73 | 0.01 | 68.21 | 101.74 | 2.97 | 0.02 | 0.001 | 3.01 | 6 | 6198 | 94 | 504922 |
| MD13-3-4 | rim | 32.66 | 0.92 | 0.00 | 67.85 | 101.42 | 2.97 | 0.02 | 0.000 | 3.01 | 6 | 7767 | 0 | 502279 |
| MD13-27-1 | int | 32.64 | 0.78 | 0.04 | 67.89 | 101.35 | 2.97 | 0.02 | 0.002 | 3.01 | 6 | 6622 | 323 | 502567 |
| MD13-27-2 | int | 32.51 | 0.81 | 0.04 | 68.02 | 101.39 | 2.96 | 0.02 | 0.002 | 3.02 | 6 | 6902 | 339 | 503515 |
| MD13-27-3 | rim | 32.62 | 0.92 | 0.01 | 68.17 | 101.72 | 2.96 | 0.02 | 0.001 | 3.02 | 6 | 7775 | 87 | 504677 |
| MD13-20-1 | int | 32.52 | 0.86 | 0.05 | 68.14 | 101.57 | 2.96 | 0.02 | 0.003 | 3.02 | 6 | 7275 | 425 | 504403 |
| MD13-20-2 | - | 32.79 | 0.80 | 0.00 | 68.10 | 101.69 | 2.97 | 0.02 | 0.000 | 3.01 | 6 | 6792 | 0 | 504129 |
| MD13-20-3 | int | 32.48 | 0.73 | 0.04 | 67.68 | 100.93 | 2.97 | 0.02 | 0.002 | 3.01 | 6 | 6224 | 307 | 501035 |
| MD13-8-1 | rim | 32.63 | 1.03 | 0.01 | 68.21 | 101.88 | 2.96 | 0.03 | 0.000 | 3.01 | 6 | 8733 | 47 | 504966 |
| MD13-8-2 | - | 32.52 | 0.89 | 0.00 | 68.22 | 101.62 | 2.95 | 0.02 | 0.000 | 3.02 | 6 | 7538 | 0 | 505003 |
| MD13-8-3 | rim | 32.65 | 0.90 | 0.00 | 67.98 | 101.53 | 2.97 | 0.02 | 0.000 | 3.01 | 6 | 7657 | 0 | 503226 |
| MD13-8-4 | | 32.66 | 0.80 | 0.06 | 67.80 | 101.31 | 2.97 | 0.02 | 0.003 | 3.01 | 6 | 6741 | 449 | 501923 |
| MD13-17-1 | cent | 32.71 | 0.87 | 0.07 | 67.94 | 101.59 | 2.97 | 0.02 | 0.003 | 3.01 | 6 | 7402 | 543 | 502930 |
| MD13-17-2 | rim | 32.61 | 0.78 | 0.00 | 68.13 | 101.52 | 2.96 | 0.02 | 0.000 | 3.02 | 6 | 6614 | 0 | 504389 |
| MD13-33-1 | int | 32.94 | 0.87 | 0.01 | 67.73 | 101.55 | 2.98 | 0.02 | 0.001 | 2.99 | 6 | 7351 | 102 | 501376 |
| MD13-33-2 | cent | 32.86 | 0.85 | 0.05 | 68.20 | 101.96 | 2.97 | 0.02 | 0.003 | 3.01 | 6 | 7207 | 425 | 504848 |
| MD13-33-3 | rim | 32.79 | 0.82 | 0.00 | 68.29 | 101.90 | 2.97 | 0.02 | 0.000 | 3.01 | 6 | 6970 | 0 | 505573 |
| MD13-33-4 | rim | 32.75 | 0.87 | 0.03 | 67.95 | 101.60 | 2.97 | 0.02 | 0.001 | 3.01 | 6 | 7343 | 228 | 503034 |
| MD13-34-1 | cent | 32.71 | 0.99 | 0.12 | 67.98 | 101.80 | 2.97 | 0.03 | 0.006 | 3.00 | 6 | 8420 | 929 | 503234 |
| MD13-34-2 | int | 32.77 | 0.90 | 0.12 | 67.58 | 101.37 | 2.98 | 0.02 | 0.006 | 2.99 | 6 | 7631 | 913 | 500310 |
| MD13-34-3 | rim | 32.72 | 0.98 | 0.06 | 67.96 | 101.72 | 2.97 | 0.03 | 0.003 | 3.00 | 6 | 8292 | 449 | 503093 |
| MD13-50-1 | cent | 32.67 | 0.78 | 0.06 | 68.04 | 101.56 | 2.97 | 0.02 | 0.003 | 3.01 | 6 | 6605 | 488 | 503730 |
| MD13-50-2 | rim | 32.61 | 0.77 | 0.03 | 68.04 | 101.44 | 2.96 | 0.02 | 0.002 | 3.02 | 6 | 6503 | 260 | 503663 |
| MD13-50-3 | rim | 32.54 | 0.90 | 0.03 | 67.47 | 100.94 | 2.97 | 0.02 | 0.002 | 3.00 | 6 | 7665 | 260 | 499466 |

| | | IN wt % | | | | | Cation | | | | | In ppm | | |
|---|---|---|---|---|---|---|---|---|---|---|---|---|---|---|
| SL NO | | SiO2 | HfO2 | Y2O3 | ZrO2 | Total | Si | Hf | Y | Zr | SUM | Hf | Y | Zr |
| MD22B-7-1 | cent | 32.94 | 0.78 | 0.05 | 66.54 | 100.31 | 3.01 | 0.02 | 0.002 | 2.97 | 6 | 6614 | 386 | 492581 |
| MD22B-7-2 | int | 32.87 | 0.83 | 0.04 | 65.90 | 99.64 | 3.02 | 0.02 | 0.002 | 2.95 | 6 | 7029 | 283 | 487880 |
| MD22B-14-1 | rim | 32.98 | 0.77 | 0.05 | 66.63 | 100.42 | 3.01 | 0.02 | 0.002 | 2.97 | 6 | 6529 | 362 | 493225 |
| MD22B-14-2 | cent | 32.93 | 0.70 | 0.04 | 66.67 | 100.33 | 3.01 | 0.02 | 0.002 | 2.97 | 6 | 5952 | 276 | 493528 |
| MD22B-14-3 | cent | 33.00 | 0.70 | 0.09 | 66.30 | 100.09 | 3.02 | 0.02 | 0.004 | 2.96 | 6 | 5961 | 709 | 490841 |
| MD22B-14-4 | rim | 33.00 | 0.70 | 0.03 | 66.86 | 100.58 | 3.01 | 0.02 | 0.001 | 2.97 | 6 | 5910 | 220 | 494942 |
| MD22B-13-1 | rim | 32.56 | 0.74 | 0.00 | 66.90 | 100.20 | 2.99 | 0.02 | 0.000 | 2.99 | 6 | 6258 | 0 | 495253 |
| MD22B-13-3 | cent | 32.66 | 0.67 | 0.11 | 66.56 | 100.01 | 3.00 | 0.02 | 0.005 | 2.98 | 6 | 5664 | 866 | 492773 |
| MD22B-13-4 | rim | 32.83 | 0.78 | 0.00 | 66.50 | 100.10 | 3.01 | 0.02 | 0.000 | 2.97 | 6 | 6605 | 0 | 492270 |
| MD22B-11-1 | rim | 33.06 | 0.67 | 0.02 | 66.30 | 100.05 | 3.02 | 0.02 | 0.001 | 2.96 | 6 | 5706 | 134 | 490834 |
| MD22B-11-2 | cent | 32.99 | 0.64 | 0.06 | 66.76 | 100.44 | 3.01 | 0.02 | 0.003 | 2.97 | 6 | 5444 | 433 | 494195 |
| MD22B-11-3 | rim | 32.83 | 0.67 | 0.03 | 66.57 | 100.11 | 3.01 | 0.02 | 0.001 | 2.97 | 6 | 5681 | 236 | 492847 |
| MD22B-16-1 | rim | 32.95 | 0.79 | 0.00 | 66.70 | 100.45 | 3.01 | 0.02 | 0.000 | 2.97 | 6 | 6724 | 31 | 493795 |
| MD22B-16-2 | - | 32.91 | 0.81 | 0.00 | 66.50 | 100.22 | 3.01 | 0.02 | 0.000 | 2.97 | 6 | 6843 | 0 | 492322 |
| MD22B-16-3 | rim | 32.90 | 1.07 | 0.01 | 66.13 | 100.11 | 3.02 | 0.03 | 0.001 | 2.96 | 6 | 9073 | 87 | 489568 |
| MD22B-21-1 | int | 32.63 | 0.70 | 0.07 | 66.33 | 99.72 | 3.00 | 0.02 | 0.003 | 2.98 | 6 | 5927 | 512 | 491034 |
| MD22B-21-2 | cent | 32.47 | 0.76 | 0.06 | 66.26 | 99.55 | 3.00 | 0.02 | 0.003 | 2.98 | 6 | 6410 | 504 | 490552 |
| MD22B-21-3 | rim | 32.76 | 0.83 | 0.01 | 66.38 | 99.97 | 3.01 | 0.02 | 0.000 | 2.97 | 6 | 7004 | 71 | 491374 |
| MD22B-23-1 | int | 33.10 | 1.03 | 0.04 | 65.77 | 99.94 | 3.03 | 0.03 | 0.002 | 2.94 | 6 | 8750 | 276 | 486918 |
| MD22B-23-2 | cent | 32.86 | 0.66 | 0.03 | 66.50 | 100.04 | 3.01 | 0.02 | 0.001 | 2.97 | 6 | 5579 | 220 | 492262 |
| MD22B-23-3 | rim | 32.78 | 0.68 | 0.00 | 66.21 | 99.67 | 3.01 | 0.02 | 0.000 | 2.97 | 6 | 5783 | 0 | 490153 |
| MD22B-27-1 | rim | 33.24 | 0.92 | 0.11 | 66.01 | 100.28 | 3.03 | 0.02 | 0.005 | 2.94 | 6 | 7835 | 858 | 488672 |
| MD22B-27-2 | cent | 33.15 | 0.89 | 0.14 | 66.12 | 100.30 | 3.03 | 0.02 | 0.007 | 2.94 | 6 | 7555 | 1102 | 489494 |
| MD22B-27-3 | rim | 33.10 | 1.23 | 0.08 | 66.22 | 100.63 | 3.02 | 0.03 | 0.004 | 2.95 | 6 | 10395 | 638 | 490204 |
| MD22B-29-1 | rim | 32.97 | 1.13 | 0.09 | 65.69 | 99.88 | 3.03 | 0.03 | 0.004 | 2.94 | 6 | 9607 | 701 | 486288 |
| MD22B-29-2 | int | 32.92 | 1.03 | 0.07 | 65.87 | 99.89 | 3.02 | 0.03 | 0.004 | 2.95 | 6 | 8691 | 567 | 487658 |
| MD22B-29-3 | cent | 33.02 | 1.08 | 0.19 | 65.95 | 100.23 | 3.02 | 0.03 | 0.009 | 2.94 | 6 | 9149 | 1465 | 488220 |
| MD22B-29-4 | rim | 32.97 | 1.07 | 0.13 | 65.79 | 99.96 | 3.02 | 0.03 | 0.006 | 2.94 | 6 | 9073 | 992 | 487058 |
| MD22B-35-1 | cent | 32.96 | 0.68 | 0.09 | 67.19 | 100.93 | 3.00 | 0.02 | 0.004 | 2.98 | 6 | 5800 | 701 | 497415 |
| MD22B-35-2 | cent | 32.96 | 0.76 | 0.07 | 67.07 | 100.85 | 3.00 | 0.02 | 0.003 | 2.98 | 6 | 6427 | 520 | 496519 |
| MD22B-35-3 | int | 33.05 | 0.75 | 0.06 | 66.82 | 100.68 | 3.01 | 0.02 | 0.003 | 2.97 | 6 | 6317 | 480 | 494691 |
| MD22B-35-4 | rim | 32.88 | 0.74 | 0.02 | 67.17 | 100.81 | 3.00 | 0.02 | 0.001 | 2.98 | 6 | 6258 | 189 | 497245 |
| MD22B-35-5 r | rim | 32.95 | 0.90 | 0.04 | 66.27 | 100.16 | 3.02 | 0.02 | 0.002 | 2.96 | 6 | 7597 | 283 | 490626 |
| MD22B-48-1 | cent | 32.89 | 1.25 | 0.11 | 65.90 | 100.15 | 3.02 | 0.03 | 0.005 | 2.95 | 6 | 10616 | 850 | 487858 |
| MD22B-48-2 | rim | 33.01 | 1.24 | 0.06 | 66.58 | 100.88 | 3.01 | 0.03 | 0.003 | 2.96 | 6 | 10505 | 472 | 492862 |

| | | IN wt % | | | | | Cation | | | | | In ppm | | |
|---|---|---|---|---|---|---|---|---|---|---|---|---|---|---|
| SL NO | | SiO2 | HfO2 | Y2O3 | ZrO2 | Total | Si | Hf | Y | Zr | SUM | Hf | Y | Zr |
| MD26-2-1 | core | 32.73 | 1.07 | 0.13 | 65.71 | 99.64 | 3.02 | 0.03 | 0.006 | 2.95 | 6 | 9081 | 1000 | 486459 |
| MD26-2-2 | rim | 32.89 | 1.17 | 0.07 | 66.03 | 100.16 | 3.02 | 0.03 | 0.003 | 2.95 | 6 | 9946 | 559 | 488798 |
| MD26-2-3 | - | 32.86 | 2.12 | 0.00 | 65.21 | 100.19 | 3.02 | 0.06 | 0.000 | 2.92 | 6 | 17967 | 0 | 482764 |
| MD26-2-4 | - | 33.14 | 1.09 | 0.00 | 65.59 | 99.82 | 3.04 | 0.03 | 0.000 | 2.93 | 6 | 9276 | 0 | 485541 |
| MD26-9-1 | core | 32.75 | 0.91 | 0.56 | 65.39 | 99.61 | 3.02 | 0.02 | 0.027 | 2.94 | 6 | 7716 | 4378 | 484112 |
| MD26-9-2 | rim | 33.13 | 1.13 | 0.05 | 66.27 | 100.58 | 3.02 | 0.03 | 0.003 | 2.95 | 6 | 9581 | 425 | 490560 |
| MD26-9-3 | rim | 34.13 | 1.08 | 0.01 | 63.97 | 99.19 | 3.12 | 0.03 | 0.000 | 2.85 | 6 | 9157 | 55 | 473577 |
| MD26-24-1 | core | 33.17 | 0.92 | 0.46 | 65.99 | 100.53 | 3.03 | 0.02 | 0.022 | 2.93 | 6 | 7809 | 3598 | 488502 |
| MD26-24-2 | rim | 33.30 | 1.09 | 0.01 | 66.45 | 100.84 | 3.03 | 0.03 | 0.001 | 2.94 | 6 | 9225 | 102 | 491907 |
| MD26-24-3 | int | 33.08 | 1.15 | 0.04 | 66.11 | 100.38 | 3.02 | 0.03 | 0.002 | 2.95 | 6 | 9759 | 315 | 489405 |
| MD26-28-1 | core | 32.81 | 1.07 | 0.56 | 65.09 | 99.53 | 3.03 | 0.03 | 0.027 | 2.93 | 6 | 9081 | 4409 | 481854 |
| MD26-28-2 | core | 33.20 | 1.05 | 0.21 | 66.43 | 100.89 | 3.02 | 0.03 | 0.010 | 2.95 | 6 | 8894 | 1614 | 491803 |
| MD26-28-3 | int | 33.13 | 1.13 | 0.16 | 65.84 | 100.27 | 3.03 | 0.03 | 0.008 | 2.94 | 6 | 9615 | 1260 | 487414 |
| MD26-28-4 | int | 33.07 | 1.15 | 0.11 | 66.30 | 100.62 | 3.02 | 0.03 | 0.005 | 2.95 | 6 | 9742 | 850 | 490789 |
| MD26-28-5 | rim | 33.16 | 1.27 | 0.05 | 66.48 | 100.96 | 3.02 | 0.03 | 0.003 | 2.95 | 6 | 10743 | 409 | 492144 |
| MD26-28-6 | rim | 33.39 | 1.41 | 0.01 | 65.80 | 100.62 | 3.04 | 0.04 | 0.001 | 2.92 | 6 | 11964 | 110 | 487125 |
| MD26-31-1 | rim | 33.34 | 1.07 | 0.08 | 66.23 | 100.73 | 3.03 | 0.03 | 0.004 | 2.94 | 6 | 9098 | 606 | 490330 |
| MD26-31-2 | core | 33.03 | 1.41 | 0.19 | 65.72 | 100.35 | 3.02 | 0.04 | 0.009 | 2.93 | 6 | 11972 | 1520 | 486540 |
| MD26-31-3 | rim | 33.08 | 1.31 | 0.08 | 66.03 | 100.50 | 3.02 | 0.03 | 0.004 | 2.94 | 6 | 11074 | 661 | 488813 |
| MD26-31-4 | int | 33.02 | 1.33 | 0.11 | 65.78 | 100.25 | 3.02 | 0.03 | 0.005 | 2.94 | 6 | 11277 | 858 | 486992 |
| MD26-36-1 | rim | 33.04 | 1.02 | 0.12 | 66.09 | 100.26 | 3.02 | 0.03 | 0.006 | 2.95 | 6 | 8632 | 961 | 489227 |
| MD26-36-2 | int | 33.00 | 1.02 | 0.16 | 66.17 | 100.35 | 3.02 | 0.03 | 0.008 | 2.95 | 6 | 8606 | 1236 | 489886 |
| MD26-36-3 | int | 32.90 | 1.00 | 0.40 | 66.34 | 100.63 | 3.00 | 0.03 | 0.019 | 2.95 | 6 | 8437 | 3134 | 491093 |
| MD26-36-4 | rim | 33.09 | 1.16 | 0.06 | 65.88 | 100.19 | 3.03 | 0.03 | 0.003 | 2.94 | 6 | 9827 | 496 | 487687 |
| MD26-38-1 | core | 32.87 | 0.95 | 0.50 | 66.17 | 100.49 | 3.01 | 0.02 | 0.024 | 2.95 | 6 | 8055 | 3906 | 489879 |
| MD26-38-2 | core | 32.85 | 0.93 | 0.55 | 65.57 | 99.90 | 3.02 | 0.02 | 0.027 | 2.94 | 6 | 7902 | 4307 | 485400 |
| MD26-38-3 | rim | 33.08 | 1.12 | 0.01 | 66.29 | 100.50 | 3.02 | 0.03 | 0.000 | 2.95 | 6 | 9454 | 47 | 490760 |
| MD26-49-1 | core | 33.34 | 0.96 | 0.30 | 65.70 | 100.30 | 3.04 | 0.03 | 0.014 | 2.92 | 6 | 8174 | 2339 | 486370 |
| MD26-49-2 | core | 33.13 | 1.10 | 0.20 | 65.87 | 100.30 | 3.03 | 0.03 | 0.010 | 2.94 | 6 | 9285 | 1606 | 487650 |
| MD26-49-3 | rim | 33.12 | 1.15 | 0.01 | 66.61 | 100.89 | 3.01 | 0.03 | 0.001 | 2.96 | 6 | 9751 | 94 | 493106 |
| MD26-52-1 | core | 33.10 | 0.99 | 0.44 | 65.24 | 99.76 | 3.04 | 0.03 | 0.021 | 2.92 | 6 | 8411 | 3441 | 482935 |
| MD26-52-2 | rim | 33.16 | 1.11 | 0.02 | 66.37 | 100.67 | 3.02 | 0.03 | 0.001 | 2.95 | 6 | 9429 | 189 | 491352 |
| MD26-50-1 | int | 33.03 | 0.83 | 0.00 | 66.52 | 100.39 | 3.02 | 0.02 | 0.000 | 2.96 | 6 | 7021 | 0 | 492470 |
| MD26-50-2 | int | 33.03 | 0.85 | 0.05 | 66.30 | 100.23 | 3.02 | 0.02 | 0.002 | 2.96 | 6 | 7199 | 354 | 490811 |
| MD26-50-3 | int | 33.17 | 0.80 | 0.00 | 66.80 | 100.76 | 3.02 | 0.02 | 0.000 | 2.96 | 6 | 6749 | 0 | 494491 |
| MD26-54-1 | core | 32.93 | 0.88 | 0.59 | 65.09 | 99.48 | 3.03 | 0.02 | 0.029 | 2.92 | 6 | 7487 | 4622 | 481846 |
| MD26-54-2 | rim | 33.07 | 1.19 | 0.05 | 66.27 | 100.58 | 3.02 | 0.03 | 0.003 | 2.95 | 6 | 10073 | 425 | 490567 |
| MD26-58-1 | core | 33.09 | 0.73 | 0.03 | 67.02 | 100.86 | 3.01 | 0.02 | 0.001 | 2.97 | 6 | 6207 | 197 | 496142 |
| MD26-58-2 | rim | 33.20 | 0.89 | 0.01 | 67.00 | 101.09 | 3.01 | 0.02 | 0.000 | 2.96 | 6 | 7512 | 39 | 495979 |
| MD26-58-3 | rim | 33.24 | 0.84 | 0.02 | 66.69 | 100.79 | 3.02 | 0.02 | 0.001 | 2.96 | 6 | 7156 | 150 | 493691 |

| | | IN wt % | | | | | Cation | | | | | In ppm | | |
|---|---|---|---|---|---|---|---|---|---|---|---|---|---|---|
| SL NO | | SiO2 | HfO2 | Y2O3 | ZrO2 | Total | Si | Hf | Y | Zr | SUM | Hf | Y | Zr |
| MD8-1-1 | rim | 32.01 | 1.09 | 0.06 | 66.96 | 100.12 | 2.95 | 0.03 | 0.002 | 3.01 | 6 | 9217 | 488 | 495720 |
| MD8-1-2 | cent | 31.99 | 1.07 | 0.05 | 67.25 | 100.36 | 2.95 | 0.03 | 0.002 | 3.02 | 6 | 9081 | 409 | 497830 |
| MD8-1-3 | int | 32.14 | 1.03 | 0.02 | 68.02 | 101.21 | 2.94 | 0.03 | 0.001 | 3.03 | 6 | 8699 | 173 | 503530 |
| MD8-1-4 | rim | 32.08 | 1.13 | 0.00 | 66.91 | 100.12 | 2.96 | 0.03 | 0.000 | 3.01 | 6 | 9590 | 0 | 495305 |
| MD8-1-5 | int | 32.22 | 1.05 | 0.06 | 67.02 | 100.34 | 2.96 | 0.03 | 0.002 | 3.01 | 6 | 8869 | 457 | 496156 |
| MD8-6-1 | rim | 32.36 | 1.07 | 0.06 | 67.77 | 101.25 | 2.95 | 0.03 | 0.002 | 3.02 | 6 | 9030 | 449 | 501709 |
| MD8-6-2 c | cent | 32.48 | 0.91 | 0.10 | 67.99 | 101.47 | 2.96 | 0.02 | 0.003 | 3.02 | 6 | 7682 | 787 | 503308 |
| MD8-6-3 | cent | 32.24 | 0.99 | 0.08 | 68.03 | 101.34 | 2.94 | 0.03 | 0.003 | 3.03 | 6 | 8386 | 646 | 503596 |
| MD8-6-4 r | int | 32.30 | 1.01 | 0.02 | 67.61 | 100.94 | 2.96 | 0.03 | 0.001 | 3.02 | 6 | 8530 | 165 | 500539 |
| MD8-6-5 | rim | 32.30 | 1.07 | 0.03 | 67.84 | 101.24 | 2.95 | 0.03 | 0.001 | 3.02 | 6 | 9106 | 205 | 502220 |
| MD8-6-6 | rim | 32.44 | 1.01 | 0.04 | 67.35 | 100.83 | 2.97 | 0.03 | 0.001 | 3.00 | 6 | 8547 | 276 | 498614 |
| MD8-5-1 | int | 32.55 | 0.94 | 0.07 | 67.78 | 101.35 | 2.96 | 0.02 | 0.002 | 3.01 | 6 | 7996 | 575 | 501805 |
| MD8-5-2 | int | 32.53 | 1.03 | 0.07 | 67.86 | 101.49 | 2.96 | 0.03 | 0.002 | 3.01 | 6 | 8759 | 575 | 502345 |
| MD8-5-3 | cent | 32.54 | 1.01 | 0.07 | 67.86 | 101.48 | 2.96 | 0.03 | 0.002 | 3.01 | 6 | 8530 | 567 | 502368 |
| MD8-5-4 | rim | 32.04 | 1.05 | 0.01 | 67.04 | 100.14 | 2.96 | 0.03 | 0.000 | 3.02 | 6 | 8911 | 47 | 496282 |
| MD8-5-5 | int | 32.46 | 0.94 | 0.06 | 67.18 | 100.64 | 2.97 | 0.02 | 0.002 | 3.00 | 6 | 7979 | 433 | 497311 |
| MD8-5-6 | rim | 32.59 | 1.16 | 0.01 | 67.64 | 101.40 | 2.97 | 0.03 | 0.000 | 3.00 | 6 | 9827 | 79 | 500761 |
| MD8-2-1 | core | 32.47 | 1.41 | 0.36 | 66.92 | 101.15 | 2.97 | 0.04 | 0.012 | 2.98 | 6 | 11930 | 2811 | 495394 |
| MD8-2-2 | core | 32.43 | 1.27 | 0.34 | 66.94 | 100.98 | 2.97 | 0.03 | 0.011 | 2.99 | 6 | 10785 | 2654 | 495549 |
| MD8-2-3 | core | 32.27 | 1.25 | 0.37 | 67.22 | 101.11 | 2.95 | 0.03 | 0.012 | 3.00 | 6 | 10624 | 2898 | 497600 |
| MD8-2-5 | rim | 32.52 | 1.54 | 0.06 | 67.54 | 101.66 | 2.95 | 0.04 | 0.003 | 3.01 | 6 | 13066 | 488 | 499984 |
| MD8-3-1 | core | 32.28 | 1.33 | 0.20 | 67.44 | 101.24 | 2.94 | 0.04 | 0.003 | 3.01 | 6 | 11260 | 1567 | 499229 |
| MD8-3-2 | core | 32.26 | 0.95 | 0.63 | 66.40 | 100.25 | 2.95 | 0.03 | 0.006 | 3.01 | 6 | 8064 | 4992 | 491581 |
| MD8-3-3 | core | 32.22 | 0.88 | 0.45 | 66.65 | 100.20 | 2.97 | 0.02 | 0.015 | 2.99 | 6 | 7436 | 3520 | 493403 |
| MD8-3-4 | core | 31.92 | 0.85 | 0.55 | 65.79 | 99.12 | 2.97 | 0.02 | 0.018 | 2.99 | 6 | 7233 | 4354 | 487043 |
| MD8-3-5 | core | 32.31 | 0.82 | 0.51 | 67.07 | 100.71 | 2.96 | 0.02 | 0.017 | 3.00 | 6 | 6970 | 4000 | 496482 |
| MD8-3-6 | core | 32.23 | 0.76 | 0.39 | 67.03 | 100.41 | 2.96 | 0.02 | 0.013 | 3.00 | 6 | 6427 | 3039 | 496253 |
| MD8-3-7 | int | 32.40 | 1.30 | 0.23 | 66.88 | 100.80 | 2.97 | 0.03 | 0.007 | 2.99 | 6 | 11023 | 1780 | 495083 |
| MD8-4-1 | rim | 32.42 | 1.37 | 0.10 | 67.38 | 101.27 | 2.96 | 0.04 | 0.003 | 3.00 | 6 | 11642 | 764 | 498829 |
| MD8-4-2 | int | 32.35 | 1.46 | 0.15 | 66.92 | 100.87 | 2.97 | 0.04 | 0.005 | 2.99 | 6 | 12354 | 1165 | 495416 |
| MD8-4-3 | int | 32.30 | 1.44 | 0.16 | 66.72 | 100.62 | 2.97 | 0.04 | 0.005 | 2.99 | 6 | 12193 | 1291 | 493943 |
| MD8-4-4 | int | 32.27 | 1.38 | 0.21 | 66.48 | 100.33 | 2.97 | 0.04 | 0.007 | 2.98 | 6 | 11667 | 1677 | 492114 |
| MD8-4-5 | core | 32.50 | 0.85 | 0.17 | 67.54 | 101.06 | 2.97 | 0.02 | 0.006 | 3.01 | 6 | 7241 | 1346 | 499999 |
| MD8-4-6 | core | 32.36 | 0.99 | 0.39 | 67.08 | 100.81 | 2.96 | 0.03 | 0.013 | 3.00 | 6 | 8420 | 3031 | 496586 |

| | | IN wt % | | | | | Cation | | | | | In ppm | | |
|---|---|---|---|---|---|---|---|---|---|---|---|---|---|---|
| SL NO | | SiO2 | HfO2 | Y2O3 | ZrO2 | Total | Si | Hf | Y | Zr | SUM | Hf | Y | Zr |
| MD22A-4-1 | rim | 32.33 | 1.07 | 0.14 | 67.62 | 101.16 | 2.95 | 0.03 | 0.005 | 3.01 | 6 | 9089 | 1134 | 500583 |
| MD22A-4-2 | int | 32.51 | 1.26 | 0.13 | 67.52 | 101.41 | 2.96 | 0.03 | 0.004 | 3.00 | 6 | 10675 | 1000 | 499851 |
| MD22A-4-3 | core | 32.38 | 1.09 | 0.22 | 67.36 | 101.04 | 2.96 | 0.03 | 0.007 | 3.00 | 6 | 9268 | 1693 | 498644 |
| MD22A-4-4 | int | 31.92 | 0.86 | 1.35 | 65.13 | 99.26 | 2.97 | 0.02 | 0.045 | 2.96 | 6 | 7250 | 10654 | 482180 |
| MD22A-4-5 | rim | 32.41 | 1.03 | 0.25 | 67.48 | 101.16 | 2.96 | 0.03 | 0.008 | 3.00 | 6 | 8708 | 1953 | 499577 |
| MD22A-4-6 | rim | 32.57 | 1.20 | 0.09 | 67.78 | 101.64 | 2.96 | 0.03 | 0.003 | 3.00 | 6 | 10192 | 717 | 501790 |
| MD22A-4-7 | int | 32.50 | 1.20 | 0.12 | 67.71 | 101.54 | 2.96 | 0.03 | 0.004 | 3.01 | 6 | 10200 | 976 | 501250 |
| MD22A-4-8 | core | 32.61 | 1.23 | 0.05 | 67.24 | 101.14 | 2.97 | 0.03 | 0.002 | 2.99 | 6 | 10455 | 425 | 497785 |
| MD22A-4-9 | rim | 32.55 | 1.37 | 0.01 | 67.71 | 101.64 | 2.96 | 0.04 | 0.000 | 3.00 | 6 | 11608 | 94 | 501250 |
| MD22A-13-1 | rim | 32.51 | 1.23 | 0.09 | 68.10 | 101.94 | 2.95 | 0.03 | 0.003 | 3.01 | 6 | 10412 | 740 | 504167 |
| MD22A-13-2 | int | 32.63 | 1.31 | 0.08 | 67.79 | 101.82 | 2.96 | 0.03 | 0.003 | 3.00 | 6 | 11124 | 661 | 501857 |
| MD22A-13-3 | core | 32.49 | 1.07 | 0.34 | 67.58 | 101.47 | 2.96 | 0.03 | 0.011 | 3.00 | 6 | 9030 | 2685 | 500273 |
| MD22A-13-4 | int | 32.60 | 1.31 | 0.12 | 67.47 | 101.50 | 2.97 | 0.03 | 0.004 | 2.99 | 6 | 11091 | 976 | 499443 |
| MD22A-13-5 | rim | 32.66 | 1.05 | 0.15 | 68.04 | 101.89 | 2.96 | 0.03 | 0.005 | 3.01 | 6 | 8861 | 1173 | 503671 |
| MD22A-14-1 | rim | 32.87 | 1.14 | 0.07 | 67.49 | 101.57 | 2.98 | 0.03 | 0.002 | 2.99 | 6 | 9632 | 551 | 499606 |
| MD22A-14-2 | int | 32.68 | 1.05 | 0.15 | 67.62 | 101.51 | 2.97 | 0.03 | 0.005 | 3.00 | 6 | 8928 | 1213 | 500554 |
| MD22A-14-3 | core | 32.73 | 1.03 | 0.17 | 67.34 | 101.27 | 2.98 | 0.03 | 0.006 | 2.99 | 6 | 8750 | 1370 | 498488 |
| MD22A-14-4 | int | 32.77 | 1.04 | 0.21 | 67.74 | 101.76 | 2.97 | 0.03 | 0.007 | 2.99 | 6 | 8827 | 1661 | 501442 |
| MD22A-14-5 | rim | 32.78 | 1.15 | 0.05 | 67.63 | 101.61 | 2.98 | 0.03 | 0.001 | 2.99 | 6 | 9785 | 362 | 500672 |
| MD22A-7-1 | rim | 32.60 | 1.16 | 0.07 | 67.95 | 101.78 | 2.96 | 0.03 | 0.002 | 3.01 | 6 | 9810 | 543 | 503056 |
| MD22A-7-2 | int | 32.61 | 1.27 | 0.11 | 67.58 | 101.57 | 2.97 | 0.03 | 0.004 | 3.00 | 6 | 10726 | 898 | 500295 |
| MD22A-7-3 | near | 32.65 | 0.83 | 0.62 | 66.33 | 100.42 | 2.99 | 0.02 | 0.020 | 2.96 | 6 | 6995 | 4874 | 491048 |
| MD22A-7-4 | rim | 32.60 | 1.08 | 0.14 | 67.32 | 101.14 | 2.97 | 0.03 | 0.005 | 2.99 | 6 | 9123 | 1118 | 498377 |
| MD22A-8-1 | rim | 32.65 | 1.27 | 0.20 | 67.03 | 101.15 | 2.98 | 0.03 | 0.006 | 2.98 | 6 | 10777 | 1575 | 496238 |
| MD22A-8-2 | int | 32.68 | 1.15 | 0.13 | 67.85 | 101.82 | 2.96 | 0.03 | 0.004 | 3.00 | 6 | 9776 | 1047 | 502257 |
| MD22A-8-3 | core | 32.80 | 0.98 | 0.16 | 67.44 | 101.38 | 2.98 | 0.03 | 0.005 | 2.99 | 6 | 8318 | 1252 | 499258 |
| MD22A-8-4 | core | 32.25 | 0.88 | 0.60 | 66.73 | 100.47 | 2.96 | 0.02 | 0.019 | 2.99 | 6 | 7470 | 4701 | 494032 |

| | | IN wt % | | | | | Cation | | | | | In ppm | | |
|---|---|---|---|---|---|---|---|---|---|---|---|---|---|---|
| SL NO | | SiO2 | HfO2 | Y2O3 | ZrO2 | Total | Si | Hf | Y | Zr | SUM | Hf | Y | Zr |
| MD22A-8-5 | rim | 32.83 | 1.37 | 0.08 | 66.99 | 101.27 | 2.99 | 0.04 | 0.003 | 2.97 | 6 | 11591 | 614 | 495949 |
| MD22A-23-1 | rim | 32.71 | 1.01 | 0.08 | 67.57 | 101.37 | 2.97 | 0.03 | 0.002 | 3.00 | 6 | 8572 | 598 | 500250 |
| MD22A-23-2 | rim | 32.62 | 1.02 | 0.07 | 67.81 | 101.52 | 2.97 | 0.03 | 0.002 | 3.01 | 6 | 8682 | 543 | 501968 |
| MD22A-23-3 | rim | 32.48 | 1.07 | 0.19 | 68.03 | 101.76 | 2.95 | 0.03 | 0.006 | 3.01 | 6 | 9047 | 1472 | 503611 |
| MD22A-23-5 | rim | 32.76 | 1.01 | 0.10 | 67.83 | 101.69 | 2.97 | 0.03 | 0.003 | 3.00 | 6 | 8530 | 748 | 502160 |
| MD22A-23-6 | near | 32.34 | 1.06 | 0.34 | 67.10 | 100.84 | 2.96 | 0.03 | 0.011 | 3.00 | 6 | 9013 | 2654 | 496704 |
| MD22A-24-1 r | rim | 32.76 | 0.95 | 0.07 | 67.81 | 101.59 | 2.97 | 0.02 | 0.002 | 3.00 | 6 | 8030 | 543 | 502012 |
| MD22A-24-2 c | core | 32.63 | 0.80 | 0.29 | 67.88 | 101.59 | 2.96 | 0.02 | 0.009 | 3.01 | 6 | 6758 | 2260 | 502479 |
| MD22A-31-1 | rim | 32.61 | 1.22 | 0.14 | 67.42 | 101.39 | 2.97 | 0.03 | 0.004 | 2.99 | 6 | 10370 | 1071 | 499095 |
| MD22A-31-2 | int | 32.46 | 1.06 | 0.23 | 67.08 | 100.83 | 2.97 | 0.03 | 0.007 | 2.99 | 6 | 9005 | 1795 | 496601 |
| MD22A-31-3 | core | 31.74 | 1.28 | 0.13 | 66.39 | 99.53 | 2.95 | 0.03 | 0.004 | 3.01 | 6 | 10819 | 992 | 491456 |
| MD22A-31-4 | rim | 32.18 | 1.04 | 0.09 | 66.54 | 99.85 | 2.97 | 0.03 | 0.003 | 3.00 | 6 | 8835 | 717 | 492581 |
| MD22A-33-1 | rim | 32.70 | 1.15 | 0.01 | 67.81 | 101.67 | 2.97 | 0.03 | 0.000 | 3.00 | 6 | 9759 | 39 | 502020 |
| MD22A-33-2 | core | 32.54 | 1.02 | 0.21 | 67.13 | 100.90 | 2.97 | 0.03 | 0.007 | 2.99 | 6 | 8649 | 1646 | 496971 |
| MD22A-33-3 | core | 32.58 | 1.01 | 0.17 | 67.23 | 100.99 | 2.97 | 0.03 | 0.006 | 2.99 | 6 | 8521 | 1370 | 497681 |
| MD22A-33-4 | int | 32.50 | 1.27 | 0.09 | 67.85 | 101.70 | 2.96 | 0.03 | 0.003 | 3.01 | 6 | 10768 | 677 | 502264 |
| MD22A-36-1 r2 | rim | 32.45 | 1.10 | 0.12 | 68.00 | 101.67 | 2.95 | 0.03 | 0.004 | 3.02 | 6 | 9293 | 937 | 503397 |
| MD22A-36-2 | core | 32.60 | 1.26 | 0.12 | 67.69 | 101.66 | 2.96 | 0.03 | 0.004 | 3.00 | 6 | 10658 | 913 | 501102 |
| MD22A-36-3 | core | 32.39 | 1.06 | 0.36 | 66.86 | 100.67 | 2.97 | 0.03 | 0.012 | 2.99 | 6 | 9005 | 2811 | 494965 |
| MD22A-36-4 | int | 32.52 | 1.15 | 0.14 | 67.42 | 101.22 | 2.97 | 0.03 | 0.004 | 3.00 | 6 | 9725 | 1079 | 499140 |
| MD22A-36-5 | rim | 32.45 | 1.07 | 0.26 | 67.25 | 101.03 | 2.97 | 0.03 | 0.008 | 3.00 | 6 | 9081 | 2024 | 497859 |
| MD22A-36-6 r1 | rim | 32.53 | 1.36 | 0.02 | 67.87 | 101.77 | 2.96 | 0.04 | 0.001 | 3.01 | 6 | 11498 | 150 | 502449 |
| MD22A-60-1 | rim | 32.61 | 1.09 | 0.06 | 67.91 | 101.67 | 2.96 | 0.03 | 0.002 | 3.01 | 6 | 9242 | 465 | 502760 |
| MD22A-60-2 | core | 32.58 | 1.03 | 0.13 | 67.96 | 101.69 | 2.96 | 0.03 | 0.004 | 3.01 | 6 | 8708 | 1031 | 503108 |
| MD22A-60-4 | core | 32.56 | 1.20 | 0.19 | 67.71 | 101.65 | 2.96 | 0.03 | 0.006 | 3.00 | 6 | 10132 | 1457 | 501265 |
| MD22A-60-5 | rim | 32.58 | 1.13 | 0.00 | 67.93 | 101.64 | 2.96 | 0.03 | 0.000 | 3.01 | 6 | 9590 | 0 | 502864 |
| MD22A-61-1 | rim | 32.56 | 1.07 | 0.20 | 67.30 | 101.13 | 2.97 | 0.03 | 0.006 | 2.99 | 6 | 9056 | 1543 | 498207 |
| MD22A-61-2 | core | 32.53 | 1.02 | 0.25 | 67.71 | 101.51 | 2.96 | 0.03 | 0.008 | 3.00 | 6 | 8682 | 1976 | 501265 |
| MD22A-61-3 | rim | 32.37 | 1.01 | 0.16 | 67.70 | 101.25 | 2.95 | 0.03 | 0.005 | 3.01 | 6 | 8572 | 1283 | 501176 |
| MD22A-61-4 | rim | 32.38 | 1.37 | 0.12 | 68.03 | 101.90 | 2.94 | 0.04 | 0.004 | 3.02 | 6 | 11582 | 961 | 503641 |
| MD22A-61-5 | rim | 32.45 | 1.19 | 0.12 | 67.58 | 101.34 | 2.96 | 0.03 | 0.004 | 3.01 | 6 | 10115 | 945 | 500258 |
| MD22A-52-3 | int | 32.21 | 0.98 | 0.52 | 66.62 | 100.33 | 2.97 | 0.03 | 0.017 | 2.99 | 6 | 8326 | 4087 | 493188 |
| MD22A-52-4 | rim | 32.36 | 1.24 | 0.13 | 67.66 | 101.39 | 2.95 | 0.03 | 0.004 | 3.01 | 6 | 10522 | 1008 | 500887 |
| MD22A-78-1 | rim | 32.32 | 1.59 | 0.16 | 66.23 | 100.29 | 2.98 | 0.04 | 0.005 | 2.98 | 6 | 13465 | 1252 | 490308 |
| MD22A-78-2 | int | 32.44 | 1.46 | 0.11 | 67.51 | 101.52 | 2.96 | 0.04 | 0.003 | 3.00 | 6 | 12362 | 850 | 499784 |
| MD22A-78-3 | core | 32.28 | 1.06 | 0.63 | 66.41 | 100.38 | 2.97 | 0.03 | 0.020 | 2.98 | 6 | 9005 | 4921 | 491618 |

| | | IN wt % | | | | | Cation | | | | | In ppm | | |
|---|---|---|---|---|---|---|---|---|---|---|---|---|---|---|
| SL NO | | SiO2 | HfO2 | Y2O3 | ZrO2 | Total | Si | Hf | Y | Zr | SUM | Hf | Y | Zr |
| MD22A-78-4 | rim | 32.64 | 1.30 | 0.12 | 67.41 | 101.47 | 2.97 | 0.03 | 0.004 | 2.99 | 6 | 11040 | 976 | 499051 |
| MD22A-84-1 | rim | 32.44 | 1.08 | 0.06 | 67.76 | 101.34 | 2.96 | 0.03 | 0.002 | 3.01 | 6 | 9166 | 496 | 501605 |
| MD22A-84-2 | core | 32.47 | 1.33 | 0.20 | 67.47 | 101.47 | 2.96 | 0.03 | 0.006 | 3.00 | 6 | 11252 | 1583 | 499503 |
| MD22A-84-3 | rim | 32.59 | 1.01 | 0.08 | 67.75 | 101.43 | 2.97 | 0.03 | 0.003 | 3.01 | 6 | 8538 | 654 | 501575 |
| MD22A-112-1 | rim | 32.28 | 0.89 | 0.12 | 67.57 | 100.86 | 2.96 | 0.02 | 0.004 | 3.02 | 6 | 7538 | 921 | 500228 |
| MD22A-112-2 | core | 32.40 | 1.15 | 0.07 | 67.83 | 101.45 | 2.95 | 0.03 | 0.002 | 3.01 | 6 | 9725 | 559 | 502175 |
| MD22A-112-3 | rim | 32.45 | 0.99 | 0.17 | 67.91 | 101.51 | 2.95 | 0.03 | 0.005 | 3.01 | 6 | 8386 | 1323 | 502701 |
| MD22A-121-1 | rim | 32.59 | 1.31 | 0.09 | 67.76 | 101.74 | 2.96 | 0.03 | 0.003 | 3.00 | 6 | 11091 | 669 | 501605 |
| MD22A-121-2 | int | 32.78 | 1.38 | 0.09 | 67.48 | 101.73 | 2.98 | 0.04 | 0.003 | 2.99 | 6 | 11709 | 717 | 499547 |
| MD22A-121-3 | core | 32.70 | 1.32 | 0.15 | 67.15 | 101.32 | 2.98 | 0.03 | 0.005 | 2.98 | 6 | 11175 | 1205 | 497126 |
| MD22A-121-4 | int | 32.67 | 1.33 | 0.18 | 67.44 | 101.62 | 2.97 | 0.03 | 0.006 | 2.99 | 6 | 11243 | 1441 | 499266 |
| MD22A-121-5 | rim | 32.65 | 1.18 | 0.19 | 67.53 | 101.55 | 2.97 | 0.03 | 0.006 | 2.99 | 6 | 9997 | 1480 | 499932 |
| MD22A-144-1 | rim | 32.54 | 1.34 | 0.10 | 67.61 | 101.58 | 2.96 | 0.03 | 0.003 | 3.00 | 6 | 11328 | 811 | 500487 |
| MD22A-144-2 | int | 32.52 | 1.09 | 0.12 | 67.89 | 101.61 | 2.96 | 0.03 | 0.004 | 3.01 | 6 | 9208 | 921 | 502597 |
| MD22A-144-3 | core | 32.50 | 1.08 | 0.28 | 68.12 | 101.98 | 2.95 | 0.03 | 0.009 | 3.01 | 6 | 9157 | 2220 | 504255 |
| MD22A-144-4 | int | 32.52 | 1.31 | 0.14 | 67.57 | 101.53 | 2.96 | 0.03 | 0.005 | 3.00 | 6 | 11065 | 1126 | 500184 |
| MD22A-144-5 | rim | 32.52 | 1.01 | 0.15 | 67.35 | 101.03 | 2.97 | 0.03 | 0.005 | 3.00 | 6 | 8598 | 1165 | 498577 |
| MD22A-144-6 | rim | 32.44 | 0.98 | 0.13 | 67.94 | 101.48 | 2.95 | 0.03 | 0.004 | 3.02 | 6 | 8276 | 1000 | 502960 |
| MD22A-134-1 r | rim | 32.24 | 1.10 | 0.38 | 67.08 | 100.80 | 2.96 | 0.03 | 0.012 | 3.00 | 6 | 9327 | 2953 | 496586 |
| MD22A-134-2 | int | 32.43 | 1.38 | 0.02 | 67.98 | 101.81 | 2.95 | 0.04 | 0.001 | 3.01 | 6 | 11701 | 181 | 503226 |
| MD22A-134-3 c | core | 32.40 | 1.43 | 0.01 | 68.09 | 101.93 | 2.95 | 0.04 | 0.000 | 3.02 | 6 | 12091 | 102 | 504033 |
| MD22A-134-4 | rim | 32.29 | 1.06 | 0.05 | 68.59 | 101.99 | 2.93 | 0.03 | 0.002 | 3.04 | 6 | 8988 | 394 | 507750 |
| MD17A-2-1 | int | 32.52 | 1.06 | 0.27 | 65.30 | 99.15 | 3.01 | 0.03 | 0.013 | 2.95 | 6 | 9022 | 2150 | 483379 |
| MD17A-2-2 | rim | 32.76 | 1.09 | 0.03 | 65.55 | 99.43 | 3.02 | 0.03 | 0.001 | 2.95 | 6 | 9217 | 228 | 485289 |
| MD17A-2-3 | cent | 32.42 | 0.87 | 0.26 | 65.48 | 99.03 | 3.01 | 0.02 | 0.013 | 2.96 | 6 | 7402 | 2079 | 484748 |
| MD17A-2-4 | rim | 32.60 | 1.00 | 0.05 | 65.87 | 99.52 | 3.01 | 0.03 | 0.003 | 2.96 | 6 | 8479 | 402 | 487613 |
| MD17A-11-1 | int | 32.75 | 1.06 | 0.24 | 65.53 | 99.58 | 3.02 | 0.03 | 0.012 | 2.94 | 6 | 8979 | 1921 | 485111 |
| MD17A-11-2 | int | 32.57 | 1.06 | 0.24 | 65.31 | 99.18 | 3.02 | 0.03 | 0.012 | 2.95 | 6 | 8962 | 1898 | 483453 |
| MD17A-11-3 | cent | 32.67 | 1.11 | 0.11 | 65.15 | 99.04 | 3.03 | 0.03 | 0.005 | 2.94 | 6 | 9446 | 835 | 482328 |
| MD17A-11-4 | rim | 32.65 | 0.98 | 0.11 | 65.13 | 98.87 | 3.03 | 0.03 | 0.005 | 2.94 | 6 | 8292 | 866 | 482165 |
| MD17A-11-5 | rim | 32.46 | 0.98 | 0.10 | 65.39 | 98.92 | 3.01 | 0.03 | 0.005 | 2.96 | 6 | 8267 | 772 | 484045 |
| MD17A-13-1 | rim | 32.55 | 0.95 | 0.20 | 64.86 | 98.55 | 3.03 | 0.03 | 0.010 | 2.94 | 6 | 8080 | 1559 | 480136 |
| MD17A-13-2 | cent | 32.57 | 0.97 | 0.07 | 65.28 | 98.89 | 3.02 | 0.03 | 0.003 | 2.95 | 6 | 8259 | 535 | 483238 |
| MD17A-13-3 | rim | 32.61 | 1.08 | 0.21 | 65.13 | 99.03 | 3.02 | 0.03 | 0.010 | 2.94 | 6 | 9140 | 1630 | 482157 |
| MD17A-70-1 | cent | 32.66 | 1.03 | 0.13 | 65.63 | 99.45 | 3.01 | 0.03 | 0.006 | 2.95 | 6 | 8691 | 1039 | 485851 |
| MD17A-70-2 | cent | 32.64 | 1.05 | 0.20 | 65.11 | 99.00 | 3.02 | 0.03 | 0.010 | 2.94 | 6 | 8878 | 1575 | 481972 |
| MD17A-70-3 | rim | 32.85 | 1.08 | 0.09 | 64.97 | 98.99 | 3.04 | 0.03 | 0.005 | 2.93 | 6 | 9191 | 740 | 480936 |
| MD17A-70-4 | - | 32.39 | 0.98 | 0.10 | 65.46 | 98.93 | 3.01 | 0.03 | 0.005 | 2.96 | 6 | 8343 | 795 | 484578 |
| MD17A-70-5 | rim | 32.27 | 0.99 | 0.11 | 65.17 | 98.54 | 3.01 | 0.03 | 0.005 | 2.96 | 6 | 8403 | 858 | 482446 |
| MD17A-70-6 | rim | 32.56 | 1.05 | 0.10 | 65.58 | 99.29 | 3.01 | 0.03 | 0.005 | 2.96 | 6 | 8937 | 787 | 485474 |
| MD17A-117-1 | rim | 32.61 | 1.07 | 0.11 | 65.46 | 99.24 | 3.02 | 0.03 | 0.005 | 2.95 | 6 | 9030 | 827 | 484600 |
| MD17A-117-2 | rim | 32.52 | 1.02 | 0.08 | 65.51 | 99.13 | 3.01 | 0.03 | 0.004 | 2.96 | 6 | 8615 | 638 | 484956 |
| MD17A-117-3 | cent | 32.68 | 0.99 | 0.26 | 65.18 | 99.10 | 3.02 | 0.03 | 0.013 | 2.94 | 6 | 8386 | 2008 | 482513 |
| MD17A-128-1 | rim | 32.72 | 1.01 | 0.05 | 65.66 | 99.44 | 3.02 | 0.03 | 0.003 | 2.95 | 6 | 8538 | 402 | 486096 |
| MD17A-128-2 | cent | 32.80 | 1.07 | 0.08 | 65.90 | 99.85 | 3.02 | 0.03 | 0.004 | 2.95 | 6 | 9089 | 598 | 487858 |

| | | IN wt % | | | | | Cation | | | | | In ppm | | |
|---|---|---|---|---|---|---|---|---|---|---|---|---|---|---|
| SL NO | | SiO2 | HfO2 | Y2O3 | ZrO2 | Total | Si | Hf | Y | Zr | SUM | Hf | Y | Zr |
| MD17A-128-3 | int | 32.73 | 1.12 | 0.01 | 65.29 | 99.15 | 3.03 | 0.03 | 0.001 | 2.94 | 6 | 9488 | 110 | 483349 |
| MD17A-128-4 | rim | 32.83 | 1.05 | 0.00 | 65.47 | 99.34 | 3.03 | 0.03 | 0.000 | 2.94 | 6 | 8903 | 0 | 484652 |
| MD17A-139-1 | int | 32.55 | 1.07 | 0.19 | 65.16 | 98.97 | 3.02 | 0.03 | 0.009 | 2.95 | 6 | 9056 | 1457 | 482387 |
| MD17A-139-2 | rim | 32.68 | 1.06 | 0.12 | 65.48 | 99.35 | 3.02 | 0.03 | 0.006 | 2.95 | 6 | 8979 | 961 | 484778 |
| MD17A-139-3 | rim | 32.62 | 1.04 | 0.11 | 65.38 | 99.14 | 3.02 | 0.03 | 0.005 | 2.95 | 6 | 8818 | 843 | 484001 |
| MD17A-139-4 | cent | 32.50 | 1.07 | 0.28 | 64.90 | 98.75 | 3.02 | 0.03 | 0.014 | 2.94 | 6 | 9106 | 2181 | 480432 |
| MD17A-156-1 | rim | 32.68 | 1.09 | 0.00 | 65.60 | 99.37 | 3.02 | 0.03 | 0.000 | 2.95 | 6 | 9225 | 8 | 485629 |
| MD17A-156-2 | rim | 33.09 | 1.05 | 0.00 | 64.86 | 99.00 | 3.05 | 0.03 | 0.000 | 2.92 | 6 | 8869 | 0 | 480173 |
| MD17A-156-3 | cent | 32.59 | 1.12 | 0.02 | 65.36 | 99.09 | 3.02 | 0.03 | 0.001 | 2.95 | 6 | 9522 | 173 | 483830 |
| MD17A-156-4 | int | 32.66 | 1.12 | 0.02 | 65.06 | 98.86 | 3.03 | 0.03 | 0.001 | 2.94 | 6 | 9496 | 157 | 481617 |
| MD17A-205-1 | int | 31.34 | 1.06 | 0.03 | 67.85 | 100.28 | 2.90 | 0.03 | 0.001 | 3.07 | 6 | 8988 | 228 | 502308 |
| MD17A-205-2 | cent | 31.56 | 1.09 | 0.03 | 67.54 | 100.22 | 2.92 | 0.03 | 0.001 | 3.05 | 6 | 9276 | 205 | 500028 |
| MD17A-205-3 | rim | 31.16 | 1.00 | 0.00 | 67.66 | 99.82 | 2.90 | 0.03 | 0.000 | 3.07 | 6 | 8479 | 0 | 500880 |
| MD17A-234-2 | cent | 32.23 | 1.11 | 0.24 | 64.50 | 98.09 | 3.02 | 0.03 | 0.012 | 2.94 | 6 | 9446 | 1882 | 477523 |
| MD17A-234-3 | rim | 32.88 | 1.07 | 0.02 | 64.27 | 98.23 | 3.06 | 0.03 | 0.001 | 2.91 | 6 | 9039 | 118 | 475769 |
| MD17A-234-4 | rim | 32.84 | 1.10 | 0.04 | 64.97 | 98.95 | 3.04 | 0.03 | 0.002 | 2.93 | 6 | 9335 | 283 | 480995 |
| MD17A-234-5 | cent | 32.38 | 1.15 | 0.21 | 64.69 | 98.43 | 3.02 | 0.03 | 0.010 | 2.94 | 6 | 9751 | 1614 | 478915 |
| MD32-1-2 | rim | 32.08 | 1.48 | 0.06 | 65.13 | 98.74 | 2.99 | 0.04 | 0.003 | 2.96 | 6 | 12507 | 465 | 482120 |
| MD32-1-3 | int | 31.98 | 1.32 | 0.14 | 65.17 | 98.60 | 2.99 | 0.04 | 0.007 | 2.97 | 6 | 11175 | 1079 | 482431 |
| MD32-1-5 | core | 32.24 | 1.43 | 0.15 | 65.03 | 98.85 | 3.00 | 0.04 | 0.007 | 2.95 | 6 | 12108 | 1189 | 481387 |
| MD32-1-6 | core | 31.95 | 1.36 | 0.18 | 65.06 | 98.55 | 2.99 | 0.04 | 0.009 | 2.97 | 6 | 11531 | 1449 | 481654 |
| MD32-1-7 | int | 32.08 | 1.38 | 0.15 | 65.17 | 98.77 | 2.99 | 0.04 | 0.007 | 2.96 | 6 | 11676 | 1173 | 482446 |
| MD32-1-8 | int | 32.15 | 1.46 | 0.14 | 65.41 | 99.16 | 2.99 | 0.04 | 0.007 | 2.97 | 6 | 12337 | 1134 | 484230 |
| MD32-1-9 | rim | 32.25 | 1.31 | 0.07 | 64.90 | 98.54 | 3.01 | 0.03 | 0.004 | 2.95 | 6 | 11116 | 559 | 480477 |
| MD32-3-1 | core | 31.96 | 1.35 | 0.32 | 64.91 | 98.55 | 2.99 | 0.04 | 0.016 | 2.96 | 6 | 11472 | 2535 | 480536 |
| MD32-3-2 | core | 32.00 | 1.33 | 0.21 | 64.98 | 98.52 | 2.99 | 0.04 | 0.011 | 2.96 | 6 | 11294 | 1685 | 481032 |
| MD32-3-3 | rim | 32.22 | 0.99 | 0.09 | 66.18 | 99.48 | 2.98 | 0.03 | 0.004 | 2.99 | 6 | 8352 | 685 | 489938 |
| MD32-3-4 | rim | 32.37 | 1.00 | 0.09 | 65.85 | 99.30 | 3.00 | 0.03 | 0.004 | 2.97 | 6 | 8454 | 717 | 487465 |
| MD-32-2-1 | rim | 32.69 | 1.18 | 0.00 | 65.73 | 99.60 | 3.01 | 0.03 | 0.000 | 2.95 | 6 | 10031 | 0 | 486584 |
| MD-32-2-2 | core | 32.36 | 1.55 | 0.14 | 64.76 | 98.81 | 3.01 | 0.04 | 0.007 | 2.94 | 6 | 13168 | 1063 | 479403 |
| MD-32-2-3 | core | 31.98 | 2.02 | 0.27 | 63.68 | 97.95 | 3.01 | 0.05 | 0.014 | 2.92 | 6 | 17119 | 2150 | 471423 |
| MD-32-2-4 | core | 32.62 | 1.25 | 0.05 | 65.61 | 99.52 | 3.01 | 0.03 | 0.002 | 2.95 | 6 | 10590 | 386 | 485711 |
| MD-32-2-5 | core | 32.30 | 1.73 | 0.21 | 64.74 | 98.98 | 3.01 | 0.05 | 0.010 | 2.94 | 6 | 14660 | 1646 | 479292 |
| MD-32-2-6 | int | 32.54 | 1.69 | 0.03 | 64.99 | 99.25 | 3.02 | 0.04 | 0.002 | 2.94 | 6 | 14296 | 260 | 481128 |
| MD-32-2-7 | rim | 32.65 | 1.07 | 0.01 | 65.79 | 99.51 | 3.01 | 0.03 | 0.000 | 2.96 | 6 | 9073 | 47 | 487021 |
| MD-32-7-1 | core | 32.48 | 1.43 | 0.15 | 65.09 | 99.15 | 3.01 | 0.04 | 0.008 | 2.94 | 6 | 12150 | 1197 | 481854 |
| MD-32-7-3 | rim | 32.35 | 1.95 | 0.08 | 64.72 | 99.10 | 3.01 | 0.05 | 0.004 | 2.94 | 6 | 16526 | 638 | 479100 |
| MD-32-7-4 | rim | 32.50 | 1.75 | 0.01 | 64.68 | 98.93 | 3.02 | 0.05 | 0.000 | 2.93 | 6 | 14804 | 55 | 478789 |
| MD-32-10-1 | core | 32.41 | 1.44 | 0.28 | 64.88 | 99.01 | 3.01 | 0.04 | 0.014 | 2.94 | 6 | 12193 | 2165 | 480321 |
| MD-32-10-2 | rim | 32.73 | 0.87 | 0.10 | 65.46 | 99.16 | 3.02 | 0.02 | 0.005 | 2.95 | 6 | 7402 | 795 | 484578 |
| MD-32-10-3 | rim | 32.68 | 1.05 | 0.01 | 65.67 | 99.40 | 3.02 | 0.03 | 0.000 | 2.96 | 6 | 8894 | 39 | 486170 |
| MD-32-16-1 | core | 32.56 | 2.17 | 0.07 | 64.94 | 99.74 | 3.01 | 0.06 | 0.004 | 2.93 | 6 | 18391 | 583 | 480729 |
| MD-32-16-2 | rim | 32.74 | 0.96 | 0.08 | 65.75 | 99.53 | 3.02 | 0.03 | 0.004 | 2.95 | 6 | 8165 | 654 | 486710 |
| MD-32-16-3 | rim | 32.82 | 1.00 | 0.00 | 66.43 | 100.25 | 3.01 | 0.03 | 0.000 | 2.97 | 6 | 8479 | 0 | 491796 |

| | | IN wt % | | | | | Cation | | | | | In ppm | | |
|---|---|---|---|---|---|---|---|---|---|---|---|---|---|---|
| SL NO | | SiO2 | HfO2 | Y2O3 | ZrO2 | Total | Si | Hf | Y | Zr | SUM | Hf | Y | Zr |
| MD-32-15-1 | core | 32.38 | 1.92 | 0.16 | 64.12 | 98.58 | 3.02 | 0.05 | 0.008 | 2.92 | 6 | 16297 | 1244 | 474703 |
| MD-32-15-2 | core | 32.37 | 1.91 | 0.17 | 64.08 | 98.52 | 3.02 | 0.05 | 0.008 | 2.92 | 6 | 16161 | 1315 | 474347 |
| MD-32-15-3 | rim | 31.45 | 1.36 | 0.00 | 67.86 | 100.67 | 2.91 | 0.04 | 0.000 | 3.06 | 6 | 11506 | 0 | 502397 |
| MD-32-21-1 | core | 32.49 | 1.68 | 0.18 | 64.88 | 99.23 | 3.01 | 0.04 | 0.009 | 2.93 | 6 | 14211 | 1417 | 480321 |
| MD-32-21-2 | core | 32.73 | 1.62 | 0.21 | 65.20 | 99.76 | 3.02 | 0.04 | 0.010 | 2.93 | 6 | 13761 | 1630 | 482653 |
| MD-32-21-3 | rim | 32.88 | 0.92 | 0.07 | 66.63 | 100.49 | 3.00 | 0.02 | 0.003 | 2.97 | 6 | 7758 | 559 | 493269 |
| MD-32-42-1 | rim | 32.74 | 1.48 | 0.02 | 65.55 | 99.79 | 3.02 | 0.04 | 0.001 | 2.94 | 6 | 12583 | 126 | 485289 |
| MD-32-42-2 | core | 32.52 | 1.42 | 0.21 | 65.14 | 99.28 | 3.01 | 0.04 | 0.010 | 2.94 | 6 | 12023 | 1630 | 482202 |
| MD-32-42-3 | rim | 32.73 | 0.99 | 0.00 | 65.65 | 99.37 | 3.02 | 0.03 | 0.000 | 2.95 | 6 | 8394 | 16 | 485992 |
| MD-32-42-4 | rim | 32.55 | 1.55 | 0.10 | 65.38 | 99.57 | 3.01 | 0.04 | 0.005 | 2.95 | 6 | 13142 | 748 | 483986 |
| MD-32-90-1 | rim | 32.71 | 1.05 | 0.05 | 65.95 | 99.76 | 3.01 | 0.03 | 0.002 | 2.96 | 6 | 8894 | 370 | 488235 |
| MD-32-90-2 | core | 32.29 | 1.75 | 0.37 | 63.76 | 98.17 | 3.03 | 0.05 | 0.018 | 2.91 | 6 | 14813 | 2882 | 472030 |
| MD-32-90-3 | rim | 32.59 | 1.59 | 0.08 | 64.97 | 99.23 | 3.02 | 0.04 | 0.004 | 2.94 | 6 | 13473 | 638 | 480988 |
| MD-32-74-1 | core | 32.54 | 1.66 | 0.04 | 65.00 | 99.24 | 3.02 | 0.04 | 0.002 | 2.94 | 6 | 14067 | 323 | 481195 |
| MD-32-74-2 | rim | 32.93 | 1.00 | 0.02 | 65.54 | 99.49 | 3.03 | 0.03 | 0.001 | 2.94 | 6 | 8445 | 134 | 485200 |
| MD-32-83-1 | rim | 32.75 | 0.90 | 0.05 | 65.76 | 99.45 | 3.02 | 0.02 | 0.002 | 2.96 | 6 | 7614 | 354 | 486784 |
| MD-32-83-2 | int | 32.67 | 0.87 | 0.07 | 65.68 | 99.30 | 3.02 | 0.02 | 0.003 | 2.96 | 6 | 7385 | 559 | 486222 |
| MD-32-83-3 | cent | 32.64 | 1.01 | 0.03 | 65.89 | 99.57 | 3.01 | 0.03 | 0.001 | 2.96 | 6 | 8572 | 205 | 487791 |
| MD-32-83-4 | rim | 32.86 | 0.91 | 0.03 | 65.26 | 99.06 | 3.04 | 0.02 | 0.001 | 2.94 | 6 | 7741 | 205 | 483127 |
| MD-32-88-2 | core | 32.84 | 1.12 | 0.13 | 63.28 | 97.37 | 3.08 | 0.03 | 0.006 | 2.89 | 6 | 9522 | 1024 | 468440 |
| MD-32-88-3 | int | 32.62 | 1.53 | 0.08 | 64.54 | 98.76 | 3.03 | 0.04 | 0.004 | 2.93 | 6 | 12939 | 614 | 477797 |
| MD-32-88-4 | rim | 32.69 | 1.59 | 0.02 | 65.10 | 99.40 | 3.02 | 0.04 | 0.001 | 2.93 | 6 | 13490 | 142 | 481928 |
| MD-32-79-1 | core | 32.84 | 1.28 | 0.21 | 65.31 | 99.63 | 3.03 | 0.03 | 0.010 | 2.93 | 6 | 10853 | 1622 | 483460 |
| MD-32-79-2 | core | 32.60 | 1.35 | 0.21 | 64.92 | 99.08 | 3.02 | 0.04 | 0.010 | 2.93 | 6 | 11472 | 1661 | 480625 |
| MD-32-79-3 | core | 32.79 | 1.31 | 0.13 | 64.78 | 99.01 | 3.04 | 0.03 | 0.006 | 2.92 | 6 | 11124 | 1016 | 479596 |
| MD-32-93-1 | core | 32.73 | 0.97 | 0.09 | 66.13 | 99.92 | 3.01 | 0.03 | 0.004 | 2.96 | 6 | 8225 | 685 | 489575 |
| MD-32-93-2 | core | 32.57 | 1.10 | 0.12 | 65.10 | 98.88 | 3.02 | 0.03 | 0.006 | 2.94 | 6 | 9293 | 961 | 481906 |
| MD-32-93-3 | rim | 32.80 | 0.93 | 0.04 | 65.74 | 99.50 | 3.02 | 0.02 | 0.002 | 2.95 | 6 | 7869 | 307 | 486636 |
| MD-32-93-4 | core | 32.66 | 0.93 | 0.05 | 65.57 | 99.22 | 3.02 | 0.02 | 0.003 | 2.96 | 6 | 7911 | 417 | 485444 |
| MD-32-93-5 | rim | 32.81 | 1.02 | 0.03 | 65.93 | 99.79 | 3.02 | 0.03 | 0.001 | 2.96 | 6 | 8682 | 205 | 488109 |
| MD-32-93-6 | rim | 32.77 | 1.06 | 0.02 | 65.70 | 99.55 | 3.02 | 0.03 | 0.001 | 2.95 | 6 | 8996 | 126 | 486377 |
| MD-32-98-1 | int | 32.66 | 1.41 | 0.01 | 65.02 | 99.10 | 3.03 | 0.04 | 0.000 | 2.94 | 6 | 11955 | 47 | 481373 |
| MD-32-98-2 | core | 32.75 | 0.94 | 0.07 | 65.45 | 99.20 | 3.03 | 0.02 | 0.003 | 2.95 | 6 | 7945 | 520 | 484497 |
| MD-32-98-3 | rim | 32.74 | 1.00 | 0.07 | 66.03 | 99.83 | 3.01 | 0.03 | 0.003 | 2.96 | 6 | 8462 | 512 | 488783 |
| MD-32-98-4 | core | 32.94 | 0.95 | 0.14 | 65.63 | 99.66 | 3.03 | 0.02 | 0.007 | 2.94 | 6 | 8038 | 1126 | 485851 |
| MD-32-98-5 | core | 32.95 | 0.93 | 0.11 | 65.98 | 99.98 | 3.02 | 0.02 | 0.005 | 2.95 | 6 | 7885 | 882 | 488472 |
| MD-32-107-1 | rim | 32.55 | 1.02 | 0.00 | 65.48 | 99.05 | 3.02 | 0.03 | 0.000 | 2.96 | 6 | 8623 | 0 | 484756 |
| MD-32-107-3 | core | 32.50 | 1.28 | 0.25 | 64.90 | 98.93 | 3.02 | 0.03 | 0.012 | 2.94 | 6 | 10836 | 1976 | 480462 |
| MD-32-107-4 | int | 32.61 | 0.94 | 0.08 | 65.74 | 99.37 | 3.01 | 0.02 | 0.004 | 2.96 | 6 | 8004 | 654 | 486666 |
| MD-32-107-5 | rim | 32.56 | 1.00 | 0.03 | 65.37 | 98.96 | 3.02 | 0.03 | 0.002 | 2.95 | 6 | 8479 | 268 | 483919 |

| | | IN wt % | | | | | Cation | | | | | In ppm | | |
|---|---|---|---|---|---|---|---|---|---|---|---|---|---|---|
| SL NO | | SiO2 | HfO2 | Y2O3 | ZrO2 | Total | Si | Hf | Y | Zr | SUM | Hf | Y | Zr |
| MD-32-107-6 | rim | 32.70 | 0.94 | 0.07 | 65.23 | 98.93 | 3.03 | 0.02 | 0.003 | 2.95 | 6 | 7945 | 528 | 482868 |
| MD-32-115-1 | core | 32.83 | 0.97 | 0.11 | 65.54 | 99.44 | 3.03 | 0.03 | 0.005 | 2.95 | 6 | 8208 | 843 | 485170 |
| MD-32-115-2 | core | 32.60 | 2.14 | 0.09 | 64.97 | 99.80 | 3.01 | 0.06 | 0.004 | 2.93 | 6 | 18179 | 693 | 480966 |
| MD-32-115-3 | core | 32.77 | 1.51 | 0.02 | 65.44 | 99.73 | 3.02 | 0.04 | 0.001 | 2.94 | 6 | 12761 | 118 | 484438 |
| MD-32-115-4 | core | 32.66 | 1.63 | 0.03 | 65.49 | 99.81 | 3.01 | 0.04 | 0.001 | 2.94 | 6 | 13846 | 205 | 484830 |
| MD-32-115-5 | rim | 32.99 | 1.03 | 0.06 | 65.13 | 99.20 | 3.04 | 0.03 | 0.003 | 2.93 | 6 | 8691 | 441 | 482157 |
| MD-32-114-1 | rim | 32.68 | 1.07 | 0.00 | 65.82 | 99.57 | 3.01 | 0.03 | 0.000 | 2.96 | 6 | 9039 | 0 | 487295 |
| MD-32-114-2 | core | 32.66 | 1.59 | 0.13 | 65.00 | 99.38 | 3.02 | 0.04 | 0.007 | 2.93 | 6 | 13448 | 1047 | 481202 |
| MD-32-114-3 | core | 32.72 | 1.48 | 0.18 | 65.30 | 99.69 | 3.02 | 0.04 | 0.009 | 2.94 | 6 | 12515 | 1441 | 483431 |
| MD-32-114-4 | int | 32.50 | 2.21 | 0.14 | 64.59 | 99.44 | 3.01 | 0.06 | 0.007 | 2.92 | 6 | 18730 | 1087 | 478167 |
| MD-32-114-5 | rim | 32.56 | 1.64 | 0.06 | 64.50 | 98.77 | 3.03 | 0.04 | 0.003 | 2.93 | 6 | 13889 | 496 | 477516 |
| MD-32-111-1 | rim | 32.75 | 1.32 | 0.19 | 64.81 | 99.06 | 3.03 | 0.03 | 0.009 | 2.93 | 6 | 11184 | 1457 | 479788 |
| MD-32-111-2 | core | 32.64 | 1.39 | 0.24 | 64.50 | 98.76 | 3.03 | 0.04 | 0.012 | 2.92 | 6 | 11760 | 1858 | 477464 |
| MD-32-111-3 | core | 32.72 | 1.69 | 0.13 | 64.32 | 98.87 | 3.04 | 0.04 | 0.006 | 2.91 | 6 | 14346 | 1016 | 476191 |
| MD-32-111-4 | core | 32.71 | 1.31 | 0.16 | 64.73 | 98.91 | 3.03 | 0.03 | 0.008 | 2.93 | 6 | 11065 | 1260 | 479181 |
| MD-32-111-5 | int | 32.69 | 1.59 | 0.01 | 65.19 | 99.49 | 3.02 | 0.04 | 0.001 | 2.94 | 6 | 13490 | 94 | 482594 |
| MD-32-111-6 | rim | 32.97 | 1.05 | 0.06 | 65.30 | 99.38 | 3.04 | 0.03 | 0.003 | 2.93 | 6 | 8903 | 449 | 483438 |
| MD2-2-1 | rim | 32.84 | 2.08 | 0.03 | 65.44 | 100.39 | 3.02 | 0.05 | 0.002 | 2.93 | 6 | 17602 | 260 | 484460 |
| MD2-2-2 | int | 32.76 | 1.32 | 0.18 | 65.47 | 99.73 | 3.02 | 0.03 | 0.009 | 2.94 | 6 | 11192 | 1394 | 484704 |
| MD2-2-3 | core | 32.83 | 1.09 | 0.26 | 66.06 | 100.23 | 3.01 | 0.03 | 0.013 | 2.95 | 6 | 9242 | 2024 | 489005 |
| MD2-14-1 | rim | 32.79 | 1.12 | 0.30 | 65.32 | 99.53 | 3.02 | 0.03 | 0.015 | 2.94 | 6 | 9454 | 2370 | 483571 |
| MD2-14-2 | core | 32.91 | 1.20 | 0.28 | 65.96 | 100.34 | 3.01 | 0.03 | 0.013 | 2.95 | 6 | 10158 | 2181 | 488280 |
| MD2-14-3 | rim | 32.45 | 1.45 | 0.58 | 65.14 | 99.61 | 3.00 | 0.04 | 0.028 | 2.94 | 6 | 12286 | 4535 | 482202 |
| MD2-15-1 | core | 32.58 | 1.32 | 0.76 | 64.11 | 98.77 | 3.03 | 0.04 | 0.038 | 2.91 | 6 | 11218 | 5984 | 474614 |
| MD2-15-2 | rim | 32.58 | 1.79 | 0.34 | 64.49 | 99.20 | 3.02 | 0.05 | 0.017 | 2.92 | 6 | 15135 | 2654 | 477434 |
| MD2-23-1 | rim | 32.59 | 1.50 | 0.17 | 65.29 | 99.54 | 3.01 | 0.04 | 0.008 | 2.94 | 6 | 12702 | 1323 | 483334 |
| MD2-23-2 | int | 32.82 | 1.07 | 0.13 | 65.85 | 99.87 | 3.02 | 0.03 | 0.006 | 2.95 | 6 | 9047 | 1024 | 487502 |
| MD2-23-3 | core | 32.83 | 1.02 | 0.33 | 65.67 | 99.85 | 3.02 | 0.03 | 0.016 | 2.94 | 6 | 8674 | 2606 | 486185 |
| MD2-23-4 | rim | 32.73 | 0.99 | 0.13 | 66.30 | 100.15 | 3.00 | 0.03 | 0.006 | 2.97 | 6 | 8369 | 1024 | 490841 |
| MD2-42-1 | core | 32.92 | 1.01 | 0.26 | 65.84 | 100.03 | 3.02 | 0.03 | 0.013 | 2.94 | 6 | 8589 | 2031 | 487399 |
| MD2-42-3 | rim | 32.86 | 1.36 | 0.10 | 66.01 | 100.34 | 3.01 | 0.04 | 0.005 | 2.95 | 6 | 11565 | 819 | 488694 |
| MD2-36-1 | core | 32.78 | 1.22 | 0.19 | 65.46 | 99.65 | 3.02 | 0.03 | 0.009 | 2.94 | 6 | 10353 | 1480 | 484608 |
| MD2-36-2 | rim | 32.76 | 1.31 | 0.05 | 66.11 | 100.23 | 3.01 | 0.03 | 0.002 | 2.96 | 6 | 11074 | 386 | 489390 |
| MD2-36-3 | rim | 32.73 | 1.84 | 0.10 | 64.93 | 99.60 | 3.02 | 0.05 | 0.005 | 2.92 | 6 | 15618 | 764 | 480684 |
| MD2-36-4 | rim | 32.74 | 1.48 | 0.39 | 65.22 | 99.82 | 3.02 | 0.04 | 0.019 | 2.93 | 6 | 12515 | 3063 | 482809 |
| MD2-62-1 | rim | 33.02 | 1.83 | 0.10 | 65.64 | 100.58 | 3.02 | 0.05 | 0.005 | 2.93 | 6 | 15500 | 748 | 485911 |
| MD2-62-2 | core | 32.96 | 1.23 | 0.09 | 66.20 | 100.48 | 3.01 | 0.03 | 0.004 | 2.95 | 6 | 10455 | 724 | 490042 |
| MD2-62-3 | core | 32.80 | 0.90 | 0.42 | 65.80 | 99.93 | 3.01 | 0.02 | 0.021 | 2.95 | 6 | 7657 | 3339 | 487140 |
| MD2-62-4 | rim | 32.94 | 1.30 | 0.07 | 65.59 | 99.90 | 3.03 | 0.03 | 0.003 | 2.94 | 6 | 11040 | 543 | 485541 |
| MD2-68-1 | core | 32.60 | 0.98 | 0.76 | 64.87 | 99.21 | 3.02 | 0.03 | 0.037 | 2.93 | 6 | 8343 | 5961 | 480210 |
| MD2-68-2 | rim | 32.91 | 1.13 | 0.04 | 66.51 | 100.59 | 3.01 | 0.03 | 0.002 | 2.96 | 6 | 9564 | 339 | 492359 |

| | | IN wt % | | | | | Cation | | | | | In ppm | | |
|---|---|---|---|---|---|---|---|---|---|---|---|---|---|---|
| SL NO | | SiO2 | HfO2 | Y2O3 | ZrO2 | Total | Si | Hf | Y | Zr | SUM | Hf | Y | Zr |
| MD2-80-1 | rim | 33.03 | 0.93 | 0.04 | 66.33 | 100.32 | 3.02 | 0.02 | 0.002 | 2.96 | 6 | 7852 | 291 | 491026 |
| MD2-80-2 | core | 33.02 | 0.94 | 0.01 | 66.14 | 100.12 | 3.02 | 0.02 | 0.001 | 2.95 | 6 | 7987 | 94 | 489642 |
| MD2-80-3 | rim | 32.80 | 0.88 | 0.31 | 65.85 | 99.84 | 3.01 | 0.02 | 0.015 | 2.95 | 6 | 7428 | 2441 | 487517 |
| MD2-78-1 | rim | 32.77 | 1.37 | 0.29 | 65.23 | 99.65 | 3.02 | 0.04 | 0.014 | 2.93 | 6 | 11582 | 2252 | 482890 |
| MD2-78-2 | int | 31.90 | 1.06 | 0.47 | 65.12 | 98.54 | 2.98 | 0.03 | 0.023 | 2.97 | 6 | 8962 | 3709 | 482054 |
| MD2-78-3 | core | 32.60 | 1.15 | 0.81 | 64.62 | 99.18 | 3.02 | 0.03 | 0.040 | 2.92 | 6 | 9759 | 6362 | 478389 |
| MD2-78-4 | core | 32.85 | 1.36 | 0.08 | 65.90 | 100.19 | 3.01 | 0.04 | 0.004 | 2.95 | 6 | 11557 | 606 | 487835 |
| MD2-78-5 | int | 33.02 | 1.21 | 0.06 | 65.37 | 99.65 | 3.04 | 0.03 | 0.003 | 2.93 | 6 | 10234 | 449 | 483964 |
| MD2-78-6 | rim | 32.67 | 1.27 | 0.23 | 65.76 | 99.92 | 3.01 | 0.03 | 0.011 | 2.95 | 6 | 10785 | 1772 | 486829 |
| MD6-10-1 | core | 32.85 | 0.95 | 0.32 | 65.67 | 99.79 | 3.02 | 0.02 | 0.016 | 2.94 | 6 | 8030 | 2535 | 486118 |
| MD6-10-2 | int | 32.90 | 1.17 | 0.10 | 65.66 | 99.83 | 3.02 | 0.03 | 0.005 | 2.94 | 6 | 9887 | 787 | 486059 |
| MD6-10-3 | rim | 32.80 | 1.80 | 0.01 | 66.00 | 100.61 | 3.00 | 0.05 | 0.000 | 2.95 | 6 | 15296 | 47 | 488620 |
| MD6-11-1 | core | 33.00 | 1.20 | 0.13 | 65.89 | 100.21 | 3.02 | 0.03 | 0.006 | 2.94 | 6 | 10149 | 1000 | 487747 |
| MD6-11-2 | rim | 33.03 | 1.20 | 0.21 | 65.59 | 100.02 | 3.03 | 0.03 | 0.010 | 2.93 | 6 | 10209 | 1614 | 485526 |
| MD6-62-1 | core | 32.82 | 1.44 | 0.11 | 65.81 | 100.18 | 3.01 | 0.04 | 0.005 | 2.95 | 6 | 12201 | 850 | 487177 |
| MD6-62-2 | core | 32.86 | 1.08 | 0.29 | 65.46 | 99.68 | 3.02 | 0.03 | 0.014 | 2.94 | 6 | 9132 | 2244 | 484593 |
| MD6-62-3 | rim | 33.08 | 1.31 | 0.01 | 66.22 | 100.62 | 3.02 | 0.03 | 0.000 | 2.95 | 6 | 11107 | 55 | 490256 |
| MD6-62-4 | int | 32.67 | 1.85 | 0.24 | 64.84 | 99.59 | 3.02 | 0.05 | 0.012 | 2.92 | 6 | 15652 | 1898 | 480018 |
| MD6-67-1 | core | 32.97 | 1.22 | 0.21 | 65.25 | 99.64 | 3.03 | 0.03 | 0.010 | 2.93 | 6 | 10353 | 1630 | 483009 |
| MD6-67-2 | rim | 32.84 | 1.92 | 0.00 | 65.62 | 100.38 | 3.01 | 0.05 | 0.000 | 2.94 | 6 | 16271 | 0 | 485770 |
| MD6-80-1 | core | 32.97 | 0.99 | 0.19 | 66.01 | 100.15 | 3.02 | 0.03 | 0.009 | 2.95 | 6 | 8369 | 1457 | 488679 |
| MD6-80-2 | int | 32.95 | 1.05 | 0.14 | 66.35 | 100.49 | 3.01 | 0.03 | 0.007 | 2.96 | 6 | 8928 | 1087 | 491167 |
| MD6-80-3 | int | 33.03 | 1.01 | 0.08 | 65.47 | 99.59 | 3.04 | 0.03 | 0.004 | 2.93 | 6 | 8581 | 622 | 484660 |
| MD6-84a-1 | core | 32.97 | 1.09 | 0.10 | 65.58 | 99.74 | 3.03 | 0.03 | 0.005 | 2.94 | 6 | 9200 | 795 | 485496 |
| MD6-84a-2 | rim | 32.89 | 1.39 | 0.00 | 64.97 | 99.25 | 3.04 | 0.04 | 0.000 | 2.93 | 6 | 11760 | 8 | 480966 |
| MD6-84a-3 | core | 32.88 | 0.96 | 0.15 | 65.70 | 99.69 | 3.02 | 0.03 | 0.007 | 2.95 | 6 | 8114 | 1173 | 486370 |
| MD6-84b-1 | core | 32.87 | 1.08 | 0.37 | 65.45 | 99.77 | 3.02 | 0.03 | 0.018 | 2.94 | 6 | 9166 | 2945 | 484512 |
| MD6-84b-2 | int | 32.98 | 1.60 | 0.00 | 65.20 | 99.79 | 3.03 | 0.04 | 0.000 | 2.92 | 6 | 13558 | 24 | 482690 |
| MD6-84b-3 | rim | 32.85 | 1.71 | 0.01 | 64.98 | 99.55 | 3.03 | 0.05 | 0.000 | 2.92 | 6 | 14499 | 47 | 481025 |
| MD6-85-1 | core | 32.98 | 1.28 | 0.05 | 65.40 | 99.70 | 3.03 | 0.03 | 0.002 | 2.93 | 6 | 10887 | 362 | 484134 |
| MD6-85-2 | core | 32.97 | 1.25 | 0.11 | 65.74 | 100.08 | 3.02 | 0.03 | 0.005 | 2.94 | 6 | 10633 | 882 | 486695 |
| MD6-85-3 | int | 32.84 | 1.38 | 0.18 | 65.48 | 99.88 | 3.02 | 0.04 | 0.009 | 2.94 | 6 | 11684 | 1394 | 484756 |
| MD6-85-4 | rim | 32.45 | 1.79 | 0.41 | 64.75 | 99.39 | 3.01 | 0.05 | 0.020 | 2.93 | 6 | 15169 | 3205 | 479329 |
| MD6-95-1 | core | 32.83 | 0.96 | 0.30 | 65.64 | 99.73 | 3.02 | 0.03 | 0.015 | 2.94 | 6 | 8157 | 2370 | 485896 |
| MD6-95-2 | core | 32.76 | 1.08 | 0.29 | 64.92 | 99.05 | 3.03 | 0.03 | 0.014 | 2.93 | 6 | 9149 | 2260 | 480595 |
| MD6-95-3 | int | 32.86 | 1.39 | 0.11 | 65.79 | 100.15 | 3.02 | 0.04 | 0.005 | 2.94 | 6 | 11794 | 843 | 487051 |
| MD6-95-4 | rim | 32.90 | 1.98 | 0.06 | 65.01 | 99.96 | 3.03 | 0.05 | 0.003 | 2.92 | 6 | 16797 | 504 | 481247 |
| MD6-117-1 | core | 32.69 | 1.68 | 0.31 | 64.22 | 98.90 | 3.04 | 0.04 | 0.015 | 2.91 | 6 | 14270 | 2402 | 475421 |

| | | IN wt % | | | | | Cation | | | | | In ppm | | |
|---|---|---|---|---|---|---|---|---|---|---|---|---|---|---|
| SL NO | | SiO2 | HfO2 | Y2O3 | ZrO2 | Total | Si | Hf | Y | Zr | SUM | Hf | Y | Zr |
| MD6-117-2 | int | 32.70 | 1.97 | 0.12 | 64.45 | 99.24 | 3.03 | 0.05 | 0.006 | 2.91 | 6 | 16661 | 945 | 477146 |
| MD6-117-3 | rim | 32.77 | 1.81 | 0.00 | 65.26 | 99.84 | 3.02 | 0.05 | 0.000 | 2.93 | 6 | 15364 | 0 | 483112 |
| MD6-117-4 | rim | 32.97 | 1.95 | 0.00 | 65.00 | 99.91 | 3.03 | 0.05 | 0.000 | 2.92 | 6 | 16492 | 0 | 481180 |
| MD6-118-1 | core | 32.64 | 0.99 | 0.80 | 64.53 | 98.96 | 3.03 | 0.03 | 0.039 | 2.92 | 6 | 8420 | 6299 | 477745 |
| MD6-118-2 | core | 32.44 | 1.82 | 0.22 | 64.62 | 99.10 | 3.02 | 0.05 | 0.011 | 2.93 | 6 | 15423 | 1717 | 478352 |
| MD6-118-3 | rim | 33.00 | 2.00 | 0.00 | 64.51 | 99.51 | 3.04 | 0.05 | 0.000 | 2.90 | 6 | 16966 | 0 | 477597 |
| MD6-118-4 | rim | 32.67 | 2.08 | 0.01 | 64.20 | 98.95 | 3.04 | 0.06 | 0.000 | 2.91 | 6 | 17602 | 47 | 475258 |
| MD6-121-3 | core | 32.82 | 1.63 | 0.23 | 64.69 | 99.38 | 3.03 | 0.04 | 0.012 | 2.92 | 6 | 13812 | 1843 | 478915 |
| MD6-121-4 | int | 32.91 | 1.36 | 0.17 | 64.69 | 99.14 | 3.04 | 0.04 | 0.009 | 2.92 | 6 | 11548 | 1362 | 478893 |
| MD6-121-5 | rim | 32.85 | 1.63 | 0.03 | 64.90 | 99.40 | 3.03 | 0.04 | 0.001 | 2.92 | 6 | 13838 | 220 | 480418 |
| MD6-124-1 | core | 32.84 | 1.51 | 0.00 | 65.20 | 99.55 | 3.03 | 0.04 | 0.000 | 2.93 | 6 | 12829 | 0 | 482639 |
| MD6-124-2 | int | 32.96 | 1.50 | 0.00 | 64.79 | 99.26 | 3.04 | 0.04 | 0.000 | 2.92 | 6 | 12702 | 0 | 479670 |
| MD6-124-3 | rim | 32.85 | 1.61 | 0.04 | 64.95 | 99.45 | 3.03 | 0.04 | 0.002 | 2.92 | 6 | 13617 | 307 | 480832 |
| MD6-135-1 | core | 32.67 | 1.74 | 0.19 | 64.66 | 99.26 | 3.03 | 0.05 | 0.009 | 2.92 | 6 | 14720 | 1488 | 478708 |
| MD6-135-2 | core | 32.78 | 1.27 | 0.15 | 64.85 | 99.05 | 3.03 | 0.03 | 0.007 | 2.93 | 6 | 10760 | 1189 | 480055 |
| MD6-135-3 | core | 32.85 | 1.12 | 0.16 | 65.27 | 99.39 | 3.03 | 0.03 | 0.008 | 2.94 | 6 | 9454 | 1244 | 483194 |
| MD6-135-4 | int | 32.89 | 1.05 | 0.12 | 65.31 | 99.37 | 3.03 | 0.03 | 0.006 | 2.94 | 6 | 8911 | 976 | 483490 |
| MD6-135-5 | rim | 32.47 | 1.88 | 0.30 | 64.05 | 98.70 | 3.03 | 0.05 | 0.015 | 2.91 | 6 | 15949 | 2362 | 474177 |
| MD6-135-6 | rim | 32.76 | 1.16 | 0.19 | 65.03 | 99.14 | 3.03 | 0.03 | 0.009 | 2.93 | 6 | 9870 | 1512 | 481387 |
| MD6-135-7 | rim | 32.61 | 1.71 | 0.24 | 64.17 | 98.73 | 3.03 | 0.05 | 0.012 | 2.91 | 6 | 14516 | 1866 | 475028 |
| MD6-135-8 | rim | 32.78 | 1.91 | 0.03 | 64.97 | 99.69 | 3.03 | 0.05 | 0.001 | 2.92 | 6 | 16161 | 228 | 480988 |
| MD6-136-2 | core | 32.69 | 1.37 | 0.17 | 64.73 | 98.97 | 3.03 | 0.04 | 0.009 | 2.93 | 6 | 11616 | 1370 | 479226 |
| MD6-136-3 | core | 32.84 | 1.30 | 0.09 | 65.27 | 99.50 | 3.03 | 0.03 | 0.004 | 2.93 | 6 | 11057 | 693 | 483186 |
| MD6-136-4 | int | 32.69 | 1.36 | 0.10 | 65.05 | 99.19 | 3.03 | 0.04 | 0.005 | 2.94 | 6 | 11514 | 772 | 481550 |
| MD6-136-5 | rim | 32.77 | 1.53 | 0.01 | 64.64 | 98.96 | 3.04 | 0.04 | 0.000 | 2.92 | 6 | 13007 | 79 | 478552 |
| MD29-1-1 | rim | 32.47 | 1.08 | 0.02 | 67.56 | 101.13 | 2.96 | 0.03 | 0.001 | 3.01 | 6 | 9183 | 150 | 500132 |
| MD29-1-2 | core | 32.42 | 1.65 | 0.11 | 67.25 | 101.43 | 2.96 | 0.04 | 0.003 | 2.99 | 6 | 13999 | 827 | 497844 |
| MD29-32-1 | core | 32.54 | 1.56 | 0.07 | 67.23 | 101.40 | 2.97 | 0.04 | 0.002 | 2.99 | 6 | 13185 | 551 | 497718 |
| MD29-32-2 | rim | 32.54 | 1.57 | 0.08 | 67.48 | 101.67 | 2.96 | 0.04 | 0.003 | 2.99 | 6 | 13329 | 614 | 499562 |
| MD29-23-2 | rim | 32.29 | 1.01 | 0.05 | 66.12 | 99.47 | 2.99 | 0.03 | 0.002 | 2.98 | 6 | 8589 | 378 | 489457 |
| MD29-23-3 | rim | 32.53 | 1.15 | 0.02 | 67.99 | 101.69 | 2.96 | 0.03 | 0.001 | 3.01 | 6 | 9776 | 150 | 503330 |
| MD29-31-1 | core | 32.21 | 1.33 | 0.13 | 67.82 | 101.49 | 2.94 | 0.03 | 0.004 | 3.02 | 6 | 11277 | 1047 | 502094 |
| MD29-31-2 | core | 32.06 | 1.15 | 0.28 | 67.36 | 100.85 | 2.94 | 0.03 | 0.009 | 3.02 | 6 | 9725 | 2205 | 498651 |
| MD29-31-3 | int | 32.24 | 1.27 | 0.05 | 67.29 | 100.85 | 2.96 | 0.03 | 0.002 | 3.01 | 6 | 10726 | 386 | 498155 |
| MD29-31-4 | rim | 32.32 | 1.37 | 0.06 | 67.67 | 101.42 | 2.95 | 0.04 | 0.002 | 3.01 | 6 | 11608 | 465 | 500954 |
| MD29-31-5 | rim | 32.24 | 1.72 | 0.01 | 67.35 | 101.32 | 2.95 | 0.04 | 0.000 | 3.00 | 6 | 14592 | 110 | 498562 |
| MD29-33-1 | rim | 32.58 | 1.54 | 0.04 | 67.50 | 101.65 | 2.96 | 0.04 | 0.001 | 2.99 | 6 | 13024 | 276 | 499680 |
| MD29-33-2 | core | 32.55 | 1.55 | 0.05 | 67.49 | 101.63 | 2.96 | 0.04 | 0.001 | 3.00 | 6 | 13100 | 362 | 499643 |
| MD29-33-4 | rim | 32.50 | 1.52 | 0.03 | 67.31 | 101.35 | 2.97 | 0.04 | 0.001 | 2.99 | 6 | 12854 | 213 | 498281 |

| | | IN wt % | | | | | Cation | | | | | In ppm | | |
|---|---|---|---|---|---|---|---|---|---|---|---|---|---|---|
| SL NO | | SiO2 | HfO2 | Y2O3 | ZrO2 | Total | Si | Hf | Y | Zr | SUM | Hf | Y | Zr |
| MD29-42-1 | core | 32.16 | 1.41 | 0.65 | 65.00 | 99.22 | 2.99 | 0.04 | 0.022 | 2.95 | 6 | 11913 | 5134 | 481195 |
| MD29-42-2 | int | 32.44 | 1.26 | 0.16 | 67.43 | 101.28 | 2.96 | 0.03 | 0.005 | 3.00 | 6 | 10658 | 1228 | 499206 |
| MD29-42-3 | rim | 32.38 | 1.34 | 0.04 | 67.73 | 101.49 | 2.95 | 0.03 | 0.001 | 3.01 | 6 | 11345 | 276 | 501427 |
| MD29-42-4 | rim | 32.50 | 1.39 | 0.03 | 67.74 | 101.66 | 2.96 | 0.04 | 0.001 | 3.01 | 6 | 11777 | 252 | 501442 |
| MD29-65-1 | rim | 32.49 | 1.58 | 0.01 | 67.60 | 101.68 | 2.96 | 0.04 | 0.000 | 3.00 | 6 | 13414 | 47 | 500421 |
| MD29-65-2 | core | 32.48 | 1.02 | 0.22 | 67.50 | 101.21 | 2.96 | 0.03 | 0.007 | 3.00 | 6 | 8640 | 1709 | 499673 |
| MD29-65-3 | core | 32.47 | 0.84 | 0.29 | 67.36 | 100.97 | 2.97 | 0.02 | 0.009 | 3.00 | 6 | 7156 | 2299 | 498651 |
| MD29-65-4 | core | 32.32 | 1.61 | 0.13 | 67.33 | 101.38 | 2.95 | 0.04 | 0.004 | 3.00 | 6 | 13609 | 1008 | 498422 |
| MD29-65-5 | rim | 32.10 | 2.71 | 0.12 | 65.30 | 100.23 | 2.97 | 0.07 | 0.004 | 2.95 | 6 | 22944 | 906 | 483446 |
| MD29-66-1 | core | 32.23 | 1.31 | 0.11 | 67.46 | 101.10 | 2.95 | 0.03 | 0.004 | 3.01 | 6 | 11099 | 890 | 499384 |
| MD29-66-2 | core | 32.44 | 1.35 | 0.29 | 67.39 | 101.48 | 2.96 | 0.04 | 0.009 | 3.00 | 6 | 11472 | 2291 | 498918 |
| MD29-66-3 | int | 32.43 | 1.64 | 0.05 | 67.31 | 101.43 | 2.96 | 0.04 | 0.002 | 3.00 | 6 | 13939 | 378 | 498303 |
| MD29-66-4 | rim | 32.36 | 1.38 | 0.11 | 67.10 | 100.95 | 2.96 | 0.04 | 0.004 | 3.00 | 6 | 11709 | 866 | 496734 |
| MD29-67-1 | core | 32.29 | 1.31 | 0.18 | 67.16 | 100.94 | 2.96 | 0.03 | 0.006 | 3.00 | 6 | 11124 | 1433 | 497148 |
| MD29-67-2 | core | 32.31 | 1.32 | 0.23 | 67.58 | 101.45 | 2.95 | 0.03 | 0.007 | 3.01 | 6 | 11201 | 1819 | 500324 |
| MD29-67-3 | int | 32.47 | 1.38 | 0.04 | 67.79 | 101.68 | 2.96 | 0.04 | 0.001 | 3.01 | 6 | 11676 | 331 | 501812 |
| MD29-70-1 | cent | 32.43 | 1.26 | 0.04 | 67.59 | 101.32 | 2.96 | 0.03 | 0.001 | 3.01 | 6 | 10684 | 346 | 500369 |
| MD29-70-2 | rim | 32.31 | 0.93 | 0.13 | 68.31 | 101.68 | 2.94 | 0.02 | 0.004 | 3.03 | 6 | 7919 | 1000 | 505662 |
| MD29-73-1 | rim | 32.14 | 1.09 | 0.00 | 67.96 | 101.19 | 2.94 | 0.03 | 0.000 | 3.03 | 6 | 9208 | 0 | 503086 |
| MD29-73-2 | int | 32.37 | 1.48 | 0.05 | 67.18 | 101.08 | 2.96 | 0.04 | 0.002 | 3.00 | 6 | 12507 | 417 | 497319 |
| MD29-73-3 | core | 32.20 | 1.15 | 0.26 | 66.32 | 99.93 | 2.97 | 0.03 | 0.008 | 2.99 | 6 | 9768 | 2016 | 490982 |
| MD29-86-1 | rim | 32.45 | 1.07 | 0.02 | 68.20 | 101.74 | 2.95 | 0.03 | 0.001 | 3.02 | 6 | 9073 | 126 | 504885 |
| MD29-86-2 | core | 32.08 | 1.26 | 0.33 | 67.71 | 101.37 | 2.93 | 0.03 | 0.011 | 3.02 | 6 | 10692 | 2559 | 501257 |
| MD29-86-3 | rim | 32.16 | 0.97 | 0.05 | 68.06 | 101.25 | 2.94 | 0.03 | 0.002 | 3.03 | 6 | 8216 | 394 | 503878 |
| MD29-90-1 | core | 31.96 | 1.45 | 0.33 | 66.75 | 100.48 | 2.95 | 0.04 | 0.011 | 3.00 | 6 | 12252 | 2591 | 494128 |
| MD29-90-2 | core | 32.20 | 0.96 | 0.24 | 67.57 | 100.98 | 2.95 | 0.03 | 0.008 | 3.02 | 6 | 8165 | 1921 | 500236 |
| MD29-90-3 | rim | 32.10 | 1.56 | 0.05 | 67.53 | 101.23 | 2.94 | 0.04 | 0.002 | 3.02 | 6 | 13202 | 402 | 499888 |
| MD29-90-4 | rim | 32.35 | 1.15 | 0.02 | 68.08 | 101.60 | 2.95 | 0.03 | 0.001 | 3.02 | 6 | 9717 | 134 | 504018 |
| MD29-91-1 | rim | 32.30 | 1.37 | 0.04 | 67.43 | 101.15 | 2.96 | 0.04 | 0.001 | 3.01 | 6 | 11650 | 315 | 499177 |
| MD29-91-2 | core | 32.41 | 1.05 | 0.25 | 68.09 | 101.80 | 2.95 | 0.03 | 0.008 | 3.02 | 6 | 8911 | 1976 | 504041 |
| MD29-91-3 | core | 32.39 | 1.01 | 0.13 | 68.53 | 102.06 | 2.94 | 0.03 | 0.004 | 3.03 | 6 | 8547 | 1047 | 507350 |
| MD29-91-4 | rim | 32.34 | 1.01 | 0.02 | 68.11 | 101.48 | 2.95 | 0.03 | 0.001 | 3.03 | 6 | 8589 | 150 | 504218 |
| MD29-91-5 | rim | 32.33 | 1.08 | 0.03 | 67.97 | 101.41 | 2.95 | 0.03 | 0.001 | 3.02 | 6 | 9183 | 244 | 503175 |
| MD29-91-6 | rim | 32.53 | 1.05 | 0.02 | 67.91 | 101.51 | 2.96 | 0.03 | 0.001 | 3.01 | 6 | 8886 | 150 | 502730 |
| MD29-94-1 | core | 32.00 | 1.04 | 0.49 | 66.43 | 99.95 | 2.96 | 0.03 | 0.016 | 3.00 | 6 | 8810 | 3874 | 491766 |
| MD29-94-2 | rim | 32.16 | 1.16 | 0.02 | 67.76 | 101.10 | 2.94 | 0.03 | 0.001 | 3.02 | 6 | 9861 | 157 | 501598 |
| MD29-97-1 | int | 32.21 | 1.01 | 0.07 | 68.70 | 101.99 | 2.93 | 0.03 | 0.002 | 3.04 | 6 | 8538 | 520 | 508608 |
| MD29-97-2 | int | 32.21 | 1.59 | 0.07 | 67.05 | 100.92 | 2.96 | 0.04 | 0.002 | 3.00 | 6 | 13482 | 520 | 496401 |
| MD29-97-3 | core | 32.23 | 1.30 | 0.25 | 67.54 | 101.32 | 2.95 | 0.03 | 0.008 | 3.01 | 6 | 11023 | 1937 | 499962 |
| MD29-97-4 | rim | 32.20 | 1.49 | 0.04 | 67.68 | 101.40 | 2.94 | 0.04 | 0.001 | 3.02 | 6 | 12608 | 283 | 501042 |
| MD29-97-5 | core | 32.20 | 1.16 | 0.18 | 67.60 | 101.14 | 2.95 | 0.03 | 0.006 | 3.02 | 6 | 9810 | 1409 | 500472 |

| | | IN wt % | | | | | Cation | | | | | In ppm | | |
|---|---|---|---|---|---|---|---|---|---|---|---|---|---|---|
| SL NO | | SiO2 | HfO2 | Y2O3 | ZrO2 | Total | Si | Hf | Y | Zr | SUM | Hf | Y | Zr |
| MD29-97-6 | rim | 32.10 | 1.49 | 0.02 | 67.87 | 101.48 | 2.93 | 0.04 | 0.001 | 3.03 | 6 | 12625 | 126 | 502449 |
| MD29-102-1 | rim | 32.32 | 1.37 | 0.03 | 67.96 | 101.68 | 2.94 | 0.04 | 0.001 | 3.02 | 6 | 11591 | 252 | 503108 |
| MD29-102-2 | int | 32.30 | 1.09 | 0.21 | 67.01 | 100.59 | 2.96 | 0.03 | 0.007 | 3.00 | 6 | 9208 | 1614 | 496053 |
| MD29-102-3 | core | 32.20 | 1.16 | 0.25 | 66.94 | 100.54 | 2.96 | 0.03 | 0.008 | 3.00 | 6 | 9819 | 1953 | 495535 |
| MD29-102-4 | core | 31.94 | 1.24 | 0.44 | 66.93 | 100.56 | 2.94 | 0.03 | 0.014 | 3.01 | 6 | 10514 | 3488 | 495505 |
| MD29-102-5 | int | 32.13 | 1.39 | 0.24 | 67.06 | 100.83 | 2.95 | 0.04 | 0.008 | 3.00 | 6 | 11786 | 1913 | 496460 |
| MD29-104-1 | core | 32.69 | 1.53 | 0.48 | 63.94 | 98.65 | 3.04 | 0.04 | 0.016 | 2.90 | 6 | 12973 | 3787 | 473363 |
| MD29-104-2 | core | 32.16 | 1.20 | 0.20 | 66.94 | 100.50 | 2.96 | 0.03 | 0.006 | 3.00 | 6 | 10166 | 1567 | 495542 |
| MD29-104-3 | core | 32.09 | 1.20 | 0.50 | 66.07 | 99.85 | 2.97 | 0.03 | 0.016 | 2.98 | 6 | 10149 | 3945 | 489101 |
| MD29-104-4 | rim | 32.02 | 1.79 | 0.08 | 66.33 | 100.23 | 2.96 | 0.05 | 0.003 | 2.99 | 6 | 15186 | 661 | 491056 |
| MD29-104-5 | rim | 32.30 | 1.31 | 0.04 | 68.03 | 101.68 | 2.94 | 0.03 | 0.001 | 3.02 | 6 | 11065 | 299 | 503648 |
| MD29-107-2 | int | 31.91 | 1.34 | 0.13 | 66.95 | 100.32 | 2.95 | 0.04 | 0.004 | 3.01 | 6 | 11370 | 992 | 495631 |
| MD29-107-3 | core | 32.04 | 1.17 | 0.18 | 67.16 | 100.54 | 2.95 | 0.03 | 0.006 | 3.01 | 6 | 9895 | 1378 | 497171 |
| MD29-107-4 | int | 32.11 | 1.32 | 0.11 | 67.89 | 101.43 | 2.94 | 0.03 | 0.004 | 3.03 | 6 | 11175 | 866 | 502582 |
| MD29-107-5 | int | 32.10 | 1.33 | 0.08 | 67.98 | 101.49 | 2.93 | 0.03 | 0.003 | 3.03 | 6 | 11269 | 638 | 503278 |
| MD29-107-6 | rim | 32.00 | 1.30 | 0.13 | 67.23 | 100.66 | 2.94 | 0.03 | 0.004 | 3.02 | 6 | 11031 | 1039 | 497681 |
| MD33-2-1 | core | 32.96 | 1.27 | 0.22 | 65.82 | 100.26 | 3.02 | 0.03 | 0.011 | 2.94 | 6 | 10743 | 1701 | 487243 |
| MD33-2-2 | rim | 32.98 | 1.70 | 0.00 | 65.33 | 100.01 | 3.03 | 0.04 | 0.000 | 2.93 | 6 | 14397 | 31 | 483668 |
| MD33-22-1 | core | 33.01 | 1.19 | 0.33 | 65.31 | 99.83 | 3.03 | 0.03 | 0.016 | 2.93 | 6 | 10107 | 2559 | 483497 |
| MD33-22-2 | core | 32.78 | 1.37 | 0.18 | 65.48 | 99.82 | 3.02 | 0.04 | 0.009 | 2.94 | 6 | 11591 | 1449 | 484778 |
| MD33-22-3 | int | 32.92 | 1.37 | 0.15 | 65.57 | 99.99 | 3.02 | 0.04 | 0.007 | 2.94 | 6 | 11574 | 1150 | 485393 |
| MD33-22-4 | int | 32.99 | 1.37 | 0.08 | 65.45 | 99.88 | 3.03 | 0.04 | 0.004 | 2.93 | 6 | 11582 | 591 | 484526 |
| MD33-22-5 | rim | 33.17 | 1.51 | 0.11 | 65.17 | 99.96 | 3.04 | 0.04 | 0.005 | 2.91 | 6 | 12829 | 843 | 482439 |
| MD33-22-6 | core | 33.00 | 1.31 | 0.11 | 65.74 | 100.16 | 3.02 | 0.03 | 0.006 | 2.94 | 6 | 11107 | 890 | 486644 |
| MD33-22-7 | rim | 32.94 | 1.43 | 0.12 | 65.01 | 99.50 | 3.04 | 0.04 | 0.006 | 2.92 | 6 | 12142 | 937 | 481291 |
| MD33-25-1 | core | 32.49 | 1.32 | 0.12 | 65.58 | 99.52 | 3.00 | 0.03 | 0.006 | 2.96 | 6 | 11218 | 961 | 485511 |
| MD33-25-2 | rim | 32.73 | 1.64 | 0.00 | 65.63 | 100.00 | 3.01 | 0.04 | 0.000 | 2.94 | 6 | 13880 | 0 | 485859 |
| MD33-25-3 | int | 32.43 | 1.28 | 0.67 | 64.24 | 98.62 | 3.02 | 0.03 | 0.033 | 2.92 | 6 | 10836 | 5283 | 475539 |
| MD33-27-1 | core | 32.90 | 1.10 | 0.15 | 66.51 | 100.66 | 3.00 | 0.03 | 0.007 | 2.96 | 6 | 9352 | 1142 | 492388 |
| MD33-27-2 | core | 32.98 | 1.19 | 0.11 | 66.18 | 100.46 | 3.01 | 0.03 | 0.005 | 2.95 | 6 | 10124 | 835 | 489953 |
| MD33-27-3 | int | 32.80 | 1.51 | 0.00 | 66.08 | 100.40 | 3.01 | 0.04 | 0.000 | 2.95 | 6 | 12837 | 0 | 489212 |
| MD33-27-4 | int | 32.79 | 1.41 | 0.08 | 65.77 | 100.05 | 3.01 | 0.04 | 0.004 | 2.95 | 6 | 11930 | 638 | 486910 |

| | | IN wt % | | | | | Cation | | | | | In ppm | | |
|---|---|---|---|---|---|---|---|---|---|---|---|---|---|---|
| SL NO | | SiO2 | HfO2 | Y2O3 | ZrO2 | Total | Si | Hf | Y | Zr | SUM | Hf | Y | Zr |
| MD33-27-5 | rim | 33.65 | 1.47 | 0.01 | 64.67 | 99.80 | 3.08 | 0.04 | 0.000 | 2.88 | 6 | 12481 | 39 | 478767 |
| MD33-28-1 | core | 32.84 | 1.32 | 0.24 | 65.70 | 100.10 | 3.02 | 0.03 | 0.012 | 2.94 | 6 | 11150 | 1913 | 486362 |
| MD33-28-2 | core | 32.80 | 1.39 | 0.23 | 65.67 | 100.09 | 3.01 | 0.04 | 0.011 | 2.94 | 6 | 11769 | 1803 | 486133 |
| MD33-28-3 | int | 32.73 | 1.48 | 0.08 | 65.39 | 99.68 | 3.02 | 0.04 | 0.004 | 2.94 | 6 | 12583 | 614 | 484060 |
| MD33-28-4 | rim | 32.82 | 1.38 | 0.09 | 65.50 | 99.78 | 3.02 | 0.04 | 0.004 | 2.94 | 6 | 11667 | 717 | 484882 |
| MD33-29-1 | core | 32.85 | 1.40 | 0.09 | 65.66 | 100.00 | 3.02 | 0.04 | 0.004 | 2.94 | 6 | 11879 | 724 | 486088 |
| MD33-29-2 c | core | 32.73 | 1.18 | 0.29 | 65.04 | 99.23 | 3.03 | 0.03 | 0.014 | 2.93 | 6 | 9988 | 2260 | 481513 |
| MD33-29-3 r | rim | 32.57 | 1.77 | 0.00 | 64.72 | 99.06 | 3.02 | 0.05 | 0.000 | 2.93 | 6 | 14974 | 0 | 479152 |
| MD33-29-5 | int | 32.75 | 1.44 | 0.04 | 65.30 | 99.53 | 3.02 | 0.04 | 0.002 | 2.94 | 6 | 12201 | 331 | 483379 |
| MD33-29-6 | rim | 32.63 | 1.68 | 0.00 | 65.98 | 100.29 | 3.00 | 0.04 | 0.000 | 2.96 | 6 | 14279 | 0 | 488472 |
| MD33-43-1 | core | 32.72 | 1.51 | 0.36 | 65.35 | 99.94 | 3.01 | 0.04 | 0.017 | 2.93 | 6 | 12837 | 2795 | 483793 |
| MD33-43-2 | int | 32.68 | 1.92 | 0.09 | 65.36 | 100.06 | 3.01 | 0.05 | 0.005 | 2.94 | 6 | 16280 | 732 | 483890 |
| MD33-43-3 | int | 32.54 | 2.36 | 0.16 | 64.90 | 99.96 | 3.01 | 0.06 | 0.008 | 2.92 | 6 | 20027 | 1252 | 480477 |
| MD33-43-4 | rim | 32.91 | 1.60 | 0.05 | 65.13 | 99.68 | 3.03 | 0.04 | 0.002 | 2.93 | 6 | 13549 | 362 | 482180 |
| MD33-43-5 | core | 32.85 | 1.25 | 0.09 | 66.05 | 100.24 | 3.01 | 0.03 | 0.004 | 2.95 | 6 | 10565 | 724 | 488983 |
| MD33-43-6 | int | 32.95 | 1.43 | 0.00 | 65.73 | 100.11 | 3.02 | 0.04 | 0.000 | 2.94 | 6 | 12116 | 0 | 486562 |
| MD33-43-7 | int | 32.73 | 1.36 | 0.05 | 66.12 | 100.26 | 3.00 | 0.04 | 0.002 | 2.96 | 6 | 11514 | 362 | 489494 |
| MD33-43-8 | int | 32.75 | 1.16 | 0.11 | 65.98 | 100.00 | 3.01 | 0.03 | 0.005 | 2.96 | 6 | 9836 | 882 | 488413 |
| MD33-46-1 | core | 32.84 | 1.57 | 0.34 | 65.31 | 100.07 | 3.02 | 0.04 | 0.017 | 2.93 | 6 | 13329 | 2685 | 483520 |
| MD33-46-2 | core | 32.66 | 1.56 | 0.14 | 65.27 | 99.62 | 3.02 | 0.04 | 0.007 | 2.94 | 6 | 13219 | 1102 | 483194 |
| MD33-46-3 | rim | 33.07 | 1.53 | 0.00 | 65.44 | 100.04 | 3.03 | 0.04 | 0.000 | 2.93 | 6 | 12930 | 0 | 484460 |
| MD33-46-4 | core | 32.79 | 1.49 | 0.19 | 65.19 | 99.66 | 3.02 | 0.04 | 0.009 | 2.93 | 6 | 12591 | 1480 | 482616 |
| MD33-46-5 | rim | 32.89 | 1.61 | 0.00 | 65.68 | 100.18 | 3.02 | 0.04 | 0.000 | 2.94 | 6 | 13660 | 0 | 486236 |
| MD33-62-1 | core | 32.89 | 1.40 | 0.19 | 65.54 | 100.02 | 3.02 | 0.04 | 0.009 | 2.93 | 6 | 11905 | 1520 | 485156 |
| MD33-62-2 | core | 32.99 | 1.20 | 0.21 | 65.96 | 100.35 | 3.02 | 0.03 | 0.010 | 2.94 | 6 | 10141 | 1638 | 488294 |
| MD33-62-3 | core | 32.73 | 1.42 | 0.16 | 65.40 | 99.71 | 3.02 | 0.04 | 0.008 | 2.94 | 6 | 12066 | 1244 | 484127 |
| MD33-62-4 | int | 32.84 | 1.35 | 0.12 | 65.63 | 99.95 | 3.02 | 0.04 | 0.006 | 2.94 | 6 | 11464 | 953 | 485889 |
| MD33-62-5 | rim | 32.94 | 1.53 | 0.00 | 65.45 | 99.92 | 3.03 | 0.04 | 0.000 | 2.93 | 6 | 12973 | 0 | 484526 |
| MD33-58-1 | rim | 33.14 | 1.41 | 0.06 | 65.65 | 100.26 | 3.03 | 0.04 | 0.003 | 2.93 | 6 | 11921 | 441 | 486014 |
| MD33-58-2 | core | 33.11 | 1.81 | 0.11 | 65.20 | 100.22 | 3.04 | 0.05 | 0.005 | 2.91 | 6 | 15305 | 827 | 482646 |
| MD33-58-3 | core | 32.83 | 1.82 | 0.38 | 64.79 | 99.81 | 3.03 | 0.05 | 0.019 | 2.91 | 6 | 15389 | 3008 | 479626 |
| MD33-58-4 | int | 32.81 | 1.75 | 0.18 | 65.38 | 100.12 | 3.02 | 0.05 | 0.009 | 2.93 | 6 | 14864 | 1417 | 483986 |
| MD33-58-5 | rim | 33.00 | 1.57 | 0.11 | 65.98 | 100.66 | 3.02 | 0.04 | 0.005 | 2.94 | 6 | 13321 | 843 | 488428 |
| MD33-58-6 | core | 33.10 | 1.81 | 0.32 | 64.54 | 99.76 | 3.05 | 0.05 | 0.016 | 2.90 | 6 | 15339 | 2496 | 477760 |
| MD33-58-7 | int | 33.10 | 1.48 | 0.12 | 65.20 | 99.90 | 3.04 | 0.04 | 0.006 | 2.92 | 6 | 12540 | 953 | 482676 |
| MD33-77-1 | core | 32.81 | 1.26 | 0.07 | 66.21 | 100.35 | 3.01 | 0.03 | 0.003 | 2.96 | 6 | 10675 | 512 | 490182 |
| MD33-77-2 | core | 32.94 | 1.23 | 0.06 | 66.14 | 100.38 | 3.01 | 0.03 | 0.003 | 2.95 | 6 | 10463 | 504 | 489627 |
| MD33-77-3 | core | 32.74 | 1.58 | 0.23 | 65.70 | 100.26 | 3.01 | 0.04 | 0.011 | 2.94 | 6 | 13405 | 1819 | 486399 |
| MD33-77-4 | int | 32.95 | 1.53 | 0.07 | 65.95 | 100.50 | 3.02 | 0.04 | 0.003 | 2.94 | 6 | 12947 | 512 | 488250 |
| MD33-77-5 | rim | 32.96 | 1.34 | 0.02 | 66.07 | 100.39 | 3.02 | 0.04 | 0.001 | 2.95 | 6 | 11396 | 142 | 489116 |
| MD33-128-1 | core | 32.95 | 1.22 | 0.08 | 66.08 | 100.33 | 3.02 | 0.03 | 0.004 | 2.95 | 6 | 10327 | 646 | 489168 |
| MD33-128-4 | int | 33.14 | 1.59 | 0.11 | 65.96 | 100.80 | 3.02 | 0.04 | 0.005 | 2.93 | 6 | 13516 | 866 | 488302 |
| MD33-134-1 | core | 33.04 | 1.09 | 0.14 | 66.27 | 100.54 | 3.02 | 0.03 | 0.007 | 2.95 | 6 | 9276 | 1102 | 490560 |
| MD33-134-3 | core | 33.04 | 1.08 | 0.04 | 65.83 | 99.99 | 3.03 | 0.03 | 0.002 | 2.94 | 6 | 9149 | 346 | 487317 |
| MD33-134-4 | int | 33.04 | 1.23 | 0.08 | 65.71 | 100.06 | 3.03 | 0.03 | 0.004 | 2.94 | 6 | 10455 | 591 | 486436 |
| MD33-134-5 | int | 32.93 | 2.37 | 0.10 | 65.01 | 100.41 | 3.02 | 0.06 | 0.005 | 2.91 | 6 | 20112 | 772 | 481262 |

| | | IN wt % | | | | | Cation | | | | | In ppm | | |
|---|---|---|---|---|---|---|---|---|---|---|---|---|---|---|
| SL NO | | SiO2 | HfO2 | Y2O3 | ZrO2 | Total | Si | Hf | Y | Zr | SUM | Hf | Y | Zr |
| MD33-134-6 | int | 32.93 | 2.17 | 0.09 | 65.83 | 101.02 | 3.01 | 0.06 | 0.004 | 2.93 | 6 | 18399 | 709 | 487325 |
| MD33-134-7 | rim | 32.97 | 1.76 | 0.18 | 65.89 | 100.80 | 3.01 | 0.05 | 0.009 | 2.94 | 6 | 14923 | 1441 | 487754 |
| MD33-134-8 | rim | 33.06 | 1.73 | 0.02 | 65.25 | 100.06 | 3.03 | 0.05 | 0.001 | 2.92 | 6 | 14677 | 118 | 483016 |
| MD33-142-1 | rim | 32.98 | 1.25 | 0.11 | 65.50 | 99.84 | 3.03 | 0.03 | 0.005 | 2.93 | 6 | 10582 | 858 | 484889 |
| MD33-142-2 | int | 32.92 | 1.33 | 0.10 | 65.71 | 100.06 | 3.02 | 0.03 | 0.005 | 2.94 | 6 | 11277 | 787 | 486466 |
| MD33-142-3 | core | 32.86 | 1.24 | 0.19 | 66.00 | 100.29 | 3.01 | 0.03 | 0.009 | 2.95 | 6 | 10531 | 1488 | 488613 |
| MD33-142-4 | core | 32.73 | 1.16 | 0.45 | 65.78 | 100.12 | 3.01 | 0.03 | 0.022 | 2.95 | 6 | 9802 | 3575 | 486992 |
| MD33-142-5 | rim | 33.07 | 1.41 | 0.11 | 65.80 | 100.39 | 3.02 | 0.04 | 0.005 | 2.93 | 6 | 11981 | 835 | 487110 |
| MD33-148-1 | rim | 32.91 | 1.36 | 0.07 | 65.94 | 100.27 | 3.02 | 0.04 | 0.003 | 2.95 | 6 | 11557 | 512 | 488124 |
| MD33-148-2 | int | 32.94 | 1.35 | 0.04 | 66.68 | 101.00 | 3.00 | 0.03 | 0.002 | 2.96 | 6 | 11404 | 276 | 493625 |
| MD33-148-3 | core | 32.91 | 1.49 | 0.01 | 65.97 | 100.38 | 3.01 | 0.04 | 0.000 | 2.95 | 6 | 12651 | 79 | 488369 |
| MD33-148-4 | int | 33.02 | 1.38 | 0.02 | 65.63 | 100.05 | 3.03 | 0.04 | 0.001 | 2.93 | 6 | 11735 | 126 | 485844 |
| MD33-148-5 | rim | 33.14 | 1.20 | 0.09 | 65.85 | 100.27 | 3.03 | 0.03 | 0.004 | 2.94 | 6 | 10141 | 701 | 487502 |
| MD33-160-1 | core | 32.69 | 1.37 | 0.47 | 64.79 | 99.32 | 3.02 | 0.04 | 0.023 | 2.92 | 6 | 11633 | 3669 | 479618 |
| MD33-160-2 | core | 32.91 | 1.13 | 0.23 | 65.65 | 99.92 | 3.02 | 0.03 | 0.011 | 2.94 | 6 | 9590 | 1787 | 486022 |
| MD33-160-3 | core | 32.83 | 1.55 | 0.07 | 65.99 | 100.44 | 3.01 | 0.04 | 0.003 | 2.95 | 6 | 13134 | 551 | 488502 |
| MD33-160-4 | int | 32.98 | 1.59 | 0.03 | 65.92 | 100.51 | 3.02 | 0.04 | 0.001 | 2.94 | 6 | 13456 | 220 | 487998 |
| MD33-160-5 | rim | 32.95 | 1.71 | 0.00 | 65.82 | 100.47 | 3.02 | 0.04 | 0.000 | 2.94 | 6 | 14499 | 0 | 487251 |
| MD14-7-1 | core | 33.08 | 1.01 | 0.13 | 65.85 | 100.06 | 3.03 | 0.03 | 0.006 | 2.94 | 6 | 8521 | 1016 | 487465 |
| MD14-7-2 | rim | 33.15 | 1.02 | 0.00 | 66.16 | 100.34 | 3.03 | 0.03 | 0.000 | 2.95 | 6 | 8682 | 0 | 489775 |
| MD14-13-1 | core | 33.20 | 0.96 | 0.13 | 66.21 | 100.50 | 3.03 | 0.03 | 0.006 | 2.94 | 6 | 8165 | 1047 | 490138 |
| MD14-13-2 | int | 33.16 | 0.98 | 0.04 | 66.43 | 100.60 | 3.02 | 0.03 | 0.002 | 2.95 | 6 | 8292 | 291 | 491752 |
| MD14-13-3 | rim | 33.16 | 0.96 | 0.02 | 66.22 | 100.37 | 3.03 | 0.03 | 0.001 | 2.95 | 6 | 8174 | 181 | 490227 |
| MD14-18-1 | core | 32.89 | 0.91 | 0.40 | 65.70 | 99.90 | 3.02 | 0.02 | 0.019 | 2.94 | 6 | 7673 | 3142 | 486399 |
| MD14-18-2 | int | 33.07 | 0.99 | 0.12 | 65.59 | 99.78 | 3.03 | 0.03 | 0.006 | 2.93 | 6 | 8428 | 969 | 485563 |
| MD14-18-3 | int | 33.01 | 1.12 | 0.01 | 66.21 | 100.35 | 3.02 | 0.03 | 0.001 | 2.95 | 6 | 9496 | 110 | 490145 |
| MD14-18-4 | rim | 33.10 | 1.10 | 0.00 | 66.21 | 100.42 | 3.02 | 0.03 | 0.000 | 2.95 | 6 | 9352 | 0 | 490145 |
| MD14-18-5 | core | 32.94 | 1.02 | 0.18 | 65.91 | 100.04 | 3.02 | 0.03 | 0.009 | 2.95 | 6 | 8606 | 1394 | 487910 |
| MD14-18-6 | rim | 33.14 | 1.11 | 0.03 | 65.89 | 100.17 | 3.03 | 0.03 | 0.002 | 2.94 | 6 | 9429 | 244 | 487754 |
| MD14-24-1 | rim | 32.99 | 1.13 | 0.01 | 66.19 | 100.32 | 3.02 | 0.03 | 0.000 | 2.95 | 6 | 9615 | 63 | 489990 |
| MD14-24-2 | int | 32.80 | 0.91 | 0.33 | 65.48 | 99.52 | 3.02 | 0.02 | 0.016 | 2.94 | 6 | 7690 | 2614 | 484719 |
| MD14-24-3 | core | 32.95 | 1.10 | 0.02 | 66.14 | 100.21 | 3.02 | 0.03 | 0.001 | 2.95 | 6 | 9352 | 165 | 489627 |
| MD14-24-4 | rim | 32.96 | 1.05 | 0.14 | 66.45 | 100.60 | 3.01 | 0.03 | 0.007 | 2.96 | 6 | 8878 | 1094 | 491937 |
| MD14-33-1 | rim | 32.88 | 0.98 | 0.10 | 65.93 | 99.88 | 3.02 | 0.03 | 0.005 | 2.95 | 6 | 8284 | 795 | 488058 |
| MD14-33-3 | core | 32.80 | 0.97 | 0.10 | 65.92 | 99.79 | 3.02 | 0.03 | 0.005 | 2.96 | 6 | 8182 | 819 | 487984 |
| MD14-33-4 c | int | 32.81 | 0.95 | 0.41 | 65.43 | 99.59 | 3.02 | 0.02 | 0.020 | 2.94 | 6 | 8013 | 3189 | 484408 |
| MD14-33-5 r | rim | 32.93 | 1.04 | 0.03 | 65.93 | 99.92 | 3.02 | 0.03 | 0.001 | 2.95 | 6 | 8827 | 220 | 488043 |
| MD14-43-1 | core | 32.83 | 1.06 | 0.64 | 64.74 | 99.27 | 3.03 | 0.03 | 0.031 | 2.92 | 6 | 8979 | 5024 | 479285 |
| MD14-43-2 | core | 32.87 | 1.07 | 0.39 | 65.46 | 99.78 | 3.02 | 0.03 | 0.019 | 2.94 | 6 | 9047 | 3063 | 484600 |
| MD14-43-3 | int | 32.87 | 1.44 | 0.14 | 65.76 | 100.22 | 3.02 | 0.04 | 0.007 | 2.94 | 6 | 12235 | 1134 | 486806 |
| MD14-43-4 | rim | 32.96 | 1.12 | 0.00 | 65.67 | 99.75 | 3.03 | 0.03 | 0.000 | 2.94 | 6 | 9513 | 24 | 486162 |
| MD14-48-1 | rim | 33.08 | 1.17 | 0.03 | 66.04 | 100.31 | 3.02 | 0.03 | 0.001 | 2.94 | 6 | 9887 | 197 | 488857 |
| MD14-48-2 | core | 32.61 | 1.01 | 0.55 | 64.80 | 98.97 | 3.02 | 0.03 | 0.027 | 2.93 | 6 | 8555 | 4307 | 479737 |
| MD14-48-3 | rim | 33.11 | 1.19 | 0.02 | 66.18 | 100.49 | 3.02 | 0.03 | 0.001 | 2.95 | 6 | 10048 | 126 | 489945 |
| MD14-48-4 | int | 32.92 | 0.99 | 0.21 | 65.74 | 99.86 | 3.02 | 0.03 | 0.010 | 2.94 | 6 | 8360 | 1677 | 486688 |
| MD14-48-5 | rim | 33.23 | 1.16 | 0.00 | 66.16 | 100.55 | 3.03 | 0.03 | 0.000 | 2.94 | 6 | 9836 | 0 | 489768 |
| MD14-70-1 c | core | 32.71 | 0.99 | 0.87 | 64.66 | 99.22 | 3.03 | 0.03 | 0.043 | 2.92 | 6 | 8386 | 6811 | 478663 |
| MD14-70-2 r | rim | 32.93 | 0.96 | 0.08 | 66.51 | 100.48 | 3.01 | 0.03 | 0.004 | 2.96 | 6 | 8165 | 646 | 492366 |
| MD14-70-3 | rim | 32.92 | 1.05 | 0.07 | 66.18 | 100.21 | 3.01 | 0.03 | 0.003 | 2.96 | 6 | 8869 | 528 | 489945 |
| MD14-79-1 | core | 32.73 | 0.92 | 0.77 | 64.53 | 98.95 | 3.03 | 0.02 | 0.038 | 2.92 | 6 | 7818 | 6039 | 477738 |

| | | IN wt % | | | | | Cation | | | | | In ppm | | |
|---|---|---|---|---|---|---|---|---|---|---|---|---|---|---|
| SL NO | | SiO2 | HfO2 | Y2O3 | ZrO2 | Total | Si | Hf | Y | Zr | SUM | Hf | Y | Zr |
| MD14-79-2 | int | 33.08 | 1.08 | 0.07 | 66.05 | 100.28 | 3.02 | 0.03 | 0.004 | 2.94 | 6 | 9132 | 567 | 488983 |
| MD14-79-3 | rim | 32.94 | 1.08 | 0.04 | 66.05 | 100.10 | 3.02 | 0.03 | 0.002 | 2.95 | 6 | 9140 | 283 | 488939 |
| MD14-86-1 | core | 32.96 | 1.18 | 0.07 | 65.56 | 99.76 | 3.03 | 0.03 | 0.003 | 2.94 | 6 | 9971 | 528 | 485363 |
| MD14-86-2 | core | 32.90 | 0.97 | 0.01 | 66.08 | 99.96 | 3.02 | 0.03 | 0.000 | 2.96 | 6 | 8199 | 63 | 489175 |
| MD14-86-3 | int | 32.75 | 1.01 | 0.09 | 65.53 | 99.37 | 3.02 | 0.03 | 0.004 | 2.95 | 6 | 8521 | 677 | 485119 |
| MD14-86-4 | rim | 32.92 | 1.07 | 0.00 | 65.79 | 99.78 | 3.02 | 0.03 | 0.000 | 2.95 | 6 | 9073 | 0 | 487066 |
| MD14-128-1 | rim | 32.91 | 1.10 | 0.05 | 66.63 | 100.68 | 3.00 | 0.03 | 0.002 | 2.97 | 6 | 9352 | 370 | 493225 |
| MD14-128-2 | core | 32.55 | 0.92 | 0.69 | 64.94 | 99.11 | 3.02 | 0.02 | 0.034 | 2.93 | 6 | 7801 | 5441 | 480766 |
| MD14-128-3 | rim | 32.95 | 1.13 | 0.03 | 65.91 | 100.02 | 3.02 | 0.03 | 0.002 | 2.95 | 6 | 9556 | 244 | 487895 |
| MD14-128-4 | rim | 32.87 | 1.03 | 0.08 | 66.06 | 100.04 | 3.02 | 0.03 | 0.004 | 2.95 | 6 | 8759 | 591 | 489050 |
| MD14-130-1 | rim | 32.93 | 1.10 | 0.04 | 65.69 | 99.75 | 3.03 | 0.03 | 0.002 | 2.94 | 6 | 9285 | 299 | 486296 |
| MD14-130-2 | core | 32.95 | 0.93 | 0.06 | 65.99 | 99.93 | 3.02 | 0.02 | 0.003 | 2.95 | 6 | 7869 | 488 | 488524 |
| MD-38-23-1 | rim | 32.47 | 1.13 | 0.01 | 65.06 | 98.66 | 3.02 | 0.03 | 0.000 | 2.95 | 6 | 9547 | 79 | 481632 |
| MD-38-27-3 | core | 32.57 | 1.23 | 0.14 | 65.16 | 99.10 | 3.02 | 0.03 | 0.007 | 2.94 | 6 | 10429 | 1118 | 482365 |
| MD-38-27-5 | rim | 32.60 | 1.36 | 0.12 | 65.24 | 99.32 | 3.02 | 0.04 | 0.006 | 2.94 | 6 | 11506 | 906 | 483001 |
| MD-38-27-6 | rim | 32.61 | 1.50 | 0.12 | 65.07 | 99.29 | 3.02 | 0.04 | 0.006 | 2.94 | 6 | 12727 | 937 | 481698 |
| MD-38-32-2 | rim | 32.65 | 1.24 | 0.02 | 65.98 | 99.90 | 3.01 | 0.03 | 0.001 | 2.96 | 6 | 10539 | 173 | 488480 |
| MD-38-32-3 | rim | 32.73 | 1.10 | 0.00 | 65.57 | 99.39 | 3.02 | 0.03 | 0.000 | 2.95 | 6 | 9285 | 0 | 485378 |
| MD-38-47-1 | rim | 32.58 | 1.48 | 0.04 | 64.41 | 98.51 | 3.03 | 0.04 | 0.002 | 2.92 | 6 | 12549 | 339 | 476798 |
| MD-38-47-2 | int | 32.68 | 1.11 | 0.00 | 65.01 | 98.80 | 3.03 | 0.03 | 0.000 | 2.94 | 6 | 9395 | 0 | 481291 |
| MD-38-48-1 | rim | 32.65 | 1.07 | 0.10 | 66.02 | 99.84 | 3.01 | 0.03 | 0.005 | 2.96 | 6 | 9089 | 787 | 488716 |
| MD-38-48-2 | core | 32.73 | 1.08 | 0.03 | 65.79 | 99.63 | 3.02 | 0.03 | 0.001 | 2.96 | 6 | 9149 | 197 | 487058 |
| MD-38-48-3 | rim | 32.85 | 1.06 | 0.07 | 64.90 | 98.89 | 3.04 | 0.03 | 0.004 | 2.93 | 6 | 9022 | 567 | 480455 |
| MD-38-116-1 | rim | 31.43 | 1.09 | 0.06 | 62.84 | 95.42 | 3.02 | 0.03 | 0.003 | 2.95 | 6 | 9251 | 433 | 465234 |
| MD-38-116-2 | int | 32.65 | 1.01 | 0.00 | 65.40 | 99.06 | 3.02 | 0.03 | 0.000 | 2.95 | 6 | 8564 | 0 | 484134 |
| MD-38-116-3 | int | 32.56 | 1.05 | 0.06 | 65.58 | 99.25 | 3.01 | 0.03 | 0.003 | 2.96 | 6 | 8878 | 433 | 485518 |
| MD-38-116-4 | core | 32.63 | 1.05 | 0.03 | 65.93 | 99.64 | 3.01 | 0.03 | 0.001 | 2.96 | 6 | 8886 | 228 | 488102 |
| MD-38-127-1 | rim | 32.72 | 1.19 | 0.03 | 65.62 | 99.56 | 3.02 | 0.03 | 0.001 | 2.95 | 6 | 10124 | 197 | 485777 |
| MD-38-129-1 | rim | 32.61 | 1.16 | 0.03 | 64.92 | 98.72 | 3.03 | 0.03 | 0.001 | 2.94 | 6 | 9827 | 213 | 480618 |
| MD-38-129-3 | int | 32.50 | 1.38 | 0.12 | 65.15 | 99.15 | 3.01 | 0.04 | 0.006 | 2.95 | 6 | 11718 | 906 | 482335 |
| MD-38-129-4 | core | 32.53 | 1.28 | 0.07 | 65.12 | 99.00 | 3.02 | 0.03 | 0.003 | 2.95 | 6 | 10870 | 543 | 482076 |
| MD-38-129-5 | int | 32.45 | 1.29 | 0.18 | 64.68 | 98.60 | 3.02 | 0.03 | 0.009 | 2.94 | 6 | 10946 | 1394 | 478811 |
| MD-38-129-6 | rim | 32.63 | 1.10 | 0.01 | 65.66 | 99.40 | 3.01 | 0.03 | 0.000 | 2.96 | 6 | 9361 | 39 | 486096 |
| MD-38-129-7 | rim | 32.64 | 1.32 | 0.10 | 65.11 | 99.17 | 3.02 | 0.03 | 0.005 | 2.94 | 6 | 11218 | 764 | 481995 |
| MD-38-132-1 | rim | 32.54 | 1.08 | 0.11 | 65.44 | 99.17 | 3.01 | 0.03 | 0.005 | 2.95 | 6 | 9166 | 843 | 484445 |
| MD-38-132-2 | int | 32.47 | 1.08 | 0.06 | 65.33 | 98.93 | 3.01 | 0.03 | 0.003 | 2.96 | 6 | 9174 | 472 | 483601 |
| MD-38-132-3 | core | 32.51 | 1.11 | 0.07 | 65.36 | 99.05 | 3.01 | 0.03 | 0.004 | 2.95 | 6 | 9378 | 583 | 483845 |
| MD-38-132-4 | rim | 32.44 | 1.14 | 0.09 | 65.28 | 98.95 | 3.01 | 0.03 | 0.005 | 2.95 | 6 | 9675 | 732 | 483260 |

| | | IN wt % | | | | | Cation | | | | | In ppm | | |
|---|---|---|---|---|---|---|---|---|---|---|---|---|---|---|
| SL NO | | SiO2 | HfO2 | Y2O3 | ZrO2 | Total | Si | Hf | Y | Zr | SUM | Hf | Y | Zr |
| MD-38-132-5 | core | 32.44 | 1.09 | 0.05 | 64.93 | 98.51 | 3.02 | 0.03 | 0.002 | 2.95 | 6 | 9208 | 386 | 480655 |
| MD-38-147-1 | rim | 32.33 | 1.05 | 0.00 | 65.30 | 98.69 | 3.01 | 0.03 | 0.000 | 2.96 | 6 | 8928 | 0 | 483446 |
| MD-38-147-2 | rim | 32.48 | 1.06 | 0.13 | 65.52 | 99.19 | 3.01 | 0.03 | 0.006 | 2.96 | 6 | 9013 | 992 | 485015 |
| MD-38-147-4 | - | 32.42 | 1.08 | 0.03 | 65.55 | 99.08 | 3.01 | 0.03 | 0.001 | 2.96 | 6 | 9174 | 220 | 485274 |
| MD-38-156-1 | rim | 32.53 | 1.33 | 0.01 | 65.25 | 99.12 | 3.02 | 0.04 | 0.001 | 2.95 | 6 | 11269 | 102 | 483068 |
| MD-38-156-2 | core | 32.51 | 0.93 | 0.26 | 64.99 | 98.69 | 3.02 | 0.02 | 0.013 | 2.94 | 6 | 7885 | 2016 | 481136 |
| MD-38-156-3 | int | 32.41 | 0.97 | 0.05 | 65.49 | 98.92 | 3.01 | 0.03 | 0.002 | 2.96 | 6 | 8259 | 362 | 484815 |
| MD-38-156-4 | rim | 32.51 | 1.32 | 0.03 | 65.58 | 99.44 | 3.01 | 0.03 | 0.001 | 2.96 | 6 | 11192 | 236 | 485474 |
| MD-38-143-1 | rim | 32.46 | 1.32 | 0.12 | 65.46 | 99.36 | 3.01 | 0.03 | 0.006 | 2.96 | 6 | 11150 | 945 | 484608 |
| MD-38-143-2 | int | 32.47 | 1.08 | 0.22 | 65.40 | 99.17 | 3.01 | 0.03 | 0.011 | 2.95 | 6 | 9132 | 1748 | 484186 |
| MD-38-143-3 | core | 32.27 | 1.05 | 0.22 | 65.12 | 98.65 | 3.01 | 0.03 | 0.011 | 2.96 | 6 | 8861 | 1724 | 482054 |
| MD-38-143-5 | rim | 32.37 | 1.19 | 0.14 | 65.10 | 98.80 | 3.01 | 0.03 | 0.007 | 2.95 | 6 | 10107 | 1087 | 481950 |
| MD-38-165-1 | core | 32.30 | 0.92 | 0.54 | 64.83 | 98.59 | 3.01 | 0.02 | 0.027 | 2.95 | 6 | 7826 | 4220 | 479914 |
| MD-38-165-2 | rim | 32.46 | 1.16 | 0.07 | 65.39 | 99.07 | 3.01 | 0.03 | 0.003 | 2.96 | 6 | 9844 | 528 | 484060 |
| MD-38-165-3 | rim | 32.61 | 1.22 | 0.06 | 65.29 | 99.18 | 3.02 | 0.03 | 0.003 | 2.95 | 6 | 10353 | 488 | 483349 |
| MD-38-183-1 | rim | 32.48 | 1.13 | 0.06 | 65.52 | 99.19 | 3.01 | 0.03 | 0.003 | 2.96 | 6 | 9573 | 457 | 485045 |
| MD-38-183-2 | core | 32.36 | 0.95 | 0.25 | 65.17 | 98.73 | 3.01 | 0.03 | 0.012 | 2.96 | 6 | 8021 | 1953 | 482483 |
| MD-38-183-3 | int | 32.30 | 1.12 | 0.11 | 65.53 | 99.05 | 3.00 | 0.03 | 0.005 | 2.97 | 6 | 9471 | 827 | 485119 |
| MD-38-183-4 | rim | 32.50 | 1.34 | 0.05 | 65.37 | 99.26 | 3.01 | 0.04 | 0.002 | 2.95 | 6 | 11345 | 378 | 483949 |
| MD-38-185-1 | rim | 32.51 | 1.35 | 0.00 | 65.49 | 99.35 | 3.01 | 0.04 | 0.000 | 2.96 | 6 | 11481 | 0 | 484808 |
| MD-38-185-2 | core | 32.46 | 0.94 | 0.23 | 65.02 | 98.65 | 3.02 | 0.02 | 0.012 | 2.95 | 6 | 7928 | 1843 | 481328 |
| MD-38-185-3 | rim | 32.48 | 1.19 | 0.04 | 65.25 | 98.95 | 3.01 | 0.03 | 0.002 | 2.95 | 6 | 10115 | 276 | 483016 |

## *Appendix 4.2. Garnet Major Element Analyses of Mt Daniel Samples recalculated on the basis of Oxygen=24*

| Sample No | MD2-3-1 | MD2-3-2 | MD2-3-3 | MD2-3-4 | MD2-3-5 | MD2-3-6 | MD2-2-1 | MD2-2-2 | MD2-2-3 | MD2-2-4 | MD2-2-5 | MD2-2-6 |
|---|---|---|---|---|---|---|---|---|---|---|---|---|
| SiO2 | 38.28 | 38.51 | 38.25 | 38.42 | 38.26 | 38.28 | 38.04 | 38.29 | 38.39 | 38.38 | 38.24 | 38.13 |
| FeO | 30.99 | 30.05 | 31.14 | 29.64 | 30.1 | 29.78 | 29.77 | 30.46 | 30.08 | 28.79 | 29.49 | 28.21 |
| TiO2 | 0.01 | 0.03 | 0.03 | 0.02 | 0.01 | 0.04 | 0.02 | 0.02 | 0.05 | 0.03 | 0.03 | 0.04 |
| MgO | 2.91 | 2.13 | 2.92 | 2.27 | 2.3 | 1.86 | 2.24 | 2.25 | 2.47 | 2.04 | 2.44 | 2.31 |
| CaO | 5.54 | 8.09 | 5.59 | 7.97 | 6.71 | 8.49 | 8.15 | 7.7 | 7.19 | 9.05 | 7.35 | 9.36 |
| Al2O3 | 21.26 | 21.2 | 21.25 | 20.98 | 21.18 | 21.25 | 20.93 | 20.99 | 21.16 | 21.11 | 21.13 | 20.88 |
| MnO | 1.46 | 1.03 | 1.37 | 1.10 | 1.31 | 1.07 | 0.94 | 1.01 | 1.10 | 0.79 | 1.11 | 0.95 |
| Total | 100.45 | 101.04 | 100.55 | 100.40 | 99.87 | 100.76 | 100.09 | 100.73 | 100.44 | 100.19 | 99.79 | 99.88 |
| Si | 6.06 | 6.07 | 6.05 | 6.08 | 6.09 | 6.05 | 6.05 | 6.06 | 6.07 | 6.08 | 6.08 | 6.06 |
| Fe | 4.10 | 3.96 | 4.12 | 3.92 | 4.00 | 3.94 | 3.96 | 4.03 | 3.98 | 3.81 | 3.92 | 3.75 |
| Ti | 0.00 | 0.00 | 0.00 | 0.00 | 0.00 | 0.00 | 0.00 | 0.00 | 0.01 | 0.00 | 0.00 | 0.00 |
| Mg | 0.69 | 0.50 | 0.69 | 0.54 | 0.55 | 0.44 | 0.53 | 0.53 | 0.58 | 0.48 | 0.58 | 0.55 |
| Ca | 0.94 | 1.37 | 0.95 | 1.35 | 1.14 | 1.44 | 1.39 | 1.31 | 1.22 | 1.53 | 1.25 | 1.59 |
| Al | 3.97 | 3.93 | 3.96 | 3.91 | 3.97 | 3.96 | 3.92 | 3.91 | 3.94 | 3.94 | 3.96 | 3.91 |
| Mn | 0.20 | 0.14 | 0.18 | 0.15 | 0.18 | 0.14 | 0.13 | 0.14 | 0.15 | 0.11 | 0.15 | 0.13 |

| Sample No | MD13-grt1-1 | MD13-grt1-2 | MD13-grt1-3 | MD13-grt1-4 | MD13-grt1-5 | MD13-grt1-6 | MD13-grt1-7 | MD13-grt1-8 | MD13-grt1-9 | MD13-grt1-10 | MD13-grt1-11 | MD13-grt2-1 |
|---|---|---|---|---|---|---|---|---|---|---|---|---|
| SiO2 | 39.13 | 38.75 | 39.26 | 39.13 | 39.29 | 39.04 | 38.81 | 38.38 | 38.88 | 38.79 | 38.73 | 38.65 |
| FeO | 25.5 | 26.87 | 25.87 | 26.47 | 26.25 | 25.5 | 26.48 | 25.88 | 26.38 | 26.8 | 26.11 | 26.89 |
| TiO2 | 0.08 | 0.11 | 0.05 | 0.11 | 0.08 | 0.06 | 0.08 | 0.04 | 0.08 | 0.06 | 0.06 | 0.06 |
| MgO | 5.56 | 4.65 | 5.52 | 5.27 | 5.49 | 5.64 | 5.51 | 5.79 | 5.35 | 5.42 | 5.62 | 5.52 |
| CaO | 9.32 | 9.2 | 9.16 | 8.96 | 8.58 | 8.65 | 8.58 | 7.74 | 8.22 | 8.34 | 8.56 | 7.88 |
| Al2O3 | 21.91 | 21.7 | 21.88 | 21.81 | 22.02 | 21.75 | 21.74 | 21.8 | 21.74 | 22.05 | 21.85 | 21.88 |
| MnO | 0.21 | 0.38 | 0.17 | 0.24 | 0.26 | 0.26 | 0.27 | 0.24 | 0.31 | 0.30 | 0.34 | 0.32 |
| Total | 101.71 | 101.66 | 101.92 | 101.98 | 101.97 | 100.89 | 101.47 | 99.87 | 100.96 | 101.76 | 101.27 | 101.20 |
| Si | 5.99 | 5.98 | 6.00 | 5.99 | 6.00 | 6.01 | 5.97 | 5.98 | 6.00 | 5.96 | 5.96 | 5.97 |
| Fe | 3.26 | 3.47 | 3.31 | 3.39 | 3.35 | 3.28 | 3.41 | 3.37 | 3.41 | 3.44 | 3.36 | 3.47 |
| Ti | 0.01 | 0.01 | 0.01 | 0.01 | 0.01 | 0.01 | 0.01 | 0.01 | 0.01 | 0.01 | 0.01 | 0.01 |
| Mg | 1.27 | 1.07 | 1.26 | 1.20 | 1.25 | 1.29 | 1.26 | 1.34 | 1.23 | 1.24 | 1.29 | 1.27 |
| Ca | 1.53 | 1.52 | 1.50 | 1.47 | 1.40 | 1.43 | 1.41 | 1.29 | 1.36 | 1.37 | 1.41 | 1.30 |
| Al | 3.95 | 3.94 | 3.94 | 3.93 | 3.96 | 3.95 | 3.94 | 4.00 | 3.96 | 3.99 | 3.97 | 3.98 |
| Mn | 0.03 | 0.05 | 0.02 | 0.03 | 0.03 | 0.03 | 0.04 | 0.03 | 0.04 | 0.04 | 0.04 | 0.04 |

| Sample No | MD13-grt2-2 | MD13-grt2-3 | MD13-grt2-4 | MD13-grt2-5 | MD13-grt2-6 | MD13-grt2-7 | MD13-grt2-8 | MD13-grt2-9 | MD22B-1-1 | MD22B-1-2 | MD22B-1-3 | MD22B-1-4 |
|---|---|---|---|---|---|---|---|---|---|---|---|---|
| SiO2 | 38.52 | 38.92 | 38.66 | 38.74 | 38.98 | 38.7 | 38.81 | 38.86 | 38.62 | 39.17 | 39.55 | 39.82 |
| FeO | 26.55 | 25.51 | 25.03 | 26.96 | 25.38 | 25.75 | 25.27 | 25.63 | 26.28 | 25.27 | 24.23 | 23.38 |
| TiO2 | 0.10 | 0.07 | 0.07 | 0.05 | 0.09 | 0.05 | 0.05 | 0.08 | 0.07 | 0.07 | 0.07 | 0.12 |
| MgO | 5.5 | 6.75 | 6.59 | 5.56 | 6.71 | 5.71 | 6.69 | 6.34 | 3.76 | 5.18 | 6.81 | 7.25 |
| CaO | 7.8 | 7.87 | 7.47 | 7.94 | 7.76 | 7.69 | 7.8 | 7.72 | 8.46 | 8.78 | 8.7 | 8.72 |
| Al2O3 | 21.9 | 22.04 | 21.77 | 21.6 | 22.01 | 21.68 | 21.79 | 21.8 | 21.7 | 21.6 | 21.76 | 22.04 |
| MnO | 0.30 | 0.26 | 0.32 | 0.33 | 0.33 | 0.45 | 0.28 | 0.34 | 1.10 | 0.52 | 0.23 | 0.19 |
| Total | 100.67 | 101.42 | 99.90 | 101.18 | 101.26 | 100.02 | 100.69 | 100.77 | 99.99 | 100.59 | 101.35 | 101.53 |
| Si | 5.97 | 5.95 | 5.99 | 5.98 | 5.97 | 6.01 | 5.97 | 5.99 | 0.64 | 0.65 | 0.66 | 0.66 |
| Fe | 3.44 | 3.26 | 3.24 | 3.48 | 3.25 | 3.35 | 3.25 | 3.30 | 0.37 | 0.35 | 0.34 | 0.33 |
| Ti | 0.01 | 0.01 | 0.01 | 0.01 | 0.01 | 0.01 | 0.01 | 0.01 | 0.00 | 0.00 | 0.00 | 0.00 |
| Mg | 1.27 | 1.54 | 1.52 | 1.28 | 1.53 | 1.32 | 1.54 | 1.46 | 0.09 | 0.13 | 0.17 | 0.18 |
| Ca | 1.29 | 1.29 | 1.24 | 1.31 | 1.27 | 1.28 | 1.29 | 1.27 | 0.15 | 0.16 | 0.16 | 0.16 |
| Al | 4.00 | 3.97 | 3.97 | 3.93 | 3.97 | 3.97 | 3.95 | 3.96 | 0.43 | 0.42 | 0.43 | 0.43 |
| Mn | 0.04 | 0.03 | 0.04 | 0.04 | 0.04 | 0.06 | 0.04 | 0.04 | 0.02 | 0.01 | 0.00 | 0.00 |

| Sample No | MD22B-1-5 | MD22B-1-6 | MD22B-1-7 | MD22B-1-8 | MD22B-1-9 | MD22B-1-10 | MD22B-1-11 | MD22B-1-12 | MD22B-2-1 | MD22B-2-2 | MD22B-2-3 | MD22B-2-4 |
|---|---|---|---|---|---|---|---|---|---|---|---|---|
| SiO2 | 39.38 | 39.86 | 39.46 | 39.28 | 39.35 | 39.59 | 38.89 | 39.48 | 39.43 | 39.46 | 39.36 | 39.73 |
| FeO | 24.32 | 23.34 | 24.47 | 25.5 | 24.56 | 24.51 | 26.72 | 23.78 | 23.88 | 24.8 | 25.14 | 23.63 |
| TiO2 | 0.09 | 0.10 | 0.10 | 0.07 | 0.07 | 0.08 | 0.11 | 0.09 | 0.08 | 0.09 | 0.07 | 0.11 |
| MgO | 6.02 | 7.41 | 6.43 | 5.55 | 6.86 | 6.83 | 4.59 | 7.1 | 6.15 | 5.59 | 5.89 | 7.08 |
| CaO | 9.02 | 8.77 | 9.06 | 8.61 | 8.48 | 8.61 | 9.12 | 8.93 | 9.41 | 9.31 | 9.2 | 9.23 |
| Al2O3 | 21.43 | 21.89 | 21.71 | 21.91 | 21.65 | 21.9 | 21.54 | 21.68 | 21.56 | 21.6 | 21.75 | 21.55 |
| MnO | 0.33 | 0.14 | 0.27 | 0.40 | 0.21 | 0.27 | 0.60 | 0.16 | 0.26 | 0.34 | 0.29 | 0.20 |
| Total | 100.59 | 101.51 | 101.50 | 101.32 | 101.18 | 101.79 | 101.58 | 101.22 | 100.77 | 101.19 | 101.71 | 101.53 |
| Si | 0.66 | 0.66 | 0.66 | 0.65 | 0.65 | 0.66 | 0.65 | 0.66 | 0.66 | 0.66 | 0.66 | 0.66 |
| Fe | 0.34 | 0.32 | 0.34 | 0.35 | 0.34 | 0.34 | 0.37 | 0.33 | 0.33 | 0.35 | 0.35 | 0.33 |
| Ti | 0.00 | 0.00 | 0.00 | 0.00 | 0.00 | 0.00 | 0.00 | 0.00 | 0.00 | 0.00 | 0.00 | 0.00 |
| Mg | 0.15 | 0.18 | 0.16 | 0.14 | 0.17 | 0.17 | 0.11 | 0.18 | 0.15 | 0.14 | 0.15 | 0.18 |
| Ca | 0.16 | 0.16 | 0.16 | 0.15 | 0.15 | 0.15 | 0.16 | 0.16 | 0.17 | 0.17 | 0.16 | 0.16 |
| Al | 0.42 | 0.43 | 0.43 | 0.43 | 0.42 | 0.43 | 0.42 | 0.43 | 0.42 | 0.42 | 0.43 | 0.42 |
| Mn | 0.00 | 0.00 | 0.00 | 0.01 | 0.00 | 0.00 | 0.01 | 0.00 | 0.00 | 0.00 | 0.00 | 0.00 |

| Sample No | MD22B-2-5 | MD22B-2-7 | MD22B-2-8 | MD22B-2-9 | MD22B-2a.1 | MD22B-2a.4 | MD22B-2a.5 | MD22B-2a.6 | MD22B-2a.7 | MD22B-2a.8 | MD22B-2a.9 | MD26-grt1-1 |
|---|---|---|---|---|---|---|---|---|---|---|---|---|
| SiO2 | 39.73 | 39.19 | 39.59 | 39.47 | 39.19 | 39.75 | 39.45 | 39.07 | 38.78 | 39.62 | 39.25 | 38.98 |
| FeO | 23.75 | 24.84 | 23.37 | 23.14 | 25.68 | 23.3 | 24.69 | 25.35 | 25.62 | 23.49 | 23.8 | 23.56 |
| TiO2 | 0.17 | 0.09 | 0.20 | 0.20 | 0.09 | 0.15 | 0.13 | 0.13 | 0.06 | 0.15 | 0.12 | 0.06 |
| MgO | 7.2 | 5.39 | 6.86 | 6.6 | 5.31 | 6.68 | 6.18 | 5.36 | 5.03 | 6.82 | 6.71 | 4.97 |
| CaO | 9.27 | 9.21 | 9.21 | 9.34 | 9.03 | 9.83 | 9.04 | 9.49 | 9.19 | 9.69 | 9.52 | 10.7 |
| Al2O3 | 21.68 | 21.4 | 21.49 | 21.54 | 21.62 | 21.17 | 21.78 | 21.4 | 21.52 | 21.64 | 21.71 | 21.87 |
| MnO | 0.16 | 0.37 | 0.20 | 0.27 | 0.41 | 0.19 | 0.25 | 0.32 | 0.51 | 0.24 | 0.21 | 0.34 |
| Total | 101.96 | 100.49 | 100.92 | 100.56 | 101.33 | 101.08 | 101.52 | 101.12 | 100.71 | 101.65 | 101.33 | 100.48 |
| Si | 0.66 | 0.65 | 0.66 | 0.66 | 0.65 | 0.66 | 0.66 | 0.65 | 0.65 | 0.66 | 0.65 | 6.01 |
| Fe | 0.33 | 0.35 | 0.33 | 0.32 | 0.36 | 0.32 | 0.34 | 0.35 | 0.36 | 0.33 | 0.33 | 3.04 |
| Ti | 0.00 | 0.00 | 0.00 | 0.00 | 0.00 | 0.00 | 0.00 | 0.00 | 0.00 | 0.00 | 0.00 | 0.01 |
| Mg | 0.18 | 0.13 | 0.17 | 0.16 | 0.13 | 0.17 | 0.15 | 0.13 | 0.12 | 0.17 | 0.17 | 1.14 |
| Ca | 0.17 | 0.16 | 0.16 | 0.17 | 0.16 | 0.18 | 0.16 | 0.17 | 0.16 | 0.17 | 0.17 | 1.77 |
| Al | 0.43 | 0.42 | 0.42 | 0.42 | 0.42 | 0.42 | 0.43 | 0.42 | 0.42 | 0.42 | 0.43 | 3.98 |
| Mn | 0.00 | 0.01 | 0.00 | 0.00 | 0.01 | 0.00 | 0.00 | 0.00 | 0.01 | 0.00 | 0.00 | 0.04 |

| Sample No | MD26-grt1-2 | MD26-grt1-3 | MD26-grt1-4 | MD26-grt1-5 | MD26-grt1-6 | MD26-grt1-7 | MD26-grt1-8 | MD26-grt1-9 | MD26-grt1-10 | MD26-grt3-1 | MD26-grt3-2 | MD26-grt3-3 |
|---|---|---|---|---|---|---|---|---|---|---|---|---|
| SiO2 | 38.67 | 38.82 | 38.8 | 38.67 | 38.65 | 38.81 | 38.69 | 38.73 | 38.9 | 38.96 | 38.92 | 38.84 |
| FeO | 22.25 | 24.21 | 24.3 | 24.82 | 25.34 | 24.89 | 26.08 | 25.15 | 24.18 | 26.18 | 26.35 | 25.85 |
| TiO2 | 0.06 | 0.06 | 0.19 | 0.07 | 0.12 | 0.14 | 0.27 | 0.07 | 0.05 | 0.03 | 0.06 | 0.05 |
| MgO | 5.09 | 5.13 | 5.23 | 5.22 | 5.38 | 5.35 | 4.84 | 5.59 | 5.63 | 6.43 | 6.34 | 6.55 |
| CaO | 10.57 | 10.31 | 9.77 | 9.62 | 9.22 | 9.05 | 8.99 | 9.01 | 9.21 | 7.45 | 7.54 | 7.07 |
| Al2O3 | 21.7 | 21.92 | 21.66 | 21.82 | 21.8 | 21.75 | 21.68 | 21.74 | 21.56 | 21.95 | 21.84 | 21.88 |
| MnO | 0.32 | 0.38 | 0.33 | 0.35 | 0.33 | 0.40 | 0.42 | 0.36 | 0.39 | 0.39 | 0.38 | 0.35 |
| Total | 98.65 | 100.84 | 100.28 | 100.57 | 100.84 | 100.39 | 100.96 | 100.65 | 99.92 | 101.39 | 101.43 | 100.59 |
| Si | 6.04 | 5.98 | 6.01 | 5.98 | 5.97 | 6.01 | 5.99 | 5.98 | 6.03 | 5.97 | 5.97 | 5.99 |
| Fe | 2.91 | 3.12 | 3.15 | 3.21 | 3.27 | 3.22 | 3.37 | 3.25 | 3.13 | 3.36 | 3.38 | 3.33 |
| Ti | 0.01 | 0.01 | 0.02 | 0.01 | 0.01 | 0.02 | 0.03 | 0.01 | 0.01 | 0.00 | 0.01 | 0.01 |
| Mg | 1.19 | 1.18 | 1.21 | 1.20 | 1.24 | 1.23 | 1.12 | 1.29 | 1.30 | 1.47 | 1.45 | 1.51 |
| Ca | 1.77 | 1.70 | 1.62 | 1.59 | 1.53 | 1.50 | 1.49 | 1.49 | 1.53 | 1.22 | 1.24 | 1.17 |
| Al | 4.00 | 3.98 | 3.95 | 3.98 | 3.97 | 3.97 | 3.95 | 3.96 | 3.94 | 3.97 | 3.95 | 3.97 |
| Mn | 0.04 | 0.05 | 0.04 | 0.05 | 0.04 | 0.05 | 0.05 | 0.05 | 0.05 | 0.05 | 0.05 | 0.05 |

| Sample No | MD26-grt3-4 | MD26-grt3-5 | MD26-grt3-6 | MD26-grt3-7 | MD26-grt3-8 | MD26-grt3-9 | MD26-grt3-10 | MD26-grt2-1 | MD26-grt2-2 | MD26-grt2-3 | MD26-grt2-4 | MD26-grt2-5 |
|---|---|---|---|---|---|---|---|---|---|---|---|---|
| SiO2 | 39.13 | 38.9 | 39.01 | 38.79 | 38.3 | 38.51 | 38.66 | 39.01 | 38.6 | 38.89 | 39.08 | 38.69 |
| FeO | 25.74 | 26.21 | 26.61 | 27.66 | 26.82 | 26.67 | 26.94 | 25.29 | 27.26 | 25.65 | 24.97 | 25.62 |
| TiO2 | 0.08 | 0.06 | 0.07 | 0.06 | 0.07 | 0.05 | 0.02 | 0.06 | 0.07 | 0.04 | 0.06 | 0.09 |
| MgO | 6.44 | 6.69 | 6.3 | 5.41 | 4.57 | 5.91 | 5.48 | 6.3 | 5.37 | 6.55 | 6.43 | 4.37 |
| CaO | 7.09 | 6.98 | 6.94 | 6.94 | 7.88 | 7.3 | 7.2 | 7.47 | 7.37 | 7.44 | 7.65 | 8.49 |
| Al2O3 | 21.93 | 21.77 | 21.87 | 21.76 | 21.58 | 21.91 | 21.93 | 21.88 | 21.82 | 21.99 | 21.99 | 21.75 |
| MnO | 0.47 | 0.39 | 0.41 | 0.44 | 0.57 | 0.41 | 0.38 | 0.33 | 0.51 | 0.33 | 0.33 | 0.41 |
| Total | 100.87 | 101.00 | 101.21 | 101.05 | 99.79 | 100.77 | 100.61 | 100.34 | 101.01 | 100.89 | 100.50 | 99.42 |
| Si | 6.01 | 5.98 | 5.99 | 6.00 | 6.01 | 5.96 | 5.99 | 6.02 | 5.98 | 5.98 | 6.01 | 6.06 |
| Fe | 3.31 | 3.37 | 3.42 | 3.58 | 3.52 | 3.45 | 3.49 | 3.26 | 3.53 | 3.30 | 3.21 | 3.35 |
| Ti | 0.01 | 0.01 | 0.01 | 0.01 | 0.01 | 0.01 | 0.00 | 0.01 | 0.01 | 0.01 | 0.01 | 0.01 |
| Mg | 1.47 | 1.53 | 1.44 | 1.25 | 1.07 | 1.36 | 1.27 | 1.45 | 1.24 | 1.50 | 1.47 | 1.02 |
| Ca | 1.17 | 1.15 | 1.14 | 1.15 | 1.32 | 1.21 | 1.20 | 1.23 | 1.22 | 1.22 | 1.26 | 1.42 |
| Al | 3.97 | 3.95 | 3.96 | 3.97 | 3.99 | 4.00 | 4.01 | 3.98 | 3.98 | 3.98 | 3.99 | 4.01 |
| Mn | 0.06 | 0.05 | 0.05 | 0.06 | 0.08 | 0.05 | 0.05 | 0.04 | 0.07 | 0.04 | 0.04 | 0.05 |

| Sample No | MD26-grt2-6 | MD26-grt2-7 | MD26-grt2-8 | MD26-grt2-9 | MD8-grt3-1 | MD8-grt3-2 | MD8-grt3-3 | MD8-grt3-4 | MD8-grt3-5 | MD8-grt3-6 | MD8-grt3-7 | MD8-grt3-8 |
|---|---|---|---|---|---|---|---|---|---|---|---|---|
| SiO2 | 38.99 | 38.88 | 39.14 | 38.97 | 37.56 | 38.2 | 37.96 | 38.21 | 37.9 | 37.94 | 38.21 | 38.27 |
| FeO | 25.61 | 24.75 | 24.82 | 24.34 | 24.21 | 24.26 | 24.74 | 25.27 | 24.97 | 26.89 | 24.06 | 26.16 |
| TiO2 | 0.08 | 0.10 | 0.13 | 0.10 | 0.05 | 0.00 | 0.06 | 0.06 | 0.03 | 0.07 | 0.13 | 0.07 |
| MgO | 6.15 | 6.15 | 6.16 | 5.97 | 2.16 | 2.35 | 2.22 | 2.48 | 2.87 | 2.9 | 2.14 | 2.74 |
| CaO | 8.33 | 8.76 | 8.97 | 8.97 | 9.55 | 9.59 | 10.03 | 9.11 | 10.18 | 8.16 | 9.65 | 8.73 |
| Al2O3 | 21.83 | 21.91 | 21.92 | 21.97 | 20.81 | 21.12 | 21.01 | 20.99 | 21.16 | 21.14 | 21.14 | 20.96 |
| MnO | 0.40 | 0.35 | 0.29 | 0.32 | 5.32 | 4.88 | 5.15 | 4.61 | 3.22 | 4.17 | 5.42 | 4.14 |
| Total | 101.39 | 100.90 | 101.43 | 100.64 | 99.66 | 100.40 | 101.17 | 100.73 | 100.33 | 101.27 | 100.75 | 101.07 |
| Si | 5.98 | 5.97 | 5.98 | 5.99 | 6.00 | 6.03 | 5.98 | 6.03 | 5.98 | 5.97 | 6.02 | 6.02 |
| Fe | 3.28 | 3.18 | 3.17 | 3.13 | 3.24 | 3.20 | 3.26 | 3.33 | 3.30 | 3.54 | 3.17 | 3.44 |
| Ti | 0.01 | 0.01 | 0.01 | 0.01 | 0.01 | 0.00 | 0.01 | 0.01 | 0.00 | 0.01 | 0.02 | 0.01 |
| Mg | 1.41 | 1.41 | 1.40 | 1.37 | 0.51 | 0.55 | 0.52 | 0.58 | 0.68 | 0.68 | 0.50 | 0.64 |
| Ca | 1.37 | 1.44 | 1.47 | 1.48 | 1.64 | 1.62 | 1.69 | 1.54 | 1.72 | 1.38 | 1.63 | 1.47 |
| Al | 3.94 | 3.97 | 3.95 | 3.98 | 3.92 | 3.93 | 3.90 | 3.90 | 3.94 | 3.92 | 3.93 | 3.89 |
| Mn | 0.05 | 0.05 | 0.04 | 0.04 | 0.72 | 0.65 | 0.69 | 0.62 | 0.43 | 0.56 | 0.72 | 0.55 |

| Sample No | MD8-grt3-9 | MD8-grt3-10 | MD8-grt3-11 | MD8-grt3-12 | MD8-grt3-13 | MD8-grt3-14 | MD8-grt3-15 | MD8-grt4-1 | MD8-grt4-2 | MD8-grt4-3 | MD8-grt4-4 | MD8-grt4-5 |
|---|---|---|---|---|---|---|---|---|---|---|---|---|
| SiO2 | 38.38 | 38.19 | 38.2 | 37.98 | 38.34 | 38.11 | 37.93 | 37.57 | 38.14 | 38.04 | 38.07 | 38.43 |
| FeO | 25.15 | 25.87 | 24.97 | 26.08 | 25 | 26.29 | 24.23 | 25.97 | 25.64 | 24.39 | 26.02 | 26.67 |
| TiO2 | 0.06 | 0.07 | 0.08 | 0.03 | 0.00 | 0.06 | 0.07 | 0.04 | 0.01 | 0.06 | 0.00 | 0.04 |
| MgO | 2.41 | 2.29 | 2.4 | 2.88 | 2.81 | 2.58 | 2.08 | 2.62 | 2.47 | 1.77 | 2.42 | 2.99 |
| CaO | 9.56 | 8.88 | 9.78 | 8.99 | 10.22 | 8.69 | 10.05 | 9 | 9.2 | 9.72 | 8.98 | 8.92 |
| Al2O3 | 21.23 | 21.05 | 21.09 | 20.99 | 21.2 | 21.1 | 21.25 | 21.06 | 21.11 | 20.74 | 21.22 | 21.19 |
| MnO | 4.55 | 4.84 | 4.83 | 3.48 | 3.21 | 4.71 | 5.09 | 4.30 | 4.62 | 6.27 | 4.90 | 2.96 |
| Total | 101.34 | 101.19 | 101.35 | 100.43 | 100.78 | 101.54 | 100.70 | 100.56 | 101.19 | 100.99 | 101.61 | 101.20 |
| Si | 6.02 | 6.02 | 6.00 | 6.01 | 6.02 | 5.99 | 5.99 | 5.96 | 6.00 | 6.02 | 5.98 | 6.02 |
| Fe | 3.30 | 3.41 | 3.28 | 3.45 | 3.28 | 3.45 | 3.20 | 3.44 | 3.37 | 3.23 | 3.42 | 3.49 |
| Ti | 0.01 | 0.01 | 0.01 | 0.00 | 0.00 | 0.01 | 0.01 | 0.00 | 0.00 | 0.01 | 0.00 | 0.00 |
| Mg | 0.56 | 0.54 | 0.56 | 0.68 | 0.66 | 0.60 | 0.49 | 0.62 | 0.58 | 0.42 | 0.57 | 0.70 |
| Ca | 1.61 | 1.50 | 1.65 | 1.52 | 1.72 | 1.46 | 1.70 | 1.53 | 1.55 | 1.65 | 1.51 | 1.50 |
| Al | 3.92 | 3.91 | 3.90 | 3.91 | 3.92 | 3.91 | 3.95 | 3.94 | 3.92 | 3.87 | 3.93 | 3.91 |
| Mn | 0.60 | 0.65 | 0.64 | 0.47 | 0.43 | 0.63 | 0.68 | 0.58 | 0.62 | 0.84 | 0.65 | 0.39 |

| Sample No | MD2-3-1 | MD2-3-2 | MD2-3-3 | MD2-3-4 | MD2-3-5 | MD2-3-6 | MD2-2-1 | MD2-2-2 | MD2-2-3 | MD2-2-4 | MD2-2-5 | MD2-2-6 | MD2-2-7 | MD2-2-8 | MD2-2-9 | MD2-2-10 | MD2-1-1 | MD2-1-2 | MD2-1-3 |
|---|---|---|---|---|---|---|---|---|---|---|---|---|---|---|---|---|---|---|---|
| SiO2 | 38.28 | 38.51 | 38.25 | 38.42 | 38.26 | 38.28 | 38.04 | 38.29 | 38.39 | 38.38 | 38.24 | 38.13 | 38.47 | 38.33 | 38.06 | 38.25 | 38.1 | 38.36 | 38.41 |
| FeO | 30.99 | 30.05 | 31.14 | 29.64 | 30.1 | 29.78 | 29.77 | 30.46 | 30.08 | 28.79 | 29.49 | 28.21 | 29.11 | 29.34 | 30.01 | 30.52 | 29.11 | 28.57 | 29.63 |
| TiO2 | 0.01 | 0.03 | 0.03 | 0.02 | 0.01 | 0.04 | 0.02 | 0.02 | 0.05 | 0.03 | 0.03 | 0.04 | 0.03 | 0.03 | 0.02 | 0.03 | 0.03 | 0.04 | 0.02 |
| MgO | 2.91 | 2.13 | 2.92 | 2.27 | 2.3 | 1.86 | 2.24 | 2.25 | 2.47 | 2.04 | 2.44 | 2.31 | 2 | 1.97 | 2.1 | 1.7 | 2.18 | 2.66 | 2.64 |
| CaO | 5.54 | 8.09 | 5.59 | 7.97 | 6.71 | 8.49 | 8.15 | 7.7 | 7.19 | 9.05 | 7.35 | 9.36 | 9.57 | 8.85 | 7.63 | 8 | 9.24 | 8.01 | 7.47 |
| Al2O3 | 21.26 | 21.2 | 21.25 | 20.98 | 21.18 | 21.25 | 20.93 | 20.99 | 21.16 | 21.11 | 21.13 | 20.88 | 21.05 | 20.87 | 21.12 | 20.81 | 20.79 | 21 | 21.08 |
| MnO | 1.46 | 1.03 | 1.37 | 1.10 | 1.31 | 1.07 | 0.94 | 1.01 | 1.10 | 0.79 | 1.11 | 0.95 | 0.82 | 1.10 | 1.16 | 1.19 | 1.08 | 1.26 | 1.41 |
| Total | 100.45 | 101.04 | 100.55 | 100.40 | 99.87 | 100.76 | 100.09 | 100.73 | 100.44 | 100.19 | 99.79 | 99.88 | 101.04 | 100.48 | 100.11 | 100.49 | 100.52 | 99.90 | 100.66 |
| Si | 6.06 | 6.07 | 6.05 | 6.08 | 6.09 | 6.05 | 6.05 | 6.06 | 6.07 | 6.08 | 6.08 | 6.06 | 6.06 | 6.07 | 6.05 | 6.08 | 6.04 | 6.08 | 6.06 |
| Fe | 4.10 | 3.96 | 4.12 | 3.92 | 4.00 | 3.94 | 3.96 | 4.03 | 3.98 | 3.81 | 3.92 | 3.75 | 3.83 | 3.89 | 3.99 | 4.06 | 3.86 | 3.79 | 3.91 |
| Ti | 0.00 | 0.00 | 0.00 | 0.00 | 0.00 | 0.00 | 0.00 | 0.00 | 0.01 | 0.00 | 0.00 | 0.00 | 0.00 | 0.00 | 0.00 | 0.00 | 0.00 | 0.01 | 0.00 |
| Mg | 0.69 | 0.50 | 0.69 | 0.54 | 0.55 | 0.44 | 0.53 | 0.53 | 0.58 | 0.48 | 0.58 | 0.55 | 0.47 | 0.47 | 0.50 | 0.40 | 0.52 | 0.63 | 0.62 |
| Ca | 0.94 | 1.37 | 0.95 | 1.35 | 1.14 | 1.44 | 1.39 | 1.31 | 1.22 | 1.53 | 1.25 | 1.59 | 1.61 | 1.50 | 1.30 | 1.36 | 1.57 | 1.36 | 1.26 |
| Al | 3.97 | 3.93 | 3.96 | 3.91 | 3.97 | 3.96 | 3.92 | 3.91 | 3.94 | 3.94 | 3.96 | 3.91 | 3.91 | 3.90 | 3.96 | 3.90 | 3.88 | 3.92 | 3.92 |
| Mn | 0.20 | 0.14 | 0.18 | 0.15 | 0.18 | 0.14 | 0.13 | 0.14 | 0.15 | 0.11 | 0.15 | 0.13 | 0.11 | 0.15 | 0.16 | 0.16 | 0.14 | 0.17 | 0.19 |

| Sample No | MD2-1-4 | MD2-1-5 | MD2-1-6 | MD2-1-7 | MD2-1-8 | MD6-2-1 | MD6-2-2 | MD6-2-3 rim | MD6-2-4 | MD6-2-5 | MD6-2-6 | MD6-2-7 | MD6-1-1 | MD6-1-2 | MD6-1-3 | MD6-1-4 | MD6-1-5 | MD6-1-6 | MD6-1-7 |
|---|---|---|---|---|---|---|---|---|---|---|---|---|---|---|---|---|---|---|---|
| SiO2 | 38.34 | 38.25 | 38.05 | 38.25 | 38.49 | 38.21 | 38.22 | 37.75 | 38.26 | 38.36 | 38.05 | 38.36 | 38.29 | 38.26 | 38 | 38.12 | 38.05 | 38.36 | 38.06 |
| FeO | 30.46 | 28.98 | 30.22 | 29.52 | 28.76 | 30.03 | 29.12 | 30.13 | 29.76 | 30.18 | 29.86 | 30.2 | 29.72 | 29.96 | 29.29 | 30.41 | 29.37 | 30.28 | 30.22 |
| TiO2 | 0.03 | 0.02 | 0.03 | 0.04 | 0.02 | 0.04 | 0.03 | 0.05 | 0.05 | 0.06 | 0.03 | 0.04 | 0.08 | 0.05 | 0.04 | 0.04 | 0.06 | 0.03 | 0.02 |
| MgO | 2.28 | 1.9 | 1.1477 | 2.2 | 2.25 | 2.93 | 3.04 | 2.94 | 2.82 | 2.84 | 2.82 | 2.96 | 2.77 | 2.92 | 2.89 | 2.95 | 1.86 | 2.95 | 2.07 |
| CaO | 7.2 | 7.59 | 8.14 | 8.14 | 8.99 | 8.15 | 8.09 | 8.64 | 8.73 | 7.99 | 8.83 | 7.71 | 8.69 | 8.06 | 7.95 | 7.58 | 9.86 | 8.09 | 8.35 |
| Al2O3 | 20.94 | 20.94 | 21.13 | 21.07 | 21.02 | 20.58 | 21.02 | 20.87 | 20.97 | 20.4 | 21.02 | 21.1 | 20.01 | 20.88 | 20.64 | 20.63 | 20.61 | 21 | 20.88 |
| MnO | 1.11 | 1.15 | 1.56 | 0.99 | 0.93 | 0.73 | 0.62 | 0.38 | 0.46 | 0.60 | 0.37 | 0.60 | 0.57 | 0.69 | 0.79 | 0.59 | 0.58 | 0.55 | 0.56 |
| Total | 100.35 | 98.83 | 100.28 | 100.21 | 100.46 | 100.67 | 100.14 | 100.76 | 101.05 | 100.43 | 100.98 | 100.97 | 100.14 | 100.81 | 99.60 | 100.32 | 100.38 | 101.27 | 100.16 |
| Si | 6.08 | 6.13 | 6.07 | 6.07 | 6.08 | 6.05 | 6.05 | 5.98 | 6.02 | 6.08 | 6.00 | 6.04 | 6.09 | 6.04 | 6.06 | 6.05 | 6.05 | 6.03 | 6.06 |
| Fe | 4.04 | 3.88 | 4.03 | 3.92 | 3.80 | 3.97 | 3.85 | 3.99 | 3.92 | 4.00 | 3.94 | 3.97 | 3.95 | 3.95 | 3.91 | 4.04 | 3.90 | 3.98 | 4.02 |
| Ti | 0.00 | 0.00 | 0.00 | 0.01 | 0.00 | 0.00 | 0.00 | 0.01 | 0.01 | 0.01 | 0.00 | 0.00 | 0.01 | 0.01 | 0.00 | 0.00 | 0.01 | 0.00 | 0.00 |
| Mg | 0.54 | 0.45 | 0.27 | 0.52 | 0.53 | 0.69 | 0.72 | 0.69 | 0.66 | 0.67 | 0.66 | 0.69 | 0.66 | 0.69 | 0.69 | 0.70 | 0.44 | 0.69 | 0.49 |
| Ca | 1.22 | 1.30 | 1.39 | 1.38 | 1.52 | 1.38 | 1.37 | 1.47 | 1.47 | 1.36 | 1.49 | 1.30 | 1.48 | 1.36 | 1.36 | 1.29 | 1.68 | 1.36 | 1.42 |
| Al | 3.92 | 3.96 | 3.97 | 3.94 | 3.91 | 3.84 | 3.92 | 3.89 | 3.89 | 3.81 | 3.90 | 3.91 | 3.75 | 3.88 | 3.88 | 3.86 | 3.86 | 3.89 | 3.92 |
| Mn | 0.15 | 0.16 | 0.21 | 0.13 | 0.12 | 0.10 | 0.08 | 0.05 | 0.06 | 0.08 | 0.05 | 0.08 | 0.08 | 0.09 | 0.11 | 0.08 | 0.08 | 0.07 | 0.07 |

| Sample No | MD6-1-8 | MD6-3-1 | MD6-3-2 | MD6-3-3 | MD6-3-4 | MD6-3-5 | MD6-3-6 | MD6-3-7 | MD6-3-8 | MD6-3-9 | MD6-3-10 | MD-29-2-1 | MD-29-2-2 | MD-29-2-3 | MD-29-2-4 | MD-29-2-5 | MD-29-2-6 | MD-29-2-7 |
|---|---|---|---|---|---|---|---|---|---|---|---|---|---|---|---|---|---|---|
| SiO2 | 38.47 | 38.34 | 38.32 | 38.08 | 38.11 | 38.35 | 38.43 | 38.37 | 38.01 | 37.96 | 38.25 | 38.66 | 38.78 | 38.52 | 38.76 | 38.44 | 38.67 | 38.85 |
| FeO | 29.69 | 29.9 | 29.63 | 29.97 | 30.19 | 29.23 | 29.36 | 29.89 | 28.12 | 30.01 | 29.86 | 25.73 | 26.1 | 26.52 | 25.38 | 25.57 | 26.67 | 24.34 |
| TiO2 | 0.02 | 0.03 | 0.05 | 0.05 | 0.06 | 0.05 | 0.04 | 0.02 | 0.06 | 0.05 | 0.04 | 0.04 | 0.04 | 0.06 | 0.06 | 0.04 | 0.06 | 0.06 |
| MgO | 2.88 | 2.79 | 3.01 | 2.91 | 2.74 | 2.85 | 2.28 | 2.78 | 1.5746 | 2.9 | 2.44 | 3.27 | 3.29 | 3.02 | 3.11 | 3.28 | 3.15 | 2.78 |
| CaO | 8.05 | 8.48 | 8 | 7.79 | 8.13 | 8.91 | 9.34 | 8.15 | 9.8 | 7.96 | 8.71 | 10.88 | 10.64 | 10.07 | 11.54 | 10.32 | 9.68 | 11.92 |
| Al2O3 | 20.95 | 20.8 | 20.76 | 20.75 | 20.99 | 20.96 | 20.78 | 20.93 | 20.58 | 20.69 | 21.01 | 21.08 | 20.95 | 20.89 | 21.13 | 21.12 | 21.16 | 21.11 |
| MnO | 0.59 | 0.49 | 0.63 | 0.54 | 0.46 | 0.56 | 0.41 | 0.41 | 1.26 | 0.49 | 0.47 | 0.60 | 0.76 | 0.98 | 0.68 | 0.73 | 0.91 | 0.94 |
| Total | 100.65 | 100.84 | 100.41 | 100.10 | 100.68 | 100.91 | 100.64 | 100.56 | 99.40 | 100.07 | 100.78 | 100.27 | 100.56 | 100.06 | 100.67 | 99.50 | 100.30 | 100.00 |
| Si | 6.06 | 6.05 | 6.06 | 6.05 | 6.02 | 6.03 | 6.07 | 6.06 | 6.08 | 6.04 | 6.04 | 6.06 | 6.07 | 6.07 | 6.05 | 6.06 | 6.07 | 6.09 |
| Fe | 3.91 | 3.94 | 3.92 | 3.98 | 3.99 | 3.85 | 3.88 | 3.95 | 3.76 | 3.99 | 3.94 | 3.37 | 3.41 | 3.49 | 3.31 | 3.37 | 3.50 | 3.19 |
| Ti | 0.00 | 0.00 | 0.01 | 0.01 | 0.01 | 0.01 | 0.01 | 0.00 | 0.01 | 0.01 | 0.00 | 0.00 | 0.00 | 0.01 | 0.01 | 0.01 | 0.01 | 0.01 |
| Mg | 0.68 | 0.66 | 0.71 | 0.69 | 0.65 | 0.67 | 0.54 | 0.65 | 0.38 | 0.69 | 0.57 | 0.76 | 0.77 | 0.71 | 0.72 | 0.77 | 0.74 | 0.65 |
| Ca | 1.36 | 1.43 | 1.36 | 1.33 | 1.38 | 1.50 | 1.58 | 1.38 | 1.68 | 1.36 | 1.47 | 1.83 | 1.78 | 1.70 | 1.93 | 1.74 | 1.63 | 2.00 |
| Al | 3.89 | 3.87 | 3.87 | 3.88 | 3.91 | 3.89 | 3.87 | 3.89 | 3.88 | 3.88 | 3.91 | 3.89 | 3.86 | 3.88 | 3.89 | 3.92 | 3.91 | 3.90 |
| Mn | 0.08 | 0.07 | 0.08 | 0.07 | 0.06 | 0.08 | 0.05 | 0.06 | 0.17 | 0.07 | 0.06 | 0.08 | 0.10 | 0.13 | 0.09 | 0.10 | 0.12 | 0.12 |

| Sample No | MD-29-2-8 | MD-29-2-9 | MD-29-2-10 | MD-29-4-1 | MD-29-4-2 | MD-29-4-3 | MD-29-4-4 | MD-29-4-5 | MD-29-4-6 | MD-29-3-1 | MD-29-3-2 | MD-29-3-3 | MD-29-3-4 | MD-29-3-5 | MD-29-3-6 | MD-29-3-7 |
|---|---|---|---|---|---|---|---|---|---|---|---|---|---|---|---|---|
| SiO2 | 38.63 | 38.22 | 38.63 | 38.8 | 38.56 | 38.65 | 38.55 | 38.67 | 38.69 | 38.28 | 38.68 | 38.21 | 38.57 | 38.49 | 38.56 | 38.52 |
| FeO | 27.54 | 26.33 | 24.86 | 25.76 | 26.19 | 26.4 | 25.86 | 25.61 | 26.87 | 26.68 | 25.93 | 27.02 | 24.91 | 24.59 | 26.08 | 26.1 |
| TiO2 | 0.07 | 0.03 | 0.05 | 0.06 | 0.05 | 0.07 | 0.05 | 0.04 | 0.05 | 0.03 | 0.04 | 0.02 | 0.07 | 0.04 | 0.05 | 0.05 |
| MgO | 3.56 | 3.93 | 2.98 | 3.27 | 3.34 | 3.39 | 3.24 | 3.41 | 3.52 | 3.37 | 3.48 | 3.46 | 3.01 | 3.11 | 3.2 | 3.14 |
| CaO | 8.78 | 9.13 | 10.58 | 11.5 | 10.68 | 10.48 | 10.17 | 10.24 | 10.05 | 9.62 | 9.46 | 9.73 | 12.07 | 11.08 | 10.56 | 10.4 |
| Al2O3 | 21.05 | 21.37 | 21.2 | 21.01 | 20.82 | 21.13 | 20.88 | 21.46 | 21.03 | 21.02 | 20.89 | 21.03 | 21.13 | 21.15 | 20.94 | 21.28 |
| MnO | 0.92 | 0.75 | 1.15 | 0.65 | 0.85 | 0.78 | 0.85 | 0.81 | 0.61 | 0.91 | 0.94 | 0.98 | 0.67 | 0.74 | 0.78 | 0.93 |
| Total | 100.55 | 99.76 | 99.45 | 101.06 | 100.49 | 100.90 | 99.60 | 100.24 | 100.82 | 99.91 | 99.42 | 100.46 | 100.44 | 99.20 | 100.17 | 100.42 |
| Si | 6.06 | 6.01 | 6.09 | 6.04 | 6.05 | 6.03 | 6.08 | 6.05 | 6.04 | 6.04 | 6.10 | 6.01 | 6.03 | 6.07 | 6.06 | 6.04 |
| Fe | 3.61 | 3.46 | 3.27 | 3.35 | 3.43 | 3.45 | 3.41 | 3.35 | 3.51 | 3.52 | 3.42 | 3.55 | 3.26 | 3.24 | 3.43 | 3.42 |
| Ti | 0.01 | 0.00 | 0.01 | 0.01 | 0.01 | 0.01 | 0.01 | 0.00 | 0.01 | 0.00 | 0.00 | 0.00 | 0.01 | 0.00 | 0.01 | 0.01 |
| Mg | 0.83 | 0.92 | 0.70 | 0.76 | 0.78 | 0.79 | 0.76 | 0.79 | 0.82 | 0.79 | 0.82 | 0.81 | 0.70 | 0.73 | 0.75 | 0.73 |
| Ca | 1.47 | 1.54 | 1.79 | 1.92 | 1.79 | 1.75 | 1.72 | 1.72 | 1.68 | 1.63 | 1.60 | 1.64 | 2.02 | 1.87 | 1.78 | 1.75 |
| Al | 3.89 | 3.96 | 3.94 | 3.86 | 3.85 | 3.89 | 3.88 | 3.95 | 3.87 | 3.91 | 3.88 | 3.90 | 3.90 | 3.93 | 3.88 | 3.93 |
| Mn | 0.12 | 0.10 | 0.15 | 0.09 | 0.11 | 0.10 | 0.11 | 0.11 | 0.08 | 0.12 | 0.13 | 0.13 | 0.09 | 0.10 | 0.10 | 0.12 |

| Sample No | MD-29-3-8 | MD-29-3-9 | MD-29-3-10 | MD-29-3-11 | MD33-3-1 | MD33-3-2 | MD33-3-3 | MD33-3-4 | MD33-3-5 | MD33-3-6 | MD33-3-7 | MD33-3-8 | MD33-3-9 | MD33-3-10 | MD33-1-1 | MD33-1-2 |
|---|---|---|---|---|---|---|---|---|---|---|---|---|---|---|---|---|
| SiO2 | 38.2 | 38.59 | 38.58 | 38.6 | 38.99 | 38.69 | 38.55 | 38.58 | 38.48 | 38.44 | 38.24 | 38.63 | 38.89 | 38.48 | 38.68 | 38.69 |
| FeO | 26.11 | 26.38 | 26.26 | 25.89 | 26.89 | 28.57 | 28.33 | 28.48 | 28.22 | 24.81 | 25.04 | 28.2 | 26.9 | 26.72 | 28.12 | 27.84 |
| TiO2 | 0.05 | 0.09 | 0.06 | 0.04 | 0.06 | 0.07 | 0.07 | 0.06 | 0.07 | 0.04 | 0.06 | 0.05 | 0.05 | 0.08 | 0.12 | 0.06 |
| MgO | 3.25 | 3.37 | 3.38 | 3.32 | 3.19 | 3.69 | 3.71 | 3.81 | 3.76 | 1.3956 | 1.467 | 3.46 | 2.94 | 2.7 | 3.54 | 3.65 |
| CaO | 10.6 | 9.29 | 10.23 | 10.61 | 10.6 | 9.09 | 9.18 | 9.07 | 9.02 | 10.7 | 10.52 | 8.88 | 10.96 | 10.87 | 8.98 | 9.51 |
| Al2O3 | 21.06 | 21.01 | 21.14 | 21.17 | 21.22 | 20.79 | 20.95 | 20.92 | 21.17 | 20.56 | 20.77 | 20.94 | 21.14 | 20.87 | 20.64 | 21.15 |
| MnO | 0.83 | 0.89 | 0.80 | 0.84 | 0.58 | 0.50 | 0.48 | 0.50 | 0.59 | 2.82 | 2.92 | 0.64 | 0.63 | 0.88 | 0.54 | 0.50 |
| Total | 100.10 | 99.62 | 100.45 | 100.48 | 101.53 | 101.40 | 101.27 | 101.42 | 101.31 | 98.77 | 99.02 | 100.80 | 101.51 | 100.60 | 100.62 | 101.40 |
| Si | 6.01 | 6.08 | 6.04 | 6.04 | 6.05 | 6.04 | 6.02 | 6.02 | 6.00 | 6.15 | 6.11 | 6.05 | 6.05 | 6.05 | 6.07 | 6.02 |
| Fe | 3.44 | 3.48 | 3.44 | 3.39 | 3.49 | 3.73 | 3.70 | 3.71 | 3.68 | 3.32 | 3.35 | 3.70 | 3.50 | 3.51 | 3.69 | 3.62 |
| Ti | 0.01 | 0.01 | 0.01 | 0.01 | 0.01 | 0.01 | 0.01 | 0.01 | 0.01 | 0.01 | 0.01 | 0.01 | 0.01 | 0.01 | 0.01 | 0.01 |
| Mg | 0.76 | 0.79 | 0.79 | 0.77 | 0.74 | 0.86 | 0.86 | 0.89 | 0.87 | 0.33 | 0.35 | 0.81 | 0.68 | 0.63 | 0.83 | 0.85 |
| Ca | 1.79 | 1.57 | 1.72 | 1.78 | 1.76 | 1.52 | 1.54 | 1.52 | 1.51 | 1.83 | 1.80 | 1.49 | 1.83 | 1.83 | 1.51 | 1.59 |
| Al | 3.91 | 3.90 | 3.90 | 3.90 | 3.88 | 3.82 | 3.85 | 3.85 | 3.89 | 3.88 | 3.91 | 3.87 | 3.87 | 3.86 | 3.82 | 3.88 |
| Mn | 0.11 | 0.12 | 0.11 | 0.11 | 0.08 | 0.07 | 0.06 | 0.07 | 0.08 | 0.38 | 0.40 | 0.08 | 0.08 | 0.12 | 0.07 | 0.07 |

| Sample No | MD33-1-3 | MD33-1-4 | MD33-1-5 | MD33-1-6 | MD33-1-7 | MD33-1-8 | MD-33-2-1 | MD-33-2-2 | MD-33-2-3 | MD-33-2-4 | MD-33-2-5 | MD-33-2-6 | MD-33-2-7 | MD-33-2-8 | MD-33-2-9 | MD-33-2-10 |
|---|---|---|---|---|---|---|---|---|---|---|---|---|---|---|---|---|
| SiO2 | 38.59 | 38.73 | 38.56 | 38.63 | 38.68 | 38.52 | 38.59 | 38.85 | 38.88 | 38.59 | 38.73 | 38.83 | 38.76 | 38.61 | 38.72 | 38.48 |
| FeO | 28.35 | 27.66 | 28.31 | 27.66 | 26.36 | 28.04 | 25.9 | 27.96 | 26.09 | 27.89 | 26.52 | 26.12 | 27.51 | 27.4 | 26.96 | 26.35 |
| TiO2 | 0.07 | 0.07 | 0.04 | 0.04 | 0.04 | 0.07 | 0.04 | 0.05 | 0.07 | 0.07 | 0.05 | 0.07 | 0.06 | 0.05 | 0.04 | 0.08 |
| MgO | 3.61 | 3.71 | 3.73 | 3.41 | 3.31 | 3.02 | 3.02 | 3.69 | 3.16 | 3.69 | 2.69 | 2.88 | 3.26 | 3.39 | 3.04 | 2.86 |
| CaO | 9.3 | 9.09 | 8.45 | 9.7 | 10.94 | 10.11 | 11.47 | 9.5 | 11.52 | 9.24 | 11.06 | 11.09 | 10.05 | 9.95 | 10.34 | 10.24 |
| Al2O3 | 21.3 | 21.09 | 20.97 | 21.21 | 21.1 | 20.98 | 21.19 | 21.19 | 21.47 | 21 | 21.49 | 21.14 | 21.02 | 21.17 | 21.29 | 21.34 |
| MnO | 0.60 | 0.56 | 0.49 | 0.50 | 0.36 | 0.66 | 0.50 | 0.45 | 0.37 | 0.50 | 0.86 | 0.65 | 0.63 | 0.43 | 0.75 | 0.82 |
| Total | 101.82 | 100.92 | 100.55 | 101.15 | 100.80 | 101.40 | 100.71 | 101.69 | 101.56 | 100.97 | 101.40 | 100.78 | 101.30 | 101.00 | 101.13 | 100.17 |
| Si | 5.99 | 6.05 | 6.05 | 6.03 | 6.04 | 6.02 | 6.03 | 6.03 | 6.02 | 6.03 | 6.02 | 6.06 | 6.04 | 6.03 | 6.04 | 6.05 |
| Fe | 3.68 | 3.61 | 3.71 | 3.61 | 3.44 | 3.66 | 3.38 | 3.63 | 3.38 | 3.65 | 3.45 | 3.41 | 3.59 | 3.58 | 3.52 | 3.46 |
| Ti | 0.01 | 0.01 | 0.00 | 0.00 | 0.01 | 0.01 | 0.00 | 0.01 | 0.01 | 0.01 | 0.01 | 0.01 | 0.01 | 0.01 | 0.00 | 0.01 |
| Mg | 0.84 | 0.86 | 0.87 | 0.79 | 0.77 | 0.70 | 0.70 | 0.85 | 0.73 | 0.86 | 0.62 | 0.67 | 0.76 | 0.79 | 0.71 | 0.67 |
| Ca | 1.55 | 1.52 | 1.42 | 1.62 | 1.83 | 1.69 | 1.92 | 1.58 | 1.91 | 1.55 | 1.84 | 1.86 | 1.68 | 1.66 | 1.73 | 1.72 |
| Al | 3.90 | 3.88 | 3.88 | 3.90 | 3.88 | 3.86 | 3.90 | 3.87 | 3.92 | 3.87 | 3.94 | 3.89 | 3.86 | 3.90 | 3.91 | 3.95 |
| Mn | 0.08 | 0.07 | 0.07 | 0.07 | 0.05 | 0.09 | 0.07 | 0.06 | 0.05 | 0.07 | 0.11 | 0.09 | 0.08 | 0.06 | 0.10 | 0.11 |

| Sample No | MD-33-4-1 | MD-33-4-2 | MD-33-4-3 | MD-33-4-4 | MD-33-4-5 | MD-33-4-6 | MD-33-4-7 | MD-33-4-8 | MD-33-4-9 | MD14-grt4-1 | MD14-grt4-2 | MD14-grt4-3 | MD14-grt4-4 | MD14-grt3-1 | MD14-grt3-2 |
|---|---|---|---|---|---|---|---|---|---|---|---|---|---|---|---|
| SiO2 | 38.62 | 38.82 | 38.91 | 38.99 | 38.61 | 38.73 | 39.4 | 38.62 | 38.79 | 39.5 | 37.91 | 37.97 | 38.25 | 37.92 | 37.98 |
| FeO | 27.09 | 27.17 | 27.33 | 26.85 | 26.89 | 26.93 | 24.42 | 27.25 | 27.57 | 25.94 | 27.39 | 27.15 | 27.82 | 26.83 | 27.31 |
| TiO2 | 0.06 | 0.03 | 0.07 | 0.06 | 0.07 | 0.05 | 0.05 | 0.07 | 0.04 | 0.0467 | 0.0313 | 0.1049 | 0.0442 | 0.0465 | 0.0615 |
| MgO | 3 | 3.2 | 3.15 | 3 | 3.26 | 3.33 | 3.42 | 3.2 | 3.44 | 3.51 | 3.26 | 2.78 | 3.07 | 2.25 | 2.26 |
| CaO | 10.83 | 10.98 | 10.35 | 10.85 | 10.64 | 10.62 | 11.89 | 10.58 | 9.68 | 10.41 | 9.42 | 10.5 | 9.48 | 10.7 | 10.48 |
| Al2O3 | 21.07 | 21.3 | 21.47 | 21.3 | 21.38 | 21.02 | 21.59 | 21.45 | 20.82 | 22.05 | 20.93 | 20.79 | 21.24 | 21.23 | 21.1 |
| MnO | 0.63 | 0.47 | 0.53 | 0.62 | 0.47 | 0.46 | 0.21 | 0.54 | 0.46 | 0.4443 | 0.4921 | 0.6431 | 0.5555 | 0.7648 | 0.8062 |
| Total | 101.30 | 101.97 | 101.81 | 101.67 | 101.32 | 101.14 | 100.98 | 101.71 | 100.80 | 101.901 | 99.4334 | 99.938 | 100.4597 | 99.7413 | 99.9977 |
| Si | 6.03 | 6.01 | 6.03 | 6.04 | 6.01 | 6.04 | 6.08 | 5.99 | 6.07 | 6.06 | 6.02 | 6.02 | 6.02 | 6.01 | 6.02 |
| Fe | 3.53 | 3.52 | 3.54 | 3.48 | 3.50 | 3.51 | 3.15 | 3.54 | 3.61 | 3.33 | 3.64 | 3.60 | 3.66 | 3.56 | 3.62 |
| Ti | 0.01 | 0.00 | 0.01 | 0.01 | 0.01 | 0.01 | 0.01 | 0.01 | 0.00 | 0.01 | 0.00 | 0.01 | 0.01 | 0.01 | 0.01 |
| Mg | 0.70 | 0.74 | 0.73 | 0.69 | 0.76 | 0.77 | 0.79 | 0.74 | 0.80 | 0.80 | 0.77 | 0.66 | 0.72 | 0.53 | 0.53 |
| Ca | 1.81 | 1.82 | 1.72 | 1.80 | 1.77 | 1.77 | 1.97 | 1.76 | 1.62 | 1.71 | 1.60 | 1.78 | 1.60 | 1.82 | 1.78 |
| Al | 3.87 | 3.89 | 3.92 | 3.89 | 3.92 | 3.86 | 3.93 | 3.92 | 3.84 | 3.98 | 3.92 | 3.88 | 3.94 | 3.97 | 3.94 |
| Mn | 0.08 | 0.06 | 0.07 | 0.08 | 0.06 | 0.06 | 0.03 | 0.07 | 0.06 | 0.06 | 0.07 | 0.09 | 0.07 | 0.10 | 0.11 |

| Sample No | MD14-grt3-3 | MD14-grt3-4 | MD14-grt3-5 | MD14-grt3-6 | MD14-grt3a-1 | MD14-grt3a-2 | MD14-grt3a-3 | MD14-grt3a-4 | MD14-grt3a-5 | MD14-grt3a-6 |
|---|---|---|---|---|---|---|---|---|---|---|
| SiO2 | 37.92 | 38.33 | 38.03 | 38.23 | 38.21 | 38.41 | 38.02 | 38.07 | 37.98 | 38.04 |
| FeO | 27.79 | 27.52 | 27.86 | 26.74 | 27.27 | 27.32 | 27.52 | 28.05 | 26.52 | 27.25 |
| TiO2 | 0.0388 | 0.0551 | 0.0356 | 0.0476 | 0.0465 | 0.0496 | 0.055 | 0.124 | 0.1038 | 0.0151 |
| MgO | 2.89 | 3.05 | 3.55 | 2.91 | 2.35 | 2.57 | 2.2 | 2.58 | 2.16 | 2.61 |
| CaO | 9.92 | 9.87 | 9.69 | 10.47 | 10.48 | 10.46 | 10.22 | 10.14 | 10.58 | 9.43 |
| Al2O3 | 21.19 | 21.29 | 21.27 | 21.41 | 21.42 | 21.09 | 20.86 | 20.85 | 20.84 | 21.7 |
| MnO | 0.4992 | 0.5503 | 0.4703 | 0.3782 | 0.7265 | 0.7211 | 0.7442 | 0.6152 | 0.7595 | 0.7989 |
| Total | 100.248 | 100.6654 | 100.9059 | 100.1858 | 100.503 | 100.6207 | 99.6192 | 100.4292 | 98.9433 | 99.844 |
| Si | 5.99 | 6.01 | 5.96 | 6.01 | 6.01 | 6.04 | 6.05 | 6.02 | 6.06 | 6.01 |
| Fe | 3.67 | 3.61 | 3.65 | 3.52 | 3.59 | 3.59 | 3.66 | 3.71 | 3.54 | 3.60 |
| Ti | 0.00 | 0.01 | 0.00 | 0.01 | 0.01 | 0.01 | 0.01 | 0.01 | 0.01 | 0.00 |
| Mg | 0.68 | 0.71 | 0.83 | 0.68 | 0.55 | 0.60 | 0.52 | 0.61 | 0.51 | 0.61 |
| Ca | 1.68 | 1.66 | 1.63 | 1.76 | 1.77 | 1.76 | 1.74 | 1.72 | 1.81 | 1.60 |
| Al | 3.94 | 3.94 | 3.93 | 3.97 | 3.97 | 3.91 | 3.91 | 3.88 | 3.92 | 4.04 |
| Mn | 0.07 | 0.07 | 0.06 | 0.05 | 0.10 | 0.10 | 0.10 | 0.08 | 0.10 | 0.11 |

## *Appendix 5.1. Trace Element analyses of Zircons*

| Element | MD15-20-1 | MD15-14-1 | MD15-47-1 | MD15-50-1 | MD15-101-1 | MD15-110-1 | MD15-145-1 | MD13-3-1 | MD13-8-2 | MD13-17-1 | MD13-16-1 | MD13-20-1 | MD13-27-1 | MD13-33-1 | MD13-34-1 |
|---|---|---|---|---|---|---|---|---|---|---|---|---|---|---|---|
| P31 | 164.22 | 181.2 | 178.05 | 237.54 | 208.35 | 236.99 | 153.58 | 394.33 | 415.31 | 343.47 | 262.03 | 351.82 | 354.96 | 411.41 | 1200.05 |
| Ca43 | 339.26 | 303.4 | 191.04 | 420.64 | 261.04 | 279.94 | 389.17 | <45.75 | 63.97 | <43.35 | <42.24 | <43.42 | <42.68 | <49.85 | 496.66 |
| Ti49 | 21.89 | 19.07 | 14.38 | 23.65 | 28.26 | 26.23 | 23.57 | 16.07 | 13.55 | 10.07 | 10.08 | 9.82 | 11.66 | 9.22 | 9.89 |
| Sr88 | 0.211 | 0.2 | 0.155 | 1.349 | 0.18 | 1.589 | 0.17 | <0.079 | 0.093 | <0.078 | <0.073 | <0.074 | <0.074 | <0.087 | 1.197 |
| Y89 | 604.71 | 998.03 | 492.91 | 1042.92 | 954.1 | 454.43 | 323.59 | 379.04 | 395.06 | 549.54 | 196.58 | 338.1 | 230.49 | 327.61 | 787.32 |
| Nb93 | 0.751 | 0.771 | 1.093 | 0.841 | 0.774 | 0.985 | 0.789 | 0.243 | 0.177 | 0.186 | 0.136 | 0.14 | 0.197 | 0.182 | 0.652 |
| La139 | 0.015 | 0.0428 | 0.0066 | 0.038 | 0.0371 | <0.0061 | 0.0061 | <0.0192 | <0.0220 | <0.0187 | <0.0180 | <0.0192 | <0.0169 | <0.0215 | 0.063 |
| Ce140 | 12.6 | 20.97 | 16.36 | 18.49 | 17.38 | 15.42 | 13.02 | 1.683 | 1.646 | 1.965 | 0.861 | 1.291 | 1.122 | 1.627 | 9.89 |
| Pr141 | 0.1481 | 0.558 | 0.0509 | 0.414 | 0.347 | 0.071 | 0.0451 | 0.0553 | 0.0635 | 0.12 | 0.0152 | 0.0324 | 0.0144 | 0.052 | 0.438 |
| Nd146 | 2.293 | 8.23 | 0.987 | 6.28 | 5.43 | 1.249 | 0.741 | 0.83 | 1.022 | 2.13 | 0.299 | 0.656 | 0.26 | 0.778 | 5.31 |
| Sm147 | 3.9 | 10.44 | 2.101 | 9.06 | 8.15 | 2.42 | 1.621 | 1.637 | 1.714 | 3.08 | 0.66 | 1.443 | 0.691 | 1.432 | 6.12 |
| Eu153 | 0.599 | 1.37 | 0.346 | 1.311 | 1.177 | 0.382 | 0.282 | 0.617 | 0.694 | 1.347 | 0.264 | 0.527 | 0.307 | 0.556 | 1.232 |
| Gd157 | 16.19 | 33.93 | 9.62 | 29.54 | 29.8 | 9.79 | 7.41 | 7.78 | 8.37 | 13.5 | 3.36 | 7.18 | 3.98 | 6.89 | 23.51 |
| Tb159 | 4.98 | 9.38 | 3.33 | 8.97 | 8.58 | 3.28 | 2.388 | 2.43 | 2.6 | 3.94 | 1.182 | 2.23 | 1.338 | 2.145 | 6.5 |
| Dy163 | 57.5 | 103.95 | 42.28 | 103.8 | 94.77 | 40.07 | 29.18 | 31.42 | 32.78 | 47.22 | 15.27 | 28.25 | 18.21 | 27.52 | 73.95 |
| Ho165 | 19.98 | 34.1 | 15.71 | 35.19 | 31.58 | 14.68 | 10.29 | 11.93 | 12.37 | 17.61 | 6.12 | 10.84 | 7.09 | 10.35 | 25.19 |
| Er166 | 88.7 | 149.45 | 75.72 | 156.49 | 138.87 | 67.62 | 48.67 | 55.38 | 58.04 | 81.44 | 30.13 | 50.21 | 34.73 | 47.97 | 105.59 |
| Tm169 | 18.82 | 31.01 | 17.24 | 31.61 | 28.59 | 14.81 | 10.72 | 11.98 | 12.48 | 16.91 | 6.71 | 10.69 | 7.86 | 10.33 | 20.43 |
| Yb173 | 163.32 | 274.43 | 162.41 | 279.59 | 248.3 | 133.04 | 100.45 | 118.69 | 123.96 | 167.46 | 68.67 | 106.7 | 79.62 | 102.26 | 178.39 |
| Lu175 | 30.63 | 48.28 | 30.66 | 50.92 | 46.01 | 25.8 | 19.32 | 26.28 | 27.87 | 36.48 | 15.48 | 23.26 | 18.21 | 22.54 | 35.08 |
| Hf178 | 9650 | 9887.43 | 10031.59 | 10616.69 | 9768.71 | 10913.48 | 9675.44 | 7767.48 | 7657.25 | 7402.85 | 6173.28 | 6792.31 | 6622.71 | 7207.82 | 7631.81 |
| Th232 | 181.51 | 331.07 | 184.72 | 290.24 | 288.57 | 152.05 | 122.77 | 18.84 | 23.99 | 25.78 | 7.79 | 14.6 | 13.5 | 18.63 | 249.13 |
| U238 | 169.11 | 292.16 | 243.61 | 265.83 | 244.34 | 191.73 | 155.96 | 29.44 | 36.38 | 36.7 | 15.82 | 23.45 | 25.46 | 27.84 | 195.21 |
| Th/U | 1.1 | 1.1 | 0.8 | 1.1 | 1.2 | 0.8 | 0.8 | 0.6 | 0.7 | 0.7 | 0.5 | 0.6 | 0.5 | 0.7 | 1.3 |
| Ce/Ce* | 66 | 33 | 219 | 36 | 38 | nd | 192 | nd | nd | nd | nd | nd | nd | nd | 14.597333 |
| Eu/Eu* | 0.2 | 0.2 | 0.2 | 0.2 | 0.2 | 0.2 | 0.2 | 0.5 | 0.6 | 0.6 | 0.5 | 0.5 | 0.6 | 0.5 | 0.3 |
| T C | 815 | 801 | 774 | 823 | 841 | 833 | 822 | 784 | 768 | 742 | 742 | 739 | 755 | 734 | 740 |

| Element | MD13-50 | MD22b-13-1 | MD22B-14-1 | MD22B-16-1 | MD22B-21-1 | MD22B-29-1 | MD22B-35-1 | MD22B-35-2 | MD22B-48-1 | MD22B-7-1 | MD22B-11-1 | MD22B-23-1 | MD26-24-1 | MD26-28-1 |
|---|---|---|---|---|---|---|---|---|---|---|---|---|---|---|
| P31 | 327.45 | 189.29 | 908.81 | 313.46 | 249.63 | 555.43 | 284.44 | 240.31 | 283.46 | 254.43 | 205.93 | 362.26 | 153.58 | 2441.67 |
| Ca43 | <40.95 | <41.96 | 2150.7 | <57.79 | <57.56 | <64.97 | <61.80 | <60.87 | <55.18 | 727.95 | 259.34 | 536.27 | <55.61 | 4482.84 |
| Ti49 | 9.21 | 11.28 | 57.3 | 29.14 | 28.17 | 13.7 | 36.01 | 25.05 | 4.44 | 39.25 | 24.14 | 50.09 | 4.65 | 17.9 |
| Sr88 | <0.070 | 0.141 | 4.51 | 0.113 | 0.074 | 0.224 | 1.151 | <0.062 | 0.084 | 0.345 | <0.104 | <0.172 | 0.095 | 15.27 |
| Y89 | 244.65 | 357.84 | 316.99 | 508.49 | 506.91 | 168.67 | 456.97 | 318.16 | 576.73 | 476.15 | 285.68 | 545.74 | 229.83 | <0.0095 |
| Nb93 | 0.155 | 0.227 | 0.298 | 0.325 | 0.24 | 1.493 | 0.318 | 0.379 | 0.748 | 0.374 | 0.276 | 0.476 | 0.964 | 5.01 |
| La139 | <0.0166 | 0.0214 | 0.0681 | 0.0135 | 0.0214 | 0.0361 | 0.0186 | <0.0035 | <0.0033 | 0.0102 | 0.0062 | 0.0133 | <0.0029 | 0.735 |
| Ce140 | 1.127 | 3.06 | 11.68 | 3.13 | 3.08 | 33.2 | 2.82 | 3.45 | 7.79 | 3.71 | 2.19 | 3.69 | 7.94 | 37.08 |
| Pr141 | 0.0142 | 0.086 | 0.219 | 0.1869 | 0.1829 | 0.449 | 0.1272 | 0.0275 | 0.0344 | 0.1067 | 0.0659 | 0.1484 | 0.0456 | 1.113 |
| Nd146 | 0.432 | 1.143 | 2.67 | 2.139 | 2.33 | 7.13 | 1.644 | 0.498 | 0.719 | 1.67 | 1.069 | 2.04 | 0.86 | 15.01 |
| Sm147 | 0.855 | 1.532 | 3.37 | 2.79 | 2.91 | 12.22 | 2.32 | 1.092 | 1.778 | 2.48 | 1.59 | 3.07 | 1.806 | 23.21 |
| Eu153 | 0.322 | 0.753 | 1.52 | 1.261 | 1.323 | 6.33 | 1.059 | 0.556 | 0.596 | 1.053 | 0.751 | 1.337 | 1.052 | 3.56 |
| Gd157 | 4.42 | 6.6 | 14.4 | 12.05 | 12.01 | 47.49 | 10.11 | 6.03 | 10.58 | 11.03 | 6.38 | 12.95 | 8.83 | 108.07 |
| Tb159 | 1.453 | 2.033 | 4.01 | 3.57 | 3.51 | 12.56 | 3.07 | 1.97 | 3.59 | 3.41 | 2.015 | 4.2 | 2.657 | 31.56 |
| Dy163 | 19.83 | 26.38 | 49.81 | 43.19 | 43.53 | 138.98 | 38.21 | 25.48 | 46.98 | 42.68 | 25.53 | 49.86 | 33.25 | 376.57 |
| Ho165 | 7.8 | 10.8 | 18.89 | 16.26 | 16.2 | 47.94 | 14.44 | 9.96 | 18.35 | 15.85 | 9.36 | 18.02 | 12.36 | 133.63 |
| Er166 | 37.11 | 53.8 | 87.1 | 74.17 | 73.95 | 206.26 | 67.18 | 47.35 | 86.46 | 75.18 | 47.62 | 86.02 | 55.12 | 559.49 |
| Tm169 | 8.02 | 12.3 | 18.49 | 15.74 | 15.6 | 40.81 | 14.36 | 10.31 | 18.16 | 16.77 | 11.09 | 19.62 | 11.81 | 106.41 |
| Yb173 | 79.19 | 129.94 | 182.76 | 155.53 | 154.4 | 384.3 | 144.75 | 105.47 | 177.22 | 159.55 | 114.97 | 189.42 | 115.04 | 945.72 |
| Lu175 | 17.74 | 29.52 | 37.96 | 32.53 | 32.81 | 78.93 | 31.19 | 22.47 | 35.91 | 32.67 | 24.52 | 39.03 | 22.41 | 169.79 |
| Hf178 | 6504 | 5664.5 | 5961.29 | 6724.47 | 6410.72 | 8691.78 | 6427.68 | 7597.89 | 10506.46 | 7029.74 | 5681.46 | 8751.14 | 7809.88 | 9081.85 |
| Th232 | 12.53 | 16.92 | 49.38 | 13.37 | 15.39 | 90.14 | 12.78 | 20.67 | 38.55 | 14.99 | 8.11 | 11.35 | 67.1 | 405.17 |
| U238 | 21.62 | 33.8 | 32.1 | 19.48 | 26.95 | 72.66 | 20.1 | 35.06 | 74.81 | 27.18 | 20.58 | 25.26 | 187.27 | 378.62 |
| Th/U | 0.6 | 0.5 | 1.5 | 0.7 | 0.6 | 1.2 | 0.6 | 0.6 | 0.5 | 0.6 | 0.4 | 0.4 | 0.4 | 1.1 |
| Ce/Ce* | nd | 17 | 23 | 15 | 12 | 64 | 14 | nd | nd | 28 | 27 | 20 | nd | 10 |
| Eu/Eu* | 0.5 | 0.7 | 0.7 | 0.7 | 0.7 | 0.8 | 0.7 | 0.7 | 0.4 | 0.6 | 0.7 | 0.6 | 0.8 | 0.2 |
| T C | 734 | 752 | 922 | 845 | 841 | 769 | 868 | 829 | 674 | 877 | 825 | 906 | 678 | 795 |

| Element | MD26-36-1 | MD26-50-1 | MD26-52-1 | MD26-54-1 | MD26-49-1 | MD8-5-1 | MD8-1-1 | MD8-6-1 | MD8-6-2 | MD22A-7-1 | MD22A-14-1 | MD22A-13-1 | MD22A-23-1 |
|---|---|---|---|---|---|---|---|---|---|---|---|---|---|
| P31 | 153.94 | 170.41 | 305.01 | 598.61 | 609.65 | 176.67 | 269.36 | 212.70 | 112.58 | 1465.81 | 1064.35 | 592.91 | 937.91 |
| Ca43 | <50.27 | <50.61 | <45.94 | <53.51 | <62.28 | 398.36 | 699.72 | 297.23 | 235.99 | 1616.52 | 380.55 | <56.27 | <44.50 |
| Ti49 | 4.06 | 11.72 | 6.11 | 36.89 | 17.95 | 17.93 | 8.99 | 44.72 | 28.12 | 3.91 | 9.61 | 4.72 | 17.12 |
| Sr88 | 0.236 | 0.071 | 0.263 | 0.856 | 0.344 | 0.19 | 0.25 | 0.20 | 0.14 | 2.12 | 0.68 | <0.103 | 0.21 |
| Y89 | 196.05 | 147.36 | 104.15 | <0.0094 | <0.0113 | 315.30 | 490.53 | 921.59 | 234.31 | 862.14 | 1665.93 | 1365.41 | 1075.56 |
| Nb93 | 0.774 | 0.173 | 1.833 | 5.69 | 7.37 | 0.48 | 0.51 | 0.56 | 0.30 | 3.36 | 4.90 | 4.23 | 2.05 |
| La139 | 0.0229 | <0.0027 | 0.0214 | 0.0717 | 0.0234 | 0.01 | 0.01 | 0.09 | <0.0045 | 5.88 | 0.03 | <0.025 | 0.03 |
| Ce140 | 7.58 | 1.011 | 9.66 | 30.57 | 35.07 | 8.00 | 10.80 | 11.05 | 6.00 | 29.42 | 17.11 | 15.32 | 6.69 |
| Pr141 | 0.0644 | 0.0155 | 0.22 | 0.835 | 0.347 | 0.10 | 0.17 | 0.54 | 0.05 | 2.35 | 0.10 | 0.07 | 0.20 |
| Nd146 | 1.086 | 0.175 | 3.84 | 15.55 | 6.34 | 1.59 | 2.91 | 6.86 | 0.87 | 11.64 | 1.59 | 1.41 | 2.80 |
| Sm147 | 2.18 | 0.341 | 7.53 | 30.01 | 14.2 | 2.53 | 4.71 | 7.99 | 1.68 | 4.03 | 3.71 | 3.55 | 5.24 |
| Eu153 | 0.96 | 0.1734 | 1.752 | 6.15 | 3.25 | 0.48 | 0.93 | 1.43 | 0.35 | 0.45 | 0.81 | 0.57 | 0.59 |
| Gd157 | 10.83 | 2.107 | 39.48 | 135.27 | 84.24 | 9.16 | 17.51 | 26.69 | 7.13 | 12.61 | 22.28 | 20.21 | 23.74 |
| Tb159 | 3.27 | 0.73 | 12.07 | 39.02 | 26.1 | 2.67 | 4.69 | 7.46 | 2.06 | 4.26 | 8.33 | 7.27 | 7.51 |
| Dy163 | 41.2 | 10.36 | 148.94 | 455.47 | 321.51 | 29.08 | 49.64 | 86.67 | 23.17 | 61.09 | 123.17 | 104.38 | 95.70 |
| Ho165 | 15.87 | 4.45 | 53.8 | 158.17 | 114.67 | 10.08 | 15.92 | 30.22 | 7.74 | 26.02 | 53.13 | 43.33 | 34.48 |
| Er166 | 71.78 | 23.71 | 234.62 | 660.55 | 481.79 | 45.48 | 67.25 | 131.65 | 34.62 | 131.82 | 272.78 | 215.02 | 152.08 |
| Tm169 | 15.06 | 5.56 | 45.3 | 122.97 | 91.05 | 10.03 | 13.71 | 25.71 | 7.22 | 29.16 | 60.51 | 45.49 | 29.54 |
| Yb173 | 145 | 60.81 | 409.47 | 1060.85 | 796.54 | 90.48 | 118.16 | 216.60 | 65.45 | 291.48 | 606.57 | 444.73 | 272.99 |
| Lu175 | 27.55 | 13.75 | 76.94 | 197.2 | 149.69 | 17.96 | 22.40 | 40.85 | 12.62 | 62.52 | 131.53 | 94.72 | 52.94 |
| Hf178 | 8632.42 | 7021.26 | 8411.95 | 7487.65 | 9751.75 | 8530.67 | 8869.86 | 7682.69 | 8530.67 | 10726.93 | 11091.56 | 11091.56 | 8573.06 |
| Th232 | 70.61 | 7.3 | 146.2 | 430.7 | 234.85 | 106.46 | 153.71 | 325.90 | 56.30 | 162.05 | 159.13 | 180.43 | 20.66 |
| U238 | 185.5 | 23.01 | 215.62 | 380.18 | 246 | 143.52 | 131.17 | 282.86 | 67.16 | 331.28 | 334.05 | 321.78 | 35.82 |
| Th/U | 0.4 | 0.3 | 0.7 | 1.1 | 1.0 | 0.7 | 1.2 | 1.2 | 0.8 | 0.5 | 0.5 | 0.6 | 0.6 |
| Ce/Ce* | 48 | nd | 35 | 31 | 95 | 70 | 63 | 12 | nd | 2 | 78 | nd | 21 |
| Eu/Eu* | 0.6 | 0.6 | 0.3 | 0.3 | 0.3 | 0.3 | 0.3 | 0.3 | 0.3 | 0.2 | 0.3 | 0.2 | 0.2 |
| T C | 667 | 755 | 699 | 870 | 795 | 795 | 732 | 892 | 841 | 665 | 737 | 679 | 791 |

| Element | MD22A-24-1 | MD22A-24-2 | MD22A-31-1 | MD22A-36-1 | MD22A-36-2 | MD22A-60-1 | MD22A-121-1 | MD22A-134-1 | MD22A-134-2 | MD22A-144-1 | MD17A-2-1 | MD17A-2-2 | MD17A-11-1 | MD17A-11-2 |
|---|---|---|---|---|---|---|---|---|---|---|---|---|---|---|
| P31 | 439.65 | 196.38 | 708.78 | 474.06 | 512.71 | 1069.63 | 499.24 | 575.92 | 672.31 | 630.86 | 401.06 | 449.71 | 295.64 | 403.08 |
| Ca43 | <39.69 | 36.30 | 107.71 | <56.41 | <38.63 | <49.22 | <51.76 | 97.05 | <64.14 | 66.18 | <141.43 | <138.08 | 262.59 | 237.71 |
| Ti49 | 2.60 | 2.93 | 5.25 | 4.09 | 2.56 | 5.77 | 2.56 | 6.55 | 4.76 | 3.52 | 20.02 | 11.47 | 17.87 | 18.58 |
| Sr88 | 0.18 | 0.06 | 0.28 | 0.21 | 0.15 | 0.25 | 0.18 | 0.23 | 0.20 | 0.14 | 0.14 | 0.24 | 0.15 | 0.19 |
| Y89 | 1359.20 | 236.65 | 1594.58 | 952.67 | 924.65 | 2105.25 | 767.22 | 1043.22 | 1011.39 | 1002.39 | 1547.47 | 1355.15 | 1022.84 | 1198.00 |
| Nb93 | 2.24 | 0.96 | 4.25 | 3.41 | 4.10 | 6.49 | 3.00 | 2.01 | 3.07 | 3.55 | 2.20 | 1.26 | 1.84 | 1.90 |
| La139 | <0.0183 | <0.0128 | 0.28 | <0.025 | <0.0172 | <0.0187 | 0.10 | 0.06 | <0.026 | 0.23 | 0.01 | 0.02 | 0.01 | 0.01 |
| Ce140 | 10.03 | 3.92 | 16.79 | 12.29 | 11.35 | 23.71 | 11.43 | 11.94 | 11.98 | 14.95 | 38.78 | 28.43 | 23.66 | 28.34 |
| Pr141 | 0.13 | 0.01 | 0.19 | 0.02 | 0.03 | 0.13 | 0.06 | 0.11 | 0.05 | 0.12 | 0.18 | 0.23 | 0.13 | 0.16 |
| Nd146 | 2.14 | 0.16 | 2.19 | 0.56 | 0.59 | 2.52 | 0.62 | 1.65 | 1.02 | 0.95 | 3.59 | 4.29 | 2.51 | 2.95 |
| Sm147 | 4.67 | 0.38 | 3.93 | 1.82 | 1.78 | 6.18 | 1.35 | 3.28 | 2.43 | 2.16 | 8.08 | 8.53 | 5.14 | 6.19 |
| Eu153 | 0.82 | 0.06 | 0.75 | 0.21 | 0.22 | 1.07 | 0.18 | 0.40 | 0.32 | 0.23 | 5.13 | 4.60 | 2.96 | 3.74 |
| Gd157 | 24.56 | 2.72 | 23.01 | 11.90 | 11.53 | 38.29 | 9.10 | 18.12 | 14.12 | 13.23 | 47.65 | 38.14 | 27.01 | 32.82 |
| Tb159 | 8.44 | 1.14 | 8.40 | 4.57 | 4.37 | 13.26 | 3.66 | 6.23 | 5.30 | 4.99 | 14.24 | 11.12 | 8.04 | 9.82 |
| Dy163 | 112.51 | 16.75 | 120.96 | 68.57 | 66.86 | 182.42 | 54.21 | 84.29 | 74.99 | 73.88 | 158.67 | 127.05 | 94.96 | 114.85 |
| Ho165 | 45.22 | 7.35 | 50.43 | 29.78 | 29.52 | 71.68 | 23.77 | 33.51 | 31.55 | 31.51 | 51.03 | 43.76 | 32.71 | 39.10 |
| Er166 | 216.44 | 38.70 | 248.57 | 154.21 | 150.83 | 334.46 | 125.29 | 159.36 | 158.65 | 162.43 | 213.30 | 195.60 | 146.88 | 171.90 |
| Tm169 | 45.84 | 8.99 | 53.02 | 35.10 | 33.46 | 68.66 | 28.38 | 33.59 | 35.53 | 36.55 | 41.71 | 40.42 | 30.59 | 35.90 |
| Yb173 | 432.20 | 91.35 | 515.45 | 355.75 | 331.77 | 643.01 | 286.52 | 322.98 | 361.21 | 369.59 | 353.99 | 365.92 | 282.12 | 320.75 |
| Lu175 | 91.42 | 20.01 | 108.43 | 77.88 | 71.29 | 131.32 | 63.33 | 66.89 | 78.12 | 79.83 | 65.52 | 73.19 | 53.55 | 62.25 |
| Hf178 | 8030.36 | 6758.39 | 9005.53 | 11498.59 | 9293.84 | 9242.97 | 11710.58 | 9327.76 | 12092.17 | 11328.99 | 7402.85 | 8479.79 | 8980.09 | 8293.23 |
| Th232 | 121.39 | 24.90 | 184.60 | 111.05 | 123.42 | 468.68 | 116.26 | 140.11 | 130.34 | 151.52 | 95.67 | 72.03 | 45.91 | 62.25 |
| U238 | 209.47 | 81.36 | 318.04 | 269.11 | 276.31 | 544.81 | 262.28 | 217.43 | 269.00 | 327.84 | 75.78 | 62.93 | 54.76 | 65.49 |
| Th/U | 0.6 | 0.3 | 0.6 | 0.4 | 0.4 | 0.9 | 0.4 | 0.6 | 0.5 | 0.5 | 1.3 | 1.1 | 0.8 | 1.0 |
| Ce/Ce* | nd | nd | 18 | nd | nd | nd | 37 | 36 | nd | 22 | 240 | 111 | 208 | 202 |
| Eu/EU* | 0.2 | 0.2 | 0.2 | 0.1 | 0.1 | 0.2 | 0.2 | 0.2 | 0.2 | 0.1 | 0.8 | 0.8 | 0.8 | 0.8 |
| T C | 635 | 643 | 687 | 668 | 634 | 695 | 634 | 705 | 680 | 657 | 806 | 753 | 795 | 799 |

| Element | MD17A-13-1 | MD17A-13-2 | MD17A-70-1 | MD17A-70-2 | MD17A-117-1 | MD17A-139-1 | MD17A-156-1 | MD17A-205-1 | MD17A-234-1 | MD32-1-1 | MD32-1-2 | MD32-2-1 | MD32-3-1 |
|---|---|---|---|---|---|---|---|---|---|---|---|---|---|
| P31 | 456.90 | 370.80 | 569.36 | 548.72 | 538.84 | 464.33 | 602.25 | 417.43 | 711.82 | 257.44 | 2716.12 | 149.40 | 247.63 |
| Ca43 | <179.59 | <176.83 | 210.05 | <148.96 | <198.87 | 169.69 | <205.30 | <265.64 | <207.32 | 863.60 | 4377.54 | <144.47 | 140.77 |
| Ti49 | 13.75 | 9.03 | 16.68 | 29.68 | 10.55 | 18.05 | 26.73 | 9.34 | 18.74 | 17.10 | 7.19 | 6.23 | 3.63 |
| Sr88 | 0.17 | <0.069 | 0.19 | 0.15 | 0.20 | 0.25 | 0.12 | <0.108 | 0.19 | 0.19 | 13.48 | 0.42 | 0.22 |
| Y89 | 1347.47 | 1115.90 | 1445.65 | 2355.60 | 1484.61 | 1496.65 | 1891.74 | 1186.67 | 2266.36 | 778.85 | 1569.82 | 357.48 | 696.29 |
| Nb93 | 1.88 | 1.41 | 1.36 | 3.23 | 1.25 | 1.49 | 2.69 | 1.28 | 2.41 | 2.29 | 8.17 | 4.98 | 3.61 |
| La139 | 0.02 | 0.03 | 0.02 | 0.01 | 0.01 | 0.01 | 0.02 | 0.02 | 0.05 | <0.0050 | 0.02 | <0.0026 | 0.01 |
| Ce140 | 31.14 | 25.88 | 31.65 | 62.79 | 19.69 | 34.01 | 50.58 | 23.70 | 55.83 | 14.49 | 33.79 | 7.75 | 15.36 |
| Pr141 | 0.23 | 0.38 | 0.27 | 0.29 | 0.13 | 0.20 | 0.25 | 0.27 | 0.61 | 0.05 | 0.07 | 0.02 | 0.04 |
| Nd146 | 4.17 | 6.48 | 4.97 | 5.58 | 2.53 | 3.96 | 4.89 | 4.78 | 10.49 | 1.19 | 1.45 | 0.39 | 0.69 |
| Sm147 | 8.51 | 10.82 | 9.66 | 12.83 | 6.12 | 8.80 | 11.53 | 8.65 | 19.94 | 3.04 | 3.99 | 1.34 | 1.86 |
| Eu153 | 4.92 | 5.33 | 5.26 | 8.28 | 3.71 | 5.06 | 7.01 | 4.52 | 10.31 | 1.78 | 0.48 | 0.67 | 0.33 |
| Gd157 | 41.39 | 38.39 | 41.43 | 79.46 | 31.85 | 42.66 | 63.16 | 35.91 | 78.80 | 16.28 | 25.97 | 9.64 | 11.36 |
| Tb159 | 11.98 | 10.37 | 11.80 | 22.81 | 10.14 | 12.65 | 17.96 | 10.12 | 21.44 | 5.50 | 9.81 | 3.29 | 4.37 |
| Dy163 | 134.03 | 112.08 | 136.01 | 250.46 | 127.32 | 142.28 | 197.42 | 114.91 | 231.60 | 70.15 | 140.92 | 36.88 | 62.72 |
| Ho165 | 43.67 | 36.50 | 46.37 | 78.78 | 47.19 | 48.95 | 63.49 | 38.91 | 74.91 | 26.06 | 55.83 | 11.97 | 25.09 |
| Er166 | 189.88 | 158.35 | 208.41 | 321.45 | 227.56 | 215.42 | 266.63 | 174.69 | 318.83 | 127.78 | 287.66 | 51.94 | 129.01 |
| Tm169 | 38.40 | 32.41 | 43.16 | 61.60 | 50.11 | 44.34 | 52.33 | 36.22 | 63.80 | 27.98 | 65.38 | 10.75 | 29.59 |
| Yb173 | 337.75 | 291.62 | 392.56 | 517.72 | 477.04 | 398.05 | 451.23 | 331.36 | 556.50 | 265.83 | 623.74 | 100.13 | 278.97 |
| Lu175 | 65.24 | 57.35 | 80.31 | 94.23 | 102.11 | 80.17 | 87.15 | 69.06 | 110.31 | 55.16 | 126.01 | 20.78 | 55.77 |
| Hf178 | 8081.24 | 8259.31 | 8878.34 | 9192.09 | 8386.51 | 9056.41 | 9226.01 | 8479.79 | 9751.75 | 12507.68 | 11532.51 | 10031.59 | 8454.35 |
| Th232 | 74.27 | 58.96 | 77.94 | 170.81 | 30.94 | 92.25 | 141.63 | 55.04 | 157.92 | 71.96 | 620.07 | 36.05 | 91.84 |
| U238 | 63.83 | 50.22 | 69.69 | 119.03 | 41.15 | 74.56 | 102.40 | 49.48 | 111.00 | 101.04 | 953.55 | 587.67 | 413.14 |
| Th/U | 1.2 | 1.2 | 1.1 | 1.4 | 0.8 | 1.2 | 1.4 | 1.1 | 1.4 | 0.7 | 0.7 | 0.1 | 0.2 |
| Ce/Ce* | 129 | 59 | 104 | 248 | 137 | 196 | 185 | 76 | 77 | nd | 211 | nd | 243 |
| Eu/EU* | 0.8 | 0.8 | 0.8 | 0.8 | 0.8 | 0.8 | 0.8 | 0.8 | 0.8 | 0.8 | 0.1 | 0.6 | 0.2 |
| T C | 770 | 732 | 788 | 847 | 746 | 796 | 835 | 735 | 799 | 790 | 713 | 701 | 659 |

| Element | MD32-7-1 | MD32-10-2 | MD32-16-1 | MD32-21-1 | MD32-21-2 | MD32-8-1 | MD2-80-1 | MD2-62-1 | MD2-124-1 | MD2-129-1 | MD6-80-1 | MD6-84b-1 | MD6-85-1 |
|---|---|---|---|---|---|---|---|---|---|---|---|---|---|
| P31 | 323.01 | 200.45 | 194.39 | 238.86 | 1040.61 | 282.27 | 285.84 | 319.79 | 768.25 | 341.53 | 386.94 | 161.15 | 1092.73 |
| Ca43 | 288.36 | 304.43 | 190.53 | 122.06 | 2564.59 | <145.84 | 479.75 | 362.79 | 835.72 | 1061.38 | 586.76 | 366.57 | <242.51 |
| Ti49 | 6.54 | 13.66 | 12.75 | 3.77 | 18.66 | 41.65 | 11.54 | 3.18 | 3.69 | 4.08 | 5.02 | 4.87 | 4.54 |
| Sr88 | 0.42 | 0.15 | 0.14 | 0.23 | 10.47 | 0.27 | 0.22 | 0.27 | 0.50 | 0.16 | 0.32 | <0.121 | 0.51 |
| Y89 | 1279.99 | 812.00 | 677.74 | 743.29 | 3829.44 | 1531.03 | 1658.52 | 993.54 | 1405.88 | 1091.16 | 1870.19 | 254.31 | 2570.69 |
| Nb93 | 3.29 | 2.24 | 1.64 | 2.49 | 5.75 | 5.11 | 0.94 | 10.46 | 33.06 | 10.06 | 8.37 | 6.25 | 52.06 |
| La139 | 0.01 | <0.0028 | 0.00 | 0.00 | 0.28 | 0.01 | 0.04 | <0.0068 | <0.0056 | <0.0076 | 0.02 | <0.0053 | 0.01 |
| Ce140 | 18.76 | 12.32 | 10.35 | 5.64 | 30.72 | 31.90 | 9.34 | 11.21 | 8.61 | 18.22 | 9.89 | 7.64 | 27.03 |
| Pr141 | 0.09 | 0.05 | 0.05 | 0.07 | 0.62 | 0.20 | 0.27 | 0.06 | 0.01 | 0.07 | 0.22 | 0.02 | 0.04 |
| Nd146 | 1.97 | 1.16 | 0.98 | 1.29 | 9.82 | 3.87 | 4.19 | 1.14 | 0.11 | 1.45 | 4.01 | 0.31 | 0.97 |
| Sm147 | 5.04 | 2.69 | 2.41 | 2.80 | 19.05 | 7.96 | 7.37 | 3.02 | 0.88 | 4.03 | 8.57 | 1.49 | 3.51 |
| Eu153 | 0.78 | 1.63 | 1.45 | 0.41 | 2.18 | 4.58 | 3.43 | 0.37 | 0.18 | 0.54 | 1.29 | 0.60 | 0.11 |
| Gd157 | 27.48 | 15.60 | 13.49 | 15.76 | 95.33 | 41.83 | 40.05 | 17.96 | 8.90 | 24.33 | 44.56 | 11.59 | 27.64 |
| Tb159 | 9.50 | 5.48 | 4.59 | 5.58 | 31.76 | 13.17 | 12.45 | 6.37 | 4.99 | 8.34 | 14.81 | 3.89 | 13.21 |
| Dy163 | 123.57 | 72.75 | 62.27 | 75.78 | 404.67 | 165.60 | 151.95 | 87.30 | 96.38 | 107.02 | 186.12 | 35.54 | 207.74 |
| Ho165 | 45.08 | 28.35 | 23.65 | 28.47 | 150.18 | 59.29 | 55.66 | 33.94 | 46.92 | 39.41 | 68.87 | 8.60 | 88.84 |
| Er166 | 212.02 | 139.47 | 118.09 | 140.40 | 704.20 | 270.16 | 264.81 | 172.02 | 286.01 | 182.81 | 311.69 | 27.39 | 467.91 |
| Tm169 | 45.18 | 30.96 | 25.92 | 31.18 | 148.70 | 55.48 | 56.11 | 37.15 | 76.72 | 36.85 | 64.15 | 4.19 | 103.75 |
| Yb173 | 408.49 | 288.23 | 248.45 | 294.50 | 1309.75 | 497.53 | 527.02 | 351.62 | 801.70 | 313.19 | 555.54 | 32.33 | 962.02 |
| Lu175 | 77.99 | 60.44 | 52.29 | 60.44 | 254.49 | 96.34 | 111.43 | 71.58 | 167.78 | 61.25 | 108.13 | 5.79 | 187.10 |
| Hf178 | 14805.71 | 7402.85 | 8166.03 | 7759.00 | 13762.69 | 8479.79 | 7428.29 | 10455.58 | 11481.63 | 14263.00 | 8369.55 | 14500.43 | 15170.34 |
| Th232 | 209.59 | 66.14 | 42.94 | 104.18 | 712.42 | 197.44 | 363.17 | 149.37 | 32.05 | 370.71 | 160.49 | 34.69 | 389.52 |
| U238 | 732.84 | 91.73 | 62.29 | 378.49 | 913.74 | 168.34 | 275.76 | 540.32 | 1095.31 | 525.37 | 363.92 | 1173.22 | 1549.83 |
| Th/U | 0.3 | 0.7 | 0.7 | 0.3 | 0.8 | 1.2 | 1.32 | 0.28 | 0.03 | 0.71 | 0.44 | 0.03 | 0.25 |
| Ce/Ce* | 171 | nd | 189 | 82 | 18 | 212 | 23 | nd | nd | nd | 39 | nd | 358 |
| Eu/EU* | 0.2 | 0.8 | 0.8 | 0.2 | 0.2 | 0.8 | 0.6 | 0.2 | 0.2 | 0.2 | 0.2 | 0.4 | 0.0 |
| T C | 705 | 769 | 763 | 662 | 799 | 884 | 754 | 649 | 660 | 668 | 684 | 681 | 676 |

| Element | MD6-124-1 | MD6-124-2 | MD6-12-1 | MD6-67-1 | MD6-62-1 | MD6-95-1 | MD6-138-1 | MD29-1-1 | MD29-33-1 | MD29-70-1 | MD29-65-1 | MD29-65-2 | MD29-66-1 | MD29-90-1 |
|---|---|---|---|---|---|---|---|---|---|---|---|---|---|---|
| P31 | 104.68 | 96.52 | 159.37 | 180.14 | 399.58 | 210.44 | 73.78 | 163.45 | 114.36 | 188.77 | 376.63 | 342.52 | 233.29 | 1028.16 |
| Ca43 | 435.34 | 573.89 | 576.38 | 326.30 | 556.60 | 345.17 | 327.77 | 272.02 | 214.82 | 453.85 | <358.58 | <170.05 | <196.89 | 401.66 |
| Ti49 | 3.34 | 3.26 | 3.59 | 4.32 | 3.70 | 4.04 | 3.73 | 3.69 | 3.40 | 5.09 | 7.99 | 4.40 | 3.14 | 8.38 |
| Sr88 | 0.22 | <0.137 | 0.13 | 0.24 | 0.21 | 0.17 | 0.14 | 0.12 | 0.12 | 0.13 | 0.27 | 0.20 | 0.17 | 0.54 |
| Y89 | 279.16 | 237.17 | 322.49 | 292.82 | 780.64 | 330.45 | 57.21 | 444.52 | 299.93 | 268.73 | 790.62 | 1583.85 | 677.88 | 2527.26 |
| Nb93 | 6.67 | 4.94 | 12.44 | 16.23 | 23.51 | 9.59 | 3.39 | 2.99 | 7.31 | 1.20 | 6.26 | 4.65 | 4.66 | 26.92 |
| La139 | <0.0056 | <0.0061 | 0.00 | <0.0043 | <0.0027 | 0.00 | <0.0031 | <0.0028 | 0.00 | <0.0041 | <0.0064 | 0.01 | <0.0035 | 0.00 |
| Ce140 | 4.30 | 4.12 | 10.44 | 7.64 | 9.03 | 6.68 | 2.22 | 7.50 | 3.92 | 8.08 | 12.86 | 15.94 | 9.50 | 20.57 |
| Pr141 | 0.01 | 0.01 | 0.02 | 0.01 | 0.01 | 0.01 | 0.01 | 0.01 | 0.01 | 0.02 | 0.02 | 0.21 | 0.03 | 0.04 |
| Nd146 | 0.29 | 0.27 | 0.51 | 0.24 | 0.29 | 0.21 | 0.19 | 0.27 | 0.19 | 0.37 | 0.37 | 3.84 | 0.59 | 0.87 |
| Sm147 | 1.82 | 1.33 | 2.47 | 1.16 | 1.04 | 1.05 | 0.98 | 1.08 | 1.27 | 1.07 | 1.30 | 8.22 | 1.77 | 3.40 |
| Eu153 | 1.20 | 0.88 | 0.75 | 0.42 | 0.26 | 0.33 | 0.68 | 0.31 | 0.57 | 0.55 | 0.34 | 1.63 | 0.14 | 0.14 |
| Gd157 | 16.00 | 11.57 | 22.03 | 11.72 | 8.93 | 9.16 | 8.87 | 7.42 | 11.01 | 5.64 | 9.49 | 43.54 | 11.00 | 27.30 |
| Tb159 | 5.21 | 3.73 | 6.62 | 4.29 | 4.08 | 3.55 | 2.40 | 2.82 | 3.90 | 1.87 | 3.95 | 14.10 | 4.19 | 13.60 |
| Dy163 | 43.60 | 34.13 | 54.62 | 41.96 | 64.38 | 38.43 | 14.17 | 39.10 | 38.77 | 24.19 | 59.59 | 178.51 | 58.18 | 220.44 |
| Ho165 | 9.05 | 7.62 | 11.18 | 9.85 | 27.93 | 10.94 | 1.90 | 15.02 | 9.59 | 8.92 | 25.35 | 64.25 | 23.06 | 93.53 |
| Er166 | 24.13 | 22.24 | 29.97 | 29.16 | 154.11 | 43.56 | 3.54 | 74.60 | 29.52 | 42.35 | 138.41 | 292.31 | 115.71 | 508.39 |
| Tm169 | 3.38 | 3.18 | 4.22 | 4.19 | 35.60 | 8.58 | 0.40 | 16.69 | 4.50 | 9.20 | 33.85 | 59.59 | 26.12 | 122.93 |
| Yb173 | 23.47 | 22.99 | 31.58 | 30.80 | 337.76 | 77.11 | 2.46 | 158.32 | 30.93 | 85.91 | 350.29 | 519.83 | 253.21 | 1192.66 |
| Lu175 | 4.01 | 4.01 | 5.97 | 6.13 | 68.29 | 15.17 | 0.45 | 31.96 | 4.65 | 17.46 | 76.97 | 96.57 | 53.74 | 231.64 |
| Hf178 | 13618.54 | 12829.92 | 15424.73 | 16272.71 | 15653.68 | 16798.46 | 14279.96 | 9183.61 | 12855.36 | 10684.53 | 22946.30 | 7156.94 | 11710.58 | 12253.29 |
| Th232 | 17.10 | 15.74 | 67.74 | 47.67 | 36.27 | 32.12 | 7.64 | 103.88 | 3.69 | 30.11 | 36.94 | 279.45 | 138.12 | 305.86 |
| U238 | 1277.97 | 902.81 | 1241.00 | 1188.39 | 636.82 | 686.61 | 240.78 | 301.18 | 1052.61 | 93.19 | 986.42 | 372.33 | 469.38 | 4357.42 |
| Th/U | 0.01 | 0.02 | 0.05 | 0.04 | 0.06 | 0.05 | 0.03 | 0.34 | 0.00 | 0.32 | 0.04 | 0.75 | 0.29 | 0.07 |
| Ce/Ce* | nd | nd | 355 | nd | nd | 312 | nd | nd | 211 | nd | nd | 75 | nd | 394 |
| Eu/Eu* | 0.7 | 0.7 | 0.3 | 0.4 | 0.3 | 0.3 | 0.7 | 0.3 | 0.5 | 0.7 | 0.3 | 0.3 | 0.1 | 0.0 |
| T C | 653 | 651 | 658 | 672 | 661 | 667 | 661 | 660 | 654 | 685 | 722 | 674 | 648 | 726 |

| Element | MD29-91-1 | MD29-91-2 | MD29-104-1 | MD29-104-2 | MD33-25-1 | MD33-27-1 | MD-33-29-1 | MD33-29-2 | MD33-43-1 | MD33-46-1 | MD-33-58-1 | MD33-62-1 | MD33-148-1 |
|---|---|---|---|---|---|---|---|---|---|---|---|---|---|
| P31 | 244.51 | 230.83 | 411.79 | 383.72 | 464.22 | 413.06 | 109.31 | 407.50 | 295.21 | 1090.19 | 474.66 | 301.95 | 236.06 |
| Ca43 | 306.29 | <180.83 | 308.64 | <188.03 | <67.59 | 147.14 | <57.38 | <56.14 | <49.18 | 76.94 | <47.86 | <48.55 | <45.45 |
| Ti49 | 5.03 | 3.38 | 5.48 | 8.71 | 7.01 | 7.15 | 3.75 | 4.09 | 3.12 | 5.24 | 3.74 | 2.93 | 3.20 |
| Sr88 | 0.12 | 0.17 | 0.37 | 0.33 | 0.45 | 0.61 | 0.07 | 0.32 | 0.14 | 0.94 | 0.22 | 0.23 | 0.05 |
| Y89 | 424.51 | 1221.85 | 1290.46 | 2791.92 | 20.93 | 1213.00 | 43.77 | 0.00 | 796.70 | 1448.00 | 0.00 | 0.00 | 478.46 |
| Nb93 | 2.71 | 2.40 | 16.37 | 5.58 | 5.71 | 4.24 | 2.15 | 3.07 | 1.19 | 4.51 | 15.50 | 5.49 | 2.43 |
| La139 | <0.0035 | 0.01 | <0.0044 | 0.01 | 0.00 | <0.0031 | <0.0030 | 0.01 | 0.00 | 0.04 | <0.0026 | 0.02 | <0.0024 |
| Ce140 | 9.84 | 10.82 | 12.96 | 22.54 | 19.13 | 10.07 | 4.09 | 9.16 | 11.88 | 31.80 | 12.56 | 11.96 | 5.05 |
| Pr141 | 0.02 | 0.13 | 0.03 | 0.31 | 0.20 | 0.04 | 0.01 | 0.20 | 0.05 | 0.08 | 0.03 | 0.04 | 0.01 |
| Nd146 | 0.39 | 2.77 | 0.83 | 6.10 | 4.10 | 0.89 | 0.27 | 4.05 | 0.91 | 1.38 | 0.76 | 0.93 | 0.26 |
| Sm147 | 1.18 | 6.04 | 2.66 | 14.69 | 10.29 | 2.47 | 1.04 | 9.04 | 2.15 | 3.39 | 3.21 | 2.58 | 0.79 |
| Eu153 | 0.48 | 0.88 | 0.27 | 1.68 | 0.82 | 0.24 | 0.44 | 1.00 | 0.47 | 0.67 | 0.09 | 0.21 | 0.08 |
| Gd157 | 7.11 | 30.64 | 20.43 | 79.29 | 60.65 | 16.63 | 4.96 | 50.64 | 11.59 | 20.27 | 25.57 | 18.38 | 5.84 |
| Tb159 | 2.52 | 10.02 | 8.05 | 25.37 | 20.59 | 6.16 | 1.02 | 16.60 | 4.06 | 7.58 | 10.35 | 7.15 | 2.37 |
| Dy163 | 35.23 | 128.19 | 117.88 | 317.77 | 274.01 | 88.79 | 7.01 | 212.34 | 56.22 | 111.23 | 150.82 | 104.37 | 36.15 |
| Ho165 | 13.92 | 47.46 | 47.97 | 113.73 | 105.57 | 36.26 | 1.35 | 78.87 | 23.10 | 47.17 | 61.59 | 44.54 | 15.33 |
| Er166 | 72.21 | 222.62 | 244.57 | 514.81 | 481.72 | 176.99 | 3.55 | 348.71 | 117.96 | 248.76 | 293.96 | 224.73 | 78.57 |
| Tm169 | 17.54 | 46.07 | 55.31 | 102.14 | 98.06 | 38.22 | 0.52 | 67.91 | 27.35 | 58.81 | 60.75 | 49.22 | 17.77 |
| Yb173 | 173.55 | 403.37 | 517.31 | 871.00 | 897.68 | 369.07 | 3.93 | 607.94 | 290.13 | 622.17 | 562.48 | 480.42 | 181.86 |
| Lu175 | 35.54 | 77.06 | 104.46 | 163.72 | 165.51 | 71.99 | 0.61 | 116.08 | 62.95 | 135.37 | 106.46 | 96.77 | 35.90 |
| Hf178 | 11651.23 | 8912.25 | 15187.30 | 10167.26 | 11218.76 | 11931.06 | 14975.30 | 9989.19 | 9836.55 | 13219.98 | 12541.60 | 10141.82 | 10141.82 |
| Th232 | 34.24 | 119.52 | 358.65 | 398.48 | 317.54 | 237.47 | 22.44 | 243.68 | 96.71 | 299.26 | 442.98 | 269.43 | 65.70 |
| U238 | 368.44 | 361.99 | 1025.12 | 644.87 | 656.66 | 394.19 | 670.70 | 436.25 | 182.29 | 490.90 | 537.80 | 277.03 | 250.31 |
| Th/U | 0.09 | 0.33 | 0.35 | 0.62 | 0.48 | 0.60 | 0.03 | 0.56 | 0.53 | 0.61 | 0.82 | 0.97 | 0.26 |
| Ce/Ce* | nd | 91 | nd | 88 | 174 | nd | nd | 52 | 242 | 137 | nd | 111 | nd |
| Eu/Eu* | 0.5 | 0.2 | 0.1 | 0.2 | 0.1 | 0.1 | 0.6 | 0.1 | 0.3 | 0.2 | 0.0 | 0.1 | 0.1 |
| T C | 684 | 654 | 691 | 729 | 711 | 712 | 662 | 668 | 648 | 687 | 661 | 643 | 650 |

| Element | MD33-160-1 | MD33-160-2 | MD33-142-1 | MD33-134-1 | MD33-2-1 | MD33-2-2 | MD14-7-1 | MD14-13-1 | MD14-33-1 | MD14-33-2 | MD14-70-1 | MD14-70-2 | MD14-86-1 |
|---|---|---|---|---|---|---|---|---|---|---|---|---|---|
| P31 | 504.69 | 311.60 | 241.18 | 674.22 | 82.14 | 369.34 | 585.53 | 630.84 | 1682.50 | 774.28 | 517.89 | 2638.13 | 587.76 |
| Ca43 | <55.04 | <50.40 | <56.06 | <103.84 | 700.92 | <240.02 | 58.73 | <39.56 | <43.60 | <50.07 | <50.71 | 70.32 | <49.42 |
| Ti49 | 5.82 | 3.28 | 3.28 | 7.80 | 6.82 | 3.19 | 3.87 | 2.84 | 14.68 | 7.21 | 4.34 | 39.31 | 3.02 |
| Sr88 | 0.26 | 0.22 | 0.10 | 0.35 | 0.22 | 0.38 | 0.08 | <0.068 | 0.21 | <0.088 | 0.15 | 0.73 | <0.088 |
| Y89 | 0.00 | 703.00 | 401.36 | 1695.00 | 46.49 | 2173.59 | 812.36 | 646.33 | 2373.59 | 549.01 | 404.13 | 3146.91 | 320.41 |
| Nb93 | 6.09 | 3.64 | 4.26 | 5.50 | 2.23 | 2.69 | 1.59 | 1.33 | 5.35 | 1.23 | 0.92 | 5.56 | 1.03 |
| La139 | 0.01 | 0.00 | 0.00 | 0.01 | <0.0058 | <0.022 | <0.0168 | <0.0169 | 0.05 | 0.10 | <0.020 | 0.07 | <0.0205 |
| Ce140 | 18.41 | 7.22 | 4.67 | 30.96 | 4.68 | 10.12 | 7.28 | 6.77 | 29.63 | 7.28 | 4.11 | 39.87 | 5.16 |
| Pr141 | 0.22 | 0.02 | 0.01 | 0.09 | 0.01 | 0.15 | 0.06 | 0.04 | 0.56 | 0.04 | 0.01 | 0.83 | 0.02 |
| Nd146 | 4.26 | 0.48 | 0.17 | 1.88 | 0.27 | 3.55 | 1.36 | 1.02 | 9.41 | 0.71 | 0.46 | 13.35 | 0.38 |
| Sm147 | 9.62 | 1.41 | 0.56 | 4.48 | 1.07 | 9.39 | 3.20 | 2.23 | 18.84 | 1.72 | 1.05 | 26.91 | 0.83 |
| Eu153 | 1.01 | 0.15 | 0.19 | 1.10 | 0.49 | 1.11 | 0.63 | 0.53 | 3.32 | 0.41 | 0.31 | 3.47 | 0.30 |
| Gd157 | 54.90 | 9.54 | 4.34 | 26.48 | 5.38 | 53.98 | 15.34 | 11.99 | 92.08 | 9.20 | 5.88 | 132.80 | 4.90 |
| Tb159 | 18.76 | 3.75 | 1.74 | 9.67 | 1.11 | 17.68 | 5.23 | 4.02 | 28.25 | 3.33 | 2.20 | 41.47 | 1.85 |
| Dy163 | 247.75 | 55.16 | 29.42 | 141.43 | 7.71 | 223.07 | 69.40 | 53.81 | 342.49 | 44.16 | 30.48 | 502.93 | 24.87 |
| Ho165 | 93.36 | 23.14 | 14.36 | 60.53 | 1.44 | 79.65 | 26.87 | 21.11 | 121.22 | 17.85 | 12.05 | 177.27 | 10.09 |
| Er166 | 415.36 | 115.45 | 79.51 | 315.10 | 3.83 | 357.68 | 121.44 | 97.15 | 506.51 | 84.05 | 61.20 | 749.66 | 48.75 |
| Tm169 | 83.89 | 26.49 | 18.42 | 74.40 | 0.55 | 71.96 | 24.49 | 20.17 | 95.28 | 17.57 | 13.59 | 141.06 | 10.91 |
| Yb173 | 769.04 | 268.28 | 185.86 | 792.32 | 3.67 | 615.70 | 225.44 | 190.44 | 824.34 | 170.88 | 138.54 | 1211.91 | 112.67 |
| Lu175 | 131.31 | 52.34 | 38.39 | 167.50 | 0.61 | 111.26 | 47.17 | 40.50 | 156.37 | 36.04 | 31.58 | 224.19 | 25.21 |
| Hf178 | 11634.27 | 13457.42 | 11981.94 | 20114.05 | 14398.68 | 10743.89 | 8522.18 | 8166.03 | 8013.40 | 8827.46 | 8166.03 | 8386.51 | 9073.37 |
| Th232 | 537.45 | 93.70 | 63.60 | 293.83 | 23.17 | 219.37 | 78.19 | 78.56 | 480.25 | 60.05 | 39.44 | 688.72 | 49.61 |
| U238 | 818.00 | 454.60 | 307.71 | 589.00 | 627.31 | 372.82 | 179.99 | 179.46 | 453.11 | 147.44 | 171.13 | 650.05 | 203.64 |
| Th/U | 0.66 | 0.21 | 0.21 | 0.50 | 0.04 | 0.59 | 0.43 | 0.44 | 1.06 | 0.41 | 0.23 | 1.06 | 0.24 |
| Ce/Ce* | 87 | 167 | 204 | 299 | nd | nd | nd | nd | 45 | 30 | nd | 42 | nd |
| Eu/Eu* | 0.1 | 0.1 | 0.4 | 0.3 | 0.6 | 0.2 | 0.3 | 0.3 | 0.2 | 0.3 | 0.4 | 0.2 | 0.4 |
| T C | 696 | 652 | 652 | 720 | 708 | 650 | 664 | 641 | 776 | 713 | 673 | 877 | 646 |

| Element | MD14-86-2 | MD14-86-3 | MD14-128-1 | MD38-23-1 | MD38-23-2 | MD38-27-1 | MD38-32-1 | MD38-47-1 | MD38-48-1 | MD38-116-1 | MD38-127-1 | MD38-129-1 | MD38-132-1 |
|---|---|---|---|---|---|---|---|---|---|---|---|---|---|
| P31 | 1784.28 | 1162.79 | 822.44 | 201.35 | 1126.12 | 288.72 | 356.56 | 339.04 | 290.83 | 132.48 | 774.10 | 151.42 | 145.21 |
| Ca43 | 268.63 | <40.70 | <64.14 | <98.28 | 1519.21 | <115.97 | <98.33 | <134.61 | 183.66 | 140.55 | 305.59 | <83.76 | 84.00 |
| Ti49 | 3.96 | 3.89 | 3.02 | 5.89 | 4.27 | 12.84 | 5.07 | 6.48 | 5.15 | 5.30 | 25.75 | 3.92 | 3.37 |
| Sr88 | 0.93 | <0.073 | 0.20 | 0.19 | 2.26 | 0.46 | 0.16 | 0.27 | 0.24 | 0.19 | 1.70 | 0.12 | 0.20 |
| Y89 | 1032.23 | 712.83 | 311.25 | 772.47 | 1173.45 | 1655.63 | 1368.97 | 2151.18 | 1401.50 | 493.96 | 3805.94 | 505.48 | 425.93 |
| Nb93 | 2.05 | 1.32 | 0.96 | 2.21 | 3.81 | 1.55 | 2.97 | 1.91 | 2.40 | 1.14 | 5.77 | 1.23 | 1.05 |
| La139 | 0.02 | <0.0169 | <0.025 | <0.0039 | 0.24 | 0.01 | 0.01 | 0.02 | 0.01 | 0.01 | 0.15 | <0.0033 | 0.01 |
| Ce140 | 11.99 | 6.49 | 6.57 | 8.36 | 12.76 | 9.55 | 12.07 | 14.13 | 9.66 | 6.50 | 27.96 | 6.15 | 6.54 |
| Pr141 | 0.14 | 0.06 | 0.02 | 0.05 | 0.15 | 0.19 | 0.11 | 0.37 | 0.11 | 0.03 | 0.71 | 0.03 | 0.04 |
| Nd146 | 2.20 | 0.99 | 0.44 | 1.03 | 1.87 | 3.66 | 2.16 | 6.72 | 2.33 | 0.58 | 12.06 | 0.57 | 0.74 |
| Sm147 | 4.56 | 2.23 | 0.93 | 2.62 | 3.79 | 7.20 | 4.87 | 12.40 | 5.71 | 1.55 | 23.53 | 1.49 | 1.53 |
| Eu153 | 0.99 | 0.73 | 0.30 | 0.44 | 0.59 | 1.64 | 1.16 | 2.90 | 0.79 | 0.40 | 5.02 | 0.30 | 0.49 |
| Gd157 | 21.90 | 13.04 | 4.93 | 15.11 | 22.39 | 33.35 | 27.66 | 55.32 | 30.97 | 8.91 | 110.11 | 9.11 | 8.13 |
| Tb159 | 7.23 | 4.58 | 1.74 | 5.17 | 7.82 | 10.93 | 9.06 | 17.25 | 10.22 | 3.16 | 33.24 | 3.19 | 2.74 |
| Dy163 | 93.86 | 60.06 | 24.70 | 68.53 | 103.87 | 142.19 | 120.50 | 207.24 | 130.45 | 42.26 | 389.60 | 42.95 | 35.65 |
| Ho165 | 35.32 | 23.58 | 9.87 | 25.92 | 39.61 | 54.72 | 45.77 | 74.53 | 48.48 | 16.39 | 136.31 | 16.68 | 14.03 |
| Er166 | 158.93 | 105.65 | 48.12 | 124.27 | 189.80 | 265.96 | 214.94 | 342.02 | 226.31 | 80.90 | 594.42 | 81.87 | 69.60 |
| Tm169 | 31.74 | 22.26 | 11.07 | 26.17 | 40.23 | 57.81 | 45.44 | 70.47 | 46.91 | 17.86 | 117.19 | 17.81 | 15.81 |
| Yb173 | 292.62 | 209.14 | 112.57 | 238.28 | 359.33 | 529.45 | 412.51 | 619.14 | 419.07 | 167.64 | 987.02 | 166.84 | 154.31 |
| Lu175 | 59.14 | 43.22 | 24.66 | 46.66 | 70.64 | 105.08 | 80.60 | 119.50 | 81.55 | 34.47 | 187.94 | 33.84 | 33.29 |
| Hf178 | 8199.95 | 9073.37 | 9556.72 | 9548.24 | 9548.24 | 11507.07 | 9285.37 | 12550.08 | 9149.69 | 9251.45 | 10124.86 | 9828.07 | 9166.65 |
| Th232 | 115.78 | 82.21 | 56.37 | 79.80 | 148.53 | 176.17 | 215.05 | 204.61 | 151.70 | 58.85 | 418.28 | 57.98 | 67.11 |
| U238 | 189.16 | 153.65 | 157.88 | 199.39 | 297.67 | 300.99 | 397.30 | 276.51 | 446.96 | 156.06 | 566.49 | 126.02 | 432.05 |
| Th/U | 0.61 | 0.54 | 0.36 | 0.40 | 0.50 | 0.59 | 0.54 | 0.74 | 0.34 | 0.38 | 0.74 | 0.46 | 0.16 |
| Ce/Ce* | 52 | nd | nd | nd | 16 | 51 | 100 | 38 | 82 | 117 | 21 | nd | 103 |
| Eu/Eu* | 0.3 | 0.4 | 0.4 | 0.2 | 0.2 | 0.3 | 0.3 | 0.3 | 0.2 | 0.3 | 0.3 | 0.3 | 0.4 |
| T C | 666 | 664 | 646 | 696 | 671 | 763 | 685 | 704 | 686 | 688 | 832 | 665 | 654 |

| Element | MD38-143-1 | MD38-147-1 | MD38-156-1 | MD38-183-1 |
|---|---|---|---|---|
| P31 | 280.01 | 304.83 | 250.37 | 174.22 |
| Ca43 | <80.81 | <90.68 | 63.44 | <160.06 |
| Ti49 | 4.19 | 9.53 | 10.18 | 3.29 |
| Sr88 | 0.14 | 0.55 | 0.34 | 0.07 |
| Y89 | 1317.11 | 2377.29 | 2064.35 | 450.27 |
| Nb93 | 2.82 | 2.16 | 2.31 | 0.82 |
| La139 | 0.00 | 0.04 | 0.03 | <0.0062 |
| Ce140 | 8.52 | 15.35 | 13.20 | 5.79 |
| Pr141 | 0.09 | 0.43 | 0.36 | 0.02 |
| Nd146 | 1.84 | 7.69 | 6.55 | 0.42 |
| Sm147 | 4.58 | 14.06 | 13.28 | 1.27 |
| Eu153 | 0.51 | 3.29 | 2.81 | 0.31 |
| Gd157 | 26.64 | 64.31 | 62.60 | 7.30 |
| Tb159 | 9.45 | 19.85 | 18.73 | 2.62 |
| Dy163 | 122.41 | 235.41 | 220.05 | 36.36 |
| Ho165 | 45.88 | 83.51 | 76.58 | 14.67 |
| Er166 | 212.70 | 378.41 | 336.45 | 74.89 |
| Tm169 | 43.59 | 76.85 | 66.62 | 17.12 |
| Yb173 | 378.99 | 669.27 | 567.27 | 165.86 |
| Lu175 | 72.21 | 127.69 | 105.93 | 34.53 |
| Hf178 | 8861.38 | 9014.01 | 7886.20 | 9573.68 |
| Th232 | 166.64 | 252.46 | 226.26 | 66.13 |
| U238 | 306.33 | 290.86 | 312.01 | 200.10 |
| Th/U | 0.54 | 0.87 | 0.73 | 0.33 |
| Ce/Ce* | 102 | 30 | 30 | nd |
| Eu/Eu* | 0.1 | 0.3 | 0.3 | 0.3 |
| T C | 670 | 737 | 743 | 652 |

## *Appendix 5.2. Trace Element Analyses of Garnets*

| Element | MD22B-grt3-1 | MD22B-grt3-2 | MD22B-grt3-3 | MD22B-grt1-1 | MD22B-grt1-2 | MD22B-grt1-3 | MD22B-grt1-3B | MD13-grt-1-1 | MD13-grt-1-2 | MD13-grt-1-3 | MD13-grt-1-4 | MD13-grt-2-1 |
|---|---|---|---|---|---|---|---|---|---|---|---|---|
| P | 97.65 | 110.76 | 88.28 | 96.54 | 85.86 | 86.76 | 91.58 | 50.94 | 56.58 | 346.47 | 46.89 | 52.89 |
| Ca | 66538.66 | 65966.88 | 66753.06 | 62750.74 | 62178.98 | 64751.91 | 64751.91 | 59606.07 | 55317.86 | 61321.35 | 65466.61 | 55746.68 |
| Ti | 677.78 | 979.24 | 1312.8 | 616.39 | 412.61 | 653.85 | 661.2 | 303.42 | 277.79 | 332 | 380.06 | 336.56 |
| Sr | <0.059 | 0.113 | 0.201 | 0.109 | 19.42 | 0.112 | 0.256 | 0.521 | 0.106 | 2.47 | 0.135 | 0.113 |
| Y | 50.57 | 43.33 | 32.28 | 119.03 | 97.9 | 77.04 | 79.4 | 128.17 | 106.92 | 99.68 | 145.31 | 133.77 |
| Zr | 6.81 | 20.36 | 15 | 12.98 | 4.27 | 9 | 12.06 | 3.01 | 3.17 | 3.19 | 2.83 | 3.93 |
| Nb | <0.034 | <0.030 | <0.031 | <0.029 | 0.071 | <0.028 | <0.027 | <0.029 | <0.026 | <0.026 | <0.030 | <0.030 |
| La | 0.0058 | 0.0056 | 0.0072 | 0.0154 | 0.013 | <0.0054 | 0.006 | <0.0166 | <0.0149 | 0.169 | 0.132 | <0.0172 |
| Ce | 0.1446 | 0.1788 | 0.1455 | 0.314 | 0.1078 | 0.1893 | 0.1954 | 0.0962 | 0.109 | 0.794 | 0.653 | 0.182 |
| Pr | 0.1065 | 0.1117 | 0.0922 | 0.2397 | 0.0747 | 0.126 | 0.1406 | 0.0591 | 0.0642 | 0.184 | 0.1388 | 0.099 |
| Nd | 1.984 | 1.808 | 1.637 | 4.53 | 1.549 | 2.58 | 2.81 | 1.295 | 1.229 | 2.29 | 1.85 | 1.79 |
| Sm | 3.41 | 2.83 | 2.72 | 8.08 | 3.87 | 5.66 | 6.11 | 2.32 | 2.14 | 2.8 | 2.53 | 2.75 |
| Eu | 1.556 | 1.039 | 0.973 | 3.26 | 2.029 | 2.53 | 2.69 | 1.556 | 1.478 | 1.8 | 1.733 | 1.731 |
| Gd | 7.2 | 6.58 | 5.96 | 18.82 | 12.48 | 12.72 | 13.86 | 8.36 | 7.85 | 9.04 | 8.68 | 9.27 |
| Tb | 1.326 | 1.228 | 1.034 | 3.52 | 2.578 | 2.245 | 2.45 | 3.53 | 3.2 | 3.43 | 3.55 | 3.67 |
| Dy | 9.43 | 8.42 | 6.6 | 23.62 | 18.66 | 14.73 | 16.06 | 19.16 | 17.08 | 16.8 | 20.61 | 20.57 |
| Ho | 1.898 | 1.687 | 1.23 | 4.63 | 3.78 | 3.05 | 3.17 | 4.39 | 3.71 | 3.3 | 4.94 | 4.64 |
| Er | 5.37 | 4.53 | 3.19 | 12.49 | 10.49 | 8.77 | 8.63 | 14.75 | 12.05 | 9.77 | 18.16 | 15.48 |
| Tm | 0.752 | 0.614 | 0.432 | 1.659 | 1.408 | 1.23 | 1.169 | 2.088 | 1.662 | 1.236 | 2.77 | 2.114 |
| Yb | 4.95 | 4.05 | 2.748 | 10.44 | 9.24 | 7.98 | 7.44 | 16.95 | 13.02 | 9.55 | 24.29 | 16.67 |
| Lu | 0.669 | 0.539 | 0.386 | 1.384 | 1.213 | 1.183 | 1.009 | 2.326 | 1.846 | 1.179 | 3.66 | 2.237 |
| Hf | 0.165 | 0.341 | 0.232 | 0.24 | 0.1454 | 0.264 | 0.347 | 0.0545 | 0.0612 | 0.06 | 0.053 | 0.0609 |
| Th | <0.0026 | <0.00224 | 0.0068 | <0.00205 | <0.00217 | <0.00207 | <0.00184 | <0.0047 | <0.0038 | <0.0030 | 0.0057 | <0.0048 |
| U | <0.0025 | <0.0021 | 0.0036 | <0.00259 | <0.00180 | <0.00215 | <0.0028 | <0.0045 | <0.0042 | <0.0026 | <0.0049 | <0.0043 |

| Element | MD13-grt-2-2 | MD13-grt-2-3 | MD13-grt-2-4 | MD13-grt-2-5 | MD26-grt1-3 | MD26-grt1-4 | MD26-grt3-1 | MD26-grt3-2 | MD26-grt3-3 | MD26-grt2-1 | MD26-grt2-2 | MD26-grt2-3 |
|---|---|---|---|---|---|---|---|---|---|---|---|---|
| P | 144.9 | 64.86 | 154.88 | 110.85 | 125.7 | 127.08 | 101.94 | 121.4 | 75.22 | 107.95 | 97.51 | 74.56 |
| Ca | 55460.8 | 56747.26 | 53388.16 | 56318.44 | 64680.44 | 65823.96 | 49600.25 | 50529.36 | 53245.22 | 53388.16 | 54674.62 | 64108.68 |
| Ti | 385.43 | 394.41 | 412.95 | 460.45 | 493.98 | 400.11 | 354.99 | 366.28 | 350.26 | 328.97 | 329.58 | 320.35 |
| Sr | 1.708 | <0.082 | 0.184 | 5.05 | 0.278 | 0.129 | 0.033 | 0.089 | 0.0507 | 0.194 | 0.051 | 0.085 |
| Y | 146.33 | 170.23 | 119.85 | 102.01 | 95.15 | 104.6 | 91.53 | 112.53 | 81.25 | 145.06 | 178.02 | 115.56 |
| Zr | 4.35 | 5.99 | 4.38 | 5.01 | 2.53 | 2.41 | 3.41 | 3.16 | 2.56 | 2.47 | 2.71 | 2.6 |
| Nb | <0.024 | <0.026 | <0.030 | <0.030 | 0.0136 | <0.0088 | <0.0086 | <0.0078 | <0.0079 | <0.0087 | <0.0088 | <0.0077 |
| La | <0.0160 | <0.0166 | <0.0161 | <0.0178 | 0.0139 | 0.0109 | 0.0055 | 0.0068 | 0.0075 | 0.0152 | 0.0069 | 0.0104 |
| Ce | 0.22 | 0.209 | 0.172 | 0.188 | 0.215 | 0.212 | 0.1143 | 0.1374 | 0.1414 | 0.175 | 0.1482 | 0.206 |
| Pr | 0.1076 | 0.1111 | 0.0952 | 0.1114 | 0.1172 | 0.1214 | 0.0717 | 0.0823 | 0.0828 | 0.0966 | 0.0838 | 0.1319 |
| Nd | 2.02 | 1.99 | 1.595 | 1.96 | 1.96 | 2.07 | 1.226 | 1.335 | 1.394 | 1.459 | 1.365 | 1.97 |
| Sm | 2.83 | 3.04 | 2.63 | 3.15 | 3.31 | 3.49 | 2.17 | 2.23 | 2.44 | 2.53 | 2.41 | 3.45 |
| Eu | 1.822 | 1.842 | 1.668 | 1.895 | 2.043 | 2.18 | 1.292 | 1.311 | 1.416 | 1.46 | 1.428 | 2.1 |
| Gd | 9.39 | 10.08 | 8.73 | 9.85 | 9.74 | 10.55 | 6.97 | 7.22 | 7.37 | 8.58 | 8.45 | 10.54 |
| Tb | 3.86 | 4.2 | 3.42 | 3.55 | 2.17 | 2.36 | 1.688 | 1.839 | 1.718 | 2.28 | 2.43 | 2.58 |
| Dy | 21.61 | 24.24 | 18.73 | 17.46 | 16.11 | 17.72 | 14.13 | 16.08 | 13.35 | 20.92 | 23.49 | 20.63 |
| Ho | 5.13 | 5.95 | 4.2 | 3.57 | 3.29 | 3.65 | 3.25 | 4.01 | 2.89 | 5.31 | 6.35 | 4.33 |
| Er | 18.21 | 22.14 | 14.45 | 11.49 | 9.43 | 10.88 | 10.18 | 13.77 | 8.68 | 17.4 | 23.1 | 11.98 |
| Tm | 2.64 | 3.32 | 2.035 | 1.522 | 1.381 | 1.657 | 1.672 | 2.31 | 1.303 | 2.72 | 3.9 | 1.615 |
| Yb | 22.35 | 28.85 | 16.81 | 12.2 | 9.63 | 11.78 | 12.36 | 18.1 | 9.55 | 19.28 | 30.56 | 9.79 |
| Lu | 3.29 | 4.28 | 2.31 | 1.655 | 1.323 | 1.773 | 1.945 | 2.9 | 1.371 | 2.85 | 4.86 | 1.306 |
| Hf | 0.088 | 0.085 | 0.086 | 0.092 | 0.0633 | 0.05 | 0.0764 | 0.065 | 0.0392 | 0.0493 | 0.0445 | 0.0343 |
| Th | <0.0038 | <0.0050 | <0.0041 | <0.0051 | <0.00169 | <0.00160 | <0.00154 | <0.00163 | <0.0028 | 0.0017 | <0.00182 | <0.00139 |
| U | <0.0043 | <0.0035 | <0.0043 | 0.0054 | 0.0018 | 0.003 | 0.00166 | <0.00139 | <0.00174 | <0.00164 | 0.0024 | <0.00160 |

| Element | MD8-grt3-1 | MD8-grt3-2 | MD8-grt3-3 | MD8-grt3-4 | MD8-grt4-1 | MD8-grt4-2 | MD8-grt4-4 | MD2-grt1-1 | MD2-grt1-2 | MD2-grt1-3 | MD2-grt2-1 | MD2-grt2-2 |
|---|---|---|---|---|---|---|---|---|---|---|---|---|
| P | 44.95 | 105.49 | 78.67 | 104.95 | 69.89 | 125.04 | 122.67 | 42.52 | 39.22 | 50.01 | 45.12 | 38.37 |
| Ca | 65109.25 | 58319.6 | 73042.44 | 62107.5 | 64323.09 | 64180.13 | 69468.92 | 66038.37 | 53388.16 | 58176.66 | 58248.13 | 51387 |
| Ti | 264.91 | 293.5 | 229.8 | 253.18 | 252.83 | 265.71 | 351.35 | 239.02 | 180.2 | 212.41 | 214.87 | 182.28 |
| Sr | <0.090 | 0.088 | <0.095 | <0.082 | <0.092 | <0.083 | 47.84 | <0.0199 | 0.412 | <0.0199 | 0.122 | 0.042 |
| Y | 152.77 | 132.07 | 100.59 | 122.21 | 155.13 | 140.21 | 137.63 | 397.78 | 739.12 | 709.3 | 579.14 | 790.53 |
| Zr | 3.36 | 3.87 | 1.84 | 3.07 | 2.75 | 3.02 | 4.16 | 1.87 | 1.94 | 2.23 | 1.94 | 2.07 |
| Nb | <0.0250 | 0.026 | <0.029 | <0.026 | <0.023 | <0.030 | <0.025 | <0.0094 | <0.0098 | <0.0093 | <0.0101 | <0.0091 |
| La | <0.0172 | <0.0146 | <0.0164 | <0.0164 | <0.0187 | <0.0168 | <0.0139 | 0.0025 | 0.0029 | <0.0024 | 0.0048 | 0.0027 |
| Ce | 0.0283 | 0.0234 | 0.0206 | 0.0258 | 0.0268 | 0.029 | 0.0347 | 0.0486 | 0.0712 | 0.0637 | 0.0806 | 0.0905 |
| Pr | 0.0348 | 0.0236 | 0.0179 | 0.0275 | 0.0305 | 0.0232 | 0.0275 | 0.0371 | 0.0578 | 0.0606 | 0.0582 | 0.0763 |
| Nd | 0.874 | 0.755 | 0.442 | 0.585 | 0.769 | 0.529 | 0.835 | 0.841 | 1.322 | 1.381 | 1.3 | 1.695 |
| Sm | 2.25 | 2.24 | 1.5 | 1.82 | 1.97 | 1.84 | 2.26 | 3.95 | 5.86 | 5.91 | 5.36 | 6.76 |
| Eu | 1.53 | 1.462 | 1.783 | 1.772 | 1.708 | 1.813 | 1.709 | 2.87 | 2.52 | 2.81 | 2.97 | 2.49 |
| Gd | 8.43 | 7.91 | 9.11 | 8.68 | 9.42 | 9.45 | 8.88 | 24.96 | 35.6 | 36.59 | 32.26 | 40.03 |
| Tb | 2.23 | 2.002 | 2.15 | 2.24 | 2.33 | 2.45 | 2.19 | 8.18 | 12.58 | 12.58 | 10.9 | 13.8 |
| Dy | 21.13 | 19.18 | 14.9 | 17.56 | 21.55 | 19.34 | 19.01 | 71.03 | 119.53 | 117.37 | 98.7 | 130.21 |
| Ho | 5.06 | 4.26 | 3.22 | 3.78 | 5.15 | 4.66 | 4.31 | 14.56 | 27.24 | 26.02 | 21.2 | 29.19 |
| Er | 18.1 | 14.71 | 10.79 | 12.54 | 17.73 | 16.97 | 15.45 | 37.35 | 76.05 | 71.32 | 56.13 | 81.15 |
| Tm | 2.67 | 2.19 | 1.506 | 1.825 | 2.55 | 2.49 | 2.38 | 4.25 | 9.53 | 8.81 | 6.64 | 10.1 |
| Yb | 23.11 | 19.4 | 12.85 | 16.61 | 21.79 | 22.44 | 21.9 | 21.32 | 50.06 | 46.42 | 34.25 | 53.24 |
| Lu | 3.36 | 2.76 | 1.805 | 2.37 | 3.03 | 3.23 | 3.27 | 2.57 | 6.02 | 5.6 | 4 | 6.34 |
| Hf | 0.075 | 0.083 | 0.05 | 0.086 | 0.081 | 0.09 | 0.112 | 0.0383 | 0.0375 | 0.0366 | 0.0389 | 0.04 |
| Th | <0.0052 | <0.0090 | 0.0039 | <0.0046 | <0.0051 | <0.0033 | 0.0201 | <0.00194 | <0.0033 | <0.0040 | 0.0059 | <0.00179 |
| U | <0.0045 | <0.0038 | 0.0117 | <0.0053 | 0.0039 | 0.0036 | <0.0046 | 0.004 | 0.0061 | 0.0109 | 0.0095 | 0.0121 |

| Element | MD2-grt2-3 | MD2-grt3-1 | MD2-grt3-2 | MD2-grt3-3 | MD6-grt2-1 | MD6-grt2-2 | MD6-grt2-3 | MD6-grt2-4 | MD6-grt1-1 | MD6-grt1-2 | MD6-grt1-3 | MD6-grt1-3a |
|---|---|---|---|---|---|---|---|---|---|---|---|---|
| P | 32.35 | 29.65 | 35.7 | 37.71 | 53.17 | 33.13 | 157.17 | 56.21 | 49.46 | 38.37 | 65.58 | 212.69 |
| Ca | 66896.01 | 60678.11 | 39594.43 | 56961.66 | 62393.39 | 58248.13 | 57104.61 | 61750.16 | 70469.52 | 56818.73 | 62107.5 | 62107.5 |
| Ti | 239.37 | 214.87 | 155.27 | 193.15 | 363.72 | 304.96 | 326.55 | 380.38 | 367.63 | 285.85 | 264.58 | 854.9 |
| Sr | 0.027 | 0.044 | 0.034 | 0.029 | 0.034 | 0.044 | 0.089 | <0.022 | <0.046 | 0.031 | 1.73 | 1.78 |
| Y | 487.92 | 422.78 | 1009.71 | 642.51 | 96.95 | 589.17 | 542.63 | 102.61 | 81.17 | 818.06 | 243.16 | 145.92 |
| Zr | 1.92 | 1.46 | 2.28 | 1.98 | 5.48 | 4.07 | 3.68 | 5.25 | 2.82 | 3.48 | 3.7 | 4.85 |
| Nb | <0.0096 | <0.0100 | 0.0095 | <0.0104 | <0.0110 | <0.0112 | 0.0593 | <0.0105 | <0.0117 | <0.0107 | 0.0189 | 1.36 |
| La | <0.0027 | <0.0026 | 0.0054 | <0.0029 | 0.0061 | 0.0076 | 0.0236 | 0.0041 | <0.0034 | 0.0111 | 0.004 | 0.012 |
| Ce | 0.0621 | 0.0213 | 0.1312 | 0.0376 | 0.1274 | 0.298 | 0.254 | 0.1406 | 0.0466 | 0.281 | 0.0884 | 0.137 |
| Pr | 0.0548 | 0.0194 | 0.1187 | 0.0352 | 0.1029 | 0.225 | 0.172 | 0.1025 | 0.0413 | 0.207 | 0.0728 | 0.0885 |
| Nd | 1.141 | 0.512 | 2.73 | 0.926 | 2.19 | 4.33 | 3.25 | 2.11 | 0.949 | 4.12 | 1.604 | 1.84 |
| Sm | 4.86 | 2.7 | 9.46 | 4.93 | 7.39 | 11.91 | 9.45 | 7.01 | 3.52 | 12.11 | 6.28 | 6.72 |
| Eu | 3.13 | 1.932 | 1.677 | 2.5 | 4.2 | 5.32 | 4.22 | 3.99 | 2.71 | 3.82 | 3.63 | 3.91 |
| Gd | 29.6 | 19.26 | 47.24 | 33.06 | 35.48 | 51.49 | 44.24 | 34 | 18.93 | 60.55 | 36.72 | 37.43 |
| Tb | 10.04 | 6.68 | 15.59 | 11.11 | 7.39 | 14.03 | 12.53 | 7.05 | 4.45 | 17.87 | 9.65 | 8.84 |
| Dy | 88.65 | 63.68 | 152.4 | 102.85 | 34.4 | 110.88 | 103.9 | 34.51 | 24.67 | 151.31 | 61.59 | 47.29 |
| Ho | 17.93 | 14.91 | 37.32 | 23.26 | 3.73 | 22.32 | 21.73 | 4.18 | 3.25 | 32.38 | 8.95 | 5.71 |
| Er | 45.4 | 45.29 | 116.83 | 67.06 | 5.68 | 57.81 | 56.19 | 7.4 | 5.91 | 87.57 | 17.59 | 9.68 |
| Tm | 5.12 | 6.22 | 16.95 | 8.73 | 0.531 | 7.22 | 6.91 | 0.769 | 0.629 | 11.79 | 2.02 | 1.022 |
| Yb | 25.2 | 35.76 | 104.01 | 49.43 | 2.72 | 44.9 | 42.35 | 4.35 | 3.7 | 76.17 | 12.12 | 5.64 |
| Lu | 2.85 | 4.63 | 13.63 | 6.09 | 0.336 | 6.25 | 5.94 | 0.601 | 0.542 | 12.11 | 1.618 | 0.764 |
| Hf | 0.0471 | 0.0269 | 0.0435 | 0.0228 | 0.1334 | 0.0943 | 0.0723 | 0.1014 | 0.0505 | 0.0711 | 0.0814 | 0.0883 |
| Th | <0.0025 | <0.0046 | <0.00197 | <0.0021 | <0.0039 | <0.00185 | <0.00187 | 0.00202 | <0.0020 | <0.0023 | <0.00190 | <0.0021 |
| U | 0.0075 | 0.003 | 0.0111 | 0.0071 | 0.011 | 0.0383 | 0.038 | 0.0129 | 0.0061 | 0.0268 | 0.0077 | 0.0146 |

| Element | MD6-grt3-1 | MD6-grt3-2 | MD6-grt3-3 | MD29-grt3-1 | MD29-grt3-2 | MD29-grt3-3 | MD29-grt3-4 | MD29-grt4-1a | MD29-grt4-1b | MD29-grt4-2 | MD29-grt4-3 | MD29-grt4-4 |
|---|---|---|---|---|---|---|---|---|---|---|---|---|
| P | 46.62 | 37.03 | 9.39 | 44.43 | 40.21 | 43.79 | 32.31 | 52.21 | 59.95 | 38.4 | 84.2 | 38.43 |
| Ca | 66753.07 | 58248.13 | 60606.64 | 75758.3 | 66395.72 | 73113.9 | 68754.23 | 82190.61 | 82190.61 | 76330.06 | 74900.66 | 72685.09 |
| Ti | 303.49 | 247.95 | 270.75 | 300.61 | 402.35 | 354.62 | 286.2 | 406.21 | 411.53 | 274.79 | 329.72 | 263.69 |
| Sr | 0.28 | <0.019 | <0.023 | 0.068 | 0.028 | 0.034 | 0.071 | 6.24 | 2.631 | 0.107 | 0.12 | <0.031 |
| Y | 144.38 | 355.14 | 345.92 | 380.37 | 358.52 | 533.96 | 417.13 | 121.6 | 142.13 | 445.92 | 590.93 | 706.42 |
| Zr | 2.18 | 1.38 | 3.39 | 3.64 | 5.74 | 5.04 | 3.69 | 3.31 | 3.14 | 2.95 | 4.69 | 3.34 |
| Nb | <0.0095 | 0.0145 | <0.0092 | 0.0474 | 0.0173 | 0.0472 | <0.0142 | 0.0266 | <0.0133 | <0.0143 | 0.0424 | 0.0336 |
| La | 0.0074 | 0.0029 | 0.0073 | <0.0023 | 0.0032 | 0.0026 | 0.0043 | <0.0024 | 0.0051 | 0.0039 | 0.0042 | 0.0031 |
| Ce | 0.0555 | 0.0551 | 0.13 | 0.0662 | 0.074 | 0.033 | 0.0852 | 0.0371 | 0.0525 | 0.047 | 0.0587 | 0.0825 |
| Pr | 0.0307 | 0.056 | 0.1011 | 0.0561 | 0.0781 | 0.0401 | 0.0744 | 0.0324 | 0.0452 | 0.0469 | 0.0593 | 0.0766 |
| Nd | 0.669 | 1.265 | 2.11 | 1.452 | 2.096 | 1.133 | 1.738 | 0.77 | 1.094 | 1.219 | 1.719 | 1.834 |
| Sm | 2.65 | 4.96 | 7.08 | 6.34 | 7.26 | 5.76 | 7.19 | 4.06 | 5.12 | 5.86 | 7.33 | 7.54 |
| Eu | 1.958 | 2.52 | 3.34 | 3.206 | 2.47 | 2.565 | 3.165 | 2.783 | 3.247 | 2.927 | 2.744 | 2.928 |
| Gd | 16.17 | 31.41 | 37.6 | 32.9 | 27.22 | 30.88 | 35.92 | 21.99 | 26.09 | 33.21 | 38.28 | 40.1 |
| Tb | 4.4 | 9.25 | 10.29 | 9 | 6.94 | 9.2 | 10.01 | 5.04 | 6 | 9.67 | 11.55 | 12.74 |
| Dy | 31.08 | 72.62 | 75.23 | 68.29 | 55.41 | 85.38 | 77.66 | 28.98 | 34.85 | 79.38 | 102.36 | 119.52 |
| Ho | 5.52 | 14.2 | 13.99 | 13.24 | 11.93 | 20.62 | 15.14 | 4.17 | 4.93 | 16.63 | 22.86 | 28.58 |
| Er | 13.49 | 34.76 | 33.78 | 34.99 | 35.54 | 65.45 | 38.89 | 8.48 | 9.99 | 44.97 | 65.85 | 84.86 |
| Tm | 1.824 | 4.26 | 4.16 | 4.69 | 5.39 | 9.8 | 4.93 | 0.984 | 1.142 | 5.96 | 9.31 | 11.77 |
| Yb | 12.6 | 27.07 | 26.34 | 29.71 | 36.69 | 65.35 | 29.91 | 5.55 | 6.62 | 37.01 | 59.57 | 74.48 |
| Lu | 1.957 | 4.11 | 4.15 | 4 | 5.08 | 9.2 | 3.89 | 0.679 | 0.888 | 5.03 | 7.98 | 10.29 |
| Hf | 0.0388 | 0.06 | 0.0573 | 0.0489 | 0.1077 | 0.1101 | 0.059 | 0.0469 | 0.0539 | 0.041 | 0.0926 | 0.0534 |
| Th | <0.00178 | <0.00163 | 0.0035 | <0.0024 | <0.00164 | 0.0165 | <0.0022 | <0.0026 | <0.00230 | 0.0023 | <0.00146 | <0.0026 |
| U | 0.0025 | 0.0058 | 0.0237 | 0.0162 | 0.017 | 0.0157 | 0.0194 | 0.0105 | 0.0181 | 0.0173 | 0.0296 | 0.0212 |

| Element | MD33-grt1-1 | MD33-grt1-2 | MD33-grt1-3 | MD33-grt1-4 | MD33-grt4-1 | MD33-grt4-2 | MD33-grt4-3 | MD33-grt3-1 | MD33-grt3-2 | MD33-grt3-3 | MD33-grt3-4 | MD14-grt3-1 |
|---|---|---|---|---|---|---|---|---|---|---|---|---|
| P | 48.99 | 58.06 | 59.26 | 48.17 | 38.59 | 39.88 | 41.33 | 42.99 | 50.86 | 43.37 | 23.31 | 37.39 |
| Ca | 78188.3 | 69326 | 64966.32 | 64180.14 | 69183.05 | 76044.19 | 73971.55 | 64823.38 | 64466.04 | 65609.55 | 77687.99 | 74829.2 |
| Ti | 368.96 | 428.6 | 587.97 | 344.82 | 323.67 | 324.77 | 362.02 | 338.25 | 411.99 | 353.6 | 379.51 | 337.07 |
| Sr | 0.413 | <0.061 | <0.059 | <0.058 | 0.089 | <0.065 | <0.058 | 0.095 | <0.059 | 0.697 | 0.09 | <0.081 |
| Y | 147.67 | 288.51 | 357.79 | 266.94 | 122.66 | 159.45 | 132.06 | 349.02 | 537.1 | 313.36 | 333.31 | 133.6 |
| Zr | - | - | - | - | - | - | - | - | - | - | - | 3.56 |
| Nb | 0.0329 | <0.0142 | <0.0135 | 0.0134 | <0.0135 | 0.0393 | <0.0136 | <0.0147 | <0.0140 | 0.0127 | <0.0140 | <0.028 |
| La | <0.0021 | 0.0113 | 0.0088 | 0.003 | <0.0022 | <0.0024 | <0.00212 | 0.0113 | 0.0109 | <0.0021 | 0.0027 | <0.0158 |
| Ce | 0.0204 | 0.2679 | 0.2271 | 0.104 | 0.0241 | 0.0279 | 0.0172 | 0.2687 | 0.2417 | 0.0448 | 0.0073 | 0.153 |
| Pr | 0.0237 | 0.1889 | 0.1591 | 0.0873 | 0.0214 | 0.0273 | 0.0678 | 0.1853 | 0.1626 | 0.0445 | 0.0274 | 0.114 |
| Nd | 0.625 | 3.55 | 3.19 | 1.993 | 0.623 | 0.794 | 0.469 | 3.36 | 3.14 | 1.199 | 0.849 | 2.65 |
| Sm | 3.02 | 8.4 | 7.89 | 6 | 2.77 | 3.37 | 2.296 | 7.93 | 7.26 | 4.18 | 3.56 | 4.92 |
| Eu | 2.023 | 3.45 | 3.34 | 2.765 | 1.886 | 2.35 | 1.708 | 3.2 | 3.068 | 2.072 | 1.916 | 6.61 |
| Gd | 16.3 | 28.96 | 28.01 | 24.18 | 14.78 | 18.7 | 13.83 | 27.88 | 27.83 | 20.35 | 18.75 | 14.49 |
| Tb | 3.88 | 6.91 | 7.05 | 5.85 | 3.4 | 4.42 | 3.31 | 7.02 | 7.88 | 5.37 | 5.25 | 5.05 |
| Dy | 28.54 | 54.21 | 59.59 | 47.52 | 24.03 | 30.79 | 24.54 | 59.5 | 76.75 | 48.25 | 49.22 | 23.26 |
| Ho | 6.05 | 11.32 | 14.01 | 10.13 | 4.83 | 5.89 | 5.04 | 13.72 | 20.87 | 12.42 | 13.61 | 4.8 |
| Er | 17.98 | 30.34 | 42.7 | 28.06 | 13.46 | 15.66 | 14.3 | 40.15 | 70.91 | 41.38 | 46.71 | 14.2 |
| Tm | 2.681 | 3.83 | 6.15 | 3.6 | 1.86 | 2.085 | 2.047 | 5.14 | 11.28 | 6.38 | 7.29 | 1.718 |
| Yb | 19.56 | 22.18 | 40.08 | 21.19 | 12.67 | 13.6 | 14.17 | 29.17 | 77.97 | 43.85 | 51.52 | 12.64 |
| Lu | 3.47 | 2.87 | 5.98 | 2.749 | 2.02 | 1.919 | 2.163 | 3.79 | 12.37 | 6.83 | 8.31 | 1.667 |
| Hf | 0.0499 | 0.1124 | 0.1502 | 0.1075 | 0.0615 | 0.0553 | 0.0632 | 0.1128 | 0.259 | 0.0907 | 0.0991 | 0.0514 |
| Th | 0.00467 | 0.0022 | <0.00161 | <0.00210 | <0.00153 | 0.00168 | <0.00142 | <0.0034 | 0.0076 | 0.018 | 0.007 | <0.0040 |
| U | 0.00174 | 0.0303 | 0.0232 | 0.0172 | <0.00150 | <0.0019 | 0.00415 | 0.0171 | 0.0234 | 0.0076 | 0.0057 | 0.0104 |

| Element | MD14-grt3-2 | MD14-grt3-3 | MD14-grt3-4 | MD14-grt3a-1 | MD14-grt3a-2 | MD14-grt3a-3 | MD14-grt3a-4 |
|---|---|---|---|---|---|---|---|
| P | 129.85 | 46.08 | 1316.44 | 56.1 | 88.49 | 80.23 | 56.71 |
| Ca | 69254.53 | 70898.35 | 76473.02 | 67396.31 | 72470.7 | 74757.73 | 74900.66 |
| Ti | 332.03 | 296.94 | 548.62 | 307.54 | 495.79 | 425.19 | 337.43 |
| Sr | 1.47 | 0.084 | 20.38 | 9.24 | 8.4 | 0.147 | 1.027 |
| Y | 87.18 | 94.74 | 66.24 | 95.01 | 99.18 | 113.12 | 100.09 |
| Zr | 4.1 | 3.09 | 2.7 | 3.13 | 3.39 | 4.01 | 3.7 |
| Nb | 0.047 | <0.026 | 0.313 | 0.043 | 0.758 | 0.194 | 0.05 |
| La | <0.0144 | <0.0128 | <0.0166 | <0.0132 | <0.0153 | <0.0161 | <0.0149 |
| Ce | 0.0596 | 0.0421 | 0.0438 | 0.0429 | 0.0344 | 0.0316 | 0.0334 |
| Pr | 0.0538 | 0.0462 | 0.0313 | 0.0483 | 0.0244 | 0.0373 | 0.0354 |
| Nd | 1.388 | 1.276 | 0.777 | 1.264 | 1.118 | 1.198 | 1.169 |
| Sm | 3.38 | 3.43 | 2.31 | 3.08 | 3.03 | 3.35 | 3.22 |
| Eu | 5.12 | 5.02 | 3.52 | 4.28 | 4.6 | 4.86 | 4.92 |
| Gd | 11.69 | 11.23 | 8.46 | 10.39 | 10.88 | 12.09 | 11.63 |
| Tb | 3.74 | 3.74 | 2.66 | 3.46 | 3.55 | 4.1 | 3.75 |
| Dy | 15.91 | 16.8 | 11.84 | 16.1 | 16.83 | 19.5 | 17.2 |
| Ho | 3 | 3.38 | 2.5 | 3.6 | 3.69 | 4.34 | 3.53 |
| Er | 8.66 | 10.07 | 7.83 | 11.93 | 12.09 | 13.65 | 10.74 |
| Tm | 1.034 | 1.239 | 1.09 | 1.573 | 1.515 | 1.653 | 1.338 |
| Yb | 7.81 | 8.88 | 9.4 | 12.36 | 11.7 | 11.8 | 9.79 |
| Lu | 1.01 | 1.19 | 1.342 | 1.712 | 1.597 | 1.528 | 1.243 |
| Hf | 0.0675 | 0.0466 | 0.044 | 0.062 | 0.076 | 0.069 | 0.059 |
| Th | <0.0034 | <0.0030 | 0.0063 | <0.0041 | <0.0043 | <0.0056 | <0.0056 |
| U | <0.0142 | 0.0036 | 0.0283 | 0.0036 | 0.0065 | <0.0053 | <0.0034 |

## *Appendix 5.3. Trace Element Analyses of Rutiles*

| Element | MD26-rt1 | MD26-rt-2 | MD26-rt-3 | MD26-rt-4 | MD26-rt-5 | MD13-rt-1 | MD13-rt-2 | MD13-rt-3 |
|---|---|---|---|---|---|---|---|---|
| P | 3232 | 7 | 2638 | 21 | 47 | 38 | <23.06 | <24.76 |
| C | 5453 | 221 | 3835 | 217 | <76.28 | 697 | 427 | <431.66 |
| Ti | 599508 | 599508 | 599508 | 599508 | 599508 | 599508 | 599508 | 599508 |
| Sr | 20.13 | 2.02 | 12.47 | 2.02 | 2.01 | 22.91 | 1.78 | 1.81 |
| Y | 1.93 | 0.17 | 2.23 | 0.25 | 0.16 | 0.47 | 0.12 | 0.15 |
| Zr | 101 | 187 | 166 | 201 | 270 | 161 | 193 | 181 |
| Nb | 379 | 574 | 325 | 411 | 150 | 308 | 323 | 335 |
| La1 | 0.008 | 0.002 | 0.007 | <0.0021 | <0.0022 | <0.0199 | <0.030 | <0.035 |
| Ce | 0.043 | <0.0062 | 0.065 | 0.056 | <0.0052 | 0.037 | <0.0159 | 0.049 |
| Pr | 0.007 | 0.010 | 0.018 | <0.00151 | <0.00159 | <0.0081 | <0.0130 | <0.0140 |
| Nd | 0.078 | <0.0107 | 0.176 | <0.0107 | <0.0096 | 0.047 | <0.058 | <0.102 |
| Sm | 0.055 | <0.0099 | 0.137 | <0.0104 | <0.0110 | <0.048 | <0.065 | <0.083 |
| Eu | 0.028 | <0.00170 | 0.044 | 0.004 | 0.003 | <0.0188 | <0.030 | <0.028 |
| Gd | 0.182 | <0.0086 | 0.307 | 0.014 | <0.0082 | 0.042 | <0.043 | <0.044 |
| Tb | 0.040 | 0.002 | 0.063 | 0.003 | <0.00092 | 0.015 | <0.0097 | <0.0120 |
| Dy | 0.263 | <0.0078 | 0.388 | 0.037 | <0.0041 | 0.085 | <0.0246 | <0.0153 |
| Ho | 0.063 | 0.005 | 0.080 | 0.020 | 0.004 | 0.015 | 0.005 | <0.0070 |
| Er | 0.205 | <0.0034 | 0.226 | <0.0148 | <0.0030 | 0.071 | <0.033 | <0.034 |
| Tm | 0.028 | <0.00119 | 0.028 | 0.041 | 0.018 | 0.009 | <0.0052 | <0.0039 |
| Yb | 0.159 | <0.0070 | 0.152 | 0.012 | 0.014 | 0.060 | <0.048 | <0.045 |
| Lu | 0.026 | <0.00117 | 0.034 | 0.002 | 0.003 | 0.010 | <0.0072 | 0.008 |
| Hf | 6.27 | 9.65 | 9.89 | 12.11 | 13.40 | 8.69 | 9.75 | 9.23 |
| Ta | 25.59 | 139.32 | 12.95 | 16.64 | 2.11 | 14.06 | 13.20 | 87.03 |
| Pb | 0.28 | 0.32 | 0.39 | 0.36 | 0.26 | 3.81 | 0.48 | 1.29 |
| Th | <0.00157 | <0.00158 | <0.0030 | 0.001 | <0.00131 | <0.0070 | <0.0080 | <0.0104 |
| U | 0.17 | 0.29 | 0.22 | 0.15 | 0.81 | 0.18 | 0.34 | 0.47 |
| T C | 561 | 606 | 597 | 611 | 634 | 594 | 608 | 603 |

| Element | MD13-rt-4 | MD13-rt-6 | MD22B-rt-1 | MD22B-rt-2 | MD22B-rt-3 | MD22B-rt-4 | MD22B-rt-5 | MD22B-rt-6 |
|---|---|---|---|---|---|---|---|---|
| P | <24.09 | 32 | 47 | 364 | 6 | 73 | 225 | 129 |
| C | <424.75 | <351.29 | 1116 | 1152 | 381 | 441 | 252 | 335 |
| Ti | 599508 | 599508 | 599508 | 599508 | 599508 | 599508 | 599508 | 599508 |
| Sr | 1.86 | 1.81 | 1.95 | 2.46 | 1.84 | 4.40 | 1.90 | 1.84 |
| Y | 0.13 | 0.83 | 0.33 | 0.22 | 0.18 | 0.23 | 0.19 | 0.15 |
| Zr | 230 | 234 | 371 | 145 | 277 | 290 | 439 | 352 |
| Nb | 513 | 296 | 489 | 471 | 475 | 492 | 504 | 480 |
| La1 | <0.030 | <0.027 | 0.026 | 0.021 | 0.019 | 0.034 | 0.045 | 0.036 |
| Ce | <0.0186 | <0.0157 | 0.171 | 0.074 | 0.066 | 0.099 | 0.044 | 0.049 |
| Pr | <0.0138 | <0.0099 | 0.037 | 0.006 | 0.002 | 0.008 | 0.005 | 0.005 |
| Nd | <0.089 | <0.077 | 0.069 | 0.027 | <0.0138 | <0.0141 | 0.020 | 0.019 |
| Sm | <0.076 | <0.074 | 0.011 | <0.0158 | <0.0153 | 0.017 | <0.0144 | <0.0141 |
| Eu | <0.030 | 0.048 | 0.006 | 0.007 | <0.0026 | 0.017 | 0.003 | <0.0022 |
| Gd | <0.039 | 0.093 | <0.0066 | 0.028 | <0.0091 | 0.020 | 0.013 | 0.012 |
| Tb | <0.0078 | 0.020 | 0.032 | <0.00137 | 0.003 | 0.002 | 0.009 | 0.010 |
| Dy | <0.035 | 0.173 | 0.023 | 0.031 | 0.045 | 0.019 | 0.014 | 0.013 |
| Ho | <0.0069 | 0.039 | 0.015 | 0.006 | <0.00123 | 0.007 | 0.006 | <0.0054 |
| Er | <0.043 | 0.152 | <0.0035 | 0.014 | <0.0040 | 0.013 | 0.013 | 0.005 |
| Tm | <0.0072 | 0.013 | 0.034 | 0.051 | 0.039 | 0.020 | 0.007 | 0.059 |
| Yb | <0.064 | 0.111 | <0.0030 | 0.016 | 0.006 | 0.025 | 0.016 | <0.0100 |
| Lu | <0.0068 | 0.013 | 0.013 | 0.018 | <0.0046 | 0.004 | 0.020 | 0.006 |
| Hf | 11.40 | 12.98 | 19.62 | 9.20 | 16.97 | 16.17 | 20.38 | 18.76 |
| Ta | 79.14 | 9.19 | 18.37 | 21.90 | 23.84 | 16.07 | 53.99 | 28.76 |
| Pb | 0.14 | 0.36 | 0.11 | 0.46 | 1.23 | 0.46 | 0.29 | 0.35 |
| Th | <0.0080 | <0.0079 | 0.015 | 0.003 | <0.0059 | <0.00177 | 0.003 | <0.00176 |
| U | 0.44 | 0.43 | 1.64 | 0.26 | 0.51 | 1.37 | 2.35 | 0.96 |
| T C | 621 | 622 | 660 | 587 | 636 | 640 | 675 | 656 |

*Appendix 6-Hf Isotope Analyses of Zircons from Mt Daniel Rock Groups*

| Spot | MD15-1a | MD15-2 | MD15-8-1 | MD15-8 | MD15-16 | MD15-18 | MD15-20 |
|---|---|---|---|---|---|---|---|
| $^{176}Hf/^{177}Hf$ | 0.282841 | 0.282845 | 0.282836 | 0.282849 | 0.282848 | 0.282855 | 0.282860 |
| ±2 s | 0.000016 | 0.000025 | 0.000020 | 0.000020 | 0.000014 | 0.000012 | 0.000016 |
| $^{178}Hf/^{177}Hf$ | 1.467351 | 1.467444 | 1.467361 | 1.467226 | 1.467298 | 1.467253 | 1.467273 |
| ± 2 se | 0.000047 | 0.000106 | 0.000047 | 0.000051 | 0.000037 | 0.000026 | 0.000035 |
| $^{180}Hf/^{177}Hf$ | 1.886861 | 1.887097 | 1.886885 | 1.886780 | 1.886822 | 1.886801 | 1.886907 |
| ± 2 se | 0.000063 | 0.000118 | 0.000085 | 0.000080 | 0.000062 | 0.000044 | 0.000060 |
| $^{176}Lu/^{177}Hf$ | 0.00046 | 0.00036 | 0.00048 | 0.00048 | 0.00048 | 0.00042 | 0.00031 |
| ± 2 se | 0.000022 | 0.000021 | 0.000034 | 0.000035 | 0.000016 | 0.000007 | 0.000015 |
| $^{176}Yb/^{177}Hf$ | 0.0145 | 0.0111 | 0.0146 | 0.0151 | 0.0143 | 0.0132 | 0.0097 |
| ± 2 se | 0.000540 | 0.000897 | 0.000974 | 0.001054 | 0.000410 | 0.000260 | 0.000474 |
| Yb/Hf | 0.021 | 0.016 | 0.021 | 0.021 | 0.020 | 0.019 | 0.014 |
| total Hf (v) | 26.9 | 21.8 | 19.0 | 20.4 | 25.4 | 27.2 | 24.8 |
| Age Ma | 125 | 125 | 125 | 125 | 125 | 125 | 123 |
| ± 2 se | 3 | 3 | 3 | 3 | 3 | 3 | 3 |
| CHUR(t) | 0.2827 | 0.2827 | 0.2827 | 0.2827 | 0.2827 | 0.2827 | 0.2827 |
| $^{176}Hf/^{177}Hf$ (i) | 0.282840 | 0.282844 | 0.282835 | 0.282848 | 0.282847 | 0.282854 | 0.282859 |
| ± 2 se | 0.000016 | 0.000025 | 0.000020 | 0.000020 | 0.000014 | 0.000012 | 0.000016 |
| e Hf (t) | 5.2 | 5.3 | 5.0 | 5.4 | 5.4 | 5.7 | 5.8 |
| ± 2 se | 0.55 | 0.90 | 0.70 | 0.71 | 0.50 | 0.42 | 0.55 |
| Age Ma (Chosen except core) | 125 | 125 | 125 | 125 | 125 | 125 | 125 |
| ± 2 se | 2 | 2 | 2 | 2 | 2 | 2 | 2 |
| CHUR(t=mean age) | 0.28269 | 0.28269 | 0.28269 | 0.28269 | 0.28269 | 0.28269 | 0.28269 |
| 176Hf/177Hf(i) | 0.2828402 | 0.2828442 | 0.2828348 | 0.2828482 | 0.2828470 | 0.2828544 | 0.2828594 |
| ±2se | 0.0000157 | 0.0000254 | 0.0000199 | 0.0000201 | 0.0000143 | 0.0000118 | 0.0000156 |
| eHf(t= avg mean age Ma) | 5.2 | 5.3 | 5.0 | 5.4 | 5.4 | 5.7 | 5.8 |
| ± 2 se | 0.6 | 0.9 | 0.7 | 0.7 | 0.5 | 0.4 | 0.6 |
| eNd | 1.6 | 1.6 | 1.6 | 1.6 | 1.6 | 1.6 | 1.6 |

Abbreviations are used in Appendix 6: c=core and r=rim for the zircons which have inherited core and rim structures. Grain no (s) without any abbreviations are without inherited cores and of Early Cretaceous age.

| Spot | MD15-20-2 | MD15-29 | MD15-56 | MD15-63 | MD15-64 | MD15-68 | MD15-81 |
|---|---|---|---|---|---|---|---|
| $^{176}Hf/^{177}Hf$ | 0.282860 | 0.282846 | 0.282853 | 0.282837 | 0.282848 | 0.282830 | 0.282851 |
| ±2 se | 0.000015 | 0.000018 | 0.000014 | 0.000014 | 0.000015 | 0.000020 | 0.000013 |
| $^{178}Hf/^{177}Hf$ | 1.467253 | 1.467373 | 1.467268 | 1.467291 | 1.467225 | 1.467346 | 1.467262 |
| ± 2 se | 0.000032 | 0.000049 | 0.000048 | 0.000029 | 0.000035 | 0.000046 | 0.000040 |
| $^{180}Hf/^{177}Hf$ | 1.886837 | 1.886983 | 1.886832 | 1.886822 | 1.886783 | 1.886869 | 1.886784 |
| ± 2 se | 0.000054 | 0.000074 | 0.000074 | 0.000050 | 0.000056 | 0.000078 | 0.000055 |
| $^{176}Lu/^{177}Hf$ | 0.00032 | 0.00071 | 0.00036 | 0.00051 | 0.00040 | 0.00044 | 0.00066 |
| ± 2 se | 0.000010 | 0.000037 | 0.000006 | 0.000018 | 0.000007 | 0.000015 | 0.000011 |
| $^{176}Yb/^{177}Hf$ | 0.0100 | 0.0219 | 0.0107 | 0.0154 | 0.0120 | 0.0134 | 0.0182 |
| ± 2 se | 0.000361 | 0.000986 | 0.000221 | 0.000570 | 0.000234 | 0.000489 | 0.000330 |
| Yb/Hf | 0.014 | 0.031 | 0.015 | 0.022 | 0.017 | 0.019 | 0.026 |
| total Hf (v) | 23.8 | 24.3 | 24.9 | 30.4 | 25.2 | 29.1 | 27.7 |
| Age Ma | 123 | 123 | 125 | 125 | 127 | 125 | 129 |
| ± 2 se | 3 | 3 | 3 | 3 | 3 | 3 | 3 |
| CHUR(t) | 0.2827 | 0.2827 | 0.2827 | 0.2827 | 0.2827 | 0.2827 | 0.2827 |
| $^{176}Hf/^{177}Hf$ (i) | 0.282860 | 0.282844 | 0.282852 | 0.282836 | 0.282847 | 0.282829 | 0.282849 |
| ± 2 se | 0.000015 | 0.000018 | 0.000014 | 0.000014 | 0.000015 | 0.000020 | 0.000013 |
| e Hf (t) | 5.8 | 5.3 | 5.6 | 5.0 | 5.5 | 4.8 | 5.6 |
| ± 2 se | 0.52 | 0.64 | 0.50 | 0.51 | 0.51 | 0.71 | 0.45 |
| Age Ma (Chosen except core) | 125 | 125 | 125 | 125 | 125 | 125 | 125 |
| ± 2 se | 2 | 2 | 2 | 2 | 2 | 2 | 2 |
| CHUR(t=mean age) | 0.28269 | 0.28269 | 0.28269 | 0.28269 | 0.28269 | 0.28269 | 0.28269 |
| 176Hf/177Hf(i) | 0.2828597 | 0.2828445 | 0.2828524 | 0.2828362 | 0.2828472 | 0.2828291 | 0.2828491 |
| ±2se | 0.0000146 | 0.0000182 | 0.0000142 | 0.0000145 | 0.0000145 | 0.0000202 | 0.0000128 |
| eHf(t= avg mean age Ma) | 5.8 | 5.3 | 5.6 | 5.0 | 5.4 | 4.8 | 5.5 |
| ± 2 se | 0.5 | 0.6 | 0.5 | 0.5 | 0.5 | 0.7 | 0.5 |
| eNd | 1.6 | 1.6 | 1.6 | 1.6 | 1.6 | 1.6 | 1.6 |

| Spot | MD15-101 | MD15-110 | MD15-125 | MD15-127 | MD15-132 | MD15-135 | MD15-146 |
|---|---|---|---|---|---|---|---|
| $^{176}Hf/^{177}Hf$ | 0.282839 | 0.282848 | 0.282850 | 0.282848 | 0.282849 | 0.282838 | 0.282828 |
| ±2 se | 0.000015 | 0.000013 | 0.000012 | 0.000011 | 0.000015 | 0.000019 | 0.000019 |
| $^{178}Hf/^{177}Hf$ | 1.467307 | 1.467274 | 1.467297 | 1.467278 | 1.467359 | 1.467323 | 1.467346 |
| ± 2 se | 0.000045 | 0.000037 | 0.000029 | 0.000034 | 0.000056 | 0.000061 | 0.000071 |
| $^{180}Hf/^{177}Hf$ | 1.887007 | 1.886857 | 1.886808 | 1.886842 | 1.886918 | 1.886925 | 1.886947 |
| ± 2 se | 0.000067 | 0.000048 | 0.000055 | 0.000052 | 0.000094 | 0.000074 | 0.000073 |
| $^{176}Lu/^{177}Hf$ | 0.00050 | 0.00037 | 0.00059 | 0.00053 | 0.00047 | 0.00065 | 0.00050 |
| ± 2 se | 0.000012 | 0.000002 | 0.000008 | 0.000010 | 0.000012 | 0.000013 | 0.000006 |
| $^{176}Yb/^{177}Hf$ | 0.0137 | 0.0099 | 0.0174 | 0.0157 | 0.0136 | 0.0193 | 0.0151 |
| ± 2 se | 0.000399 | 0.000037 | 0.000197 | 0.000348 | 0.000360 | 0.000487 | 0.000218 |
| Yb/Hf | 0.020 | 0.014 | 0.025 | 0.022 | 0.019 | 0.027 | 0.021 |
| total Hf (v) | 28.9 | 26.3 | 28.2 | 28.1 | 26.2 | 26.6 | 27.4 |
| Age Ma | 125 | 125 | 125 | 125 | 125 | 125 | 125 |
| ± 2 se | 3 | 3 | 3 | 3 | 3 | 3 | 3 |
| CHUR(t) | 0.2827 | 0.2827 | 0.2827 | 0.2827 | 0.2827 | 0.2827 | 0.2827 |
| $^{176}Hf/^{177}Hf$ (i) | 0.282837 | 0.282847 | 0.282849 | 0.282847 | 0.282848 | 0.282837 | 0.282826 |
| ± 2 se | 0.000015 | 0.000013 | 0.000012 | 0.000011 | 0.000015 | 0.000019 | 0.000019 |
| e Hf (t) | 5.1 | 5.4 | 5.5 | 5.4 | 5.4 | 5.0 | 4.7 |
| ± 2 se | 0.55 | 0.47 | 0.44 | 0.40 | 0.53 | 0.66 | 0.69 |
| Age Ma (Chosen except core) | 125 | 125 | 125 | 125 | 125 | 125 | 125 |
| ± 2 se | 2 | 2 | 2 | 2 | 2 | 2 | 2 |
| CHUR(t=mean age) | 0.28269 | 0.28269 | 0.28269 | 0.28269 | 0.28269 | 0.28269 | 0.28269 |
| 176Hf/177Hf(i) | 0.2828375 | 0.2828472 | 0.2828486 | 0.2828467 | 0.2828483 | 0.2828365 | 0.2828264 |
| ±2se | 0.0000154 | 0.0000133 | 0.0000123 | 0.0000112 | 0.0000151 | 0.0000187 | 0.0000194 |
| eHf(t= avg mean age Ma) | 5.1 | 5.4 | 5.5 | 5.4 | 5.4 | 5.0 | 4.7 |
| ± 2 se | 0.5 | 0.5 | 0.4 | 0.4 | 0.5 | 0.7 | 0.7 |
| eNd | 1.6 | 1.6 | 1.6 | 1.6 | 1.6 | 1.6 | 1.6 |

| Spot | MD15-151 | MD15-161 | MD13-12 | MD13-16 | MD13-27 | MD13-28 | MD13-29 |
|---|---|---|---|---|---|---|---|
| $^{176}Hf/^{177}Hf$ | 0.282853 | 0.282845 | 0.282781 | 0.282777 | 0.282801 | 0.282790 | 0.282786 |
| ±2 se | 0.000016 | 0.000013 | 0.000016 | 0.000012 | 0.000017 | 0.000018 | 0.000018 |
| $^{178}Hf/^{177}Hf$ | 1.467304 | 1.467315 | 1.467250 | 1.467293 | 1.467280 | 1.467316 | 1.467297 |
| ± 2 se | 0.000055 | 0.000047 | 0.000034 | 0.000034 | 0.000037 | 0.000032 | 0.000031 |
| $^{180}Hf/^{177}Hf$ | 1.886840 | 1.886828 | 1.886840 | 1.886897 | 1.886831 | 1.886895 | 1.886835 |
| ± 2 se | 0.000071 | 0.000065 | 0.000056 | 0.000065 | 0.000066 | 0.000067 | 0.000067 |
| $^{176}Lu/^{177}Hf$ | 0.00049 | 0.00051 | 0.00049 | 0.00043 | 0.00033 | 0.00047 | 0.00057 |
| ± 2 se | 0.000025 | 0.000020 | 0.000008 | 0.000001 | 0.000001 | 0.000002 | 0.000017 |
| $^{176}Yb/^{177}Hf$ | 0.0145 | 0.0155 | 0.0148 | 0.0127 | 0.0098 | 0.0139 | 0.0171 |
| ± 2 se | 0.000669 | 0.000602 | 0.000273 | 0.000052 | 0.000046 | 0.000063 | 0.000577 |
| Yb/Hf | 0.021 | 0.022 | 0.021 | 0.018 | 0.014 | 0.020 | 0.024 |
| total Hf (v) | 25.1 | 30.1 | 20.9 | 21.1 | 20.3 | 20.4 | 22.8 |
| Age Ma | 125 | 126 | 114 | 111 | 122 | 125 | 125 |
| ± 2 se | 3 | 3 | 6 | 6 | 4 | 3 | 3 |
| CHUR(t) | 0.2827 | 0.2827 | 0.2827 | 0.2827 | 0.2827 | 0.2827 | 0.2827 |
| $^{176}Hf/^{177}Hf$ (i) | 0.282851 | 0.282844 | 0.282780 | 0.282776 | 0.282800 | 0.282789 | 0.282784 |
| ± 2 se | 0.000016 | 0.000013 | 0.000016 | 0.000012 | 0.000017 | 0.000018 | 0.000018 |
| e Hf (t) | 5.6 | 5.3 | 2.8 | 2.6 | 3.7 | 3.3 | 3.2 |
| ± 2 se | 0.58 | 0.48 | 0.58 | 0.44 | 0.59 | 0.62 | 0.64 |
| Age Ma (Chosen except core) | 125 | 125 | 123 | 123 | 123 | 123 | 123 |
| ± 2 se | 2 | 2 | 6 | 6 | 6 | 6 | 6 |
| CHUR(t=mean age) | 0.28269 | 0.28269 | 0.28270 | 0.28270 | 0.28270 | 0.28270 | 0.28270 |
| 176Hf/177Hf(i) | 0.2828514 | 0.2828439 | 0.2827798 | 0.2827755 | 0.2828002 | 0.2827889 | 0.2827842 |
| ±2se | 0.0000164 | 0.0000135 | 0.0000164 | 0.0000124 | 0.0000167 | 0.0000176 | 0.0000181 |
| eHf(t= avg mean age Ma) | 5.6 | 5.3 | 3.0 | 2.8 | 3.7 | 3.3 | 3.1 |
| ± 2 se | 0.6 | 0.5 | 0.6 | 0.4 | 0.6 | 0.6 | 0.6 |
| eNd | 1.6 | 1.6 | 2.7 | 2.7 | 2.7 | 2.7 | 2.7 |

| Spot | MD13-30 | MD13-31 | MD13-32 | MD13-34 | MD13-42 | MD13-48 | MD22b-3 |
|---|---|---|---|---|---|---|---|
| $^{176}Hf/^{177}Hf$ | 0.282785 | 0.282798 | 0.282784 | 0.282874 | 0.282797 | 0.282803 | 0.282810 |
| ±2 se | 0.000015 | 0.000017 | 0.000014 | 0.000013 | 0.000016 | 0.000015 | 0.000015 |
| $^{178}Hf/^{177}Hf$ | 1.467271 | 1.467302 | 1.467283 | 1.467240 | 1.467273 | 1.467251 | 1.467306 |
| ± 2 se | 0.000035 | 0.000034 | 0.000031 | 0.000033 | 0.000046 | 0.000037 | 0.000036 |
| $^{180}Hf/^{177}Hf$ | 1.886837 | 1.886818 | 1.886801 | 1.886790 | 1.886845 | 1.886796 | 1.886784 |
| ± 2 se | 0.000062 | 0.000062 | 0.000062 | 0.000059 | 0.000063 | 0.000060 | 0.000059 |
| $^{176}Lu/^{177}Hf$ | 0.00043 | 0.00045 | 0.00038 | 0.00050 | 0.00046 | 0.00047 | 0.00056 |
| ± 2 se | 0.000011 | 0.000012 | 0.000002 | 0.000013 | 0.000005 | 0.000006 | 0.000001 |
| $^{176}Yb/^{177}Hf$ | 0.0127 | 0.0132 | 0.0112 | 0.0144 | 0.0120 | 0.0120 | 0.0172 |
| ± 2 se | 0.000352 | 0.000387 | 0.000041 | 0.000390 | 0.000147 | 0.000114 | 0.000083 |
| Yb/Hf | 0.018 | 0.019 | 0.016 | 0.020 | 0.017 | 0.017 | 0.024 |
| total Hf (v) | 22.6 | 20.4 | 22.3 | 24.8 | 19.7 | 19.9 | 22.0 |
| Age Ma | 126 | 126 | 125 | 119 | 125 | 125 | 120 |
| ± 2 se | 4 | 5 | 3 | 3 | 5 | 3 | 4 |
| CHUR(t) | 0.2827 | 0.2827 | 0.2827 | 0.2827 | 0.2827 | 0.2827 | 0.2827 |
| $^{176}Hf/^{177}Hf$ (i) | 0.282784 | 0.282796 | 0.282783 | 0.282873 | 0.282795 | 0.282802 | 0.282809 |
| ± 2 se | 0.000015 | 0.000017 | 0.000014 | 0.000013 | 0.000016 | 0.000015 | 0.000015 |
| e Hf (t) | 3.2 | 3.6 | 3.1 | 6.2 | 3.6 | 3.8 | 3.9 |
| ± 2 se | 0.52 | 0.61 | 0.50 | 0.47 | 0.57 | 0.53 | 0.54 |
| Age Ma (Chosen except core) | 123 | 123 | 123 | 123 | 123 | 123 | 122 |
| ± 2 se | 6 | 6 | 6 | 6 | 6 | 6 | 2 |
| CHUR(t=mean age) | 0.28270 | 0.28270 | 0.28270 | 0.28270 | 0.28270 | 0.28270 | 0.28270 |
| 176Hf/177Hf(i) | 0.2827837 | 0.2827965 | 0.2827834 | 0.2828727 | 0.2827955 | 0.2828017 | 0.2828090 |
| ±2se | 0.0000147 | 0.0000172 | 0.0000140 | 0.0000134 | 0.0000162 | 0.0000151 | 0.0000153 |
| eHf(t= avg mean age Ma) | 3.1 | 3.6 | 3.1 | 6.3 | 3.5 | 3.7 | 4.0 |
| ± 2 se | 0.5 | 0.6 | 0.5 | 0.5 | 0.6 | 0.5 | 0.5 |
| eNd | 2.7 | 2.7 | 2.7 | 2.7 | 2.7 | 2.7 | 1.2 |

| Spot | MD22b-4 | MD22b-7 | MD22b-12 | MD22b-16 | MD22b-19 | MD22b-23 | MD22b-24 |
|---|---|---|---|---|---|---|---|
| $^{176}Hf/^{177}Hf$ | 0.282818 | 0.282834 | 0.282804 | 0.282801 | 0.282794 | 0.282805 | 0.282802 |
| ±2 se | 0.000016 | 0.000027 | 0.000019 | 0.000015 | 0.000024 | 0.000018 | 0.000018 |
| $^{178}Hf/^{177}Hf$ | 1.467269 | 1.467249 | 1.467317 | 1.467249 | 1.467317 | 1.467292 | 1.467288 |
| ± 2 se | 0.000036 | 0.000050 | 0.000042 | 0.000032 | 0.000042 | 0.000040 | 0.000042 |
| $^{180}Hf/^{177}Hf$ | 1.886863 | 1.886796 | 1.886847 | 1.886763 | 1.886851 | 1.886901 | 1.886850 |
| ± 2 se | 0.000061 | 0.000078 | 0.000071 | 0.000076 | 0.000092 | 0.000072 | 0.000069 |
| $^{176}Lu/^{177}Hf$ | 0.00040 | 0.00100 | 0.00073 | 0.00064 | 0.00068 | 0.00073 | 0.00054 |
| ± 2 se | 0.000002 | 0.000020 | 0.000010 | 0.000003 | 0.000032 | 0.000014 | 0.000008 |
| $^{176}Yb/^{177}Hf$ | 0.0125 | 0.0276 | 0.0206 | 0.0206 | 0.0182 | 0.0219 | 0.0166 |
| ± 2 se | 0.000028 | 0.000542 | 0.000216 | 0.000100 | 0.000812 | 0.000505 | 0.000242 |
| Yb/Hf | 0.018 | 0.039 | 0.029 | 0.029 | 0.026 | 0.031 | 0.024 |
| total Hf (v) | 18.4 | 11.3 | 16.7 | 15.1 | 14.7 | 15.2 | 19.0 |
| Age Ma | 114 | 120 | 120 | 121 | 120 | 120 | 123 |
| ± 2 se | 7 | 4 | 4 | 5 | 4 | 4 | 4 |
| CHUR(t) | 0.2827 | 0.2827 | 0.2827 | 0.2827 | 0.2827 | 0.2827 | 0.2827 |
| $^{176}Hf/^{177}Hf$ (i) | 0.282817 | 0.282832 | 0.282802 | 0.282800 | 0.282792 | 0.282803 | 0.282801 |
| ± 2 se | 0.000016 | 0.000027 | 0.000019 | 0.000015 | 0.000024 | 0.000018 | 0.000018 |
| e Hf (t) | 4.1 | 4.7 | 3.7 | 3.6 | 3.3 | 3.7 | 3.7 |
| ± 2 se | 0.56 | 0.96 | 0.69 | 0.54 | 0.83 | 0.63 | 0.64 |
| Age Ma (Chosen except core) | 122 | 122 | 122 | 122 | 122 | 122 | 122 |
| ± 2 se | 2 | 2 | 2 | 2 | 2 | 2 | 2 |
| CHUR(t=mean age) | 0.28270 | 0.28270 | 0.28270 | 0.28270 | 0.28270 | 0.28270 | 0.28270 |
| 176Hf/177Hf(i) | 0.2828166 | 0.2828317 | 0.2828022 | 0.2827996 | 0.2827921 | 0.2828029 | 0.2828006 |
| ±2se | 0.0000157 | 0.0000271 | 0.0000194 | 0.0000152 | 0.0000236 | 0.0000179 | 0.0000180 |
| eHf(t= avg mean age Ma) | 4.3 | 4.8 | 3.7 | 3.7 | 3.4 | 3.8 | 3.7 |
| ± 2 se | 0.6 | 1.0 | 0.7 | 0.5 | 0.8 | 0.6 | 0.6 |
| eNd | 1.2 | 1.2 | 1.2 | 1.2 | 1.2 | 1.2 | 1.2 |

| Spot | MD22b-26 | MD22b-27 | MD22b-33 | MD22b-35 | MD22b-40 | MD22b-42 | MD22b-55 |
|---|---|---|---|---|---|---|---|
| $^{176}Hf/^{177}Hf$ | 0.282800 | 0.282766 | 0.282804 | 0.282808 | 0.282814 | 0.282814 | 0.282800 |
| ±2 se | 0.000019 | 0.000017 | 0.000017 | 0.000018 | 0.000015 | 0.000015 | 0.000014 |
| $^{178}Hf/^{177}Hf$ | 1.467313 | 1.467282 | 1.467274 | 1.467299 | 1.467293 | 1.467300 | 1.467272 |
| ± 2 se | 0.000043 | 0.000046 | 0.000041 | 0.000046 | 0.000039 | 0.000036 | 0.000038 |
| $^{180}Hf/^{177}Hf$ | 1.886846 | 1.886863 | 1.886857 | 1.886844 | 1.886780 | 1.886800 | 1.886802 |
| ± 2 se | 0.000064 | 0.000074 | 0.000071 | 0.000071 | 0.000065 | 0.000062 | 0.000055 |
| $^{176}Lu/^{177}Hf$ | 0.00063 | 0.00156 | 0.00087 | 0.00059 | 0.00043 | 0.00048 | 0.00075 |
| ± 2 se | 0.000014 | 0.000010 | 0.000005 | 0.000016 | 0.000009 | 0.000006 | 0.000006 |
| $^{176}Yb/^{177}Hf$ | 0.0188 | 0.0467 | 0.0263 | 0.0177 | 0.0129 | 0.0142 | 0.0218 |
| ± 2 se | 0.000473 | 0.000312 | 0.000090 | 0.000520 | 0.000309 | 0.000166 | 0.000230 |
| Yb/Hf | 0.027 | 0.067 | 0.037 | 0.025 | 0.018 | 0.020 | 0.031 |
| total Hf (v) | 17.3 | 19.5 | 17.9 | 17.0 | 17.3 | 22.9 | 19.7 |
| Age Ma | 120 | 122 | 120 | 128 | 120 | 121 | 126 |
| ± 2 se | 4 | 3 | 4 | 4 | 4 | 4 | 5 |
| CHUR(t) | 0.2827 | 0.2827 | 0.2827 | 0.2827 | 0.2827 | 0.2827 | 0.2827 |
| $^{176}Hf/^{177}Hf$ (i) | 0.282798 | 0.282763 | 0.282802 | 0.282807 | 0.282813 | 0.282813 | 0.282799 |
| ± 2 se | 0.000019 | 0.000017 | 0.000017 | 0.000018 | 0.000015 | 0.000015 | 0.000014 |
| e Hf (t) | 3.6 | 2.3 | 3.7 | 4.1 | 4.1 | 4.1 | 3.7 |
| ± 2 se | 0.66 | 0.61 | 0.62 | 0.64 | 0.54 | 0.53 | 0.50 |
| Age Ma (Chosen except core) | 122 | 122 | 122 | 122 | 122 | 122 | 122 |
| ± 2 se | 2 | 2 | 2 | 2 | 2 | 2 | 2 |
| CHUR(t=mean age) | 0.28270 | 0.28270 | 0.28270 | 0.28270 | 0.28270 | 0.28270 | 0.28270 |
| 176Hf/177Hf(i) | 0.2827983 | 0.2827626 | 0.2828024 | 0.2828071 | 0.2828131 | 0.2828125 | 0.2827987 |
| ±2se | 0.0000188 | 0.0000174 | 0.0000175 | 0.0000181 | 0.0000153 | 0.0000150 | 0.0000143 |
| eHf(t= avg mean age Ma) | 3.6 | 2.3 | 3.8 | 3.9 | 4.1 | 4.1 | 3.6 |
| ± 2 se | 0.7 | 0.6 | 0.6 | 0.6 | 0.5 | 0.5 | 0.5 |
| eNd | 1.2 | 1.2 | 1.2 | 1.2 | 1.2 | 1.2 | 1.2 |

| Spot | MD26-10 | MD26-23 | MD26-27 | MD26-32 | MD26-48 | MD26-50 | MD26-63 |
|---|---|---|---|---|---|---|---|
| $^{176}Hf/^{177}Hf$ | 0.282783 | 0.282785 | 0.282781 | 0.282797 | 0.282780 | 0.282791 | 0.282804 |
| ±2 se | 0.000016 | 0.000017 | 0.000026 | 0.000016 | 0.000027 | 0.000018 | 0.000014 |
| $^{178}Hf/^{177}Hf$ | 1.467220 | 1.467258 | 1.467264 | 1.467264 | 1.467341 | 1.467270 | 1.467255 |
| ± 2 se | 0.000061 | 0.000042 | 0.000134 | 0.000044 | 0.000113 | 0.000071 | 0.000033 |
| $^{180}Hf/^{177}Hf$ | 1.886845 | 1.886877 | 1.886904 | 1.886859 | 1.886931 | 1.886838 | 1.886798 |
| ± 2 se | 0.000069 | 0.000061 | 0.000120 | 0.000063 | 0.000130 | 0.000078 | 0.000059 |
| $^{176}Lu/^{177}Hf$ | 0.00038 | 0.00029 | 0.00043 | 0.00046 | 0.00050 | 0.00042 | 0.00043 |
| ± 2 se | 0.000007 | 0.000008 | 0.000012 | 0.000003 | 0.000017 | 0.000012 | 0.000005 |
| $^{176}Yb/^{177}Hf$ | 0.0111 | 0.0082 | 0.0114 | 0.0136 | 0.0131 | 0.0109 | 0.0117 |
| ± 2 se | 0.000194 | 0.000227 | 0.000386 | 0.000062 | 0.000404 | 0.000295 | 0.000157 |
| Yb/Hf | 0.016 | 0.012 | 0.016 | 0.019 | 0.019 | 0.016 | 0.017 |
| total Hf (v) | 16.7 | 18.8 | 14.7 | 17.5 | 15.0 | 14.7 | 20.0 |
| Age Ma | 126 | 123 | 127 | 128 | 126 | 125 | 125 |
| ± 2 se | 5 | 4 | 5 | 4 | 5 | 4 | 4 |
| CHUR(t) | 0.2827 | 0.2827 | 0.2827 | 0.2827 | 0.2827 | 0.2827 | 0.2827 |
| $^{176}Hf/^{177}Hf$ (i) | 0.282782 | 0.282784 | 0.282780 | 0.282796 | 0.282779 | 0.282790 | 0.282803 |
| ± 2 se | 0.000016 | 0.000017 | 0.000026 | 0.000016 | 0.000027 | 0.000018 | 0.000014 |
| e Hf (t) | 3.1 | 3.1 | 3.1 | 3.7 | 3.0 | 3.4 | 3.9 |
| ± 2 se | 0.57 | 0.59 | 0.91 | 0.56 | 0.95 | 0.64 | 0.51 |
| Age Ma (Chosen except core) | 124 | 124 | 124 | 124 | 124 | 124 | 124 |
| ± 2 se | 6 | 6 | 6 | 6 | 6 | 6 | 6 |
| CHUR(t=mean age) | 0.28270 | 0.28270 | 0.28270 | 0.28270 | 0.28270 | 0.28270 | 0.28270 |
| 176Hf/177Hf(i) | 0.2827821 | 0.2827843 | 0.2827799 | 0.2827960 | 0.2827789 | 0.2827903 | 0.2828035 |
| ±2se | 0.0000161 | 0.0000168 | 0.0000257 | 0.0000159 | 0.0000269 | 0.0000181 | 0.0000144 |
| eHf(t= avg mean age Ma) | 3.1 | 3.2 | 3.0 | 3.6 | 3.0 | 3.4 | 3.8 |
| ± 2 se | 0.6 | 0.6 | 0.9 | 0.6 | 1.0 | 0.6 | 0.5 |
| eNd | 0.3 | 0.3 | 0.3 | 0.3 | 0.3 | 0.3 | 0.3 |

| Spot | MD26-64c | MD26-31c | MD26-37c | MD26-54c | MD8-1 | MD8-5 | MD8-6 |
|---|---|---|---|---|---|---|---|
| $^{176}Hf/^{177}Hf$ | 0.282744 | 0.282687 | 0.282674 | 0.282695 | 0.282862 | 0.282852 | 0.282864 |
| ±2 se | 0.000017 | 0.000015 | 0.000027 | 0.000019 | 0.000014 | 0.000018 | 0.000015 |
| $^{178}Hf/^{177}Hf$ | 1.467262 | 1.467247 | 1.467251 | 1.467268 | 1.467259 | 1.467272 | 1.467287 |
| ± 2 se | 0.000037 | 0.000056 | 0.000049 | 0.000029 | 0.000045 | 0.000058 | 0.000075 |
| $^{180}Hf/^{177}Hf$ | 1.886777 | 1.886852 | 1.886975 | 1.886857 | 1.886820 | 1.886904 | 1.886787 |
| ± 2 se | 0.000056 | 0.000059 | 0.000085 | 0.000056 | 0.000061 | 0.000076 | 0.000077 |
| $^{176}Lu/^{177}Hf$ | 0.00327 | 0.00178 | 0.00347 | 0.00328 | 0.00027 | 0.00044 | 0.00049 |
| ± 2 se | 0.000053 | 0.000054 | 0.000132 | 0.000037 | 0.000005 | 0.000010 | 0.000013 |
| $^{176}Yb/^{177}Hf$ | 0.1028 | 0.0576 | 0.1057 | 0.0988 | 0.0082 | 0.0120 | 0.0141 |
| ± 2 se | 0.001835 | 0.001881 | 0.004108 | 0.001218 | 0.000248 | 0.000364 | 0.000346 |
| Yb/Hf | 0.146 | 0.082 | 0.150 | 0.140 | 0.012 | 0.017 | 0.020 |
| total Hf (v) | 22.5 | 27.2 | 12.4 | 20.9 | 26.0 | 22.4 | 21.9 |
| Age Ma | 311 | 306 | 377 | 356 | 107 | 118 | 114 |
| ± 2 se | 6 | 6 | 8 | 8 | 3 | 5 | 3 |
| CHUR(t) | 0.2826 | 0.2826 | 0.2825 | 0.2826 | 0.2827 | 0.2827 | 0.2827 |
| $^{176}Hf/^{177}Hf$ (i) | 0.282725 | 0.282677 | 0.282650 | 0.282673 | 0.282862 | 0.282851 | 0.282863 |
| ± 2 se | 0.000017 | 0.000015 | 0.000027 | 0.000019 | 0.000014 | 0.000018 | 0.000015 |
| e Hf (t) | 5.2 | 3.4 | 4.0 | 4.3 | 5.5 | 5.4 | 5.7 |
| ± 2 se | 0.61 | 0.54 | 0.96 | 0.67 | 0.50 | 0.62 | 0.53 |
| Age Ma (Chosen except core) | - | - | - | - | 112 | 112 | 112 |
| ± 2 se | - | - | - | - | 12 | 12 | 12 |
| CHUR(t=mean age) | - | - | - | - | 0.28270 | 0.28270 | 0.28270 |
| 176Hf/177Hf(i) | - | - | - | - | 0.2828618 | 0.2828507 | 0.2828630 |
| ±2se | - | - | - | - | 0.0000141 | 0.0000175 | 0.0000150 |
| eHf(t= avg mean age Ma) | - | - | - | - | 5.6 | 5.2 | 5.7 |
| ± 2 se | - | - | - | - | 0.5 | 0.6 | 0.5 |
| eNd | - | - | - | - | -1.0 | -1.0 | -1.0 |

| Spot | MD8-2c | MD8-3c | MD8-4c | MD22a-3 | MD22a-18r | MD22a-6c | MD22a-9c |
|---|---|---|---|---|---|---|---|
| $^{176}Hf/^{177}Hf$ | 0.282705 | 0.282749 | 0.282733 | 0.282753 | 0.282701 | 0.282697 | 0.282702 |
| ±2 se | 0.000012 | 0.000018 | 0.000011 | 0.000017 | 0.000021 | 0.000019 | 0.000021 |
| $^{178}Hf/^{177}Hf$ | 1.467286 | 1.467254 | 1.467285 | 1.467274 | 1.467305 | 1.467264 | 1.467219 |
| ± 2 se | 0.000032 | 0.000031 | 0.000028 | 0.000038 | 0.000052 | 0.000055 | 0.000065 |
| $^{180}Hf/^{177}Hf$ | 1.886817 | 1.886838 | 1.886866 | 1.886799 | 1.886801 | 1.886808 | 1.886793 |
| ± 2 se | 0.000047 | 0.000057 | 0.000046 | 0.000058 | 0.000082 | 0.000074 | 0.000076 |
| $^{176}Lu/^{177}Hf$ | 0.00141 | 0.00373 | 0.00165 | 0.00186 | 0.00032 | 0.00118 | 0.00152 |
| ± 2 se | 0.000021 | 0.000125 | 0.000023 | 0.000040 | 0.000018 | 0.000012 | 0.000028 |
| $^{176}Yb/^{177}Hf$ | 0.0416 | 0.1070 | 0.0455 | 0.0748 | 0.0128 | 0.0493 | 0.0653 |
| ± 2 se | 0.000739 | 0.003376 | 0.000676 | 0.000938 | 0.000923 | 0.000540 | 0.001613 |
| Yb/Hf | 0.059 | 0.152 | 0.064 | 0.106 | 0.018 | 0.070 | 0.093 |
| total Hf (v) | 33.2 | 26.7 | 34.0 | 28.87 | 19.16 | 24.71 | 20.55 |
| Age Ma | 300 | 330 | 310 | 129 | 125 | 357 | 352 |
| ± 2 se | 7 | 7 | 7 | 4 | 4 | 8 | 7 |
| CHUR(t) | 0.2826 | 0.2826 | 0.2826 | 0.2827 | 0.2827 | 0.2826 | 0.2826 |
| $^{176}Hf/^{177}Hf$ (i) | 0.282697 | 0.282726 | 0.282724 | 0.282749 | 0.282700 | 0.282689 | 0.282692 |
| ± 2 se | 0.000012 | 0.000018 | 0.000011 | 0.000017 | 0.000021 | 0.000019 | 0.000021 |
| e Hf (t) | 3.9 | 5.6 | 5.1 | 2.0 | 0.2 | 4.9 | 4.9 |
| ± 2 se | 0.42 | 0.62 | 0.40 | 0.62 | 0.74 | 0.68 | 0.76 |
| Age Ma (Chosen except core) | - | - | - | 125 | 125 | - | - |
| ± 2 se | - | - | - | 18 | 18 | - | - |
| CHUR(t=mean age) | - | - | - | 0.28269 | 0.28269 | - | - |
| 176Hf/177Hf(i) | - | - | - | 0.2827488 | 0.2827005 | - | - |
| ±2se | - | - | - | 0.0000174 | 0.0000209 | - | - |
| eHf(t= avg mean age Ma) | - | - | - | 1.9 | 0.2 | - | - |
| ± 2 se | - | - | - | 0.6 | 0.7 | - | - |
| eNd | - | - | - | -1.2 | -1.2 | - | - |

| Spot | MD22a-12c-1 | MD22a-12c-2 | MD22a-14c | MD22a-22c | MD22a-32c | MD17a-1 | MD17a-2 |
|---|---|---|---|---|---|---|---|
| $^{176}Hf/^{177}Hf$ | 0.282677 | 0.282672 | 0.282682 | 0.282696 | 0.282665 | 0.282901 | 0.282844 |
| ±2 se | 0.000034 | 0.000024 | 0.000031 | 0.000014 | 0.000023 | 0.000035 | 0.000020 |
| $^{178}Hf/^{177}Hf$ | 1.467315 | 1.467235 | 1.467275 | 1.467267 | 1.467283 | 1.467295 | 1.467310 |
| ± 2 se | 0.000080 | 0.000054 | 0.000064 | 0.000042 | 0.000052 | 0.000053 | 0.000045 |
| $^{180}Hf/^{177}Hf$ | 1.886816 | 1.886824 | 1.886884 | 1.886792 | 1.886850 | 1.886816 | 1.886906 |
| ± 2 se | 0.000129 | 0.000082 | 0.000116 | 0.000058 | 0.000071 | 0.000109 | 0.000088 |
| $^{176}Lu/^{177}Hf$ | 0.00100 | 0.00143 | 0.00057 | 0.00103 | 0.00222 | 0.00181 | 0.00107 |
| ± 2 se | 0.000021 | 0.000036 | 0.000005 | 0.000022 | 0.000055 | 0.000030 | 0.000033 |
| $^{176}Yb/^{177}Hf$ | 0.0387 | 0.0611 | 0.0244 | 0.0407 | 0.0902 | 0.0635 | 0.0361 |
| ± 2 se | 0.001148 | 0.001821 | 0.000172 | 0.000706 | 0.003075 | 0.001395 | 0.000687 |
| Yb/Hf | 0.055 | 0.087 | 0.035 | 0.058 | 0.128 | 0.090 | 0.051 |
| total Hf (v) | 17.24 | 16.85 | 8.97 | 29.76 | 25.99 | 12.3 | 18.0 |
| Age Ma | 329 | 359 | 363 | 335 | 314 | 120 | 120 |
| ± 2 se | 9 | 11 | 8 | 8 | 7 | 4 | 3 |
| CHUR(t) | 0.2826 | 0.2825 | 0.2825 | 0.2826 | 0.2826 | 0.2827 | 0.2827 |
| $^{176}Hf/^{177}Hf$ (i) | 0.282671 | 0.282662 | 0.282678 | 0.282690 | 0.282652 | 0.282897 | 0.282841 |
| ± 2 se | 0.000034 | 0.000024 | 0.000031 | 0.000014 | 0.000023 | 0.000035 | 0.000020 |
| e Hf (t) | 3.7 | 4.0 | 4.7 | 4.5 | 2.7 | 7.0 | 5.1 |
| ± 2 se | 1.22 | 0.86 | 1.11 | 0.49 | 0.81 | 1.25 | 0.71 |
| Chosen Cret | - | - | - | - | - | 116 | 116 |
| ± 2 se | - | - | - | - | - | 4 | 4 |
| CHUR(t=mean age) | - | - | - | - | - | 0.28270 | 0.28270 |
| 176Hf/177Hf(i) | - | - | - | - | - | 0.2828970 | 0.2828414 |
| ±2se | - | - | - | - | - | 0.0000353 | 0.0000201 |
| Hf(t= avg mean age Ma | - | - | - | - | - | 7.0 | 5.0 |
| ± 2 se | - | - | - | - | - | 1.2 | 0.7 |
| eNd | - | - | - | - | - | 2.3 | 2.3 |

| Spot | MD17a-11 | MD17a-13-1 | MD17a-13-2 | MD17a-18 | MD17a-21 | MD17a-30 | MD17a-37 |
|---|---|---|---|---|---|---|---|
| $^{176}Hf/^{177}Hf$ | 0.282856 | 0.282860 | 0.282868 | 0.282882 | 0.282848 | 0.282875 | 0.282871 |
| ±2 se | 0.000017 | 0.000016 | 0.000016 | 0.000026 | 0.000016 | 0.000017 | 0.000028 |
| $^{178}Hf/^{177}Hf$ | 1.467314 | 1.467224 | 1.467280 | 1.467336 | 1.467291 | 1.467301 | 1.467317 |
| ± 2 se | 0.000052 | 0.000032 | 0.000030 | 0.000051 | 0.000032 | 0.000034 | 0.000068 |
| $^{180}Hf/^{177}Hf$ | 1.886943 | 1.886804 | 1.886806 | 1.886793 | 1.886853 | 1.887122 | 1.886804 |
| ± 2 se | 0.000093 | 0.000055 | 0.000057 | 0.000095 | 0.000067 | 0.000076 | 0.000120 |
| $^{176}Lu/^{177}Hf$ | 0.00097 | 0.00116 | 0.00139 | 0.00140 | 0.00108 | 0.00130 | 0.00072 |
| ± 2 se | 0.000009 | 0.000024 | 0.000030 | 0.000025 | 0.000058 | 0.000021 | 0.000034 |
| $^{176}Yb/^{177}Hf$ | 0.0351 | 0.0412 | 0.0466 | 0.0528 | 0.0377 | 0.0471 | 0.0253 |
| ± 2 se | 0.000708 | 0.000825 | 0.000969 | 0.001353 | 0.002295 | 0.000916 | 0.001258 |
| Yb/Hf | 0.050 | 0.058 | 0.066 | 0.075 | 0.053 | 0.067 | 0.036 |
| total Hf (v) | 22.0 | 19.2 | 18.6 | 16.4 | 22.9 | 23.6 | 16.2 |
| Age Ma | 120 | 120 | 120 | 120 | 116 | 116 | 120 |
| ± 2 se | 3 | 3 | 3 | 3 | 3 | 3 | 3 |
| CHUR(t) | 0.2827 | 0.2827 | 0.2827 | 0.2827 | 0.2827 | 0.2827 | 0.2827 |
| $^{176}Hf/^{177}Hf$ (i) | 0.282854 | 0.282857 | 0.282865 | 0.282878 | 0.282846 | 0.282872 | 0.282870 |
| ± 2 se | 0.000017 | 0.000016 | 0.000016 | 0.000026 | 0.000016 | 0.000017 | 0.000028 |
| e Hf (t) | 5.5 | 5.7 | 5.9 | 6.4 | 5.2 | 6.1 | 6.1 |
| ± 2 se | 0.60 | 0.55 | 0.58 | 0.92 | 0.55 | 0.60 | 0.99 |
| Age Ma (Chosen except core) | 116 | 116 | 116 | 116 | 116 | 116 | 116 |
| ± 2 se | 4 | 4 | 4 | 4 | 4 | 4 | 4 |
| CHUR(t=mean age) | 0.28270 | 0.28270 | 0.28270 | 0.28270 | 0.28270 | 0.28270 | 0.28270 |
| 176Hf/177Hf(i) | 0.2828539 | 0.2828574 | 0.2828652 | 0.2828785 | 0.2828458 | 0.2828722 | 0.2828699 |
| ±2se | 0.0000169 | 0.0000155 | 0.0000164 | 0.0000261 | 0.0000155 | 0.0000168 | 0.0000280 |
| eHf(t= avg mean age Ma) | 5.4 | 5.6 | 5.8 | 6.3 | 5.2 | 6.1 | 6.0 |
| ± 2 se | 0.6 | 0.5 | 0.6 | 0.9 | 0.5 | 0.6 | 1.0 |
| eNd | 2.3 | 2.3 | 2.3 | 2.3 | 2.3 | 2.3 | 2.3 |

| Spot | MD17a-38 | MD17a-51 | MD17a-72 | MD32-1c | MD32-2c | MD32-10c-actual | MD32-16c |
|---|---|---|---|---|---|---|---|
| $^{176}Hf/^{177}Hf$ | 0.282856 | 0.282866 | 0.282881 | 0.282675 | 0.282694 | 0.282688 | 0.282649 |
| ±2 se | 0.000017 | 0.000017 | 0.000018 | 0.000023 | 0.000020 | 0.000033 | 0.000021 |
| $^{178}Hf/^{177}Hf$ | 1.467247 | 1.467253 | 1.467283 | 1.467288 | 1.467281 | 1.467291 | 1.467275 |
| ± 2 se | 0.000032 | 0.000038 | 0.000032 | 0.000035 | 0.000038 | 0.000052 | 0.000036 |
| $^{180}Hf/^{177}Hf$ | 1.886861 | 1.886829 | 1.886917 | 1.886845 | 1.886885 | 1.886889 | 1.886875 |
| ± 2 se | 0.000064 | 0.000059 | 0.000067 | 0.000062 | 0.000068 | 0.000104 | 0.000073 |
| $^{176}Lu/^{177}Hf$ | 0.00125 | 0.00114 | 0.00133 | 0.00091 | 0.00175 | 0.00143 | 0.00140 |
| ± 2 se | 0.000009 | 0.000027 | 0.000051 | 0.000003 | 0.000011 | 0.000028 | 0.000071 |
| $^{176}Yb/^{177}Hf$ | 0.0443 | 0.0378 | 0.0433 | 0.0308 | 0.0561 | 0.0447 | 0.0459 |
| ± 2 se | 0.000191 | 0.000740 | 0.001546 | 0.000070 | 0.000367 | 0.000941 | 0.002391 |
| Yb/Hf | 0.063 | 0.054 | 0.061 | 0.044 | 0.079 | 0.063 | 0.065 |
| total Hf (v) | 19.0 | 20.9 | 22.0 | 11.0 | 12.1 | 5.5 | 11.6 |
| Age Ma | 118 | 119 | 119 | 333 | 342 | 345 | 339 |
| ± 2 se | 3 | 4 | 4 | 7 | 8 | 7 | 7 |
| CHUR(t) | 0.2827 | 0.2827 | 0.2827 | 0.2826 | 0.2826 | 0.2826 | 0.2826 |
| $^{176}Hf/^{177}Hf$ (i) | 0.282853 | 0.282864 | 0.282878 | 0.282669 | 0.282683 | 0.282678 | 0.282640 |
| ± 2 se | 0.000017 | 0.000017 | 0.000018 | 0.000023 | 0.000020 | 0.000033 | 0.000021 |
| e Hf (t) | 5.5 | 5.9 | 6.4 | 3.7 | 4.4 | 4.3 | 2.8 |
| ± 2 se | 0.61 | 0.62 | 0.62 | 0.82 | 0.71 | 1.16 | 0.74 |
| Age Ma (Chosen except core) | 116 | 116 | 116 | - | - | - | - |
| ± 2 se | 4 | 4 | 4 | - | - | - | - |
| CHUR(t=mean age) | 0.28270 | 0.28270 | 0.28270 | - | - | - | - |
| 176Hf/177Hf(i) | 0.2828529 | 0.2828640 | 0.2828781 | - | - | - | - |
| ±2se | 0.0000171 | 0.0000175 | 0.0000175 | - | - | - | - |
| eHf(t= avg mean age Ma) | 5.4 | 5.8 | 6.3 | - | - | - | - |
| ± 2 se | 0.6 | 0.6 | 0.6 | - | - | - | - |
| eNd | 2.3 | 2.3 | 2.3 | - | - | - | - |

| Spot | MD32-21c | MD32-1r-2 | MD32-2r | MD32-10r | MD32-16r | MD32-21r | MD32-83c |
|---|---|---|---|---|---|---|---|
| $^{176}Hf/^{177}Hf$ | 0.282666 | 0.282860 | 0.282756 | 0.282810 | 0.282781 | 0.282818 | 0.282838 |
| ±2 se | 0.000024 | 0.000026 | 0.000051 | 0.000049 | 0.000023 | 0.000021 | 0.000017 |
| $^{178}Hf/^{177}Hf$ | 1.467271 | 1.467257 | 1.467312 | 1.467319 | 1.467245 | 1.467245 | 1.467247 |
| ± 2 se | 0.000040 | 0.000043 | 0.000081 | 0.000072 | 0.000039 | 0.000036 | 0.000032 |
| $^{180}Hf/^{177}Hf$ | 1.886824 | 1.886773 | 1.886791 | 1.887002 | 1.886837 | 1.886853 | 1.886826 |
| ± 2 se | 0.000082 | 0.000088 | 0.000171 | 0.000135 | 0.000076 | 0.000069 | 0.000074 |
| $^{176}Lu/^{177}Hf$ | 0.00160 | 0.00059 | 0.00023 | 0.00217 | 0.00087 | 0.00074 | 0.00151 |
| ± 2 se | 0.000040 | 0.000010 | 0.000011 | 0.000077 | 0.000010 | 0.000017 | 0.000058 |
| $^{176}Yb/^{177}Hf$ | 0.0507 | 0.0184 | 0.0064 | 0.0635 | 0.0266 | 0.0230 | 0.0394 |
| ± 2 se | 0.001071 | 0.000410 | 0.000289 | 0.001849 | 0.000348 | 0.000532 | 0.001507 |
| Yb/Hf | 0.072 | 0.026 | 0.009 | 0.090 | 0.038 | 0.033 | 0.056 |
| total Hf (v) | 10.2 | 7.9 | 5.3 | 5.2 | 9.0 | 10.5 | 16.7 |
| Age Ma | 324 | 122 | 127 | 126 | 129 | 121 | 112 |
| ± 2 se | 7 | 4 | 3 | 4 | 4 | 5 | 6 |
| CHUR(t) | 0.2826 | 0.2827 | 0.2827 | 0.2827 | 0.2827 | 0.2827 | 0.2827 |
| $^{176}Hf/^{177}Hf$ (i) | 0.282656 | 0.282858 | 0.282756 | 0.282805 | 0.282779 | 0.282816 | 0.282834 |
| ± 2 se | 0.000024 | 0.000026 | 0.000051 | 0.000049 | 0.000023 | 0.000021 | 0.000017 |
| e Hf (t) | 3.0 | 5.7 | 2.2 | 3.9 | 3.1 | 4.2 | 4.7 |
| ± 2 se | 0.87 | 0.92 | 1.79 | 1.74 | 0.82 | 0.74 | 0.61 |
| Age Ma (Chosen except core) | - | 120 | 120 | 120 | 120 | 120 | 120 |
| ± 2 se | - | 6 | 6 | 6 | 6 | 6 | 6 |
| CHUR(t=mean age) | - | 0.28270 | 0.28270 | 0.28270 | 0.28270 | 0.28270 | 0.28270 |
| 176Hf/177Hf(i) | - | 0.2828585 | 0.2827558 | 0.2828048 | 0.2827790 | 0.2828165 | 0.2828341 |
| ±2se | - | 0.0000260 | 0.0000507 | 0.0000491 | 0.0000233 | 0.0000210 | 0.0000171 |
| eHf(t= avg mean age Ma) | - | 5.7 | 2.1 | 3.8 | 2.9 | 4.2 | 4.8 |
| ± 2 se | - | 0.9 | 1.8 | 1.7 | 0.8 | 0.7 | 0.6 |
| eNd | - | -0.6 | -0.6 | -0.6 | -0.6 | -0.6 | -0.6 |

| Spot | MD32-94 | MD32-95c | MD32-100 | MD32-108 | MD32-109 | MD2-1c | MD2-21c |
|---|---|---|---|---|---|---|---|
| $^{176}Hf/^{177}Hf$ | 0.282784 | 0.282759 | 0.282838 | 0.282853 | 0.282835 | 0.282707 | 0.282725 |
| ±2 se | 0.000016 | 0.000020 | 0.000019 | 0.000030 | 0.000021 | 0.000022 | 0.000022 |
| $^{178}Hf/^{177}Hf$ | 1.467233 | 1.467249 | 1.467238 | 1.467286 | 1.467256 | 1.467190 | 1.467255 |
| ± 2 se | 0.000030 | 0.000029 | 0.000036 | 0.000050 | 0.000045 | 0.000048 | 0.000038 |
| $^{180}Hf/^{177}Hf$ | 1.886763 | 1.886803 | 1.886804 | 1.886929 | 1.886817 | 1.886744 | 1.886830 |
| ± 2 se | 0.000062 | 0.000056 | 0.000065 | 0.000080 | 0.000069 | 0.000072 | 0.000076 |
| $^{176}Lu/^{177}Hf$ | 0.00061 | 0.00077 | 0.00117 | 0.00197 | 0.00169 | 0.00130 | 0.00209 |
| ± 2 se | 0.000049 | 0.000069 | 0.000014 | 0.000035 | 0.000050 | 0.000051 | 0.000065 |
| $^{176}Yb/^{177}Hf$ | 0.0181 | 0.0214 | 0.0353 | 0.0563 | 0.0521 | 0.0459 | 0.0713 |
| ± 2 se | 0.001474 | 0.001834 | 0.000471 | 0.001021 | 0.001569 | 0.001764 | 0.002063 |
| Yb/Hf | 0.026 | 0.030 | 0.050 | 0.080 | 0.074 | 0.065 | 0.101 |
| total Hf (v) | 18.2 | 19.3 | 13.5 | 8.3 | 13.6 | 16.7 | 14.5 |
| Age Ma | 119 | 121 | 119 | 122 | 112 | 348 | 310 |
| ± 2 se | 3 | 3 | 6 | 5 | 5 | 10 | 9 |
| CHUR(t) | 0.2827 | 0.2827 | 0.2827 | 0.2827 | 0.2827 | 0.2826 | 0.2826 |
| $^{176}Hf/^{177}Hf$ (i) | 0.282782 | 0.282757 | 0.282835 | 0.282849 | 0.282832 | 0.282699 | 0.282713 |
| ± 2 se | 0.000016 | 0.000020 | 0.000019 | 0.000030 | 0.000021 | 0.000022 | 0.000022 |
| e Hf (t) | 3.0 | 2.1 | 4.8 | 5.4 | 4.6 | 5.1 | 4.7 |
| ± 2 se | 0.55 | 0.70 | 0.69 | 1.05 | 0.73 | 0.78 | 0.78 |
| Age Ma (Chosen except core) | 120 | 120 | 120 | 120 | 120 | - | - |
| ± 2 se | 6 | 6 | 6 | 6 | 6 | - | - |
| CHUR(t=mean age) | 0.28270 | 0.28270 | 0.28270 | 0.28270 | 0.28270 | - | - |
| 176Hf/177Hf(i) | 0.2827824 | 0.2827573 | 0.2828351 | 0.2828487 | 0.2828316 | - | - |
| ±2se | 0.0000156 | 0.0000198 | 0.0000195 | 0.0000297 | 0.0000206 | - | - |
| eHf(t= avg mean age Ma) | 3.0 | 2.1 | 4.9 | 5.3 | 4.7 | - | - |
| ± 2 se | 0.6 | 0.7 | 0.7 | 1.1 | 0.7 | - | - |
| eNd | -0.6 | -0.6 | -0.6 | -0.6 | -0.6 | - | - |

| Spot | MD2-41c | MD2-80c | MD2-118c | MD2-23r | MD2-124r | MD2-149r | MD6-124c |
|---|---|---|---|---|---|---|---|
| $^{176}Hf/^{177}Hf$ | 0.282697 | 0.282690 | 0.282724 | 0.282742 | 0.282720 | 0.282693 | 0.282648 |
| ±2 se | 0.000020 | 0.000023 | 0.000055 | 0.000031 | 0.000047 | 0.000049 | 0.000011 |
| $^{178}Hf/^{177}Hf$ | 1.467262 | 1.467241 | 1.467294 | 1.467259 | 1.467299 | 1.467139 | 1.467265 |
| ± 2 se | 0.000034 | 0.000056 | 0.000071 | 0.000048 | 0.000068 | 0.000091 | 0.000048 |
| $^{180}Hf/^{177}Hf$ | 1.886850 | 1.886786 | 1.887489 | 1.886884 | 1.886900 | 1.886969 | 1.886839 |
| ± 2 se | 0.000068 | 0.000088 | 0.000210 | 0.000100 | 0.000134 | 0.000171 | 0.000046 |
| $^{176}Lu/^{177}Hf$ | 0.00149 | 0.00118 | 0.00317 | 0.00145 | 0.00181 | 0.00164 | 0.00004 |
| ± 2 se | 0.000018 | 0.000050 | 0.000341 | 0.000013 | 0.000028 | 0.000034 | 0.000001 |
| $^{176}Yb/^{177}Hf$ | 0.0517 | 0.0382 | 0.1012 | 0.0425 | 0.0467 | 0.0451 | 0.0012 |
| ± 2 se | 0.000645 | 0.001532 | 0.011805 | 0.000318 | 0.000874 | 0.000856 | 0.000027 |
| Yb/Hf | 0.073 | 0.054 | 0.143 | 0.060 | 0.066 | 0.064 | 0.002 |
| total Hf (v) | 13.7 | 9.5 | 8.5 | 7.7 | 10.5 | 11.7 | 28.9 |
| Age Ma | 322 | 326 | 305 | 140 | 144 | 140 | 120 |
| ± 2 se | 9 | 10 | 11 | 4 | 4 | 6 | 2 |
| CHUR(t) | 0.2826 | 0.2826 | 0.2826 | 0.2827 | 0.2827 | 0.2827 | 0.2827 |
| $^{176}Hf/^{177}Hf$ (i) | 0.282688 | 0.282683 | 0.282706 | 0.282738 | 0.282716 | 0.282689 | 0.282648 |
| ± 2 se | 0.000020 | 0.000023 | 0.000055 | 0.000031 | 0.000047 | 0.000049 | 0.000011 |
| e Hf (t) | 4.1 | 4.0 | 4.4 | 1.9 | 1.2 | 0.1 | -1.8 |
| ± 2 se | 0.72 | 0.82 | 1.96 | 1.08 | 1.68 | 1.74 | 0.40 |
| Age Ma (Chosen except core) | - | - | - | 140 | 140 | 140 | 110 |
| ± 2 se | - | - | - | 6 | 6 | 6 | 8 |
| CHUR(t=mean age) | - | - | - | 0.28269 | 0.28269 | 0.28269 | 0.28270 |
| 176Hf/177Hf(i) | - | - | - | 0.2827381 | 0.2827157 | 0.2826886 | 0.2826479 |
| ±2se | - | - | - | 0.0000307 | 0.0000474 | 0.0000491 | 0.0000113 |
| eHf(t= avg mean age Ma) | - | - | - | 1.9 | 1.1 | 0.1 | -2.0 |
| ± 2 se | - | - | - | 1.1 | 1.7 | 1.7 | 0.4 |
| eNd | - | - | - | -1.4 | -1.4 | -1.4 | -4.1 |

| Spot | MD6-84a-r | MD6-84a-c | MD6-130c | MD6-62c | MD29-1c | MD29-6c | MD29-69c |
|---|---|---|---|---|---|---|---|
| $^{176}Hf/^{177}Hf$ | 0.282657 | 0.282661 | 0.282609 | 0.282708 | 0.282689 | 0.282670 | 0.282675 |
| ±2 se | 0.000063 | 0.000032 | 0.000023 | 0.000022 | 0.000010 | 0.000016 | 0.000013 |
| $^{178}Hf/^{177}Hf$ | 1.467332 | 1.467316 | 1.467294 | 1.467278 | 1.467280 | 1.467269 | 1.467274 |
| ± 2 se | 0.000163 | 0.000114 | 0.000088 | 0.000070 | 0.000028 | 0.000032 | 0.000026 |
| $^{180}Hf/^{177}Hf$ | 1.886966 | 1.886927 | 1.886794 | 1.886900 | 1.886832 | 1.886981 | 1.886821 |
| ± 2 se | 0.000201 | 0.000131 | 0.000092 | 0.000077 | 0.000045 | 0.000050 | 0.000044 |
| $^{176}Lu/^{177}Hf$ | 0.00042 | 0.00137 | 0.00088 | 0.00153 | 0.00077 | 0.00108 | 0.00120 |
| ± 2 se | 0.000078 | 0.000021 | 0.000023 | 0.000060 | 0.000020 | 0.000059 | 0.000017 |
| $^{176}Yb/^{177}Hf$ | 0.0122 | 0.0429 | 0.0241 | 0.0454 | 0.0216 | 0.0352 | 0.0368 |
| ± 2 se | 0.002278 | 0.000761 | 0.000648 | 0.001826 | 0.000642 | 0.002024 | 0.000703 |
| Yb/Hf | 0.017 | 0.061 | 0.034 | 0.065 | 0.031 | 0.050 | 0.052 |
| total Hf (v) | 5.5 | 16.0 | 21.9 | 13.8 | 38.1 | 28.0 | 31.6 |
| Age Ma | 108 | 327 | 320 | 323 | 302 | 309 | 304 |
| ± 2 se | 2 | 6 | 6 | 6 | 6 | 6 | 6 |
| CHUR(t) | 0.2827 | 0.2826 | 0.2826 | 0.2826 | 0.2826 | 0.2826 | 0.2826 |
| $^{176}Hf/^{177}Hf$ (i) | 0.282656 | 0.282653 | 0.282604 | 0.282699 | 0.282684 | 0.282664 | 0.282669 |
| ± 2 se | 0.000063 | 0.000032 | 0.000023 | 0.000022 | 0.000010 | 0.000016 | 0.000013 |
| e Hf (t) | -1.7 | 3.0 | 1.1 | 4.5 | 3.5 | 3.0 | 3.0 |
| ± 2 se | 2.22 | 1.12 | 0.80 | 0.77 | 0.36 | 0.57 | 0.46 |
| Age Ma (Chosen except core) | 110 | - | - | - | - | - | - |
| ± 2 se | 8 | - | - | - | - | - | - |
| CHUR(t=mean age) | 0.28270 | - | - | - | - | - | - |
| 176Hf/177Hf(i) | 0.2826560 | - | - | - | - | - | - |
| ±2se | 0.0000628 | - | - | - | - | - | - |
| eHf(t= avg mean age Ma) | -1.7 | - | - | - | - | - | - |
| ± 2 se | 2.2 | - | - | - | - | - | - |
| eNd | -4.1 | - | - | - | - | - | - |

| Spot | MD29-1r | MD29-5r | MD29-32 | MD29-33-1 | MD29-70-1 | MD29-70-2 | MD29-91-1 |
|---|---|---|---|---|---|---|---|
| $^{176}Hf/^{177}Hf$ | 0.282749 | 0.282729 | 0.282719 | 0.282713 | 0.282793 | 0.282725 | 0.282743 |
| ±2 se | 0.000013 | 0.000011 | 0.000010 | 0.000016 | 0.000017 | 0.000014 | 0.000025 |
| $^{178}Hf/^{177}Hf$ | 1.467264 | 1.467291 | 1.467293 | 1.467312 | 1.467252 | 1.467279 | 1.467249 |
| ± 2 se | 0.000037 | 0.000038 | 0.000031 | 0.000070 | 0.000090 | 0.000029 | 0.000098 |
| $^{180}Hf/^{177}Hf$ | 1.886787 | 1.886844 | 1.886832 | 1.886824 | 1.886785 | 1.886867 | 1.886861 |
| ± 2 se | 0.000049 | 0.000046 | 0.000045 | 0.000070 | 0.000069 | 0.000058 | 0.000109 |
| $^{176}Lu/^{177}Hf$ | 0.00066 | 0.00038 | 0.00012 | 0.00006 | 0.00020 | 0.00292 | 0.00060 |
| ± 2 se | 0.000021 | 0.000049 | 0.000020 | 0.000001 | 0.000007 | 0.000046 | 0.000006 |
| $^{176}Yb/^{177}Hf$ | 0.0185 | 0.0120 | 0.0043 | 0.0021 | 0.0059 | 0.0735 | 0.0154 |
| ± 2 se | 0.000551 | 0.001471 | 0.000596 | 0.000026 | 0.000212 | 0.001037 | 0.000248 |
| Yb/Hf | 0.026 | 0.017 | 0.006 | 0.003 | 0.008 | 0.104 | 0.022 |
| total Hf (v) | 33.8 | 39.7 | 42.3 | 22.0 | 21.8 | 25.2 | 13.3 |
| Age Ma | 114 | 141 | 129 | 120 | 123 | 123 | 126 |
| ± 2 se | 3 | 3 | 3 | 3 | 3 | 3 | 3 |
| CHUR(t) | 0.2827 | 0.2827 | 0.2827 | 0.2827 | 0.2827 | 0.2827 | 0.2827 |
| $^{176}Hf/^{177}Hf$ (i) | 0.282748 | 0.282728 | 0.282719 | 0.282713 | 0.282793 | 0.282719 | 0.282741 |
| ± 2 se | 0.000013 | 0.000011 | 0.000010 | 0.000016 | 0.000017 | 0.000014 | 0.000025 |
| e Hf (t) | 1.7 | 1.5 | 1.0 | 0.6 | 3.4 | 0.8 | 1.7 |
| ± 2 se | 0.47 | 0.39 | 0.36 | 0.58 | 0.59 | 0.50 | 0.90 |
| Age Ma (Chosen except core) | 122 | 122 | 122 | 122 | 122 | 122 | 122 |
| ± 2 se | 11 | 11 | 11 | 11 | 11 | 11 | 11 |
| CHUR(t=mean age) | 0.28270 | 0.28270 | 0.28270 | 0.28270 | 0.28270 | 0.28270 | 0.28270 |
| 176Hf/177Hf(i) | 0.2827478 | 0.2827278 | 0.2827191 | 0.2827130 | 0.2827929 | 0.2827187 | 0.2827413 |
| ±2se | 0.0000132 | 0.0000111 | 0.0000100 | 0.0000164 | 0.0000167 | 0.0000142 | 0.0000253 |
| eHf(t= avg mean age Ma) | 1.8 | 1.1 | 0.8 | 0.6 | 3.4 | 0.8 | 1.6 |
| ± 2 se | 0.5 | 0.4 | 0.4 | 0.6 | 0.6 | 0.5 | 0.9 |
| eNd | -2.3 | -2.3 | -2.3 | -2.3 | -2.3 | -2.3 | -2.3 |

| Spot | MD29-91-2r | MD33-2c | MD33-29c | MD33-2r | MD33-29r | MD33-43c | MD14-6-c |
|---|---|---|---|---|---|---|---|
| $^{176}Hf/^{177}Hf$ | 0.282742 | 0.282607 | 0.282615 | 0.282665 | 0.282693 | 0.282712 | 0.282658 |
| ±2 se | 0.000023 | 0.000019 | 0.000021 | 0.000016 | 0.000018 | 0.000015 | 0.000030 |
| $^{178}Hf/^{177}Hf$ | 1.467324 | 1.467258 | 1.467238 | 1.467264 | 1.467236 | 1.467237 | 1.467277 |
| ± 2 se | 0.000049 | 0.000026 | 0.000033 | 0.000030 | 0.000032 | 0.000036 | 0.000069 |
| $^{180}Hf/^{177}Hf$ | 1.886817 | 1.886888 | 1.886797 | 1.886811 | 1.886819 | 1.886914 | 1.886880 |
| ± 2 se | 0.000103 | 0.000066 | 0.000069 | 0.000064 | 0.000064 | 0.000070 | 0.000099 |
| $^{176}Lu/^{177}Hf$ | 0.00038 | 0.00120 | 0.00187 | 0.00001 | 0.00010 | 0.00054 | 0.00250 |
| ± 2 se | 0.000016 | 0.000020 | 0.000017 | 0.000000 | 0.000004 | 0.000040 | 0.000118 |
| $^{176}Yb/^{177}Hf$ | 0.0100 | 0.0504 | 0.0770 | 0.0004 | 0.0035 | 0.0195 | 0.0860 |
| ± 2 se | 0.000393 | 0.001027 | 0.000808 | 0.000014 | 0.000140 | 0.001546 | 0.004273 |
| Yb/Hf | 0.014 | 0.072 | 0.109 | 0.000 | 0.005 | 0.028 | 0.122 |
| total Hf (v) | 20.1 | 20.83 | 16.82 | 18.74 | 15.66 | 22.84 | 9.7 |
| Age Ma | 126 | 260 | 340 | 121 | 120 | 132 | 128 |
| ± 2 se | 3 | 6 | 7 | 3 | 3 | 3 | 12 |
| CHUR(t) | 0.2827 | 0.2826 | 0.2826 | 0.2827 | 0.2827 | 0.2827 | 0.2827 |
| $^{176}Hf/^{177}Hf$ (i) | 0.282741 | 0.282601 | 0.282603 | 0.282665 | 0.282693 | 0.282711 | 0.282652 |
| ± 2 se | 0.000023 | 0.000019 | 0.000021 | 0.000016 | 0.000018 | 0.000015 | 0.000030 |
| e Hf (t) | 1.7 | -0.4 | 1.5 | -1.1 | -0.2 | 0.8 | -1.4 |
| ± 2 se |  | 0.67 | 0.74 | 0.55 | 0.63 | 0.52 | 1.07 |
| Age Ma (Chosen except core) | 122 | - | - | 121 | 121 | 121 | 119 |
| ± 2 se | 11 | - | - | 4 | 4 | 4 | 12 |
| CHUR(t=mean age) | 0.28270 | - | - | 0.28270 | 0.28270 | 0.28270 | 0.28270 |
| 176Hf/177Hf(i) | 0.2827409 | - | - | 0.2826650 | 0.2826927 | 0.2827112 | 0.2826525 |
| ±2se | 0.0000227 | - | - | 0.0000156 | 0.0000177 | 0.0000148 | 0.0000303 |
| eHf(t= avg mean age Ma) | 1.6 | - | - | -1.1 | -0.1 | 0.5 | -1.6 |
| ± 2 se | 0.8 | - | - | 0.6 | 0.6 | 0.5 | 1.1 |
| eNd | -2.3 | - | - | -3.8 | -3.8 | -3.8 | 0.7 |

| Spot | MD14-89-c | MD14-50-r | MD14-64-r | MD14-10-r | MD14-10-1r | MD14-130-c-r | MD14-10-c |
|---|---|---|---|---|---|---|---|
| $^{176}Hf/^{177}Hf$ | 0.282697 | 0.282674 | 0.282729 | 0.282709 | 0.282725 | 0.282695 | 0.282712 |
| ±2 se | 0.000023 | 0.000028 | 0.000038 | 0.000028 | 0.000018 | 0.000027 | 0.000021 |
| $^{178}Hf/^{177}Hf$ | 1.467300 | 1.467349 | 1.467250 | 1.467274 | 1.467254 | 1.467288 | 1.467286 |
| ± 2 se | 0.000057 | 0.000082 | 0.000129 | 0.000084 | 0.000037 | 0.000062 | 0.000046 |
| $^{180}Hf/^{177}Hf$ | 1.886788 | 1.886957 | 1.886759 | 1.886869 | 1.886863 | 1.886813 | 1.886822 |
| ± 2 se | 0.000080 | 0.000096 | 0.000163 | 0.000116 | 0.000064 | 0.000076 | 0.000066 |
| $^{176}Lu/^{177}Hf$ | 0.00043 | 0.00060 | 0.00033 | 0.00056 | 0.00054 | 0.00195 | 0.00184 |
| ± 2 se | 0.000029 | 0.000011 | 0.000003 | 0.000004 | 0.000004 | 0.000025 | 0.000058 |
| $^{176}Yb/^{177}Hf$ | 0.0116 | 0.0172 | 0.0093 | 0.0160 | 0.0167 | 0.0647 | 0.0604 |
| ± 2 se | 0.000810 | 0.000411 | 0.000155 | 0.000061 | 0.000129 | 0.000922 | 0.002175 |
| Yb/Hf | 0.016 | 0.024 | 0.013 | 0.023 | 0.024 | 0.092 | 0.086 |
| total Hf (v) | 12.7 | 12.4 | 14.1 | 12.3 | 12.0 | 8.8 | 10.5 |
| Age Ma | 118 | 123 | 111 | 130 | 130 | 314 | 333 |
| ± 2 se | 20 | 28 | 32 | 36 | 38 | 18 | 40 |
| CHUR(t) | 0.2827 | 0.2827 | 0.2827 | 0.2827 | 0.2827 | 0.2826 | 0.2826 |
| $^{176}Hf/^{177}Hf$ (i) | 0.282696 | 0.282672 | 0.282728 | 0.282707 | 0.282724 | 0.282683 | 0.282700 |
| ± 2 se | 0.000023 | 0.000028 | 0.000038 | 0.000028 | 0.000018 | 0.000027 | 0.000021 |
| e Hf (t) | -0.1 | -0.8 | 0.9 | 0.6 | 1.1 | 3.8 | 4.8 |
| ± 2 se | 0.82 | 0.99 | 1.33 | 1.00 | 0.65 | 0.94 | 0.74 |
| Age Ma (Chosen except core) | 119 | 119 | 119 | 119 | 119 | - | - |
| ± 2 se | 12 | 12 | 12 | 12 | 12 | - | - |
| CHUR(t=mean age) | 0.28270 | 0.28270 | 0.28270 | 0.28270 | 0.28270 | - | - |
| 176Hf/177Hf(i) | 0.2826955 | 0.2826724 | 0.2827279 | 0.2827075 | 0.2827240 | - | - |
| ±2se | 0.0000233 | 0.0000281 | 0.0000376 | 0.0000281 | 0.0000185 | - | - |
| eHf(t= avg mean age Ma) | -0.1 | -0.9 | 1.1 | 0.3 | 0.9 | - | - |
| ± 2 se | 0.8 | 1.0 | 1.3 | 1.0 | 0.7 | - | - |
| eNd | 0.7 | 0.7 | 0.7 | 0.7 | 0.7 | - | - |

| Spot | MD14-79-c | MD14-50-c | MD38-2c | MD38-27c | MD38-40c | MD38-170c |
|---|---|---|---|---|---|---|
| $^{176}Hf/^{177}Hf$ | 0.282727 | 0.282728 | 0.282700 | 0.282670 | 0.282711 | 0.282688 |
| ±2 se | 0.000028 | 0.000036 | 0.000025 | 0.000017 | 0.000031 | 0.000017 |
| $^{178}Hf/^{177}Hf$ | 1.467281 | 1.467223 | 1.467296 | 1.467254 | 1.467251 | 1.467245 |
| ± 2 se | 0.000053 | 0.000080 | 0.000039 | 0.000035 | 0.000044 | 0.000041 |
| $^{180}Hf/^{177}Hf$ | 1.886822 | 1.886795 | 1.886863 | 1.886867 | 1.886722 | 1.886842 |
| ± 2 se | 0.000076 | 0.000117 | 0.000075 | 0.000064 | 0.000097 | 0.000063 |
| $^{176}Lu/^{177}Hf$ | 0.00467 | 0.00224 | 0.00150 | 0.00124 | 0.00174 | 0.00077 |
| ± 2 se | 0.000076 | 0.000077 | 0.000013 | 0.000054 | 0.000099 | 0.000057 |
| $^{176}Yb/^{177}Hf$ | 0.1435 | 0.0711 | 0.0513 | 0.0414 | 0.0581 | 0.0265 |
| ± 2 se | 0.002298 | 0.002481 | 0.000542 | 0.001920 | 0.003508 | 0.001960 |
| Yb/Hf | 0.204 | 0.101 | 0.073 | 0.059 | 0.082 | 0.038 |
| total Hf (v) | 10.2 | 11.6 | 9.7 | 15.5 | 9.1 | 14.9 |
| Age Ma | 284 | 322 | 344 | 331 | 329 | 339 |
| ± 2 se | 22 | 30 | 7 | 7 | 7 | 8 |
| CHUR(t) | 0.2826 | 0.2826 | 0.2826 | 0.2826 | 0.2826 | 0.2826 |
| $^{176}Hf/^{177}Hf$ (i) | 0.282702 | 0.282715 | 0.282690 | 0.282662 | 0.282700 | 0.282683 |
| ± 2 se | 0.000028 | 0.000036 | 0.000025 | 0.000017 | 0.000031 | 0.000017 |
| e Hf (t) | 3.8 | 5.1 | 4.7 | 3.4 | 4.7 | 4.3 |
| ± 2 se | 0.99 | 1.28 | 0.87 | 0.61 | 1.09 | 0.61 |
| Age Ma (Chosen except core) | - | - | - | - | - | - |
| ± 2 se | - | - | - | - | - | - |
| CHUR(t=mean age) | - | - | - | - | - | - |
| 176Hf/177Hf(i) | - | - | - | - | - | - |
| ±2se | - | - | - | - | - | - |
| eHf(t= avg mean age Ma) | - | - | - | - | - | - |
| ± 2 se | - | - | - | - | - | - |
| eNd | - | - | - | - | - | - |

| Spot | MD38-47c | MD38-37 |
|---|---|---|
| $^{176}Hf/^{177}Hf$ | 0.282679 | 0.282705 |
| ±2 se | 0.000016 | 0.000023 |
| $^{178}Hf/^{177}Hf$ | 1.467250 | 1.467254 |
| ± 2 se | 0.000030 | 0.000039 |
| $^{180}Hf/^{177}Hf$ | 1.886867 | 1.886851 |
| ± 2 se | 0.000053 | 0.000079 |
| $^{176}Lu/^{177}Hf$ | 0.00053 | 0.00117 |
| ± 2 se | 0.000026 | 0.000024 |
| $^{176}Yb/^{177}Hf$ | 0.0164 | 0.0380 |
| ± 2 se | 0.000843 | 0.000870 |
| Yb/Hf | 0.023 | 0.054 |
| total Hf (v) | 16.9 | 9.1 |
| Age Ma | 152 | 126 |
| ± 2 se | 4 | 3 |
| CHUR(t) | 0.2827 | 0.2827 |
| $^{176}Hf/^{177}Hf$ (i) | 0.282677 | 0.282702 |
| ± 2 se | 0.000027 | 0.000027 |
| e Hf (t) | -0.02 | 0.3 |
| ± 2 se | 0.56 | 0.83 |
| Age Ma (Chosen except core) | - | 125 |
| ± 2 se | - | - |
| CHUR(t=mean age) | - | 0.28269 |
| 176Hf/177Hf(i) | - | 0.2827021 |
| ±2se | - | 0.0000233 |
| eHf(t= avg mean age Ma) | - | 0.3 |
| ± 2 se | - | 0.8 |
| eNd | - | -1.7 |